Journal of ATMOSPHERIC and TERRESTRIAL PHYSICS

EDITORIAL ADVISORY BOARD

H. O. G. ALFVEN–STOCKHOLM · **J. BARTELS**–GÖTTINGEN · **W. J. G. BEYNON**–ABERYSTWYTH
P. M. S. BLACKETT–LONDON · **H. G. BOOKER**–ITHACA, N.Y. · **E. G. BOWEN**–SYDNEY
SIR DAVID BRUNT–LONDON · **R. BUREAU**–BAGNEUX · **S. CHAPMAN**–ALASKA
J. EGEDAL–COPENHAGEN · **V. F. HESS**–NEW YORK · **E. O. HULBURT**–WASHINGTON, D.C.
H. ISRAEL–AACHEN · **D. K. MENZEL**–CAMBRIDGE, MASS. · **S. K. MITRA**–CALCUTTA
M. NICOLET–UCCLE · **E. H. NORINDER**–UPPSALA · **J. PATON**–EDINBURGH
N. V. PUSHKOV–MOSCOW · **J. A. RATCLIFFE**–SLOUGH · **O. E. H. RYDBECK**–GOTHENBURG
J. C. W. SCOTT–OTTAWA · **SIR GEORGE SIMPSON**–LONDON · **H. SOLBERG**–OSLO
J. VELDKAMP–DE BILT · **M. WALDMEIER**–ZÜRICH

OL.
22
961

EDITOR-IN-CHIEF
SIR EDWARD APPLETON, F.R.S.
EDINBURGH

VOLUME 22
1961

PERGAMON PRESS
OXFORD • LONDON • NEW YORK • PARIS

VOL.
22
1961

CONTENTS

No. 1

K. V. V. Ramana and B. Ramachandra Rao: Investigation of ionospheric absorption on 5·65 Mc/s at Waltair 1

M. S. V. Gopal Rao and B. Ramachandra Rao: Nocturnal and seasonal variations of equatorial spread-*F* 12

A. F. El Nadi and N. Farag: The effect of light on the mobility and concentrations of large ions in air mixed with N_2O gas 23

D. Van Sabben: Ionospheric current systems of ten IGY-solar flare effects . . . 32

G. F. Fooks: The fading of radio waves reflected vertically from the ionosphere during magnetic storms 43

O. K. Garriott and A. W. Nichol: Ionospheric information deduced from the Doppler shifts of harmonic frequencies from earth satellites 50

J. S. Greenhow: Head echoes from meteor trails 64

Research Notes

H. W. Bergh and J. W. King: Ionospheric critical frequencies and magnetic parameters of the day before 74

M. Gadsden and K. Salmon: A note on the observations of twilight lithium emission made from Hallett Station 75

Book Reviews

"Upper Winds over the World", by H. Heastie and P. M. Stephenson. (Reviewed by D. H. McIntosh) 79

"Zyklen und Perioden in der Geophysik", by F. S. G. Bayer. (Reviewed by D. H. McIntosh) 79

Papers to be published in future issues 80

No. 2

R. Raghava Rao and B. Ramachandra Rao: Study of horizontal drifts in the *E*-region at Waltair 81

H. Unz: The effect of small values of $Z = \nu/\omega$ on the complex refractive index in the magneto-ionic theory 100

M. Gadsden: The relative intensities of some nitrogen bands in auroral spectra . . 105

Elisabeth Cooper: The properties of low frequency radio waves reflected from the ionosphere, calculated by the phase-integral method 122

S. Chapman and P. C. Kendall: An idealized problem of plasma dynamics that bears on geomagnetic storm theory; oblique projection 142

Research Notes

C. H. Cummack: Evidence of some geomagnetic control on the *F1*-layer 157

R. Raghava Rao and B. Ramachandra Rao: Height gradient of horizontal drifts in the *E*-region over Waltair 158

Papers to be published in future issues 160

No. 3

A. R. Thompson: Sweep frequency observations of meteor scatter bursts 161

D. E. Shemansky and A. Vallance Jones: New measurements of the night airglow spectrum in the 1·5 μ region 166

J. Wolfe: 20 Mc/s w.w.v. bursts during the last few periods of 1958δ2 176

L. H. Heisler and J. D. Whitehead: The interpretation of *F2* critical frequency measurements 186

G. H. Bazzard and C. M. Minnis: The geographical distribution of the harmonics of the annual variation in the critical frequency of the *F2*-layer at noon 192

J. E. Titheridge: The effect of collisions on the propagation of radio waves in the ionosphere 200

Research Notes
L. H. Heisler and L. D. Wilson: A new versatile ionospheric recorder . . 218
D. G. Singleton: On the apparent long term negative correlation between scintillations and spread-F 219
Book Reviews
"Science in Space", edited by L. V. Berkner and H. Odishaw. (Reviewed by Sir Edward Appleton) 221
"Antarctic Meteorology: Proceedings of the Melborne Symposium, February 1959". (Reviewed by G. Manley) 221
"Some Ionospheric Results obtained during the International Geophysical Year", scientific editor W. J. G. Beynon. (Reviewed by R. L. Smith-Rose) . . . 222
"Assualt on the Unknown", by W. Sullivan. (Reviewed by Sir Edward Appleton) 223
"Handbook of Aviation Meteorology". (Reviewed by J. Paton) 224
"Cosmic Radio Waves", by I. S. Shklovsky. (Reviewed by F. G. Smith) . . 224
"Satellite Environment Handbook", edited by F. S. Johnson. (Reviewed by Sir Edward Appleton) 225
"Tools of the Astronomer", by G. R. Miczaika and W. M. Sinton. (Reviewed by H. A. Brück) 225
"The Inversion over the Eastern North Pacific Ocean", by M. Neiburger, D. S. Johnson and Chen-Wu-Chien. (Reviewed by J. K. Bannon) 225
"Space Astrophysics", edited by W. Liller. (Reviewed by Sir Edward Appleton) 226
"Dissertations in Physics", compiled by M. L. Marckworth. (Reviewed by N. Feather) 227
Notice 228
K-Indices of geomagnetic activity for May–July 1961 229
Papers to be published in future issues 232

VOL. 22 1961

No. 4

T. Ondoh: Variations of the earth's exosphere and geomagnetic disturbances during the geomagnetic storm of 4 September 1958 233
G. S. Kent: High frequency fading of the 108 Mc/s wave radiated from an artificial earth satellite as observed at an equatorial station 255
R. Naismith and P. A. Smith: Further evidence of a long term variation in the relationship of solar activity to the ionosphere 270
W. Becker: The varying electron density profile of the F-region during magnetically quiet nights 275
R. G. Rastogi: The morphology of lunar semi-diurnal variation in f_0F2 near solar noon 290
Research Note
C. H. Cummack: The heat balance of the F-region and the saturation effect . . 298
K-indices of geomagnetic activity for August 1961 303
Papers to be published in future issues 304

AUTHOR INDEX

(B.R.) denotes a book review

Appleton E. V. (B.R.'s) 221, 223, 225, 226
Bannon J. K. (B.R.) 225
Bazzard G. H. 192
Becker W. 275
Bergh H. W. 74
Brück H. A. 225
Chapman S. 142
Cooper E. 122
Cummack C. H. 157, 298
El Nadi A. F. 23
Farag N. 23
Feather N. (B.R.) 226
Fooks G. F. 43
Gadsden M. 75, 105
Garriott O. K. 50
Greenhow J. S. 64
Heisler L. H. 186, 218
Kendall P. C. 142
Kent G. S. 255
King J. W. 74
Manley G. (B.R.) 221
McIntosh D. H. (B.R.) 79
Minnis C. M. 192
Naismith R. 270
Nichol A. W. 50
Ondoh T. 233
Paton J. (B.R.) 224
Ramana K. V. V. 1
Rao B. R. 1, 12, 81, 158
Rao M. S. V. G. 12
Rao R. R. 81, 158
Rastogi R. G. 290
Salmon K. 75
Shemansky D. E. 166
Singleton D. G. 219
Smith F. G. (B.R.) 224
Smith P. A. 270
Smith-Rose R. L. (B.R.) 222
Thompson A. R. 161
Titheridge J. E. 200
Unz H. 100
Vallance Jones A. 166
Van Sabben D. 32
Whitehead J. D. 186
Wilson L. D. 218
Wolfe J. 176

Journal of Atmospheric and Terrestrial Physics, 1961, Vol. 22, pp. 1 to 11. Pergamon Press Ltd. Printed in Northern Ireland

Investigation of ionospheric absorption on 5·65 Mc/s at Waltair

K. V. V. Ramana and B. Ramachandra Rao
Ionospheric Research Laboratories, Physics Department, Andhra University, Waltair, India

(*Received* 9 *February* 1961)

Abstract—This paper presents the results of ionospheric absorption measurements conducted at Waltair (Latitude 17·7°N, Longitude 83·3°E and Geomagnetic Latitude 7·4°N) during the International Geophysical Year and International Geophysical Co-operation periods on a frequency of 5·65 Mc/s.

The solar zenith distance variation of diurnal and seasonal data of absorption follows a law of the form

$$8{\cdot}7\,|\log_e \rho| = A_1 \,.\, (f)^{-2} \,.\, \cos^n \chi \quad \text{dB}$$

only as an approximation. The variation of the cos χ index has a significant negative correlation with Zürich relative sunspot number R.

The monthly mean diurnal variation as well as seasonal noon-time variation of absorption confirms, more precisely, to a law of the form

$$|\log_e \rho| = A' + B \,.\, F(f_0 E/f) \cos \chi \quad \text{nepers}$$

where A' is a constant expected to refer to the non-deviative absorption in lower D-region. A' is found to vary linearly with R.

A method is suggested to estimate the relative amounts of D- and E-region absorption at noon from the cos χ index data. The absorption $|\log_e \rho|$ and A' are found to vary inversely as the square of the operating frequency.

1. Introduction

Appleton and Ratcliffe (1930) were among the first to measure the apparent reflection coefficient (ρ) of radio waves reflected from the ionosphere. Appleton (1937) showed that for reflections from the F-region, the non-deviative absorption in a lower Chapman region (Chapman, 1931) is given by

$$-\log_e \rho = C \cos^{3/2} \chi \quad \text{nepers} \tag{1}$$

for the case where the operating frequency is considerably higher than the collision frequency. Here, C is a constant for a fixed operating frequency and "χ" is the solar zenith angle. Jaeger (1947) considered the overall absorption in a Chapman region and derived a general equation for the overall absorption in a Chapman layer for the cases of reflection and transmission in such a layer. For the case of transmission through a Chapman layer which is of interest in the present investigation, Jaeger has given the following expression for the overall absorption in such a layer

$$-\log_e \rho = \frac{\nu_0 H}{C} \cdot F\left(\frac{f_c}{f}\right) \cos \chi \tag{2}$$

where ν_0 is the electron collision frequency at a certain datum level h_0 (Chapman, 1931), H is the scale height and $F(f_c/f)$ is a function computed by Jaeger for various values of the ratio f_c/f where f_c is the critical frequency of the Chapman layer.

Although extensive work has been done on ionospheric absorption studies at high latitude stations, there is very little work done on this aspect at low latitude

stations. Skinner and Wright (1956) and Delobeau and Suchy (1956) are among the few who reported studies on ionospheric absorption measurements at equatorial latitudes. The authors, Rao and Ramana (1958), have reported preliminary ionospheric absorption studies on a frequency of 5·65 Mc/s for about 6 months during the International Geophysical Year. This paper embodies the results of a detailed study of ionospheric absorption on a frequency of 5·65 Mc/s for a period of 2 years and also results of a study of frequency variation of absorption.

2. Experimental Details

The experimental technique adopted for measuring the reflection coefficient and hence the value of total absorption, $|\log_e \rho|$, is the conventional vertical incidence pulse technique described earlier by Piggott (1953).

For each sample, measurement of the amplitude of the reflected echoes is carried out by varying an attenuator at the input to the receiver to keep the output constant as seen on the oscillograph. In each sample, about 100–120 measurements of the amplitudes are taken at intervals of 5 sec to minimize the errors due to fading. By taking an average of the amplitude measurements and knowing the calibration constant of the equipment, the value of the absorption $|\log_e \rho|$ is then calculated. The estimated error in the diurnal and noon absorption measurements is about ± 3 per cent. For the frequency variation study, fewer observations are taken in each sample and the estimated error varies from ± 5 to ± 10 per cent depending upon the number of amplitude measurements.

VOL. 22 1961

3. Diurnal Variation of Absorption with Solar Zenith Distance

The daily data of absorption on 5·65 Mc/s taken during the period March 1958 to February 1960 has been first utilized to study the variation of cos χ index.

Plots of $1 + \log_{10}(|\log_e \rho|)$ versus $1 + \log_{10} \cos \chi$ for 88 days during the period mentioned above showed that the points generally fall in a straight line in most of the cases. A mean straight line is drawn in each of the cases and from the slope and intercept the values of the cos χ index and the term A_1 given by the relation

$$A_1 = 8{\cdot}7\,|\log_e \rho|\,.\,f^2\,.\,(\cos^n \chi)^{-1} \quad \text{dB sec}^{-2} \tag{3}$$

are obtained for all the days. The A_1 term thus deduced is expected to be constant if the law relating absorption to cos χ, namely equation (1), were correct

There is a wide day-to-day variation in the value of n, obtained by the authors, in the range 0·8–2·0. But a majority of the values are found to be in the range 1·1–1·6, the average value of n for all the observations being 1·3. The average of n for the summer and winter seasons has also the same value. This constancy in the value of n from season to season is an interesting result which will be discussed in a later Section.

It will be interesting to compare the average value of n with the values reported by some of the earlier investigators. Best and Ratcliffe (1938) obtained a value of 1·5 for n for a set of quiet-day observations. White and Straker (1939) gave a value of 1·76 for n. But the values of the cos χ index reported by Taylor (1948),

Appleton and Piggott (1954), Davies and Hagg (1955), Mitra and Mazumdar (1957), Skinner and Wright (1956) and others vary in the range of 0·5 to unity, the most reported value being about 0·75. The average value of 1·3 obtained by the authors is neither in agreement with the theoretical value of 1·5 nor with the commonly reported value of about 0·75. A comparative study of the divergent results reported by several investigators shows that, in general, n increases with increase in the operating frequency.

We shall now examine the variation of n and A_1 with Zürich relative sunspot number and average planetary K-index (K_p) over the day. The variation of n from day to day observed at this place has a significant negative correlation with the variation of the Zürich relative sunspot number (R) and no correlation with the planetary K-index sum over the day. The correlation coefficient for the co-variation of $n - R$ is $-0{\cdot}17$ which is significant for a probability of 0·1 and, hence, the following relationship between n and R is obtained by using the method of regression coefficients

$$n = 1{\cdot}48(1 - 0{\cdot}00074R). \tag{4}$$

It follows from this relation that for the condition of zero sunspot number, the value of n will be 1·48 which is very nearly in agreement with the theoretical value of 1·5 deduced by Appleton. Thus, it appears from this relation that the absorption on 5·65 Mc/s under sunspot minimum conditions is almost non-deviative at this latitude giving a cos χ index value nearly in agreement with theory.

The correlation coefficient between the co-variations of $A_1 - R$ and $A_1 - K_p$ are positive but not significant. The term A_1 is found to vary widely from a minimum of about 300 dB sec^{-2} to about a maximum of 1900 dB sec^{-2}. Hence, it is suggested that the wide variability in the value of A_1 from day to day which showed practically no correlation with either sunspot or magnetic activity may be due to the variability in the deviative absorption due to the day-to-day variation in the E-region critical frequency.

4. Investigation of Monthly Mean Diurnal Variation Data in the Light of Jaeger's Theory

The wide variability in the value of A_1 has led the authors to seek an alternative interpretation of the 5·65 Mc/s absorption data using Jaeger's expression for total absorption in a Chapman layer which also takes into account the E-region deviative absorption. For this study, the monthly mean values of the hourly absorption data taken during the day-time for about 4 days in each month are obtained. Data for 20 months are thus available for the study. Unfortunately, due to a lack of a h'–f recorder, critical frequency data at this station is not available. The monthly mean E-region critical frequency data available in CRPL Bulletins for various low latitude stations having the same geomagnetic latitude as Waltair has been utilized to obtain the Jaeger function, $F(f_0E/f)$ for different values of (f_0E/f) during all these months.

Fig. 1 presents eight typical plots of $|\log_e \rho|$ versus $F(f_0E/f)$ cos χ for the period March to October 1958. It is interesting to note from this study that a plot of

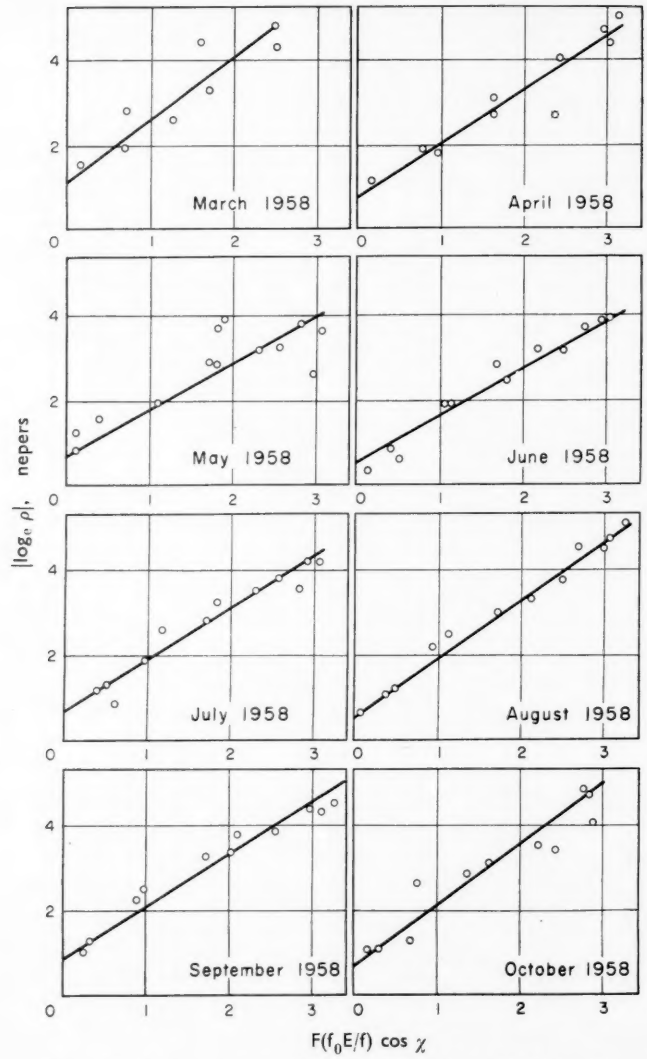

Fig. 1. Variation of monthly mean absorption with Jaeger function.

$|\log_e \rho|$ versus $F(f_0E/f) \cos \chi$ data for each of the 20 months fits closely a linear relation of the type,

$$|\log_e \rho| = A' + B \,.\, F(f_0E/f) \cos \chi \quad \text{nepers} \tag{5}$$

where A' and B are constants which are the intercept and slope of the straight line respectively in each case. The constant A' is expected to refer to the non-deviative absorption in the lower D-region, contribution due to the deviative absorption in the $F2$-layer being neglected as the critical frequency of the $F2$-layer is very much higher than the operating frequency during most part of the daylight hours. This

VOL. 22 1961

assumption is also justified by the work of MITRA and MAZUMDAR (1957) and WHITE and STRAKER (1939) who made a comparative study of the signal strengths of radio waves reflected from E_s and $F2$-layers and arrived at the conclusion that the $F2$-region absorption under these conditions is negligible.

It is interesting to note that there is a wide variation of A' with sunspot number from month to month and that a positive correlation of 0·56 exists between the co-variation of A' and monthly mean Zürich relative sunspot number $\bar{R}$. The correlation coefficient between the co-variations of A' and $\overline{\Sigma K_p}$ is also positive and its value of 0·25 is found to be less than significant for a probability of 0·01. Fig. 2

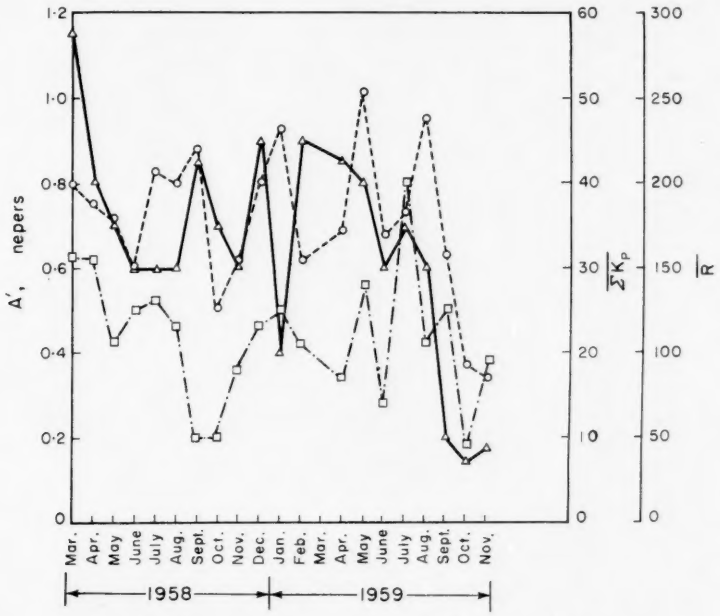

Fig. 2. Monthly variation of $A'(\triangle)$, $\overline{R}(\bigcirc)$ and $\overline{\Sigma K_p}(\square)$.

shows the variation of A', $\bar{R}$ and $\overline{\Sigma K_p}$ from month to month. The dependence of A' on $\bar{R}$ is given by the relation

$$A' = 0{\cdot}05(1 + 0{\cdot}066\ \bar{R}) \quad \text{nepers.} \tag{6}$$

It is evident from this relation that the contribution of absorption due to the lower D-region is insignificant during sunspot minimum period.

From the values of the slope B ($= \nu_0 H/C$), the electron collision frequency in the E-region at the datum level h_0 is determined, assuming a scale height of 10 km. The values thus obtained are found to vary between $2{\cdot}5 \times 10^4$ and $4{\cdot}5 \times 10^4$ c/s, the mean of these observations for the 20 months being $3{\cdot}7 \times 10^4$ c/s. This value which is expected to refer to a height of 105 km in the E-region is in reasonable agreement with the results obtained by previous investigators. A comparative study of the two methods of interpretation of the diurnal variation of absorption on 5·65 Mc/s given in Sections 3 and 4 showed that equation (5) is in better agreement with experimental observations.

5. A Method of Estimating the Relative Contributions of Noon-time D- and E-region Absorption

It is shown in the previous section that the contributions of D- and E-region absorption can be separated by assuming the E-region absorption to be varying as $F(f_0E/f)\cos\chi$. In this Section, a new method is proposed by which it is possible to estimate the ratio of noon-time E- to D-region absorption approximately from the cos χ index data. The diurnal variation data of absorption taken for each month is plotted separately to evaluate the average cos χ index, $\bar{n}$. The monthly

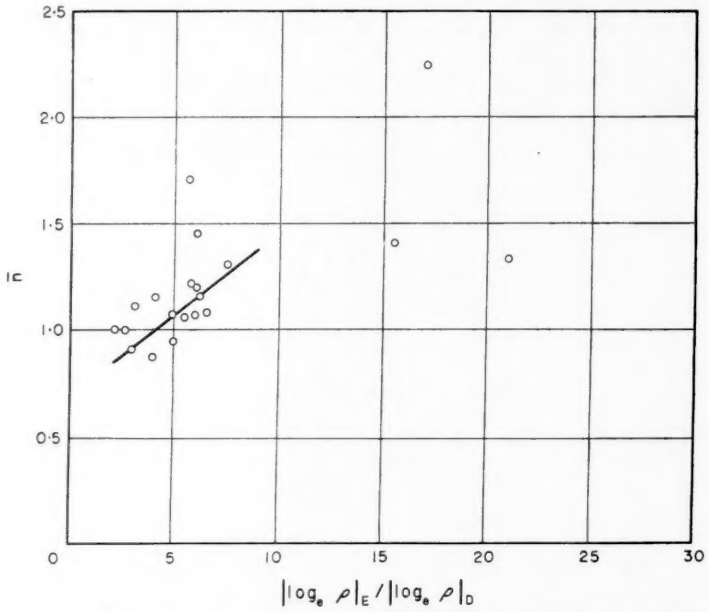

Fig. 3. Variation of the monthly mean cos χ index with the ratio of E- to D-region absorption.

mean values of the ratio of E- to D-region absorption, namely $|\log_e \rho|_E \cdot (|\log_e \rho|_D)^{-1}$ or $B \cdot (A')^{-1} F(f_0E/f)\cos\chi$ are then obtained for each month. These values are plotted with $|\log_e \rho|_E/|\log_e \rho|_D$ as abscissa and $\bar{n}$ as ordinate and shown in Fig. 3. It is clearly seen from the plot of points in Fig. 3 that the cos χ index, $\bar{n}$, increases with increase in the ratio, $|\log_e \rho|_E/|\log_e \rho|_D$. There is also a tendency for these observations to fall in a straight line in a limited range of values. It may be noted that $\bar{n}$ tends to reach values higher than 1·5 as $|\log_e \rho|_E/|\log_e \rho|_D$ increases as a result of considerable deviative absorption in the E-region. For low values of $|\log_e \rho|_E/|\log_e \rho|_D$, $\bar{n}$ should tend to zero, but observations corresponding to very low and very high values of $|\log_e \rho|_E/|\log_e \rho|_D$ are not usual. Thus, in the limited range of 2–8 for the ratio, it is possible to utilize the experimental value of n to have an idea of the ratio of E- to D-region by referring to Fig. 3. It has already been reported in an earlier Section that the average cos χ index n is the same for both summer and winter seasons at this latitude. This constancy in the value of n is

VOL. 22 1961

to be attributed to the increase in the sunspot activity observed during summer months resulting in an increase in the contribution of D-region absorption to such an extent that $|\log_e \rho|_E/|\log_e \rho|_D$ remained the same. In other words, the increase in the absorption due the E-region during summer due to higher values of f_0E is nullified by a corresponding increase in $|\log_e \rho|_D$, thus keeping the ratio constant.

6. Noon Absorption Measurements

Systematic measurements of noon-time absorption were made on a frequency of 5·65 Mc/s from the beginning of March 1958 and are continued up to date. In

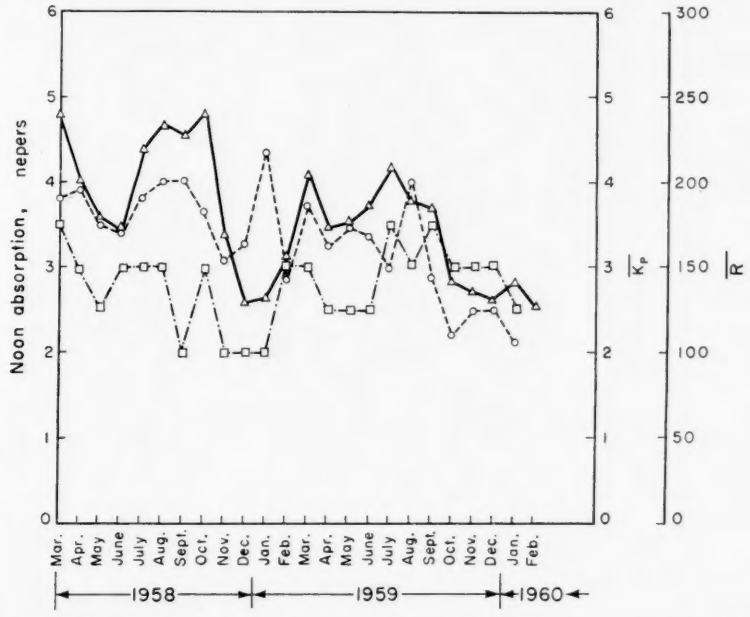

Fig. 4. Monthly variation of noon-time absorption, $\overline{R}$(○) and $\overline{K_p}$(□). △ = $|\log_e \rho|$.

these investigations, the data for the period between March 1958 and February 1960 is subjected to analysis. Data for about 10–20 days in each month is available The monthly mean noon-time absorption values have been computed for all the months.

It will be of interest to study if the variation of noon-time absorption is related to the variation in relative sunspot number. In Fig. 4 is shown a plot of noon-time absorption versus the month along with monthly mean Zürich sunspot number $\bar{R}$ and monthly mean planetary K-index $\bar{K}_p$. The correlation coefficients for the co-variation of noon-time mean $|\log_e \rho|$ with $\bar{R}$ and $\bar{K}_p$ are 0·54 and 0·36 respectively. The variation of noon-time absorption with $\bar{R}$ and $\bar{K}_p$ is represented by the following relations

$$|\log_e \rho| = 1{\cdot}42(1 + 0{\cdot}0092\bar{R})$$
$$\text{and} \qquad |\log_e \rho| = 2{\cdot}10(1 + 0{\cdot}27\bar{K}_p) \qquad (7)$$

It is found that the correlation of $|\log_e \rho|$ versus $\bar{R}$ is quite significant, a feature which also has been reported by Appleton and Piggott for high latitude observations. Davies (1960) has recently examined the absorption data on 2 Mc/s at high latitude stations in relation to the sunspot number and magnetic A_p figure and concluded that there is no well-defined correlation. In the present investigation, it is found that correlation of $|\log_e \rho|$ versus $\bar{K}_p$ is just significant for a probability of 0·1, a result which has not been reported before.

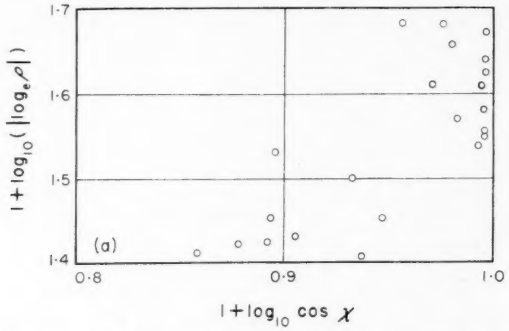

Fig. 5(a). Variation of noon absorption with $\cos \chi$. $n = 2{\cdot}16$.

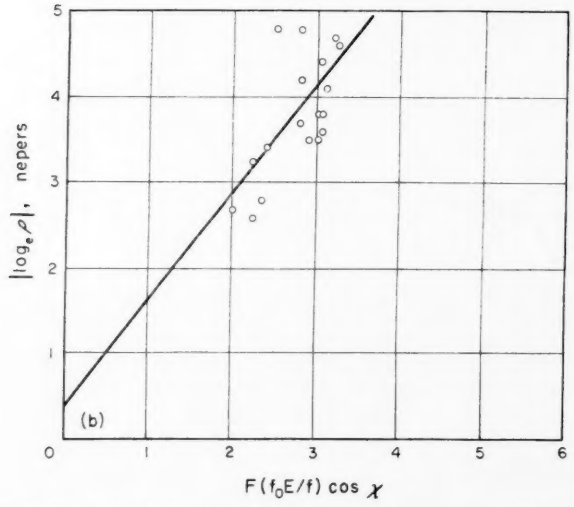

Fig. 5(b). Variation of noon absorption with Jaeger function. $\nu_0 = 3{\cdot}7 \times 10^4$; $A' = 0{\cdot}4$ nepers.

It will be interesting next to examine the variation of noon-time absorption data with solar zenith angle. To see if the absorption data, taken over the entire period, follows the relation (1), values of $1 + \log_{10}(|\log_e \rho|)$ are plotted against $1 + \log_{10} \cos \chi$ and the resultant plot is shown in Fig. 5(a). It will be seen in this plot that the points are widely scattered indicating that the simple relation (1) is no longer valid when data taken over a long interval is examined. $|\log_e \rho|$ values reduced to a common sunspot number of $\bar{R} = 100$ showed no improvement.

VOL. 22 1961

The values of $|\log_e \rho|$ are then plotted against $F(f_0E/f) \cos \chi$ as shown in Fig. 5(b). The points now lie fairly well on a straight line which is drawn using the method of least squares. From the intercept and the slope of this line, the values of A' and B are found to be 0·40 and 1·23 respectively. Here A' represents the average absorption in the lower D-region for the entire period. It will be interesting to compare this value with the value of 1·86 nepers reported by BEYNON and DAVIES (1955) for noon-time average value of A' for a frequency of 2·0 Mc/s. Considering that the non-deviative absorption in the lower D-region varies as $(f + f_L)^{-2}$, the average noon-time non-deviative absorption for 5·65 Mc/s at Waltair should be about 0·6. Hence, it may be concluded that the value of A' obtained by the authors is in reasonable agreement with the value reported by BEYNON and DAVIES.

The average summer to winter noon absorption ratio at this station is about 1·4 while the ratio of average summer to winter values of cos χ is nearly 1·2. Thus, the seasonal variation of noon-time absorption varies as the square of the cos χ index and, hence, the cos χ index for the seasonal variation is 2. SKINNER and WRIGHT also obtained a similar result for the cos χ index with regard to the seasonal variation of noon absorption. Noon-time absorption studies by APPLETON (1937), WHITE and STRAKER (1939) and WHITE and BROWN (1937) also showed departure from APPLETON'S theoretical value of 3/2 for the cos χ index.

The discrepancy in the values of n obtained from the study of seasonal variation of noon absorption and diurnal variation of absorption is due to the fact that the term A_1 in relation (3) varies widely not only from season to season but also from day to day. It is, therefore, not justifiable to deduce the value of n from a comparison of the noon-time absorption data taken in summer and winter.

7. The Variation of Absorption with Frequency

The variation of absorption with the operating frequency has been studied on two occasions. The range of frequencies used in this study are between 4·5 and 9·0 Mc/s, such that deviative absorption due to E- and F-regions is not appreciable at the times of investigation. The time of observations chosen are such that the second hop reflection is also present. The apparent coefficient of reflection (ρ) is given by the expression $\rho = 2F''/F'$ where F' and F'' are the first and second hop reflection amplitudes respectively. According to the non-deviative law, the absorption variation with frequency may be written as

$$8{\cdot}7\ |\log_e \rho| = A_1 \,.\, (f + f_L)^{-2} \,.\, \cos \chi \quad \text{dB}. \tag{8}$$

where the index n can be taken as 1·3, which is the average value of n obtained from data for 20 months as shown in Section 3. In Fig. 6(a) are presented plots of $(|\log_e \rho|)^{-1/2}$ versus the operating frequency f corresponding to the 2 days of observation. The observations for both the cases fit fairly well in the straight lines which pass through the origin showing that $f_L = 0$ and that the propagation of the ordinary ray is very nearly quasi-transverse.

In view of the fact that the diurnal variation of absorption fits more exactly the expression (5) involving the Jaeger function, it will be interesting to study the variation of $|\log_e \rho|$ with frequency by using the relation (5).

Assuming an average value for B obtained from Jaeger plots as shown in Section 4, the values of the term $BF(f_0E/f)\cos\chi$ for each operating frequency are calculated for each month. Subtracting these values from the total absorption $|\log_e \rho|$ gives the values of the lower D-region absorption $|\log_e \rho|_D$ or A' for the corresponding operating frequency f.

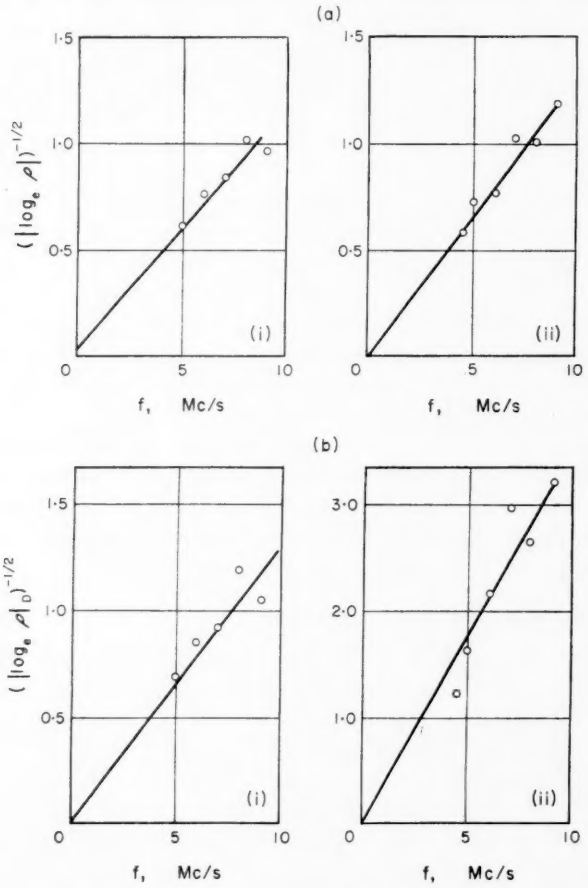

Fig. 6(a). Variation of $(|\log_e \rho|)^{-1/2}$ with f. (i) 0800 hours, 28 December 1958; (ii) 1530 hours, 1 January 1959.

Fig. 6(b). Variation of $(|\log_e \rho|_D)^{-1/2}$ with f. (i) 0800 hours, 28 December 1958; (ii) 1530 hours, 1 January 1959.

The values of $(|\log_e \rho|_D)^{-1/2}$ are then plotted against the frequency f in Mc/s for the two sets of records and the resultant plots are shown in Fig. 6(b). It can be seen that the points fall fairly well on straight lines drawn, showing that $|\log_e \rho|_D$ or A' varies inversely as the square of the operating frequency. Relation (5) can now be written as

$$8{\cdot}7\,|\log_e \rho| = A''/f^2 + 8{\cdot}7B\,.\,F(f_0E/f)\cos\chi \quad \text{dB} \tag{9}$$

VOL. 22 1961

where A'' is another constant. The frequency variation of absorption, thus, obeys both the relation (3) and (5). Since the observations are so timed that deviative absorption due to the E-region is small, the above result can be understood. It can be concluded from this study that the non-deviative absorption varies as the inverse square of the frequency, a result which is in accord with APPLETON's theory. It is interesting to note that the constant part of the non-deviative absorption due to the lower D-region also varies as the inverse square of the operating frequency.

Acknowledgement—The authors wish to acknowledge the financial assistance given by the Council of Scientific and Industrial Research (India), which enabled the present work to be carried out.

REFERENCES

APPLETON E. V.	1937	*Proc. Roy. Soc.* A **162,** 451.
APPLETON E. V. and PIGGOTT J. A.	1954	*J. Atmosph. Terr. Phys.* **5,** 141.
APPLETON E. V. and RATCLIFFE J. A.	1930	*Proc. Roy. Soc.* A **128,** 133.
BEST J. E. and RATCLIFFE J. A.	1938	*Proc. Phys. Soc. Lond.* **50,** 233.
BEYNON W. J. G. and DAVIES K.	1955	*The Physics of the Ionosphere,* Physical Society London.
CHAPMAN S.	1931	*Proc. Phys. Soc. Lond.* **43,** 26.
DAVIES K.	1960	*J. Geophys. Res.* **65,** 2285.
DAVIES K. and HAGG E. L.	1955	*J. Atmosph. Terr. Phys.* **6,** 18.
DELOBEAU F. and SUCHY K.	1956	*J. Atmosph. Terr. Phys.* **9,** 45.
JAEGER J. C.	1947	*Proc. Phys. Soc. Lond.* **59,** 87.
MITRA S. N. and MAZUMDAR S. C.	1957	*J. Atmosph. Terr. Phys.* **10,** 32.
PIGGOTT W. R.	1953	*Proc. Inst. Elect. Engrs* III **100,** 61.
RAO B. R. and RAMANA K. V. V.	1958	*J. Sci. Industr. Res.* **17,** 56
SKINNER N. J. and WRIGHT R. W.	1956	*J. Atmosph. Terr. Phys.* **9,** 103.
TAYLOR E. W.	1948	*J. Res. Nat. Bur. Stand.* **41,** 575.
WHITE F. W. G. and BROWN L. W.	1937	*Nature, Lond.* **140,** 931.
WHITE F. W. G. and STRAKER T. W.	1939	*Proc. Phys. Soc. Lond.* **51,** 865.

Journal of Atmospheric and Terrestrial Physics, 1961, Vol. 22, pp. 12 to 22. Pergamon Press Ltd. Printed in Northern Ireland

Nocturnal and seasonal variations of equatorial spread-*F*

M. S. V. Gopal Rao and B. Ramachandra Rao
Ionospheric Research Laboratories, Andhra University, Waltair

(*Received* 28 *February* 1961)

Abstract—A new classification of spread-*F* echo patterns based on the relative amplitudes of the echoes is described and discussed. The results of nocturnal and seasonal variations in spread-*F* at Waltair are presented and a comparison is made with data of other equatorial stations with particular reference to that of Kodaikanal. Differences in the seasonal behaviour of spread-*F* within a geomagnetic latitude range of 0 to $\pm 7^\circ$ are considered in relation to the equatorial electrojet.

1. Introduction

Studies on the spread-*F* (Sp-*F*) phenomenon have gained importance in recent years, particularly after the discovery of its association with radio star scintillations (Ryle and Hewish, 1950). Several estimates of the percentage occurrences of the phenomenon by the earlier investigators (Reber, 1954, 1956; Kasuaya *et al.*, 1955) indicated the general trend of the diurnal and seasonal variations and the latitude distribution of the occurrence. It has been established that Sp-*F* is fundamentally a night-time phenomenon at equatorial and mid-latitude stations (Wells, 1954).

The high latitude data showed a slow rise, a broad maximum at about 0200 hours L.T. and a fairly rapid fall at about 0500 hours L.T. in the mean diurnal variations and a more frequent occurrence of Sp-*F* during the local winters than in summers in both hemispheres as a regular seasonal feature. Reports on these features from different low latitude stations have not been consistent (Osborne, 1952; Wright *et al.*, 1956). At mid-latitudes, occurrence of Sp-*F* is itself smaller as compared with high or low latitude stations. A closer study of these features at several other low latitude stations is therefore necessary before a better picture of the phenomenon can be obtained.

Recently attempts have been made to express the intensity of the phenomenon in terms of index numbers 0–3 from a personal study of p'-f records (Briggs, 1958) or by making use of symbol *F* as it appears in the regular f_0F2 data bulletins. Although this index range is sufficient for studying the mean variations, it will be noted that the reduction of the indices is largely based on the interpretation of the individual observers and is without quantitative measurements. A more rational and quantitative index system of a wide range from 0–10 has recently been introduced by Gopala Rao *et al.* (1960). This system is found to be convenient in several analyses, the results of which will be published in due course.

This paper is intended to present some initial results, particularly the nocturnal and seasonal features of Sp-*F* as observed at Waltair (17° 43′ N geogr; 7·4°N geomag.) from November 1958 to February 1960, and to compare the results with those of other low latitude stations particularly Kodaikanal (10° 14′N geogr; 0·6°N geomag.).

2. Classification of the Echo Patterns

While making measurements by visual observation on the virtual height range of spreading of 1*F* echo, three different types of echo pattern have been indentified

VOL. 22 1961

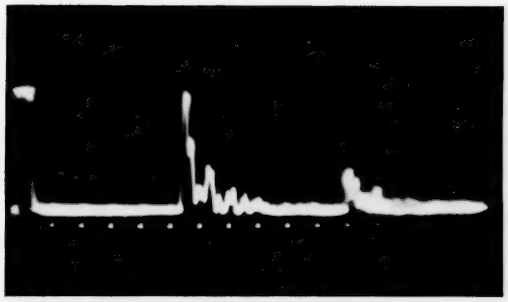

(a)

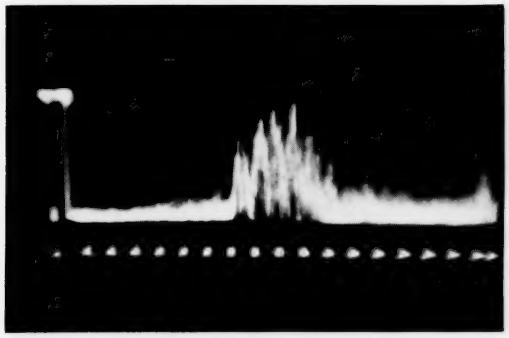

(b)

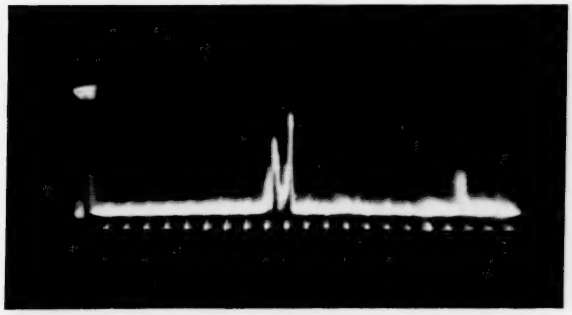

(c)

Fig. 1. Typical photographs of the three types of spread-*F* echo patterns.
(a) Type A; (b) Type B; (c) Type C.

VOL.
22
1961

and classified as "A", "B" and "C" types. If the earliest echo in the patch of echoes is the largest and has a sharp leading edge, such a patch is called type "A". Type "B" echo pattern will have its leading edge diffused and will have the largest echo occurring anywhere in the middle of the patch. In the third type classified as "C", the patch will have a diffused leading edge but the largest echo of the patch will be at the end of the patch with a maximum time delay with respect to the reference ground pulse. A typical set of photographs corresponding to these three echo patterns is shown in Figs. 1(a), (b) and (c).

Suitable conditions for the possible occurrence of these three types of echo pattern by the existing concepts of the irregularity models proposed to explain Sp-F echoes need some consideration. It is generally believed that Sp-F echoes are due to the presence of inhomogeneities in the ionization density ($\pm\Delta N$) with respect to the surrounding uniform ionization. However, the origin, sizes and the spatial distribution of these inhomogeneities are matters for discussion and of importance for any theory. A sandwich type multiple structure embeded in the regular layer, as described by ECKERSLEY (1953), may be giving rise to partial reflections really from different heights. On the other hand, blobs of perturbed ionization of convenient sizes existing in the otherwise regularly stratified ionospheric layer may produce forward- and back-scattering effects. Figs. 2 (a), (b) and (c) show three models of irregularities based on the existing concepts. With model (a) if, in addition to a regularly reflected strong echo from level A, there is partial penetration and occurrence of weak but comparable echoes from B, C and other levels above, then type A echo pattern would result. Type B echo pattern would occur when a strong reflection from level B and weaker reflections from levels like A and C are received. Similarly type C echo pattern may occur when reflections are strong from a level C, without a possibility of further penetration, together with weaker partial reflections from lower levels like B and A. From this it appears that all the three types of echo pattern have equal probability of occurrence, but the experimental facts are different. Further, in this model (a) all the bundle of spread echoes should be received practically vertically and the reflected energy should be distributed in all the echoes of the patch.

A thin scattering screen below the level of regular reflection, model (b) Fig. 2 (RENAU, 1959) will be also capable of explaining the occurrence of the three types of echo pattern. When $|\Delta N|$ is small the usual overhead echo through A in Fig. 2(b) will be strong with a sharp leading edge and will be followed by weaker echoes forward-scattered via points like B and reflected from higher levels. This corresponds to type A pattern. If $|\Delta N|$ is large enough, the overhead echo may now return with reduced amplitude, although still weaker back-scattered echoes from points like B may return earlier than the former, resulting in the type B echo pattern. Finally, if the screen has scattering centres of increasing $|\Delta N|$ to the points off the zenith such as C, then the long delayed echo through C may be stronger than other echoes including the overhead one, which results in the type C pattern. Similarly, even if the blobs of varying $|\Delta N|$ are distributed all over the F-region as shown in Fig. 2(c) the occurrence of all the three types of echo patterns will be possible.

Here at Waltair, under violent conditions of Sp-F, i.e. around the hours of

maximum Sp-*F* index, type B echo pattern occurred mostly on all the frequencies. Under moderate conditions both A and B types occurred at random at different frequencies. The type C pattern occurred very rarely at times of growth and decay process of the phenomenon. This would suggest the requirement of specially rare

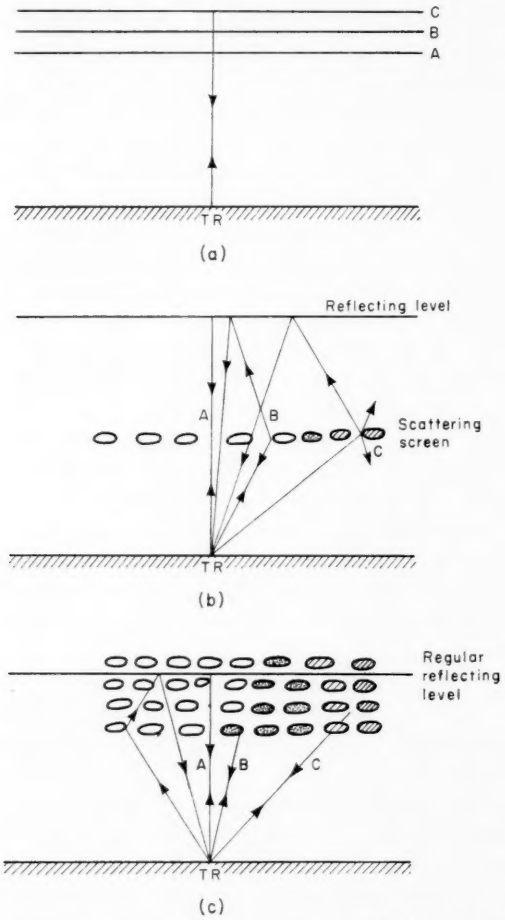

Fig. 2. Some possible models explaining spread echoes. (a) Multiply stratified structure; (b) Scattering screen below the *F*-reflection level; (c) Scattering centres in the entire *F*-region.

conditions for the occurrence of this type C echo pattern and justify the scattering models rather than the multiple structure model.

3. Time Variations of Sp-*F* on Individual Nights

The index system (0–10) adopted here is convenient in following more closely the time variations of Sp-*F* index on individual nights. Some typical variations observed at Waltair are shown in Fig. 3. Individually none of these curves are regular. But a general predominance of the phenomenon in the early half night,

VOL. 22 1961

i.e. up to 0000 hours I.S.T., is clear. The onset of the phenomenon here is generally taking place at some time around 1900 hours I.S.T. and showed normally one to two maxima in the early half night, and another, if any, in the later half night. The first Sp-*F* maximum is generally the largest and occurs at some time between 1900

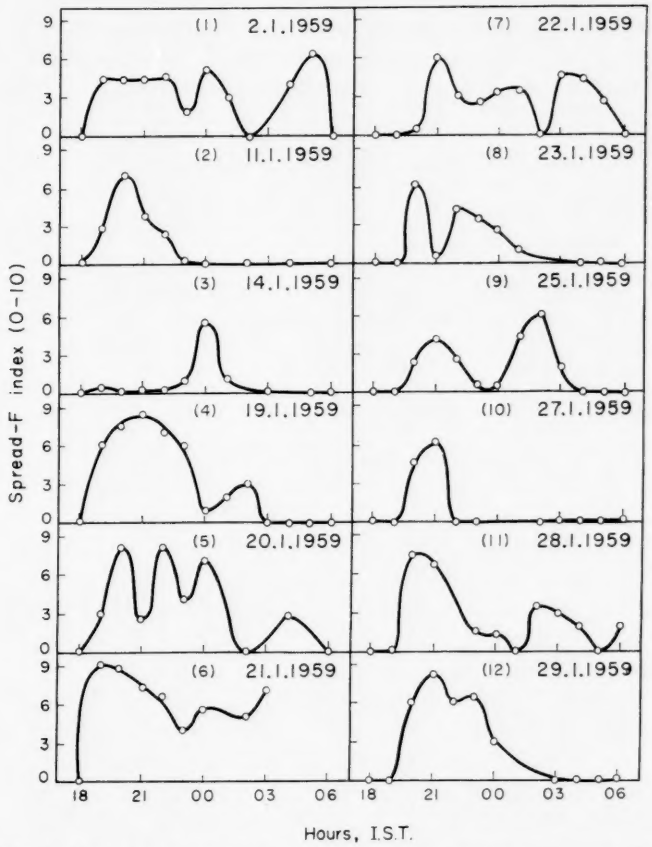

Fig. 3. Variation of spread-*F* on some individual nights of January 1959.

and 2200 hours. This peak is certain to occur earlier on magnetically quiet days and be delayed on disturbed days (curve 3 in Fig. 3). Examination of data of several other days indicated that the curves 11 and 12 of Fig. 3 are the most usual forms of variation and the curves of type 5, showing large magnitude fluctuation in shorter time intervals, have been very rare.

4. Monthly Mean Hourly Variation in Sp-*F* and *h'F*

As it is usual for many ionospheric characteristics to have smooth time variations over a day or a season, Sp-*F*, although considered as a physical irregularity of the ionosphere, also showed its own characteristic time variations on the average. It is commonly observed here that the growth and decay of spreading of the echo into a diffuse patch is a progressive phenomenon and generally varies slowly from

one hour to the next without sudden appearances and disappearances. So it is presumed that the hourly observations carried out on individual nights are representative of the general trend of variations of the intensity of Sp-*F*. Sp-*F* index at each hour is obtained as an average of the same on ten to twelve spot frequencies covering the total frequency range in which echoes are observable. These hourly indices are arranged as in Table 1 which forms the monthly data sheets; the basic material for any type of analysis. The hours between 1800 and 0600 hours correspond to two dates, so the readings are tabulated between the two relevant dates.

Table 1

Date (February 1959)	Hours I.S.T.													Night average index
	18	19	20	21	22	23	00	01	02	03	04	05	06	
1	0	0	1·8	7·2	0·5	2·2	2·6	0	0	0	0	0	0	1·1
2	0	2·6	5·8	1·3	0	0	0	0	–	0	0	0	0	0·8
3	0	0	0	0	0	0	0	–	0	1·0	0	0·2	0	0·1
4	0	0	0	0	0	0	0·3	0	0	–	0	0	0	0
5	0	0	0·6	7·9	2·9	3·4	0·7	–	3·1	5·4	–	0	0	2·2
6														

Each of the vertical columns in a month when averaged yields the monthly mean hourly values. The average of each row gives the nightly average Sp-*F* index given in the last column of Table 1.

The monthly mean hourly variations of Sp-*F* index for different months as obtained at Waltair are shown in Fig. 4. This figure also shows the monthly mean hourly variations of $h'F$ from January 1959. During the four months November 1958 to February 1959, observations were made throughout the night. But from March 1959 routine observations were made only up to 0000 hours (midnight), firstly because of the predominance of the phenomenon in the early part of the night and secondly because the method involved required manual operation and visual observations.

The main features of these curves may be summarized as follows. The variations of Sp-*F* and $h'F$ for all the months are in general similar but for a time difference in the occurrence of the peak values. In the equinoxial months Sp-*F* increased rapidly to a maximum value at 2000 hours I.S.T. and the fall in the later hours is only gradual. In other months the rise was comparatively slower and the peak is less sharp, occurring at around 2100–2200 hours I.S.T. The nature of variation and the magnitude of the peak values show gradual but readily observable changes from one month to the next. The times of maxima of $h'F$ curves and Sp-*F* curves, differed in different months as also the time delay between these maxima. The largest rise in $h'F$ takes place between 1800 and 1900 hours I.S.T. in all months except during summer solstice months when it is delayed. This could have been

VOL. 22 1961

caused by the late sunset during summer. However, the earlier sunset in winter did not effectively shift this largest rise in $h'F$ to earlier hours as may be expected. This has been carefully verified during December 1959 and January 1960 by starting observations from earlier hours. If the Sp-F phenomenon is to be connected with

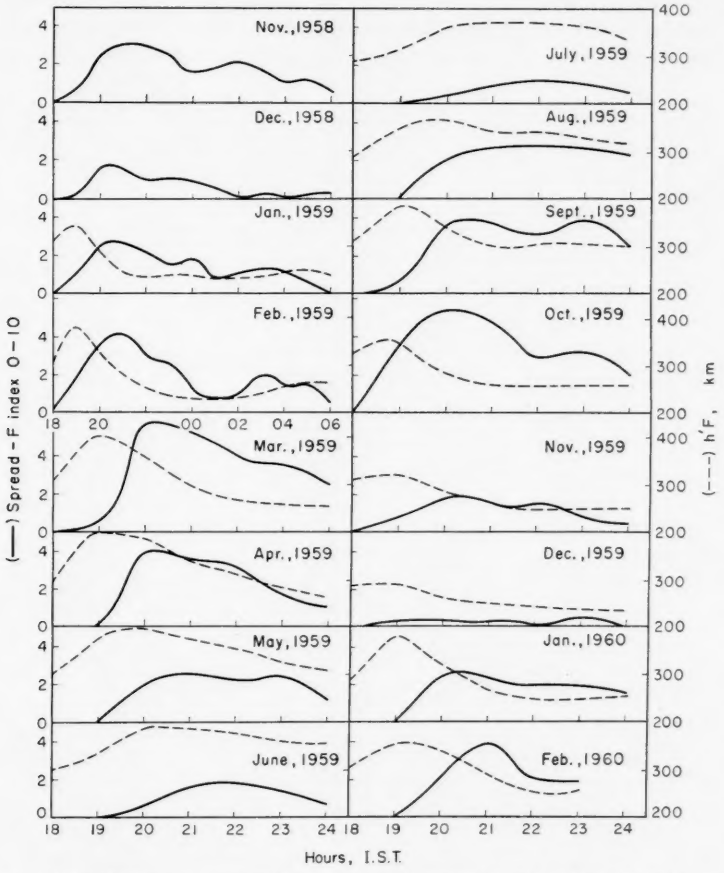

Fig. 4. Monthly mean nocturnal variations of spread-F and $h'F$ at Waltair.

the changes in $h'F$, the time delay of the Sp-F peak value with respect to the $h'F$ peak value must be considered. This aspect in relation to the recent preliminary theory of Sp-F suggested by MARTYN (1959) will be discussed in detail in a later communication.

The monthly mean nocturnal variation of Sp-F and $h'F$ at Kodaikanal for the year 1956 are shown in Fig. 5. In this case the index system in the range 0–3 after BRIGGS (1958) is adopted utilizing the regular ionospheric f_0F2 data bulletins. The variation at this station shows in general the same main features as at Waltair, although changes from one month to the next are less striking, partly because the index system adopted is less rigorous, as is also pointed out by BRIGGS. The curves, while indicating the predominance of the phenomenon during the early half night

in many months, show that the importance of Sp-*F* in the later half night increased during solsticial months. It may be noted that Wells (1954) also described a nearly similar situation at Huancayo.

5. Seasonal Variations in Sp-*F*

At Waltair, maxima during equinoxes and minima during solstices are obvious even in the nocturnal variation curves. However, in order to bring all the seasonal

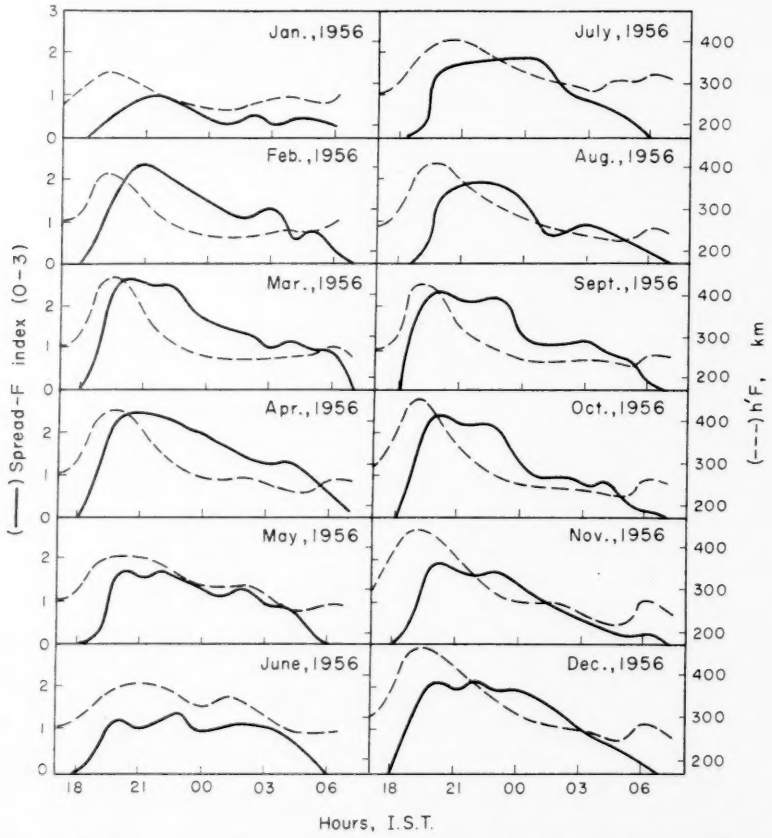

Fig. 5. Monthly mean nocturnal variations of spread-*F* and *h'F* at Kodaikanal.

features into a single curve, the monthly Sp-*F* index obtained as an average of the monthly mean hourly values is plotted for each month and shown in Fig. 6. The percentage occurrence of Sp-*F*, irrespective of the index, in the total number of hours observed in each month is also shown in the same figure. Similar plots for Kodaikanal for the years 1956–1957 and for some months of 1958 are shown in Fig. 7.

At each station there is, in general, very good similarity in the variation curves of percentage occurrence and the monthly mean Sp-*F* index in spite of the rigorous indexing system applied to Waltair data. This result is significant because it is

VOL. 22 1961

possible that the phenomenon may occur on several occasions with reduced intensity or vice versa. Thus, these curves need not be expected to be similar. The result suggests that the month of greater frequency of occurrence is also generally associated with greater intensity of Sp-*F* activity. There are, however, certain differences in these curves when examined in detail. For Waltair the autumnal equinox maxima in the two curves are displaced by 1 month. In September 1959, the

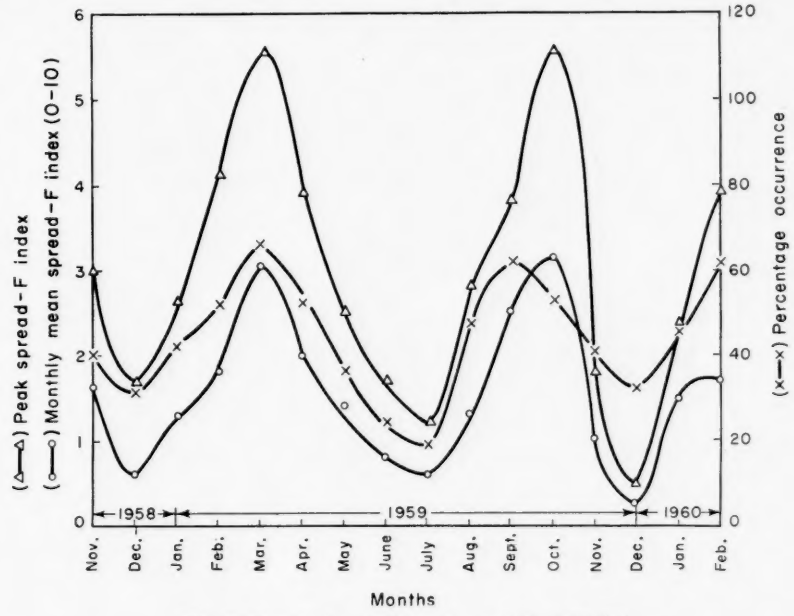

Fig. 6. Seasonal variation of spread-*F* at Waltair.

percentage occurrence was at maximum whereas the Sp-*F* index reached its maximum in October 1959.

The Kodaikanal data shows a tendency for equinoxial maxima only. There is also a tendency for minor maxima during solstice months. But it will be noted that the variations during 1957–1958 are more irregular than during 1956 when the tendency for equinoxial maxima is also greater.

In Fig. 6, a third curve is drawn showing the seasonal variation of the peak Sp-*F* index obtained from the monthly mean nocturnal curves of Fig. 4. It will be seen that the seasonal Sp-*F* characteristics at Waltair could be distinctly preserved even by this plot, which shows that it is sufficient, if routine measurements are made during a few hours around the maximum occurrence hour, to bring about the seasonal characteristics for any equatorial station.

6. Discussion of the Results

The variations in the intensity of the phenomenon on individual nights may be associated with three possible factors as follows:

(a) The growth and decay process of the irregularities at the same location;

(b) Displacement with time of contours of equal Sp-*F* index within a relatively stationary and extensive horizontal patch of irregularities;

(c) Movements of the wide patch of irregularities as a whole with varying contours of equal Sp-*F* index past a fixed observing station.

Any one or all of these factors may cause temporal variations in the phenomenon as observed at a single location.

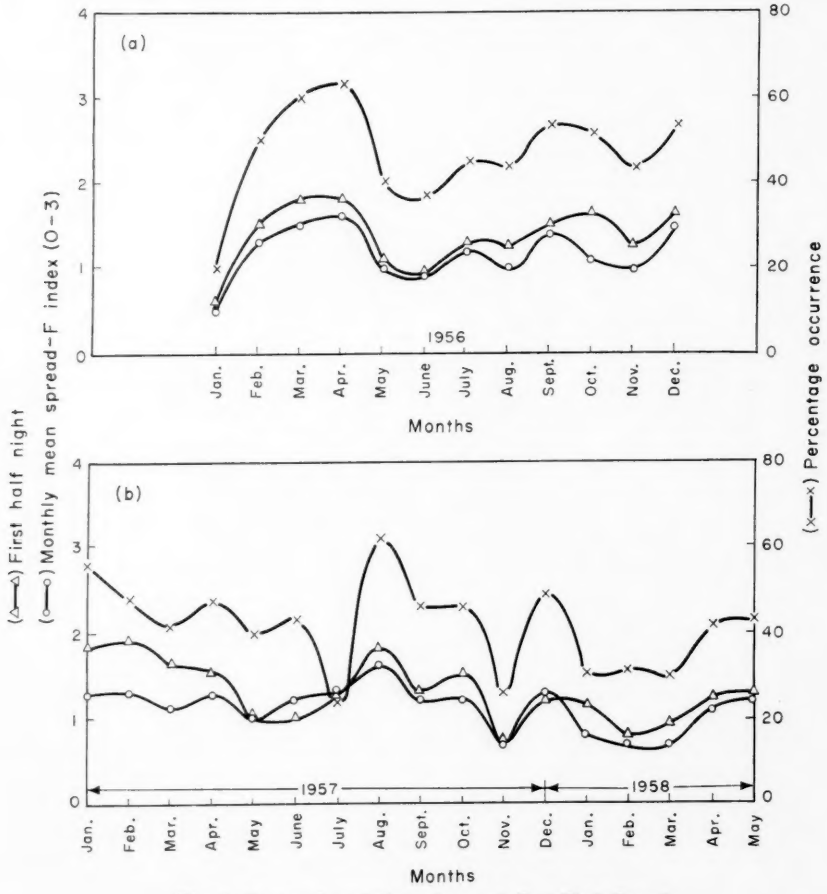

Fig. 7. Seasonal variation of spread-*F* at Kodaikanal.

The peculiar curves of the type 5 in Fig. 3 showing short time large magnitude changes which are very rare could have been caused by factors (b) and (c) rather than by (a), while the initial quick rise and the gradual fall in the later period observed in the usual curves such as 11 and 12 may be involved with the actual production and decay of the irregularities.

The nocturnal monthly mean variations of Sp-*F* at Waltair are only in broad agreement with other equatorial data but in good agreement with Singapore data reported by Osborne (1952). From Kodaikanal data averaged over the total year

VOL. 22 1961

1956, BHARGAVA (1958) showed that the percentage occurrence of Sp-*F* has a maximum at 2000 hours I.S.T. The monthly mean Sp-*F* index variation of Kodaikanal data as plotted here using the 0–3 index system shows some changes in the nature of variation when considered separately for different months. The rapid rise to a maximum at 2000 hours in the equinoxial months is similar to that observed at Waltair as also the slower rise and broadened peaks for other, especially solsticial, months. The reports from Ibadan (WRIGHT *et al.*, 1956) and Huancayo (REBER, 1956; WELLS, 1954) indicate that the main maximum in the nocturnal variation occurs at around midnight and seasonal features showed a greater percentage occurrence during local summers with only a tendency for equinoxial maxima, as at Kodaikanal also.

The seasonal variations at Kodaikanal are irregular and not as clear as at Waltair or Singapore. These irregularities need some discussion. It may be argued that the lack of second half night data for Waltair is responsible for the observed clear-cut seasonal variations. To examine this possibility, a seasonal plot is drawn (line connected by triangles, Fig. 7) for Kodaikanal, neglecting the later half (0000–0006 hours I.S.T.) night data, which follows very closely the curve in which full night data is considered. So the difference in the seasonal Sp-*F* variations between Waltair and Kodaikanal needs some explanation.

It is becoming well known that equatorial Sp-*F* activity is correlated negatively with magnetic activity and positively with *F*-region height changes, although the mechanisms of these influences are not completely clear. Being very close to the geomagnetic equator and well under the electrojet zone as compared with Waltair or Singapore, it appears that the irregular and unclear seasonal variations at Kodaikanal are to be regarded as distortions, caused by the above influences, from the otherwise smooth seasonal trend. Further it will be noted that these distortions are greater in the years 1957–1958 than during 1956 probably because of an enormous increase in the average sunspot number from 120 for 1956 to about 200 for the period considered in 1957–1958. The enhanced sunspot activity may also enhance the distorting influences. It is likely that these distortions in the seasonal Sp-*F* behaviour are confined to a narrow zone, within the equatorial electrojet. This also is probably the reason for the uncertainity in the seasonal Sp-*F* behaviour at Ibadan and Huancayo.

From the foregoing study it is clear that Sp-*F* seasonal behaviour has differences even within a geomagnetic latitude range of 0 to $\pm 7°$, and supplementation of data from more equatorial stations on these lines would further improve the picture.

Acknowledgements—The authors acknowledge with thanks the financial assistance of the Council of Scientific and Industrial Research. One of us (M. S. V. G.) is indebted to the above council for the award of a Senior Research Fellowship.

REFERENCES

BHARGAVA B. N.	1958	*Ind. J. Met. Geophys.* **9,** 1, 35.
BRIGGS B. H.	1958	*J. Atmosph. Terr. Phys.* **12,** 34.
ECKERSLEY T. L.	1953	*Proc. Phys. Soc. Lond.* B **66,** 1025.
GOPALA RAO M. S. V., RAO B. R. and PANT P. R. R.	1960	*J. Atmosph. Terr. Phys.* **17,** 345.

Kasuya I., Katano S. and Taguchi S.	1955	*J. Radio Res. Lab. Japan* **2,** 329.
Martyn D. F.	1959	*Proc. I. R. E.* **47,** 153.
Osborne B. W.	1952	*J. Atmosph. Terr. Phys.* **2,** 66.
Reber G.	1954	*J. Geophys. Res.* **59,** 257, 445.
Reber G.	1956	*J. Geophys. Res.* **61,** 157.
Renau J.	1959	*J. Geophys. Res.* **64,** 971.
Ryle M. and Hewish A.	1950	*Mon. Not. R. Astr. Soc.* **110,** 381.
Wells H. W.	1954	*J. Geophys. Res.* **59,** 273.
Wright R. W., Koster J. R. and Skinner N. J.	1956	*J. Atmosph. Terr. Phys.* **8,** 240.

VOL.
22
1961

Journal of Atmospheric and Terrestrial Physics, Vol. 22, pp. 23 to 31. Pergamon Press Ltd. Printed in Northern Ireland

The effect of light on the mobility and concentration of large ions in air mixed with N_2O gas

A. F. El Nadi* and N. Farag†
*Assiout University, Faculty of Science, Assiout, and
†Cairo University, Faculty of Science, Giza, Egypt, U.A.R.

(*Received* 13 *March* 1961)

Abstract—Investigating the action of light of a tungsten filament lamp on a mixture of air and N_2O gas, the following effects have been observed:

(1) The disappearance of some large ion groups which appear clearly when the mixture is kept in the dark;

(2) A decrease in the concentration of ions with mobilities $>$ about $0{\cdot}70 \times 10^{-4}$ and an increase in the concentration of ions with mobilities $<$ about $0{\cdot}70 \times 10^{-4}$;

(3) A decrease in the total ion concentration of the ions with mobilities ranging from $12{\cdot}5 \times 10^{-4}$ to $0{\cdot}60 \times 10^{-4}$ cm/sec : V/cm.

Both the divided electrode condenser method and the whole electrode condenser method were used in this investigation.

Introduction

The action of light on some gases was studied by Aitken (1912). He found that SO_2 gas remained free from nuclei if it was kept in the dark. If it was exposed to light, especially sunshine, then a change was effected which converted SO_2 into an active nucleus-producer.

Pealing (1915) found that when light fell on a mixture of moist air or oxygen and iodine vapour contained in a freshly cleaned glass vessel, nuclei were produced. The light required for their production need not be very intense. They usually reach their maximum size in less than 1 sec.

The influence of visible light on the mobility spectrum of large atmospheric ions was studied at Giza by Ortner and El Nadi (1955). They found that there is an increase in the ion concentration for ions with mobilities greater than about $2{\cdot}0 \times 10^{-4}$ both in daylight and in the case of light from a tungsten filament lamp. On the other hand, ions with mobilities less than $2{\cdot}0 \times 10^{-4}$ show a decrease in the ion concentration.

Verzár and Kunz (1957) showed that in a closed air mass which has a very low nucleus count, direct sunlight produces, in a few minutes, large numbers of atmospheric condensation nuclei.

In a discussion about the influence of sunlight on atmospheric condensation nuclei (Verzár, 1959), Dr. Mason suggested that the increase in the nuclei produced by sunlight resulted from the presence of trace gases. Prof. Verzár agreed that the condensation nuclei which are produced by sun rays must come from air contaminations which are present in extreme dilutions in the free atmosphere.

The present work shows the effect of light, from a 500 W tungsten filament lamp, on the mobility and concentration of large ions in a mixture of atmospheric air and N_2O gas.

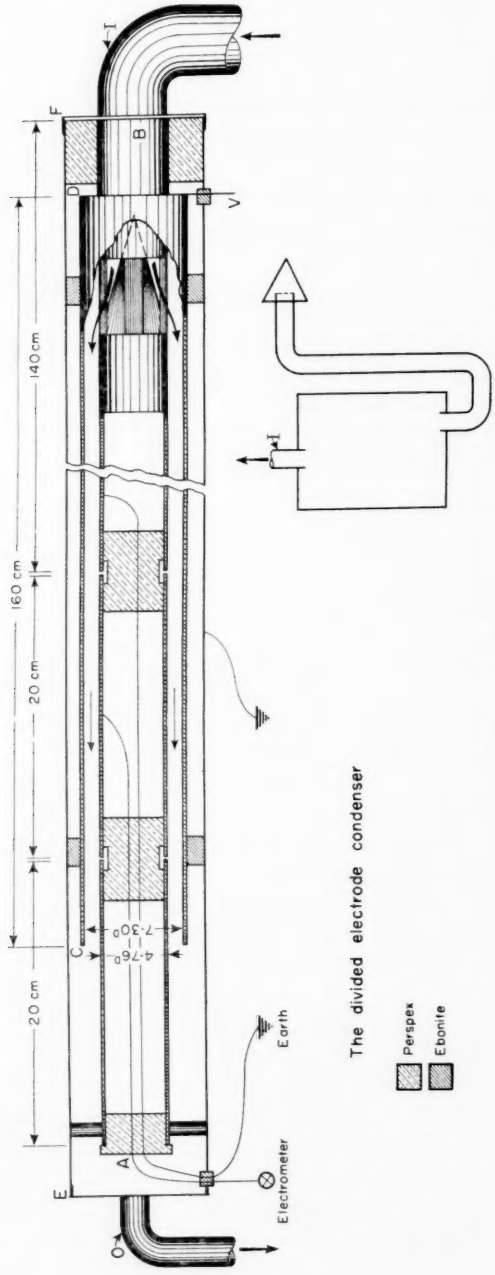

Fig. 1. Large ion counter.

VOL. 22 1961

Apparatus and Procedure

The apparatus used consisted of a cylindrical condenser composed of two concentric brass tubings (Fig. 1). The inner electrode of 4·76 cm external diameter was divided into three sections insulated from each other and fixed firmly together by Perspex cylinders. The lengths of the sections were 140, 20 and 20 cm in the direction of the air flow. The outer electrode (160 cm in length and 7·30 cm internal diameter) was connected to a variable voltage supplied by means of dry batteries placed inside a shielded box. The cylindrical condenser was well shielded by a third galvanized iron tube of 10·5 cm in diameter.

The mixture of air and N_2O gas was drawn from a rectangular wooden box of 240 l. volume, through a short tube of galvanized iron of 5 cm internal diameter, into the cylindrical condenser. The box has one of its sides (100 × 60 cm) made of glass 4 mm thick. This side was either covered by thick black paper to keep the box dark or subjected to light from a tungsten filament lamp of 500 W in a projector, with glass lenses, placed at a distance of 80 cm from the box.

Two methods were applied in this study:

(1) The divided electrode method, due to Zeleny, in which the first and third sections of the inner electrode were grounded and the second section was connected to an electrometer of the Compton type adjusted at a sensitivity of about 1800 mm/V. This was used to study the ion groups and their mobilities;

(2) The non-divided or the whole electrode method, due to McClelland, in which the first and the second sections were connected to the electrometer while the third section was grounded. This was used to study the ion concentration.

In the divided electrode method a steady flow of air containing small amounts of N_2O gas was allowed to pass through the apparatus. The potential applied to the outer electrode was varied and the current flowing to the inner electrode was measured by recording the time (t) taken by a light spot, reflected from the electrometer mirror, to move 10 mm on the scale. (The light spot was timed over 20 mm divisions and t was taken as a mean value for 10 mm divisions; the time was measured very accurately up to 0·1 of a second by using a "Venner" stop watch.) Then a curve was drawn to show the relation between $1/k$ and f, where k is the mobility of the ions and f is the corrected value of $1/t$. This curve was obtained while the mixture was kept in the dark. The mixture was then subjected to light and another complete curve was obtained.

In the whole electrode method three subsequent curves were obtained in a short time. The first curve was obtained by a flow of atmospheric air alone. The second, by a flow of a mixture of atmospheric air and N_2O gas while it was kept in the dark. The third, by the same flow of the mixture while it was subjected to light from the projector. These curves were drawn to show the relation between $1/k$ and N, where k is the mobility of ions and N is the number of ions/cm^3 (i.e. the ion concentration).

As the ion concentration (N) does not remain constant throughout the series of observations, the current was measured with a standard potential at short intervals, then every reading was corrected relative to the mean of these readings if they are within a reasonable order, otherwise the whole series was repeated.

This work has been carried out in a dark room (9 m from the ground level) in the Physics Department, Faculty of Science, Cairo University at Giza, Egypt.

Preparation of N_2O Gas

A mixture of recrystallized ammonium nitrate and pure sand in equal proportions by weight was placed in a Pyrex flask provided with a glass stopper and an outlet tube connected through a hole at the top of the suction box. The mixture was then gently heated to ensure a regular current of the gas. The gas was dried by passing it over silica jel.

$$NH_4NO_3 = N_2O + 2\,H_2O.$$

Mode of Calculation

The mobility of the ions was obtained from the formula derived by Hogg (1939):

$$k = \Phi/4\pi V\,(C_1 + C_2)$$

where Φ is the volume of air passing per second, V is the applied potential, C_1 is the capacity of the first section and C_2 that of the second section.

The ratio $(C_1 + C_2)/C_1 = (135 + 20)/135 = 1{\cdot}148$, which is less than the ratio k/k', corresponding to two adjacent ion groups, in order to assure a high resolving power.

In the case of the divided electrode method, the concentration of the ions was obtained from the formula:

$$N = \left[\frac{10}{300S} \times \frac{(C_2 + C_3)/C_2}{e\Phi} \times (C_1 + C_2)\right] \times f$$

where S is the sensitivity of the electrometer in mm/V,

f is the corrected value of $1/t$, where t is the time in seconds taken by the light spot to move 10 mm divisions,

e is the electronic charge, and

C_3 is the capacity of the electrometer and its connexions.

In the case of the whole electrode method, the concentration of the ions was obtained from the simple formula:

$$N = \frac{(C_1 + C_2 + C_3)}{300e\Phi} \times \frac{10}{S} \times f.$$

Results

1. *The divided electrode method*

In examining the characteristics obtained with the divided electrode condenser, two main points are considered: (1) The appearance of peaks corresponding to ion groups of different mobilities; (2) The ion concentration of each group which is proportional to the height of the corresponding peak over the extension to the origin of the ascending part of the next peak.

Figs. 2 and 3 are two examples, for negative and positive ions, of these characteristics.

Fig. 2 was obtained by a steady flow of a mixture of air and N_2O gas. Curve I was obtained while the mixture was kept in the dark and curve II while it was subjected to the light from the projector. Nine peaks appear clearly in the curve I representing nine groups of ions while in the curve II only seven peaks appear representing seven groups. The mobilities and ion concentration of these groups are given in Table 1.

VOL. 22 1961

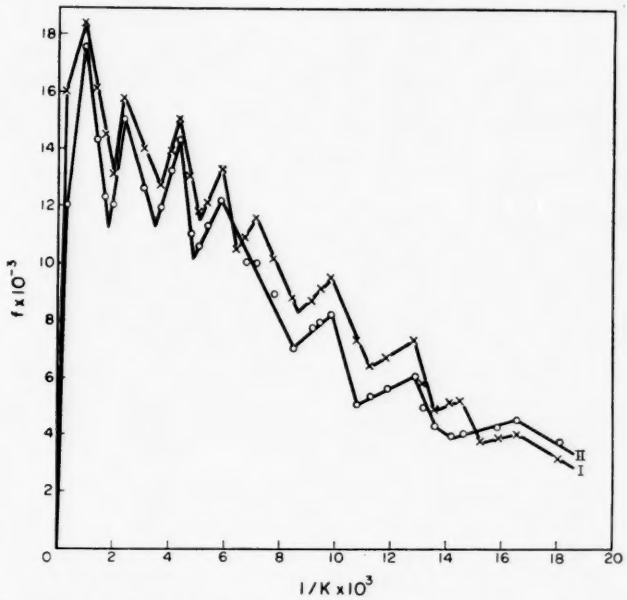

Fig. 2. Characteristics obtained by the divided electrode condenser of negative large ions. I: By a flow of a mixture of air and N_2O gas while kept in the dark. II: By a flow of a mixture of air and N_2O gas while exposed to light from a 500 W lamp.

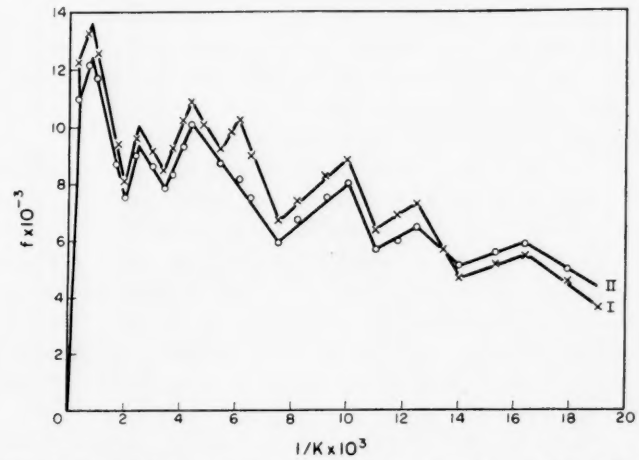

Fig. 3. Characteristics obtained by the divided electrode condenser of positive large ions. I: By a flow of a mixture of air and N_2O gas while kept in the dark. II: By a flow of a mixture of air and N_2O gas while exposed to light from a 500 W lamp.

The groups $1{\cdot}39 \times 10^{-4}$ and $0{\cdot}68 \times 10^{-4}$ disappear when the mixture is exposed to light. The two curves intersect at a point corresponding to a mobility $k = 0{\cdot}66 \times 10^{-4}$; this shows that in the presence of light, the concentration of ions with a mobility $> 0{\cdot}66 \times 10^{-4}$ decreases, while it increases for those with a mobility $< 0{\cdot}66 \times 10^{-4}$. The total ion concentration when the mixture is kept in the dark is 3420 and when subjected to light 3070 which is less by 350, i.e. by 10·2 per cent of the ions present in the dark.

The results obtained when using the divided electrode method show that when a

Table 1.

Curve I. Dark box			Curve II. Illuminated box		
$1/k$	$k \times 10^{-4}$	N/cm^3	$1/k$	$k \times 10^{-4}$	N/cm^3
1000	10·00	950	1000	10·00	900
2400	4·17	600	2400	4·17	570
4400	2·27	420	4400	2·27	410
5900	1·70	300	5900	1·70	580
7200	1·39	380			
9900	1·01	310	9900	1·01	290
12,900	0·78	220	12,900	0·78	200
(?) 14,700	0·68	140			
16,600	0·60	100	16,600	0·60	120
		3420			3070

mixture of air and N_2O gas is kept in the dark, eight ion groups could be detected. When the mixture is exposed to light, from a tungsten filament lamp, some of these groups disappear. Also, some groups show a decrease in their ion concentration while others show a corresponding increase.

Some of the results obtained in this case are collected in Table 2.

The results obtained in a previous work (El Nadi and Farag, 1961) showed that, when mixing small amounts of N_2O gas with air, eight large ion groups could be detected. The mobilities of these groups are: (10·43, 3·77, 2·32, 1·64, 1·35, 1·00, 0·78 and 0·60) $\times 10^{-4}$ for positive ions and (10·99, 3·89, 2·36, 1·66, 1·31, 1·01, 0·79 and 0·60) $\times 10^{-4}$ for negative ions. While in the case of atmospheric air alone four groups only could be detected namely: (6·93, 2·36, 1·00 and 0·60) $\times 10^{-4}$ cm/sec: V/cm. The results showed also an increase in the total ion concentration of large ions with a mobility ranging from $12{\cdot}50 \times 10^{-4}$ to $0{\cdot}60 \times 10^{-4}$ when small amounts of N_2O gas were mixed with air.

2. *The whole electrode method*

As an example of the characteristics obtained in this case, Fig. 4 was chosen for positive ions and Fig. 5 for negative ions.

Three curves were obtained in Fig. 4; curve A by a flow of air alone, curve B by a flow of air mixed with N_2O gas while the mixture is kept in the dark, and curve C by the same flow of the mixture while it was exposed to light. In the curve A four bends

VOL. 22 1961

The effect of light on the mobility and concentration of large ions in air mixed with N_2O gas

Table 2

Date 1959		Number of ions/cm³ in each group								
		N_1	N_2	N_3	N_4	N_5	N_6	N_7	N_8 (?)	N_9
29/6	Dark	990	380	240	300	310	250	200	280	190
	Light	930	310	220	270	310	230	300		210
30/6	Dark	950	600	420	300	380	310	220	140	100
	Light	900	570	410	580		290	200		120
1/7	Dark	760	410	350	250	290	250	190	200	110
	Light	740	370	330	450		240	230		140
13/7	Dark	590	370	230	190	180	180	140	130	90
	Light	570	310	210	170	150	170	180		100
15/7	Dark	1090	370	410	240	260	240	230	210	170
	Light	1030	360	370	230	230	210	330		180
4/8	Dark	820	310	280	390		250	250		180
	Light	760	290	520			220	160		190
6/8	Dark	600	330	230	290		190	140		140
	Light	550	290	210	260		170	80		150
6/8	Dark	1150		440	300	270	230	370		240
	Light	1090		590		250	210	290		250

Group 8 is not certain.

The ion concentrations of group 9 are approximate values as the groups of lower mobilities could not be detected.

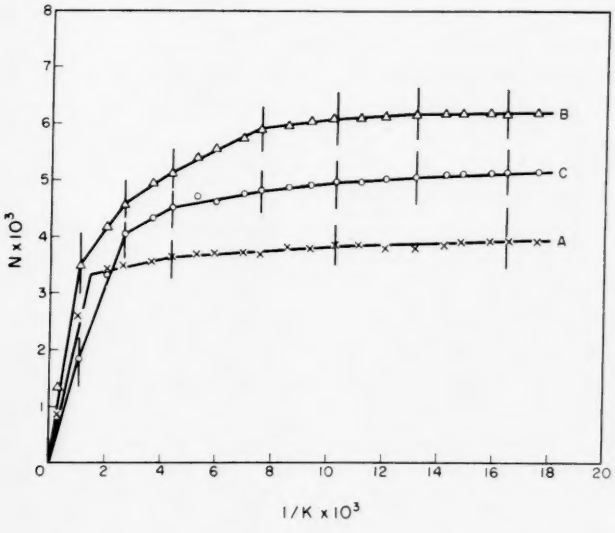

Fig. 4. Characteristics obtained by the whole electrode condenser of positive large ions. A: By a flow of air. B: By a flow of a mixture of air and N_2O gas while kept in the dark. C: By a flow of a mixture of air and N_2O gas while exposed to light from a 500 W lamp.

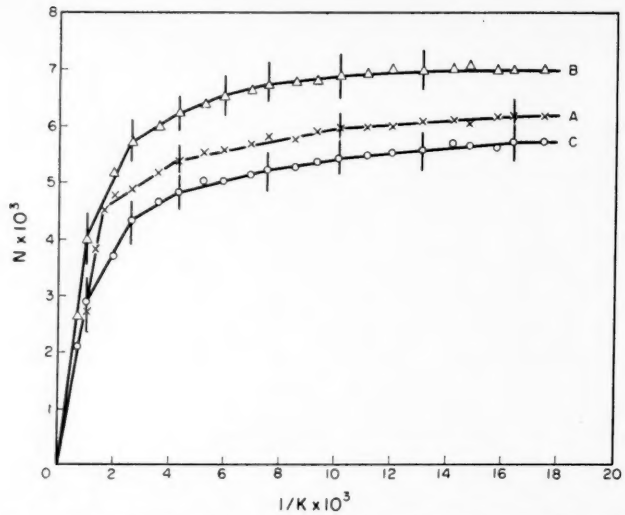

Fig. 5. Characteristics obtained by the whole electrode condenser of negative large ions.
A: By a flow of air. B: By a flow of a mixture of air and N_2O gas while kept in the dark.
C: By a flow of a mixture of air and N_2O gas while exposed to light from a 500 W lamp.

appear corresponding to four ion groups. In the curves B and C seven bends appear in each curve representing seven ion groups in each one. The total ion concentration in air alone is 3950 and in the mixture of air and N_2O gas is 6200 when the mixture is kept in the dark and 5150 when it is subjected to light. This shows that, when mixing N_2O gas with air, the total ion concentration is increased and when subjected the mixture to light the total ion concentration is decreased.

The results obtained with the whole electrode condenser confirm those obtained with the divided electrode condenser. In Tables 3 and 4 a summary is given of the results obtained with the whole electrode condenser for both positive and negative ions.

Discussion of the Results

Using the divided electrode condenser to study the action of light, of a 500 W tungsten filament lamp, on a mixture of atmospheric air and N_2O gas, the results obtained show the following behaviour:

(a) Some groups, appearing clearly when the mixture is kept in the dark, disappear in some curves when the mixture is exposed to light.

This may indicate that, in air, many unstable ion groups are present for some time until they are influenced by some factor, e.g. sunlight, especially during fair weather, and transformed gradually to more stable groups.

(b) When the mixture is exposed to light, some groups show a decrease in their ion concentration while others show a corresponding increase. Nearly in all the curves obtained in this work, the ions with a mobility $>$ about $0{\cdot}70 \times 10^{-4}$ show a decrease in their concentration while those with a mobility $<$ about $0{\cdot}70 \times 10^{-4}$ show a corresponding increase.

An explanation of this behaviour, is that it may be due to a photo-effect. This photo-effect may assist the coagulation of ions and nuclei, thus increasing their size

VOL. 22 1961

Table 3. Positive ions

Date 1959	Temp. (°C)	R.H. (%)	% of N_2O	Ion concentration		Percentage decrease
				Dark box	Illuminated box	
5/10	28·0	42	1·62	7750	6950	8·0
15/10	30·0	33	1·08	6600	5450	17·4
27/10	23·2	32	0·86	6800	6000	11·8
2/11	28·8	24	1·08	5500	4800	12·7
3/11	30·0	20	2·16	7900	6700	15·2
9/11	26·5	51	2·58	6200	5150	17·0
10/11	27·8	28	2·16	6000	5000	16·7

Table 4. Negative ions

Date 1959	Temp. (°C)	R.H. (%)	% of N_2O	Ion concentration		Percentage decrease
				Dark box	Illuminated box	
12/10	28·0	39	1·29	3950	3250	17·7
13/10	28·0	31	0·86	8000	6800	15·0
2/11	27·5	43	2·16	10,500	7800	25·7
7/11	25·8	40	1·62	5100	4400	13·7
9/11	26·2	46	1·08	6950	5700	18·0
9/11	26·0	47	1·29	6100	5500	9·9
10/11	25·2	50	1·03	7100	6000	15·5
11/11	25·2	55	2·16	6900	5250	14·0

and lowering their mobility. This is supported by the results obtained which show that, while a group disappears, the ion concentration in another group with lower mobility increases.

(c) In general the total ion concentration, when the mixture is exposed to light, is less than its value when the mixture is kept in the dark.

This may be explained by assuming an action due to light on the ions formed, raising the probability of their recombination, thus decreasing their concentration. Recombination will obviously take place more often, the greater the number of ions of each sign present in the gas, which is the case when N_2O gas is added to air.

The results obtained with the whole electrode condenser show the same behaviour.

This behaviour shows that the light effect is not simple, and needs a further study on some other trace gases such as SO_2 and H_2S which are found in the atmosphere with a relatively higher concentration than N_2O.

References

Aitken J.	1912	*Proc. Roy. Soc. Edinb.* **32,** 183.
El Nadi A. F. and Farag N.	1961	*Geofis. Pur. Appl.* **47,** 114.
Hogg A. R.	1939	*Proc. Phys. Soc. Lond.* **51,** 1014.
Ortner G. and El Nadi A. F.	1955	*J. Atmosph. Terr. Phys.* **7,** 31.
Pealing H.	1915	*Phil. Mag.* **29,** 413.
Verzár F	1959	*Geofis. Pur. Appl.* **42,** 21.
Verzár F. and Kunz Y.	1957	*Geofis. Pur. Appl.* **38,** 215.

Journal of Atmospheric and Terrestrial Physics, 1961, Vol. 22, pp. 32 to 42. Pergamon Press Ltd. Printed in Northern Ireland

Ionospheric current systems of ten IGY-solar flare effects

D. Van Sabben
Royal Netherlands Meteorological Institute, De Bilt, Netherlands

(*Received* 23 *March* 1961)

Abstract—Quantitative analysis of s.f.e. current systems shows that the northern current vortex is generally centred to the west of the southern current vortex and is relatively more intense in northern summer than the southern vortex in southern summer. The total intensity corresponds rather well with the intensity of associated solar flares and ionospheric s.w.f.'s.

The current systems of the daily variation at the time of the s.f.e.'s show the same systematic difference in longitude between *S*- and *N*-vortex centres. These centres are generally situated at a lower latitude and more to the west than those of the corresponding s.f.e.'s.

The features of asymmetry in intensity and position with respect to the equator can be described by an ionospheric current system, the meridional parts of which cross the equator in the morning and noon regions.

In a previous paper (Veldkamp and Van Sabben, 1960) the great solar flare effect (s.f.e.) of 23 March 1958 was analysed. It was presented in the well-known form of an ionospheric current system that could produce the observed deviations in the horizontal component of the earth's magnetic field, at the time of the maximum effect.

The shape of the current system of this s.f.e. proved to be distinctly different from that of the daily variation at the same moment. In view of the apparent symmetry of the s.f.e.-current system with respect to the magnetic equator, a number of other s.f.e.'s of the years 1949–1953 were re-examined and found to have the same property, though not very conclusive because of scarcity of data.

It seemed to be worth while to extend the investigation. A circular was sent to the magnetic observatories, asking for the records of nine more s.f.e.'s, which all occurred during the IGY. The selection of the s.f.e.'s was made so that their times of occurrence were distributed as well as possible over the hours of the U.T.-day. The records received were analysed and the disturbance vectors were transformed into ionospheric current vectors, again following the method that Chapman and Bartels (1940, p. 232) used to derive the current system of the S_q-variation. The resulting current systems are presented in this paper (Figs. 1–8). Two of the diagrams are not reproduced here, as they concern rather small s.f.e.'s with a great deal of uncertain data.

Contrary to the earlier published figures (Veldkamp and Van Sabben, 1960), the actual current systems have been designed in order to obtain also a quantitative description of the s.f.e.'s. This was done by drawing the consecutive streamlines at intervals corresponding to a certain fixed current intensity. The case of 23 March 1958, completed with some data received later, was re-analysed for this purpose; it is reproduced in Fig. 1, together with the current system of the daily variation at the same moment. To avoid overcrowding, the arrows for the current vectors have been omitted from this figure.

Asymmetry with Respect to the Equators

From a glance at the figures it is clear that there is in many cases a strong asymmetry with respect to the geographic equator. But it appears also that the

VOL. 22 1961

rather good symmetry with respect to the magnetic equator, found for the great effect of 23 March 1958 and the smaller effects of 1949–1953, is not a common feature of all these IGY-solar flare effects.

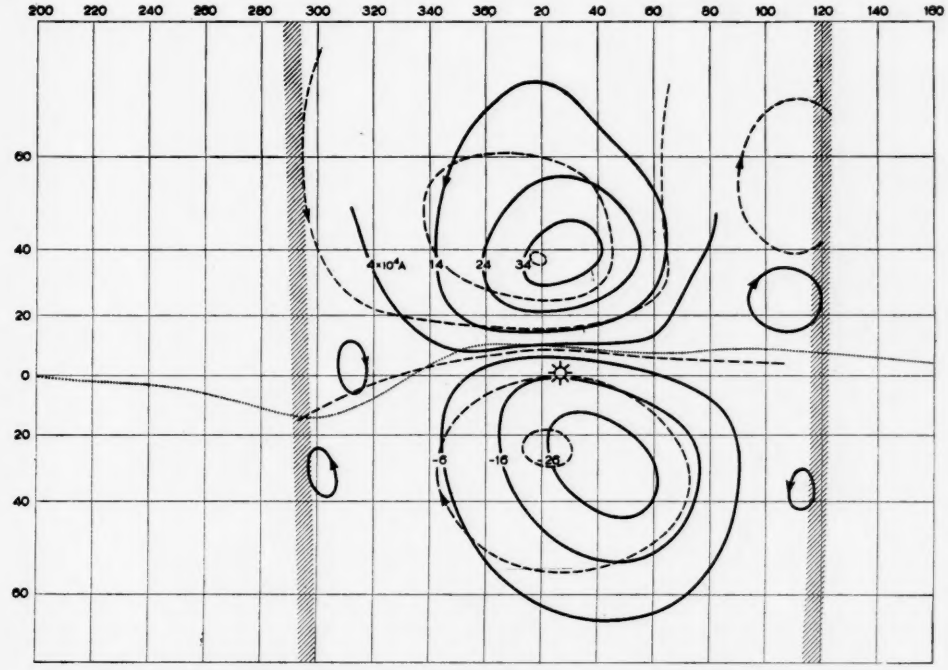

Fig. 1. Current systems of solar flare effects and daily variation, 23 March 1958, 1015 U.T. The full lines show the current system of the s.f.e. at the time of its maximum; the streamlines are provided with numbers which give the total current in units of 10^4A, flowing in between these lines and a zero line in the centre of the diagram. The dashed lines represent the current system of the daily variation at the time of the maximum s.f.e. The sub-solar point, the twilight zones and the magnetic equator are also indicated. Geographic coordinates are used.

Clearly divergent cases are those of 29 July and 16 August 1958. In most of the diagrams the equatorial current in the neighbourhood of the subsolar point has a definite south–north component, even when the slope of the magnetic equator is from north-west to south-east. This feature will be discussed later in connexion with the positions of the vortex centres.

Intensity of the Ionospheric Current Systems

The intensity of the northern (N) vortex and of the southern (S) vortex is given by the total currents J_N and J_S in units of 10^3 ampères, flowing in the regions between the centres of these vortices and an equatorial streamline, in the figures marked as zero-line. The latter has been chosen in the middle between the outermost streamlines which enclose the N- and S-vortices in the sunlit region: The sum $J = J_N + J_S$ is an index of the total intensity of the solar flare effect.

The question arises whether this index is directly related to the intensity of the corresponding solar phenomena and the intensity of associated ionospheric effects.

Table 1 summarizes a number of these data. The s.f.e.'s are arranged according to the magnitude of J. It is clear that there is a rather good agreement between

Table 1. Selected IGY solar flare effects, arranged according to magnitude, with data of associated solar flares and short wave radio fadeouts

Date	s.f.e.		Intensity		Flare				s.w.f.	
	Begin (U.T.)	Max. (U.T.)	J_N/J_S	$J = J_N + J_S$ (10^3A)	Begin (U.T.)	Max. (U.T.)	Imp. (1–3^+)	Dur. (min)	Imp. (1–3)	Dur. (min)
23 Mar. 1958	0952	1015	380/340	720	0947	1005	3^+	300	3	230
16 Aug. 1958	0434	0451	290/150	440	0433	0440	3^+	240	3	116
29 Jul. 1958	0301	0311	280/120	400	<0259	0304	3	70	3^-	84
12 Dec. 1958	1257	1301	120/170	290	1229	1304	2^+	200	3^-	30
12 Sep. 1957	1514	1518	160/110	270	1510	1516	2	90	$2\frac{1}{2}$	30
29 Mar. 1958	1340	1348	90/75	165	1339	1343	2	31	3^-	30
28 Aug. 1957	2018	2022	60/50	110	2010	2024	2^+	38	2^+	17
15 Oct. 1957	2151	2154	50/60	110	No flare reported				1	12
20 Aug. 1958	0042	0046	53/35	88	0042	0045	2^+	46	3^-	33
11 Dec. 1958	1935	1938	27/37	64	1930	1939	2	42	2	25

Figs. 2–8. Ionospheric current systems of solar flare effects. The number printed on a streamline gives the total current, flowing in between this line and a zero line in the centre of the diagram, in units of 10^4A. The arrows represent the magnetic deviation in γ's (see legend for scale); they are turned clockwise over 90° in order to indicate the overhead current density ($1\gamma \approx 1$ A/km). The heavy arrows are the s.f.e.'s, the light arrows with double heads the daily variation vectors at the same moment (called $S + L$ in the legend). Stations which recorded no effect are marked by a black dot. The sub-solar point, the twilight zones and the magnetic equator are also indicated.

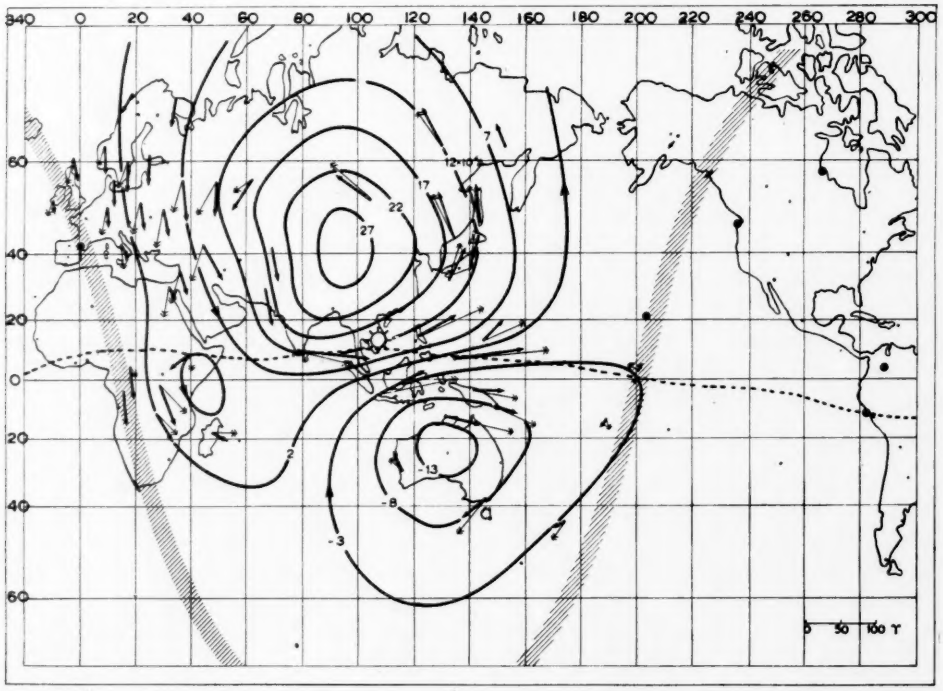

Fig. 2. Current system of solar flare effect, 16 August 1958, 0451 U.T.

VOL. 22 1961

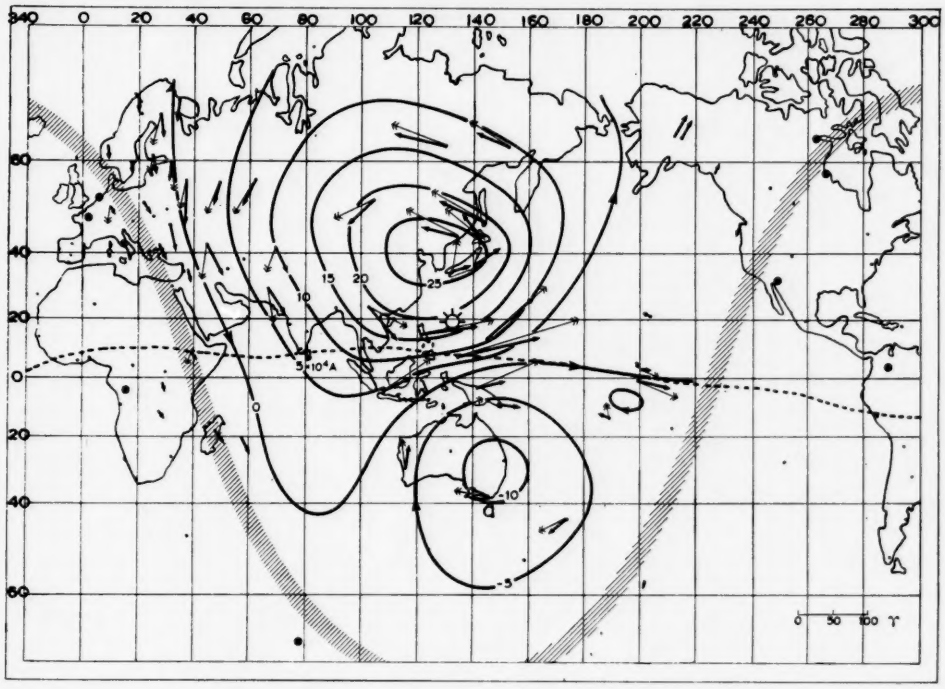

Fig. 3. Current system of solar flare effect, 29 July 1958, 0311 U.T.

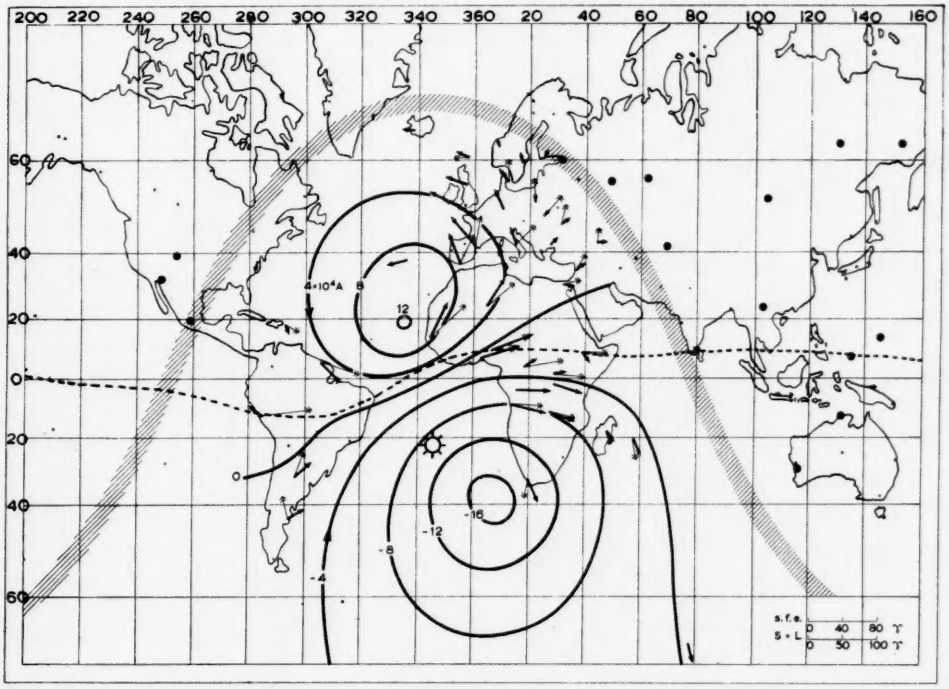

Fig. 4. Current system of solar flare effect, 12 December 1958, 1301 U.T.

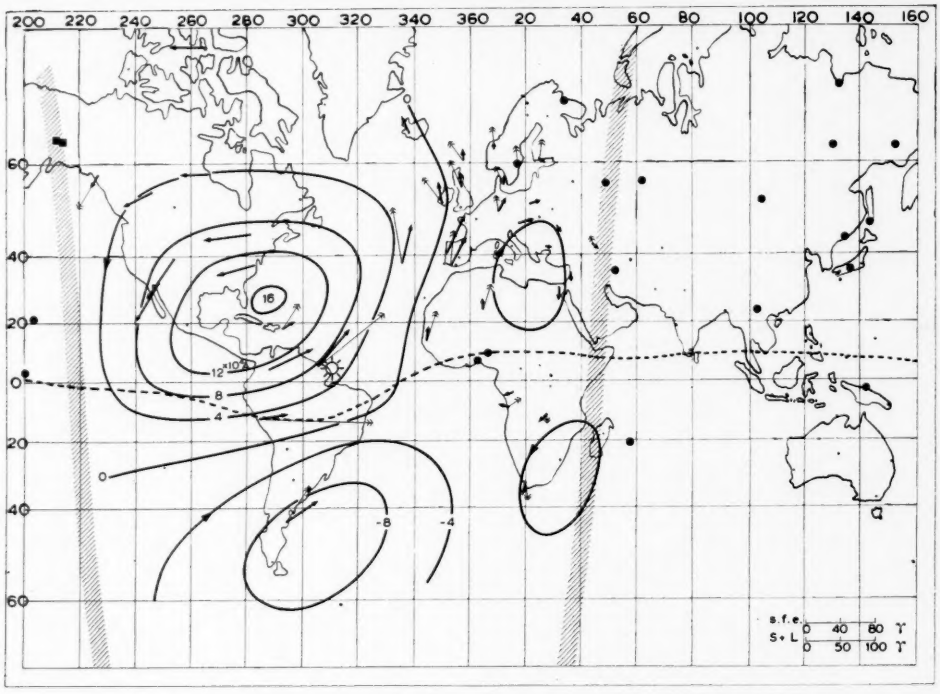

Fig. 5. Current system of solar flare effect, 12 September 1957, 1518 U.T.

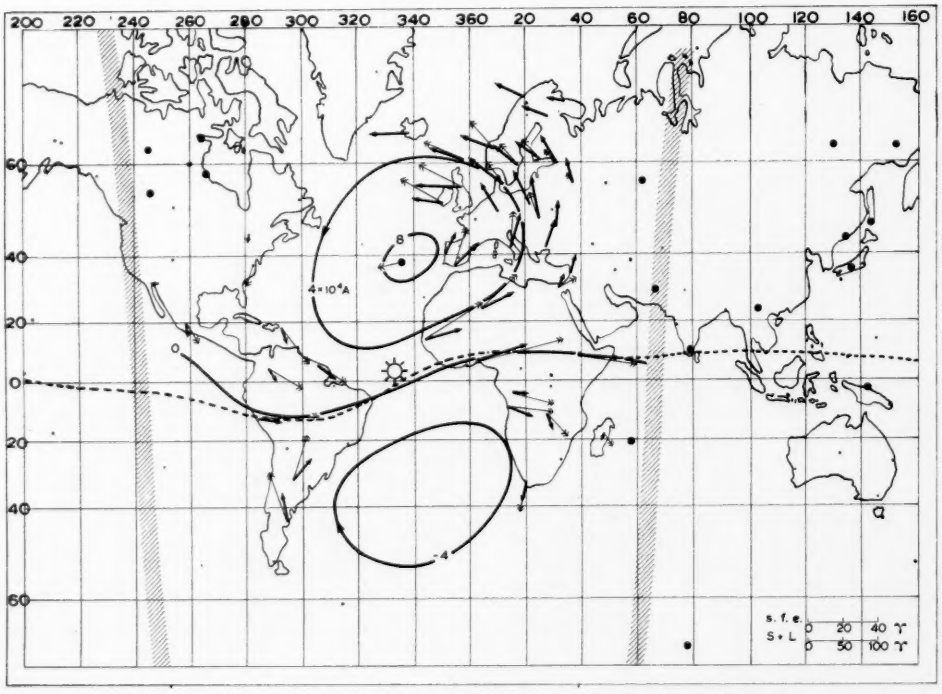

Fig. 6. Current system of solar flare effect, 29 March 1958, 1348 U.T.

VOL. 22 1961

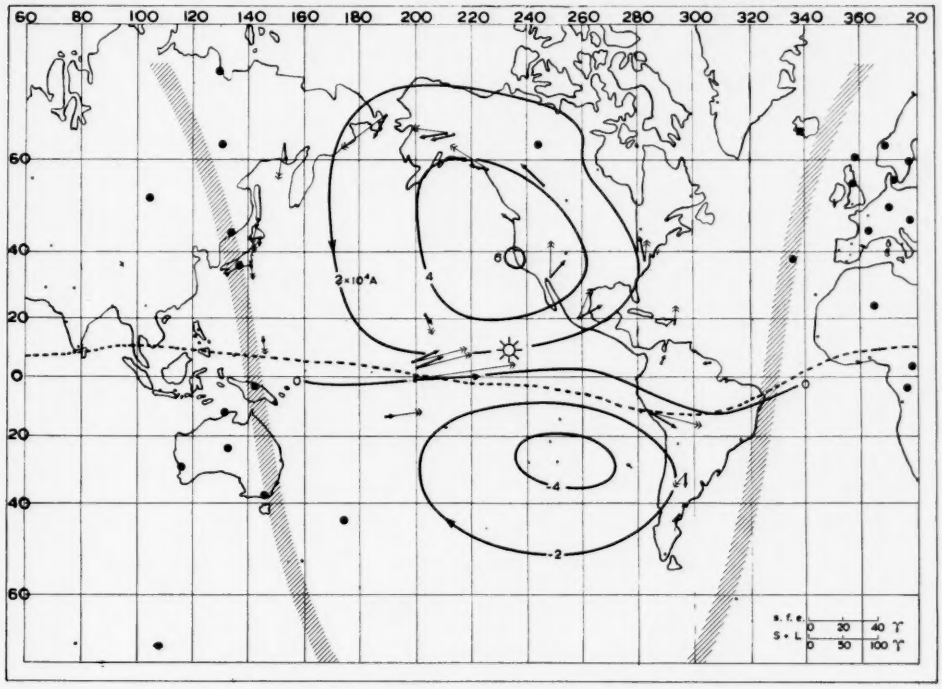

Fig. 7. Current system of solar flare effect, 28 August 1957, 2022 U.T.

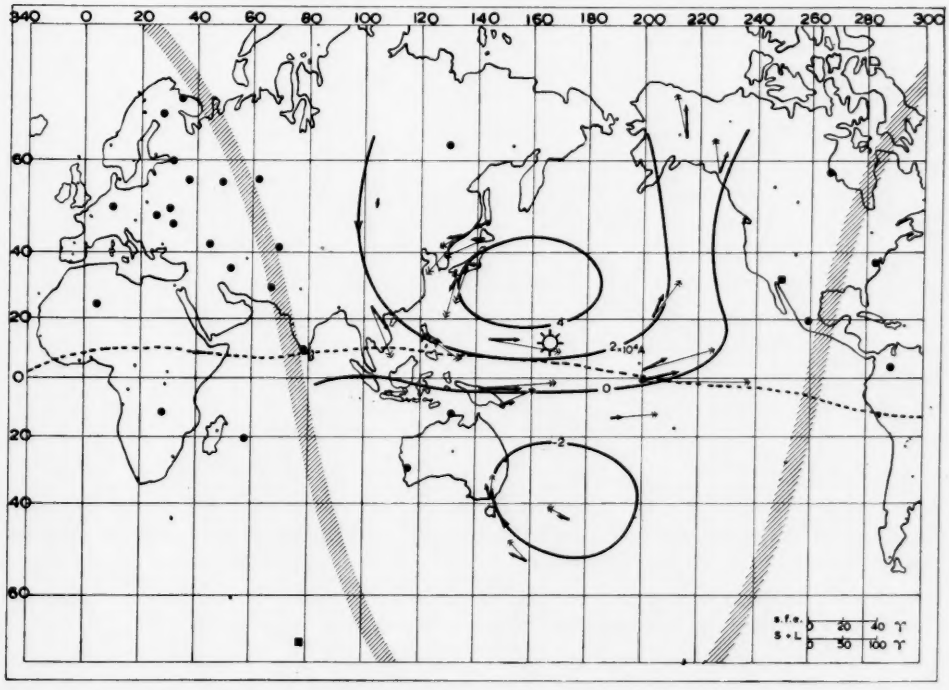

Fig. 8. Current system of solar flare effect, 20 August 1958, 0046 U.T.

J and the importance of the flares. The flare data were taken from the IGY-catalogue of WDC-A and the importance was estimated from the available reports. The data of the sudden wave fadeouts (s.w.f.) were in a similar way extracted from a list published by the radio-station NERA. The agreement between J and

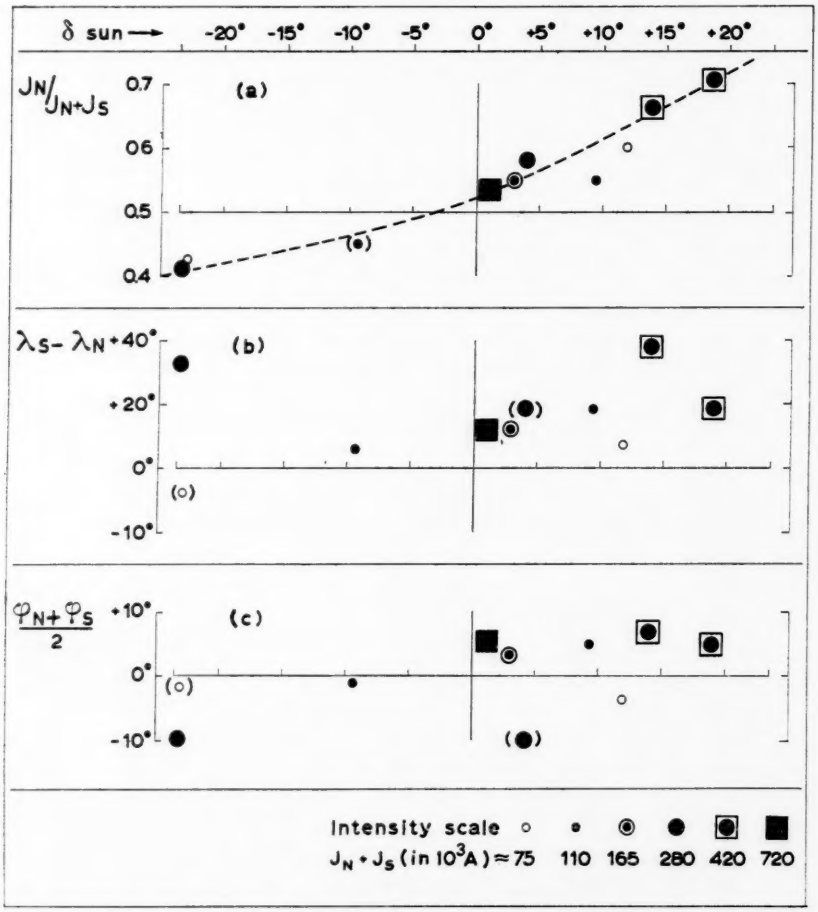

Fig. 9. Diagrams of relative intensity (a), difference in longitude (b) and mean latitude (c) of N- and S-vortex centres of solar flare effects, plotted against the solar declination (δ). Less reliable values are indicated in parentheses.

the s.w.f.'s is also rather good, especially if the latter are measured by their duration. Outbursts of solar radio noise were observed on all the occasions, except perhaps that of 15 October 1957 (when there was no flare reported either), but the correlation with their intensity seems to be less good. The same can be said of the sudden enhancements of atmospherics.

The influence of the season on the relative intensities of the N- and S-vortices

VOL. 22 1961

is shown in Fig. 9(a), where the ratio $J_N/(J_N + J_S)$ is plotted against the astronomical declination of the sun. The ratio is about 0·5 around the equinoxes, as one should expect. There seems however to be an asymmetry with respect to the northern and southern summer. In the June solstice the N-vortex takes about 75 per cent of the total current, but in the December solstice the S-vortex takes only 60 per cent.

Position of the Vortex Centres

The most consistent feature in the s.f.e.-diagrams is that the centre of the S-vortex is situated to the east of that of the N-vortex. In Fig. 9(b) the difference in geographic longitude $\lambda_S - \lambda_N$ between the centres is shown. All values of $\lambda_S - \lambda_N$ are positive, with the possible exception of that of the small effect of 11 December 1958, where the position of the S-vortex is rather uncertain. The mean lag of the S-vortex is about 18° in longitude.

The mean latitude of the N- and S-centres, $(\varphi_N + \varphi_S)/2$ $(\varphi_S < 0)$ seems to be somewhat dependent on the season. This appears from Fig. 9(c) where this quantity is plotted against the declination of the sun. The tendency is that the mean latitude is northerly when the sun is north of the equator and vice versa.

In Fig. 10 the positions of the centres are plotted on a world map, together with the subsolar points at the times of the s.f.e.'s. The intensities are entered in units of 1000 A. It is apparent that the lag of the S-centre is also present if one takes the magnetic equator as a reference line, although not as consistently as with respect to the geographic equator.

Comparison with the Daily Variation

It is of interest to compare the current system of each s.f.e. with that of the daily variation at the time of the maximum effect. To determine the daily variation, the mean traces of the magnetic components in the adjacent local time periods 2200–0200 hours L.T. were chosen as zero levels and the distance was measured between the zero level and the interpolated trace at the time of the maximum s.f.e. There were less reliable data for the daily variations than for the s.f.e.'s, because none of the periods in which the s.f.e.'s occurred were very quiet, so that it was often impossible to make a good estimate of the zero level. Therefore a number of current systems of the daily variation could not be drawn with satisfactory accuracy. Only the case of 23 March 1958 was analysed quantitatively. It is presented in the same figure as the s.f.e. (Fig. 1). The current systems of the daily variation for the other nine cases are not reproduced here, but their vortex centres are plotted in Fig. 10. Some of the southern centres are omitted however, because their positions were too uncertain.

It can be seen from Fig. 10 that:

1. The vortex centres of the daily variation are generally at a lower latitude than those of the s.f.e.'s. The mean difference in latitude is 6°.
2. With one exception, the centres are all situated to the west of the corresponding s.f.e.-vortex centres.
3. There seems to be also a systematic positive difference in longitude between the southern and northern centres, just as in the case of the s.f.e.'s.

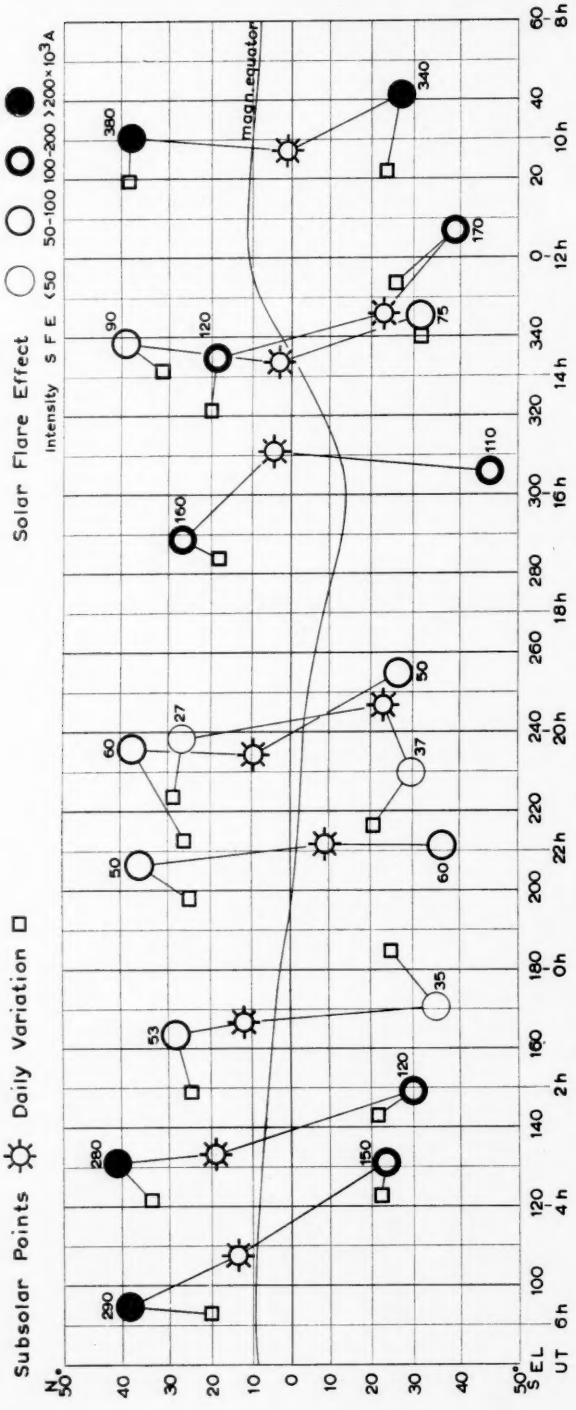

Fig. 10. Positions of vortex centres of current systems of solar flare effects and daily variations at the time of the maximum s.f.e., for the ten cases listed in Table I. Intensity of s.f.e.-vortices indicated in units of 10^3A.

VOL. 22 1961

Discussion of Results

The s.f.e. and daily variation currents are, from a dynamo-theoretical point of view, dependent on

(a) air-movements in the ionosphere of tidal-, thermal- and possibly other origin,
(b) the magnetic field of the earth at ionospheric heights (especially its vertical component),
(c) the distribution of conductivity in the ionosphere, which is, apart from its dependence on the sun's zenith angle, very probably also to a high degree governed by the magnetic field.

From (b) and (c) a tendency towards symmetry with respect to the magnetic equator can be expected. The current systems of the s.f.e.'s show this tendency as a rule (and in some cases very clearly, see Figs. 1, 4 and 6), but there are marked exceptions. A survey of the positions of the vortex centres (Fig. 10) leads to the conclusion that there is a systematic feature of asymmetry, viz. a displacement of the S-focus to the east, relative to the N-focus, both in the s.f.e.—and the daily variation current systems. A similar displacement was found by Hasegawa (1960) in his analysis of the mean track of the S_q-vortices as they moved around the earth with the sun during the second International Polar Year 1932–1933 (see also Chapman and Bartels, 1940, p. 241).

The displacement might be ascribed to a meridional current over the central part of the sunlit hemisphere, flowing from south to north in both hemispheres and crossing the equator in the region between the two vortex centres. If it is assumed that this current is part of another closed current circuit in the ionosphere, the return current from north to south should also appear in the diagrams. In Figs. 2, 3 and 5 such a current is visible in the region along the morning twilight zone.

A possible seasonal influence on latitude, as indicated in Fig. 9, so that the current systems tend to move northward and southward in phase with the sun, is in accordance with the results of Matsushita (1960), who found the same effect for the daily variation in three regions of the world (Europe, America, Far East). Furthermore the analysis of the S_q-variation of the years 1922–1933 by Vestine *et al.* (1947, pp. 164–165) indicates a reversal of sign in the daily variation of the North-component at a higher latitude during the summer than during the winter, which is also in line with the s.f.e.-results.

The systematic difference in position between the centres of the s.f.e.—and corresponding daily variation vortices might be caused by the choice of the zero level for the daily variation. Volland and Taubenheim (1958), who found the same relative displacement of the centres in the case of the s.f.e. of 31 May 1956, 0750 U.T., discussed this possibility but rejected it as improbable.

A more likely reason for this systematic difference is that the s.f.e. and daily variation currents flow for the greater parts in different layers (presumably D- and E-layer) of the ionosphere. Differences in conductivity distribution and also differences in the wind systems of these layers can then be expected. There is evidence for the latter from wind measurements, e.g. on meteor trails, which

indicate a rapid change with height of amplitude and phase of the 12-hourly atmospheric oscillation just below and in the E-layer.

The asymmetry, with respect to season, of the intensity-ratios of N- and S-vortex, might be ascribed to an asymmetry in the degree of ionization (conductivity). In fact it appears from the work of MENZEL *et al.* (1956) that the critical frequency of the E-layer was in the mean somewhat higher in the Northern Hemisphere than in the Southern Hemisphere during the sunspot maximum years 1947–1949. The authors state however that the difference is not to be regarded as significant.

Another possibility is that the dynamo e.m.f. is different in the two hemispheres. This might be caused by a systematic difference in the mean wind systems, taken over the two magnetic hemispheres. Data on ionospheric winds are however far too scarce to provide a check for such an effect.

There may be an interdependence of the asymmetry in intensity and the asymmetry in position of the N- and S-vortex centres.

If one has a superimposed current system as proposed in the first part of this discussion for the description of the latter asymmetry, with the north–south return current mainly along the morning twilight zone (left side in the figures), then the circulation of this system is such that the N-vortex will be reinforced and the S-vortex weakened. Thus both effects can be described by postulating such a superimposed current system, although the reason for its existence is not yet clear from a theoretical point of view.

Acknowledgements—I am much indebted to Prof. Dr. J. VELDKAMP for providing the stimulus and for encouraging this investigation.

Magnetograms of the following stations were used: BT, CC, RB, Di, Ti, PB, Tr, Go, Mm, So, We, Co, BD, BL, Sr, Ry, Do, Ya, Nu, Le, Ln, Lo, Cu, Si, Sv, RS, Kn, Mo, Es, Me, Wn, Wi, Ir, Sw, Ni, Vl, Gt, Ha, Ma, Db, Pr, Lw, Vi, Kv, Fu, CF, Hb, Ty, Sa, Od, Mb, Ag, Wl, Lg, Tf, Tk, IK, Eb, Ci, Aq, Fr, Ld, Ak, SM, SF, Ka, TI, Ks, Ss, As, Ky, Tu, Qu, He, C2, Ta, Zr, Ib, Ko, AA, Ho, Te, SJ, MB, Mu, Gu, Pa, Fq, Ba, Bn, Kr, Py, FI, JI, Lr, Hn, Bi, Ku, Lu, El, PM, Hu, Da, Ap, Tn, Mr, Va, Br, Wa, Pi, Hr, To, Am, Tr, MI, Mw.

REFERENCES

CHAPMAN S. and BARTELS J.	1940	*Geomagnetism*. Oxford University Press.
HASEGAWA M.	1960	*J. Geophys. Res.* **65,** 1437.
MATSUSHITA S.	1960	*J. Geophys. Res.* **65,** 3835.
MENZEL D. H., WOLBACH J. G. and GLAZER H.	1956	*J. Atmosph. Terr. Phys.* (Spec. Suppl.) **6,** 279.
VELDKAMP J. and VAN SABBEN D.	1960	*J. Atmosph. Terr. Phys.* **18,** 192.
VESTINE E. H., LANGE I., LAPORTE L. and SCOTT W. E.	1947	Publ. 580. Carnegie Inst., Washington.
VOLLAND H. and TAUBENHEIM J.	1958	*J. Atmosph. Terr. Phys.* **12,** 258.

VOL. 22 1961

Journal of Atmospheric and Terrestrial Physics, 1961, Vol. 22, pp. 43 to 49. Pergamon Press Ltd. Printed in Northern Ireland

The fading of radio waves reflected vertically from the ionosphere during magnetic storms

G. F. Fooks*
Cavendish Laboratory, Cambridge

(*Received* 24 *March* 1961)

Abstract—Some features of the reflection of radio waves from the ionosphere at vertical incidence during magnetic storms are described, and it is shown how correlation analysis can be applied to the fading at such times. The analysis shows that the irregularities in the diffraction pattern on the ground are smaller and more nearly aligned with the earth's magnetic field than they are for quiet conditions. Drift is a much more important source of fading than random changes in the pattern. The drift velocity is large, and is usually directed toward the West.

1. Introduction

When a radio wave is reflected from the ionosphere, the irregularities in electron density that are usually present cause an irregular diffraction pattern to be formed on the ground. The echo from a pulse transmitter, in magnetically quiet conditions, usually takes the form of a single pulse that fades irregularly with a quasi-period of the order of a few seconds. If the amplitude is recorded at a small number of closely-spaced points, it is possible to find the velocity of drift of the diffraction pattern using the time-delay method of Mitra (1949) and Krautkrämer (1950). Further, the correlation analysis of Briggs *et al.* (1950) and Phillips and Spencer (1955) can be applied to the records; this gives a value for the velocity of drift that is generally more accurate than that given by the time-delay method. Also, correlation analysis gives the size, axial ratio and orientation of a "characteristic ellipse" that represents an average irregularity in the diffraction pattern; and finally it gives the value of a quantity V_c which has the dimensions of a velocity and which is related to the rate at which the pattern undergoes random changes as it moves. Fooks and Jones (1961) have given results obtained by these methods at Cambridge for magnetically quiet conditions.

In the observations described in this paper, the same methods of analysis were applied to the fading during magnetic storms. The reflections are then often unusual in several respects, and corresponding changes in the methods of observation are necessary. The characteristics of reflections from the ionosphere during magnetic storms are discussed in Section 2. A brief description of the experimental apparatus and method is given in Section 3, and the results are presented and discussed in Section 4.

2. Characteristics of Reflections during Magnetic Storms

The fading during magnetic storms can be very rapid; fading periods as short as 1/10 sec are observed occasionally. Also, previous observations (reviewed by Briggs and Spencer, 1954) have shown that there is a tendency for the velocity of drift to be larger than for quiet conditions. There is evidence that these large velocities occur more frequently at night than during the day. Briggs and Spencer

* Now at D.S.I.R. Radio Research Station, Slough, Bucks.

give details of measurements of drift made during the magnetic storm of 26–27 May 1952; on that occasion the storm began at 0600 U.T. on 26 May, but the drift velocities showed no unusual behaviour until about 1800 hours on that day.

There is a tendency in middle latitudes for spread-*F* echoes to occur during times of magnetic disturbance (Wright *et al.*, 1956). The different parts of a spread echo appear to fade independently of each other, so that in order to make useful records of the amplitude it is necessary to isolate a part of the spread echo by means of a narrow strobing pulse, and measure the peak amplitude occurring within the strobe. Measurements of drift and results obtained by correlation analysis using such records will then refer only to those parts of the reflecting layer that contribute to the observed part of the spread echo. The validity of results obtained with this limitation is considered in Section 4.

There is a tendency, again in the middle latitudes, for the critical frequency of the *F2*-layer to decrease at times of magnetic disturbance (Appleton *et al.*, 1937). In severe storms the critical frequency becomes very low, and observations are often impossible with the transmitters normally used for observations of fading and drifts at Cambridge. Also, there is frequently more absorption during magnetic storms than at other times, and observations are difficult with the available power from the transmitters.

3. Apparatus and Method of Calculation

Pulses from a local transmitter, in the frequency range 2·0–4·0 Mc/s were reflected from the ionosphere at vertical incidence, and were received on three crossed-loop aerials, arranged to accept only the "ordinary" circularly polarized component of the downcoming wave (Phillips, 1951). The aerials were placed at the corners of a right-angled triangle; the sides containing the right angle lay North–South and East–West, and were 130 m in length. Three similar receivers were used, together with a strobing arrangement to select the required echo or the required part of a spread echo. The strobed outputs of the receivers were displayed as horizontal displacements on three 1 in. cathode-ray tubes mounted side-by-side, and the variations in amplitude were recorded on a continuously moving 35 mm film. To record the fastest fading TRI-X film was used, and was passed through the camera at a rate of about 40 cm/min.

After processing, the parts of the film required for further analysis were enlarged optically and traced onto paper. For correlation analysis, portions of record showing twenty or more cycles of fading were selected, and 240 to 360 equally spaced ordinates were measured on each of the three fading curves. The auto- and cross-correlation functions of the curves, for time displacements up to ± 20 times the spacing of the ordinates, were calculated on an automatic digital computer. The graphical method of Phillips and Spencer (1955) was used in the subsequent calculations to determine the parameters of the diffraction pattern on the ground.

4. Results

Table 1 gives the periods of magnetic disturbance during which observations were made, and the range of values of the magnetic *K*-index for the occasions when correlation analysis was applied to the records.

VOL. 22 1961

The records are far from complete for any of these periods. It was often impossible to obtain records with the available equipment, either because the critical frequency was too low or the absorption too great. In addition, there were many occasions when the correlation between the fading at the three receivers was very low; at such times it was not possible to apply either correlation or time-delay analysis to the records. Useful records are available for rather less than half the total time during the disturbed periods mentioned above.

Table 1. Correlation analysis during magnetic storms

Date	K
25–26 September 1958	4–6
17–18 December 1958	4–6
15 July 1959	7
17–18 July 1959	6–7
31 March–1 April 1960	6–9

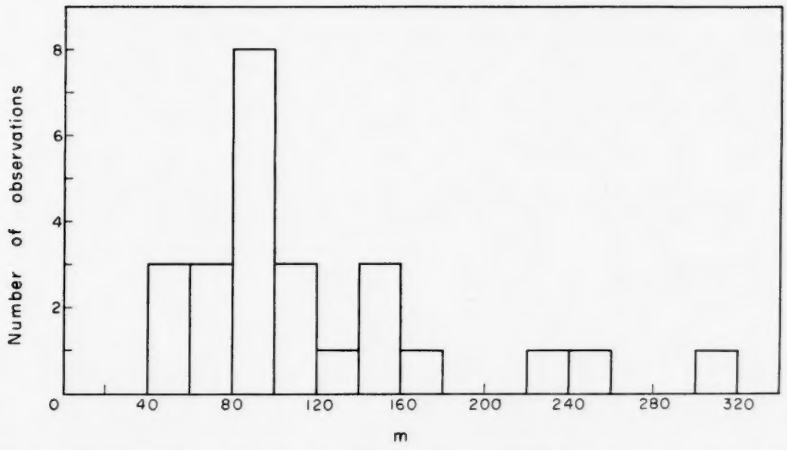

Fig. 1. Histogram for the semi-minor axis of the characteristic ellipse. For much of the time the correlation between the receivers was too small to measure, and so the maximum between 80 and 100 m is only apparent.

Correlation analysis was carried out on twenty-five records. Of these, five were of reflections from the E-region and twenty from the F-region; three were taken during the day, and twenty-two at night. There were no significant differences between these various groups, and in this Section all the results are presented together. The results for quiet conditions quoted for comparison are those given by Fooks and Jones (1961).

The lengths of the semi-minor axis of the characteristic ellipse are shown in histogram form in Fig. 1. Most of the values are considerably smaller than the median values obtained for quiet conditions; these were 235 m, 296 m and 140 m for the E-region, and for the F-region by day and night respectively. It should be

noted that the storm results are for occasions when measurements were possible with the aerial spacing of 130 m. The scale of the pattern was certainly smaller than 50 m for much of the time, but such occasions were unsuitable for analysis because of the low correlations between the fading at the three receivers.

If the ionosphere behaves as a diffracting screen that imposes phase variations much greater than 1 rad on an incident wave-front, the irregularities in the pattern on the ground will be smaller than the irregularities in the ionosphere (Hewish,

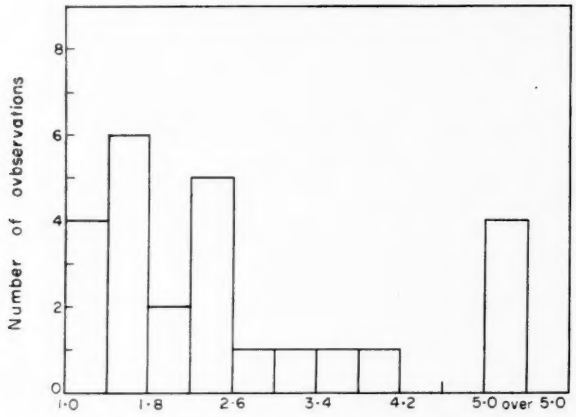

Fig. 2. Histogram for the axial ratio of the characteristic ellipse. Median = 2·0.

1951; Ratcliffe, 1956). This is almost certainly the case during storms, and at present it is not possible to say by how much the irregularities in the pattern on the ground are smaller than the structure in the ionosphere.

Fig. 2 gives a histogram for the values of the axial ratio of the characteristic ellipse. The median value (2·0) is not greatly different from the median values found for quiet conditions (1·5 for E-region, 1·6 for F-region by day, 1·8 for F-region by night), but there is a larger range of values, and on eight occasions the axial ratio was greater than 3·0.

The directions of the major axis of the characteristic ellipse are shown as a polar histogram in Fig. 3. There is a clear tendency for the major axis to lie close to the magnetic meridian.

Any elongation of the irregularities at the level of reflection in the ionosphere will be reproduced in the axial ratio and orientation of the characteristic ellipse of the diffraction pattern on the ground. We conclude that during magnetic storms the irregularities in the ionosphere tend to be aligned with the earth's magnetic field. For quiet conditions this tendency is present only for waves reflected from the F-region by night, and then to a less marked extent.

In all but six cases, the value of $(V_c)_V/V$ (as defined by Fooks and Jones, 1961) was not significantly different from zero. We may therefore say that drift is much more important in producing the fading during storms than are random changes in the diffraction pattern. This does not necessarily mean that random changes are completely absent; the accuracy in the measurement of $(V_c)_V/V$ is poor, and when

VOL. 22 1961

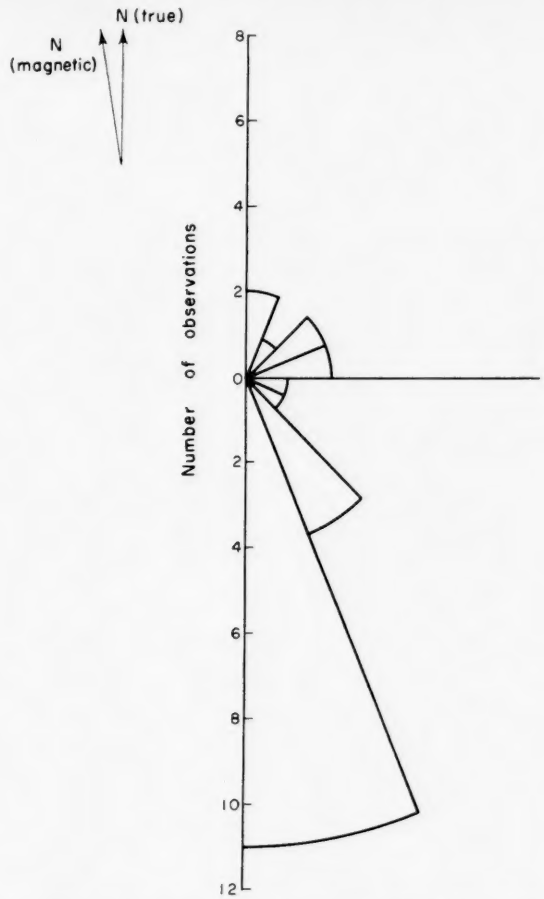

Fig. 3. Polar histogram for the direction of the major axis of the characteristic ellipse.

this quantity has a value much less than 1·0 the errors lie mainly in the determination of $(V_c)_V$, i.e. in the estimate of the contribution of random changes to the fading (FOOKS and JONES, 1961).

In a spread echo it may well be that the parts of the layer contributing to the selected part of the echo are not all at the same height. If there were large differences in velocity between these parts of the layer, correlation analysis would be expected to give an appreciable value of $(V_c)_V/V$.

On one occasion records were taken of the fading within a spread echo at three different virtual heights, all within a period of 5 min. The results of correlation analysis of the three records are given in Table 2.

Measurements of the velocity and direction of drift are considered further below; in fact the differences between these quantities for the three records in Table 2 are probably not significant, and also the values of $(V_c)_V/V$ are not significantly different from zero. These results are consistent with the conclusion that there are

Table 2. Correlation analysis of three records taken between 0038 and 0043 U.T., 18 December 1958. Frequency 2·0 Mc/s

Virtual height (km)	Velocity of drift (m/sec)	Direction of drift (°E of N)	$\frac{(V_c)_V}{V}$	Length of minor axis (m)	Axial ratio	Direction of major axis (°E of N)
400	277	230	0·3	150	2·4	177
550	224	270	0·2	90	3·4	170
700	250	270	0	105	2·5	164

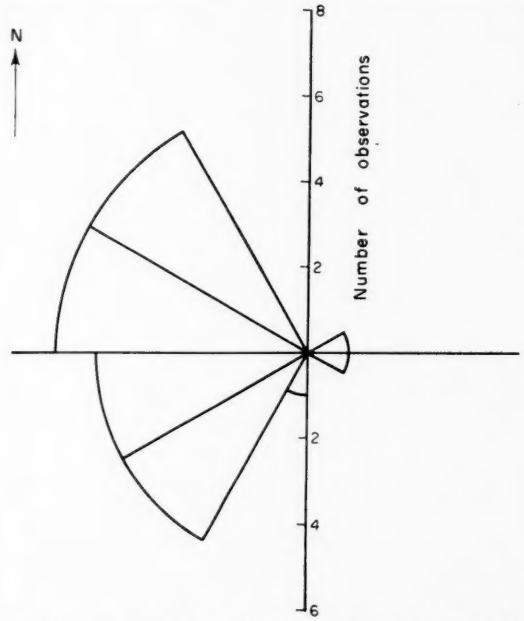

Fig. 4. Polar histogram for the directions of drift found by correlation analysis.

not large differences between the velocities of drift of the parts of the ionosphere at different heights contributing to a spread echo. Because of group retardation, the range of heights concerned is of course much less than the range of virtual heights from which the waves are apparently reflected.

It appears, therefore, that a small part of a spread echo may be selected and used by itself for measurements of drift at times of magnetic disturbance.

Fig. 4 gives a polar histogram for the directions of drift found by correlation analysis. On most occasions there was a large component of the velocity of drift toward the West.

The accuracy of measurements of the velocity of drift is affected by the tendency for the direction of elongation of the pattern to lie close to the NS direction. The EW component of the velocity is more accurately determined than the NS component, whether the time-delay method or correlation analysis is used for measurement. Also, the directions found by the time-delay method are biased towards the

VOL. 22 1961

direction perpendicular to the direction of elongation, i.e. roughly EW in this case. However, in view of the low value of $(V_e)_V/V$, the values of the EW component found by the time-delay method should be reasonably accurate.

The EW component of the velocity of drift was found by the time-delay method on twenty-nine occasions in addition to those for which correlation analysis was used; there was general agreement in the results obtained by the two methods. The values obtained showed great variability; the velocity in the ionosphere ranged from 100 to 1800 m/sec and was usually directed toward the West, though on two occasions large velocities toward the East were observed.

There was corresponding variability in the NS component, but the mean NS component was small.

These results for the velocity of drift are similar to those reported by Briggs and Spencer (1954).

Acknowledgements—The work described in this paper forms part of a programme of research on ionospheric irregularities, supported by a grant from the Department of Scientific and Industrial Research, and the author was in receipt of a maintenance grant from the same Department.

Thanks are due to the Director of the Cambridge University Mathematical Laboratory for permission to use the digital computer EDSAC 2.

The author also wishes to express his thanks to the Computing staff of the Radio Section of the Cavendish Laboratory for their assistance with the analysis of the records, and to Mr. J. A. Ratcliffe and Dr. B. H. Briggs for much helpful advice and discussion.

References

Appleton E. V., Naismith R. and Ingram L. J.	1937	*Phil. Trans.* A **236,** 191.
Briggs B. H., Phillips G. J. and Shinn D. H.	1950	*Proc. Phys. Soc. Lond.* B **63,** 106.
Briggs B. H. and Spencer M.	1954	*Rep. Progr. Phys.* **17,** 245.
Fooks G. F. and Jones I. L.	1961	*J. Atmosph. Terr. Phys.* **20,** 229.
Hewish A.	1951	*Proc. Roy. Soc.* A **209,** 81.
Krautkrämer J.	1950	*Arch. Elektr. Übertr.* **4,** 133.
Mitra S. N.	1949	*Proc. Instn Elect. Engrs* III **96,** 441.
Phillips G. J.	1951	*Proc. Instn Elect. Engrs* III **98,** 237.
Phillips G. J. and Spencer M.	1955	*Proc. Phys. Soc. Lond.* B **68,** 481.
Ratcliffe J. A.	1956	*Rep. Progr. Phys.* **19,** 188.
Wright R. W., Koster J. R. and Skinner N. J.	1956	*J. Atmosph. Terr. Phys.* **8,** 240.

Journal of Atmospheric and Terrestrial Physics, 1961, Vol. 22, pp. 50 to 63. Pergamon Press Ltd. Printed in Northern Ireland

Ionospheric information deduced from the Doppler shifts of harmonic frequencies from earth satellites

O. K. Garriott and A. W. Nichol
Cavendish Laboratory, Cambridge

(*Received* 5 *April* 1961)

Abstract—A very simple method is derived for the calculation of ionospheric electron content from the observation of the Doppler shifts on two harmonically related frequencies. A more complicated technique, involving digital computers, may be used to calculate the variations of electron content during the satellite's passage. These methods have been applied to five passages of 1958δ2 (Sputnik III) in March 1960. The results indicate the existence of appreciable ionization as low as 90 km, and are consistent with the absence of a valley between the *E*- and *F1*-regions near local noon. Irregularities in electron content were found below a height of 175 km, with variations in content of several per cent and horizontal extents of 50–200 km.

1. Introduction

It has long been recognized that a study of the Doppler shift imposed on radio transmissions from artificial earth satellites can yield important information about the electron density in the ionosphere (Weekes, 1958; Aitchison and Weekes, 1959; Hibberd and Thomas, 1959). Early attempts to relate the Doppler data to ionospheric quantities were of limited success, because the ionospheric effect is so small that it could not be accurately measured. At a frequency of 20 Mc/s the maximum Doppler shift is about 500 c/s, and the effect of the ionosphere is to change this by about 20 c/s or less. As the absolute value of the transmitted frequency is usually not known to within 20 c/s, the ionospheric effect is left in doubt.

A simple way to avoid these difficulties lies in the use of two harmonically related satellite transmissions. In the absence of an ionosphere the Doppler shifts imparted to the two frequencies would be in the same ratio as the oscillator frequencies, and the received signals would therefore maintain their harmonic relation. However, the dispersive effect of the ionosphere is larger at the lower frequency, and thus the total Doppler shifts will not be in the precise proportion of the oscillator frequencies. By noting the departure from the exact harmonic relation at the ground receiving station the ionospheric contribution is immediately obtained without any detailed knowledge of the exact frequencies of the oscillators in the satellite, and we no longer require the oscillators to be of high stability. An analogous experiment in rockets has been pioneered by Seddon (1953), and electron contents have been obtained by Ross (1960a,b) from satellite observations. The results of Ross were obtained by using the 20 Mc/s fundamental and the second harmonic of the transmitter in 1958δ2 (Sputnik III). He used a local oscillator near 20 Mc/s and its second harmonic to obtain related audio beat notes from the two transmissions. The frequency of the beat note obtained from the 20 Mc/s signal was doubled and compared with that from the 40 Mc/s signal. These two audio tones then produced a final beat frequency (a few cycles per second) which was related to the electron content of the ionosphere.

VOL. 22 1961

In this paper measurement of electron content and of the horizontal variations in electron content will be presented, based on observations of the 20 and 40 Mc/s signals from 1958δ2. The measurements were obtained by using a receiver which contained a 40 Mc/s oscillator locked in phase to the received satellite harmonic. The frequency of this "phase locked" oscillator was divided by two and compared with the received 20 Mc/s fundamental signal from the satellite. Fig. 1 is an example of the recorded beat; its frequency was determined by measuring the period occupied by a small number of cycles. The frequency of the beat was again a measure of the electron content, as will be shown below.

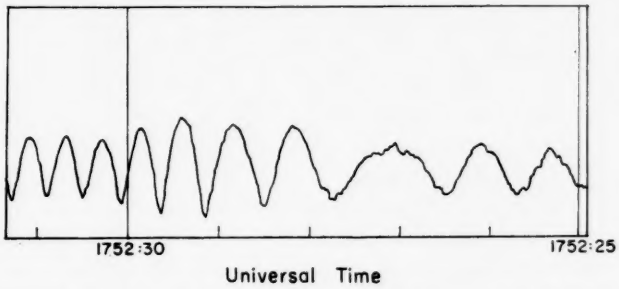

Fig. 1. Record of the beat (differential Doppler) between the 20 Mc/s signal and a frequency equal to half that of the 40 Mc/s signal from 1958δ2.

2. Electron Content of the Ionosphere

The phase path between the satellite and the receiver is given by

$$P = \int \mu \, ds = \int \left(1 - \frac{\alpha N}{f^2}\right)^{\frac{1}{2}} \sec \chi \, dh \tag{1}$$

where μ = refractive index,
N = electron density,
f = wave frequency,
χ = angle between the ray and the vertical,
α = 80·6 in m.k.s. units.

In this expression the Earth's magnetic field has been ignored and the integral (as in all the equations below) is to be taken along the ray path. The phase path will usually be shorter than the straight line range (R) to the satellite, and the difference in their lengths will be called the *phase path defect:*

$$\Delta P \equiv R - P \tag{2}$$

$$= R - \int \mu \sec \chi \, dh \tag{3}$$

$$= [R - \int ds] - \int (\mu - 1) \sec \chi \, dh \tag{4}$$

$$= [R - \int ds] - \overline{\sec \chi} \int (\mu - 1) \, dh \tag{5}$$

$$= [R - \int ds] + \overline{\sec \chi} \; \bar{g} \left(\frac{\alpha}{2f^2}\right) \int N \, dh \tag{6}$$

where, from (5)

$$\overline{\sec \chi} \equiv \frac{[R - \int ds] - \Delta P}{\int (\mu - 1)\, dh} \tag{7}$$

and, from (5) and (6)

$$\left.\begin{aligned} \bar{g} &\equiv -\frac{\int (\mu - 1)\, dh}{(\alpha/2f^2) \int N\, dh} \\ &= \frac{\int [(\alpha N/2f^2) + \tfrac{1}{2}(\alpha N/2f^2)^2 + \ldots]\, dh}{(\alpha/2f^2) \int N\, dh} \\ &\simeq 1 \text{ for } \frac{\alpha N}{2f^2} \ll 1 \end{aligned}\right\} \tag{8}$$

The value of $\overline{\sec \chi}$ is approximately the same as that of $\sec \chi$ averaged along the ionospheric portion of the ray path; however the above definition makes its meaning precise. The factor $\bar{g}$ provides a small correction to (6) to account for the higher order terms in the expansion of $(\mu - 1)$, which have been omitted from the integral. The term $(R - \int ds)$ has a negative value, and shows how much the geometrical length of the ray path has been lengthened by refraction. Its magnitude is, of course, smallest at the zenith and at higher frequencies.

The three quantities $(R - \int ds)$, $\overline{\sec \chi}$ and $\bar{g}$ cannot be determined from the observation of the signal from a satellite, although they can be computed for a particular passage of a satellite and a model ionosphere if a digital computer is available. Later in this paper we shall present some of these computations, and it will be noted that all these quantities are relatively insensitive to changes in the model ionosphere which is assumed. Then, using the observed values of ΔP as a function of time in equation (6), the variations of electron content with position of the satellite will be calculated for the real ionosphere. Before this is done, however, a simple method of estimating electron content will be given in Section 3, requiring neither a digital computer nor even an accurate ephemeris. Comparisons with real height profiles computed from ionograms will be made in Section 4.

VOL. 22 1961

3. An Approximate Method

We now wish to make two approximations in the calculation of electron content, $\int N\, dh$, although we shall return to the full expression (6) for the determination of the variations of electron content. First, refraction and the higher order terms in the expansion of $(\mu - 1)$ are neglected, leaving

$$\Delta P \simeq \overline{\sec \chi} \left(\frac{\alpha}{2f^2}\right) \int N\, dh \tag{9}$$

Dividing both sides by R,

$$\frac{\Delta P}{R} \simeq \frac{\overline{\sec \chi}}{h_s \sec \hat{\chi}} \left(\frac{\alpha}{2f^2}\right) \int N\, dh \tag{10}$$

where $h_s \sec \hat{\chi} = R$. Sec χ will take the value $\sec \hat{\chi}$ at a point near the mid point of the ray.

The second approximation is that $\overline{\sec \chi} \simeq \sec \hat{\chi}$, which is sufficiently accurate for

satellites below about 800 km, at zenith angles less than 45°, and when refraction is not too serious. We now have

$$\frac{\Delta P}{R} \simeq \frac{\alpha}{2h_s f^2} \int N\, dh \equiv \mathscr{R} \tag{11}$$

It will be seen that $\mathscr{R}$ is constant for a satellite moving in a circular orbit, if the ionosphere is spherically stratified. For this case

$$\left(\frac{\dot{\Delta P}}{\dot{R}}\right) = \left(\frac{\ddot{\Delta P}}{\ddot{R}}\right) = \mathscr{R} \tag{12}$$

in which the dot indicates differentiation with respect to time. It is important to note that these equations may be used with no orbital data available except the approximate satellite height. A corresponding derivation has been given by Garriott and Bracewell (1961) and the result is very similar to an equation developed by Ross (1960a) by other means.

The quantity $(\dot{\Delta P}/\lambda)$, where λ is the free space wavelength, is the difference between the Doppler frequency shift observed for free space transmission and that observed in the presence of the ionosphere. We shall call this quantity the *Doppler shift offset*. The quantity which we *observe* is the beat between the 20 Mc/s signal and a frequency equal to half that of the 40 Mc/s signal. We shall call this the *differential Doppler;* it is given by

$$\delta = \frac{(\dot{\Delta P}_{20}) - (\dot{\Delta P}_{40})}{\lambda_{20}} \tag{13}$$

As, from (11), ΔP is proportional to f^{-2} (to first order), the differential Doppler is $\frac{3}{4}$ of the 20 Mc/s Doppler offset.

Values of $(\dot{\Delta P}_{20})$ as a function of time have been obtained for five passages of 1958δ2 in the last 10 days of March 1960, only a few days before the final demise of the satellite, using the phase locked receiver mentioned above. Data relating to these passages are shown in Table 1. The transmissions had become continuous (rather than pulsed), which greatly assisted operation of the phase locked receiver. The height of the satellite was only about 175 km; thus the measurements relate only to the lower part of the ionosphere up to this height (which was below the F-region peak). The receiver was located at Stanford University, at a latitude of

Table 1. Observations of 1958δ2 at Stanford, March 1960

Date	Time of closest approach (P.S.T.)	Height (km)	Minimum zenith (degr.)
21	1307	176	33
24	1141	174	67
25	1141	173	<10
26	1139	172	57
31	0931	168	71

37·4°N, so that NW to SE passages were very near perigee at the time of the observations. In addition, during the last few weeks of the satellite's lifetime the orbit was nearly circular.

Fig. 2 shows the 40 Mc/s Doppler shift and the Doppler offset at 20 Mc/s obtained

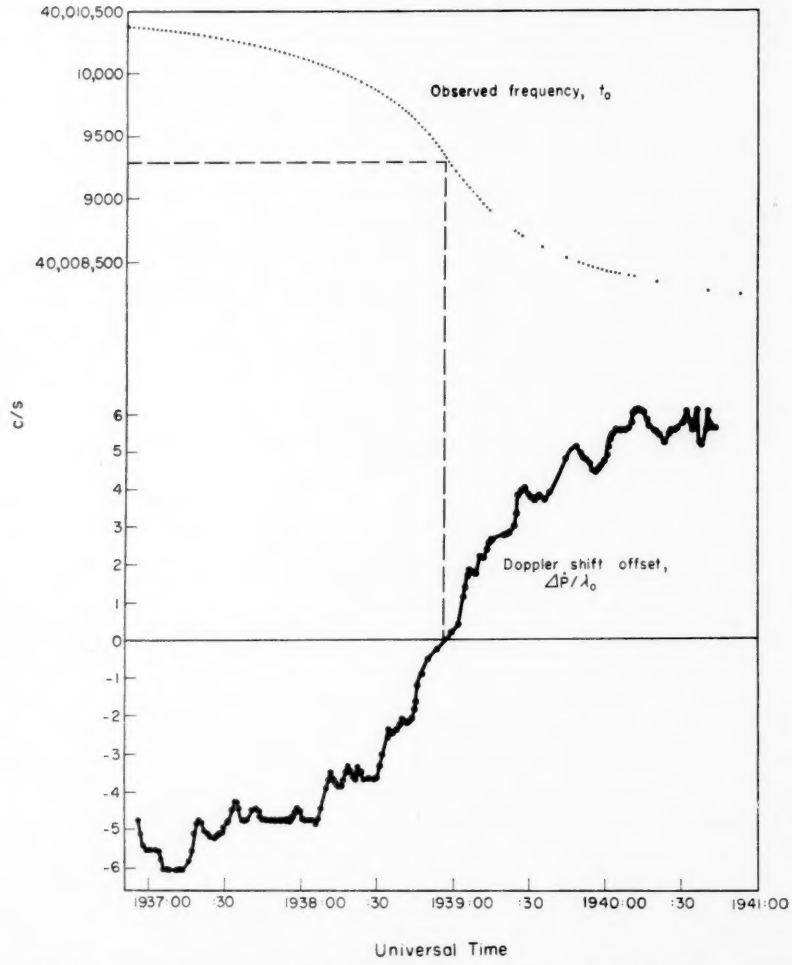

Fig. 2. Doppler shift on 40 Mc/s (upper curve) and Doppler shift offset (lower curve) obtained from 1958δ2, 26 March 1960. The irregularities in the Doppler shift offset curve correspond to variations in the electron content between the observer and the satellite.

on 26 March 1960. We have multiplied the observed differential Doppler by 4/3 to obtain the full Doppler shift offset at 20 Mc/s. The values so obtained are accurate to about 0·1 c/s. The rather large fluctuations are clearly related to ionospheric irregularities, and the last part of this paper will be devoted to their study. The value of $\dot{R}$ is readily obtained by multiplying the Doppler shift on 40 Mc/s by λ_{40}.

VOL. 22 1961

Fig. 3 shows the ratio $(\dot{\Delta P}/\dot{R})$ for the passage shown in Fig. 2. As predicted by (12), the ratio is approximately constant except for the fluctuations due to ionospheric irregularities. The value of $\mathscr{R}$ is seen to be about $1{\cdot}15 \times 10^{-2}$ which implies an electron content of $1{\cdot}96 \times 10^{16}$ electrons/m^2. In a similar manner electron contents were obtained for 21, 24, 25 and 31 March 1960.

The height of the satellite was so low that the plasma frequency never exceeded 6·5 Mc/s at any point of the ray path. Thus the wave frequency of 20 Mc/s was high

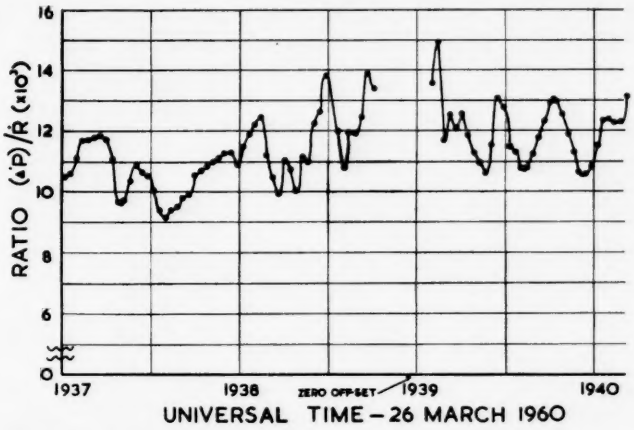

Fig. 3. Variation in the quantity $\dot{\Delta P}/\dot{R}$, whose average value corresponds to the electron content of the ionosphere.

enough to ensure that the approximations made above are sufficiently accurate. It is believed that the values of electron content obtained by this method are accurate to better than 10 per cent. The values of electron content used in the next section will be those obtained from the more accurate analysis of Section 5, and it is believed that the error in them is less than 5 per cent.

4. Comparison with Real Height Profiles

Since the satellite was well below the *F2* peak density, the values of electron content may be compared with the real height profiles of electron density computed from ionograms recorded near the time of the satellite's passage. In order to make this comparison it is necessary to know the satellite's height. The most accurate orbital data available appear to be the Ephemeris ϕ published by the Smithsonian Astrophysical Observatory. From this the height of the satellite at a latitude of 37·4°N (for the NW to SE passages) was determined as a function of date. The accuracy of these heights is estimated to be ± 3 km (D.V. Mechau, private communication). Unfortunately, the ephemeris was only completed up to 18 March 1960, and it was therefore necessary to extend it for nearly 2 weeks, as shown by Fig. 4. Therefore there is considerable doubt as to the correct height by 31 March.

Near the time of each satellite passage an ionogram was recorded and then reduced to a real height profile using Budden matrix coefficients and assuming that the electron density was a monotonic increasing function of height. The lowest

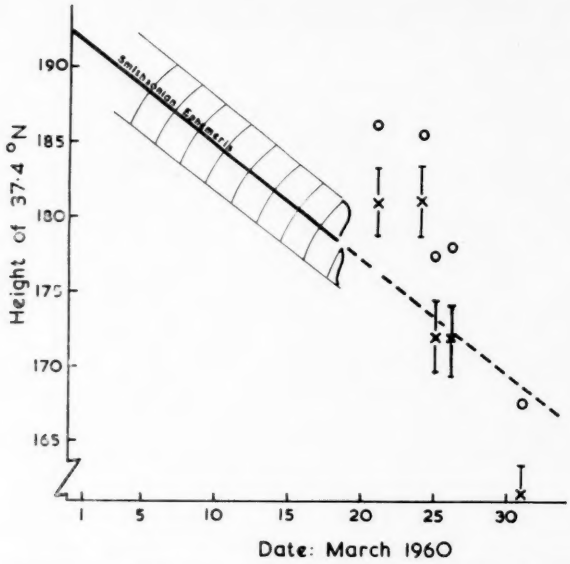

Fig. 4. The height of 1958δ2 during March 1960. The open circles show the height h at which $\int_0^h N\,dh$ for the electron density profile becomes equal to the electron content deduced from the satellite observations. The crosses are the values of h obtained when allowance is made for low-lying ionization, the vertical bars showing the effect on h of a ± 5 per cent variation in content. The limits of error of the Smithsonian Ephemeris are indicated by the shaded area.

VOL. 22 1961

frequency at which the virtual height was recorded was 1·8 Mc/s in all cases, and it was initially assumed that there was no ionization below the virtual height (100–110 km) observed at this frequency. One of the profiles obtained is shown in Fig. 5 as a solid line. If the profile is to be consistent with the satellite measurements, the value of $\int N\,dh$ up to the height of the satellite as computed from the profile must equal that derived from the Doppler measurements. We therefore computed the height for which $\int_0^h N\,dh$ for the profile was equal to the observed electron content. These heights for each of the five days studied are shown in Fig. 4 as open circles, and may be compared with the actual heights of the satellite from the ephemeris, indicated by the extension of the solid line. The open circles (except that for 31 March) all lie above the satellite's height, implying the existence of an important amount of ionization below 100 km.

In order to allow for the effect of low-lying ionization it was assumed that at frequencies below 1·8 Mc/s the virtual height was 90 km. This is equivalent to assuming ionization having a plasma frequency of 1·6 Mc/s at this height. The effect of this on the calculated profile is shown in Fig. 5 as a broken line. The revised profiles were again integrated and the new height calculated at which the integral of the profile became equal to the electron content from the satellite measurements. These heights are shown in Fig. 4 as crosses, with the effect of a ± 5 per cent variation in electron content indicated by vertical bars.

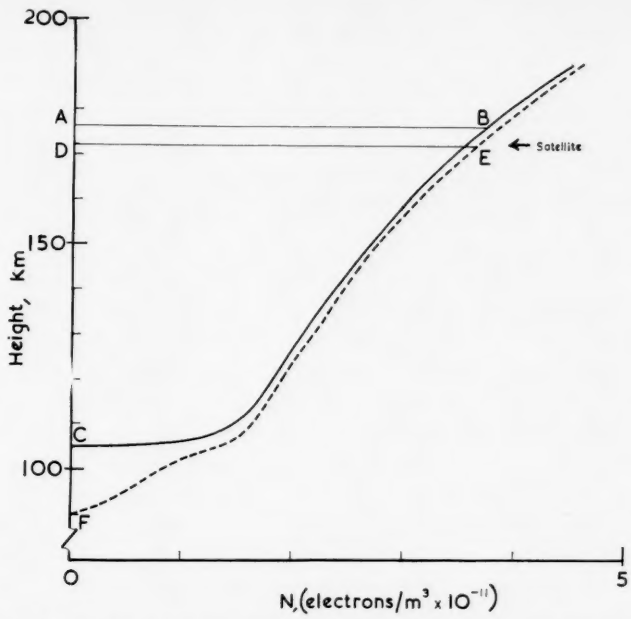

Fig. 5. The solid line is the profile of electron density computed from the ionogram on 25 March, assuming $h'_{\min} = 106$ km, while the broken curve is that obtained after allowing for low-lying ionization by taking $h'_{\min} = 90$ km. The area ABC is equal to the area DEF, and both are equal to the electron content obtained from the satellite observations. The heights A and D correspond to the circle and cross respectively in Fig. 4.

These results suggest that in the vicinity of local noon it is necessary to take account of low-lying ionization by assuming a minimum virtual height of about 90 km in calculating real height profiles, even when the minimum virtual height observed is 100–110 km at a frequency of 1·8 Mc/s. (This does not imply that our profile of ionization is at all accurate below 100 km, only that the integral of the profile to a height of about 175 km agrees with that deduced from the Doppler measurements.)

We can now consider the possibility of there being a "valley" between the E- and $F1$-regions, so that the true amount of ionization above the E-layer is less than that indicated by the profile. In this case the reduction in electron content in the valley must be offset by an equal increase in content below the E-layer peak. On 21 and 24 March it does not seem possible to include any appreciable valley and maintain agreement with the electron content from the satellite measurements, even if this has been overestimated by as much as 5 per cent and the maximum reasonable number of electrons are included below the E-region peak density. On 25 and 26 March, a valley containing 3×10^{15} electrons/m^2 might be possible, if the satellite results were reduced by 5 per cent and the height of the satellite were 3 km above the extrapolated curve.

The data from 31 March are noticeably different from those of the other four days. The initial ionogram reduction implied a height for the satellite which agreed reasonably well with the extrapolated Smithsonian curve (see Fig. 4). The electron

content from the satellite measurement on this date was only about two-thirds of that obtained a few days earlier. However, since the satellite was only about a week from the end of its lifetime, there is a greater uncertainty in its correct height. 31 March was the day of a large magnetic storm, and it is possible that its effects were noticeable below the height of the satellite. In addition the passage was near 0930 hours local time, about 2 hr earlier than on the other two days, and the effect of low lying ionization should have been smaller.

5. Variations in Electron Content

If the phase path defect ΔP is known as a function of time, equation (6) or (9) may be used to calculate $\int N\,dh$ as a function of time. The quantity so determined may be called the "electron content" although it is clear that the integration in fact takes place along an oblique ray path. The Doppler shift offset $(\dot{\Delta P}/\lambda)$ may be integrated as a function of time by simply counting the beats between the two 20 Mc/s frequencies discussed earlier. This determines the variation of ΔP with time except for an integration constant whose numerical value may be determined by converting the value of electron content, calculated as described in the previous section, to a value of ΔP at some convenient time, say at the point of closest approach. Then ΔP at any other time may be tabulated.

We have used (6) for the calculation of electron content with the aid of a computer program developed by one of us (A.W.N.). This program uses an iterative process to trace the path of a ray between the satellite and the observer through a specified model ionosphere, and calculates the expected Doppler shift and the values of P, $\overline{\sec\chi}$, $\bar{g}$ and $\int ds$ along the ray path. The calculation is confined to the plane containing the observer, the satellite and the centre of the Earth, deviations from this plane being ignored. The position of the satellite at a given instant is first calculated from orbital elements, and its zenith distance at the observer is taken as the direction of arrival for the first trial ray. The path of this ray is then traced from the observer to the satellite as a sequence of straight lines through a series of elementary spherical shells of thickness Δr, concentric with the Earth. At an intersection of the ray with a boundary between shells the angular deviation is calculated, using Snell's law with refractive indices corresponding to points in the model ionosphere at a distance $\frac{1}{2}\Delta r$ above and below the point of refraction. It is assumed that the refractive index is given by

$$\mu = \left(1 - \frac{\alpha N}{f^2}\right)^{\frac{1}{2}} \tag{14}$$

so that the results are very near the mean of those for the two magneto-ionic modes. Local electron densities are obtained by non-linear interpolation in a table of electron densities up to the F-region peak, and above this as an analytic function. It is therefore possible to make direct use of electron density profiles obtained from ionograms, without any restrictions on the continuity of derivatives.

When the ray reaches the height of the satellite, the miss distance is used to calculate a new value for the direction of arrival. After the second trial account is taken of the effect produced by the previous correction, giving a rapidly convergent

VOL. 22 1961

iterative process. When the error has been reduced to the required value the integrals are calculated along the final ray path, and the Doppler shift calculated from

$$D = \frac{\mu_s f}{C} (\mathbf{V}.\mathbf{r}) \tag{15}$$

where $\mathbf{V}$ is the relative satellite velocity and $\mathbf{r}$ a unit vector along the ray at the satellite.

This process requires from two to four iterations for a frequency of 20 Mc/s, and the computation takes an average of 30 sec using the EDSAC 2 computer at the University Mathematical Laboratory, Cambridge. The results for a particular model ionosphere have been compared with those from the very accurate method described by CAPON (1961). A model having a maximum density of $1{\cdot}5 \times 10^{12}$ m^{-3} at 300 km was used, with a satellite orbit passing the observer at zenith distances which varied during the passage from 20° to 75°, at a height varying from 800 to 1000 km. The two programs gave results differing by less than 1 per cent in the Doppler shift offset at 20 Mc/s.

It is also possible, although with less accuracy, to determine the effects on the Doppler shift of gradients and irregularities in the electron density of the ionosphere. Lateral deviations of the ray are still ignored, but the refraction at a shell boundary is calculated relative, not to the vertical at this point, but to the component of **grad** μ lying in the plane of propagation. This component of **grad** μ is computed from the values of μ at points $\frac{1}{2}\Delta r$ above and below both the point of refraction and the intersection with the preceding shell boundary. Gradients of ionization are defined by

$$N = (k_1\, d\lambda + k_2\, d\phi + 1).\ N(h + k_3\, d\lambda + k_4\, d\phi)$$

where the function $N(h)$ is the tabulated function of electron density with height above the observer, $d\lambda$ and $d\phi$ are the geographic latitude and longitude expressed relative to the observer, and $k_1 \ldots k_4$ are constants. Irregular structure may be in the form of blobs or tubes of extra ionization, or periodic variations of extra ionization expressed as a Fourier synthesis. It has been found that the program works satisfactorily provided that Δr is appreciably less than the scale of the irregularities: a value $\Delta r = 5$ km has been used in the calculations discussed here.

In order to apply this analysis to the observations, which were made after the end of the accurate Smithsonian Ephemeris, it was necessary to use approximate orbital elements published for prediction purposes by the Smithsonian Astrophysical Observatory and by the "Spacetrack" organization. The least reliable of these elements were the longitude of the ascending node and the time of nodal crossing. These have been adjusted to fit the origin of the time scale and the maximum slope of the computed Doppler curves for 40 Mc/s to those of the observed curves. The adjustments required are of the order of 2° in longitude and 10 sec in time, and it is thought that after adjustment the time of passage is correct to ± 1 sec.

The ray paths for 20 and 40 Mc/s were traced at 15 sec intervals for each pass, using two ionospheric models derived from the ionograms by assuming values for $h'_{\min}$ of 90 km and the $h'_{\min}$ observed at 1·8 Mc/s. It was found that ΔP was not precisely proportional to f^{-2}, so that the factor of 4/3, assumed in Section 3 for the

conversion of differential Doppler to Doppler shift offset, was in error by up to 5 per cent at a zenith angle of 70°. This arises from the difference in the paths taken by the two rays, the term $(R - \int ds)$ in (6) becoming comparable with ΔP at large zenith angles. Fig. 6 is a plot of the variation of these two quantities for 25 March,

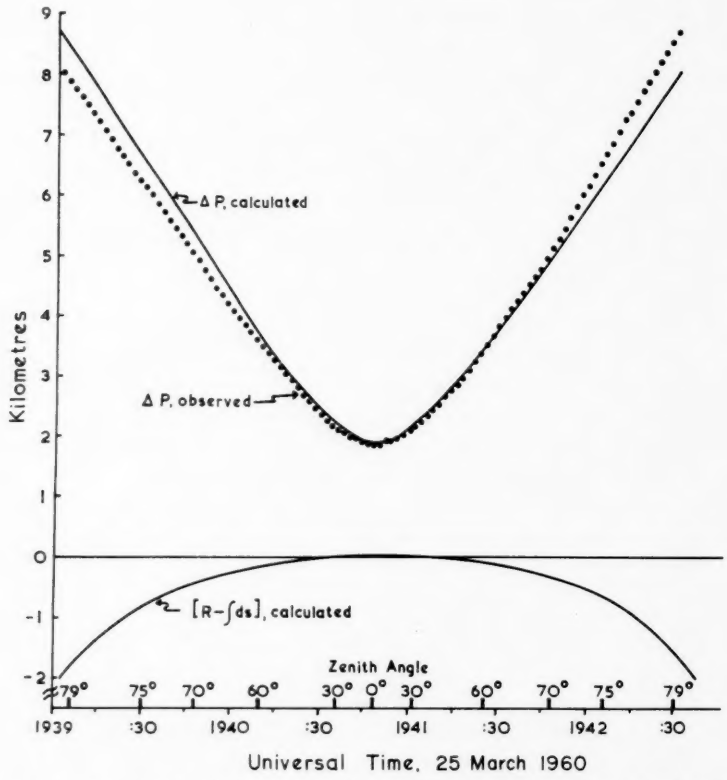

Fig. 6. The variations in the quantities ΔP and $(R - \int ds)$ with time calculated for the passage of 1958δ2 on 25 March 1960, when the satellite passed near to the zenith. The model ionosphere used corresponded to the observed ionogram. The deviation of the observed values of ΔP (shown dotted) from the calculated curve indicates the presence of a gradient of electron density.

to illustrate their relative magnitudes. A correction factor deduced from the calculations for the model ionosphere was plotted against time, and interpolated values used to convert the observed differential Doppler to 20 Mc/s Doppler shift offset.

The computed Doppler offset for the two model ionospheres was compared with the observed values, and a model giving a satisfactory fit was chosen. On some occasions it was found that one model gave a better fit up to the time of closest approach, and the other model gave a better fit thereafter, indicating the presence of gradients of electron density. The effect of gradients can also be seen from the divergence of the calculated and observed curves of ΔP in Fig. 6.

The curve of ΔP against time obtained by integrating the observed Doppler

VOL. 22 1961

offset was compared with that calculated for the chosen model, and the integration constant determined. The observed values of ΔP at 2 sec intervals were substituted in (6), together with the corresponding values of $(R - \int ds)$, $\overline{\sec \chi}$ and $\bar{g}$ obtained from the calculations. This gave the variation of $\int N\,dh$ with time. The absolute values of $\int N\,dh$ obtained in this manner differ by about 5 per cent from those obtained from (11), indicating the effects of the approximations made in deriving that equation, particularly that of assuming that $\sec \hat{\chi} = \overline{\sec \chi}$. The more accurate results of the computer calculations have been used in plotting Fig. 4.

The basic assumption made in this analysis is that the smooth variation of $\sec \chi$ and $(R - \int ds)$ obtained by calculation from the simple models is an adequate representation of their behaviour in the real ionosphere. In order to check this assumption a calculation was made using one of the model ionospheres with the addition of a density gradient and irregular ionization. The irregularities consisted of additional ionization at a height of 130 km, decaying to zero in 30 km above and below this height and varying periodically along the path of the satellite. Although the irregularity introduced large variations in ΔP and in the Doppler shift offset, comparable with those observed, the values of $\overline{\sec \chi}$ and $(R - \int ds)$ were little changed and continued to vary smoothly with time. It therefore appears that the computed variations of $\int N\,dh$ will represent the true variations in electron content. As this quantity represents an average over the region between the observer and the satellite, it is difficult to determine the precise form of the irregularities. It is, however, possible to determine their integrated content and approximate scale.

Fig. 7 shows the calculated values of $\int N\,dh$ as functions of time for the five days. There is a significant horizontal gradient in most cases, with an increasing electron content towards the South. The slope of these curves was found to be very sensitive to the precise time chosen for the closest approach of the satellite. However, the calculated horizontal gradients are consistent with those to be expected from predictions of f_0E. Of particular interest are the variations of electron content with time which were observed on all of the recorded passages. As the speed of the satellite is much higher than drift velocities to be expected in the E-region, these variations may be taken to be true spatial variations. They are a few per cent in magnitude, and have a horizontal extent of the order of 50–200 km. Although the variations in content are quite small, they give rise to rather large variations in the Doppler shift offset (see Fig. 2). This permits a very accurate measurement of their deviations in content to be made.

Records of ground back-scatter were examined at the times of the satellite passages and no sporadic-E patches were found (R. D. Egan, private communication). The origin of the irregularities found in this work is still unknown, but they appear to be part of the normal ionospheric region, since they were found on all these passages of this satellite.

6. Conclusions

A very simple yet reasonably accurate method has been demonstrated for the determination of electron content when transmissions on harmonically related frequencies from earth satellites are available. The method requires neither accurate orbital data nor high speed digital computers. A more detailed analysis,

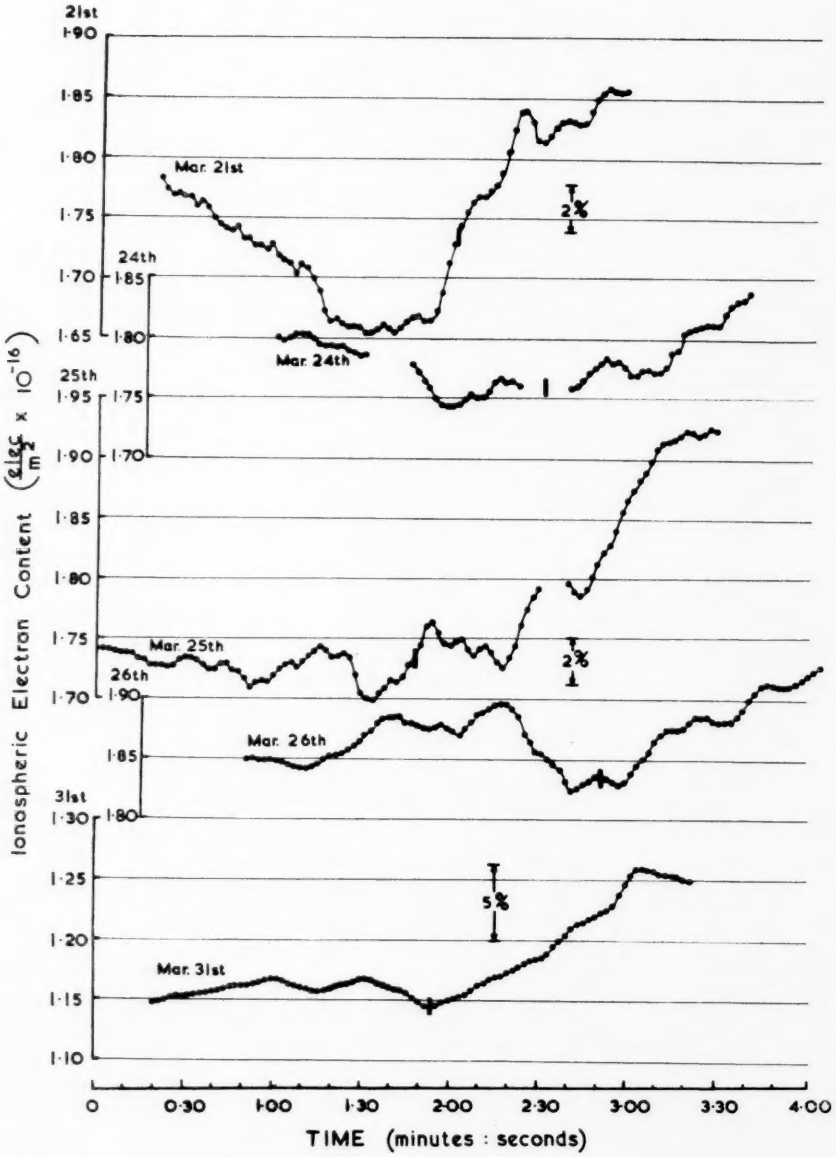

Fig. 7. The deduced variations of electron content with the position of the satellite during the five passages of 1958δ2. The vertical bars indicate the times of closest approach.

VOL. 22 1961

using computers, permits the variations of electron content with the position of the satellite during a passage to be deduced. The procedure involves:

(a) Estimation of the content from equation (11) or by other means;
(b) Calculation of $(R - \int ds)$, $\bar{g}$ and $\overline{\sec \chi}$ for a model ionosphere;
(c) Determination of ΔP against time from the differential Doppler record and the results of step (a);
(d) Calculation of $\int N\,dh$ as a function of time from equation (6).

These same techniques (with perhaps a modification to allow for a vertical velocity component and a horizontal gradient in equation (11)) should be directly applicable to the study of the Ionospheric Beacon satellite and the Transit series of satellites.

This analysis has been applied to observations of the transmissions from 1958δ2 It has been found that near local noon it was necessary to lower the minimum virtual height assumed in a real height reduction to about 90 km, some 10–15 km below the virtual height observed at 1·8 Mc/s. This was necessary to bring the electron content determined from the satellite observations into agreement with the integral of the electron density profile. The data were consistent with the absence of a valley between the *E*- and *F1*-regions. These arguments were based on a height for the satellite determined from an extrapolation of the Smithsonian Ephemeris ϕ. Irregularities of a few per cent in electron content were found on each occasion, with horizontal scales between 50 and 200 km.

Acknowledgements—The Doppler shift measurements used in this paper were made at Stanford University under grant NsG 30–60 from the National Aeronautics and Space Administration. Mr. S. C. Hall and Mr. F. de Mendonca recorded the data and also undertook the exacting task of measuring the Doppler shift offset as a function of time. We are indebted to Dr. Ray Egan for the survey of his back-scatter records for sporadic-*E* occurrence, to Dr. K. Weekes for a number of most helpful discussions, and to the Director of the Cambridge University Mathematical Laboratory for permission to use the computer EDSAC 2. One of us (O. K. G.) is now at the Cavendish Laboratory as a National Science Foundation Fellow.

References

Aitchison G. J. and Weekes K.	1959	*J. Atmosph. Terr. Phys.* **14,** 236.
Capon I. N.	1961	*Proc. Phys. Soc. Lond.* **77,** 377.
Garriott O. K. and Bracewell R. N.	1961	*Advances in Geophysics* VIII (Ed. by H. Landsberg). In press.
Hibberd F. H. and Thomas J. A.	1959	*J. Atmosph. Terr. Phys.* **17,** 71.
Ross W. J.	1960a	*J. Geophys. Res.* **65,** 2601.
Ross W. J.	1960b	*J. Geophys. Res.* **65,** 2607.
Seddon J. C.	1953	*J. Geophys. Res.* **58,** 323.
Weekes K.	1958	*J. Atmosph. Terr. Phys.* **12,** 335.

Journal of Atmospheric and Terrestrial Physics, 1961, Vol. 22, pp. 64 to 73. Pergamon Press Ltd. Printed in Northern Ireland

Head echoes from meteor trails

J. S. Greenhow
Royal Radar Establishment, Malvern

(*Received* 27 *April* 1961)

Abstract—The "head" echoes associated with ionization produced by bright meteors, when observed at radio wavelengths of a few metres, are discussed. It is shown that many of these phenomena are not true "head" echoes in the sense that they are obtained from a localized region close to, and travelling with, the meteor itself, as supposed previously. Instead the reflecting region may be as long as 100 km, with the ionization persisting for many seconds after the passage of the meteor. These echoes are explained on the basis that the ionized columns behave as rough reflectors, losing completely the highly specular reflecting properties associated with faint meteor trails. The finite duration and spread in range of an echo, and the variation in echo intensity along the trail, are explained quantitatively in this way. It is not necessary to postulate any mechanism for the production or dispersal of ionization, other than the normal processes of collision, diffusion and attachment.

1. Introduction

Immediately after formation the ionized trail produced by a meteor appears to be very linear, and this trail behaves as a specular reflector for radio waves. In the case of back-scatter an echo is obtained from the first Fresnel zone near the foot of the perpendicular to the trail, S, and as the meteor passes through successive Fresnel zones near S, the well-known diffraction effects are observed (Davies and Ellyett, 1949). A short time after formation the ionized column becomes distorted due to irregular winds and echo components may be obtained from other ranges. Changes in range of 0–100 m sec^{-1} are observed, as the trail drifts with the wind velocity. Occasionally, however, very bright meteors give rise to a so-called "head" echo. This echo apparently originates from a region very close to the meteor itself, and the range varies with the line of sight component of meteor velocity as the meteor approaches and recedes from the specular point. Changes in range of some tens of kilometers per second may be observed (Hey *et al.*, 1947; McKinley and Millman, 1949a). On a range–time display the echo describes a hyperbola. No satisfactory explanation of the head echo has yet been given, and it is the purpose of this paper to discuss a mechanism which accounts quantitatively for the characteristics of this phenomenon.

2. The Head Echo

(a) *Previous theories*

Browne and Kaiser (1953) have suggested that the head echo is due to diffraction at the discontinuity in ionization at the end of the ionized column. In this case the echo intensity is given by extending the simple Fresnel diffraction pattern for a considerable distance along the trail. With this mechanism the echo intensity falls very rapidly when the meteor is far removed from S. For example, when the off specular angle is 45°, the echo intensity is 60 dB below the broadside echo from the first Fresnel zone, at a wavelength of 9 m. This explanation has been criticized strongly by McKinley (1955), whose measurements show that the echo intensity varies quite slowly over path lengths of many Fresnel zones on

VOL. 22 1961

either side of S. Indeed, the head echo intensity may exceed that due to the main broadside echo even when the meteor is 45° away from the specular point. McKinley suggests that the head echo is due to a ball of ionization which surrounds the meteor, produced by some method other than the normal collision processes, the ionization persisting for about 10^{-3}–10^{-4} sec after the passage of the meteor.

Both of these explanations assume that the problem is to account for an extremely short lived echo associated with a localized region very close to the meteor itself. Thus with the diffraction and moving ball mechanisms, the echo duration from a given small element of trail should be limited to the time taken for the meteor to traverse the element. A corollary is that the echoes should show no extension in range. These fundamental assumptions appear to be erroneous. Inspection of the examples of head echoes published by McKinley and Millman (1949a,b), McKinley (1955) and Millman (1959), show that although these conditions sometimes appear to be satisfied over parts of a meteor path, this is by no means the general behaviour of a head echo. When a meteor is at a given point in its trajectory the echo is frequently spread in range by many kilometers, showing that a length of trail extending a considerable distance behind the meteor is giving rise to the echo. Furthermore, the echo may persist for many seconds after the passage of the meteor. Thus the moving ball hypothesis is not tenable. It is clear that these "head" echoes are not necessarily obtained from a localized region moving with the meteor itself, but are due to the ionization left behind in the trail. Thus the characteristics of this type of "head" echo which require explanation are:

(i) The echo may be obtained from a length of trail extending some tens of kilometers behind a meteor, down to a limit imposed by the transmitter pulse length (usually about 1 km).

(ii) The echo from a given part of the meteor path may persist from a small fraction of a second after the passage of the meteor, up to several hundred seconds.

(iii) The trail may show a complete lack of the usual specular reflecting properties shown by the absence of any enhancement in echo amplitude as the first Fresnel zone is formed. A possible explanation of these effects will now be considered.

(b) *The rough trail mechanism*

The finite duration of a head echo shows that we are concerned with an over-critically dense reflection mechanism (Greenhow, 1952), with the echo duration determined by the processes of diffusion and attachment. Thus conditions (i) and (ii) in the previous Section are readily explained on the assumption that the ionized column is produced behind a very bright meteor by the normal collision processes. Depending upon the height and initial electron density the echo duration from a given part of the trail can vary from a small fraction of a second up to several hundred seconds, the duration being determined by the time taken for the electron density to fall below the critical value n_c through the effects of diffusion and attachment. The maximum permissible spread in range of the echo is then determined by the length of trail behind the meteor in which the electron density exceeds n_c. This length can vary between zero at some point along the early part of the meteor path, up to many tens of kilometers.

However, effects (i) and (ii) would not be observed if the trail retained the highly specular properties associated with faint meteors, as no appreciable echo would be obtained except from the first Fresnel zone near the right angle point. On the other hand (iii) shows that the trails of these very bright meteors lose completely their specular reflecting properties, and the only logical explanation of this effect is that the ionized columns are rough compared with at least one quarter of the observing wavelength. This is only 1–2 m over the range of wavelengths at

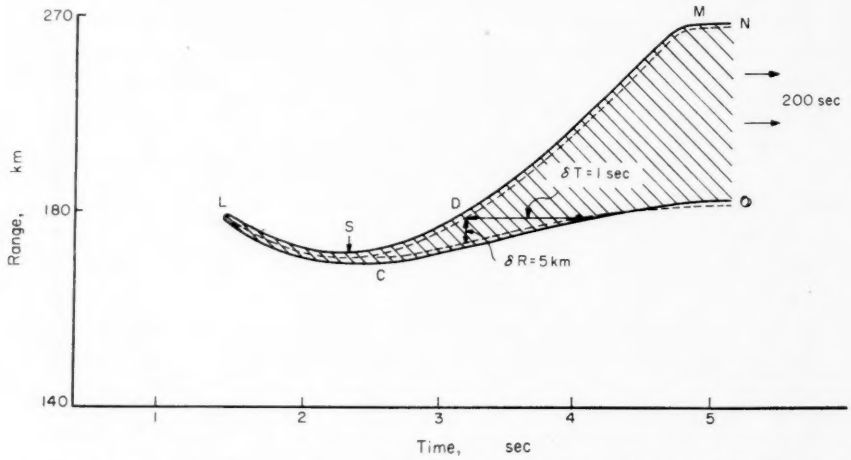

Fig. 1. The range–time envelope of a meteor head echo observed by McKINLEY (1955) (cross-hatched region). The broken lines *LSMNOC* show the theoretical range–time envelope for a rough trail.

which head echoes have been observed, and it will be shown later that a roughness of this order is quite likely to occur with the very large meteors associated with head echoes.

Two very good examples of head echoes have been published by McKINLEY (1955) together with details of the echo characteristics. One of these echoes will be considered in some detail, and it will be shown that a rough trail mechanism gives a good quantitative explanation of the variations in echo intensity, duration and range spread along the path of the meteor.

3. THE ANALYSIS OF A TYPICAL HEAD ECHO

(a) *Description of the echo*

The range–time variations of the echo observed by McKINLEY on 10 August 1953 are reproduced in Fig. 1 (McKINLEY, 1955). The broken curves *LSM* in the figure is the hyperbola which describes the range variations which would be followed by an echo from a region close to the meteor itself. The point *S* corresponds to the time at which the meteor crosses the perpendicular to the trail, and is the nearest point of approach at a range of 169 km. Over the length of path *L* to *C* the echo shows no spread in range or duration greater than the limitations imposed by the pulse length. Beyond *C*, however, the echo is extended in both

VOL. 22 1961

range and time. For example, when the meteor is at the point D the echo is spread in range by 5 km, showing that the reflecting region extends for a distance of 20 km back along the trail. The echo duration from a section of the trail near D is 1 sec, and in this time the meteor has travelled 60 km further along the track.

The characteristics of this echo will now be considered in greater detail.

(b) *Variation of echo duration along the path of the meteor*

In order to predict the variations of echo duration along the path of the meteor, the variations of electron line density α along the trail are required. The ionization curve for this particular meteor is not known, and the theoretical curve given by

$$\frac{\alpha}{\alpha_{max}} = \frac{9}{4} \cdot \frac{\rho}{\rho_{max}} (1 - \tfrac{1}{3}\rho/\rho_{max})^2 \qquad (1)$$

will therefore be adopted (HERLOFSON, 1947). ρ is the air density, and α_{max} the air density at the point of maximum linear electron density α_{max}. This equation represents the average behaviour of a bright meteor, although in any individual example there may be quite large irregular variations from the mean curve. It will be assumed that the echo duration is determined by the time taken for the ionization to diffuse below the critical electron density. The absolute height scale for the meteor is not known, but because of its high velocity (60 km/sec) and the low inclination of its path to the horizontal (15°), the height of maximum ionization is likely to be about 100 km. The attachment time constant above this height is greater than 100 sec (DAVIS *et al.*, 1959), and as the echo duration is less than this value except at one or two points, the loss of electrons by attachment to neutral molecules will be neglected.

Thus the echo duration from any point on the trail is given by

$$T \propto \frac{\alpha}{D} \propto \alpha\rho \qquad (2)$$

where D is the diffusion coefficient (GREENHOW, 1952), and substituting (2) in (1) gives for the echo duration from any point on the trail, relative to the maximum duration T_{max}

$$\frac{T}{T_{max}} = \frac{9}{4} (\rho/\rho_{max})^2 (1 - \tfrac{1}{3}\rho/\rho_{max})^2 \qquad (3)$$

The form of this curve as a function of height is shown in Fig. 2. Height is measured in units of the scale height H, relative to the point of maximum ionization P. The observed variations of echo duration with height, measured at a number of points along the meteor trail, are also shown in Fig. 2. The theoretical duration curve is fitted to the experimental points for values of $T_{max} = 200$ sec and $H = 7$ km. The observed profile is irregular, but even so the theoretical curve defines the height variation of echo duration quite closely. Thus below P the theoretical duration falls from 200 sec to zero in only half a scale height, while above P the duration decreases exponentially with height and the theoretical value falls to 0·1 per cent of T_{max} in approximately four scale heights. There is

good agreement between theory and experiment over this factor of 1000 in duration. Altogether the head echo was recorded up to an altitude of seven scale heights above P, but over much of the meteor path the duration could not be resolved. This is also in agreement with the theoretical curve, which shows that T falls from only 0·1 sec to 0·0004 sec between heights of $4H$ and $7H$ above P. Thus the process of diffusion readily explains the unresolvable duration of the head

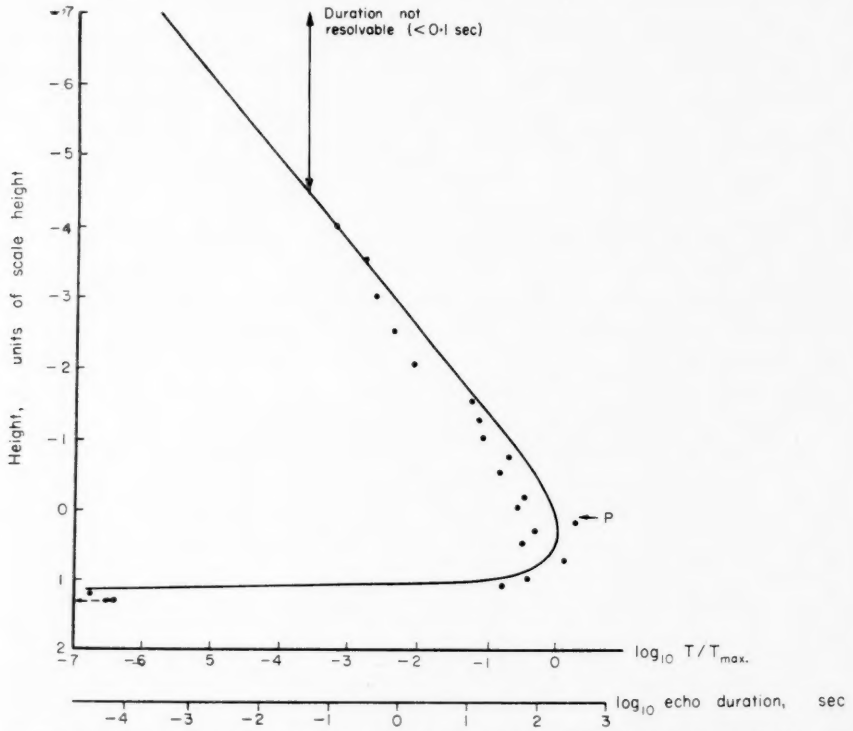

Fig. 2. The variation of echo duration T with height for a meteor following the theoretical ionization curve. Height is measured in units of the scale height H, relative to the point of maximum ionization. Log T/T_{max} is shown, where T_{max} is the maximum duration. ——— Some experimental measurements of the head echo duration for the meteor observed by MCKINLEY. The points are fitted to the theoretical curve for values of $T_{max} = 200$ sec and $H = 7$ km.

echo over the early part of the meteor trail, and yet permits durations up to several hundred seconds towards the end of the trajectory.

(c) *The spread in range of the echo*

The spread in range of the echo at any instant is determined by the length of trail behind the meteor in which the electron density is greater than the critical value, and by the aspect of the trail. Thus at the point where the echo first appears the ionization density remains greater than n_e for only 0·0004 sec (Fig. 2), and the length of the over-critically dense column can only be about 20 m for a meteor velocity of 60 km/sec. As the meteor is 20° from the specular point at this instant,

VOL. 22 1961

the range spread is reduced to only 0·3 of this value. This range difference could not be resolved with a transmitter pulse several kilometers in length, and the combined effect of the short persistence and narrow range spread is to give an echo which apparently moves with the meteor itself. On the other hand, at the point D (Fig. 1) lower down the trail, the ionization remains over-critically dense for 1 sec. In this time the meteor travels a further 60 km along its path, and an echo will now be received from this great length of trail. The long range edge of the echo will continue to extend with the line of sight component of meteor

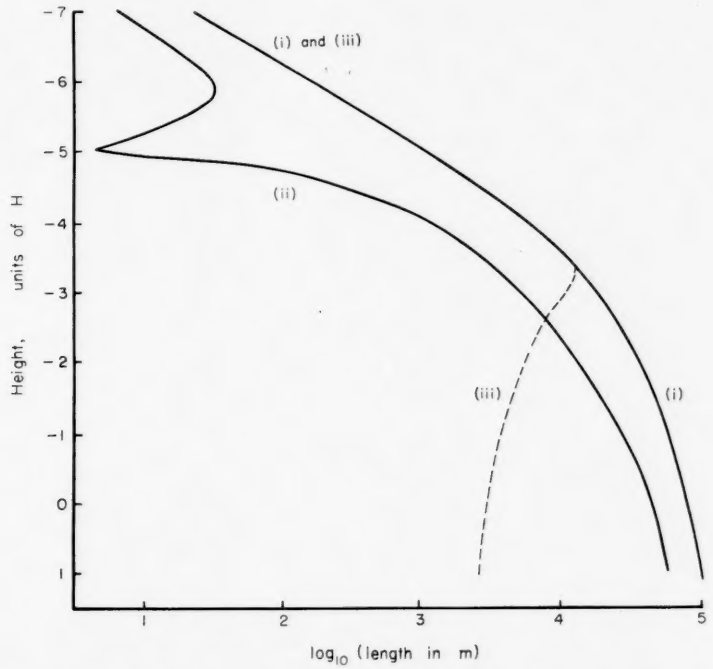

Fig. 3. Curve (i) The variation in length of the over-critically dense column of ionization behind the meteor, as a function of the height of the meteor. (ii) The spread in range of the echo. (iii) The length of the over-critically dense column contributing to the echo intensity.

velocity, while the much slower changes in range of the near edge are determined by the rate of diffusion of the ionization.

The length of the over-critically dense column behind the meteor, derived using the smooth duration curve in Fig. 2 and the velocity of the meteor, is shown for all positions of the meteor along its trajectory in Fig. 3(i). It can be seen that the length of the reflecting region varies between 20 m and 100 km. Distance along the trail has been converted to a range difference using the known aspect of the meteor track, and this is shown in Fig. 3(ii). The range spread increases from only 6 m when the echo first appears, to about 60 km near the end of the trail. The range variations of the front and back edges of the echo are superimposed on the experimental range time plot in Fig. 1. The echo duration obtained from any

point on the trail is also shown with this method of presentation. It can be seen that there is good agreement between the theoretical range–time envelope (*LSMNOC*) and the observed variations in echo duration and range.

(d) *The echo intensity*

(i) *The variation of echo intensity along the trail.* In order to determine the relative variations in echo intensity along the path of the meteor it will be assumed that α varies in the manner given by the theoretical ionization curve (equation 1). For a smooth trail the reflection coefficient is proportional to $\alpha^{\frac{1}{2}}$ (GREENHOW,

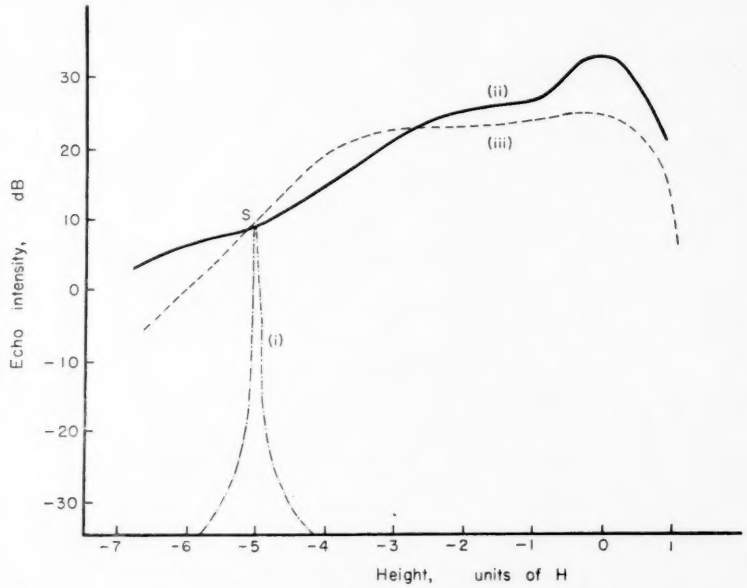

Fig. 4. The variation of echo intensity as a function of the height of the meteor. Curve (i) The diffraction head echo (BROWNE and KAISER, 1953). (ii) The observed intensity variations (MCKINLEY, 1955). (iii) The intensity variations given by the rough trail mechanism.

1952), and the changes in head echo intensity as the meteor trail is formed are given by diffraction theory (BROWNE and KAISER, 1953, curve (i) Fig. 4). The reflection is highly specular, and the intensity falls off extremely rapidly when the meteor is only a few Fresnel zones on either side of the perpendicular to the trail. The trails of faint meteors behave in this way. However, the variations in echo intensity due to the very bright meteor observed by MCKINLEY are given by the continuous curve (ii) in Fig. 4. There is no detectable enhancement as the meteor passes through the first Fresnel zone, and the echo intensity is actually a maximum when the meteor reaches a point corresponding to 40° off specular. It will therefore be assumed that the trail behaves as a rough reflector at a wavelength of 9 m, and that any short element of trail scatters almost isotropically.

If the scale of the irregularities is constant at all heights, the echo intensity at any instant will be proportional to the number of scattering centres N. N will

VOL. 22 1961

vary directly with the length of the critically dense column behind the meteor, up to the time when the range spread becomes equal to half the transmitter pulse length. Beyond this point the effective number of scattering centres is determined by the length of trail defined by this constant range difference. The length of trail which determines the echo intensity is shown by the curve (iii) in Fig. 3. The corresponding variations in echo intensity obtained by multiplying this length by a factor proportional to $\alpha^{\frac{1}{2}}$, to allow for the variations in trail radius and reflection coefficient, are shown by the broken curve (iii), Fig. 4. In view of the assumptions made about the shape of the ionization curve, and the scale of roughness along the trail, the form of the theoretical curve resembles the experimental measurements quite closely. An important feature of the theoretical curve is that the echo intensity is allowed to vary slowly as the meteor passes through the specular point, a maximum intensity being reached when the meteor is 40° off specular.

(ii) *Comparison of the echo intensity with that due to a smooth reflector.* If it is assumed that the height of maximum ionization is about 100 km, the value of α_{max} can be determined from the equation

$$\alpha = 4\pi D n_e T \tag{4}$$

(Greenhow, 1952). For $D \sim 10^5$ cm^2 sec^{-1}, and $n_e \sim 10^7$ cm^{-3}, $\alpha_{max} \sim 2 \times 10^{15}$ cm^{-1}. At the specular reflecting point, five scale heights above the position of α_{max}, equation (1) shows that $\alpha \sim 4 \times 10^{13}$ cm^{-1}. Substituting this value together with the parameters of the equipment used by McKinley, in the appropriate scattering equation (Greenhow, 1952), then shows that an echo about 45 dB above receiver noise should have been obtained. In fact the observed echo was only about 10 dB above noise. Near the specular region the over-critically dense length of trail is of the order of 1 km, about the same as the radius of the first Fresnel zone $[(R\lambda/2)^{1/2} \sim 850$ m]. This large discrepancy between the observed and predicted echo intensities is therefore a further clear indication that the meteor trail is behaving as a rough reflector. In order that the echo from 1 km of smooth trail should be reduced by 10^3 in intensity, it is necessary that the trail should be broken up into a large number of reflecting centres which scatter with random phases, instead of scattering in phase.

(e) *The energy liberated by the meteor*

The energy imparted to the surrounding air molecules as the meteor vaporizes can be estimated from a knowledge of the linear electron density and the probability of an evaporated meteor atom producing a free electron by collision processes. The probability of ionization is of the order of 0·1 (Greenhow and Hawkins, 1952), and for $\alpha = 2 \times 10^{15}$ cm^{-1} at the height of maximum ionization, about 2×10^{16} atoms cm^{-1} are liberated. These atoms are moving with velocities of 60 km sec^{-1} relative to surrounding air molecules, and the resultant loss of kinetic energy by the meteor is therefore 5×10^7 ergs cm^{-1}. 99 per cent of the energy is dissipated in raising the temperature of the air. The rest is used in the production of light and ionization. This is a very great influx of energy at meteor heights—the rate of injection being 5 W/cm in a small fraction of a second—and is sufficient to raise the temperature of all the air within a radius of 15 m of the meteor to over

2000°. A result of this rapid heating is likely to be the production of intense turbulence in the wake of the meteor, producing irregularities in the surface of the critically dense contour and causing the trail to behave as a rough reflector. As both the air density and α fall off approximately exponentially with height, the heating effect is almost independent of the distance along the meteor path.

In the case of meteors with $\alpha < 10^{12}$ cm^{-1}, which are known to behave as highly specular reflectors, the maximum increase in temperature over a radius of 2 m is less than 50°. The production of intense turbulence with a scale of this order is therefore unlikely.

4. HEAD ECHOES FROM SMOOTH METEOR TRAILS

The head echoes reproduced by HEY *et al.* (1947) appear to be of a different type to the majority of those published by MCKINLEY and MILLMAN. Thus, of the examples obtained during the Giacobinid meteor shower of 1946, all were extremely weak compared with the associated intense broadside echo, and showed no spread in either range or duration. These echoes appear to be true head echoes from the leading edge of an over-critically dense trail, as in a number of examples enduring echo components very much more intense than the weak head echo appeared at various points along the trail, a few tenths of a second after the passage of the meteor. This is approximately the time taken for an initially linear and smooth meteor trail to give an echo, other than from the specular region, due to large scale distortion of the trail by upper atmosphere winds (GREENHOW, 1952). Such echoes would be best explained by the diffraction mechanism, which must necessarily exist, but for the fact that they were observed only as the meteors approached the specular point. No examples of receding head echoes were recorded, which is a further major point of difference from the observations of MCKINLEY. A scattering mechanism is therefore required which enables a weak echo to be obtained as a meteor approaches the observer, but not as it recedes.

The heights of the echoes observed by HEY *et al.* were centred about 100 km, and recent measurements have shown that the initial radii of meteor trails in this region are 1–2 m (GREENHOW and HALL, 1960). As the head echoes were all associated with enduring body echoes, it is clear that these trails will behave as reflecting cylinders with radii of this order. At the front end of the trail immediately behind the meteor the diameter of the column falls to zero in some way, and if r_1 and r_2 are the two principal radii of curvature of the critically dense contour, an echoing area of the order $\pi r_1 r_2$ will be observed as the meteor approaches. For $r_1 \sim r_2 \sim 2$m the echoing area will be about 10 m^2, and as the equipment used by HEY *et al.* could detect an area of 1 m^2 at a range of 100 km, an effect of this type readily explains the approaching head echoes. This mechanism would not permit an echo to be obtained after the meteor has passed the point of closest approach to the observer.

DISCUSSION

The characteristics of certain types of "head" echoes from meteor trails have been considered on the basis of a rough trail reflecting mechanism. It has been shown that the magnitudes of the duration and range spread, and the variations of echo intensity along the track of a meteor, can be explained simply by the

VOL. 22 1961

normal processes controlling the production and decay of ionization in a meteor trail.

Head echoes vary widely in form. On occasions the echo may be spread in range and duration along the whole of the trail (McKinley, 1956), instead of only towards the end of the path as in the example discussed. On the other hand the echo may show either increasing or decreasing range changes only (Millman, 1959). These variations are readily explained by a rough trail mechanism. The duration and range spread of the echo at any instant depends primarily upon the initial linear electron density, and upon the appropriate values of the diffusion coefficient and attachment time constant. Echoes which show only increases in range correspond to orientations such that the specular point lies off the beginning of the trail, and similarly decreasing range changes only would be observed when the specular region falls beyond the end of the trail.

The trails of the very large meteors which give rise to head echoes ($\alpha_{max} \sim 2 \times 10^{15}$ cm^{-1}) thus show a lack of specular reflecting properties, as there is no enhancement in echo intensity as the first Fresnel zone is formed. Such trails therefore behave as rough reflectors. On the other hand it is well known that the trails of fainter meteors ($\alpha \geqslant 10^{12}$ cm^{-1}), which are highly specular reflectors for radio waves, must be comparatively smooth. A second head echo presented by McKinley (1955) is interesting as it lies in the transition region between these two extremes. Although the echo intensity varied smoothly along most of the trail, there was an enhancement of about 15 dB around the specular region. In this example, for which α_{max} is only about 10^{14} electrons/cm, the trail is only just becoming significantly rough at a wavelength of 9 m. In the examples given by Hey *et al.*, which are due presumably to even smaller meteors, the trails appear to be completely smooth and the head echo is obtained by a different mechanism.

Acknowledgements—Acknowledgement is made to the Controller, H.M. Stationery Office, for permission to publish this paper.

References

Browne I. C. and Kaiser T. R.	1953	*J. Atmosph. Terr. Phys.* **4,** 1.
Davies J. G. and Ellyett C. D.	1949	*Phil. Mag.* **40,** 614.
Davis J., Greenhow J. S. and Hall J. E.	1959	*Proc. Roy. Soc.* A **253,** 121.
Greenhow J. S.	1952	*Proc. Phys. Soc.* B **65,** 169.
Greenhow J. S. and Hall J. E.	1960	*Mon. Not. R. Astr. Soc.* **121,** 183.
Greenhow J. S. and Hawkins G. S.	1952	*Nature, Lond.* **170,** 355.
Herlofson N.	1947	*Rep. Progr. Phys.* **11,** 444.
Hey J. S., Parsons S. J. and Stewart G. S.	1947	*Mon. Not. R. Astr. Soc.* **107,** 176.
McKinley D. W. R.	1955	*Meteors,* p. 65. *J. Atmosph. Terr. Phys.* Spec. Suppl. No. 2.
McKinley D. W. R.	1956	*J. Atmosph. Terr. Phys.* **8,** 76.
McKinley D. W. R. and Millman P. M.	1949a	*Proc. Inst. Radio Engrs* **37,** 364.
McKinley D. W. R. and Millman P. M.	1949b	*Canad. J. Res.* **27,** 53.
Millman P. M.	1959	*J. Geophys. Res.* **64,** 2192.

Journal of Atmospheric and Terrestrial Physics, 1961, Vol. 22, pp. 74 to 78. Pergamon Press Ltd. Printed in Northern Ireland

RESEARCH NOTES

Ionospheric critical frequencies and magnetic parameters of the day before

(*Received* 12 *May* 1961)

IT has recently been shown (KING, 1961) that the mid-day values of f_0F2 appear to be related to the equivalent planetary daily amplitude, A_p, but that the relationship is much more definite if the A_p values of the days preceding the days on which f_0F2 were obtained are used. This time lag has been further investigated for pre-sunrise ionization using ionospheric data from Cape Town (34° 08′ S, 18° 19′ E), but, instead of using A_p as a measure of magnetic activity, the 3 hr K-indices from Hermanus (34° 25′ S, 19° 14′ E) were used. In this way both ionization and magnetic parameters were confined to the same locality. It should be pointed out that the pre-sunrise relationship between f_0F2 and A_p is a striking negative one in summer and a positive, but less pronounced, one during the 3 month mid-winter period (KING and GRAHAM, 1961).

Fig. 1(b) shows plots of the correlation between f_0F2 for 0300 and 0500 hours S.A.S.T. and the sum of the K-indices for different 24 hr periods, i.e. between f_0F2 for 0300 and 0500 hours and the sum of eight consecutive K-indices starting at different times. It is apparent that greatest correlation obtains with magnetic activity which occurred during the 24 hr

VOL. 22 1961

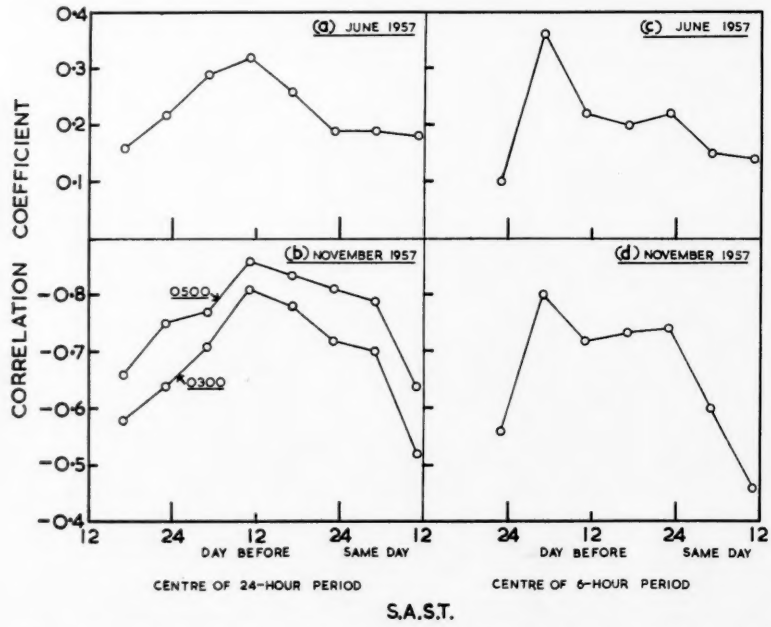

Fig. 1. Correlation between pre-sunrise f_0F2 and the sum of magnetic K-indices for various intervals.

period ending at 2300 hours on the previous day. The curves for 0300 and 0500 hours are very similar and in Figs. 1(a), (c) and (d) the mean data for these two curves is plotted. Fig. 1(a) contains data similar to Fig. 1(b) for June 1957. The correlation is slightly positive instead of strongly negative, in accordance with the seasonal effect mentioned above, but the same conclusion is apparent, viz. the period in which the most important magnetic activity occurred was the day preceding the day on which f_0F2 was measured.

In order to determine more accurately which period of magnetic activity is most strongly related to pre-sunrise ionization the next day, Figs. 1(c) and (d) were plotted showing the correlation between f_0F2 and the K-index for 6 hr periods (i.e. the sum of two 3 hr K-indices) having various centre points. It appears that the magnetic data during most of the previous day is important; there is a strong suggestion, however, that magnetic activity during the pre-sunrise period on the day before is most closely associated with f_0F2 on any day. Clearly magnetic activity during the pre-sunrise period on the same day is much less related to f_0F2 at that time.

Acknowledgements—The authors are indebted to the S.A.C.S.I.R. for supplying ionospheric data from Cape Town, and one of the authors (H. W. B.) is the recipient of a C.S.I.R. research grant. The magnetic data from Hermanus was supplied by the Union Magnetic Observatory.

H. W. Bergh
J. W. King

Department of Physics
University of Natal
Pietermaritzburg, South Africa

References

King J. W. 1961 *J. Atmosph. Terr. Phys.* **21,** 26.
King J. W. and Graham C. 1961 *J. Atmosph. Terr. Phys.* In press.

A note on the observations of twilight lithium emission made from Hallett Station*

(*Received* 23 *May* 1961)

Observations of quite strong twilight emission from atomic lithium were made in 1958 from two stations in Antarctica (Gadsden and Salmon, 1958; Delannoy, 1960). Subsequent searches from northern stations for this emission have met with partial success (Vallance Jones, 1959; Kvifte, 1959); the reported intensities have been of approximately the same order of magnitude as those reported by Delannoy and Weill (1958) at Dumont d'Urville Base during 1957 and 1958. The significant enhancement of lithium emission during August and September 1958 reported by Gadsden and Salmon and later, in more detail, by Delannoy (1960) was ascribed by Barber (1959) to residual debris from a thermonuclear device. Vallance Jones (1959) alternatively suggests a possible seasonal enhancement.

The spectrograph film records for 1959 from both Hallett Station and Scott Base, Antarctica, have now been examined and no lithium emission has been found during any month when suitable twilight exposures are possible. It seems probable, therefore, that any

* This work has been carried out with the assistance of a contract with the Air Force Cambridge Research Center, Bedford, Mass., U.S.A.

seasonal effect in lithium emission intensity is not large enough to account for the August/September 1958 observations. (The photograph of Fig. 1 indicates how plainly the lithium emission appeared on the spectrograms during these months.) Thus, BARBER's suggestion that the emission came from thermonuclear debris remains as a possible explanation of the marked enhancement.

The Hallett spectrograms have been microphotometered to yield the ratio of the emission intensity of lithium to that of sodium; the measurements were made near solar zenith distances of 98–100° and so refer to the "plateau" of intensity (DELANNOY, 1960). The absolute intensity of lithium emission cannot be obtained from the spectrograms because of the design of the instrument, which was to enable the collection of auroral synoptic data.

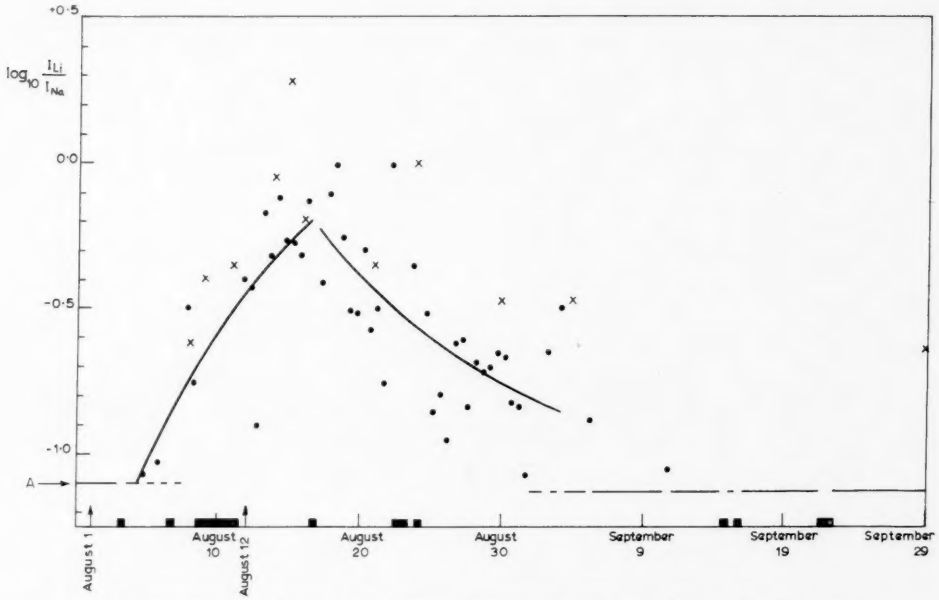

Fig. 2. Measurements of the relative intensity ratio plotted logarithmically. ● Measurements from Hallett Station; × Measurements from Dumont d'Urville Base (DELANNOY, 1960). A = Approximate minimal measurement level. ■ Indicates spectrograph not operating in twilight.

(The exposures, during twilight, were of only a few minutes in duration; the actual length of the exposure can be uncertain in some cases to as much as 50 per cent.) Furthermore, determination of the intensity ratio enables cloudy evenings to be used: this means an almost continuous set of determinations can be obtained. Similarly, reciprocity failure of the photographic emulsion may be ignored (JONES, 1954). The relative intensities were measured at three points along the geomagnetic meridan—at the zenith, and at a zenith distance of approximately 60°—and a mean taken to give a weighted mean intensity ratio. Since the sodium doublet was unresolved on the spectra, the sodium intensity refers to the sum of the doublet component intensities.

The measurements of the relative intensity ratio are plotted logarithmically in Fig. 2. Before 5 August and after 11 September no lithium emission was detected on the spectrograms and it is assumed that the ratio outside this period was less than approximately 0·08, the estimated minimum measurable ratio.

VOL. 22 1961

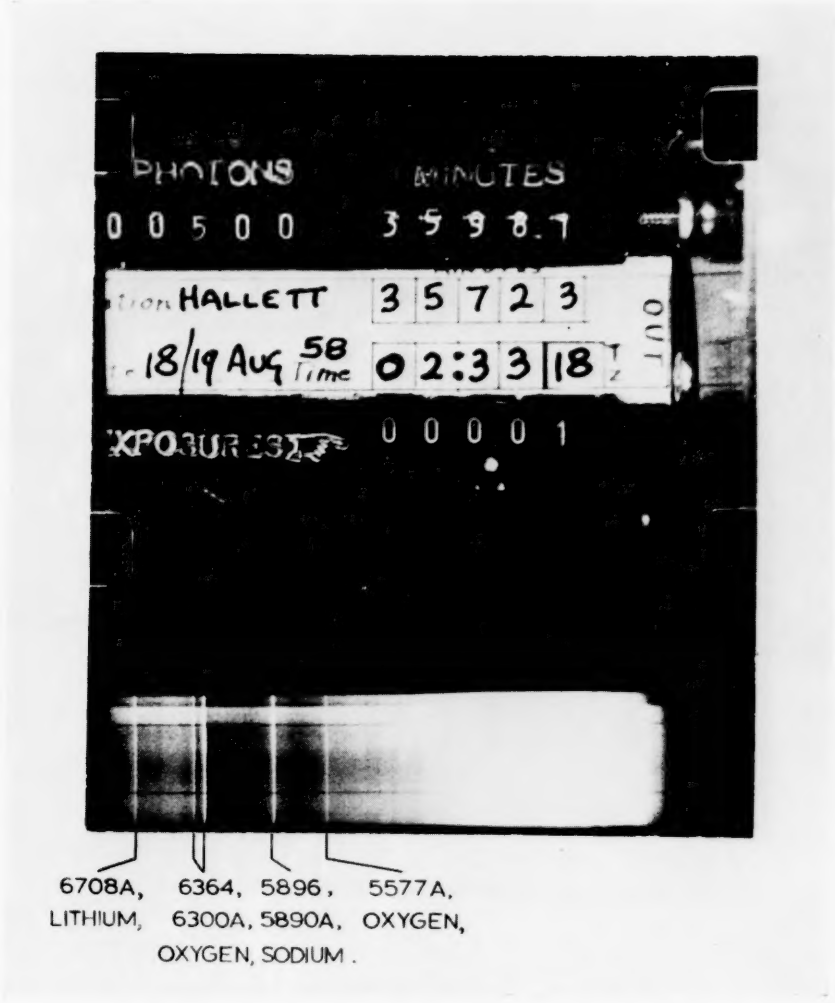

Fig. 1. Twilight spectrogram from Hallett Station 18 August 1958. In the direction perpendicular to the dispersion, the lower edge of the spectrogram corresponds to the northern horizon, the centre to the zenith, and the upper edge of the spectrogram to the southern horizon.

VOL.
22
1961

It will be seen that the intensity ratio rises fairly abruptly to a maximum around 16 August, thereafter falling a little less rapidly back below the measurable level. Also plotted in Fig. 2 are two curves, fitted by least squares to the data before and after 17 August. It will be noticed that no second broad maximum or definite change in the rate of decay after 17 August is detectable over the large scatter of the individual observations.

Changes in intensity ratio may be due to changes in the intensity of either the lithium emission or the sodium emission. Since the exposure duration from twilight to twilight is roughly constant, some indication of which intensity is affecting the intensity ratio so markedly may be given by comparing the correlation coefficients of the measured sodium or lithium intensities with the intensity ratios. These are found to be:

Sodium intensity with the intensity ratio:

$-0{\cdot}24$ (not significant according to Student's t-test)

Lithium intensity with the intensity ratio:

$+0{\cdot}70$ (highly significant according to Student's t-test).

It is thus suggested that the majority of the variation shown in the figure is due to a variation in the lithium emission intensity and not to a variation in the sodium emission intensity. This suggestion is supported by plotting, on the same scale, the observations of DELANNOY (1960); DELANNOY was using a spectrograph of dispersion 50 Å/mm and limited himself to observations of absolute intensity on eleven clear evenings during this period. His observations are shown in the figure as crosses; on these eleven evenings, he found the absolute intensity of sodium to be constant normally to within a factor of two, while the lithium intensity varies by more than a factor of ten. It is plain from Fig. 2 that DELANNOY's observations show a systematically greater intensity ratio (greater by a factor of approximately 1·9); this seems somewhat too great to be dismissed as due to differences in the reduction of the data. It may indicate a genuine station variation in the intensity of either or both of the lithium and sodium emissions.

In our original (1958) note on these observations, we deduce a possible variation in height of the lithium layer, relative to that of the sodium, from changes in the times at which the twilight enhancements of the lithium and sodium lines reached the zenith at Hallett Station. These times were easily deduced by visual measurement of the spectra since the exposure times were short enough to show the twilight enhancement advancing progressively across the sky. At the time of publication, microphotometer measurements of the spectra could not be made; the presence of great scatter in the relative intensity measurements suggests that these relative height estimates may quite easily be confused by patchiness of the emissions in the sky. Therefore, we suggest that, although conditions for a simple geometrical determination of relative height are good during August and September at Hallett, these measures are not given any weight.

It will be recalled that two thermonuclear devices were exploded by United States authorities at the beginning of August 1958; one on 1 August and the second on 12 August. Obviously, if the lithium emission is due to debris from these two bombs, the initial rise of the intensity ratio shown in the figure must be due to debris from the first explosion. The intensity ratio measures show that the second explosion cannot have produced similar effects. From magnetic and ionospheric data (MATSUSHITA, 1959) it has been suggested that the second explosion took place at a lower height than the first one. Later official information* gave the height of the 1 August explosion as 60 km and the 12 August explosion as 30 km. This difference in height may well account for the difference in the magnitude of the effects on the lithium emission intensity; in the absence of official information, it is equally possible that no lithium was involved in the second explosion. The debris-origin hypothesis

* Quoted by MATSUSHITA as *Time Magazine*, 29 June 1959, p. 56.

thus depends on a single coincidence in time. A second maximum in the intensity ratio measures, appearing close to 25 August would have provided strong confirmation of the hypothesis; the lack of a second maximum, in the absence of full information about the natures of the two explosions, indicates that the debris hypothesis must be regarded as not proven.

M. Gadsden
K. Salmon

D.P.L. Auroral Station
Private Bag
Omakau, New Zealand

References

Barber D. R.	1959	*Nature, Lond.* **183,** 384.
Delannoy J.	1960	*Ann. Géophys.* **16,** 236.
Delannoy J. and Weill G.	1958	*C.R. Acad. Sci., Paris* **247,** 806.
Gadsden M. and Salmon K.	1958	*Nature, Lond.* **182,** 1598.
Jones L. A.	1954	*The Theory of the Photographic Process,* (Ed. by C. E. K. Mees), p. 863. Macmillan, New York.
Kvifte G.	1959	*Nature, Lond.* **183,** 1384.
Matsushita S.	1959	*J. Geophys. Res.* **64,** 1149.
Vallance Jones A.	1959	*Nature, Lond.* **183,** 1315.

VOL.
22
1961

Journal of Atmospheric and Terrestrial Physics, 1961, Vol. 22, p. 79. Pergamon Press Ltd. Printed in Northern Ireland

BOOK REVIEWS

H. HEASTIE and P. M. STEPHENSON: **Upper Winds over the World,** Parts I and II. Geophysical Memoirs No. 103. H.M.S.O., London, 1960. 217 pp., 30s.

THIS volume is a revised and extended edition of the well-known Meteorological Office Publication, Geophysical Memoir No. 85, of the same title. Based on observational data for the period 1949–1953, it shows in a variety of ways mean winds for all parts of the world except Antarctica and is the most comprehensive work of its kind yet available.

Mean heights of selected isobaric surfaces up to 100 mb (about 15,000 m) are tabulated for latitudes 80°N to 60°S and, at each latitude, for longitudes at intervals of 20°. Mean contours of the isobaric surfaces are drawn on Mercator charts for latitudes 75°N to 70°S, and on circumpolar charts for latitudes 55°N to 90°N. These chart projections are also used to show streamlines and isotachs, while cross-sections are shown of mean zonal wind component and potential temperature from 1000 to 100 mb along selected longitudes. In all cases seasonal effects are illustrated by separate representation of the data for the months January, April, July and October.

The Memoir includes discussion of the sources of data, methods of reduction and representation, and the results obtained. The variability of the upper winds is to be dealt with in a separate volume (Part III).

D. H. MCINTOSH

F. S. G. BAYER: **Zyklen und Perioden in der Geophysik.** Editorial Universidad Catolica, Chile, 1960. 130 pp.

THIS account of the geophysical researches of the author is concerned mainly with meteorology, seismology and geomagnetism but strays also into biology. It is a book which presents a very personal view of the existence and causes of periodic or quasi-periodic phenomena and in which the scientific material is interspersed with autobiographical detail.

In almost all respects the author's findings are at variance with those generally accepted or even, one would have thought, established. In the few cases where suggested periods are well known the writer's views of the causes are yet unorthodox: for example, the 27-day recurrence tendency and semi-annual period in geomagnetic disturbance are attributed to lunar and not to solar influences.

The author is content to rely throughout on a graphical technique and to infer causal relationships from curve parallelism. It is a technique which must always fail to carry conviction: the more so in this case in which the results based on it are at odds with those of the many other workers who have used much more rigorous methods of investigation.

D. H. MCINTOSH

Journal of Atmospheric and Terrestrial Physics, 1961, Vol. 22, p. 80. Pergamon Press Ltd. Printed in Northern Ireland

Papers to be published in future issues

H. Unz: The effect of small values of $Z = \nu/\omega$ on the complex refractive index in the magneto-ionic theory

R. Raghava Rao and B. Ramachandra Rao: Study of horizontal drifts in the E-region at Waltair

Elisabeth Cooper: The properties of low frequency radio waves reflected from the ionosphere, calculated by the phase-integral method

M. Gadsden: The relative intensities of some nitrogen bands in auroral spectra

A. R. Thompson: Sweep frequency observations of meteor scatter bursts

S. Chapman and P. C. Kendall: An idealized problem of plasma dynamics that bears on geomagnetic storm theory; oblique projection

D. E. Shemansky and A. Vallance Jones: New measurements of the night airglow spectrum in the 1·5 μ region

J. Wolfe: 20 Mc/s w.w.v. bursts during the last few periods of 1958δ2

L. H. Heisler and J. D. Whitehead: The interpretation of $F2$ critical frequency measurements

G. H. Bazzard and C. M. Minnis: The geographical distribution of the harmonics of the annual variation in the critical frequency of the $F2$-layer at noon

T. Ondoh: Variations of the earth's exosphere and geomagnetic disturbances during the geomagnetic storm of 4 September 1958

G. S. Kent: High frequency fading of the 108 Mc/s wave radiated from an artificial earth satellite as observed at an equatorial station

J. E. Titheridge: The effect of collisions on the propagation of radio waves in the ionosphere

R. Naismith and P. A. Smith: Further evidence of a long term variation in the relationship of solar activity to the ionosphere

VOL.
22
1961

Journal of Atmospheric and Terrestrial Physics, 1961, Vol. 22, pp. 81 to 99. Pergamon Press Ltd. Printed in Northern Ireland

Study of horizontal drifts in the *E*-region at Waltair

R. Raghava Rao and B. Ramachandra Rao
Ionosphere Research Laboratory, Andhra University, Waltair

(*Received* 20 *March* 1961)

Abstract—Results of analysis of drift data for the *E*-region taken at Waltair over a period of 2 years are presented in this paper. The main features of diurnal and seasonal variation of drifts in the *E*-region at this low latitude station are compared with earlier results from high latitude stations. The 24 hourly drift vector is predominent in all seasons. This shows clockwise rotation in all seasons except summer. The 12 hourly drift vector is invariably smaller than the 24 hourly drift vector and shows clockwise rotation in all seasons. The steady component is generally directed towards SSE. The polar plots of 24 hourly and 12 hourly drift vectors show highly elliptical forms, the major axes being oriented nearly along E–W and N–S respectively. The results are compared with the winds deduced for *E*-region levels from S_q-variations.

1. Introduction

Considerable work has been done in recent years on the study of horizontal drifts in the different regions of the ionosphere using radio methods. Briggs and Spencer (1954) have reviewed the different methods employed for measuring ionospheric drifts and summarized the main results obtained up to the year 1954. Among the various radio methods available, the spaced receiver method of Mitra (1949) is widely used by several investigators for routine measurement of drifts. Systematic measurement of ionospheric drifts were made at Cambridge by using the spaced-receiver method over a number of years prior to the International Geophysical Year. Study of ionospheric drifts has been recognized as one of the major projects of the IGY and IGC programmes on ionospheric studies and it has recently been suggested that at least some stations should undertake a long range programme of drift studies covering a period of at least one sunspot cycle. Waltair (Geograph. lat. 17°43′N; Long. 83°18′E; Geomagn. lat. 7·4°N) is one of the few low latitude stations which has participated in the IGY and IGC programmes and is continuing these studies. The programme of drift measurements at Waltair actually started in the year 1954 by taking observations at a few selected hours during daytime, but this was intensified from the beginning of the IGY up to date by the initiation of round-the-clock observations for a period of at least 6 days in a month. The spaced-receiver method due to Mitra is used after modifying the recording technique by using a triple-beam oscillograph for taking drift records. The complete details about the experimental set-up and the preliminary results of drifts measurements obtained for the *E*- and *F2*- regions have been first reported by Rao *et al.* (1956). In a recent communication, Rao and Rao (1959) reported the results of analysis of *F1*- and *F2*-region measurements taken at Waltair for a period of over 2 years and discussed the essential differences in the behaviour of horizontal drifts at high and low latitude stations. The importance of the *E*-region drift measurements from Waltair cannot be over-emphasized as they form the first systematic study of drifts at a low latitude station. The results of a detailed study of *E*-region drifts for a period of 2 years from June 1957

to May 1959 which includes the IGY and part of the IGC periods are presented in this communication.

2. Some Experimental Details

Almost all the drift records were taken at hourly intervals on a frequency of 2·5 Mc/s for about 6–8 days in each month including about three consecutive World Days. All the observations refer to a virtual height range of 100–110 km. Drift records were not taken at times when there was either very slow or very fast fading and also when there was spreading of the reflected echo. As the observations were taken in the sunspot maximum period at a low latitude station, noon-time absorption was quite high and hence it was not possible to get useful records around noon-time on some days during the first year of observations. This difficulty was overcome during the second year by increasing the power of the transmitter from 2·5 to 3·5 kW and by increasing the height of the transmitting and receiving antennas nearer to the desired $\lambda/4$ height required for maximum efficiency. Previous investigators at high latitude stations experienced difficulty in getting sufficient number of drift records during the night-time due to the low critical frequency of the E-region. As the frequency of occurrence of E_s is quite high during night-time at this station, sufficient number of useful drift records could be obtained during night-time by lowering the frequency below the normal value of 2·5 Mc/s whenever fE_s is low. Out of about 3000 drift records taken during the period of 2 years, nearly one-fourth had to be rejected due to heavy noise and dissimilarity in the fading records. The remaining records are subjected to analysis by the usual similar fades method as described in the IGY manual.

VOL. 22 1961

3. Diurnal and Seasonal Variation of Drift Speeds

(*a*) *Results*

All the available observations of the E-region drift speeds taken over a period of the 2 years 1957–1959 are grouped together and a histogram of the percentage occurrence of the drift speeds against the corresponding range of drift speeds is shown in Fig. 1. It can be easily seen from this figure that the speeds generally fall in the range of 30–180 m/sec. The histogram shows a maximum of occurrence of drift speeds in the range of 60–105 m/sec. The histogram shows two peaks in the ranges of 60–75 and 90–105 m/sec. Hence the most probable drift speed may be taken as 83 m/sec which is also nearly the same as the average drift speed for all the observations leaving out extremely high and low values. It may be noted that drift speeds below 30 m/sec and above 150 m/sec are comparatively very rare.

With a view to studying the seasonal variation, if any, separate histograms are drawn for all the observations taken during the four seasons of the year. As there is not much variation in the histograms for the 2 years, the seasonal curves, for the year 1958–1959 only, are reproduced in Fig. 2. From the figure it is clear that the frequency of occurrence has a single maximum for all the seasons except winter for which two maxima are observed with a minimum in between. The maximum frequency of occurrence is found in the velocity range of 60–75 m/sec for the summer months. There is clear evidence for the shift of this maximum

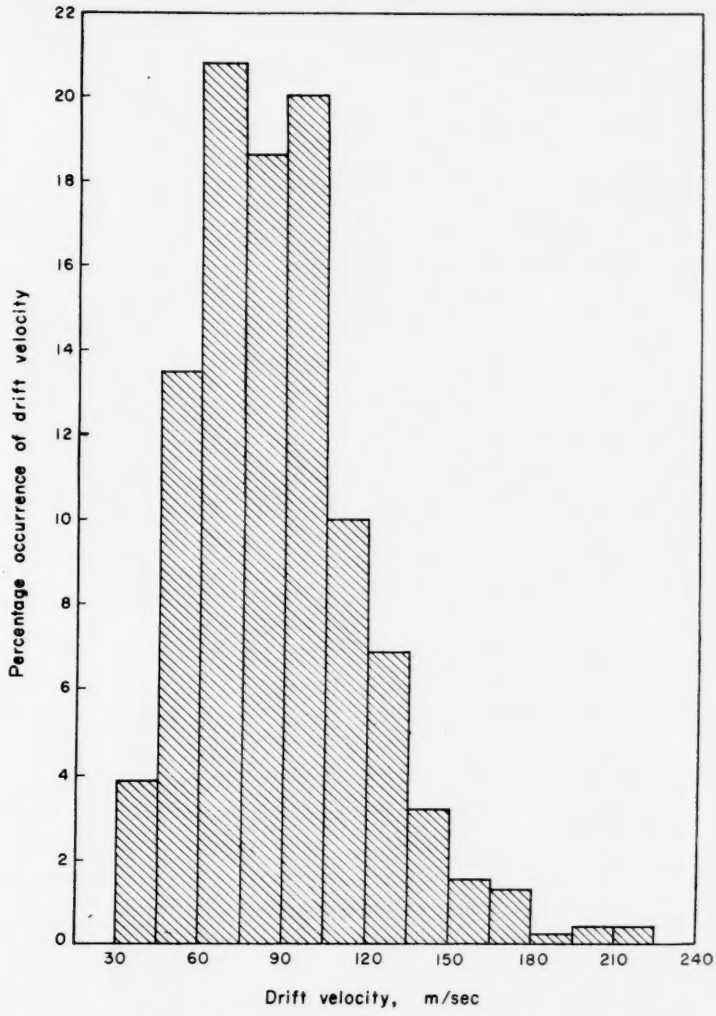

Fig. 1. Histogram of *E*-region drift speeds for the years 1957–1959.

to a higher velocity range of 75–90 m/sec in autumn and 90–105 m/sec in spring. During the summer, the frequency of occurrence rises rapidly from 30 to 70 m/sec and falls at a slow rate for higher velocity. The effect is less prominent for the autumn season. In the spring season, on the other hand, the percentage of occurrence of drift speeds rises slowly in the velocity range of 30–100 m/sec while it falls rather abruptly for higher values.

With a view to studying the seasonal changes in the difference between mean night-time drift speed and the mean day-time drift speed, the values of night-time and day-time drift speeds are averaged for each season in each year, excluding a few observations giving very high and very low values, and these are presented in

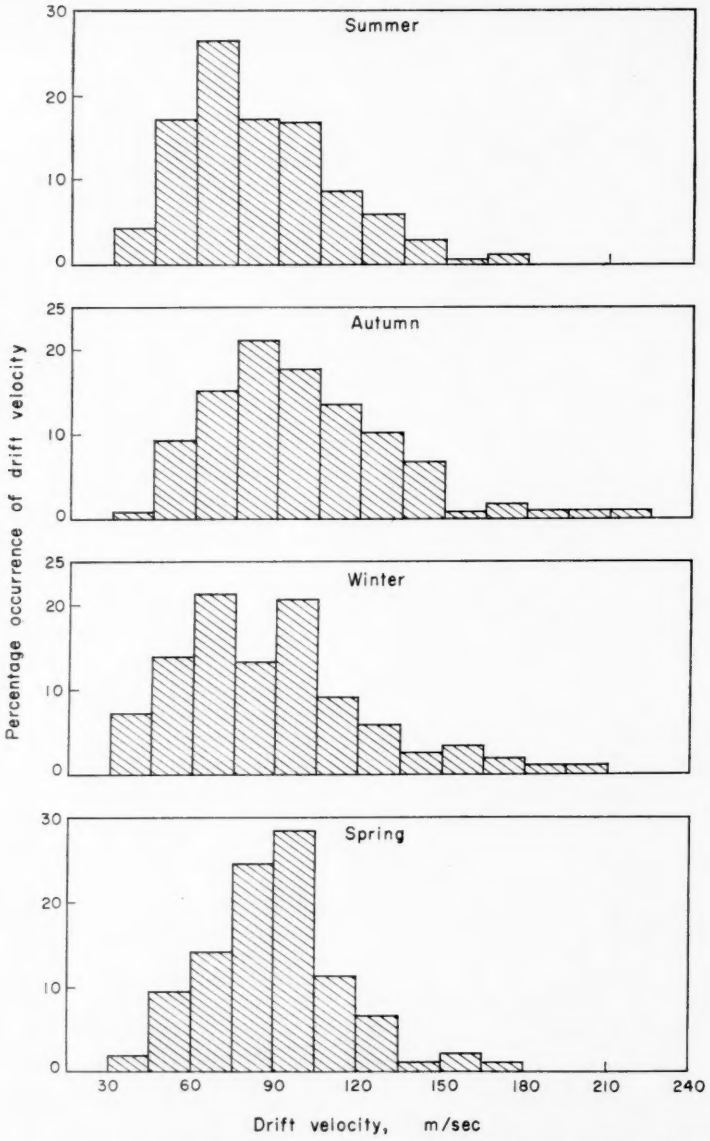

Fig. 2. Histograms of E-region drift speeds for different seasons.

Table 1 along with differences between the day and night values. Both in autumn 1957 and spring 1958 the night-time drift measurements are fewer in number than the corresponding day-time observations and as such there may be some amount of uncertainty in the night-time averages for these seasons as compared with the others.

It can be seen from this table that in all the seasons except autumn 1957 the

VOL. 22 1961

night-time average drift speed is higher than the day-time drift speed though the difference is not in general very high. This difference, as shown in the last column, is greater in summer than in the other seasons for both the years. The only exception to the general behaviour is noticed in autumn 1957, the day-time drift speed for which is higher than the night-time value. Even during autumn 1958, day-time average drift speed has almost the same value as that of night-time value, the difference being much less than that shown in other seasons for both

Table 1. Seasonal variation of day and night averages of E-region drift speeds

Season	Average drift speed during night (m/sec)	Average drift speed during day (m/sec)	Difference
Summer 1957	87·1	69·9	+17·2
1958	87·0	75·5	+11·5
Autumn 1957	83·9	93·5	−9·4
1958	88·4	87·0	+1·4
Winter 1957–1958	79·7	75·5	+4·2
1958–1959	86·2	81·2	+5·0
Spring 1958	83·3	79·8	+3·5
1959	89·4	82·3	+7·1
Yearly average			
1957–1958	83·3	81·7	+1·6
1958–1959	87·9	81·3	+6·6
Total average	86·0	81·0	+5·0

years. A possible explanation for this peculiar behaviour in this season is afforded by the predominant occurrence of the blanketing type of E_s in the month of August at this station giving rise to very high values of velocities during day-time. The frequency of occurrence of blanketing type of E_s is very high in the month of August for both these years and this feature has been noticed also during 1959. Since the data of August is included in the season, it appears that it has contributed a considerable number of high values for the day-time drift speeds in autumn. The reason for the difference being more prominent in 1957 may be partly due to lack of sufficient number of observations during night-time for all the 3 months in that season.

Comparing the variation of day-time average drifts from season to season for each year, it can be seen from the table that the summer values are miminum for both the years while the autumn values are maximum. It is well known that sporadic-E is very frequent at low latitudes particularly during summer months. In fact the sporadic-E occurrence at this latitude in summer months is almost as regular as normal E-layer at higher latitudes, showing a maximum of fE_s at noon. Generally patchy type of E_s is present during summer at this station.

But in August complete blanketing type of E_s occurs very frequently during day-time at this station. This may be partly responsible for the low velocities in summer and high velocities in autumn during daylight hours. The night-time average drift speed shows a regular seasonal variation with a minimum in winter and a maximum in summer months, the difference being quite prominent for the observations taken during 1957. In general the night-time average drift speed is always higher than the day-time average, this difference being quite significant for the observations of 1958–1959.

If the drift speeds of both day and night times for each year are averaged, it is found that the values are 81·2 and 83·6 for the years 1957–1958 and 1958–1959 respectively. There is thus a general trend of increase of drift speed from 1957–1958 to 1958–1959. Rao *et al.* (1956) obtained at this station an average drift speed of 65 m/sec for the E-region from observations taken during the year 1954. As the year 1954 is the sunspot minimum year, it may be easily seen that there is a general increase of drift speed in E-region with sunspot activity reaching almost a maximum during 1958.

With a view to studying the diurnal variation of drift speeds, the values of drift speeds obtained at hourly intervals are averaged for all days in each season and the resulting plot for all the seasons is shown in Fig. 3 along with the combined average for the year. A smoothed curve is also drawn to show the general trend of variation from day to night. A striking confirmation observed from this plot is the large day-to-night difference in drift speeds for summer, as noticed from Table 1. An interesting feature noticed for all the seasons is the occurrence of a minimum around midnight followed by a maximum which is strikingly prominent, particularly in autumn and spring. The time of occurrence of this maximum is earlier in summer and winter and later in autumn and spring. It may, however be noted that the average drift speed undergoes large fluctuations only during night-time, the range of variation being sometimes as much as 50 m/sec.

VOL. 22 1961

(b) Discussion

Krautkramer (1950) gave E-region drift speeds in the range of 25–200 m/sec with a most frequent value of about 90 m/sec. Phillips (1952) obtained drift speeds in the range of 10–200 m/sec for summer and 20–250 m/sec for winter, with a most frequent value of about 100 m/sec in winter and 70 m/sec in summer. Salzberg and Greenstone (1951) obtained 70 m/sec as the representative E-region drift speed for the year and this increased to 100 m/sec in winter. But Phillips and Salzberg and Greenstone did not separate the data for E- and F-regions. Chapman (1953) gave 80 m/sec as the most probable value of E-region drift speed. No appreciable difference in speed between day and night has been noticed by these workers. Summarizing all the available data on E-region drift speeds of previous workers from high latitude stations, Briggs and Spencer concluded that 80 m/sec may be taken as a representative value for E-region drifts and that the winter drifts speeds are higher than those of summer months. It can be easily seen that the most probable drift speed of about 83 m/sec observed at this latitude for the E-region compares favourably with the value of 80 m/sec reported for high latitude stations. But almost all the data on which Briggs and Spencer

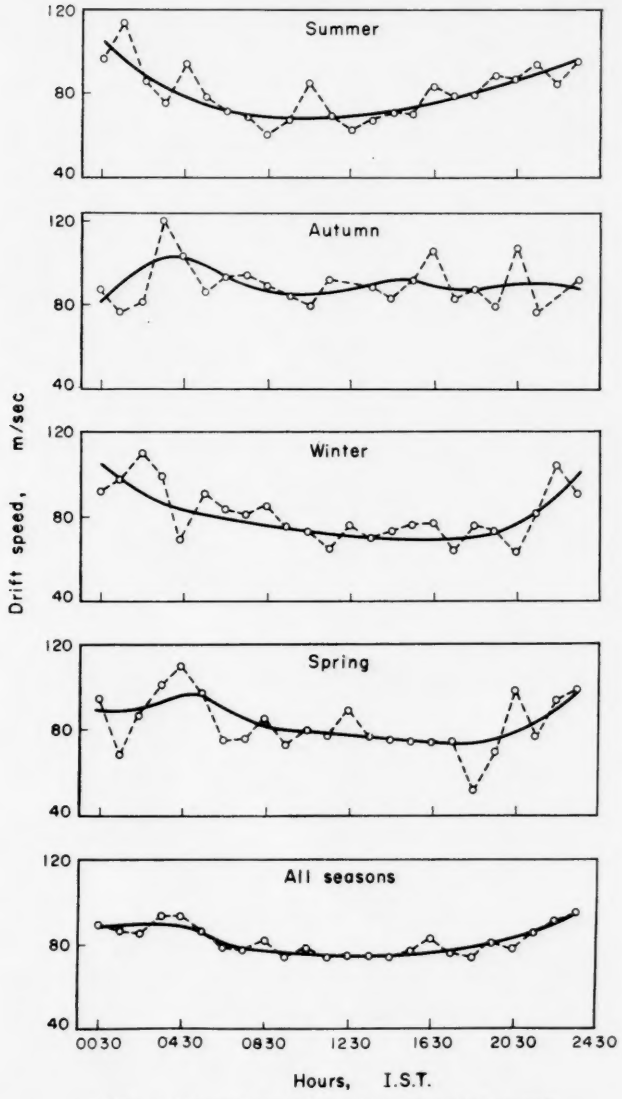

Fig. 3. Diurnal variation of E-region drift speeds.

based their conclusions were taken in the years round about the sunspot minimum period, and the value 80 m/sec, which was the average drift speed at high latitude stations, might have increased just as it happened here at Waltair during the sunspot of maximum period. The fact that the most probable drift speed in summer of about 67 m/sec is less than the most probable value in other seasons, is in agreement with a similar feature noticed by high-latitude workers. As the summer observations at Waltair refer mostly to E_s-layer drifts it will be interesting to compare the summer drift speeds with those obtained by HARVEY (1955) at Sydney.

Table 2. Results of harmonic analysis of E-region drifts for different months (t = local solar hour angle)

Month	N–S component	E–W component
June 1957	$-19{\cdot}5 + 24{\cdot}0 \sin (t + 29^\circ) + 36{\cdot}0 \sin (2t + 68^\circ)$	$+14{\cdot}5 + 73{\cdot}0 \sin (t + 70^\circ) + 39{\cdot}0 \sin (2t + 302^\circ)$
June 1958	$+15{\cdot}1 + 31{\cdot}0 \sin (t + 66^\circ) + 62{\cdot}0 \sin (2t + 97^\circ)$	$+29{\cdot}7 + 59{\cdot}0 \sin (t + 72^\circ) + 28{\cdot}0 \sin (2t + 81^\circ)$
July 1957	$-28{\cdot}8 + 3{\cdot}8 \sin (t + 282^\circ) + 28{\cdot}0 \sin (2t + 103^\circ)$	$-3{\cdot}5 + 69{\cdot}0 \sin (t + 74^\circ) + 32{\cdot}0 \sin (2t + 34^\circ)$
July 1958	$-29{\cdot}4 + 46{\cdot}0 \sin (t + 258^\circ) + 36{\cdot}8 \sin (2t + 87^\circ)$	$+12{\cdot}0 + 62{\cdot}6 \sin (t + 39^\circ) + 33{\cdot}7 \sin (2t + 3^\circ)$
Aug. 1957	$-58{\cdot}9 + 4{\cdot}1 \sin (t + 214^\circ) + 30{\cdot}0 \sin (2t + 99^\circ)$	$+1{\cdot}3 + 96{\cdot}0 \sin (t + 51^\circ) + 8{\cdot}0 \sin (2t + 44^\circ)$
Aug. 1958	$-59{\cdot}0 + 1{\cdot}1 \sin (t + 225^\circ) + 33{\cdot}0 \sin (2t + 94^\circ)$	$-2{\cdot}6 + 101{\cdot}0 \sin (t + 54^\circ) + 9{\cdot}5 \sin (2t + 349^\circ)$
Sept. 1957	$-21{\cdot}5 + 9{\cdot}0 \sin (t + 129^\circ) + 51{\cdot}5 \sin (2t + 134^\circ)$	$+0{\cdot}8 + 74{\cdot}5 \sin (t + 54^\circ) + 19{\cdot}0 \sin (2t + 332^\circ)$
Sept. 1958	$-8{\cdot}8 + 57{\cdot}5 \sin (t + 119^\circ) + 16{\cdot}1 \sin (2t + 145^\circ)$	$-4{\cdot}0 + 90{\cdot}0 \sin (t + 44^\circ) + 7{\cdot}8 \sin (2t + 284^\circ)$
Oct. 1957	$-23{\cdot}9 + 15{\cdot}0 \sin (t + 199^\circ) + 42{\cdot}0 \sin (2t + 82^\circ)$	$+12{\cdot}3 + 70{\cdot}3 \sin (t + 69^\circ) + 5{\cdot}6 \sin (2t + 284^\circ)$
Oct. 1958	$-14{\cdot}1 + 5{\cdot}2 \sin (t + 71^\circ) + 56{\cdot}0 \sin (2t + 68^\circ)$	$+24{\cdot}1 + 73{\cdot}0 \sin (t + 65^\circ) + 17{\cdot}0 \sin (2t + 252^\circ)$
Nov. 1957	$-12{\cdot}2 + 16{\cdot}0 \sin (t + 105^\circ) + 48{\cdot}0 \sin (2t + 44^\circ)$	$+13{\cdot}8 + 89{\cdot}0 \sin (t + 66^\circ) + 15{\cdot}0 \sin (2t + 232^\circ)$
Nov. 1958	$-26{\cdot}1 + 26{\cdot}0 \sin (t + 129^\circ) + 45{\cdot}0 \sin (2t + 43^\circ)$	$+19{\cdot}4 + 97{\cdot}0 \sin (t + 68^\circ) + 17{\cdot}5 \sin (2t + 225^\circ)$
Dec. 1957	$-17{\cdot}2 + 50{\cdot}0 \sin (t + 64^\circ) + 16{\cdot}0 \sin (2t + 38^\circ)$	$+5{\cdot}7 + 84{\cdot}0 \sin (t + 51^\circ) + 21{\cdot}0 \sin (2t + 18^\circ)$
Dec. 1958	$-14{\cdot}0 + 52{\cdot}6 \sin (t + 71^\circ) + 25{\cdot}7 \sin (2t + 19^\circ)$	$+8{\cdot}4 + 76{\cdot}4 \sin (t + 36^\circ) + 28{\cdot}0 \sin (2t + 335^\circ)$
Jan. 1958	$-10{\cdot}9 + 11{\cdot}4 \sin (t + 118^\circ) + 56{\cdot}4 \sin (2t + 2^\circ)$	$-0{\cdot}15 + 65{\cdot}0 \sin (t + 63^\circ) + 36{\cdot}9 \sin (2t + 359^\circ)$
Jan. 1959	$-19{\cdot}6 + 28{\cdot}0 \sin (t + 174^\circ) + 42{\cdot}0 \sin (2t + 14^\circ)$	$+10{\cdot}5 + 80{\cdot}2 \sin (t + 49^\circ) + 15{\cdot}0 \sin (2t + 326^\circ)$
Feb. 1958	$-22{\cdot}3 + 20{\cdot}0 \sin (t + 151^\circ) + 36{\cdot}0 \sin (2t + 54^\circ)$	$+11{\cdot}0 + 60{\cdot}0 \sin (t + 56^\circ) + 41{\cdot}0 \sin (2t + 340^\circ)$
Feb. 1959	$-14{\cdot}5 + 16{\cdot}7 \sin (t + 93^\circ) + 29{\cdot}5 \sin (2t + 21^\circ)$	$+21{\cdot}9 + 90{\cdot}2 \sin (t + 50^\circ) + 10{\cdot}0 \sin (2t + 285^\circ)$
Mar. 1958	$-33{\cdot}2 + 17{\cdot}0 \sin (t + 100^\circ) + 38{\cdot}0 \sin (2t + 92^\circ)$	$-9{\cdot}0 + 71{\cdot}0 \sin (t + 46^\circ) + 37{\cdot}0 \sin (2t + 346^\circ)$
Mar. 1959	$-25{\cdot}5 + 39{\cdot}0 \sin (t + 112^\circ) + 18{\cdot}5 \sin (2t + 92^\circ)$	$+7{\cdot}0 + 88{\cdot}0 \sin (t + 55^\circ) + 18{\cdot}5 \sin (2t + 1^\circ)$
Apr. 1958	$-9{\cdot}7 + 23{\cdot}0 \sin (t + 170^\circ) + 49{\cdot}0 \sin (2t + 54^\circ)$	$-4{\cdot}8 + 54{\cdot}0 \sin (t + 60^\circ) + 44{\cdot}0 \sin (2t + 333^\circ)$
Apr. 1959	$-27{\cdot}8 + 18{\cdot}0 \sin (t + 73^\circ) + 31{\cdot}0 \sin (2t + 104^\circ)$	$+11{\cdot}0 + 86{\cdot}0 \sin (t + 36^\circ) + 12{\cdot}0 \sin (2t + 317^\circ)$
May 1958	$-21{\cdot}8 + 3{\cdot}0 \sin (t + 228^\circ) + 53{\cdot}0 \sin (2t + 93^\circ)$	$-0{\cdot}13 + 84{\cdot}0 \sin (t + 50^\circ) + 19{\cdot}0 \sin (2t + 336^\circ)$
May 1959	$-12{\cdot}0 + 14{\cdot}0 \sin (t + 86^\circ) + 36{\cdot}0 \sin (2t + 107^\circ)$	$+10{\cdot}0 + 78{\cdot}0 \sin (t + 48^\circ) + 8{\cdot}0 \sin (2t + 312^\circ)$

HARVEY used a spaced-transmitter technique similar to MUNRO (1950) and obtained E_s drift speeds in the range of 40–80 m/sec with a most frequent value of 60 m/sec, which is of the same order of magnitude as the value obtained by us for summer months.

Curiously enough the most probable drift speed seems to be higher in spring at this latitude. Other workers have not reported any significant differences in day- to night-time values of drift speeds but it appears quite certain from results presented here that night-time values are generally higher than day-time values.

4. HARMONIC ANALYSIS OF E-REGION DRIFTS

(*a*) *Results*

With a view to examining the 24 and 12 hourly periodicities in the diurnal variation of E-region drifts, the north–south (N–S) and east–west (E–W) components of the drifts are plotted against the local time of observation. Points for the observations of all the days in each month are plotted in one graph, and a mean curve is drawn as judged by eye, following the methods employed by BRIGGS and SPENCER. The resulting curves thus obtained for all the 24 months are subjected to harmonic analysis to obtain the steady, 24 and 12 hourly components, and the results are presented in Table 2. With a view to studying the seasonal changes in the steady and periodic components of drift, seasonal average curves are obtained in the same manner as above by drawing mean curves through a plot of all the observations of the N–S and E–W components for each season. The diurnal variation curves of the N–S and E–W components thus obtained for all the four seasons in each year are presented in Figs. 4 (a) and (b). These curves are then subjected to harmonic analysis and the results thus obtained are presented in Table 3.

The following are the main conclusions drawn from a careful study of the seasonal curves of the N–S and E–W drift components and the results of the harmonic analysis of the monthly and seasonal curves:

(1) The N–S component is generally towards north for some hours around midnight and noon, the duration for which it is northward being 6–9 hr around midnight and 3–4 hr around noon. In general the N–S component changes over from north to south in the early morning hours. There will be again a midday reversal to north direction occurring around noon, the time of transition being different for different months. The change-over again from south to north occurs in the early part of the night at about 2100 hours in all seasons except summer.

(2) The E–W component is always towards east during the major part of the night and generally west during daytime. The eastward drift changes over to west generally at about 0900 hours. The change-over to east again occurs in the early part of the night around 2100 hours. This transition time is about the same as that of the N–S component from south to north. A prominent feature of the E–W curves is that they show a trend of 24 hourly variation, without, in general, any reversal of direction around noon as in the case of N–S components, though they show a small hump after noon in most of the curves, indicating a tendency towards eastward change.

(3) The steady component is significant, and the general range of variation

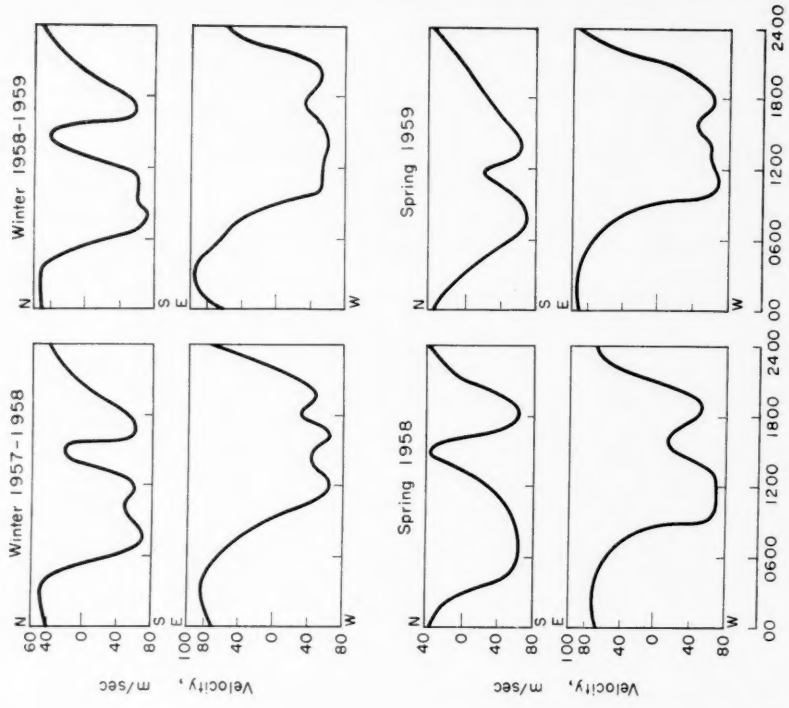

Fig. 4(b). Average diurnal variations of N–S and E–W components for winter and spring.

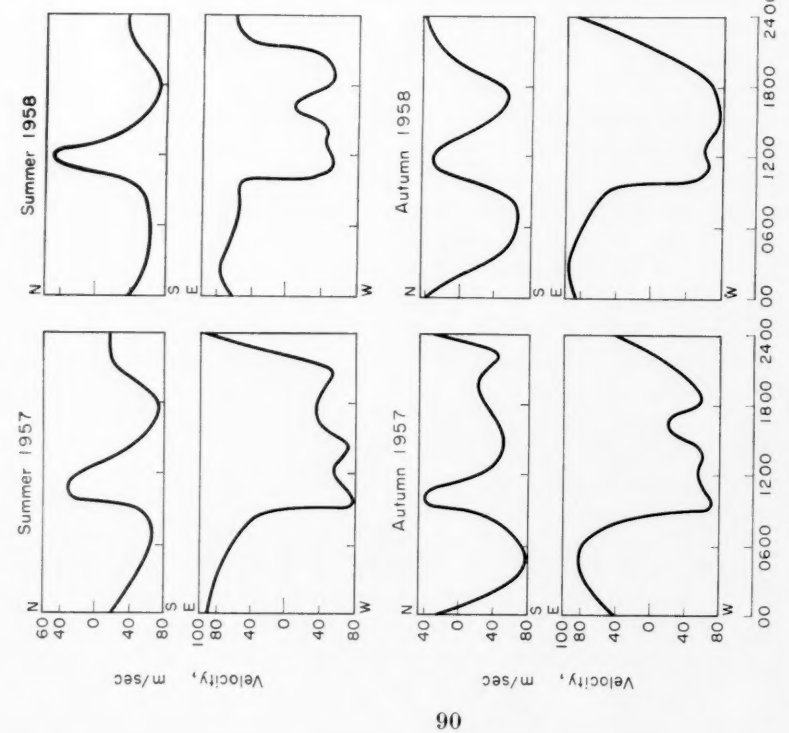

Fig. 4(a). Average diurnal variations of N–S and E–W components for summer and autumn.

VOL. 22 1961

is from 10 to 40 m/sec for the N–S components and 1–25 m/sec for E–W components. The steady component is invariably smaller than the amplitude of the 24 hourly component but is of comparable magnitude with the semi-diurnal amplitudes. The steady N–S component is very much larger than the amplitude of the semi-diurnal component in the months of August for both the years. The steady drift reaches minimum in winter and maximum in summer for both the years. The steady N–S component is always towards south and is, in general, higher than the steady E–W component except in four months. The steady component is directed predominantly towards SSE in all months and seasons.

Table 3. Results of harmonic analysis of E-region drifts for different seasons (t = local solar hour angle)

Summer 1957	(N–S)	$-37{\cdot}7 + 9{\cdot}0 \sin(t + 291°) + 39{\cdot}0 \sin(2t + 110°)$
	(E–W)	$+1{\cdot}5 + 79{\cdot}0 \sin(t + 46°) + 19{\cdot}0 \sin(2t + 342°)$
Summer 1958	(N–S)	$-46{\cdot}0 + 26{\cdot}0 \sin(t + 314°) + 32{\cdot}3 \sin(2t + 99°)$
	(E–W)	$+12{\cdot}0 + 74{\cdot}0 \sin(t + 34°) + 2{\cdot}7 \sin(2t + 81°)$
Autumn 1957	(N–S)	$-33{\cdot}3 + 8{\cdot}0 \sin(t + 199°) + 31{\cdot}0 \sin(2t + 130°)$
	(E–W)	$-2{\cdot}2 + 67{\cdot}0 \sin(t + 37°) + 29{\cdot}4 \sin(2t + 329°)$
Autumn 1958	(N–S)	$-19{\cdot}0 + 20{\cdot}0 \sin(t + 140°) + 47{\cdot}5 \sin(2t + 101°)$
	(E–W)	$+5{\cdot}4 + 99{\cdot}0 \sin(t + 39°) + 2{\cdot}4 \sin(2t + 352°)$
Winter 1957–1958	(N–S)	$-12{\cdot}9 + 45{\cdot}0 \sin(t + 85°) + 32{\cdot}0 \sin(2t + 40°)$
	(E–W)	$+4{\cdot}0 + 76{\cdot}0 \sin(t + 41°) + 15{\cdot}5 \sin(2t + 346°)$
Winter 1958–1959	(N–S)	$-7{\cdot}0 + 42{\cdot}0 \sin(t + 92°) + 39{\cdot}0 \sin(2t + 41°)$
	(E–W)	$+3{\cdot}2 + 78{\cdot}0 \sin(t + 42°) + 21{\cdot}3 \sin(2t + 346°)$
Spring 1958	(N–S)	$-20{\cdot}0 + 30{\cdot}5 \sin(t + 136°) + 41{\cdot}0 \sin(2t + 60°)$
	(E–W)	$+1{\cdot}1 + 71{\cdot}0 \sin(t + 57°) + 22{\cdot}0 \sin(2t + 344°)$
Spring 1959	(N–S)	$-24{\cdot}0 + 42{\cdot}0 \sin(t + 99°) + 18{\cdot}8 \sin(2t + 84°)$
	(E–W)	$+8{\cdot}2 + 78{\cdot}5 \sin(t + 42°) + 11{\cdot}6 \sin(2t + 1°)$

(4) The 24 hourly drift vector is invariably predominant in all months and hence in all seasons at this latitude. Its N–S component is invariably less than the E–W component, the difference between the two being quite large. Comparing the amplitudes of the N–S components for both the years, it will be noticed that these values are higher during 1958–1959 for all seasons except winter, for which season the values are nearly the same in both the years. Such an increase in the amplitude from the first to second year of observations is not shown by the E–W component. The ratio of E–W to N–S 24 hourly periodic components is generally very high in summer and autumn and is particularly prominent for the first year, 1957–1958. The phase difference between the N–S and E–W components is generally less than 180° in all months except June and July and hence in all seasons except summer for both the years. This indicates that the 24 hourly drift vector rotates in a clockwise direction in all seasons except summer for which the rotation is anti-clockwise. This can be seen from the polar plots of the drift vectors shown in Figs. 5 and 6. There is little difference between the winter and spring polar plots of the 24 hourly drift vector for both the years, the major axes being in an ENE direction in all cases. In summer and autumn the direction of the major axes are almost in an E–W direction.

(5) The semi-diurnal component of the drift vector is always less prominent

than the diurnal component at this latitude. Considering the N–S and E–W components of the 12 hourly drift vector, it can be easily seen from Tables 2 and 3 that the N–S component is invariably higher than the E–W component for the monthly and seasonal curves, with the exception of a few months when the E–W component amplitude is only slightly higher than the N–S component. The amplitudes of the E–W component are generally lower during 1958–1959 as compared with 1957–1958 except for winter. There is no consistent year-to-year increase or decrease in the

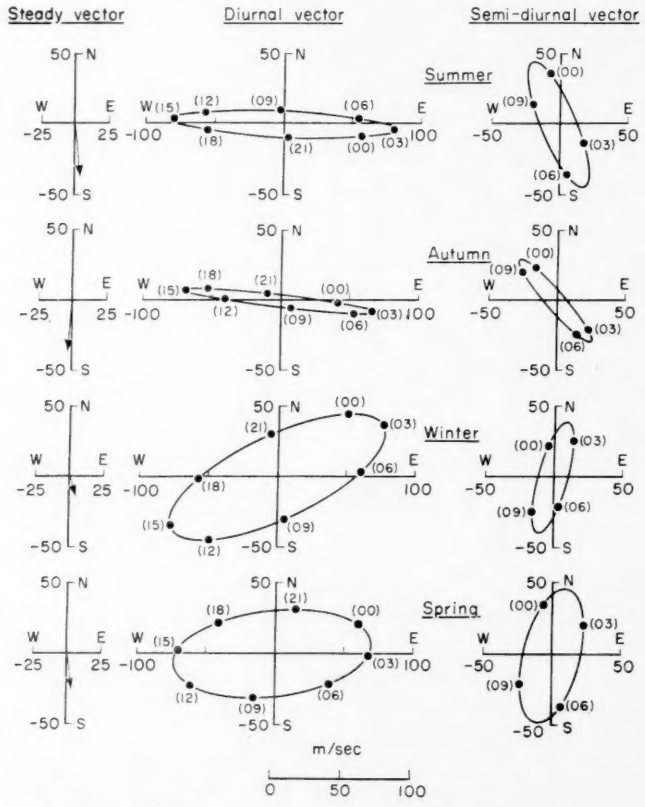

Fig. 5. Polar plots of the drift vectors in the *E*-region (1957–1958).

N–S component. During the year 1957–1958 the ratio of N–S to E–W components is generally lower, being of the order of 1 to 1·8, while during 1958–1959 the ratio is of the same order for winter and spring and very high for summer and autumn. The 12 hourly drift vector shows a clockwise sense of rotation in all seasons and in almost all months except September 1958. Polar plots of the 12 hourly drift vector, shown in Figs. 5 and 6 for all seasons, reveal clearly this clockwise rotation and high ratio of N–S to N–W component in summer and autumn 1958–1959 from the high elongation of the ellipses in a N–S direction. The polar plots for the same seasons during 1957–1958 show that their major axes are in N–W and S–E

VOL. 22 1961

directions. For winter and spring the major axes are almost in NNE and SSW directions for both the years.

(*b*) *Discussion of results of harmonic analysis*

It will be interesting to compare the results from this station with those reported from high latitude stations. Before we examine this aspect the following important difference regarding the data from Waltair and other high latitude stations may be noted. As the frequency of occurrence of E_s during night-time is

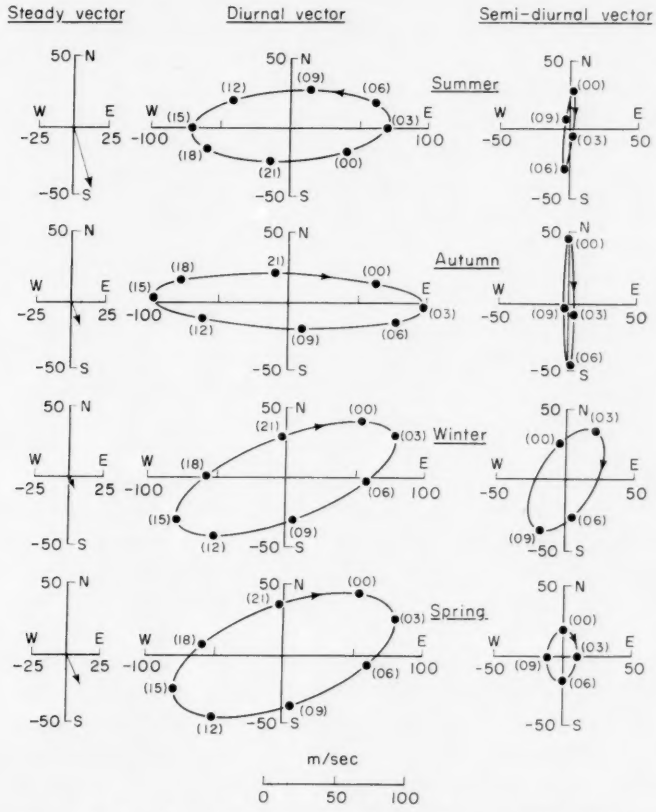

Fig. 6. Polar plots of the drift vectors in the E-region (1958–1959).

more at this station compared with the high latitude stations and as the observations for at least 6 days in each month are pooled together, sufficient number of points are available for drawing a smooth curve even for night-time hours. But as E_s occurs quite infrequently during night-time at high latitudes, those investigators have sometimes considered the night-time drift measurements on 2·4 Mc/s taken for $F2$-region reflections to be sufficiently influenced by the E-region to yield E-region drift data. This assumption of doubtful validity led to a certain amount of uncertainty in the diurnal variation curves of N–S and E–W components for high latitude stations.

Considering the Cambridge results, it appears that the steady component shows a systematic seasonal variation, the magnitude of drift being maximum in summer and the direction being towards NE in summer and SW in winter. The steady component, which is the same order as the 12 hourly component at Waltair, shows a systematic variation in magnitude only, with a maximum in summer and a minimum in winter. No systematic seasonal change in direction is observed at Waltair. Briggs and Spencer observed that the tendency of westward drift at noon gradually weakened from 1949 to 1952. A similar feature is noticed in the observation at Waltair which showed a tendency of eastward drift from year to year.

A major point of difference between the results of the present investigation and those obtained at the high latitude stations is the predominance of the 24 hourly components at this low latitude station while the 12 hourly component is reported to be the predominant one at high latitudes. Another peculiar result obtained in this study is the definite anti-clockwise sense of rotation of the 24 hourly drift vector in the summer season. As it is generally agreed that both in the *E*- and *F2*-regions the periodic component of the drift velocity vector rotates clockwise in the northern hemisphere and anti-clockwise in the southern hemisphere, it may be possible that at this low latitude the diffraction pattern has become highly elliptical in summer due to the regular occurrence of the patchy type of E_s, resulting in the radical distortion of the values of the drift velocities obtained here in that season due to high anisotropy of irregularities. It may be noted that the similar fades method gives reliable results for isotropic diffraction patterns. As there are no extensive observations from other low latitudes, these results on the 24 hourly harmonic could not be compared. However Skinner *et al.* (1958) reproduced a curve showing the diurnal variations of *E*-region drifts at Ibadan (Geogr. lat. 7°26′N; Geomagn. lat. 10·6°N). It is found that the diurnal variation curve of the E–W component at Waltair shows excellent agreement with this curve, both of them giving a transition from east to west at about 0800 hours. Night-time data was not available for Ibadan and it was reported that the N–S component is neglibly small.

Very few workers have reported the results for the 24 hourly component, but it was generally reported that the 24 hourly component is small compared with the 12 hourly component. But from Kjeller, a high latitude station, Harang and Pederson (1957) reported a higher value of the 24 hourly drift vector for summer compared with the 12 hourly component. Even the curve given for the variation of the E–W component in summer at Cambridge, by Briggs and Spencer shows predominantly diurnal behaviour. Using meteor trails for studying drift at a middle latitude station (Adelaide, Geogr. lat. 34°57′S; Geomagn. lat. 44·9°S) Elford and Robertson (1953) have reported that the 24 and 12 hourly components are of the same order of magnitude. It followed from the present investigation that the 24 hourly component is predominant compared with the 12 hourly component at a low latitude station. Examining the latitude-wise variation of relative magnitudes of 24 and 12 hourly components it appears that the 24 hourly component increases in amplitude from high latitude to low latitude in all seasons except summer. In summer it appears that the 24 hourly component is higher than the 12 hourly component at all latitudes.

VOL. 22 1961

The results of semi-diurnal harmonic analysis for N–S and E–W components at Waltair are shown in Table 4 along with those of other workers for the purpose of comparison. The following are the main points of comparison:

(1) The amplitudes of N–S and E–W components reported by BRIGGS and SPENCER from Cambridge are nearly of the same order of magnitude, while for Kjeller, HARANG and PEDERSON reported that the E–W component was very much larger than the N–S component in the 12 hourly drift vector. This feature is completely in disagreement with the results at Waltair.

Table 4. Solar 12 hourly harmonics for the *E*-region

Locality	Worker	N–S (m/sec)	E–W (m/sec)	Time	Year
Ottawa	CHAPMAN	34 sin ($2t - 10°$)	23 sin ($2t - 87°$)	Day-time	1950–1951
Cambridge	PHILLIPS	28 sin ($2t$)	28 sin ($2t - 90°$)	Day-time	1949–1951
Cambridge	BRIGGS and SPENCER	40 sin ($2t + 57°$)	45 sin ($2t - 78°$)	Winter	1949–1953
		30 sin ($2t - 30°$)	39 sin ($2t - 120°$)	Spring	
		6 sin ($2t - 66°$)	20 sin ($2t - 123°$)	Summer	
		16 sin ($2t + 30°$)	6 sin ($2t - 42°$)	Autumn	
Kjeller	HARANG and PEDERSON	14 sin ($2t - 7°$)	33 sin ($2t - 106°$)	Winter	1953–1955
		11 sin ($2t + 20°$)	33 sin ($2t - 104°$)	Spring	
		18 sin ($2t - 45°$)	38 sin ($2t - 103°$)	Summer	
		12 sin ($2t + 11°$)	23 sin ($2t - 59°$)	Autumn	
Waltair	Authors	39 sin ($2t + 41°$)	21 sin ($2t - 14°$)	Winter	1958–1959
		19 sin ($2t + 84°$)	12 sin ($2t + 1°$)	Spring	
		32 sin ($2t + 99°$)	3 sin ($2t + 81°$)	Summer	
		48 sin ($2t + 101°$)	2 sin ($2t - 8°$)	Autumn	

(2) The N–S and E–W components are both high at high latitude stations in winter, while no such consistent variation from season to season is noticed at Waltair.

(3) The 12 hourly drift vector showed clockwise rotation both at high and low latitude stations.

(4) At high latitudes the polar plots of the 12 hourly drift vector are nearly circular, while at low latitudes they are elliptical.

(5) The 12 hourly N–S component shows maximum northward drift at about 0300 and 1500 hours at Cambridge, while at Waltair the maximum occurs at 0000 and 1200 hours as can be seen from harmonic dials in Fig. 7. Thus the phase of drift vectors at Waltair differs by about 3 hr from that at high latitude stations.

(6) Cambridge results show that the 12 hourly drift vector for summer lags behind that of winter, in agreement with the theory of WILKES (1949), while at Waltair it is just the opposite as can be seen from the Fig. 7.

(*c*) *Comparison of* E- *and* F-*region drifts at Waltair*

The results of harmonic analysis of *F2* region drifts at Waltair, studied in about the same period as the present *E*-region drift results, were reported by RAO and

Rao (1959). It will therefore be interesting to compare the drift results in *E*- and *F*-regions at this station for almost the same period.

(1) The N–S and E–W components of the steady part of the drift are south and east respectively in all seasons for both *E*- and *F*-regions.

(2) The N–S component of the steady drift is greater than the E–W component in the *E*-region while the opposite is the case in the *F*-region. Thus the *E*- and *F2* region steady drifts are almost mutually perpendicular to one another, the former being towards south when the latter is towards east.

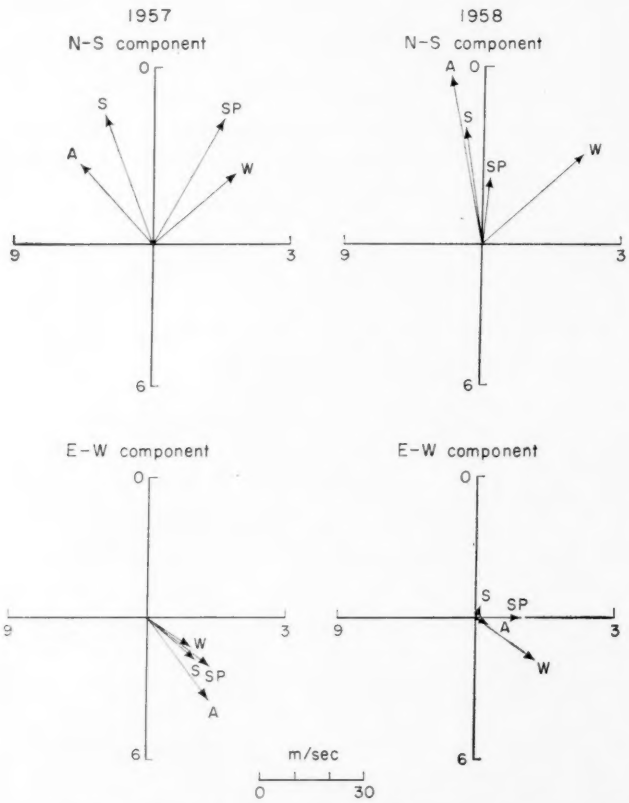

Fig. 7. Harmonic dials of the 12 hourly component. S–Summer, A–Autumn, W–Winter, SP–Spring.

(3) The magnitude of the steady component of the drift for the *F2* region is lower than that for the *E*-region. It reaches a maximum value for the *F2* region and minimum value for the *E*-region in winter.

(4) The predominant periodic component of the drift for both the *E*- and *F2* regions is the 24 hourly component.

(5) The rotation of the 24 hourly drift vector is clockwise for the *F2* region in all seasons, and for the *E*-region in all seasons except summer, when anti-clockwise sense of rotation is observed.

VOL. 22 1961

(6) The amplitudes of the N–S components of the 24 hourly drift vector are always lower than the amplitudes of E–W components. This may be due to the anisotropy of the diffraction contours which are elongated nearly along magnetic lines of force.

(7) The 12 hourly drift vector is generally very low for *F2*-region drifts, being about two to three times less than that for the *E*-region drifts.

(8) The rotation of the 12 hourly drift vector is clockwise for the *E*-region for all seasons, but for the *F2*-region the rotation does not seem to be regular in its behaviour. From the analysis of *F2*-region drift data takem during 1956–1957 and 1957–1958, the 12 hourly drift vector rotates anti-clockwise in winter season for both the years while it is clockwise for the remaining seasons in 1956–1957. During 1957–1958 the rotation is anti-clockwise for all seasons except summer.

(9) The N–S component of the 12 hourly drift vector is always greater than the E–W component for the *E*-region drifts, but no such consistent difference is noticed for the *F2*-region drifts.

(*d*) *Comparison with the theoretical results*

The motion of an irregularity in electron density relative to the surrounding ionized medium has been studied by MARTYN (1953) and later developed by CLEMMOW *et al.* (1955) for a two-dimensional model. KATO (1959) has studied recently the same problem for a three-dimensional model after making certain simplifying assumptions. He concluded that the movements of the irregularities are almost equal to that of the wind in the *E*-region on magnetically quiet days. Recently MAEDA (1959) has shown that in the lower ionosphere (*E*- and *D*-regions) the induced and electrostatic fields are nearly equally efficient in producing drift, and that the drift velocity due to these electric fields is negligible compared with the wind velocity. So it appears reasonable to assume that the layer drift in the *E*-region is almost the same as the air movements, at least on magnetically quiet days.

Attempts have been made to deduce the horizontal wind system in the ionospheric *E*-region from the dynamo theory of the geomagnetic S_q-variations by MAEDA (1955, 1957), HIRANO and KITAMURA (1956) and KATO (1956, 1957). In the last paper in this series, KATO (1957) has deduced the horizontal wind systems on both northern and southern hemispheres in the north solstice season taking into account the coriolis force. From this investigation, KATO concluded that in the northern summer the diurnal wind velocity is greater than the semi-diurnal, whereas in winter the velocity of the former is almost the same as that of the latter. The diurnal wind velocity is greater in summer than in winter and the semi-diurnal wind velocity is somewhat smaller in summer than in winter. The results of harmonic analysis of *E*-region drifts obtained experimentally at Waltair (Geomagn. lat. 7·4°N) are compared with the values for the nearest geomagnetic latitude of 10°N deduced by KATO, as shown in Table 5.

Although KATO's results show that the 24 hourly wind vector in summer is significantly higher than that in winter, no such difference has been observed at this station. However, the observed steady drift is considerably higher in summer

than in winter for both the years. But in his investigations KATO has not taken into consideration the steady winds.

The observed clockwise rotation of the semi-diurnal drift vector in all seasons is in agreement with the well-established conclusion that the semi-diurnal component of the wind rotates clockwise in the northern hemisphere. It is interesting to note from Table 5 that the observed maximum amplitude of the semi-diurnal drift vector is in fairly good agreement with the calculated magnitudes deduced

Table 5. Comparison of E-region drifts at Waltair with KATO's calculated values of winds from S_q variations

	KATO's calculated values	Observed values at Waltair				
	Summer	Summer	Autumn	Winter	Spring	Year
			Semi-diurnal			
Maximum magnitude (m/sec)	30	45	38	40	45	1957–1958
	—	32	46	40	18	1958–1959
Phase* (hours)	1130	0015	0100	0100	0030	1957–1958
	—	1130	1200	0030	1200	1958–1959
			Diurnal			
Maximum magnitude (m/sec)	66	80	67	82	75	1957–1958
	—	75	98	80	80	1958–1959
Phase* (hours)	2000	0900	2130	2115	2000	1957–1958
	—	1000	2130	2115	2115	1958–1959

* Phase shows the time when the drift vector is towards north.

by KATO. The observed time of 0030 hours when the semi-diurnal drift is generally towards north is in reasonable agreement with the calculated value of 1130 hours. From the wind system deduced by KATO, it is found that the N–S component of the semi-diurnal wind is higher than the E–W component by a factor of two. This calculated result is in excellent agreement with the observed ratio of the same order of magnitude between the N–S and E–W components of the semi-diurnal drift vector in all the seasons at this place. On the whole, there is fairly good agreement between observed and theoretical results for the case of the semi-diurnal drift vector.

Comparing the observed and calculated data for the 24 hourly component, the observed clockwise rotation of the drift vector in all seasons except summer is in agreement with the same sense of rotation from the calculations of KATO. It is interesting to see from Table 5 that the maximum amplitude of the observed diurnal component of drift is generally higher than the calculated values, but the

VOL. 22 1961

differences being not very high, the agreement may be considered as satisfactory. Considering the phase of the 24 hourly drift vector it will be seen that the observed and calculated values are generally in good agreement in all seasons except summer. Another feature of disagreement is in the relative magnitude of the E–W and N–S components. KATO's calculations show that the N–S component should be considerably higher than the E–W, but the observed polar plots of diurnal drift vector in Figs. 5 and 6 show exactly opposite behaviour, being particularly prominent in summer and autumn. This discrepancy may be partly due to the fact that the anisotropy of the diffraction contours suppress the N–S component of the drifts.

It may be noted that KATO's calculations of drifts are worked out for only periodic components and do not take into account the steady component of the wind. Even the periodic components obtained by him are on the basis of the assumption that electron density at night is 1/12 of that at noon. This may not be true, and to that extent the calculated results are uncertain.

Acknowledgement—We are indebted to the Council of Scientific and Industrial Research of India for financial support for these investigations.

REFERENCES

BRIGGS B. H. and SPENCER M.	1954	*Rep. Progr. Phys.* **17,** 245.
CHAPMAN J. H.	1953	*Canad. J. Phys.* **31,** 120.
CLEMMOW P. C., JONES M. A. and WEEKS K.	1955	*Proc. Ionosph. Conf.*, p. 136. Physical Society, London.
ELFORD W. G. and ROBERTSON D. S.	1953	*J. Atmosph. Terr. Phys.* **4,** 271.
HARANG L. and PEDERSON K.	1957	*J. Geophys. Res.* **62,** 183.
HARVEY J. A.	1955	*Austr. J. Phys.* **8,** 523.
HIRANO M. and KITAMURA T.	1956	*J. Geomagn. Geoelect.* **8,** 9.
KATO S.	1956	*J. Geomagn. Geoelect.* **8,** 24.
KATO S.	1957	*J. Geomagn. Geoelect.* **9,** 107.
KATO S.	1959	*Rep. Ionos. Space Res., Japan* **13,** 62.
KRAUTKRAMER J.	1950	*Arch. Elect. Ubertrag.* **4,** 133.
MAEDA H.	1955	*J. Geomagn. Geoelect.* **7,** 121.
MAEDA H.	1957	*J. Geomagn. Geoelect.* **9,** 86.
MAEDA H.	1959	*Rep. Ionos. Space Res., Japan* **13,** 79.
MARTYN D. F.	1953	*Phil. Trans.* A **246,** 306.
MITRA S. N.	1949	*Proc. Instn. Elect. Engrs* III **96,** 441.
MUNRO G. H.	1950	*Proc. Roy. Soc.* A **202,** 208.
PHILLIPS G. J.	1952	*J. Atmosph. Terr. Phys.* **2,** 141.
RAO B. R. and RAO E. B.	1959	*J. Atmosph. Terr. Phys.* **14,** 94.
RAO B. R., RAO M. S. and MURTY D. S. N.	1956	*J. Sci. Industr. Res.* A **15,** 75.
SALZBERG C. D. and GREENSTONE R.	1951	*J. Geophys. Res.* **56,** 521.
SKINNER N. J., HOPE J. and WRIGHT R. W.	1958	*Nature, Lond.* **182,** 1363.
WILKES M. V.	1949	*Oscillations of the Earth's Atmosphere.* Cambridge University Press.

Journal of Atmospheric and Terrestrial Physics, 1961, Vol. 22, pp. 100 to 104. Pergamon Press Ltd. Printed in Northern Ireland

The effect of small values of $Z = \nu/\omega$ on the complex refractive index in the magneto-ionic theory*

H. UNZ
Electrical Engineering Department, University of Kansas, Lawrence, Kansas

(*Received* 28 *April* 1961)

Abstract—The effect of small values of $Z = \nu/\omega$ on the general complex refractive index $n = \mu - i\chi$, which includes the magnetic field, is discussed by using McLaurin's expansion. It is shown that the refractive index μ varies only as Z^2 while the absorption coefficient χ varies as Z. For the particular case of no magnetic field the results are identical with the ones derived previously.

1. GENERAL

THE GENERAL complex refractive index n is given by the expression (RATCLIFFE, 1959, pp. 19, 37; APPLETON, 1932)

$$n^2 = 1 - X\left\{1 - iZ - \frac{\frac{1}{2}Y_T^2}{1 - X - iZ} \pm \left[\left(\frac{\frac{1}{2}Y_T^2}{1 - X - iZ}\right)^2 + Y_L^2\right]^{1/2}\right\}^{-1} \tag{1}$$

where

$$n = \mu - i\chi \tag{2}$$

where μ is the refractive index and χ represents the absorption.

A discussion of the effect of small values of Z has been given (APPLETON, 1932; RATCLIFFE, 1959, pp. 87–89) for particular cases. We are going to discuss here the effect of small values of $Z = \nu/\omega$ on the general complex refractive index; ν is the frequency of collision of electrons with heavy particles and ω is the angular wave frequency of the source. Let us rewrite equation (1) assuming that Z is the only variable quantity:

$$f(Z) = n^2 = 1 - \frac{X}{1 - iZ - \alpha \pm (\alpha^2 + Y_L^2)^{1/2}} \tag{3}$$

where

$$\alpha = \frac{\frac{1}{2}Y_T^2}{1 - X - iZ} = \alpha(Z).$$

Since we assume Z is small, we may expand (3) by McLaurin series in the form:

$$f(Z) = f(0) + Zf'(0) + \frac{Z^2}{2!}f''(0) + \cdots \tag{4}$$

where

$$f'(0) = \left.\frac{df(Z)}{dZ}\right|_{Z=0}, \qquad f''(0) = \left.\frac{d^2f(Z)}{dZ^2}\right|_{Z=0}.$$

From (3) we can write:

$$f(0) = 1 - X\left\{1 - \frac{\frac{1}{2}Y_T^2}{1 - X} \pm \left[\left(\frac{\frac{1}{2}Y_T^2}{1 - X}\right)^2 + Y_L^2\right]^{1/2}\right\}^{-1} \tag{5}$$

which is the result with no collision frequency ($\nu = 0$).

* This work has been supported in part by Contract No. DA-44-009 Eng.-3769 at the Midwest Research Institute, Kansas City, Missouri.

VOL. 22 1961

From (3) we can also get:

$$\frac{df(Z)}{dZ} = X\,\frac{-i - d\alpha/dZ \pm (\alpha d\alpha/dZ)(\alpha^2 + Y_L{}^2)^{-1/2}}{[1 - iZ - \alpha \pm (\alpha^2 + Y_L{}^2)^{1/2}]^2} \tag{6}$$

where

$$\frac{d\alpha}{dZ} = \frac{\frac{1}{2}Y_T{}^2 i}{(1 - X - iZ)^2} = \frac{i\alpha(Z)}{1 - X - iZ}.$$

From (6) we get:

$$f'(0) = \left.\frac{df(Z)}{dZ}\right|_{Z=0} = -iX\left\{1 + \frac{\frac{1}{2}Y_T{}^2}{(1-X)^2} \mp \left[\frac{(\frac{1}{2}Y_T{}^2)^2}{(1-X)^3}\right]\left[\left(\frac{\frac{1}{2}Y_T{}^2}{1-X}\right)^2 + Y_L{}^2\right]^{-1/2}\right\}$$
$$\times\left\{1 - \frac{\frac{1}{2}Y_T{}^2}{1-X} \pm \left[\left(\frac{\frac{1}{2}Y_T{}^2}{1-X}\right)^2 + Y_L{}^2\right]^{1/2}\right\}^{-2}. \tag{7}$$

Rearranging (7) we get:

$$f'(0) = -iX\,\{(1-X)^2 + \tfrac{1}{2}Y_T{}^2 \mp (\tfrac{1}{2}Y_T{}^2)^2[(\tfrac{1}{2}Y_T{}^2)^2 + (1-X)^2 Y_L{}^2]^{-1/2}\} \times$$
$$\times\left\{(1-X)^2\left(1 - \frac{\frac{1}{2}Y_T{}^2}{1-X} \pm \left[\left(\frac{\frac{1}{2}Y_T{}^2}{1-X}\right)^2 + Y_L{}^2\right]^{1/2}\right)^2\right\}^{-1}$$
$$= \frac{-iX\,\{(1-X)^2 + \frac{1}{2}Y_T{}^2 \mp (\frac{1}{2}Y_T{}^2)^2[(\frac{1}{2}Y_T{}^2)^2 + (1-X)^2\,Y_L{}^2]^{-1/2}\}}{\{1 - X - \frac{1}{2}Y_T{}^2 \pm [(\frac{1}{2}Y_T{}^2)^2 + (1-X)^2\,Y_L{}^2]^{1/2}\}^2}. \tag{8}$$

From (6) we might find now the second derivative:

$$\frac{d^2f(Z)}{dZ^2} =$$
$$= \frac{X\{-(d^2\alpha/dZ^2) \pm [(\alpha d^2\alpha/dZ^2) + (d\alpha/dZ)^2](\alpha^2 + Y_L{}^2)^{-1/2} \mp (\alpha d\alpha/dZ)^2(\alpha^2 + Y_L{}^2)^{-3/2}\}}{[1 - iZ - \alpha \pm (\alpha^2 + Y_L{}^2)^{1/2}]^2}$$
$$+ 2X\left[i + \frac{d\alpha}{dZ} \mp \frac{\alpha d\alpha/dZ}{(\alpha^2 + Y_L{}^2)^{1/2}}\right]\left\{\frac{-i - (d\alpha/dZ) \pm (\alpha d\alpha/dZ)(\alpha^2 + Y_L{}^2)^{-1/2}}{[1 - iZ - \alpha \pm (\alpha^2 + Y_L{}^2)^{1/2}]^3}\right\} \tag{9}$$

where

$$\frac{d^2\alpha}{dZ^2} = \tfrac{1}{2}Y_T{}^2\,\frac{-2}{(1 - X - iZ)^3} = \frac{-2\alpha(Z)}{(1 - X - iZ)^2}.$$

From (9) we get:

$$f''(0) = \left.\frac{d^2f(Z)}{dZ^2}\right|_{Z=0} =$$

$$= X\left\{\frac{Y_T{}^2}{(1-X)^3} \mp \frac{3(\frac{1}{2}Y_T{}^2)^2(1-X)^{-4}}{\{[\frac{1}{2}Y_T{}^2(1-X)^{-1}]^2 + Y_L{}^2\}^{1/2}} \pm \frac{[(\frac{1}{2}Y_T{}^2)^2(1-X)^{-3}]^2}{\{[\frac{1}{2}Y_T{}^2(1-X)^{-1}]^2 + Y_L{}^2\}^{3/2}}\right\}$$
$$\times\left\{1 - \frac{\frac{1}{2}Y_T{}^2}{1-X} \pm \left[\left(\frac{\frac{1}{2}Y_T{}^2}{1-X}\right)^2 + Y_L{}^2\right]^{1/2}\right\}^{-2}$$
$$+ 2X\left\{1 + \frac{\frac{1}{2}Y_T{}^2}{(1-X)^2} \mp \frac{(\frac{1}{2}Y_T{}^2)^2}{(1-X)^3}\left[\left(\frac{\frac{1}{2}Y_T{}^2}{1-X}\right)^2 + Y_L{}^2\right]^{-1/2}\right\}^2$$
$$\times\left\{1 - \frac{\frac{1}{2}Y_T{}^2}{1-X} \pm \left[\left(\frac{\frac{1}{2}Y_T{}^2}{1-X}\right)^2 + Y_L{}^2\right]^{1/2}\right\}^{-3}. \tag{10}$$

Rewriting (10) we get:

$$f''(0) = \frac{2X\{\frac{1}{2}Y_T{}^2 \mp [(\frac{1}{2}Y_T{}^2)^4 + \frac{3}{2}(\frac{1}{2}Y_T{}^2)^2 Y_L{}^2(1-X)^2][(\frac{1}{2}Y_T{}^2)^2 + (1-X)^2\, Y_L{}^2]^{-3/2}\}}{(1-X)\{1-X-\frac{1}{2}Y_T{}^2 \pm [(\frac{1}{2}Y_T{}^2)^2 + (1-X)^2 Y_L{}^2]^{1/2}\}^2}$$
$$+ \frac{2X\{(1-X)^2 + \frac{1}{2}Y_T{}^2 \mp (\frac{1}{2}Y_T{}^2)^2[(\frac{1}{2}Y_T{}^2)^2 + (1-X)^2 Y_L{}^2]^{-1/2}\}^2}{(1-X)\{1-X-\frac{1}{2}Y_T{}^2 \pm [(\frac{1}{2}Y_T{}^2)^2 + (1-X)^2 Y_L{}^2]^{1/2}\}^3}. \quad (11)$$

Substituting (5), (8), (11) in (4) we get the required expression.

2. No Magnetic Field

Let us discuss now a few particular cases. Let us assume first that there is no magnetic field $Y_L = Y_T = 0$. Then we get:

$$f(0) = 1 - X \quad (12a)$$
$$f'(0) = -iX \quad (12b)$$
$$f''(0) = 2X \quad (12c)$$

and from (12) and (4) we get:

$$f(Z) = (1-X) - iXZ + XZ^2 + \cdots \quad (13)$$

comparing with (3) with no magnetic field and small Z: $|Z| \ll 1$

$$f(Z) = 1 - \frac{X}{1-iZ} = 1 - X[1 + iZ + (iZ)^2 + (iZ)^3 + \cdots]$$
$$= 1 - X - iXZ + XZ^2 + \cdots \quad (14)$$

we see that (13) and (14) are identical. Since $f(Z) = n^2$ by assuming small Z we can write for X far from 1:

$$\begin{aligned} n &= \mu - i\chi \\ &\simeq [(1-X) - iXZ + XZ^2]^{1/2} \\ &= (1-X)^{1/2}\left(1 - \frac{iXZ}{1-X} + \frac{XZ^2}{1-X}\right)^{1/2} \\ &\simeq (1-X)^{1/2}\left[1 - \frac{iXZ}{2(1-X)} + \frac{XZ^2}{2(1-X)} + \frac{X^2Z^2}{8(1-X)^2}\right] \\ &= (1-X)^{1/2}\left[1 + \frac{XZ^2(4-3X)}{8(1-X)^2}\right] - \frac{iXZ}{2(1-X)^{1/2}} \end{aligned} \quad (15)$$

and we get for X away from 1:

$$\mu = (1-X)^{1/2}\left[1 + \frac{XZ^2(4-3X)}{8(1-X)^2}\right] \quad (16a)$$
$$\chi = \frac{XZ}{2(1-X)^{1/2}}. \quad (16b)$$

The results in (16) are identical with previous results (Appleton, 1932; Ratcliffe, 1959, pp. 87–89) for $X < 1$. It is interesting to notice in (16) that the collisions affect the refractive index only as to the second order Z^2 while they affect the absorption to the first order Z, except near $X = 1$.

VOL. 22 1961

Near $X = 1$ (15) will become:

$$n = \mu - i\chi \simeq (-iXZ + XZ^2)^{1/2} = (-iXZ)^{1/2}(1 + iZ)^{1/2}$$

$$\simeq (XZ)^{1/2}\frac{(-1+i)}{\pm\sqrt{2}}\left(1 + \frac{iZ}{2}\right) = \pm\left(\frac{XZ}{2}\right)^{1/2}\left(-1 - \frac{iZ}{2} + i - \frac{Z}{2}\right) \tag{17}$$

and from (17) we get near $X = 1$ for $|Z| \ll 1$:

$$\mu = \left(\frac{XZ}{2}\right)^{1/2}\left(1 + \frac{Z}{2}\right) \tag{18a}$$

$$\chi = \left(\frac{XZ}{2}\right)^{1/2}\left(1 - \frac{Z}{2}\right). \tag{18b}$$

Since (18) are near $X = 1$ let us substitute this value in (18) and we get

$$\mu^2 \simeq \chi^2 \simeq \frac{Z}{2} \tag{19}$$

which is identical with the result given by RATCLIFFE (1959, pp. 87–89). We see that both μ and χ near $X = 1$ are proportional to $\sqrt{Z}$ for small Z, as compared with other levels given by (16).

3. WITH MAGNETIC FIELD

Let us discuss now the case $Y_T = 0$ and $Y_L = Y$, i.e. the wave travels along the direction of the imposed steady magnetic field. We get from (5), (8) and (11):

$$f(0) = 1 - \frac{X}{1 \pm Y} \tag{20a}$$

$$f'(0) = -iX\frac{1}{(1 \pm Y)^2} \tag{20b}$$

$$f''(0) = +2X\frac{1}{(1 \pm Y)^3}. \tag{20c}$$

Substituting (20) in (4) we get:

$$n^2 = f(Z) = \left(1 - \frac{X}{1 \pm Y}\right) - \frac{iXZ}{(1 \pm Y)^2} + \frac{XZ^2}{(1 \pm Y)^3} + \cdots. \tag{21}$$

If we compare (21) with (13) we see that we have to introduce $X/(1 \pm Y)$ and $Z/(1 \pm Y)$ instead of X and Z respectively and we can continue with the same discussion as above. This has been mentioned by RATCLIFFE.

In case $Y_T = Y$, $Y_L = 0$, i.e. the wave normal is perpendicular to the imposed static magnetic field, we get from (5), (8) and (11):

$$f(0) = 1 - X\left(1 - \frac{\frac{1}{2}Y^2}{1 - X} \pm \frac{\frac{1}{2}Y^2}{1 - X}\right)^{-1} \tag{22a}$$

$$f'(0) = -iX\frac{[(1-X)^2 + \frac{1}{2}Y^2 \mp \frac{1}{2}Y^2]}{[(1-X) - \frac{1}{2}Y^2 \pm \frac{1}{2}Y^2]^2} \tag{22b}$$

$$f''(0) = +2X\frac{(\frac{1}{2}Y^2 \mp \frac{1}{2}Y^2)}{(1-X)(1-X-\frac{1}{2}Y^2 \pm \frac{1}{2}Y^2)^2} + \frac{2X[(1-X)^2 + \frac{1}{2}Y^2 \mp \frac{1}{2}Y^2]}{(1-X)(1-X-\frac{1}{2}Y^2 \pm \frac{1}{2}Y^2)^3} \tag{22c}$$

In this case again we will have to distinguish between the upper and lower signs, but the basic discussion will be quite similar.

In general we can rewrite (5), (8) and (11) as follows:

$$f(0) = 1 - Xg\,(X, Y) \tag{23a}$$

$$f'(0) = -iXp\,(X, Y) \tag{23b}$$

$$f''(0) = 2Xq\,(X, Y). \tag{23c}$$

Substituting (23) in (4) we get:

$$f(Z) = n^2 = [1 - Xg(X, Y)] - iXZp(X, Y) + XZ^2q(X, Y) + \cdots \tag{24}$$

and assuming a small Z we get for regular values of X: $(X \neq 1)$

$$n = \mu - i\chi = (1 - Xg)^{1/2}\left[1 - \frac{iXZp}{2(1 - Xg)} + \frac{XZ^2q}{2(1 - Xg)} + \frac{1}{8}\frac{X^2Z^2p^2}{(1 - Xg)^2}\right] \tag{25}$$

and from (25) we get:

$$\mu = (1 - Xg)^{1/2}\left\{1 + \frac{XZ^2}{8(1 - Xg)^2}[4q(1 - Xg) + Xp^2]\right\} \tag{26a}$$

$$\chi = \frac{Xp}{2(1 - Xg)^{1/2}}\,Z \tag{26b}$$

where (26) is our final result. The refractive index μ changes only with second order variation Z^2 while the absorption change, with the first order Z.

VOL. 22 1961

REFERENCES

APPLETON E. V. 1932 *J. Instn Elect. Engrs* **71**, 642, 649.

RATCLIFFE J. A. 1959 *The Magneto-Ionic Theory and its Applications to the Ionosphere.* Cambridge University Press.

Journal of Atmospheric and Terrestrial Physics, 1961, Vol. 22, pp. 105 to 121. Pergamon Press Ltd. Printed in Northern Ireland

The relative intensities of some nitrogen bands in auroral spectra

M. GADSDEN
D.P.L. Auroral Station, Omakau, New Zealand

(*Received* 5 *May* 1961)

Abstract—Published measurements of the relative intensities of the nitrogen second positive bands emitted from aurorae are reviewed and are found to be reasonably consistent with electron excitation of either neutral or ionized nitrogen molecules. Details of measurements made from a station, Scott Base, well within the southern auroral zone are presented and discussed. The measurements indicate clearly that electron excitation cannot be the main cause of the second positive emission observed from this station. An ionic charge exchange reaction is examined and appears likely to give rise to the population rates observed. Some consequences of the occurrence of this reaction are discussed, including the requirement that the electron density is very low during polar blackouts in regions of the atmosphere at or above the *E*-region.

ONE of the molecular band systems prominent in many spectra of the aurora is the second positive group of nitrogen. These bands, arising from the $C^3\pi - B^3\pi$ transition in the neutral nitrogen molecule, have been measured by several observers (see below) and transition probabilities for the various vibrational levels of the $C^3\pi$ state are available (BATES, 1949; NICHOLLS, 1956). Furthermore, BATES gives relative probabilities for excitation of the nitrogen molecule to the $C^3\pi$ level by electron impact with either the $N_2^+X^2\Sigma$ level or the $N_2X^1\Sigma$ level. Thus, information is available that enables quite definite analyses of intensity measurements to be made.

DISCUSSION OF PUBLISHED MEASUREMENTS

The published relative intensities of the $2PG$ bands may be tested for consistency by plotting the logarithms of the observed intensities against the logarithms of the transition probabilities weighted by the factor λ^{-4}, where λ is the wavelength of a particular band. NICHOLLS' data on relative transition probabilities, weighted by the λ^{-4} factor, are given in Table 1. If $I_{v'v''}$, $P_{v'v''}$ are the intensity and relative transition probability of the $(v' - v'')$ band and $N_{v'}$ is the population of the v' level of the upper state, then

$$I_{v'v''} \propto \frac{P_{v'v''}}{\lambda^4_{v'v''}} \cdot \frac{N_{v'}}{\sum_{v''}(P_{v'v''}/\lambda^3_{v'v''})}$$

or

$$\log I_{v'v''} = \log \frac{kN_{v'}}{\sum_{v''}(P_{v'v''}/\lambda^3_{v'v''})} + \log \frac{P_{v'v''}}{\lambda^4_{v'v''}}.$$

Since N_i is common to all the $(i - v'')$ bands and k is a constant for all the bands (since it depends on the geometry of the optical system used for the observations), a plot of $\log I_{v'v''}$ against $\log (P_{v'v''}/\lambda^4_{v'v''})$ should give a straight line for each value of v'; the slope of the lines should be unity and the intercepts will be given by $\log [kN_{v'}/\sum_{v'}(P_{v'v''}/\lambda^3_{v'v''})]$. The relative populations of the v' levels may be deduced

from the differences of the intercepts; the main value of the log $I_{v'v''}$ − log $(P_{v'v''}/\lambda^4_{v'v''})$ plot is, however, to check the observed values of $I_{v'v''}$ for consistency. With the low dispersion of spectrographs used in auroral studies and the difficulties of allowing for atmospheric absorption and overlapping of the $2PG$ bands by other auroral emissions, the observed values of $I_{v'v''}$ may show considerable errors. Such errors, unless recognized, may lead to quite misleading values of relative populations of the v' levels.

Table 1

v' \ v''	0	1	2	3	4	5	6	7	8	9	$\sum^{*}_{v''} \frac{P_{v'v''}}{\lambda^3_{v'v''}}$
0	1·000	0·616	0·226	0·068	0·018	0·004					1·000
1	0·979	0·050	0·403	0·205	0·062	0·019	0·0072				0·854
2	0·134	0·814	0·080	0·125	0·266	0·195	0·091	0·031	0·012		0·880
3	0·050	0·654	0·434	0·271		0·157	0·205	0·118	0·050	0·019	0·954
4		0·151	0·745	0·136	0·359	0·045	0·054	0·142	0·135	0·070	0·878

* Relative to unit sum for the $v' = 0$ sequence

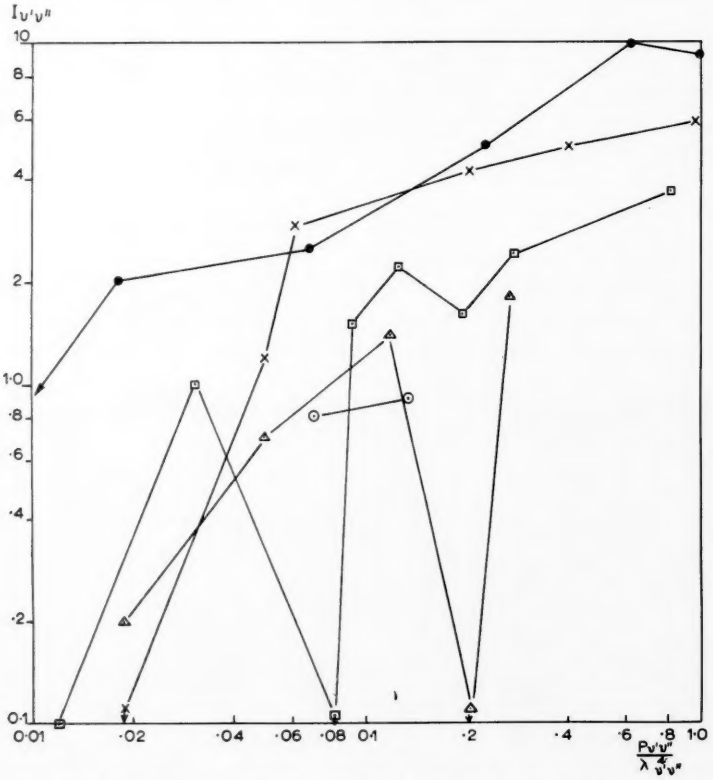

Fig. 1(a) ●, $v' = 0$; ×, $v' = 1$; ⊡, $v' = 2$; △, $v' = 3$; ○, $v' = 4$.

VOL. 22 1961

VEGARD (1956) has given the results of measurement of spectra obtained at Tromsö, the relative intensities of thirty N_2,$2PG$ bands being tabulated as the mean results of several spectra. In Fig. 1(a) these relative intensities are plotted against $P_{v'v''}/\lambda^4_{v'v''}$ It is seen that there is little resemblance, for lines of a given v' value, to straight lines of unit slope and it is impossible to deduce relative populations of the v' levels. OMHOLT (1954) has used some earlier results of VEGARD (1933), and has deduced that the relative populations of the $v' = 0$, 1, 2 levels are

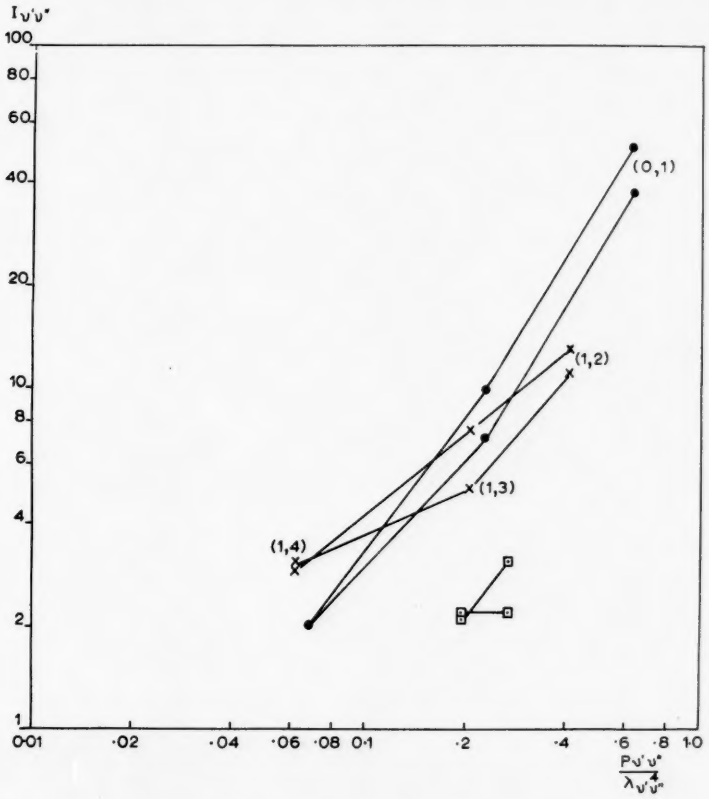

Fig. 1(b). ●, $v' = 0$; ×, $v' = 1$; ⊡, $v' = 2$.

$N_0:N_1:N_2 = 1{\cdot}0:0{\cdot}6:0{\cdot}35$. These values were obtained by considering four Δv = constant sequences separately and are probably not reliable to better than 50 per cent. In a later paper, OMHOLT (1955) gives the results of measurements of two spectra taken at a zenith distance of 60°. No correction for atmospheric extinction has been applied, and, considering Δv sequences as before, he derives the mean relative population rates

$$N_0:N_1:N_2 = 1{\cdot}00:0{\cdot}56:0{\cdot}33.$$

His measures of relative intensity are plotted in Fig. 1(b) for both spectra.

The (0, 1) band is presumably overlapped (as OMHOLT remarks) by the (1, 0)

NG band and its intensity should be disregarded. It is seen, also, that the intensity of the (1, 4) band is anomalously high and should be disregarded. Using NICHOLLS' transition probability the two spectra give $N_0:N_1:N_2 = 1{\cdot}00:0{\cdot}70,\ 0{\cdot}70:0{\cdot}24,\ 0{\cdot}34$.

PETRIE and SMALL (1952, 1954) give the relative intensities of the $2PG$ bands which are plotted in Fig. 1(c). These observations have been fully corrected for

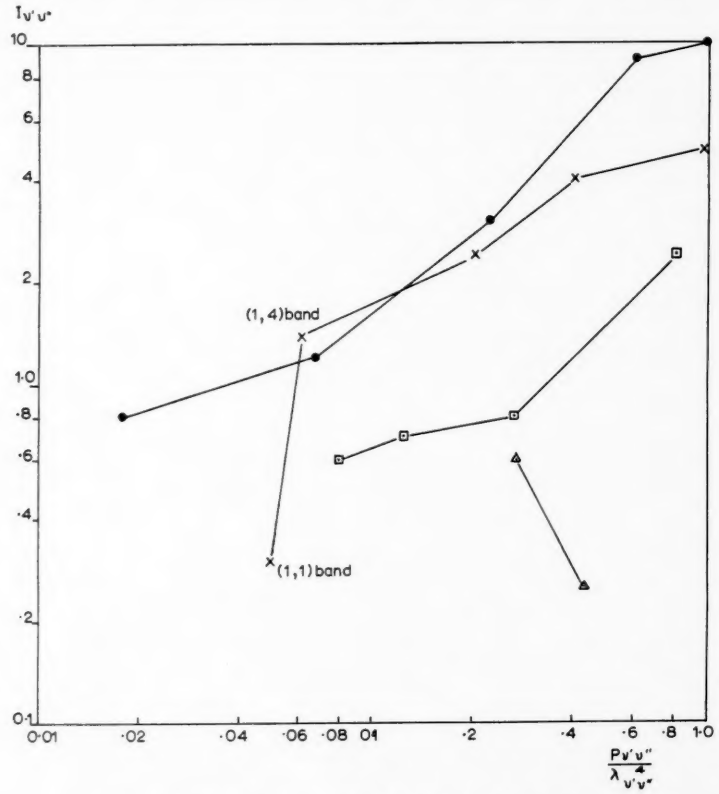

Fig. 1(c). ●, $v' = 0$; ×, $v' = 1$; ⊡, $v' = 2$; △, $v' = 3$.

atmospheric and instrumental extinction and show reasonably consistency for the $v' = 0$, 1 and 2 bands. PETRIE and SMALL remark that the (1, 1) band (marked on Fig. 1c) is abnormally weak but, since the plots of Fig. 1(c) should be straight lines of unit slope, a better interpretation is that the (1, 4) band (also marked on the figure) is approximately twice as strong as would be expected. Assigning equal statistical weight to the measured intensities (but excluding the (1, 4) band), the least squares solutions for the relative populations are:

$$N_0:N_1:N_2:N_3 = 1{\cdot}00:0{\cdot}44:0{\cdot}24:0{\cdot}09$$

—the population given for $v' = 3$ being highly uncertain. The standard deviations of these observations are in the region of 0·11 and 0·06 for the N_1 and N_2 respectively.

VOL. 22 1961

In a later paper (1953), PETRIE and SMALL have used a higher dispersion spectrograph and obtained the relative intensities plotted in Fig. 1(d). The consistency of these readings is, again, reasonable and the (1, 4) band is, again, of greater intensity than would be expected, this time by about 50 per cent. The populations derived from these measurements, excluding the (1, 4) band, are

$$N_0:N_1:N_2:N_3 = 1{\cdot}00:0{\cdot}46:0{\cdot}11:0{\cdot}10$$

—the populations for $v' = 2, 3$ depending on only two and one bands respectively. The standard deviation of these measures is in the neighbourhood of 0·03.

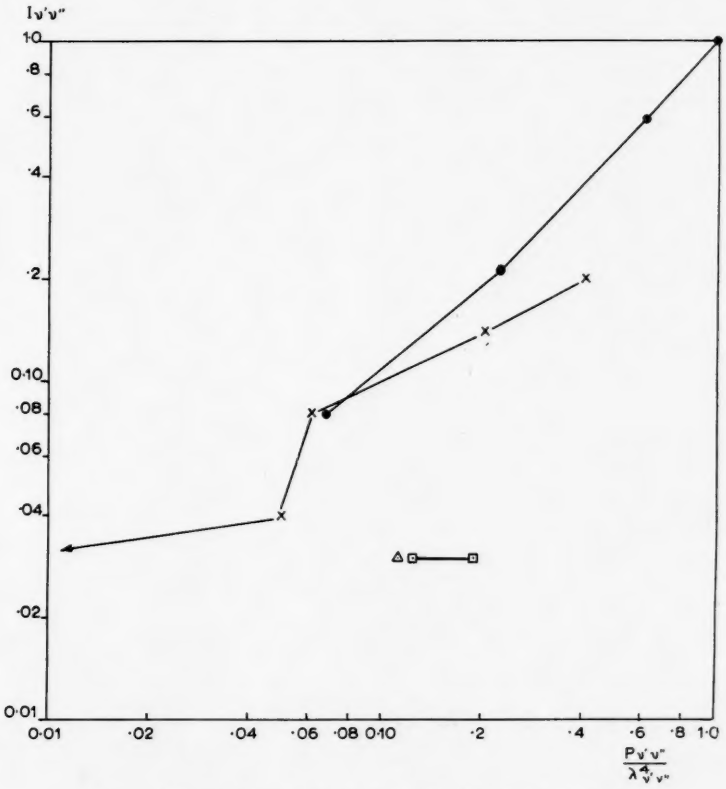

Fig. 1(d). ●, $v' = 0$; ×, $v' = 1$; ⊡, $v' = 2$; △, $v' = 3$.

HUNTEN and SHEPHERD (1955) have made probably the most numerous determinations of the intensities of the $2PG$ nitrogen bands, using a photoelectric scanning spectrometer. Their measurements, however, were limited to only one Δv sequence consisting of the (0, 2), (1, 3) and (2, 4) bands. It is thus difficult to check the consistency of their measurements; any blending of one of these bands with another emission will give a false determination of the populations. The mean populations from 275 scans on four nights of observations are:

$$N_0:N_1:N_2 = 1{\cdot}00:0{\cdot}76:0{\cdot}19$$

the range of populations between the four nights being 0·07 and 0·04 for N_1 and N_2 respectively.

SHUISKAYA (1959) has published the results of relative intensity measurements of auroral spectra in the near ultra-violet, observed from Roschino and uncorrected for atmospheric and instrumental absorption. These intensities are plotted in Fig. 1(e) and show some consistency, particularly remembering that atmospheric absorption has not been allowed for. Following the method of OMHOLT (1954) and considering only the Δv = constant sequences of bands (since these bands will

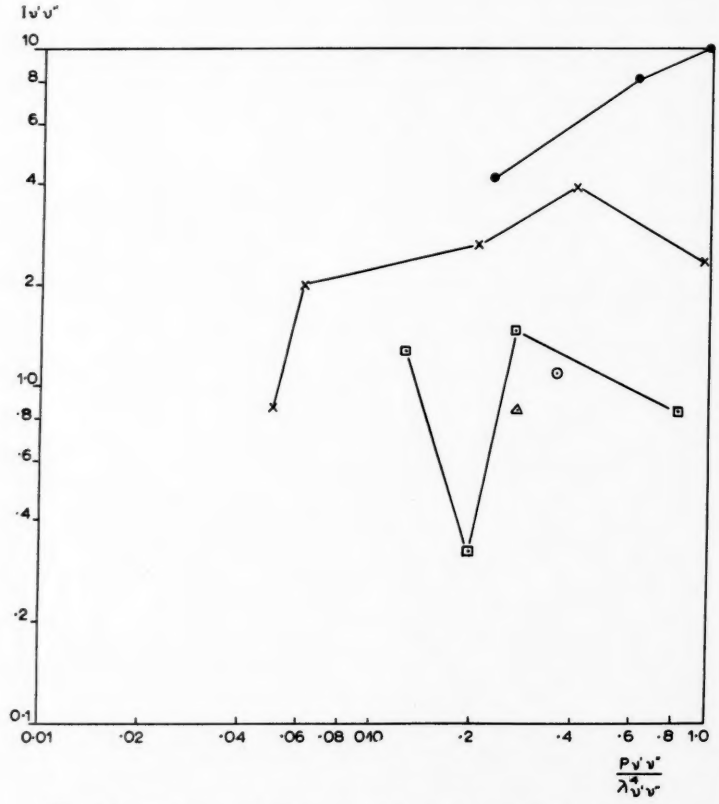

Fig. 1(e). ●, $v' = 0$; ×, $v' = 1$; ⊡, $v' = 2$; △, $v' = 3$; ⊙, $v' = 4$.

then occur in the same region of the spectrum, to a rough approximation the correction for atmospheric absorption will be the same for all the bands in the sequence), the following mean relative populations computed from SHUISKAYA's results are obtained

$$N_0:N_1:N_2:N_3:N_4 = 1{\cdot}0:0{\cdot}6:0{\cdot}4:0{\cdot}3:0{\cdot}3.$$

The populations of the $v' = 3$, 4 levels are uncertain, being computed from the intensity of one band in each case.

To summarize the information available on the relative populations of the

VOL. 22 1961

vibrational levels of the $C^3\pi$ state of the nitrogen molecule, Table 2 is given. It is probably reasonable to say that the best estimate of the relative populations is:

$$N_0 : N_1 : N_2 = 1{\cdot}0 : 0{\cdot}6 : 0{\cdot}2.$$

This does not take account of any real differences in relative populations that may occur systematically over a particular observatory; all observers, however, are agreed that

$$N_0 > N_1 > N_2.$$

Table 2

Observers	N_0	N_1	N_2	N_3	N_4	
Omholt (1954)	1·0	0·6	0·35	—	—	—
Omholt (1955)	1·00	0·70	0·24	—	—	—
	1·00	0·70	0·34	—	—	
Petrie and Small (1952)	1·00	0·44	0·24	0·09	—	N_3 uncertain
Petrie and Small (1953)	1·00	0·46	0·11	0·10	—	N_2, N_3 uncertain
Hunten and Shepherd (1955)	1·00	0·76	0·19	—	—	—
Shuiskaya (1959)	1·0	0·6	0·4	0·3	0·3	N_3, N_4 uncertain

Measurements of Spectra Obtained at Scott Base in 1959

Successful auroral spectra of the second positive group of nitrogen bands were obtained on five nights during July (11, 12, 14, 15 and 17). All of these spectra showed the $2PG$ bands strongly and in two cases the (0, 2) $2PG$ band was almost as strong as the (0, 1) NG band at 4278 Å. Fig. 2 shows a microphotometer tracing of one of the spectra, taken with photographic density as ordinate. Microphotometer tracings were taken on the first and the last spectrum obtained each night which shows the $2PG$ emission sufficiently strongly above the background to permit satisfactory reduction. Because of the very low dispersion of the spectrograph, no band structure is resolved and, for all practical purposes, the profiles of the band images are identical with the profiles of line emission images (being limited photographically in each case); this is shown in Fig. 3, which presents, side by side, tracings of the density–wavelength profile of a $2PG$ band and of the 6300/6364 atomic emission doublet. For this reason, the relative intensities have been determined from the peak density recorded in each band, with no attempt made to correct them for varying band profiles.

All measures were made on images of the zenith sky. This reduces the correction of the relative intensities for atmospheric extinction to a fairly small amount, thus keeping to a minimum errors due to uncertainty of the atmospheric extinction coefficient. Since the aurora was widely distributed over the sky during each of the exposures, Schuster's extinction correction (Schuster, 1905), has been applied:

$$I_0(\lambda) = I_\lambda(1 + \beta_\lambda x)$$

where $I_0(\lambda)$ = intensity of emission, of wavelength λ, above the atmosphere,
I_λ = observed intensity of emission, of wavelength λ,
β_λ = the Rayleigh scattering coefficient at wavelength λ,
x = air mass above the spectrograph.

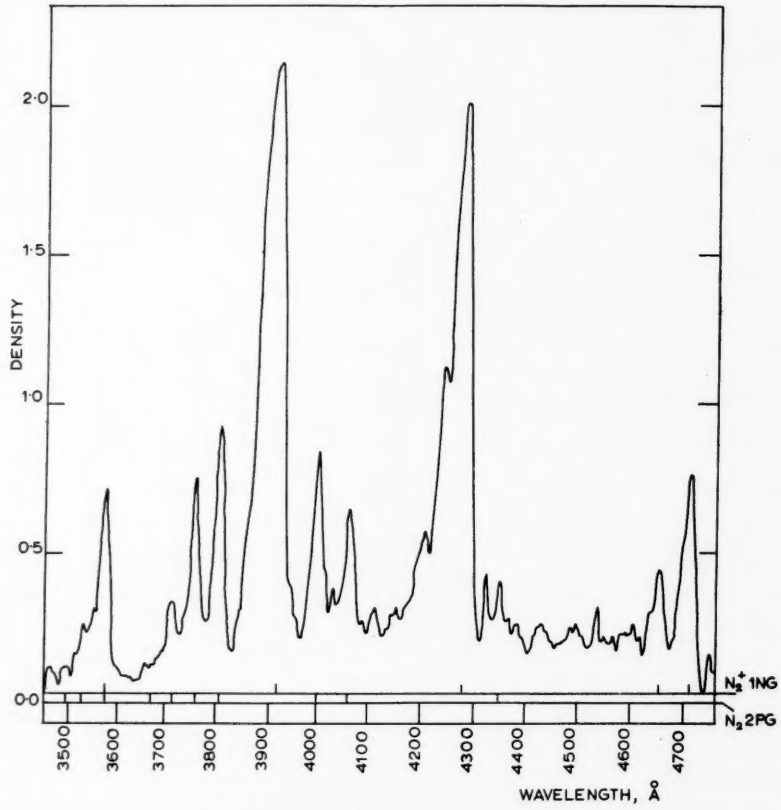

Fig. 2

This extinction correction varies quite seriously at the shorter wavelengths from the point source extinction correction

$$I_0(\lambda) = I_\lambda e^{\beta_\lambda x}.$$

At 4344 Å, the two extinction corrections are 1·27 (point source) and 1·24 (SCHUSTER). At 3500 Å, they are 1·79 (point source) and 1·58 (SCHUSTER).

The values of $P_{v'v''}/\lambda^4_{v'v''}$ given in Table 1 have been applied to the intensity measurements to give values of $N_{v'}$ for $v' = 0, 1, 2, 3, 4$. Since a photographic emulsion is essentially a detector responding logarithmically to radiation, least squares solutions of

$$\log I_{v'v''} = \log\left[kN_{v'} \Big/ \sum_{v''} \frac{P_{v'v''}}{\lambda^3_{v'v''}} \right] + \log \frac{P_{v'v''}}{\lambda^4_{v'v''}}$$

were found and the values of $kN_{v'}/kN_0$ are tabulated in Table 3.

VOL. 22 1961

Those values in italics are based on only one band and have, therefore, no check for consistency available. The values of σ_{exp} given in the next-to-bottom line of Table 3 are the expected standard deviations of the means of the N_i, calculated

Fig. 3. (a) The *OI* 6300/6364 doublet. (b) The (0, 2), (1, 3), (2, 4) $2PG$ bands.

Table 3

Date	N_1	N_2	N_3	N_4
1959 July 11	0·96	*0·31*	*0·35*	
	1·23	*0·26*	*0·12*	
12	1·64	*0·49*		
	1·10	*0·47*		
14	1·17	*0·35*		
	1·29	0·33		
15	0·79	0·34	*0·21*	*0·14*
	1·61	*0·30*		
17	1·10	*0·22*	*0·22*	
	1·02	0·20		
Mean	1·19	0·33	0·23	0·14
σ_{exp}	0·11	0·04	0·05	0·06
σ	0·26	0·10	0·08	—

from the residuals of the observed intensities. In the bottom line of the table are given the standard deviations computed from the tabulated values of the N_i. It will be noted that the expected standard deviations are smaller, in each case, than the standard deviations actually shown by the values of N_i. Snedecor's F-test (or Variance Ratio test) shows that the differences for the N_1 and N_2 values are

significant; it is therefore reasonable to assume that the relative populations are not fixed but show some variation over periods of hours and days.

The consistencies of all the band intensities were good with the exception of the (0, 4) band on both spectra of 14 July. During this night, the band was presumably blended with some emission with a wavelength within 10–20 Å of 4344 Å.

Similar measurements and reductions have been made for the negative group of N_2^+ emission bands on the same ten spectra. Because of the low resolution of

Table 4

Date	$2PG$ N_0	$1NG$ N_0
1959 July 11	3·2	10·6
	15·9	36
12	6·9	16·5
	5·0	10·9
14	3·8	8·9
	3·8	10·8
15	92	94
	4·7	15·1
17	49	47
	16·6	40
Standard deviation	17%	14%

the spectra and the relatively high population of the $v' = 0$ level of the $B^2\Sigma$ state of the N_2^+ molecule, the populations of the $v' = 1$, $v' = 2$ levels relative to that of the $v' = 0$ level are found with little precision. The means of the measures from the ten spectra were found to be $N_1 = 0{\cdot}14$ and $N_2 = 0{\cdot}08$.

Comparing the measured values of N_0 for the $2PG$ and the NG groups shows an interesting correlation. The values of N_0 are given for the two band systems in Table 4 and are plotted in Fig. 4.*

The product moment correlation coefficient between these values of N_0 for the two band systems is the highly significant value of $r = +0{\cdot}95$.

A final check on the consistency of the measurements is provided by the overlapping of the (1, 0) NG band at 3582 Å and the (0, 1) $2PG$ band at 3577 Å. Given the determined populations of the $v' = 0(2PG)$ and the mean estimate of the ratio of the $v' = 1$ and $v' = 0$ levels of the $(1NG)$ state level, it is a straightforward matter to calculate the values of $I_{1,0}(NG)$ and $I_{0,1}(2PG)$. The sum of these has been compared directly with the observed intensity of the overlapped image on the spectrograms (after correction for atmospheric extinction). The agreement is satisfactory, as can be seen from Table 5, and this provides additional confidence in the measurements of population levels.

* It should be noted that the small value of the quadratic coefficient found from least squares fitting indicates a true linear relationship between the population rates for the two band systems.

VOL. 22 1961

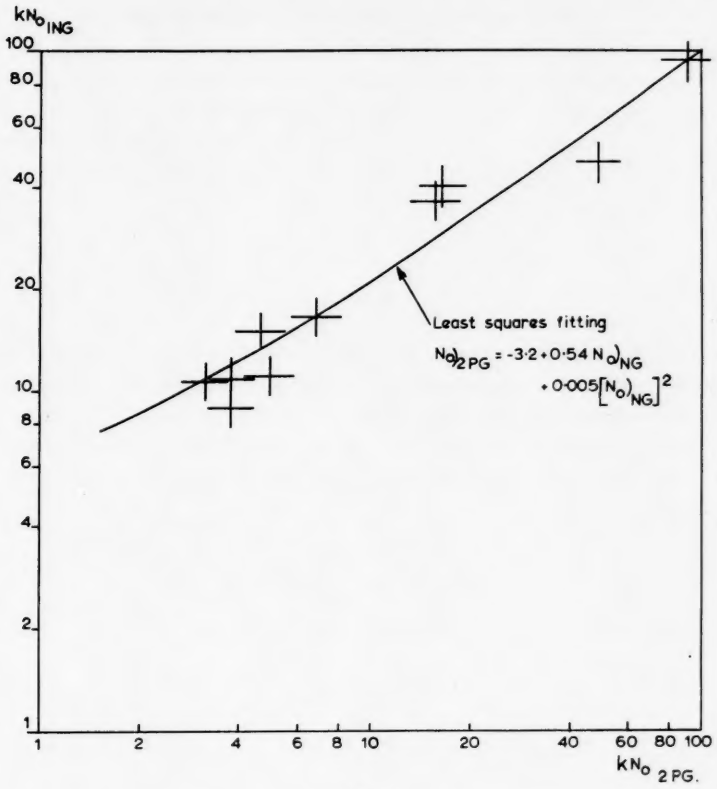

Fig. 4

Table 5

Date	$I_{calc.}$	$I_{obs.}$	Ratio $\frac{I_{obs.}}{I_{calc.}}$
1959 July 11	2·7	2·6	0·96
	13·8	8·5	0·62
12	5·4	7·0	1·30
	3·9	2·3	0·59
14	2·9	2·1	0·72
	3·0	2·8	0·93
15	63	(125)	(1·98)
	4·0	6·5	1·62
17	35	(35)	(1·00)
	13·0	(11·5)	(0·88)

The brackets around some of the observed intensities indicate uncertainty arising from the necessity for extrapolation of the emulsion characteristic curves. (It should perhaps be mentioned that these extrapolations were made before any computations of the expected intensities.)

DISCUSSION OF THE OBSERVATIONS

It is evident that the relative populations of the $C^3\pi$ vibrational levels of the nitrogen molecule derived from spectra at Scott Base differ quite markedly from those previously reported from northern hemisphere observatories.

BATES (1949) has reviewed the available values for the probability of excitation by electron collision of the $C^3\pi$ state from the ground states of both the neutral and ionized nitrogen molecule. The reactions considered in detail were thus:

$$N_2(X^1\Sigma) + e \rightarrow N_2(C^3\pi) + e \quad (1)$$

$$N_2^+(X^2\Sigma) + e \rightarrow N_2(C^3\pi) + h\nu \quad (2)$$

From the tables of theoretical transition probabilities, it is possible to predict the population rates of the vibrational levels of the $C^3\pi$ state, assuming that particular thermal distributions hold in the $N_2(X^1\Sigma)$ or $N_2^+(X^2\Sigma)$ states. BATES gives (Table 31 in his paper) the relative population rates of the $C^3\pi$ levels due to electron excitation of the $N_2(X^1\Sigma)$ state at various vibrational temperatures. This is given in Table 6.

Table 6

(Due to BATES, 1949)

$C^3\pi$ vibrational level	Vibrational temperature (°K) of $X^1\Sigma$					
	500	1000	2000	4000	6000	8000
0	1·00	1·00	1·00	1·00	1·00	1·00
1	0·60	0·58	0·56	0·60	0·66	0·71
2	0·23	0·24	0·28	0·35	0·43	0·48

Comparison with the population rates in Table 2 shows that the observations reported there are consistent, in general, with excitation by process (1) above; differences in detail are to be noted, however. It is, furthermore, obvious that the excitation observed over Scott Base in 1959 cannot be due to this process. The $v' = 1$ level has much too high a population to be excited in this manner, unless vibrational temperature of the ground state is very high; in this case the population rate of the $v' = 2$ level is too low. Table 6 has been computed for electrons with an energy somewhat above the threshold excitation energy. BATES quotes the measurements of LANGSTROTH (1935) which confirm what would be expected on general grounds—that excitation by slower electrons will decrease the relative population rates of $v' = 1$ and 2 and thus make process (1) even more unlikely.

As BATES has pointed out, similar results are obtained in the case of process (2)—either N_1 is too high, or N_2 is too low. The expected population rates are given in Table 7.

Consideration of simple thermal distributions among the vibrational levels of the $C^3\pi$ state shows that this process cannot explain the Scott Base results. Some thermal distributions are given in Table 8 and again do not account for the abnormally high population rate of the $v' = 1$ level.

VOL. 22 1961

Excitation by proton impact cannot occur directly since a change of multiplicity is involved in both the $X^1\Sigma \rightarrow C^3\pi$ and $X^2\Sigma \rightarrow C^3\pi$ transitions (Wigner's rule; MASSEY and BURHOP, 1952, p. 42). However, indirect excitation by protons can occur if the protons capture an electron first or if they produce secondary electrons which then cause excitation by collision or recombination. In this context, the observations by NICHOLLS *et al.* (1959) are of interest. They photographed spectra of the N_2 $2PG$ bands produced by firing protons into nitrogen; the $v' = 0$, 1 and 2 levels of N_2 ($C^3\pi$) were apparently enhanced relative to the

Table 7

$C^3\pi$ vibrational level	Vibrational temperature of $X^2\Sigma$ (°K)			
	500	1000	2000	4000
0	1·00	1·00	1·00	1·00
1	0·20	0·24	0·35	0·51
2	0·02	0·02	0·10	(0·3)

Table 8

v'	Temperature (°K)				
	500	1000	2000	4000	8000
0	1·00	1·00	1·00	1·00	1·00
1	0·00	0·05	0·24	0·50	0·84
2	0·00	0·00	0·06	0·25	0·70
3	0·00	0·00	0·00	0·13	0·59
4	0·00	0·00	0·00	0·07	0·50

normal discharge lamp distribution. However, no details of the enhancement are presented. Thus, it is possible that the relative population rates observed in Scott Base spectra could be caused by secondary processes during high-energy proton bombardment. No Balmer emission was noted on the Scott Base spectra used in this analysis; this is to be expected if the protons have energies approximating to 1 MeV (cf. NICHOLLS *et al.*, 1959), since at these energies the ratio of ionization to Balmer emission is very great (OMHOLT, 1959). It is relevant to note that for the period 11–17 July 1959 (inclusive) the Scott Base ionosonde showed total absorption conditions. REID and LEINBACH (1959) have reported that polar cap black-out conditions were present in the northern hemisphere during this period and have suggested that these conditions are the consequence of the injection of solar protons directly into the atmosphere inside the auroral zone.

Referring again to the work of NICHOLLS *et al.*, they find that the dominant spectral features of the proton-induced emission from nitrogen are the First Negative bands of N_2^+ and the First Positive bands of N_2 in addition to the N_2 Second Positive bands. These are interpreted as indicating that the more probable process occurring is ionization of N_2 without charge transfer:

$$H^+ + N_2 \rightarrow N_2^+ + H^+ + e.$$

The electrons are then supposed to cause excitation of N_2 or N_2^+

$$N_2^+ + e \rightarrow N_2(C^3\pi,\ B^3\pi) + h\nu$$

$$N_2 + e \rightarrow N_2(C^3\pi,\ B^3\pi) + e$$

However, these last processes have been shown to be unlikely in the case of the Scott Base observations, if N_2, N_2^+ is in thermal equilibrium in the ground state before electron collision. It is possible that the enhancement of $v' = 0, 1, 2$ population rates of $N_2(C^3\pi)$ observed by NICHOLLS *et al.* is due to non-thermal distribution of the N_2^+ $(X^2\Sigma)$ resulting from proton excitation.

Table 9

Energy level		Energy (eV)	
N_2^+ $(X^2\Sigma)$ $v' = 0$		15·72	Energy excess in $N_2 + O^-$ combination = 14·25 (13·63)
O^-		1·47 (2·09)	
N_2 $(C^3\pi)$	$v' = 5$	12·37	14·33 } Energy required in combination with $O\ ^1D$
	$v' = 4$	12·14	14·10
	$v' = 3$	11·90	13·86
	$v' = 2$	11·66	13·62
	$v' = 1$	11·42	13·38
	$v' = 0$	11·17	13·13
$O\ ^1D$		1·96	

Another possible explanation of the abnormal v' distribution observed at Scott Base invokes an ion–ion charge exchange process:

$$N_2^+(X^2\Sigma) + O^- \rightarrow N_2(C^3\pi) + O(^1D).$$

The energy balance of this process is satisfactory. Table 9 gives the energies available in the N_2^+ ion, the electron affinity of O^- and the energies required for excitation of the products (the molecular constants required have been taken from HERZBERG, 1950).

It will be noted that two energies for the electron affinity of atomic oxygen are quoted; the lower value is taken from the work of LIN and KIVEL (1959), the higher value from MASSEY and BURHOP (1952, p. 259).

The maximum cross-section for mutual neutralization processes does not occur at exact resonance (MASSEY and BURHOP, 1952, p. 621) but when the process is exothermal to the extent of about 1 eV; thus one expects that, for the lower value of electron affinity, the maximum population rate of N_2 $(C^3\pi)$ should occur for $v' = 1$ and that $v' > 4$ cannot be excited. For the higher value of electron affinity, maximum population rate should occur for $v' = 0$, and $v' > 2$ cannot be excited. Thus, if the electron affinity of oxygen be 1·47 eV, the observed high population rate of $v' = 1$, and the lack of emission from $v' > 4$ is qualitatively explained by this charge exchange process. However, if the electron affinity of oxygen is 2·09 eV, then the proposed reaction does not explain the observed population rates.

VOL. 22 1961

The charge exchange process considered above bears a close similarity to the two processes, proposed by MITRA (1943) and GHOSH (1943), and MALVILLE (1959) respectively:

$$N_2^+(X^2\Sigma) + O^- \rightarrow N_2(B^3\pi, v' = 9) + O(^1S)$$

$$N_2^+(X^2\Sigma) + O_2^-(^2\pi) \rightarrow N_2(B^3\pi) + O_2(^3\Sigma)$$

The latter process cannot excite the N_2 molecule to a level higher than 9·6 eV and is therefore incapable of exciting above the $v' = 10$ level of the $B^3\pi$ state; (with an "optimum" energy excess of 1 eV, the $v' = 5$ or 6 levels should have the highest population rates).

The first of the two processes proposes that the oxygen atom is excited to the ^1S state (4·18 eV) leaving the N_2 molecule a maximum of either 10·07 or 9·45 eV available for excitation; these energies correspond to highest v' levels of 13 or 10 in the B^3 state, and "optimum" levels around $v' = 8$ or $v' = 4$ or 5.

BATES (1949) has pointed out that the collision coefficient of the $N_2^+(X^2\Sigma)$ to $N_2(C^3\pi)$ transition is expected to be small since an internal rearrangement in the electron configuration is needed. However, since the rearrangement is the exact reverse of that which occurs in the $C^3\pi$ to $B^3\pi$ transition, it is considered that this objection does not eliminate the possibility of the process occurring. A difficulty also arises in that the process demands the presence of negative oxygen ions (formed presumably by attachment) and the absence of electrons, because the rate coefficient of the mutual neutralization process can be expected to be very much smaller than that of the straightforward N_2^+–electron recombination. Since the spectra under discussion were obtained during polar black-out conditions, this demands an ionosphere with a high electron density at low levels and a very low electron density at heights above 100 km or so. Observations made during polar black-outs by an ionospheric top-side sounding satellite should show immediately if such conditions ever occur.*

To summarize, therefore, it can be said:

(1) The relative population rates of the vibrational levels of the $N_2(C^3\pi)$ state observed from Scott Base show definite differences from those reported from stations outside the auroral zones.

(2) These relative population rates require some ionic reaction to explain them, since electron excitation from either ionized or non-ionized nitrogen cannot give the deduced rate.

(3) A possible reaction, satisfying the energy conditions, is $N_2^+(X^2\Sigma) + O^- \rightarrow N_2(C^3\pi) + O(^1D)$.

(4) An excitation process involving ionized nitrogen is particularly attractive since it suggests that a good correlation might be expected to exist between the intensity of the First Negative and Second Positive bands. Such a correlation is found, with a product moment correlation coefficient of $r = +0{\cdot}95$.

(5) The emission of the oxygen red line from the ^1D state together with the Second Positive nitrogen bands is supported by all-sky camera colour observations

* A letter by TAYLOR (1961) points out that, during a recent disturbed period, the total electron content of the ionosphere (measured by a lunar reflection technique) was exceptionally low over England.

(SANDFORD, 1961) made at the same times as seven of the spectrograph exposures. Deep red aurorae were observed to be present during five of the exposures.

(6) The relative population rates show significant variations between spectra taken a few hours or days apart. This suggests that a single process is not a sufficient explanation, but that there can be two or more excitation processes occurring during a period of 1 or 2 hr. It may well be that one process (electron excitation of neutral nitrogen at low temperatures or recombination of ionized nitrogen at high temperatures) can occur at all latitudes but with another process (charge exchange?) dominant over Scott Base, inside the auroral zone. This may explain the results of HUNTEN and SHEPHERD (given in Table 2) who find a population rate for $v' = 1$ somewhat above that found by PETRIE and SMALL, or SHUISKAYA, but definitely below that reported here. If one supposes that the demarcation line is magnetically controlled and changes its latitude with magnetic activity then it could quite easily be that Saskatoon (where the observations of PETRIE and SMALL, and HUNTEN and SHEPHERD were made) is close to the effective demarcation line of the dominance of one process or the other, and that the observations of HUNTEN and SHEPHERD were made at magnetically different periods from those of PETRIE and SMALL.

Acknowledgements—This work forms part of the research programme of the Auroral Station of the Dominion Physical Laboratory, New Zealand; I wish to acknowledge the help of Mr. B. P. SANDFORD, Senior Scientist at Scott Base, 1959, in making the spectrograms and all-sky camera records readily and rapidly available.

VOL. 22 1961

REFERENCES

BATES D. R.	1949	*Proc. Roy. Soc.* A **196,** 217.
GHOSH S. N.	1943	*Proc. Nat. Inst. Sci. India* **9,** 301.
HERZBERG G.	1950	*Spectra of Diatomic Molecules.* Van Nostrand, New York.
HUNTEN D. M. and SHEPHERD G. G.	1955	*J. Atmosph. Terr. Phys.* **6,** 64.
LANGSTROTH G. O.	1935	*Proc. Roy. Soc.* A **150,** 371.
LIN S. C. and KIVEL B.	1959	*Phys Rev.* **114,** 1026.
MALVILLE J. M.	1959	*J. Atmosph. Terr. Phys.* **16,** 59.
MASSEY H. S. W. and BURHOP E. H. S.	1952	*Electronic and Ionic Impact Phenomena.* Oxford University Press.
MITRA J. K.	1943	*Sci. & Cult.* **9,** 46.
NICHOLLS R. W.	1956	*The Airglow and the Aurorae*, p. 302. Pergamon Press, London.
NICHOLLS R. W., REEVES E. M. and BROMLEY D. A.	1959	*Proc. Phys. Soc. Lond.* **74,** 87.
OMHOLT A.	1954	*J. Atmosph. Terr. Phys.* **5,** 63.
OMHOLT A.	1955	*J. Atmosph. Terr. Phys.* **6,** 61.
OMHOLT A.	1959	*Geofys. Publ.* **20,** No. 11.
PETRIE W. and SMALL R.	1952	*J. Geophys. Res.* **57,** 51.
PETRIE W. and SMALL R.	1953	*Canad. J. Phys.* **31,** 911.
PETRIE W. and SMALL R.	1954	*Proc. Conf. Auroral Phys.*, London, Ontario, p. 61. University of Western Ontario.
REID G. C. and LEINBACH H.	1959	*J. Geophys. Res.* **64,** 1801.
SANDFORD B. P.	1961	*J. Atmosph. Terr. Phys.* **21,** 177.

Schuster A.	1905	*Astrophys. J.* **21,** 1.
Shuiskaya F. K.	1959	*Sbornik po issl. N.N.i P.C.*, Moscow, No. 1, p. 45.
Taylor G. N.	1961	*Nature, Lond.* **189,** 740.
Vegard L.	1933	*Geofys. Publ.* **10,** No. 4.
Vegard L.	1956	*Geofys. Publ.* **19,** No. 9.

OL.
22
961

Journal of Atmospheric and Terrestrial Physics, 1961, Vol. 22, pp. 122 to 141. Pergamon Press Ltd. Printed in Northern Ireland

The properties of low frequency radio waves reflected from the ionosphere, calculated by the phase-integral method

ELISABETH COOPER
Cavendish and Mathematical Laboratories, Cambridge

(*Received* 11 *May* 1961)

Abstract—This paper presents the results of some calculations of the reflecting properties of various models of the ionosphere for radio waves of moderately low frequency at vertical incidence, when allowance is made for electron collisions. The phase-integral method is used, which involves the evaluation of integrals of the complex refractive index n, or the complex group refractive index n' along paths in the complex height plane. The validity of the method and its relation to "full-wave" solutions are discussed. Results presented include a Chapman layer when the earth's magnetic field is neglected and when it is included. In all calculations, the collision frequency is assumed to be independent of height. It is concluded that the phase-integral method is likely to be the most useful for frequencies in the range 200–2000 kc/s, where a step-by-step integration is very long, and the simpler ray theory methods are not accurate enough.

1. INTRODUCTION

THE method used for calculating the reflecting properties of the ionosphere for radio waves depends upon the frequency. For high frequencies at vertical incidence, the phase and amplitude of the reflected wave are often calculated by finding the real and imaginary parts respectively of the refractive index n, and integrating them from the ground to the reflection level. This is equivalent to using a simple ray theory. It is based upon the W.K.B. approximate solutions of the wave equations, and assumes that the ionosphere is slowly varying in the sense that the change in electron density N is small within one wavelength. The reflection level is where n is zero, but when allowance is made for electron collisions, there is no real height where n is zero, and an extension of the theory is needed to deal with this.

For very low frequencies, a step-by-step integration of the differential equations has been used (BUDDEN, 1955; BARRON and BUDDEN, 1959). Here, the electron density N cannot be regarded as slowly varying, and the W.K.B. solutions are not good approximations. For frequencies greater than 200 kc/s, however, the integration requires a very large number of steps, which makes the method laborious.

In this paper an attempt is made to cover the intermediate frequency range by using the phase-integral method (ECKERSLEY, 1931, 1932a, b), which is really an extension of the simple ray theory. The main features and limitations of the phase integral method are summarized in Section 3. In Section 4 the effect of the earth's magnetic field is neglected, and the method is applied to a parabolic and a Chapman layer, to calculate equivalent heights. In Section 5 the effect of the earth's magnetic field is included, and in Section 6 the method is applied to a linear, an exponential and a Chapman layer, to calculate equivalent heights and absorbtion. Only vertical incidence is considered, and the electron collision frequency is assumed to be constant throughout each layer. This is a serious limitation, since the collision frequency cannot be regarded as constant in the actual ionosphere. A method of allowing for varying collision frequency has recently been developed, but has not yet yielded enough results to justify their presentation here. Some of

VOL. 22 1961

the integrals mentioned later were calculated on EDSAC II, the automatic digital computer in the University Mathematical Laboratory, Cambridge.

2. Notation

f	frequency of electromagnetic waves
c	velocity of electromagnetic waves in free space
k	$2\pi f/c$ the angular wave number
e, m	charge, mass of an electron
ε_0	electric permittivity of free space
N	number of electrons per unit volume
ν	collision frequency of electrons
B	magnetic induction of the earth's magnetic field
f_H	$B\lvert e\rvert/m$ the gyrofrequency
Θ	angle between the earth's magnetic field and the vertical
X	$\dfrac{Ne^2}{\varepsilon_0 m(2\pi f)^2}$ in rationalized units
Y	f_H/f
Y_L	$(f_H/f)\cos\Theta$
Y_T	$(f_H/f)\sin\Theta$
Z	$\nu/2\pi f$
f_N	plasma frequency ($X = f_N{}^2/f^2$)
n	complex refractive index given by the Appleton–Hartree formula
n'	$\dfrac{\partial}{\partial f}(nf)$ complex group refractive index
z	vertical coordinate
z_0	value of z for which $n = 0$ (in general complex)
$h'(f)$	equivalent height
ρ	reflection coefficient for amplitude
H	scale height

3. The Phase-Integral Method

For radio waves vertically incident on the ionosphere, the wave equation satisfied by the electric intensity E, when the earth's magnetic field is neglected, is

$$\frac{d^2E}{dz^2} + k^2n^2E = 0.$$

When the earth's magnetic field is allowed for, it is possible to find a field variable which satisfies the same equation, provided that the ionosphere is sufficiently slowly varying for the coupling parameter (usually denoted by ψ) to be neglected.

This equation has the two approximate W.K.B. solutions

$$n^{-\frac{1}{2}} \exp\left[ik\left(ct \pm \int_0^z n\,dz\right)\right]. \tag{3.1}$$

It can be shown that the approximation is good in an ionospheric layer in which the electron density change is small in one wavelength.

If collisions are neglected, there is often a real height z_0 where n is zero and the upgoing W.K.B. wave is converted to the downcoming W.K.B. wave. Thus reflection occurs and the reflection coefficient is

$$\rho = i \exp\left(-2ik\int_0^{z_0} n\,dz\right). \tag{3.2}$$

The validity of this statement rests upon study of the wave equation near the zero of n at $z = z_0$. If n^2 is slowly varying, the wave equation can be reduced to Stokes' equation, and the solution is an Airy integral function (BUDDEN, 1961). The factor i in (3.2) is the Stokes' constant of the Stokes' equation, but is unimportant in the present paper.

If collisions are included the refractive index becomes complex, and there is no real z_0 for which n is zero, but if n is a known analytic function of z, a complex value can be found for z_0, and the integral in (3.2) becomes a contour integral in the complex z-plane. The formula (3.1) is still valid, and (3.2) still gives the reflection coefficient provided that the zero z_0 of n is sufficiently isolated in the complex z-plane, i.e. not near another zero or any other singularity (HARTREE, 1931). This condition fails, for example, near the penetration frequency of a layer, and is mentioned in Section 4.

Alternatively, the upgoing and downcoming waves may both be represented by one W.K.B. solution

$$n^{-\frac{1}{2}} \exp\left[ik\left(ct - \int_0^z n\,dz\right)\right] \tag{3.3}$$

since the Appleton–Hartree formula gives n^2 as a function of z. One root of n^2 in (3.3) represents the upgoing wave, while the other represents the downcoming. The two roots are equal at the reflection point z_0, and if n is represented as a single-valued function on a Riemann surface, z_0 is a branch point joining the sheet containing the upgoing wave to that containing the downcoming wave. In general, n^2 is double-valued, and the Riemann surface has four sheets connected at branch points. This is considered further in Sections 4 and 5. The reflection coefficient is given by (3.2), provided that the upgoing and downcoming waves are symmetrical in n^2, and only such waves are considered in this paper.

To allow for collisions at high frequencies, some authors take the reflection height at $\mathscr{R}(z_0)$ and thus avoid an integration in the complex plane. The error in this method is usually small at high frequencies, but may not be negligible below 1 Mc/s. Also the third, or Z-trace cannot always be dealt with by this method.

VOL. 22 1961

When z_0 is complex, from (3.1) or (3.3) the reflected wave at the ground is

$$\exp\left[ik\left(ct - 2\int_0^{z_0} n\,dz\right)\right]$$

and from (3.2) the total absorption suffered by this wave is

$$-\log|\rho| = -2k\,.\,\mathscr{I}\left(\int_0^{z_0} n\,dz\right). \tag{3.4}$$

For a pulse containing a range of frequencies near f, the time of travel τ is found by expressing the condition that the phase shall be stationary with respect to f. This results in

$$c\tau = \mathscr{R}\left[2\frac{\partial}{\partial f}\left(f.\int_0^{z_0} n\,dz\right)\right].$$

Although z_0 is a function of f, n is zero when $z = z_0$ and the equivalent height thus becomes

$$h'(f) = \tfrac{1}{2}c\tau = \mathscr{R}\left(\int_0^{z_0} n'\,dz\right) \tag{3.5}$$

where

$$n' = \frac{\partial}{\partial f}(fn)\,.$$

When n is real, n' is real and is commonly called the group refractive index. In general, n' is complex and will be called the complex group refractive index.

4. Application to an Ionospheric Layer, Neglecting the Earth's Magnetic Field

4.1. *General formulae*

When the effect of the earth's magnetic field is neglected, the refractive index n is given by

$$n^2 = 1 - \frac{X}{1 - iZ}\,. \tag{4.1}$$

Thus n^2 is a single-valued function of z, and n can be represented as a single valued function on a two-sheeted Riemann surface. The only branch points are zeros of n which occur where

$$X = 1 - iZ. \tag{4.2}$$

In this paper it is assumed that ν is a constant independent of height, and hence Z is independent of z. Since X is dependent on z, the equation (4.2) can be solved for z to give the zeros of n. Only one zero is considered here, and it is chosen to satisfy the following conditions:

(a) $\mathscr{R}(z_0) > 0, \qquad \mathscr{I}(z_0) \leqslant 0.$

(b) If $Z \to 0$, $\mathscr{I}(z_0) \to 0$ and z_0 (real) takes the lowest value possible.

It is easily shown from (4.1) that

$$n' = \frac{1 - \frac{1}{2}iZ}{1 - iZ} \cdot \frac{1}{n} - \frac{\frac{1}{2}iZ}{1 - iZ} \cdot n \tag{4.3}$$

and when this is substituted in (3.5), the equivalent height becomes

$$h'(f) = \mathscr{R}\left(\frac{1 - \frac{1}{2}iZ}{1 - iZ} \cdot \int_0^{z_0} \frac{1}{n}\, dz - \frac{\frac{1}{2}iZ}{1 - iZ} \cdot \int_0^{z_0} n\, dz\right). \tag{4.4}$$

For a few very simple layers this can be evaluated analytically, but in general a numerical method must be used.

4.2. *Parabolic layer*

A parabolic layer is given by

$$f_N^2 = \begin{cases} f_p^2 \cdot \left[1 - \dfrac{(z - z_m)^2}{a^2}\right] & \text{for } 0 \leqslant |z - z_m| \leqslant a \\ 0 & \text{for } \quad |z - z_m| \geqslant a \end{cases} \tag{4.5}$$

where f_p is the penetration frequency. The equivalent height when no collisions are included is given by

$$h'(f) = z_m - a + \tfrac{1}{2}a \cdot \frac{f}{f_p} \log \frac{f_p + f}{f_p - f}. \tag{4.6}$$

When collisions are included, from (4.1) and (4.5)

$$n^2 = 1 - \frac{f_N^2}{f^2(1 - iZ)} \text{ for } 0 \leqslant |z - z_m| \leqslant a$$

$$n^2 = 1 \qquad \text{for} \qquad |z - z_m| \geqslant a.$$

Hence from (4.4)

$$h'(f) = z_m - a + \mathscr{R}\left(\frac{1 - \frac{1}{2}iZ}{1 - iZ} \int_{z_m - a}^{z_0} \left[1 - \frac{f_N^2}{f^2(1 - iZ)}\right]^{-\frac{1}{2}} dz - \frac{\frac{1}{2}iZ}{1 - iZ} \cdot \int_{z_m - a}^{z_0} \left[1 - \frac{f_N^2}{f^2(1 - iZ)}\right]^{\frac{1}{2}} dz\right). \tag{4.7}$$

The integrals of (4.7) can be evaluated analytically by means of the substitution

$$\left(\frac{f_p^2}{f'^2} - 1\right)^{\frac{1}{2}} \cosh \theta = \frac{f_p}{f'} \cdot \frac{z - z_m}{a}$$

where

$$f'^2 = f^2(1 - iZ)$$

and f' has a positive real part. The result is

$$h'(f) = z_m - a \cdot \mathscr{R}\left(\frac{1 - \frac{3}{4}iZ}{1 - iZ} - \frac{1 - \frac{3}{4}iZ}{1 - iZ} \cdot \frac{f'}{2f_p} \log \frac{f_p + f'}{f_p - f'} + \frac{\frac{1}{2}iZ}{1 - iZ} \cdot \tfrac{1}{4} \cdot \frac{f_p}{f'} \log \frac{f_p + f'}{f_p - f'}\right). \tag{4.8}$$

VOL. 22 1961

The equivalent height in (4.6), where collisions are not included, becomes infinite when $f = f_p$, but it can be seen from (4.8) that when collisions are included $h'(f)$ takes a finite value. In a parabolic profile, there are two zeros of n for any frequency f, and we expect the phase-integral method to fail when these are close together. When $\nu = 0$, the zeros coincide when $f = f_p$ and so failure is certain for

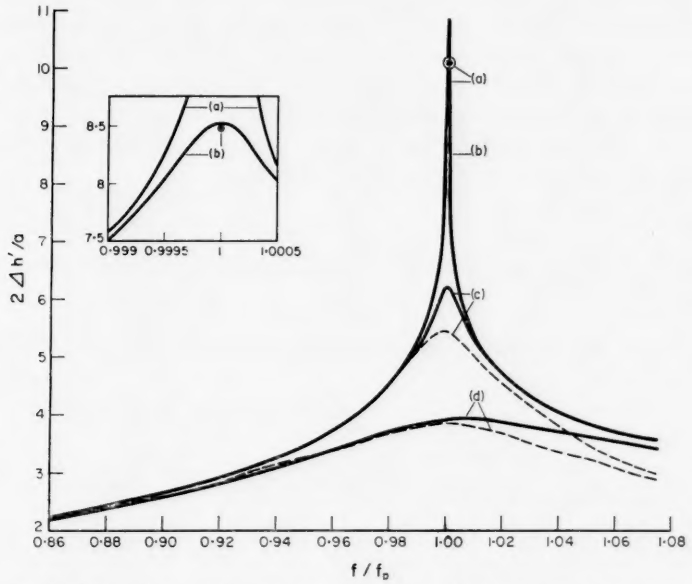

Fig. 1. To show how the equivalent height of reflection $h'(f)$ for a parabolic layer depends on frequency f when the collision frequency is independent of height, and the earth's magnetic field is neglected. The full curves are calculated by the method of this paper, and the broken curves or encircled points are "full-wave" solutions given by RYDBECK (1943). The following examples are shown:

(a) $f_p = 3{\cdot}331$ Mc/s, $a = 36$ km, $\nu = 1{\cdot}67 \times 10^3$ sec^{-1}.
(b) $f_p = 3{\cdot}331$ Mc/s, $a = 36$ km, $\nu = 1{\cdot}67 \times 10^4$ sec^{-1}.
(c) $f_p = 10$ Mc/s, $a = 0{\cdot}12$ km, $\nu = 5 \times 10^5$ sec^{-1}.
(d) $f_p = 10$ Mc/s, $a = 0{\cdot}12$ km, $\nu = 5 \times 10^6$ sec^{-1}.

The full-wave solutions are taken from curves and are therefore only approximate. For examples (a) and (b) RYDBECK only shows curves in the range $0{\cdot}99 < f/f_p < 1{\cdot}0015$. The encircled points are his maximum values.

frequencies near penetration. When $\nu \neq 0$ the zeros never coincide; their closest separation is $2a\, Z_p^{\frac{1}{2}}(1 - \frac{1}{4}Z_p^2)^{\frac{1}{4}}$, where $Z = Z_p$ when $f = f_p$, and this occurs when $f = f_p(1 - \frac{1}{2}Z_p^2)^{\frac{1}{2}}$. Therefore, if collisions are included, it should be possible to use the phase-integral method for frequencies closer to f_p than when $\nu = 0$.

The validity of the phase-integral method near f_p needs to be tested by comparison with full-wave solutions for a parabolic layer. Such solutions have been calculated by RYDBECK (1943), using parabolic cylinder functions, both with and without the inclusion of collisions, and his results are compared with those obtained by the phase-integral method in Fig. 1.

The ordinate plotted in Fig. 1 is $2\Delta h'/a$ where $\Delta h' = h'(f) - (z_m - a)$. It

should be noted that the approximate phase-integral solution for $2\Delta h'/a$ is independent of a, whereas the full-wave solution is dependent upon a. Both solutions will depend upon f_p in addition to f/f_p, since

$$Z = \frac{\nu}{2\pi} \cdot \frac{f_p}{f} \cdot \frac{1}{f_p} .$$

The examples of Fig. 1 show that there is reasonable agreement between the phase-integral method and the full-wave solutions. The curves (a) and (b) apply to a thick layer, and within the range $0{\cdot}99 \leqslant f/f_p \leqslant 1{\cdot}0015$ the solutions obtained by the two methods are indistinguishable except when $f = f_p$. The curves (c) and (d) are for a much thinner layer, and the agreement is not as good, particularly when f/f_p is large. As the reflection coefficient is then very small this is unimportant For both layers the agreement is best when ν is large.

4.3. *Chapman layer*

A more realistic layer to consider is the Chapman layer given by

$$f_N^2 = f_p^2 \exp \tfrac{1}{2}(1 - \zeta - e^{-\zeta}) \tag{4.9}$$

where $\zeta = (z - z_m)/H$, H being the scale height, which is assumed to be constant throughout the layer.

Let $\zeta = \zeta_0$ when $z = z_0$. A change of variable of integration to ζ in (4.4) gives

$$h'(f) = \mathscr{R}\left(\frac{1 - \frac{1}{2}iZ}{1 - iZ} \cdot \int_{-z_m/H}^{\zeta_0} \frac{H}{n}\, d\zeta - \frac{\frac{1}{2}iZ}{1 - iZ} \int_{-z_m/H}^{\zeta_0} H \,.\, n\, d\zeta\right).$$

This can be put into a form suitable for numerical integration, by the substitution

$$t = \frac{f_p^2}{f^2(1 - iZ)} \exp \tfrac{1}{2}(1 - \zeta - e^{-\zeta})$$

so that $n^2 = 1 - t$, and $t = 1$ when $\zeta = \zeta_0$, $t = t_1$ when $\zeta = -z_m/H$. Now $h'(f)$ becomes

$$h'(f) = H \,.\, \mathscr{R}\left(\frac{1 - \frac{1}{2}iZ}{1 - iZ} \cdot \int_{t_1}^{1} \frac{2dt}{t(1-t)^{\frac{1}{2}}(e^{-\zeta} - 1)} - \frac{\frac{1}{2}iZ}{1 - iZ} \int_{t_1}^{1} \frac{2(1-t)^{\frac{1}{2}}}{t(e^{-\zeta} - 1)}\, dt\right). \tag{4.10}$$

Since both integrands are very large near the lower limit, and the first is very large near the upper limit, it is convenient to subtract

$$\mathscr{R}(z_0) = H \,.\, \mathscr{R}\left[\int_{t_1}^{1} \frac{2dt}{t(e^{-\zeta} - 1)}\right]$$

from both sides of (4.10), and to make the further change of variable $t = \sin^2\theta$. The lower limit t_1 is proportional to the electron density near the ground, and therefore extremely small, and may now safely be replaced by zero. These changes give finally

$$\frac{h'(f) - \mathscr{R}(z_0)}{H} = \mathscr{R}\left[\frac{1 - \frac{1}{2}iZ}{1 - iZ} \cdot \int_0^{\frac{1}{2}\pi} \frac{4 \tan(\frac{1}{2}\theta)}{e^{-\zeta} - 1}\, d\theta + \frac{\frac{1}{2}iZ}{1 - iZ} \int_0^{\frac{1}{2}\pi} \frac{4 \tan(\frac{1}{2}\theta)\cos\theta}{e^{-\zeta} - 1}\, d\theta\right]. \tag{4.11}$$

VOL. 22 1961

The term $1/(e^{-\zeta} - 1)$ cannot be expressed as an explicit function of θ, and must be calculated by an iterative process, for each particular value required. The same iterative process, with $\theta = \frac{1}{2}\pi$, can be used to calculate ζ_0 and hence z_0. Gaussian quadrature was used to evaluate the integrals of (4.11), and a typical set of $h'(f)$ curves obtained is shown in Fig. 2.

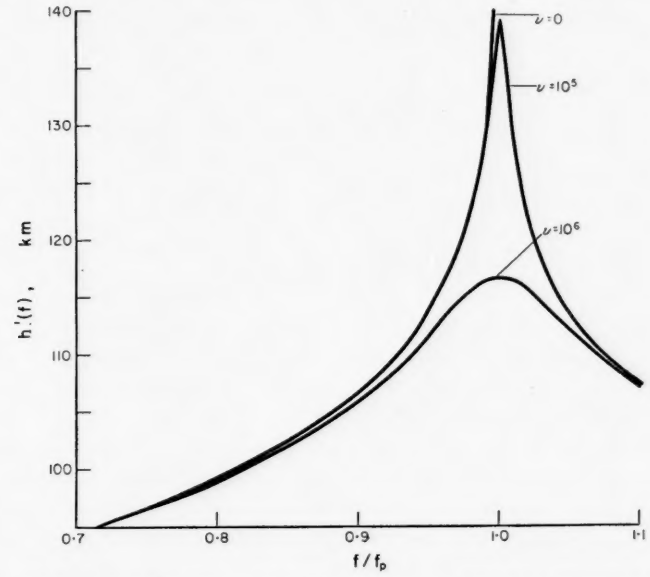

Fig. 2. To show how the equivalent height of reflection $h'(f)$ for a Chapman layer depends upon frequency f when the collision frequency is independent of height and the earth's magnetic field is neglected. For all the curves shown $f_p = 2$ Mc/s, $H = 10$ km, $z_m = 100$ km and ν is in units of sec^{-1}.

5. The Phase-Integral Method with Collisions and Magnetic Field Included

5.1. *The complex refractive index n, and the group refractive index n'.*

When the earth's magnetic field is included, the Appleton–Hartree formula (Appleton, 1932) gives for n, the complex refractive index,

$$n^2 = 1 - \frac{X(1 - X - iZ)}{D}$$

where
$$D = (1 - iZ)(1 - X - iZ) - \tfrac{1}{2}Y_T{}^2 + S \qquad (5.1)$$

and
$$S = \pm[Y_L{}^2(1 - X - iZ)^2 + \tfrac{1}{4}Y_T{}^4]^{\frac{1}{2}}$$

in which the two signs of S represent the two magneto-ionic components. The polarization of a component is given by the magneto-ionic theory as

$$R = -\frac{i}{Y_L}\left(\frac{\frac{1}{2}Y_T{}^2 - S}{1 - X - iZ}\right).$$

If the real part of S is positive the wave is called an ordinary wave in this paper, while if the real part of S is negative the wave is called extraordinary. A wave which is ordinary at low levels may sometimes become extraordinary at greater heights. Such a wave is called "initial ordinary". Similarly a wave which is extraordinary at low levels, but which becomes ordinary at greater heights is called "initial extraordinary".

The complex group refractive index n' can be found by differentiating (5.1), since

$$nn' - 1 = \tfrac{1}{2}f \cdot \frac{\partial}{\partial f}(n^2) + n^2 - 1$$

whence

$$nn' - 1 = \frac{1}{D}\left\{ - X + \tfrac{1}{2}iXZ + (1 - n^2) \times \left[1 - iZ - \tfrac{1}{2}iXZ + \frac{\tfrac{1}{2}(1 - X - iZ)(1 + X){Y_L}^2}{S}\right]\right\}. \quad (5.2)$$

The sign of S used in calculating n' for any phase integral must be such that along the path of integration in the complex plane n' is a continuous function of z.

5.2. *The Riemann surface and the branch points*

The complex refractive index n is now a four-valued function of z, and can be represented on a four-sheeted Riemann surface (ECKERSLEY, 1950; PFISTER, 1953), one sheet containing the upgoing ordinary, one the upgoing extraordinary, one the downcoming ordinary and one the downcoming extraordinary. The branch points between the upgoing and downcoming sheets are the zeros of n, while the ordinary and extraordinary sheets are connected at branch points where $S = 0$.

From (5.1) n has zeros where

$$1 - X - iZ = \begin{cases} 0 \\ \pm Y \end{cases}$$

and S has zeros where

$$1 - X - iZ \pm \tfrac{1}{2}i({Y_T}^2/Y_L) = 0.$$

Since ν and f_H are independent of z throughout this paper, the values of z for which n is zero are the solutions of

$$X(z) = \begin{cases} 1 - iZ \\ 1 - iZ \pm Y \end{cases} \quad (5.3)$$

and the values of z for which S is zero are the solutions of

$$X(z) = 1 - iZ \pm \tfrac{1}{2}i({Y_T}^2/Y_L). \quad (5.4)$$

If z_0 is the level where

$$X(z_0) = 1 - iZ$$

then $n = 0$ only if

$$S = \pm\tfrac{1}{2}{Y_T}^2$$

and only an ordinary wave is reflected. This branch point therefore joins the

VOL. 22 1961

upgoing ordinary sheet to the downcoming ordinary sheet. On the other hand, if z_0 is either of the levels where

$$X(z_0) = 1 - iZ \pm Y$$

then $n = 0$ only if

$$S = -(Y^2 - \tfrac{1}{2}Y_T{}^2)$$

and only an extraordinary wave is reflected. These branch points therefore join the upgoing extraordinary sheet to the downcoming extraordinary sheet.

A path of integration passes from an upgoing to a downcoming sheet if it goes round one of the branch points of (5.3), and passes from one polarization sheet to another, if it goes round one of the branch points of (5.4). Thus a path of integration can be taken such that it passes in succession from the upgoing ordinary sheet to the upgoing extraordinary, the downcoming extraordinary and the downcoming ordinary. It has been shown by RYDBECK (1950, 1951) in his theory of coupling, that the existence of such a component depends upon whether ν is less or greater than a critical value ω_c, where

$$\omega_c = \pi f_H \cdot \frac{\sin^2 \Theta}{\cos \Theta} .$$

The reflection properties of such a component are calculated by the phase-integral method in Section 6, and the effect of $\nu < \omega_c$ or $\nu > \omega_c$ is evident.

It should be noted that n' is infinite at the zeros of n in the appropriate polarization sheet, and at the zeros of S, i.e. at all the branch points in the Riemann sheets.

5.3. *The paths of integration*

In all the layers considered in this paper, either X is a single-valued function of z, or the electron density increases monotonically to a maximum at a height z_m, and the levels of reflection are assumed to lie below z_m. In this case, (5.3) defines three possible levels of reflection if $Y < 1$, and two possible levels if $Y > 1$. If z_0 is a possible level of reflection, the equivalent height for the component reflected at this level, calculated by the phase-integral method, is from (3.5)

$$h'(f) = \mathscr{R}\left(\int_0^{z_0} n' \, dz\right) \tag{5.5}$$

where n' is now given by (5.2).

Consider a layer for which X is an analytic function of z, such that $X = 0$ when $z = 0$. Provided a path of integration is chosen such that $dX/dz \neq 0$ at any point on it, (5.5) now gives

$$h'(f) = \mathscr{R}\left(\int_0^{X(z_0)} \frac{n'}{dX/dz} \, dX\right) \tag{5.6}$$

and the right-hand side is now a contour integral taken in the complex X-plane.

Fig. 3 has been drawn for a value of the collision frequency such that $\nu > \omega_c$. This results in the point

$$X = 1 - iZ + \tfrac{1}{2}i(Y_T{}^2/Y_L)$$

being below the real axis in the complex X-plane. Suppose

$$X(z_0) = 1 - iZ + Y.$$

Two possible paths of integration (a) and (b) are shown in Fig. 3, one of which, (b), corresponds to an initial ordinary wave and the other, (a), to an extraordinary

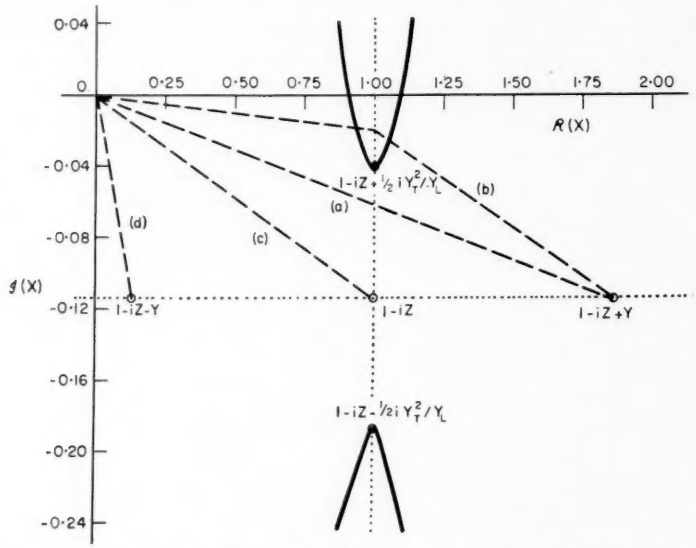

Fig. 3. The complex X-plane, showing branch points and possible paths of integration. $\nu = 10^6$ sec^{-1}, $f = 1{\cdot}4$ Mc/s, $f_H = 1{\cdot}2$ Mc/s, $\Theta = 0{\cdot}40608$ rad.

wave. This follows from consideration of the value of S along each path. The real part of S^2 changes sign on the hyperbola

$$[1 - \mathscr{R}(X)]^2 - [\mathscr{I}(X) + Z]^2 + \tfrac{1}{4}Y_T{}^4/Y_L{}^2 = 0$$

while the imaginary part changes sign on the lines

$$\mathscr{R}(X) = 1, \qquad \mathscr{I}(X) = -Z.$$

Along path (a) in Fig. 3, $\mathscr{R}(S^2)$ remains positive while $\mathscr{I}(S^2)$ changes from negative to positive values and back to zero, whereas along path (b) $\mathscr{R}(S^2)$ changes from positive to negative values and then back to positive. Fig. 4 (i) shows the variation of S^2 along the two paths for typical values of f, f_H and Θ, and Fig. 4 (ii) shows the corresponding variation of the two square roots of S^2. S must take the value $-(Y^2 - \frac{1}{2}Y_T{}^2)$ when $X = 1 - iZ + Y$ and therefore for path (a) the component reflected is extraordinary at every point of its path, whereas for path (b) the initial ordinary changes to an extraordinary wave, is reflected, and changes back to an ordinary wave on the downward path.

For frequencies greater than the gyrofrequency, this latter component is the Z-trace. For very low frequencies it is the most commonly observed reflection, being the one reflected near where $X = 1 + Y$, but having the polarization ascribed to the ordinary ray when it reaches the ground. The condition $\nu > \omega_c$

VOL. 22 1961

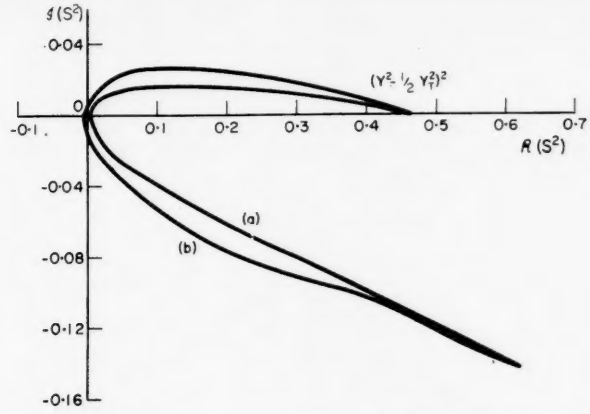

Fig. 4(i). The complex S^2-plane, showing the variation of S^2 along paths (a) and (b) of Fig. 3.

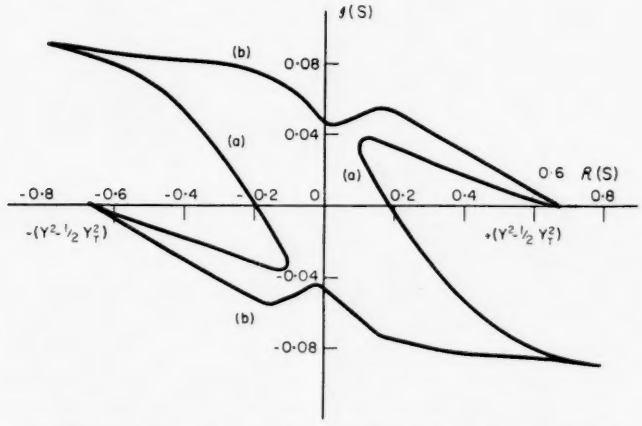

Fig. 4(ii). The complex S-plane, showing the variation of S along paths (a) and (b) of Fig. 3. The component reflected where $X = 1 - iZ + Y$ is the extraordinary for path (a) and the initial ordinary for path (b).

will generally hold for very low frequencies, since these will be reflected very low in the ionosphere, where ν is large.

Using similar arguments, the component reflected along path (c), where the height of reflection is given by

$$X(z_0) = 1 - iZ$$

is ordinary at every point, and the component reflected along path (d), where the height of reflection is given by

$$X(z_0) = 1 - iZ - Y$$

is extraordinary at every point.

The four reflected rays which have been discussed are the rays most commonly observed, and therefore of greatest interest. It appears possible to take other paths of integration, such that other reflected rays are obtained, but according to

PFISTER (1953), some of these components violate the conditions upon which the W.K.B. approximation is based. PFISTER gives the initial ordinary ray reflected at

$$X(z) = 1 - iZ - Y$$

as an example of this. BUDDEN (1961) shows that an initial extraordinary wave cannot change its polarization to ordinary and be reflected where

$$X(z) = 1 - iZ.$$

Therefore, only the four major reflected components described above have been considered in this paper.

6. Application to Linear, Exponential and Chapman Layers, with Collisions and Magnetic Field Included

Throughout this section the earth's magnetic field is taken as constant in magnitude and direction at every point of the ionized layers considered. The values used are

$$f_H = 1{\cdot}2 \text{ Mc/s}, \qquad \Theta = 23°16' = 0{\cdot}40608 \text{ rad}$$

and therefore

$$\omega_c = 0{\cdot}64030 \times 10^6 \text{ sec}^{-1}.$$

The paths of integration used to evaluate the phase integrals are (c) and (d) of Fig. 3, and a path

$$\left.\begin{aligned} X &= t[1 - iZ + \tfrac{1}{2}i(Y_T{}^2/Y_L)], \qquad 0 \leqslant t \leqslant 1 \\ X &= [1 - iZ + \tfrac{1}{2}i(Y_T{}^2/Y_L)] + s[Y - \tfrac{1}{2}i(Y_T{}^2/Y_L)], \qquad 0 \leqslant s \leqslant 1 \end{aligned}\right\} \quad (6.1)$$

from $X = 0$ to the branch point $[1 - iZ + \frac{1}{2}i(Y_T{}^2/Y_L)]$, and from there to $(1 - iZ + Y)$. If ordinary polarization is taken along the first part of this path and extraordinary along the second, ordinary and extraordinary polarizations being equal at the branch point, the initial ordinary component results, whereas if extraordinary polarization is taken along the entire path, the extraordinary component results. A check was provided on results from this path by also evaluating the phase integrals along a straight line path from $X = 0$ to $X = 1 - iZ + Y$. If $\nu < \omega_c$ the result is the extraordinary component for all frequencies, but if $\nu > \omega_c$ then the initial ordinary component results for $f < (\nu - \omega_c)f_H/\omega_c$ and the extraordinary for $f > (\nu - \omega_c)f_H/\omega_c$, care being taken to keep the polarization continuous and such that $n = 0$ at $(1 - iZ + Y)$.

Consider a linear layer

$$f_N{}^2 = \alpha z$$

for which

$$X = \frac{\alpha z}{f^2}$$

and

$$\frac{dX}{dz} = \frac{\alpha}{f^2} \neq 0.$$

Since $X = 0$, when $z = 0$, (5.6) can be used immediately, and

$$h'(f) = \frac{f^2}{\alpha}\,\mathscr{R}\left(\int_0^{X(z_0)} n'\,dX\right). \quad (6.2)$$

VOL. 22 1961

If $X(z_0) = 1 - iZ + Y$ the path of integration is given by (6.1), and hence

$$h'(f) = \frac{f^2}{\alpha} \mathscr{R}\left[\int_0^1 n' \left(1 - iZ + \tfrac{1}{2}i \frac{{Y_T}^2}{Y_L}\right) dt + \int_0^1 n' \left(Y - \tfrac{1}{2}i \frac{{Y_T}^2}{Y_L}\right) ds\right].$$

As n' has singularities at $t = 1$, and at $s = 0$, 1, it is convenient for numerical computation to put $t = \sin\theta$, and $s = \cos^2\phi$, whereupon

$$h'(f) = \frac{f^2}{\alpha} \left\{\int_0^{\pi/2} \mathscr{R}\left[n' \left(1 - iZ + \tfrac{1}{2}i \frac{{Y_T}^2}{Y_L}\right)\right] \cos\theta \, d\theta + \int_0^{\pi/2} \mathscr{R}\left[n' \left(Y - \tfrac{1}{2}i \frac{{Y_T}^2}{Y_L}\right)\right] 2 \sin\phi \cos\phi \, d\phi\right\} \quad (6.3)$$

and these integrals can be evaluated easily by Gaussian quadrature.

The total absorption of a reflected wave is given by (3.4). Application of the same set of substitutions as above to $\int_0^{z_0} n \, dz$ results in the total absorption of the components reflected at $(1 - iZ + Y)$ becoming

$$-\log|\rho| = -\frac{2kf^2}{\alpha} \left\{\int_0^{\pi/2} \mathscr{I}\left[n \left(1 - iZ + \tfrac{1}{2}i \frac{{Y_T}^2}{Y_L}\right)\right] \cos\theta \, d\theta + \int_0^{\pi/2} \mathscr{I}\left[n\left(Y - \tfrac{1}{2}i \frac{{Y_T}^2}{Y_L}\right)\right] 2 \sin\phi \cos\phi \, d\phi\right\}. \quad (6.4)$$

The integrations for $h'(f)$ and $-\log|\rho|$ can conveniently be performed in the same programme, since n has to be calculated in order to calculate n'. Curves for the initial ordinary and extraordinary components reflected at $1 - iZ + Y$ can be computed from (6.3) and (6.4). Similar expressions for $h'(f)$ and $-\log|\rho|$ can be obtained for the ordinary component reflected at $(1 - iZ)$ and for the extraordinary component reflected at $(1 - iZ + Y)$.

The result of these calculations is shown in Fig. 5. It can be seen that the magnitude of the collision frequency ν makes no appreciable difference to the $h'(f)$ curves, except to the extraordinary component, reflected at $(1 - iZ + Y)$, when f approaches the gyrofrequency f_H. This is not important, as this component is strongly absorbed as $f \to f_H$. Similar $h'(f)$ curves, with the exception of the initial ordinary ray, were obtained by SHINN (1951), using ray theory and neglecting collisions. The important point to be noticed is the difference in the absorption curves of Fig. 5(ii), in which $\nu < \omega_c$ and Fig. 5(iii) in which $\nu > \omega_c$. In the former, the absorption of the initial ordinary is four or five times that of the ordinary, whereas in the latter, the absorption of the initial ordinary is less than twice that of the ordinary.

Consider next an exponential layer for which

$${f_N}^2 = (2 \times 10^{-13})^2 \, e^{0{\cdot}6z}. \quad (6.5)$$

For such a layer, when $z = 100$ km, $f_N \approx 2$ Mc/s. From (5.3), a change to integration with respect to X gives

$$h'(f) = \mathscr{R}\left(\int_{X(0)}^{X(z_0)} \frac{n'}{0{\cdot}6X} \, dX\right) \quad (6.6)$$

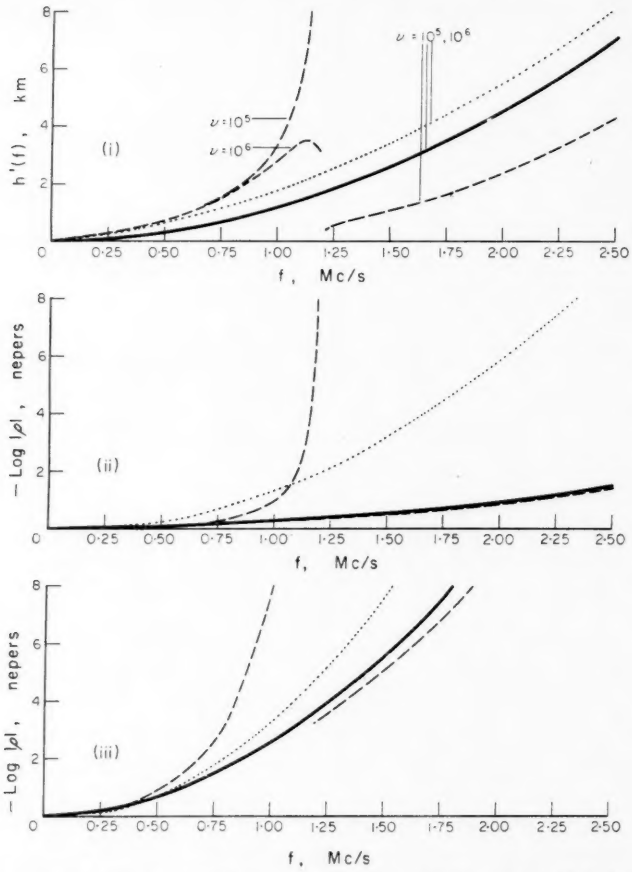

Fig. 5. Results for a linear layer $f_N{}^2 = \alpha z$, with the earth's magnetic field included and the collision frequency independent of height, showing the properties of the ordinary, extraordinary and initial ordinary waves. For all curves shown $f_H = 1{\cdot}2$ Mc/s, $\Theta = 0{\cdot}40608$ rad, $\alpha = 2$ km^{-1} sec^{-2}, $\omega_c = 6{\cdot}4030 \times 10^5$ sec^{-1}. ——— ordinary wave; – – – extraordinary wave; · · · · · initial ordinary wave.

(i) Equivalent height, $h'(f)$, curves for $\nu = 10^5$ sec^{-1} and $\nu = 10^6$ sec^{-1}.
(ii) Absorption, $-\log|\rho|$, curves for $\nu < \omega_c$; $\nu = 10^5$ sec^{-1}.
(iii) Absorption, $-\log|\rho|$, curves for $\nu > \omega_c$; $\nu = 10^6$ sec^{-1}.

where $X(0)$ is very small. Consider the component reflected at $1 - iZ - Y$, and take (d) of Fig. 3 as path of integration. Since the integrand is very large near the lower limit, it is convenient to subtract

$$\mathscr{R}(z_0) = \mathscr{R}\left(\int_{X(0)}^{X(z_0)} \frac{dX}{0{\cdot}6X}\right)$$

from both sides of (6.6), and the lower limit may then safely be replaced by zero. With a final change of variable

$$X = (1 - \tau^2)(1 - iZ - Y)$$

VOL. 22 1961

(6.6) becomes

$$h'(f) - \mathscr{R}(z_0) = \int_0^1 \frac{\mathscr{R}(n' - 1) \cdot 2\tau}{0{\cdot}6(1 - \tau^2)} \, d\tau \,. \tag{6.7}$$

Similarly the absorption for this component becomes

$$-\log |\rho| = -2k \cdot \int_0^1 \frac{2\tau \mathscr{I}(n - 1)}{0{\cdot}6(1 - \tau^2)} \, d\tau - 2k \cdot \mathscr{I}(z_0). \tag{6.8}$$

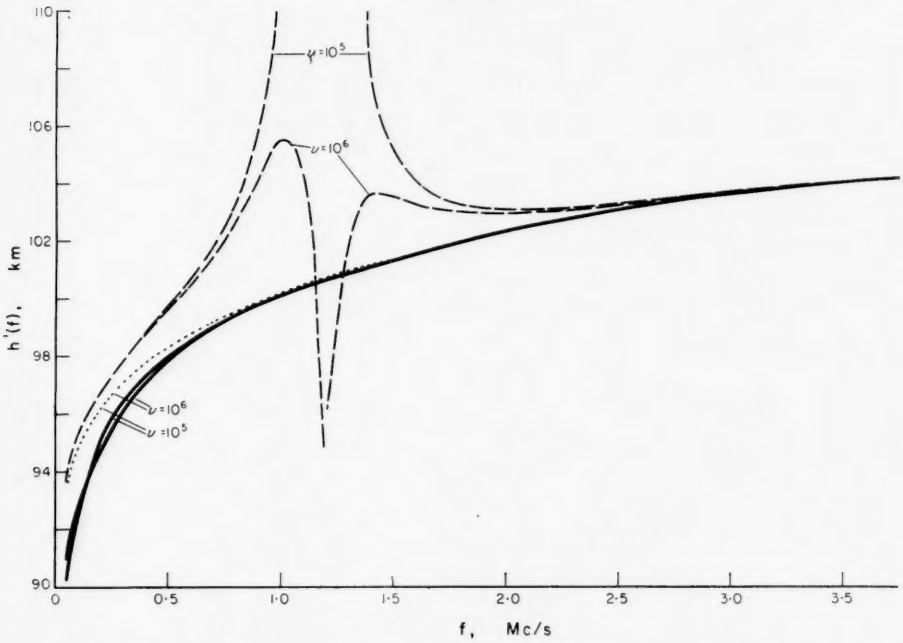

Fig. 6. Equivalent height, $h'(f)$, curves for an exponential layer with the earth's magnetic field included, showing the ordinary, initial ordinary and extraordinary waves for $\nu < \omega_c$ and $\nu > \omega_c$. $f_N^2 = (2 \times 10^{-13})^2 \, e^{0{\cdot}6z}$, $f_H = 1{\cdot}2$ Mc/s, $\Theta = 0{\cdot}40608$ rad, $\omega_c = 6{\cdot}4030 \times 10^5$ sec^{-1}. Key as in Fig. 5.

Since $X(z_0) = 1 - iZ - Y$,

$$z_0 = \frac{1}{0{\cdot}6} \log \left[\frac{f^2(1 - iZ - Y)}{(2 \times 10^{-13})^2} \right] \tag{6.9}$$

and $h'(f)$ and $-\log |\rho|$ can now easily be calculated. Similar expressions can be deduced for other reflected rays, using the paths of integration previously described. Figs. 6 and 7 show some typical results. Again the $h'(f)$ curves are very close to those for which $\nu = 0$, except for the extraordinary near f_H, where the absorption is very great. When $\nu = 10^6$ sec^{-1}, the absorption of the initial ordinary is less than that of the ordinary until $f \approx 1{\cdot}4$ Mc/s whereas when $\nu = 10^5$ sec^{-1} it is only less than that of the ordinary for $f < 200$ kc/s.

Finally consider again the Chapman layer of Section 4.3, equation (4.9) and take as an example the ordinary wave reflected where $X = (1 - iZ)$, using (c) of Fig. 3 as path of integration. The same substitutions as in Section 4 are required

to put $h'(f)$, given by (5.3), and $-\log|\rho|$, given by (3.4), in a form suitable for numerical integration. In its final form

$$h'(f) = H\left[\int_0^{\pi/2} \mathscr{R}\left(\frac{n'-1}{e^{-\zeta}-1}\right)\cdot\frac{4}{\tan\theta}\,d\theta + \mathscr{R}\left(\zeta_0 + \frac{z_m}{H}\right)\right] \tag{6.10}$$

and

$$-\log|\rho| = -2kH\left[\int_0^{\pi/2} \mathscr{I}\left(\frac{n-1}{e^{-\zeta}-1}\right)\frac{4}{\tan\theta}\,d\theta + \mathscr{I}\left(\zeta_0 + \frac{z_m}{H}\right)\right] \tag{6.11}$$

where $\zeta = (z - z_m)/H$, and

$$\sin^2\theta = \frac{f_p^2}{f^2(1 - iZ)}\exp\tfrac{1}{2}(1 - \zeta - e^{-\zeta}).$$

Similar expressions can be obtained for the other components.

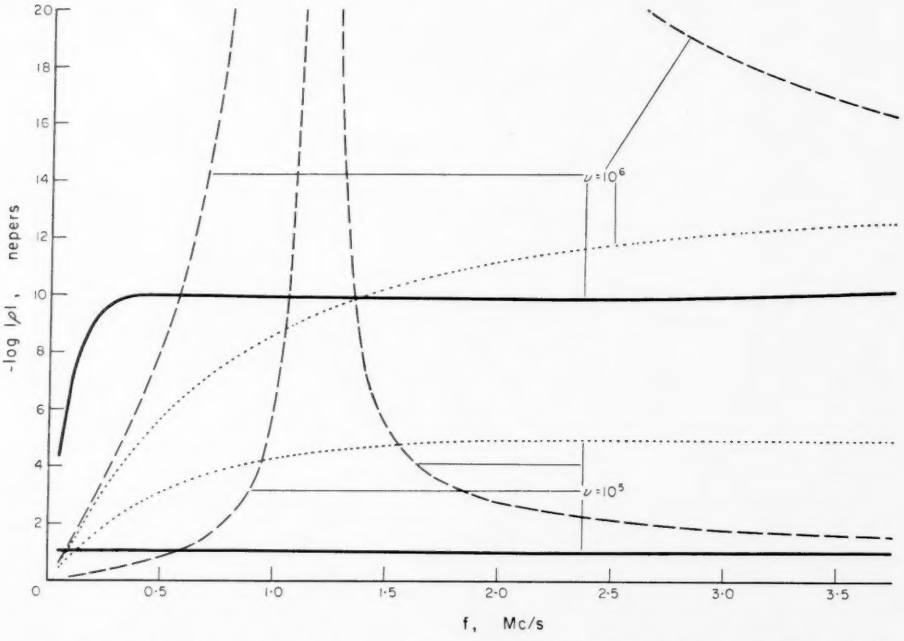

Fig. 7. Absorption, $-\log|\rho|$, curves for an exponential layer, with the earth's magnetic field included, showing the ordinary, initial ordinary and extraordinary waves for $\nu < \omega_c$ and $\nu > \omega_c$. $f_N^2 = (2 \times 10^{-13})^2 e^{0\cdot6z}$, $f_H = 1\cdot2$ Mc/s, $\Theta = 0\cdot40608$ rad, $\omega_c = 6\cdot4030 \times 10^5$ sec^{-1}. Key as in Fig. 5.

Figs. 8 and 9 show sets of curves obtained using (6.10), (6.11) and similar expressions. The penetration frequencies for the initial ordinary, ordinary and extraordinary when $\nu = 0$ are the positive solutions of

$$Cf^2 - f_p^2 = 0$$

where

$$C = \begin{cases} 1 + Y \\ 1 \\ 1 - Y \end{cases}$$

VOL. 22 1961

For the layer shown the penetration frequencies are

$$f = 1{\cdot}4881,\ 2,\ 2{\cdot}6881 \text{ Mc/s}.$$

Whereas the phase integral solution when $\nu = 0$ breaks down at these frequencies, Fig. 8 shows that when $\nu > 0$ the phase integral solutions for $h'(f)$ remain finite at and above these frequencies, although Fig. 9 shows that the absorption becomes very large. Also from Fig. 9 the initial ordinary absorption is greater

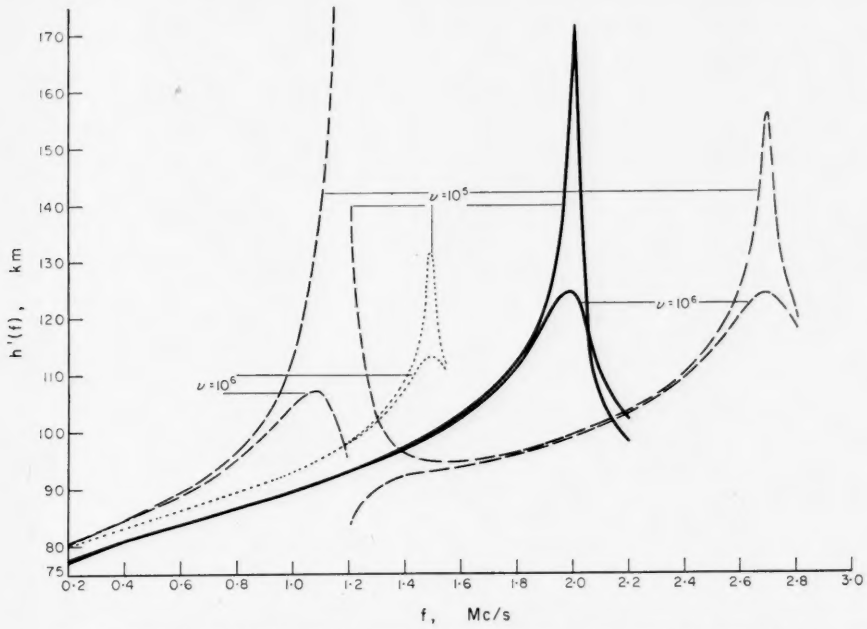

Fig. 8. Equivalent height, $h'(f)$, curves for a Chapman layer, with the earth's magnetic field included, showing the ordinary, initial ordinary and extraordinary waves for $\nu < \omega_c$ and $\nu > \omega_c$. $f_p = 2$ Mc/s, $H = 10$ km, $z_m = 100$ km, $f_H = 1{\cdot}2$ Mc/s, $\Theta = 0{\cdot}40608$ rad, $\omega_c = 6{\cdot}4030 \times 10^5$ sec^{-1}. Key as in Fig. 5.

than the ordinary when $\nu = 10^5$ sec^{-1} for all frequencies, but when $\nu = 10^6$ sec^{-1} it is less than the ordinary until $f = 0{\cdot}9$ Mc/s.

7. Conclusions

As the phase-integral method has been shown to provide good agreement with a full wave solution in a very simple case, it is likely to provide good results in more complicated cases, provided that the conditions upon which the approximation is based are fulfilled.

The method has the advantages of being more accurate than the simple ray theory, and of being valid up to and beyond the penetration frequency of a layer. It provides a straightforward method of dealing with components such as the initial ordinary reflected near $X = 1 + Y$, which is important for low frequencies if $\nu > \omega_c$. The length of the computation involved is short, depending mainly on the length of any iterative process required, and on the number of points needed

to obtain good values of the integrals—forty-eight points were taken in most examples in this paper.

It is therefore considered that the method is likely to be most useful in the frequency range 200–2000 kc/s, where a step-by-step integration is very long, and the simple ray theory methods are not sufficiently accurate. If the phase-integral method is to give a complete answer, it will be necessary to study the limiting

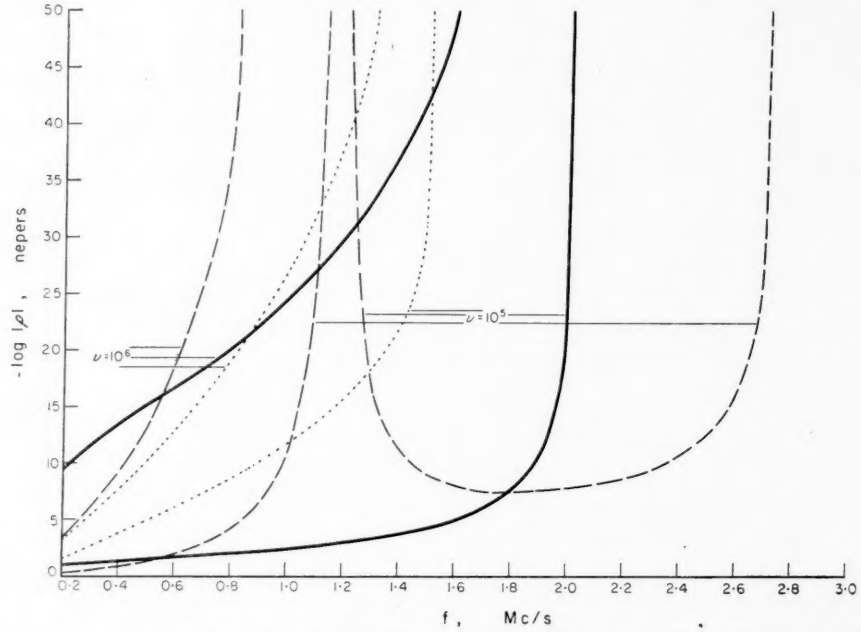

Fig. 9. Absorption, $-\log|\rho|$, curves for a Chapman layer, with the earth's magnetic field included, showing the ordinary, initial ordinary and extraordinary waves for $\nu < \omega_c$ and $\nu > \omega_c$. $f_p = 2$ Mc/s, $H = 10$ km, $z_m = 100$ km, $f_H = 1{\cdot}2$ Mc/s, $\Theta = 0{\cdot}40608$ rad, $\omega_c = 6{\cdot}4030 \times 10^5$ sec^{-1}. Key as in Fig. 5.

polarization of downcoming waves (BARRON, 1960). Coupling echoes cannot be dealt with by the phase-integral method.

Acknowledgements—I wish to thank Dr. K. G. BUDDEN for many useful suggestions and criticisms, and Dr. M. V. WILKES, Director of the University Mathematical Laboratory, Cambridge, for permission to use the computer EDSAC 2. I am indebted to the Department of Scientific and Industrial Research for a maintenance grant covering the period in which the work was carried out.

REFERENCES

APPLETON E. V.	1932	*J. Inst. Elect. Engrs* **71**, 642.
BARRON D. W.	1960	Ph.D. thesis, Cambridge.
BARRON D. W. and BUDDEN K. G.	1959	*Proc. Roy. Soc.* A **249**, 387.
BUDDEN K. G.	1955	*Proc. Roy. Soc.* A **227**, 516.
BUDDEN K. G.	1961	*Radio Waves in the Ionosphere*, p. 454. Cambridge University Press.

VOL. 22 1961

Eckersley T. L.	1931	*Proc. Roy. Soc.* A **132,** 83.
Eckersley T. L.	1932a	*Proc. Roy. Soc.* A **136,** 499.
Eckersley T. L.	1932b	*Proc. Roy. Soc.* A **137,** 158.
Eckersley T. L.	1950	*Proc. Phys. Soc. Lond.* **63,** 49.
Hartree D. R.	1931	*Proc. Roy. Soc.* A **131,** 428.
Pfister W.	1953	*J. Geophys. Res.* **58,** 29.
Rydbeck O. E. H.	1943	*Phil. Mag.* **34,** 346.
Rydbeck O. E. H.	1950	*J. Appl. Phys.* **21,** 1205.
Rydbeck O. E. H.	1951	*Chalmers Tek. Högsk. Handl.* No. 101.
Shinn D. H.	1951	Unpublished typescript, Radio Section, Cavendish Laboratory, Cambridge.

Journal of Atmospheric and Terrestrial Physics, 1961, Vol. 22, pp. 142 to 156. Pergamon Press Ltd. Printed in Northern Ireland

An idealized problem of plasma dynamics that bears on geomagnetic storm theory; oblique projection

S. CHAPMAN* and P. C. KENDALL†

(*Received* 15 *May* 1961)

Abstract—A cylindrical sheet current distribution of neutral ionized gas is situated in a permanent unidirectional magnetic field whose intensity varies as an inverse power of the distance from the axis of the cylinder. Initially every particle is projected obliquely symmetrically inward with the same speed. The motion through the field generates an electric current around the sheet, and a uniform magnetic field within the space enclosed. The sheet is retarded by the interaction between the current and the magnetic field. If the charge of either sign per unit length of the cylinder exceeds a certain value the sheet remains one—otherwise it divides into a negative and a positive sheet. The motion in the former case, which bears on the geomagnetic deflection of solar particles travelling towards the earth, is studied in detail. It has some bearing on the theory of magnetic storms, and on the shape of the hollow carved by the earth's field in solar streams, as investigated by CHAPMAN and FERRARO, and more recently by BEARD (1960), DUNGEY (1961), ZHIGULEV and ROMISHEVSKII (1959) and other writers whose work is in the press.

INTRODUCTION

IN this paper we discuss a problem that illustrates one aspect of the theory of magnetic storms. It is a simple generalization, suggested by CHAPMAN (1960), of a problem solved by him and FERRARO in 1940. Their paper was one of a series (CHAPMAN and FERRARO, 1929–1941; FERRARO, 1952) in which they sought to develop a deductive theory of magnetic storms, on the basis of certain idealized hypotheses. Their method included the conception and solution of various simple problems related in some respects to the actual phenomena. They added partly qualitative inferences and speculations suggested by their solutions. The present problem deals chiefly with the transient motion of an ionized sheet and may be contrasted with recent work involving the steady state set up by a solar corpuscular flux.

In 1952 FERRARO derived a result first proposed by MARTYN which showed that the geomagnetic field would be terminated at a point where the momentum pressure would be balanced by the magnetic pressure. This result has been used recently by various authors to infer the shape of the hollow containing the geomagnetic field. An approximate method of solution was initiated by BEARD (1960). He discussed the hollow round a point dipole. This method has since been used by SPREITER and BRIGGS (1961). The first *exact* solutions of problems of this type were derived by ZHIGULEV and ROMISHEVSKII (1959) and by DUNGEY (1961). They dealt with a two-dimensional hollow round a line dipole. It appears that the three-dimensional shape of the hollow round a point dipole has not yet been calculated exactly. However, it seems likely that SPREITER's results are close approximations.

It is interesting to note that by an extension of their 1940 paper CHAPMAN and FERRARO could have derived a curve representing the equatorial section of the

* Geophysical Institute, College, Alaska; High Altitude Observatory, Boulder, Colorado (there engaged in a programme of research sponsored by the National Bureau of Standards and the Air Force Geophysical Research Directorate.); University of Michigan, Ann Arbor, Michigan.

† On leave of absence from Bedford College, University of London.

VOL. 22 1961

hollow. In fact these authors derived the equations of motion for the present problem. We shall therefore briefly describe their work. Their 1940 paper dealt with electrons and singly charged positive ions distributed in equal numbers over a cylindrical sheet of (varying) radius R, in the presence of a magnetic field everywhere parallel to the axis. The field intensity H is M/R^n at distance R from the axis. It is convenient to think of the lines of force as directed upwards, and to call their direction northwards. Looking towards the axis, the direction to the right is eastward, and that to the left is westward. The particles move in planes normal to the axis. Energy losses due to electromagnetic radiation associated with the changing motions of the particles are ignored.

Let θ_e, θ_i denote the azimuthal angular coordinates, and U_e, V_e and U_i, V_i the radial (outward) and transverse (eastward) velocity components of a typical electron and ion when distant R from the axis. Thus

$$U_e = \dot{R}_e,\ V_e = R_e\dot{\theta}_e,\ U_i = \dot{R}_i,\ V_i = R_i\dot{\theta}_i \tag{1}$$

where the superimposed dots indicate differentiation with respect to time, t.

In terms of the masses m_e, m_i we define associated masses and transverse speeds as follows:

$$m = m_i + m_e,\ m' = m_i m_e/m,\ m'' = m' + eQ/c^2 \tag{2}$$

$$mV = m_i V_i + m_e V_e, \quad V' = V_i - V_e. \tag{3}$$

Here e denotes the positive magnitude (e.s.u.) of the charge on each particle; Q denotes the total *positive* charge per unit length of the cylinder. If there are N electrons and N ions per unit length, with number density ν per unit area,

$$Q = Ne = 2\pi R\nu e. \tag{4}$$

The sheet has angular momentum P per unit length:

$$P = NmRV. \tag{5}$$

It carries an electric current J (in e.m.u.) per unit length:

$$J = neV'/c = QV'/2\pi Rc. \tag{6}$$

This solenoidal current produces no magnetic field outside the sheet. It produces a field h inside:

$$h = 4\pi J = 2QV'/Rc. \tag{7}$$

The fields H and h have vector potentials, A, A', whose vector lines are eastward-directed circles, symmetrical about the axis:

$$A = -M/(n-2)R^{n-1}, \qquad A' = QV'/c. \tag{8}$$

The electrons and ions, moving in the magnetic field, are subject to different forces, partly radial, partly transverse. On account of the inequality of the radial forces, the sheet tends to separate into two, one occupied only by electrons, the other by ions. Any separation brings into play an electrostatic attraction, proportional to Q, between the sheets. CHAPMAN and FERRARO (1940) showed that in cases that have geomagnetic interest, Q must far exceed the least value that

suffices to prevent separation. In our discussion we suppose Q to exceed this value, so that

$$R_e = R_i = R, \qquad U_e = U_i = U \tag{9}$$

and there is only one equation of radial motion. We quote this from CHAPMAN and FERRARO (1940, Section 3.2; 1941, equation 2):

$$m\ddot{R} = (mV^2 + m''V'^2)/R + eHV'/c \tag{10}$$

Angular momentum is conserved. Hence, by (5),

$$RV = \text{constant}. \tag{11}$$

We quote the first integrals of the equations of angular momentum of the ions and electrons (CHAPMAN and FERRARO, 1941, equations 4.4, 4.5):

$$\left.\begin{aligned} m_iRV_i + eR(A + A')/c &= \text{constant} = m_iC_i \\ M_eRV_e - eR(A + A')/c &= \text{constant} = m_eC_e \end{aligned}\right\} \tag{12}$$

From these we derive the equation

$$m''RV' - eM/(n-2)cR^{n-2} = m'(C_i - C_e) = m'C = \text{constant} \tag{13}$$

by multiplying the equations (12) by m_e/m and m_i/m respectively, subtracting, and using (8).

By means of (10), (13) the right hand side of (19) can be expressed as a function of R, and integration then gives U as a function of R. Further integration gives R as a function of t. Then from (11)–(13) the various transverse speeds can be found as functions of R, and integration gives θ_e, θ_i as functions of R and hence also of t. Thus one can determine the whole motion, and also J and h.

CHAPMAN and FERRARO (1940) discussed the motion consequent on the simultaneous inward impulsion of all the particles, from radius R_0, with the same speed U_0, *radially* towards the axis. They considered all values of Q, but particularly those sufficient to maintain the unity of the sheet. As this moves inward, the ions are deflected eastward and the electrons westward, and the sheet is retarded. Finally its radial motion is halted; at that radius J and h attain their maxima. Then the sheet recedes, and J and h decrease to zero. When the original radius is regained, all is as at first, except that the radial motion is reversed, and the electrons and ions have changed their azimuth in opposite directions.

CHAPMAN and FERRARO took R_0 to be one astronomical unit—the earth's distance from the sun. But they showed that the mathematics of the problem are much simplified, without disadvantage to the geophysical applications, by taking R_0 to be infinite. In that case the most suitable time origin is the instant when the sheet is at rest and has its minimum radius. For the typical particle the angular coordinate θ is reckoned from its position at that instant.

2. Oblique Projection from Infinity

We consider the problem in a similar way, but generalized by taking the initial impulsion, from infinity, to be oblique. That is, the initial line of motion of each

VOL. 22 1961

particle, perpendicular to the axis, is at a distance B from it. Hence (5) becomes

$$P = Nm\ RV = Nm\ BU_0 \tag{14}$$

The angular momentum P and the distance B are reckoned positive if P is eastward. The case $B = 0$ is the one considered by CHAPMAN and FERRARO.

Initially, at infinity, $RV_e = RV_i = BU_0$. Hence RV' is initially and always zero. As RA, RA' are zero at infinity, the constants C_e, C_i in (12) are each BU_0, and C in (13) is zero. Thus, from (13),

$$V' = eM/(n - 2)m''\ cR^{n-1}. \tag{15}$$

Hence, by (8), (15),

$$A + A' = -m'M/(n - 2)m''R^{n-1}. \tag{16}$$

Thus (12) may be written

$$\left.\begin{aligned} \dot\theta_i &= BU_0/R^2 - em'M/(n - 2)m_i m''cR^n \\ \dot\theta_e &= BU_0/R^2 - em'M/(n - 2)m_e m''cR^n \end{aligned}\right\} \tag{17}$$

Let

$$\dot\theta_i = \dot\theta + \dot\theta_i', \qquad \dot\theta_e = \dot\theta + \dot\theta_e' \tag{18}$$

and

$$\dot\theta = BU_0/R^2 \tag{19}$$

$$\dot\theta_e' = -em'M/(n - 2)m_e m''\ cR^n, \qquad m_e\theta_e' = -m_i\theta_i'. \tag{20}$$

It is convenient, for any particle, to take θ and θ', as well as θ_e and θ_i, to be zero at its position of closest approach to the axis.

Using (15), the equation of radial motion, (10), can be written

$$\ddot R/{U_0}^2 = B^2/R^3 + (n - 1)(R_1/R)^{2n-1}/R_1 \tag{21}$$

where

$$R_1^{2n-2} = e^2M^2/(n - 2)^2 mm''c^2{U_0}^2. \tag{22}$$

By integration (16) gives:

$$(U/U_0)^2 = 1 - (B/R^2) - (R_1/R)^{2n-2}. \tag{23}$$

Thus when the initial propulsion is radial ($B = 0$), the sheet is halted ($U = 0$) at the radius R_1. It is convenient to make our equations non-dimensional, by taking R_1 as the unit of distance and U_0 as the unit of speed. Thus we write:

$$r = R/R_1, \qquad b = B/R_1 \tag{24}$$

$$u = U/U_0, \qquad v' = V'/U_0. \tag{25}$$

Hence (15) and (23) become

$$v' = (m/m'')^{1/2}/r^{n-1} \tag{26}$$

$$u^2 = 1 - (b/r)^2 - 1/r^{2n-2}. \tag{27}$$

Also, if H is the "permanent" field intensity *at the sheet surface* at any instant,

$$h/H = 2eQ/(n - 2)m''c^2. \tag{28}$$

Using (22), (24), (25), we may write (19) and (20) in the form:

$$\frac{d\theta}{dr} = \frac{b}{r^2 u}, \frac{d\theta_e'}{dr} = -\frac{2D}{r^n u} \tag{29a,b}$$

where

$$D = \frac{m'}{2m_e}\left(\frac{m}{m''}\right)^{1/2}. \tag{30}$$

3. The Solution for Large Q and $n = 3$

Following CHAPMAN and FERRARO (1940), we suppose that Q is so large* that in (2) we may ignore m' in comparison with eQ/c^2; also, as m_e/m_i is very small, we write m_i for m and m_e for m'; further, we take $n = 3$, corresponding to the distribution of the earth's dipole field in its equatorial plane. Then (22), (28) and (30) become:

$$R_1^4 = e(M/U_0)^2/m_i Q, \qquad D = \tfrac{1}{2}(m_i c^2/eQ)^{1/2} \tag{31a,b}$$

$$h/H = 2. \tag{32}$$

Thus at each instant the electric current in the sheet causes the field intensity just inside the sheet to be trebled.

It is now convenient to write

$$b^2 = 2 \cot 2\alpha. \tag{33}$$

Thus if $B = 0$ (and $b = 0$) α is $\frac{1}{4}\pi$; if b is small, α is approximately $\frac{1}{4}(\pi - b^2)$; if b is large, α is approximately $1/b^2$; and α tends to zero if B tends to infinity. The signs of B, b and α are the same.

Then (27) may be written

$$u^2 = \left(1 - \frac{\cot \alpha}{r^2}\right)\left(1 + \frac{\tan \alpha}{r^2}\right). \tag{34}$$

Let R_2 denote the minimum radius attained by the obliquely projected sheet; then, by (34),

$$R_2 = r_2 R_1 \tag{35}$$

where

$$r_2^2 = \cot \alpha = (1 + \tfrac{1}{4}b^4)^{1/2} + \tfrac{1}{2}b^2. \tag{36}$$

To integrate (29a), it is convenient to write

$$r = r_2 \sec \phi = (\cot \alpha)^{1/2} \sec \phi. \tag{37}$$

Initially $\phi = -\frac{1}{2}\pi$, and finally $\phi = \frac{1}{2}\pi$. In terms of ϕ,

$$r^2 u = \Delta \operatorname{cosec} \alpha \tan \phi \sec \phi, \qquad dr = (\cot \alpha)^{1/2} \sec \phi \tan \phi \, d\phi$$

where

$$\Delta^2 = 1 - \sin^2 \alpha \sin^2 \phi = 1 - w, \qquad w = \sin^2 \alpha \sin^2 \phi. \tag{38a,b}$$

Thus (29a) is equivalent to

$$d\theta/d\phi = (\cos 2\alpha)^{1/2}/\Delta.$$

Hence

$$\theta = (\cos 2\alpha)^{1/2} F(\alpha,\phi). \tag{39}$$

* If the ions are protons, this requires Q to be large compared to 1700 e.s.u. The values of Q that are of geophysical interest are far greater: see Table 1.

VOL. 22 1961

Here $F(\alpha, \phi)$, in the notation of JAHNKE and EMDE (1945, p. 52), denotes the incomplete elliptic integral of the first kind. The initial and final values of θ are $-\theta_2$ and θ_2, where

$$\theta_2 = (\cos 2\alpha)^{1/2} K(\sin \alpha). \tag{40}$$

When B (and α) is negative, K, θ and θ_2 are also negative. When $B = 0$, also $\theta_2 = 0$.

In the present notation, (29b) may be written

$$d\theta_e'/d\phi = -(2D \sin \alpha \cos \phi)/\Delta$$

which on integration gives

$$\theta_e' = -2D \text{ arc sin } w^{1/2}. \tag{41}$$

Initially $\phi = -\frac{1}{2}\pi$ and $\theta_e' = -\theta_{e2}'$, where

$$\theta_{e2}' = -2D|\alpha| \tag{42}$$

where $|\alpha|$ denotes the positive numerical value of α. When the projection is radial, so that $B = 0$, $\alpha = \frac{1}{4}\pi$, θ_e' has the value θ_{e1}' given by

$$\theta_{e1}' = -\tfrac{1}{2}\pi D. \tag{43}$$

Hence for any other value of B,

$$\theta_{e2}' = (4|\alpha|/\pi)\theta_{e1}'. \tag{44}$$

The larger the value of B, and consequently the smaller the value of α, the smaller is the part of the azimuthal change of θ_e and θ_i that is different for the two kinds of particle. When $B = 0$ the values of θ_{e2}' and θ_{i2}' will be denoted by θ_{e1}, θ_{i1}.

The total deflections ψ_2 of the velocity vector of the electrons and ions are given by

$$\psi_{e2} = \pm(\pi - 2\theta_2) - 2\theta_{e2}', \qquad \psi_{i2} = \pm(\pi - 2\theta_2) - 2\theta_{i2}'. \tag{45a,b}$$

The positive sign is to be taken when B (and hence also θ_2) is positive, and the negative sign when it is negative, except when B is so small that θ_{e2}' (which is always negative) or θ_{i2}' (positive) numerically exceeds θ_2. In that case the sign to be taken in (45a) is negative, and in (45b), positive. When $B = 0$ the total deflections ψ_2 will be denoted by ψ_{e1}, ψ_{i1}.

Note that

$$\left.\begin{aligned} \sin \alpha &= 2^{-1/2}[1 - 1/(1 + 4/b^4)^{1/2}]^{1/2} \\ (\cos 2\alpha)^{1/2} &= 1/(1 + 4/b^4)^{1/4} \end{aligned}\right\} \tag{46}$$

Thus θ_e and θ_i have been determined as functions of r, giving the form of the paths of the particles. The electron and ion paths are almost the same except when b is very small, because both types of path are given approximately by the relation (39) between θ and r. However, the small difference between the ionic and electronic motions, represented by the parts θ_i' and θ_e' of θ_i and θ_e, is important in that it determines the current J and the magnetic field h.

4. Numerical Illustrations: Radial Projection, $B = 0$

The case of radial projection ($B = 0$) was discussed by CHAPMAN and FERRARO

(1940) in relation to the initial increase—often sudden—of the geomagnetic field at the equator at the commencement of a magnetic storm. They took

$$M = 8 \times 10^{25} \text{ gauss cm}^3 \tag{47}$$

corresponding to the earth's dipole field moment: and

$$U_0 = 10^8 \text{ cm/sec} \tag{48}$$

corresponding in order of magnitude to the travel speed of the solar particles that are supposed to produce magnetic storms.

Here their results are illustrated for the following two values of h_1, the field produced by the electric currents in the sheet of neutral ionized gas at the instant of closest approach of the sheet ($R = R_1$):

$$h_1 = 20\gamma, \qquad h_1 = 200\gamma \tag{49}$$

where $1\gamma = 10^{-5}$ gauss. These correspond to weak and strong sudden storm commencements.

For radial projection ($b = 0$), (27) has the form

$$u^2 = 1 - 1/r^4 \tag{50}$$

and in (18),

$$\theta = 0, \quad \theta_e = \theta_e', \quad \theta_i = \theta_i' = -(m_e/m_i)\theta_e. \tag{51}$$

By (29b) and (50),

$$d\theta_e/dr = -2D/r^3(1 - 1/r^4)^{1/2} \tag{52}$$

which has the integral

$$\theta_e = \pm D[\tfrac{1}{2}\pi - \text{arc sin } (1/r^2)]. \tag{53}$$

This is the equation of the electron orbits; the minus sign corresponds to the inward motion, the plus sign to the return motion. At $R = R_1$, or $r = r_1$, $\theta_e = 0$.

The distance of closest approach, R_1, our unit of length, is given by (31a) as

$$R_1 = (e/m_iQ)^{1/4}(M/U_0)^{1/2}. \tag{54}$$

The corresponding maximum disturbing field, h_1, is given—cf. (32)—by

$$h_1 = 2M/R_1^3 = 2(m_iQU_0^2/e)^{3/4}/M^{1/2}. \tag{55}$$

These equations may be used to express R_i, Q and D in terms of our adopted values of M, U_0, and h_1, as follows:

$$R_1 = (2M/h_1)^{1/3} \tag{56}$$

$$Q = (e/m_iU_0^2)(\tfrac{1}{2}Mh_1)^{1/2} \tag{57}$$

$$D = m_icU_0/e(2Mh_1^2)^{1/3}. \tag{58}$$

Table 1 gives values of these and other related quantities, corresponding to the numerical data (47)–(49). The distance R_1 is expressed in terms of the earth's radius a (= 6370 km) as unit.

Results similar to those in Table 1 have been discussed by CHAPMAN and FERRARO (1940), FERRARO (1958) and CHAPMAN (1960). The solution of this

VOL. 22 1961

"radial" problem threw much light on the theory of the first phase of magnetic storms. The aspects specially illuminated were:

(a) the order of magnitude of the distance at which solar streams first affect the earth's field during magnetic storms;

(b) how the electrostatic attraction between the opposite charges enables the electrons to penetrate far more deeply into the field than could solitary electrons similarly projected;

(c) the nearly complete turning back of the particles that most directly approach the earth;

(d) the order of magnitude of the electric currents involved; and

(e) the time of growth of the field h_1.

Table 1. Radial projection

	$h_1 = 20\gamma$	$h_1 = 200\gamma$
R_1/a, the distance of closest approach	14·6	6·8
Q, the charge in e.s.u. per cm length of the cylinder	$2{\cdot}5 \times 10^{10}$	$5{\cdot}3 \times 10^{10}$
N, the number of ions (or electrons) per cm length of the cylinder	$5{\cdot}2 \times 10^{19}$	$1{\cdot}1 \times 10^{21}$
ν_1, the number per cm^2 at the time of closest approach	$8{\cdot}9 \times 10^{8}$	$4{\cdot}1 \times 10^{10}$
$2\theta_{e1}$, the total change (deg.) of electron azimuth (πD radians)	−1·01	−0·22
$2\theta_{i1}$, the total change (deg.) of ionic azimuth (for protons)	$5{\cdot}5 \times 10^{-3}$	$1{\cdot}2 \times 10^{-3}$
ψ_{e1}, the total deflection (deg.) of electron velocity, to 1°	−179	−180
ψ_{i1}, the total deflection (deg.) of ionic velocity, to 1°	180	180
Maximum current (amps) per cm length of cylinder, J_1	$1{\cdot}6 \times 10^{-4}$	$1{\cdot}6 \times 10^{-3}$
Current (amps) for a length of cylinder equal to one earth radius, $J_1 a$	10^5	10^6

5. Numerical Illustrations: Oblique Projection

Oblique projection of the sheet reduces its power to penetrate the magnetic field. The distance of closest approach is greater than for radial projection, in the ratio $r_2(>1)$. Table 2 and Fig. 1 indicate how r_2 varies with $b(= B/R_1)$.

The total azimuthal displacement of an electron is now given by

$$2\theta_{e2} = 2(\theta_2 + \theta_{e2}') \tag{59}$$

and that of an ion is given by

$$2\theta_{i2} = 2(\theta_2 + \theta_{i2}'). \tag{60}$$

Here θ_2 has the same sign as B, and is given by (40); θ_{e2}' is negative, and θ_{i2}' is positive, as in the case of radial projection; their values are less than in that case in the ratio $4|\alpha|/\pi$, or $(2/\pi)$ arc cot $(\frac{1}{2}b^2)$. Except for very small values of b the deflections of electrons and ions are nearly the same, though the slight difference between them determines the electric current flow, the retardation and later recession of the sheet, and the transient disturbing field. The maximum magnetic disturbance (h_2) is less than that for radial projection in the ratio $1/r_2^3$,

$$h_2/h_1 = 1/r_2^3. \tag{61}$$

Table 2 and Fig. 1 illustrate how θ_2, $\theta_{e2}'/\theta_{e1}'$ and h_2/h_1 vary with b.

Table 2

b	0	0·594	0·854	1·074	1·295	1·544	1·861	2·34	3·37	∞
α	45°	40°	35°	30°	25°	20°	15°	10°	5°	0
r_2	1	1·092	1·195	1·316	1·464	1·658	1·932	2·38	3·38	∞
θ	0	42·66°	58·01°	68·30°	75·75°	81·24°	85·21°	87·92°	89·48°	90°
$\theta_{e2}'/\theta_{e1}'$	1	0·889	0·778	0·667	0·556	0·444	0·333	0·222	0·111	0
h_2/h_1	1	0·77	0·585	0·44	0·31	0·22	0·14	0·074	0·027	0
r_3	0·765	0·877	1·008	1·16	1·34	1·56	1·87	2·34	3·37	∞

Envelope

ϕ	0	5·83°	12·63°	20·87°	31·05°	43·76°	58·98°	74·52°	85·94°	90°
x	−1	−0·775	−0·509	−0·168	0·322	1·146	2·898	8·416	47·56	∞
y	0	0·777	1·114	1·398	1·678	1·990	2·378	2·962	4·226	∞

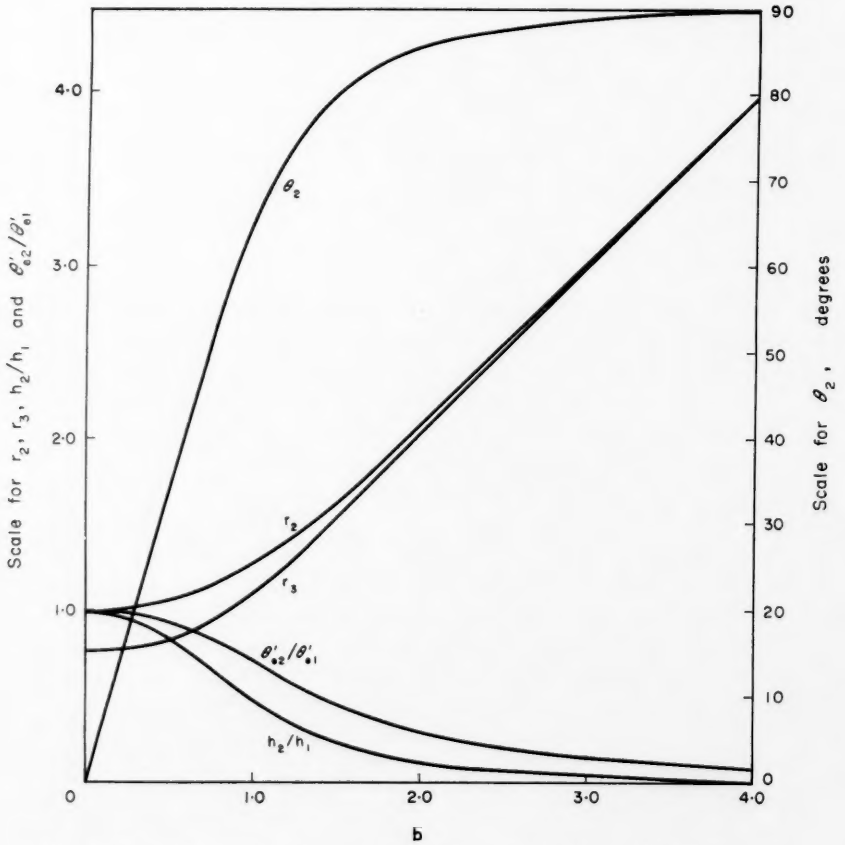

Fig. 1. r_2, r_3, $\theta_{c2}'/\theta_{c1}'$, h_2/h_1 and θ_2 as functions of b, the angular momentum.

VOL. 22 1961

Another quantity of some interest in connexion with this problem is the equivalent radius r_3 of the magnetic field, defined as the radius of a rigid elastic cylinder (without any field of force) which would deflect the particles from their initial to their final asymptotic lines of motion by elastic rebound. In this imagined case the particles travel rectilinearly along their initial asymptote until they collide with the cylinder: then they are suddenly reflected so as to move along the final asymptote of the (real) motion. In this calculation we consider only the deviation $2\theta_2$, ignoring the small relative deviations of the ions and electrons. It is easy to see that

$$r_3 = b \operatorname{cosec} \theta_2. \tag{62}$$

As b tends to zero this has the limiting value $2^{1/2}/K(\frac{1}{4}\pi)$ or 0·765; it increases with b, and as b tends to infinity, r_3/b tends to unity. Table 2 and Fig. 1 illustrate how r_3 varies with b.

The total deflection ψ_2 of the velocity of a particle (electron or ion, if we ignore the small deviations θ_{e2}', θ_{i2}') is given by

$$\psi_2 = \pi - 2\theta_2 = \pi - 2(\cos 2\alpha)^{1/2} K(\alpha). \tag{63}$$

It is not difficult to show that when b is large,

$$\psi_2 = \frac{3\pi}{4b^4}\left(1 - \frac{35}{16b^4} + \frac{385}{64b^8} + \frac{7{\cdot}3}{b^{12}} + \ldots\right) \tag{64}$$

(the last factor, 7·3, is an approximation). This formula converges rapidly for $b = 2$ and greater values. The following are values of ψ_2 from $b = 2$ onwards:

b:	2	3	4	5
ψ_2:	7·50°	1·62°	0·46°	0·22°

It is also of interest to note for what value of b the electrons return asymptotically to their original asymptote. That is,

$$\theta_{e2} = 0.$$

This corresponds to

$$\theta_2 = -\theta_{e2}'$$

or

$$(\cos 2\alpha)^{1/2} K(\alpha) = 2D\alpha.$$

The value of b is very small, and the associated value of α is nearly equal to $\frac{1}{4}\pi$. It is easily shown that

$$b_e = \pi D/2^{3/2} K(\tfrac{1}{4}\pi) = 0{\cdot}599\ D. \tag{65}$$

Thus for

$$h_1 = 20\gamma,\ b_e = 0{\cdot}00336$$

$$h_1 = 200\gamma,\ b_e = 0{\cdot}000725.$$

These values are positive, implying that an electron must be projected slightly eastward—countering the westward deflection—to return to its original asymptote. The path, however, is not quite straight. For an ion the projection must be slightly westward (b negative), and smaller in the ratio m_e/m_i.

6. The Motion of a Plane Neutral Ionized Sheet of Gas Towards the "Cylindrical" Magnetic Field

Consider an infinite *plane* sheet of neutral ionized gas, parallel to the axis of the "cylindrical" magnetic field described in Section 1, and at an infinite distance from it. Let q denote the positive charge per unit area of the sheet at any time. Suppose that every particle is simultaneously projected into the field with velocity U_0 normal to the sheet (and hence also normal to the field axis). For different particles the distance B of the initial line of motion will range from $-\infty$ to $+\infty$.

The parts of the sheet for which $\pm B$ is large will be little affected by the field. The electrons and ions will travel onward together, with little or no eastward or westward deflection, and little or no retardation. Thus these further parts of the sheet will remain almost plane, and advance with almost uniform speed U_0.

In the middle strip of the plane, where B is small, the electrons will be deflected eastward and the ions westward. Thus an eastward current will flow, but not uniformly, in a complete circuit, as in the problem earlier considered in this paper; the flow will more resemble that in a condenser. It will still involve retardation of the sheet, and a tendency to separation (in the middle strip) into two sheets, one positive and one negative. If q_0, the initial value of q, is sufficiently large, this tendency will be overcome, during the approach of this part of the sheet towards the axis. The particles for which B is least will approach closest to the axis, and be turned back most nearly directly. During the approach the sheet will bend round the axis on both sides, and its area will increase. During the recession the "stretching" of the sheet will be enhanced, as the sides ($\pm B$ large) move onward and the middle ($\pm B$ small) moves backward. This will progressively decrease the value of q, and the mutual hold of the electrons and ions on each other will weaken. Ultimately they will travel independently, uninfluenced by their earlier neighbours.

The evolution of the sheet, and of the magnetic field of the currents produced in it, will differ in many ways from that of the cylindrical sheet earlier discussed in this paper. The paths of the particles will differ from those of the particles with the same value of B in the previous cylindrical problem. But some of the latter paths may perhaps be taken as a first approximation to certain corresponding paths in the "plane sheet"–"cylindrical field" problem. Hence it is of interest to calculate the form of the sheet on this basis.

Thus we consider the section of the sheet by any plane normal to the field axis. We take this section to be the envelope of the paths of the particles, initially all moving with parallel speeds U_0. Let the direction of this initial motion be that of x, and the transverse direction be that of y. The form of each path is given in plane polar coordinates by (37) and (39). But in (39) the angle θ is reckoned from the apsidal radius. In the case now considered, all the paths have parallel initial asymptotes. Thus we must add θ_2 to the value of θ given by (39). We ignore the small relative displacements (θ_e', θ_i') of the ions and electrons.

Thus the family of the paths whose envelope we seek is given by the equations

$$r = (\cot \alpha)^{1/2} \sec \phi \tag{66}$$

$$\begin{aligned} \theta &= \theta_2 + (\cos 2\alpha)^{1/2} F(\alpha, \phi) \\ &= (\cos 2\alpha)^{1/2} [K(\alpha) + F(\alpha, \phi)]. \end{aligned} \tag{67}$$

VOL. 22 1961

Here ϕ is a parameter of the points *along* any one path, whose "family" parameter (as a whole) is α or B, given by (24) and (33).

The envelope is the curve whose points are given by (66) and (67), each for a particular value of ϕ. The value of ϕ for any path parameter α is determined by the discriminant, whose equation is

$$\frac{\partial r}{\partial \alpha}\frac{\partial \theta}{\partial \phi} = \frac{\partial r}{\partial \phi}\frac{\partial \theta}{\partial \alpha}. \tag{68}$$

This may be developed in the form

$$(2\Delta - 1/\Delta)\cot\phi = (\sec 2\alpha + 1)[F(\alpha,\phi) + K(\alpha)] - 2[E(\alpha,\phi) + E(\alpha)]. \tag{68}$$

Here $E(\alpha)$ and $E(\alpha,\phi)$ are respectively complete and incomplete elliptic integrals. $E(\alpha, \phi)$ is the integral of Δ from 0 to ϕ and $E(\alpha) = E(\alpha, \frac{1}{2}\pi)$. JAHNKE and EMDE (1945) give tables of $E(\alpha, \phi)$, $F(\alpha, \phi)$, $K(\alpha)$, $E(\alpha)$. These are helpful in determining ϕ from the discriminant for any value of α. When α is small, ϕ is approximately $\pi(\frac{1}{2} - 3\alpha^2)$; when α is nearly $\frac{1}{4}\pi$, its other limit, ϕ is approximately $(\frac{1}{4}\pi - \alpha)/K(45°)$. The value of $K(45°)$ is 1·8541. Table 2 and Fig. 2 indicate the shape of the envelope curve.

We have also numerically integrated the equation of motion applicable to the cylindrical sheet in order approximately to examine the shape of an ionized sheet as it folds around the earth's magnetic field. The successive forms thus calculated are shown in Fig. 2. Dots on these curves mark the successive positions of individual particles of the sheet. Table 3 indicates the time variation of the parameter ϕ which determines the position at any instant of a particle with given angular momentum.

7. Validity of Approximations

The equations of motion for an initially plane ionized sheet differ in two respects from those used in Section 6 in discussing the plane sheet problem.

(1) As the sheet is not always at right angles to the radius vector, both the transverse and the radial equations of motion need correction. As long as the ionized sheet is nearly plane the magnetic pressure in the real case retards only the forward motion of the sheet. In the cylindrical problems it is the radial motion which is retarded. Hence the hollow carved in the geomagnetic field as calculated in Section 6 will be too wide.

(2) The determination of the magnetic field at the sheet is a two-dimensional potential problem; the field there is no longer a simple function of H_p, the permanent magnetic field at the sheet. Hence the true equation of motion of the sheet along the normal must differ from that used in Section 6. This is a problem dealt with by other writers. FERRARO (1960) has suggested that the total magnetic field just inside the hollow might be replaced by $2fH_p$. SPREITER and BRIGGS (1961) have shown that $f = 1$, as used by BEARD, is a good approximation for two-dimensional problems. Since these other problems involved a volume flux of particles, and since the shielding of the hollow was complete, it is unsafe to compare their results with our plane sheet results. We shall therefore compare only the differential magnetic pressures at the interface.

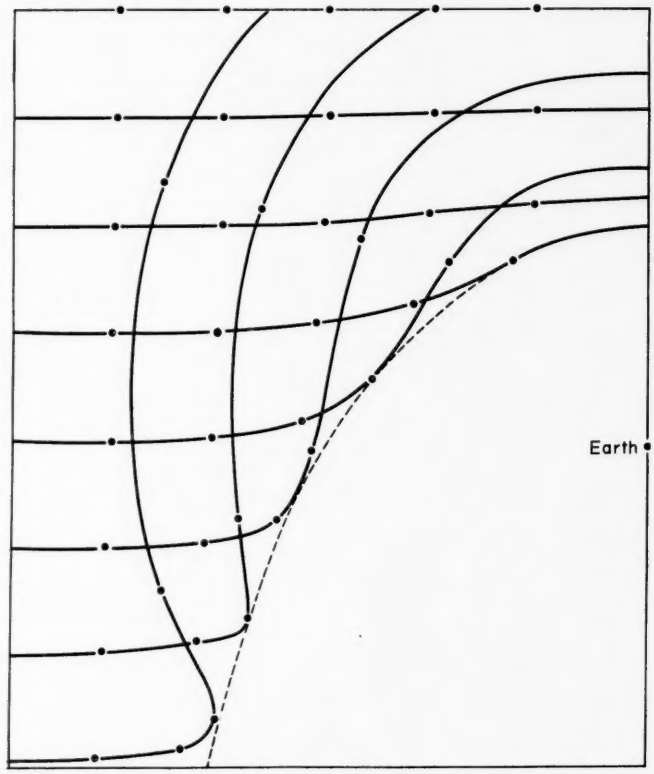

Fig. 2. The successive shapes of the initially plane sheet at intervals of 0·5 units of time. The broken line represents the shape of the envelope curve of the particle trajectories.

Table 3. Time variation of ϕ in degrees ($\phi = 0$ initially)

t \ α	5°	10°	15°	20°	25°	30°	35°	40°	45°
0·5	8·44	12·03	14·99	17·77	20·56	23·53	26·77	30·36	34·38
1·0	16·54	23·08	28·12	32·53	36·64	40·62	44·55	48·47	52·39
1·5	24·00	32·56	38·65	43·58	47·85	51·71	55·27	58·63	61·81
2·0	30·69	40·38	46·76	51·61	55·59	59·03	62·09	64·87	67·46
2·5	36·57	46·73	52·98	57·51	61·10	64·11	66·72	69·07	71·21
3·0	41·67	51·86	57·80	61·95	65·16	67·80	70·06	72·06	73·88

If the total field just inside the hollow is taken to be $2kH_p$ in the cylindrical sheet problems, the *differential* magnetic pressure at the interface will be the same as before if $(2k)^2 - 1 = (2f)^2$. The difference arises because the external field of the solenoidal current sheet is zero. We find that the altered equations of motion can be restored to their original form by changing the fundamental unit of distance R_1 (Section 2) to $[(4k^2 - 1)/8]^{1/4}R_1$. Substituting for k in terms of f, this becomes

VOL. 22 1961

$f^{1/2}2^{-1/4}R_1$. Thus $f = 1$, which is a likely value, gives an overall decrease of approximately 15 per cent in the linear dimensions of the hollow. The shape of the hollow will not be much affected, being insensitive to f.

We have assumed throughout that the charges in the sheet will never separate. CHAPMAN and FERRARO in their 1940 paper derived the condition ($Q > 2mU_0^2/e$) for non-separation in the case of zero angular momentum. They showed that for sheets that illustrate events in magnetic storms, Q is too large by many powers of ten for separation of charge: and this will be true also when there is angular momentum. In the plane sheet problem of Section 6 the density near the apex of the hollow is evidently reduced, after reflection, more than in the cylindrical problems. The reduction, however, is by a factor of order unity, so that Q will still be too large for separation. Hence our assumption that the electron and ion sheets remain together is justified.

8. Discussion

In Sections 2–5 an exact solution of a cylindrical problem is given. It concerns a cylindrical neutral sheet of plasma with given initial surface density of angular momentum which advances into a unidirectional magnetic field whose intensity at distance r from the axis varies as $1/r^3$. The initial densities of charge ($\pm$) and of angular momentum determine the particle orbits and the distance of closest approach of the sheet. This problem has a bearing on the efficiency of the geomagnetic field as a scatterer of particles in an incident solar stream. Some of the particles in the stream will be turned back toward the sun.

In Section 6 we have applied these results to discuss approximately the advance of an initially *plane* ionized sheet towards the same type of magnetic field. We conclude in Section 7 that this approach gives a wider hollow in the sheet than is actually the case. Nevertheless it does offer at least a qualitative picture of the distortion of an initially plane sheet as it advances into a field. We infer that this approximates to the equatorial section of the Chapman–Ferraro hollow.

It is possible to calculate the envelope curve of the particle trajectories. This has a bearing on the shape of the steady state hollow mentioned in the introduction. For comparison with the results derived by BEARD (1960) we take the apex of the hollow to coincide in his case and ours. The limiting width of our envelope curve of Fig. 2 and Table 2 increases indefinitely to an infinite value at infinity, whereas in BEARD'S case it remains finite. The reason appears to be that given in Section 7.

The motion of an initially plane ionized sheet and of a thin layer of ionized gas initially bounded by planes parallel to the axis of the field would certainly be similar. Such a thin layer might be emitted during a quiet period of solar activity. The equatorial section of the ejected material would then assume the various forms shown in Fig. 2.

The motion of reflected particles back towards the sun might impede the advance of any magnetic field embedded in the particle stream, particularly near the apex of the hollow.

Our method of deriving a steady state is of less interest than the methods

recently used by other writers. We conclude by referring the reader to a recent paper by SPREITER and BRIGGS (1961), which describes these in detail.

Acknowledgements—We should like to thank Professor V. C. A. FERRARO for his interest in this work. We are also grateful to the Director of the University of London Computer Unit for providing computing facilities.

REFERENCES

BEARD D. B.	1960	*J. Geophys. Res.* **65,** 3559.
CHAPMAN S.	1960	*Rev. Mod. Phys.* **32,** 919.
CHAPMAN S. and FERRARO V. C. A.	1940	*Terr. Magn. Atmos. Elect.* **45,** 245.
CHAPMAN S. and FERRARO V. C. A.	1941	*Terr. Magn. Atmos. Elect.* **46,** 1.
DUNGEY J. W.	1961	*J. Geophys. Res.* **66,** 1043.
FERRARO V. C. A.	1952	*J. Geophys. Res.* **32,** 934.
FERRARO V. C. A.	1958	*I.A.U. Symposium* No. 6, p. 295.
FERRARO V. C. A.	1960	*J. Geophys. Res.* **65,** 3951.
HURLEY J.	1961	*J. Geophys. Res.* In press
JAHNKE E. and EMDE F.	1945	*Tables of Functions.* Dover, New York.
SPREITER J. and BRIGGS B. R.	1961	*J. Geophys. Res.* In press.
ZHIGULEV V. N. and ROMISHEVSKII E. A.	1959	*Dokl. Akad. Nauk SSSR* **127,** 1001. (*Eng. Trans. Soviet Phys.-Dokl.* **4,** 859, 1960).

VOL.
22
1961

Journal of Atmospheric and Terrestrial Physics, 1961, Vol. 22, pp. 157 to 160. Pergamon Press Ltd. Printed in Northern Ireland

RESEARCH NOTES

Evidence of some geomagnetic control on the *F1*-layer

(*Received* 24 *May* 1961)

RATCLIFFE (1956) and others have given a theory of the bifurcation of the *F*-layer into *F1* and *F2*. This theory would indicate that, if the atmospheric temperature and composition is independent of latitude, then the solar zenith angle at which *F1* first appears, should also be independent of latitude. A glance at the ionograms for different stations makes it immediately obvious that it is impossible to support a hypothesis of latitude-independent atmospheric parameters. For this reason an attempt has been made, on a purely empirical basis, to answer the question "What are the factors which effect the first appearance of the *F1*-layer?"

The data considered were daily values of f_0F1 at noon for various southern hemisphere stations during 1958 with some 1957 data included, and a crude working index was devised for judging the first appearance of *F1*. This was: a full weight or doubtful value of f_0F1 tabulated counts as one; incomplete formation of *F1* (scaling symbol "*L*") counts as one half; when the 5 day running average of this index consistently exceeds one half, *F1* is judged to be present. The majority of the stations considered showed consistent use of the *F1* scaling symbols, but a few stations showed a significant over-use of the symbol *L*, and at these stations only full weight values of f_0F1 were considered. From these data the noon solar zenith angle at which *F* first bifurcated was calculated.

The results thus obtained showed an interesting property. They plotted well against geomagnetic latitude, but not nearly so well against magnetic dip or geographic latitude.

The fact that χ plots better against geomagnetic latitude than magnetic dip seems to indicate that such "*in situ*" effects as diffusion are not our primary concern, and it seems profitable to attempt an explanation from "transition" theory.

The invariant relations for the transition region have been given by CUMMACK (1961). Using this notation the third invariant is

$$P\sigma \operatorname{Ch} \chi = 1 - \frac{k}{1+r} + \left(2 - \frac{1}{1+r}\right) H \frac{\partial \log N}{\partial h} \tag{1}$$

Now Fig. 1 indicates that at any value of Ch χ the *F*-layer bifurcation is more complete at higher geomagnetic latitudes than near the geomagnetic equator. Thus at any fixed pressure P, values of N and $(\partial \log N)/\partial h$ decrease with geomagnetic latitude. In order that equation (1) still holds true either H or r must increase towards the geomagnetic pole.

Consider the case when r varies while H is fixed. As $r = \beta/\alpha N$ and $q = \beta N/1 + r$ then because the q distribution is defined, it is possible to decrease N and $(\partial \log N)/\partial h$ only by increasing β. β in turn is directly related to the concentration of some molecular constituent such as nitrogen or oxygen which increases only when the level, where diffusive separation predominates, increases with height.

It is thus concluded that in order to preserve the "transition" theory of *F1*-layer formation it seems necessary to postulate that either the atmospheric scale height or the

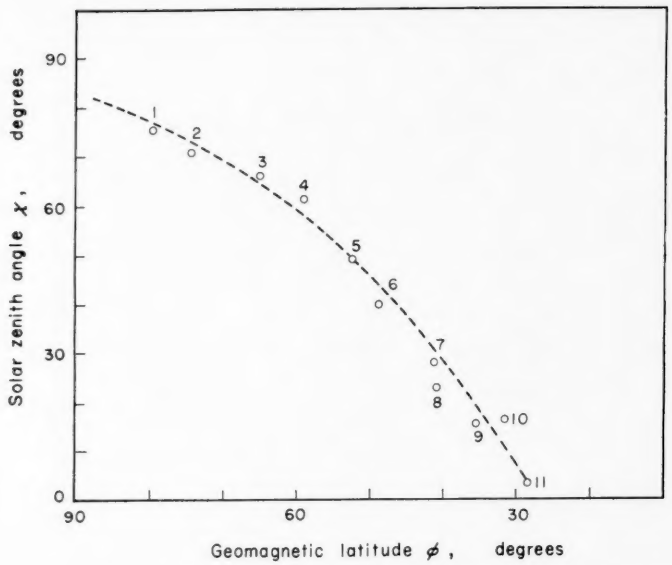

Fig. 1. A plot of the solar zenith angle χ, at which *F1* first appears, vs. geomagnetic latitude. All data southern spring 1958, except where indicated. The stations are: (1) Scott Base, (2) Cape Hallett, (3) Halley Bay (1957), (4) Campbell Island, (5) Port Lockray (1957), (6) Godley Head, (7) Canberra, (8) Watheroo, (9) Brisbane, (10) Cape Town, (11) Johannesburg.

VOL. 22 1961

atmospheric mixing process is a function of geomagnetic latitude. It should also be realized that such conclusions can be regarded as tentative until the results are checked by more refined methods.

Acknowledgement—This work is part of the research programme of the Geophysical Observatory of the New Zealand Department of Scientific and Industrial Research (Superintendent, Mr. J. W. Beagley).

C. H. Cummack

Geophysical Observatory
Christchurch, New Zealand

References

Cummack C. H. 1961 *J. Geophys. Res.* **66,** 158.
Ratcliffe J. A. 1956 *J. Atmosph. Terr. Phys.* **8,** 260.

Height gradient of horizontal drifts in the *E*-region over Waltair

(*Received* 12 *June* 1961)

Although considerable work has been done on horizontal drifts in the *E*- and *F*-regions of the ionosphere, there are very few estimates of the height gradients of drift speeds, especially for the *E*-region. The main difficulty in this estimation by the spaced

receiver method is the location of the level of the drifts. Evidence in support of the idea that the ionospheric irregularities responsible for fading are located close to the level of reflection was given by BOOKER (1955) on theoretical grounds and by JONES (1957) from the experimental study of drifts measured simultaneously on two frequencies. In this communication the authors present the results of height gradient calculation of drift speeds in the E-region over Waltair estimated on the basis of the above evidence that the drifts measured by the spaced receiver method refer to a height close to the reflection level.

E-region drift data taken on a frequency of 2·5 Mc/s for a period of 2 years from June 1957 to May 1959 is utilized in this study. Only day-time data is utilized as it has been observed that night-time reflections from the E_s-region do not show any appreciable variation in the reflection level. Day-time drift speeds in the E-region show very little variation, and since the analysis is made by considering a large number of day-time observations together, minor diurnal and seasonal variations are smoothed out. In view of the fact that E-region drift speeds at Waltair show a positive correlation with magnetic activity as reported by RAO and RAO (1961) only quiet day observations are utilized in this study. The drift speed data is grouped into three virtual height ranges corresponding to 95–105, 105–115 and 115–125 km and the averages of the drift speeds in each of these groups are taken to correspond to the virtual heights of 100, 110 and 120 km. The results thus obtained are given in Table 1 along with the gradients estimated for the two height

Table 1. Variation of average drift speed with height

Height (km)	100	110	120
Average drift speed (m/sec)	74·61	82·36	89·41
Height gradient of drift speed (m/sec/km)		0·775	0·705

ranges of 100–110 and 110–120 km. The average gradient for the entire height range is 0·74 m/sec/km. Although there is indication of a slightly lower gradient at higher levels, this result may not be regarded as significant in view of the fact that only approximate values of virtual heights are used.

Estimates of height gradients of drift speed are available for the height range of 80–100 km by the meteor method. GREENHOW (1955) has obtained a value of 2·5 m/sec/km, and ELFORD and ROBERTSON (1953) reported a value of 3·6 m/sec/km. The result obtained in the present investigation is less than that obtained by tha meteor method. WINKLEMAN (1956) reported a value of 4·9 m/sec/km for the height gradient of drift speed by the spaced receiver method from observations on a frequency of 310 kc/s taken on eleven nights. Considering the fact that our observation at Waltair refers to higher levels and a lower latitude, complete agreement with the few results so far reported from higher latitude stations is not expected.

Results from other lower latitude stations are not available for comparison.

Acknowledgement—The authors are indebted to the Council of Scientific and Industrial Research (India) for financial support of these investigations.

Ionosphere Research Laboratories
Physics Department
Andhra University
Waltair, India

R. RAGHAVA RAO
B. RAMACHANDRA RAO

REFERENCES

BOOKER H. G. 1955 *J. Atmosph. Terr. Phys.* **7**, 343.
ELFORD W. G. and ROBERTSON D. S. 1953 *J. Atmosph. Terr. Phys.* **4**, 271.

Greenhow J. S.	1954	*Phil. Mag.* **45**, 471.
Jones I. L.	1957	*Polar Atmosph. Sympos.*, Part II, p. 20. Pergamon Press, London.
Raghava Rao R. and Ramachandra Rao B.	1961	Presented at Symposium on "Upper Atmosphere and I.G.Y. Data", Delhi, February, 1961.
Winkleman R. E.	1956	AFCRC–TR–56–190 ASTIA Document No. AD110185 Radio Prop. Lab., Stanford University, California.

Papers to be published in future issues

A. R. Thompson: Sweep frequency observations of meteor scatter bursts

D. E. Shemansky and A. Vallance Jones: New measurements of the night airglow spectrum in the 1·5 μ region

J. Wolfe: 20 Mc/s w.w.v. bursts during the last few periods of 1958δ2

L. H. Heisler and J. D. Whitehead: The intepretation of *F2* critical frequency measurements

G. H. Bazzard and C. M. Minnis: The geographical distribution of the harmonics of the annual variation in the critical frequency of the *F2*-layer at noon

T. Ondoh: Variations of the earth's exosphere and geomagnetic disturbances during the geomagnetic storm of 4 September 1958

G. S. Kent: High frequency fading of the 108 Mc/s wave radiated from an artificial earth satellite as observed at an equatorial station

J. E. Titheridge: The effect of collisions on the propagation of radio waves in the ionosphere

R. Naismith and P. A. Smith: Further evidence of a long term variation in the relationship of solar activity to the ionosphere

W. Becker: The varying electron density profile of the *F*-region during magnetically quiet nights

R. K. Suryanarayana: Effect of radio fade-out on the *F2*-layer

R. G. Rastogi: The morphology of lunar semi-diurnal variation in f_0F2 near solar noon

VOL.
22
1961

Journal of Atmospheric and Terrestrial Physics, 1961, Vol. 22, pp. 161 to 165. Pergamon Press Ltd. Printed in Northern Ireland

Sweep frequency observations of meteor scatter bursts

A. R. THOMPSON
Harvard Radio Astronomy Station, Fort Davis, Texas

(*Received* 13 *May* 1961)

Abstract—Meteor scatter bursts from distant television transmitters have been observed on a sweep frequency receiver. The receiver covers the band 50–100 Mc/s, and signals at a number of frequencies are recorded from each meteor trail. The trails are of the overdense type, and the scattered signals show a characteristic frequency–time profile, persisting longer at the lower frequencies. The duration of the signals as a function of frequency agrees closely with the inverse-square relation predicted theoretically. The diurnal and seasonal variations in the number of scatter bursts observed are briefly described.

1. INTRODUCTION

THE propagation of radio signals by forward scatter from meteor trails has received much attention as a means of long distance communication at frequencies in the range 30–100 Mc/s. Experimental studies of meteor scatter in most cases have involved transmission and reception at a single frequency. The present observations concern reception of signals at a number of frequencies from each meteor trail. The signals originate from television transmitters, and are recorded on a sweep frequency receiver covering 50–100 Mc/s. The receiver is operated at a remote site in West Texas shielded by surrounding mountains, where the frequency range 50–100 Mc/s is virtually free from permanent man-made radio signals. Propagation by meteor trails causes bursts of intermittent interference in which signals are usually received on five to fifteen different frequencies. The signals start sharply and almost simultaneously, and die away after a few seconds or minutes, persisting longer at the lower frequencies. Examples of the bursts, recorded with a frequency–time display, are shown in Fig. 1. The frequencies of the signals are principally those of television channels 2–6 (54–88 Mc/s), although frequencies in the lower channels of the f.m. broadcast band also appear occasionally.

Signals in a long enduring form caused by sporadic-*E* are also recorded and persist for many minutes or hours. The occurrence of the sporadic-*E* propagation shows the characteristic seasonal distribution described by SMITH (1957) with a pronounced maximum during the summer months and a subsidiary maximum in December. On occasions the long enduring signals have been monitored with a v.h.f. communications receiver and found to be television transmissions from within the United States and Mexico. The exact locations of the stations, however, have not been identified. The observations described in this paper are concerned only with the meteor scatter propagation.

The receiving equipment has been described in detail elsewhere (THOMPSON, 1961), and is used principally to record radio bursts from the sun. The receiver sweeps through the range 50–100 Mc/s three times per second, and has an i.f. bandwidth of 100 kc/s, and a noise figure of 4 dB. The antenna to which it is connected is a single broadband dipole mounted over a plane reflecting screen and oriented so that the direction of maximum sensitivity points toward the south at

an elevation of 60°. The dipole is polarized in the plane of the meridian. The output of the receiver is displayed on an intensity-modulated cathode ray tube, and photographed continuously to provide a frequency–time display. The minimum signal strength visible on the records is about 1 μV per metre. The receiver has been operated from sunrise to sunset each day since January 1959.

2. Duration of the Scatter Bursts

The maximum observed duration of the meteor scatter bursts is approximately 4 min. The short lived bursts predominate and the mean duration at 60 Mc/s is 10 sec. Bursts of duration less than 3 sec cannot be distinguished with certainty on the records, and have been omitted from the analysis. This minimum duration indicates that the bursts are all scattered from meteor trails of the overdense type. For such trails the scattered signal strength remains approximately constant as the trail diffuses, until the electron density no longer exceeds the critical value. The signal strength then falls sharply. Thus the observed duration depends mainly on the initial trail density, and only to a lesser extent upon the power of the transmitter.

An estimate of the magnitude of the meteors may be obtained from the durations of the meteor scatter bursts. For overdense trails the duration at a given frequency is proportional to the electron line density and approximately proportional to $\sec^m \phi$, where 2ϕ is the angle subtended by the transmitter and the receiver at the reflection point (Manning, 1959). The value of m varies from 2·0 when the trail lies in the plane of propagation to 0·3 when the trail is normal to the plane of propagation. For randomly distributed trails, m has a median value of approximately 0·85. The value of ϕ is limited by the height of the trails (approximately 100 km) and the curvature of the earth to a maximum of 80°, which corresponds to a maximum propagation distance of about 2000 km. Thus for any meteor burst the factor $\sec^{0\cdot85} \phi$ must lie between 1 and 4·4. The corresponding range of line density for a 3 sec burst at 60 Mc/s is (5·0–1·2) $\times$ 10^{15} electrons per metre. A formula by Hawkins (1956a) relates the electron line density in a trail to the equivalent visual magnitude of the meteor, and thus the values of the line density given above correspond to magnitudes 1 to 2·5. The present scatter bursts are therefore produced mainly by large meteors, brighter than visual magnitude 2·5.

3. The Frequency–Time Profiles

For overdense trails, the duration of a scatter signal is theoretically predicted to vary inversely as the square of the frequency (Kaiser and Closs, 1952). This relation should hold, on average, for the frequency–time profiles of the present scatter bursts. The different frequencies in any burst originate from transmitters at different locations, involving different values of scatter angle, ϕ. However, this effect should produce random rather than systematic deviations in the frequency–time profiles. The examples in Fig. 1 show that there is some variability in the sharpness of the profiles. In the longer duration bursts, the signals often die away less sharply, because the trails become distorted by upper atmosphere winds. The long burst of 10 August 1960 shows an increase in signal strengths after 2 min, which is probably caused by the reorientation of part of the trail.

VOL. 22 1961

VOL.
22
961

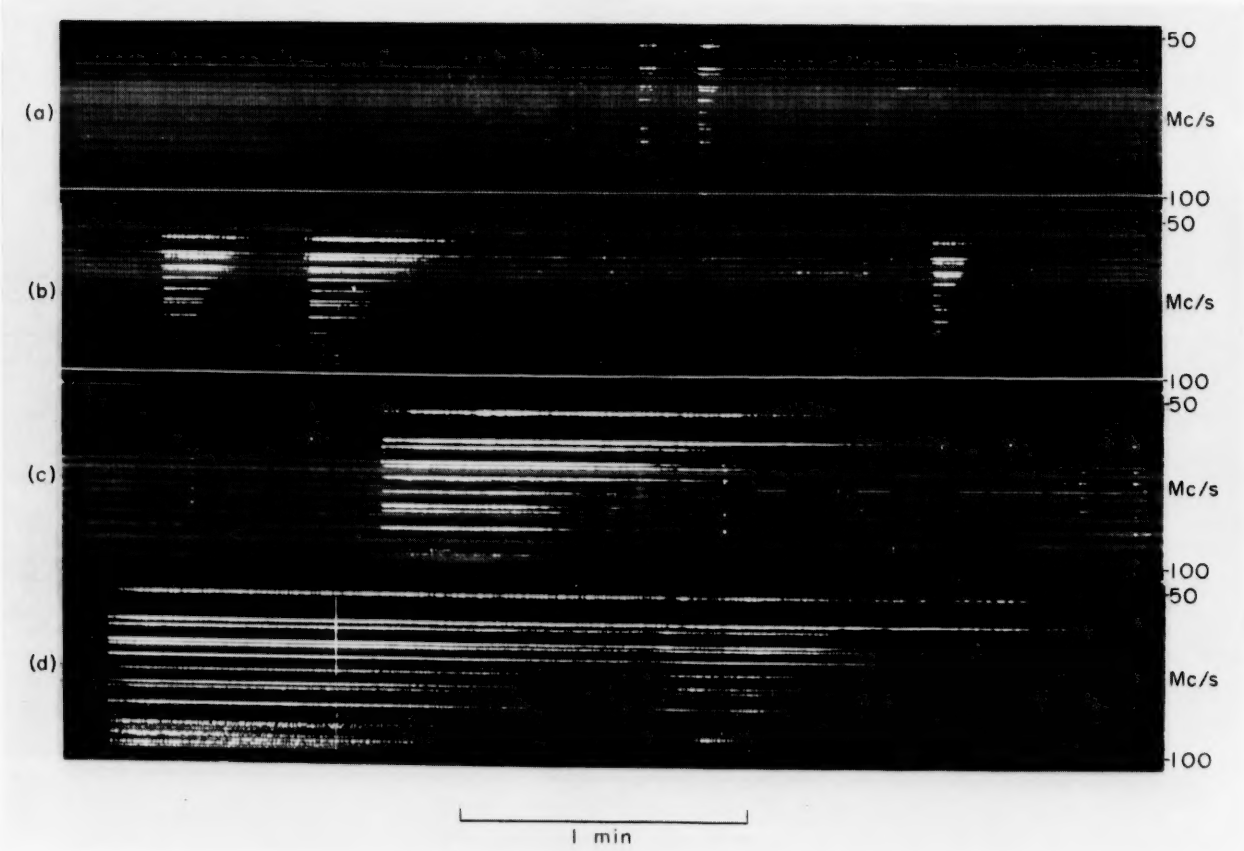

Fig. 1. Meteor scatter bursts recorded on a frequency–time display. The examples shown occurred during the periods of the Quadrantid and Perseid showers. (a) 1625–1629 U.T., 2 January 1961; (b) 1914–1918 U.T., 11 August 1959; (c) 1850–1854 U.T., 13 August 1960; (d) 1455–1459 U.T., 10 August 1960.

VOL.
22
1961

As a test of the inverse square relation, measurements were made on thirty bursts that occurred during the period of the Perseid shower in 1960. Bursts with well-defined profiles and with total durations ranging from 10 to 40 sec were selected. The frequency–time profile was traced for each of the thirty bursts, and the duration was measured at intervals of 5 Mc/s from 60 to 90 Mc/s. The values of duration for each burst were then scaled to normalize the duration at 75 Mc/s to unity. The resulting relative durations were averaged over the thirty bursts for each measured frequency, and the values obtained are shown in Fig. 2 together with

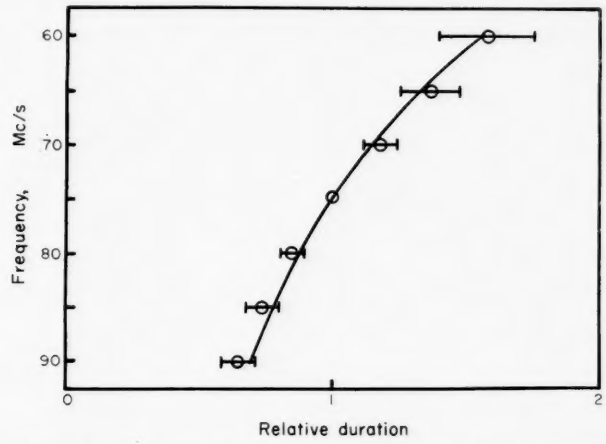

Fig. 2. The normalized frequency–time profile of meteor scatter bursts. The points show the duration at each frequency relative to that at 75 Mc/s, and are averaged over thirty bursts. The curve shows the theoretical inverse square relation between duration and frequency.

the root mean square deviations of the individual values from the mean. The points lie very close to the theoretical curve, and thus agree with the predicted inverse square relation.

4. Diurnal and Seasonal Variation

The diurnal variation in the rate of occurrence of the scatter bursts is shown in Fig. 3(a) which is based on data averaged over the year 1959. Local noon is approximately 1900 U.T. The rate shows the well-known steady decline from the morning hours to the evening. The ratio of maximum to minimum rates is 1·8 times as great as that given by Hawkins (1956b) for the diurnal variation of the total sporadic meteor rate for the same latitude. This disparity probably results from the fact that the meteors detected as scatter bursts are not uniformly selected with respect to the radiant position. The probability that a meteor trail will produce a scatter burst between a given transmitter and receiver is governed by the conditions for specular reflection, and thus depends upon the relative position and direction of the trail, as discussed, for example, by Forsyth *et al.* (1957). The probability of receiving a scatter burst from a trail whose radiant is near the zenith is very low. This condition implies a low angle of incidence at the receiving site, and, in the present case, the horizon is restricted by surrounding mountains. The

probability of receiving a scatter burst should not depend critically on the azimuth of the radiant, since the beamwidth of the receiving antenna is broad, and the signals originate from a number of transmitters at different azimuths. For long-duration trails, which become distorted by upper atmosphere winds, the original orientation is less important.

The seasonal variation of the rate of the meteor scatter bursts, based on observations during 1959 and 1960, is shown in Fig. 3(b). The high rate in August results from the Perseid meteor shower; otherwise the data refer essentially to

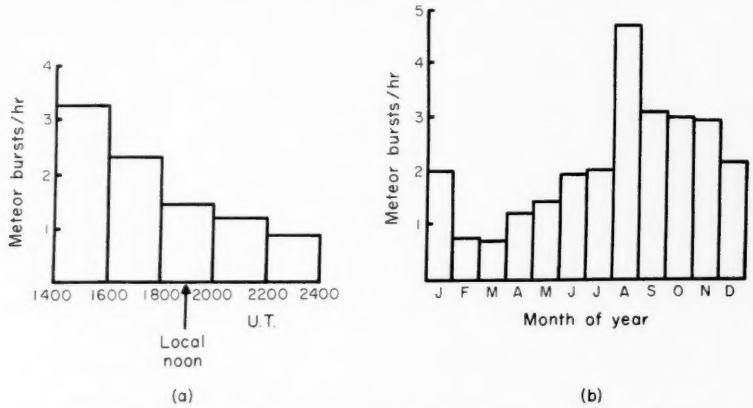

Fig. 3. The diurnal and seasonal variations in the occurrence of meteor scatter bursts. The diurnal variation is based on data for 1959 and the seasonal variation on data for 1959 and 1960. The daily observing period was 1400–2400 U.T.

sporadic meteors. The general form of the seasonal curve, with a minimum during February and March and a maximum during the latter half of the year, is in reasonable agreement with a radar survey by Evans (1960). The radar equipment used a rotating antenna to obtain complete sky coverage, and the minimum detectable trail density corresponded to visual magnitude 6.

A prominent feature on the scatter-burst records is the Perseid shower (10–14 August) during which the daily burst-rate increased by a factor of 4. Many long duration bursts were observed, and the mean duration increased to 30 sec. The records have also been examined for similar increases in the burst rate during the three other great showers; the Geminids (12–14 December), the Quadrantids (2–4 January), and the Arietids (29 May–18 June). During the Geminids, the mean daily rate increased by a factor of 2 (even though the radiant was above the horizon for only 2 hr of the daily period), and during the Quadrantids there was a similar increase of 2. During the Arietids the increase was only 1·5; a large increase in the burst rate was not expected for this shower, since it has been found to contain relatively few of the larger meteors (Browne *et al.*, 1956).

Acknowledgements—The author wishes to thank Miss M. B. Wood of the National Bureau of Standards, Boulder, Colorado, for assistance in analysis of the records, and Dr. G. S. Hawkins of Harvard College Observatory, and Dr. Alan Maxwell

VOL. 22 1961

of the Harvard Radio Astronomy Station for helpful discussions. The equipment is operated under a program sponsored by the Geophysics Research Directorate of the United States Air Force through the Sacramento Peak Observatory.

References

Browne I. C., Bullough K., Evans S. and Kaiser T. R.	1956	*Proc. Phys. Soc. Lond.* B **69,** 83.
Evans G. C.	1960	*Jodrell Bank Ann.* **1,** 280.
Forsyth P. A., Vogan E. L., Hansen D. R. and Hines C. O.	1957	*Proc. Inst. Radio Engrs* **45,** 1642.
Hawkins G. S.	1956a	*Astrophys. J.* **124,** 311.
Hawkins G. S.	1956b	*Astr. J.* **61,** 386.
Kaiser T. R. and Closs R. L.	1952	*Phil. Mag.* **43,** 1.
Manning L. A.	1959	*J. Atmosph. Terr. Phys.* **14,** 82.
Smith E. K.	1957	*Worldwide Occurrence of Sporadic-E.* National Bureau of Standards Circular No. 582.
Thompson A. R.	1961	*Astrophys. J.* **133,** 643.

Journal of Atmospheric and Terrestrial Physics, 1961, Vol. 22, pp. 166 to 175. Pergamon Press Ltd. Printed in Northern Ireland

New measurements of the night airglow spectrum in the 1·5 μ region*

D. E. Shemansky† and A. Vallance Jones
Physics Department, University of Saskatchewan, Saskatoon, Canada

(*Received* 2 *June* 1961)

Abstract—Measurements of the spectra of the night airglow emission in the 1·40–1·65 μ region have been made at a spectral slit width of 25 Å, with a grating spectrometer using a germanium photoconductive detector. The rotational fine structure of the 3,1 and 4,2 OH bands was partially resolved and the 2,0 OH band was observed for the first time. Rotational temperatures between 200 and 225°K were obtained from the *P*-branch of the 3,1 band. A mean value of 66 kR was obtained for the absolute zenith brightness of the 4,2 OH band. A van Rhijn measurement of the height of the OH emitting layer gave a value of 69 km.

1. Introduction

The first observations of the spectrum of the night airglow between 1·4 and 1·7 μ were made by Gush and Vallance Jones (1955). The absolute brightness of the emission in this spectral region was measured by Harrison and Vallance Jones (1957). The minimum spectral slit width used in these investigations was 100 Å. Recently Connes and Gush (1959, 1960), using a Michelson interferometer, have obtained measurements of the spectrum of the night airglow in this region with a resolution equivalent to a spectral slit width of 7·5 Å.

The recent availability of improved detectors for this spectral region has made it possible to attempt to obtain spectra either at higher resolution or with increased signal-to-noise ratio. In 1959 modifications were made to the spectrometer at the University of Saskatchewan so that it could be used with a germanium photoconductive detector. The improved response, so obtained, made it possible to record night airglow spectra with spectral slit widths down to 25 Å. This resolution, in conjunction with improvements in the signal-to-noise ratio, made it feasible to obtain improved rotational temperatures from the OH bands in this spectral region and to make some further measurements of the relative intensities of the OH vibrational bands. It also proved possible to make van Rhijn measurements of the height of the emitting layer for the OH bands.

2. Spectrometer

The spectrometer used in this work is a modified version of the instrument described by Gush and Vallance Jones (1955). The radiation is dispersed by a 4 × 5 in. plane diffraction grating having 600 lines/mm and blazed at 1·08 μ in the first order. Certain modifications have been made to the original instrument, including the replacement of the 120 in. collimator mirror with a 60 in. spherical mirror and the installation of an ellipsoidal mirror to form a 10:1 reduced image of the exit slit on the detector. This modification is necessary to make it possible

* The research reported in this paper has been sponsored by the Geophysics Research Directorate of the Air Force Cambridge Research Center, Air Research and Development Command, under Contract AF 19(604)–7265.

† Present address: Bristol Aero Industries, Winnipeg, Manitoba.

VOL. 22 1961

to use a dewar-mounted detector. A field mirror behind the exit slit images the grating on to the ellipsoidal mirror.

The most important change was the use of a Philco n-type gold–antimony doped germanium photoconductive detector having a noise equivalent power of about $6{\cdot}8 \times 10^{-13}$W at 1·4 μ for a bandwidth of 1 c/s. The response of the cell is sharply peaked at 1·4 μ and has fallen to 50 per cent of its maximum value by 1·7 μ. The radiation falling on the cell is modulated at a frequency of 780 c/s by an external chopper. The output from the cell is amplified by a tuned amplifier, detected by a phase-sensitive detector and applied to a pen recorder. The field of view of the spectrometer was 6·4° in zenith angle and 3·8° in azimuth angle.

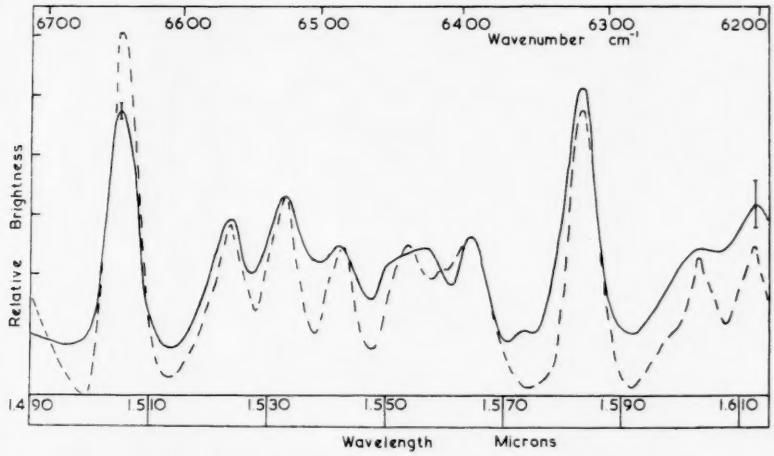

Fig. 1. Spectrum of the night airglow between 1·49 and 1·61 μ obtained with a spectral slit width of 50 Å (full curve). This spectrum is the mean of fifteen obtained on the night of the 2/3 September 1959. The dashed curve represents a synthetic spectrum calculated with a triangular resolution function and a relative intensity $I(3,1)/I(4,2) = 1{\cdot}2$. The probable error of the mean spectrum is indicated by the vertical markers through the solid curve.

3. Night Airglow Spectra

Three typical night airglow spectra obtained are shown in Figs. 1–3. Fig. 1 shows the spectrum between 1·49 and 1·61 μ obtained with a spectral slit width of 50 Å. The plotted curve represents an average of fifteen spectra. Fig. 2 shows the spectrum between 1·50 and 1·61 μ with a spectral slit width of 25 Å. Curve "a" is a mean of ten spectra and curve "b" is the mean of twenty-one spectra. These spectra were all recorded during the months of September, October and November 1959. The zenith angle of observation was 73°. Aurora present while the spectra were being obtained did not exceed intensity I and, in the case of the spectra of Figs. 1 and 2a, it is known that no visible aurora entered the field of view of the instrument. Since the spectra shown in these figures were obtained by averaging the original traces from the spectrometer, the probable errors of the mean curves were computed and are indicated graphically on each figure.

Fig. 3 shows the spectrum obtained in the wavelength range between 1·40 and 1·51 μ. This spectrum represents a single 4 min scan at a zenith distance of 0° and a

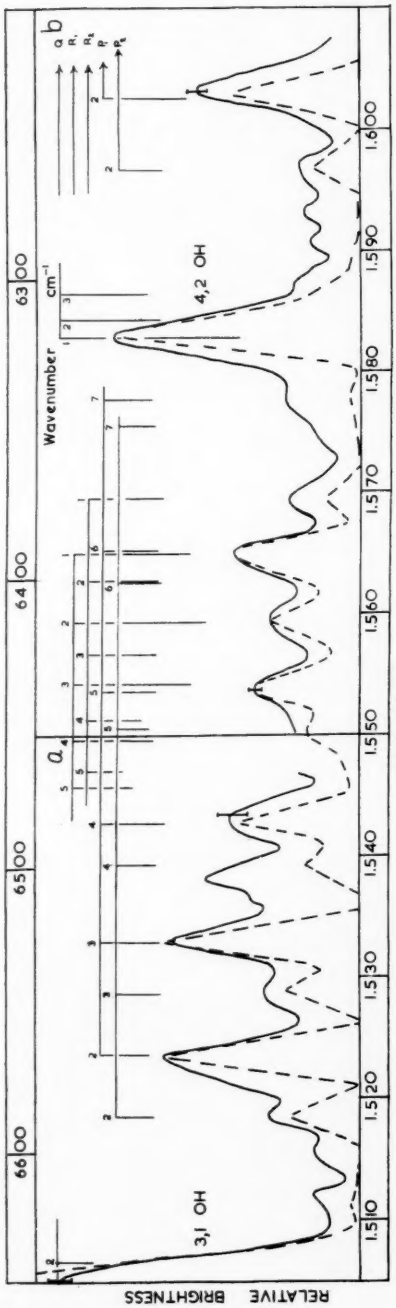

Fig. 2. Spectra of the night airglow between 1·50 and 1·61 μ with spectral slit widths of 25 Å (full curve). Curve "a" is the mean of ten spectra obtained on the night of 15/16 October 1959 while curve "b" is the mean of twenty-one spectra obtained on the night of 16/17 November 1959. The probable errors of the observed spectra are indicated by the vertical markers through the solid curve. The corresponding synthetic spectra which are shown by the dotted curves were calculated for a rotational temperature of 200°K between 1·50 and 1·55 μ and for 225°K between 1·55 and 1·61 μ. The positions of the rotational lines of the bands are shown.

VOL. 22 1961

spectral slit width of 100 Å. It was obtained on an exceptionally clear and very cold night in March 1960. As a consequence of the extremely low water vapour content of the atmosphere and the high sensitivity of the germanium cell it was possible to record these spectra which show definitely, for the first time, the branch structure of the 2,0 OH band.

The investigations referred to in Section 1 led to the conclusion that the only emission features detected in the night airglow in the 1·4–1·7 μ region were the vibration–rotation bands of OH. For comparison with the observed spectra, synthetic OH spectra have been calculated for the spectral slit widths* used in

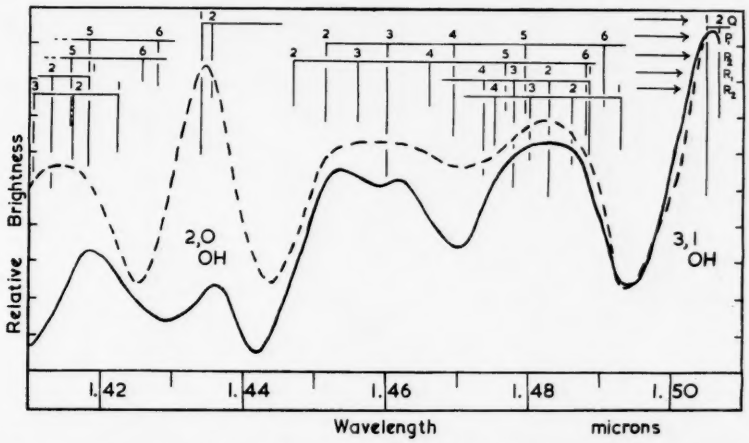

Fig. 3. Spectrum of the night airglow between 1·40 and 1·51 μ obtained with a spectral slit width of 100 Å (full curve). This curve represents a single spectrum obtained at a zenith distance of 0° on an exceptionally clear and cold night in March 1960. The dashed curve shows a synthetic spectrum calculated for a temperature of 225°K and a relative intensity $I(2,0)/I(3,1) = 0{\cdot}93$. The positions of the rotational lines are indicated.

the observations. The line intensities were calculated using the line strength factors given by Plyler *et al.* (1953) and the term values of Dieke and Crosswhite (1948) The intensity ratio between the 4,2 band and the 3,1 band, as well as the rotational temperature, were adjusted to provide the best fit with the observed spectrum. This was done in each case for the spectra shown in Figs. 1 and 2, on which the resulting synthetic spectra are also shown. While the fit obtained between the observed and synthetic spectra is on the whole good (when it is borne in mind that atmospheric water vapour absorption begins to have a noticeable effect for wavelengths shorter than 1·51 μ), it was found that there were some persistent discrepancies between the observed and calculated spectra. In particular, enhanced emission intensities were observed at 1·538 and 1·580 μ. It is possible that the enhancement at 1·58 μ corresponds to a night airglow excitation of the 0,1 $(^1\Delta_g – ^3\Sigma_g^-)0_2$ band. This band is observed in the twilight (Vallance Jones and Harrison, 1958) and the closely related atmospheric 0_2 band appears in the night

* With the exception of the synthetic spectra shown in Fig. 4 a triangular resolution function was employed. Since this does not take into account the distortion produced by the finite output–circuit time constant, exact agreement cannot be expected, especially in the troughs between peaks.

airglow. Therefore it would not be surprising if the 1·58 μ band occurred with low intensity in the night airglow.

The main conclusion to be drawn from the comparison between the observed and synthetic spectra, however, is that the attainment of higher resolution has failed to reveal with certainty the presence of emissions other than the OH bands. This is in agreement with the still higher resolution study of Connes and Gush (1960).

4. Rotational Temperatures of OH Bands

The method of estimating upper atmospheric temperatures from the rotational intensity distribution of the OH bands has been extensively employed since its introduction by Meinel (1950). References to earlier work will be found in the paper of Wallace (1960). Since the spectra obtained by Gush and Vallance Jones (1955) were not of sufficiently high resolution to provide measurements of the relative intensities of the individual rotational lines of the bands, the temperature measurements in the 1·5 μ region were made by comparing the observed spectra with synthetic spectra plotted for a series of different temperatures. While this method is not so precise as one based on a measurement of individual line intensities it does have the redeeming feature, in comparison with the photographic methods, that it is applied to data which is not subject to the well-known errors of photographic photometry.

While the spectra obtained in the work reported here were not intended primarily for the determination of temperatures it seemed worth while to make as accurate a temperature determination as possible from the data in view of the wide range of different temperatures obtained in photographic studies. Two methods were used in the reduction of the spectra, the first being that of comparison with synthetic spectra constructed for different temperatures and the second being based on the measurement of the individual line intensities.

In Fig. 4 is shown an example of the synthetic spectrum method. This figure shows synthetic spectra calculated between 1·52 and 1·55 μ for temperatures of 180, 200 and 250°K. These synthetic spectra were calculated using a resolution function of ideal triangular form modified to take into account the time constant of the output circuit. This time constant was 0·29 of the time required for the spectrometer to scan one spectral slit width. The observed mean night airglow spectrum obtained on 2/3 September 1959 is also shown. The region between 1·52 and 1·55 μ was chosen for the comparison between the observed and synthetic spectra because, as may be seen from Fig. 2, it covers the partially resolved $P_1(2)$, $P_1(3)$ and $P_1(4)$ lines of the 3,1 band. At longer wavelengths the P-branch lines of the 3,1 band overlap the R-branch lines of the 4,2 band, and consequently the match between the observed and synthetic curves becomes sensitive to the intensity ratio assumed between the two bands. At shorter wavelengths the match is affected by water vapour absorption which probably reduces the intensity of the Q-branch of the 3,1 band somewhat. The curves shown in Fig. 4 show that the best fit between the peaks of the observed and synthetic spectra is obtained for a temperature between 200 and 225°K. The agreement at wavelengths between peaks is sensitive to the value chosen for the time constant of the output circuit whereas the agreement at the line peak is relatively insensitive to this quantity. More weight was therefore

VOL. 22 1961

given to agreement at peaks of the lines. There is also the possibility mentioned in Section 3 that the observed spectrum is enhanced by some foreign emission at 1·538 μ. On this basis a temperature of 215 $\pm$ 20°K was assigned to the spectrum. The temperature obtained in this way from several spectra are set out in Table 1.

For a spectral slit width of 25 Å, the $P_1(2)$, $P_1(3)$ and $P_1(4)$ lines of the 3,1 band are free from overlapping with other lines and consequently it seemed worthwhile

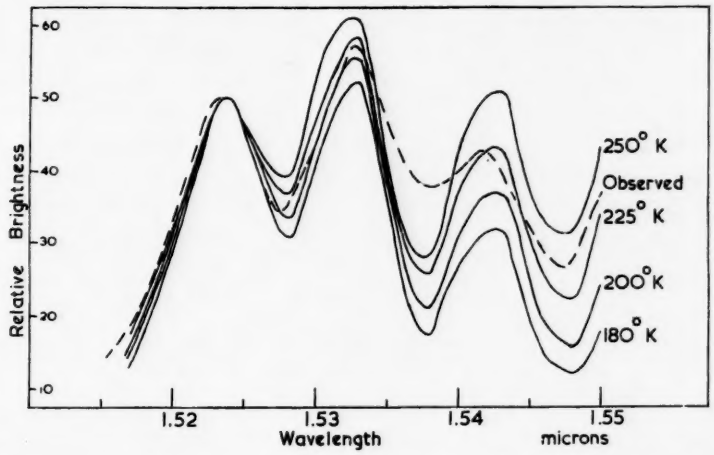

Fig. 4. Comparison between observed spectrum of Fig. 1 (dashed curve) and synthetic spectra calculated for different temperatures (full curve). For this figure the synthetic spectra were calculated using a resolution function which takes into account the distortion of the ideal triangular shape produced by the time constant of the output circuit.

Table 1. OH rotational temperatures

Date	Method	Spectral slit width (Å)	Temperature (°K)
2/3 September 1959	Synthetic spectrum	50	215 $\pm$ 20
21/22 September 1959	Synthetic spectrum	40	200 $\pm$ 50
15/16 October 1959	Line intensity plot	25	197 $\pm$ 20

to derive a value for the rotational temperature by using the usual method of analysis of plotting log $I(P)/S(K'')$ against $F(K')$. In this way a temperature of 197°K was obtained from the spectrum shown in Fig. 2. This value also is entered in Table 1.

5. Absolute and Relative Brightnesses of the $\Delta v = 2$ Bands of OH

The results obtained in the present series of measurements were used to derive absolute brightnesses for the 4,2 OH band by the same method as was employed by Harrison and Vallance Jones (1957). The standard low brightness source which was used to calibrate the spectrometer during the course of each night's observation, was recalibrated against a black-body cavity. A thick, glass filter was used to prevent long-wave radiation from entering the spectrometer and producing a

spurious stray-radiation signal. This precaution is very necessary since the standard black-body cavity temperature was set at a value between 500 and 600°K and was consequently very much brighter at longer wavelengths than in the region for which the calibration was being made. The use of the glass filter, combined with the rapid drop in cell sensitivity beyond 1·5 μ reduces the effect of stray radiation to a negligible level.

For the measurements of absolute brightness of the 4,2 band, the quantity measured from the spectra was the peak spectrometer deflection for the Q-branch. The integrated brightness for the whole band was then deduced with the help of the ratio (obtained from synthetic spectra) of the peak brightness, at a given spectral slit width, to the total band brightness. The latter ratio depends on the rotational temperature assumed; in this work a temperature of 210°K was taken in accordance with the results of Section 4.

Nine sets of spectra were used to obtain absolute brightnesses and the results are listed in Table 2.

Table 2. Observed zenith brightnesses of 4,2 OH band

Date	Spectral slit width (Å)	Zenith distance (degr.)	Brightness (kR)
2/3 September 1959	50	73	59
21/22 September 1959	50	73	65
16/17 November 1959	25	73	46
	100	80	45
14/15 January 1960	100	0	52
17/18 February 1960	25	75	101
19/20 February 1960	100	80	49
2/3 March 1960	100	80	56
	100	0	124
Mean			66

The results for the absolute brightness are all lower than the value of 175 kR given by Harrison and Vallance Jones. The latter value was obtained for an assumed rotational temperature of 260°K but the result was reduced to the zenith by multiplication by cos Z (where Z is the zenith angle) instead of the van Rhijn factor for 70 km. When the results obtained by Harrison and Vallance Jones are reduced by the method employed in this work the two corrections compensate and a value of 175 kR is again obtained. It must be concluded, therefore, that the value quoted by them refers to an occasion when the emission was exceptionally bright and that a value in the range between 40 and 70 kR is more typical of average conditions. This new value fits well with the calculations of Chamberlain and Smith (1954) and the recent results of Moroz (1960).

The relative brightnesses of the bands may also be obtained from the present results. The results shown in Fig. 1 show that a good match is obtained between the synthetic and observed spectra for a relative intensity $I(3,1)/I(4,2) = 1{\cdot}2$ when

VOL. 22 1961

the P-branch of the 3,1 is matched to the Q- and R-branches of the 4,2 band. A value for the intensity ratio between the 2,0 and 3,1 bands was obtained from the spectrum shown in Fig. 3. This spectrum was obtained on an exceptionally clear and very cold night. Since other spectra were obtained the same night at zenith distances from 0 to 80° it was possible to extrapolate the brightness of the P-branch of the 2,0 band to zero absorption and so obtain an estimate of the relative brightnesses of the 2,0 and 3,1 band. The final results obtained were: $I(2,0):I(3,1):I(4,2) = 1{\cdot}1:1{\cdot}0:0{\cdot}91$.

This result depends upon the assumption that the line strength factors of PLYLER *et al.* (1953) are correct. It was recently suggested by CONNES and GUSH (1960) that the line strength factors for the Q-branches should be reduced. This effect, if present, would require an adjustment in the above result and would lead to a reduction in intensities of the 2,0 and 3,1 bands relative to the 4,2 band since in each case the P-branch of the bands have been compared with the Q-branches of their immediate, long wavelength neighbours.

6. The Height of the Emitting Layer

The higher signal-to-noise ratio of the present series of measurements makes it feasible to apply the van Rhijn method for the measurement of the height of the emitting layer. This method, in practice, is subject to a number of uncertainties (ROACH and MEINEL, 1955). In the 1·5 μ infra-red region some of the difficulties associated with it should be less serious. The method calls for a comparison between the observed brightness of the airglow emission in the zenith direction and in one or more directions closer to the horizon. The ratios of brightnesses observed in these different directions should be a simple function of the height of the emitting layer. The sources of error are: (i) non-uniformities in the brightness in the emitting layer, (ii) the transmission losses arising from scattering and absorption in the lower atmosphere and (iii) the presence of a uniform background of emission from extra-terrestrial sources. For infra-red measurements at 1·5 μ error (iii) should be much less serious, while the part of error (ii) due to molecular scattering is reduced by an order of magnitude. Error (i) may be reduced by making a large number of measurements. There is also an additional error arising as a consequence of the finite field of the instrument. However, this effect may be taken exactly into account.

Value of the ratio $B'(80)/B'(0)$ (where $B'(Z)$ is the brightness at zenith distance Z, averaged over the field of view of the spectrometer) were calculated for a range of heights of the emitting layer. In calculating the ratio the effect of Rayleigh scattering was taken into account using an extinction coefficient of 0·0015 atm^{-1} (ALLEN, 1955). The ratios obtained were as listed in Table 3.

Table 3

h(km)	100	90	80	70	60	50
$B'(80)/B'(0)$	4·06	4·17	4·31	4·43	4·57	4·72

The experimental results comprised 185 values of the ratio $B'(80)/B'(0)$ obtained on a very clear, cold night for the P-branch of the 3,1 and the R-branch of the 4,2

OH band. The mean value of the ratio was 4·45 with a standard error of the mean of 0·09. No correction was made for extinction by dust or water vapour in view of the very cold, clear conditions. This corresponds to a height of about 69 km with a standard error of 7 km. The result is in agreement with the earlier van Rhijn measurements of Roach *et al.* (1950) and Meinel (1950) who derived a height of 70 km. In view of the possibility of systematic errors with the van Rhijn method there is no reason to believe that the present result is inconsistent with the recent rocket measurement of Lowe (1961) and of Koomen *et al.* (1960) who found a maximum emission rate between 75 and 90 km. It does, however, provide support for the view that the OH emission originates in the 60–90 km region. Additional support for this conclusion is provided by the temperature measurements since temperatures in the range between 170 and 230°K are associated with the 70–90 km region (Minzner and Ripley, 1956; Stroud *et al.*, 1960).

7. Conclusions

The use of a germanium photoconductive detector made it possible to obtain more highly resolved spectra at 1·5 μ than had been obtained previously with a spectrometer. It was found, in agreement with the even higher resolution interferometric results of Connes and Gush (1960), that there are present no strong features other than the rotation vibration bands of OH between 1·5 and 1·61 μ. It is possible that there are some weak additional features present at 1·538 and 1·580 μ.

The temperature determinations from the rotational structure of the P-branch of the 3,1 band yielded temperatures between 200 and 225°K. This result is in good agreement with the earlier value of Gush and Vallance Jones (1955) and with the results of Connes and Gush. The temperature results from the infra-red are also in satisfactory agreement with the mean value obtained photographically at Saskatoon by McPherson and Vallance Jones (1960) after the correction pointed out by Wallace (1960) has been made. It seems, therefore, that spectral observations of the kind described in this paper provide a convenient means of measuring OH temperatures with an accuracy of ± 20°K. It is likely that even better precision could be obtained by confining the measurements to the $P_1(2)$, $P_1(3)$ and $P_1(4)$ lines of the 3,1 band. In this way the accuracy of measurements of these lines of the spectrum could be very much increased and a comparison could be made between the observed and synthetic spectra using the least squares method of Connes and Gush.

VOL. 22 1961

References

Allen C. W.	1955	*Astrophysical Quantities*, p. 116. Athlone Press, London.
Chamberlain J. W. and Smith C. A.	1959	*J. Geophys. Res.* **64**, 611.
Connes J. and Gush H. P.	1959	*J. Phys. Radium* **20**, 915.
Connes J. and Gush H. P.	1960	*J. Phys. Radium* **21**, 645.
Dieke G. H. and Crosswhite H. M.	1948	Bumblebee Report No. 87, Johns Hopkins University.
Gush H. P. and Vallance Jones A.	1955	*J. Atmosph. Terr. Phys.* **7**, 285.
Harrison A. W. and Vallance Jones A.	1957	*J. Atmosph. Terr. Phys.* **11**, 192.
Koomen M. J., Paker D. M., Gulledge I. S., Cooper H. W. and Tousey R.	1960	Presented at UGGI Meeting, Helsinki.

Lowe R. P.	1961	CARDE Technical Memorandum 291/59.
McPherson D. H. and Vallance Jones A.	1960	*J. Atmosph. Terr. Phys.*, **17** 302.
Meinel A. B.	1950	*Astrophys. J.* **112,** 120.
Minzner R. A. and Ripley W. S.	1956	U.S. Air Force Surveys in Geophysics TN-56-204, No. 86.
Moroz V. I.	1960	*Dokl. Akad. Nauk SSSR* **126,** 983.
Plyer E. K., Benedict W. S. and Humphreys C. J.	1953	*J. Chem. Phys.* **21,** 398.
Roach F. E. and Meinel A. B.	1955	*Astrophys. J.* **122,** 530.
Roach F. E., Pettit H. B. and Williams D. R.	1950	*J. Geophys. Res.* **55,** 183.
Stroud W. G., Nordberg W. and Bandeen W. R.	1960	*J. Geophys. Res.* **65,** 2303.
Vallance Jones A. and Harrison A. W.	1958	*J. Atmosph. Terr. Phys.* **13,** 45.
Wallace L.	1960	*J. Geophys. Res.* **65,** 921.

Journal of Atmospheric and Terrestrial Physics, 1961, Vol. 22, pp. 176 to 185. Pergamon Press Ltd. Printed in Northern Ireland

20 Mc/s w.w.v. bursts during the last few periods of 1958δ2

J. WOLFE
Radio and Electrical Engineering Division, National Research Council, Ottawa 2, Canada

(*Received* 13 *June* 1961)

Abstract—Paper recordings of w.w.v. on 20 Mc/s were taken during the last 8 days of Sputnik III (1958δ2). The satellite was tracked during this period with an h.f. direction finder. This paper describes the methods used in trying to correlate w.w.v. enhancements with the position of the satellite. The results indicate that if Sputnik III produced detectable reflections, its ability to do so was nearly, if not completely, independent of the satellite's position.

THE DETECTION of silent satellites using c.w. reflection techniques was first reported by KRAUS (1958a). Since then several similar experiments using the same technique have been reported (KRAUS, 1958b,c,d, 1960a,b,c; HENDRICKS, 1958; ROBERTS, 1959). In these experiments the signal from a distant transmitter (usually w.w.v.) was monitored. The transmitter chosen was located such that its frequency was above the m.u.f. for all or a portion of each day. Thus small signal enhancements were easily detected because the background "noise" due to signal propagation by ionospheric reflections was absent.

A small signal is present, however, due to forward scatter and to reflections from meteor trails. These modes of propagation may produce a noisy background with characteristics similar to those of the signal we wish to detect. If such a similarity exists it is necessary to use statistical methods in order to detect the presence of satellite-enhanced signals.

Paper records from a receiver tuned to w.w.v. on 20 Mc/s were made when Sputnik III was about to fall in. The antenna was sensitive to vertical polarizations only and was about 400 ft from the receiver. A signal strength of 45 μV/m at the aerials produced full-scale deflection on the linear amplitude scale of the paper records (Figs. 2 and 9). The 1200 c/s bandwidth of the receiver was narrow enough to eliminate interference since no signals were recorded during the quiet periods of w.w.v. This bandwidth was not reduced further to ensure reception of possible Doppler-shifted w.w.v. signals (ROBERTS, 1959; KRAUS, 1960).

The satellite was tracked with an h.f. direction finder tuned to the satellite frequency (20·0045 Mc/s) (MCLEISH, 1958; WOLFE, 1958). The period and inclination of the orbit were determined. With this orbital data and a fix on the sub point of the satellite during a near approach, the position of the satellite at the time of a w.w.v. burst could be found.

A total of fifty-six significant bursts were recorded from 1500 hours (E.S.T.) on 28 March to 2400 hours (E.S.T.) on 5 April. A w.w.v. burst was considered significant if its amplitude was twice the background level and if its duration was 40 sec or more. The penwidth of the recorder was 20 sec. The time, duration and amplitude of each burst were listed.

A target area was then chosen over which Sputnik III would most likely be if

VOL. 22 1961

a satellite reflection of w.w.v. was observed. Previous reports indicate the detection of satellite induced reflections over long, as well as short distances and particularly from the northern auroral zone (KRAUS, 1960a). Thus, the area chosen includes the nearby auroral zone and is shown by the dotted lines in Fig. 1. This target is bounded by the latitudes 65°N and 35°N and by the longitudes 15°W and 135°W. The probability of finding the satellite over this section of the earth at some random instant of time was calculated. For an orbital inclination of 65° this probability is 0·10.

The positions of the satellite when the w.w.v. bursts were recorded are also shown in Fig. 1. Seven of the bursts occurred when the satellite was over the

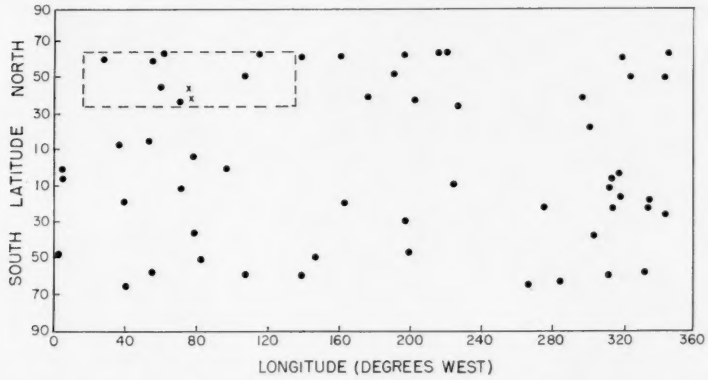

Fig. 1. The positions of Sputnik III when the fifty-six w.w.v. bursts were recorded. The dotted lines enclose the target area chosen. Ottawa and Washington are located by the two crosses in the target area.

target area and so are called "hits". The expected number of hits for randomly occurring bursts is 5·6. On statistical grounds this increase of 1·4 over the number of expected hits is not significant. This can best be shown by testing for real change changes in frequency (BEER, 1956) (This is a χ^2 test using Yates' correction and is based on a confidence level of 0·05 for 1 degree of freedom). With a 5 per cent probability, ten or more hits in fifty-six tries would be required to indicate a significant departure from a random distribution.

Approximately 50 per cent of the records could not be used in this analysis for the following reasons:

(1) w.w.v. signals were received continuously from about 1400 to 2200 hours on a number of days. These signals, propagated by normal ionospheric and scatter modes, were too strong to permit the detection of the weaker bursts. Thus a total of 43 hr of recording was rendered useless.

(2) On one occasion a great many short bursts were recorded for a period of 24 hr. A separate analysis was made over this period and will be discussed later.

(3) An interesting record was obtained on 31 March from 1600 to 2300 hours E.S.T. Very strong, enduring but irregular bursts were recorded as shown in Fig. 2. Data from a local auroral radar (48 Mc/s) indicated considerable activity during

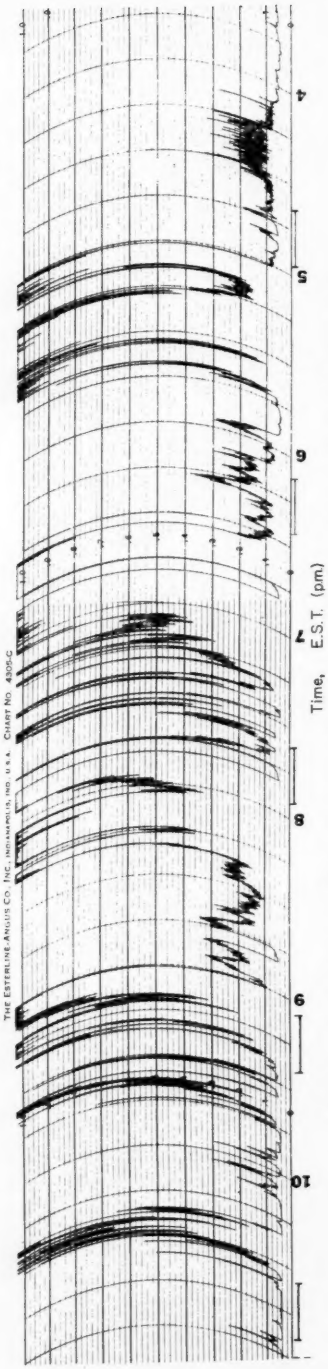

Fig. 2. Very strong, enduring but irregular w.w.v. bursts recorded on 31 March 1960, from 1600 to 2300 hours E.S.T. The solid bars along the time scale indicate the times during which the satellite was north of 45°N.

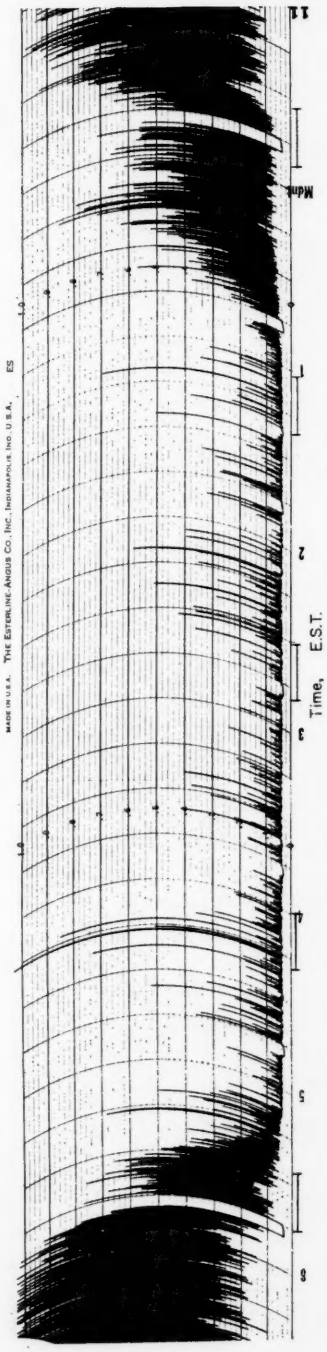

Fig. 9. An example of the frequent but short w.w.v. bursts recorded on 6 April 1960, from 0100 to 0530 hours E.S.T. Sputnik III is believed to have fallen during this period, the last official sighting being made at 0230 hours E.S.T.

VOL. 22 1961

this period. There was no apparent correlation of fine structure between the two records, possibly because of the difference in frequency. The solid lines, along the time scale in Fig. 2, indicate the times during which the satellite was north of the 45°N parallel.

(4) Equipment failure caused the loss of 20 more hours of data.

The fifty-six w.w.v. bursts were recorded during the remaining time of 107 hr. A histogram of the distribution of the 107 hr throughout the day is shown in Fig. 3(a). The distribution of the fifty-six bursts is plotted in Fig. 3(b). Note the correlation between Fig. 3(a) and Fig. 3(b). The average burst rate for each 2 hr mean is shown in Fig. 3(c).

Fig. 3 becomes much more interesting with the addition of part (d). The probability of finding the satellite over the target area as a function of time is shown in Fig. 4. At time $T = 0$ the most northerly part of the orbit is north of Ottawa (75°W). For a portion of each day the target area is not intersected by the orbital plane. This occurs when the most northerly point of the orbit is between the longitudes of 60°E and 150°E. Therefore, during one quarter of the Earth's rotation or 6 hr each day, it is impossible to score a hit. On 24 March this "dead" period was from 1600 to 2200 hours E.S.T. The precession of the orbit and the use of solar time cause the dead period to change slightly each day so that on 5 April the dead period occurred from 1300 to 1900 hours E.S.T. The solid lines in Fig. 3(d) indicate the times during which the orbital plane did not intersect the target area. The dashed lines in Fig. 3(d) indicate the times of day when the satellite traverses the longest possible path over the target area. This, of course, occurs exactly 12 hr away from the mid-point of the dead period.

Fig. 3 reveals two interesting points. The first is the fact that the burst rate does not increase when the probability of finding the satellite over the target area is greatest. If satellite-produced echoes had been detected consistently, the burst rate should have increased.

Secondly, it should be noted that the dead period each day occurs when the direct signal from w.w.v. is too large to detect small bursts. This, of course, is purely accidental, but the coincidence affects the previous results based on the probability of a hit being 0·10. If direct signals from w.w.v. were not present at any time the total number of good hours would be constant throughout the day. The histogram in Fig. 3(a) would be flat and therefore the numbers of hours and bursts recorded between 1400 and 2200 hours would be greater. These additional bursts could not have been hits since the satellite never crossed the target area during this period. Therefore, seven hits would have been observed out of $56 + n$ bursts. An approximation to n was made by multiplying the average burst rate by the number of additional hours required from 1400 to 2200 hours to make the mean number of good hours during this period and from 2200 to 1400 hours equal. The approximate value of n is 17. This would indicate seven hits out of seventy-three bursts, which is close to the 7·3 hits predicted for randomly-occurring w.w.v. bursts.

Consider now the area of each of the fifty-six bursts as the products of it amplitude and duration. The total area of the fifty-six bursts is 961 units. The total area of the seven hits is 216 units, as compared with an expected area of $7/56 \times 961$ or 120 units. Three large bursts account for 192 units of area. A list of the seven

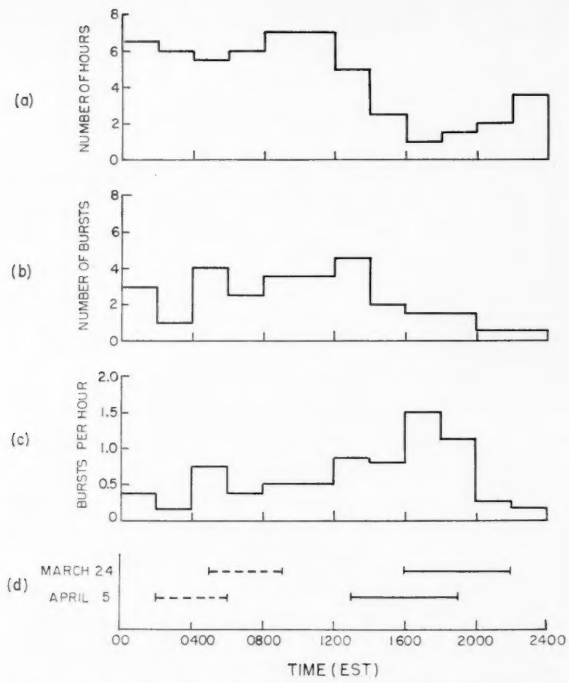

Fig. 3. (a) A histogram showing the distribution of the 107 hr of good observations throughout the day. (b) The distribution of the fifty-six w.w.v. bursts throughout the day. (c) The burst rates calculated from the 2 hr means of (a) and (b). (d) The dead period or the time during which the orbital plane did not intersect the target area (————). The time when the satellite traversed the longest possible path over the target area (– – – –).

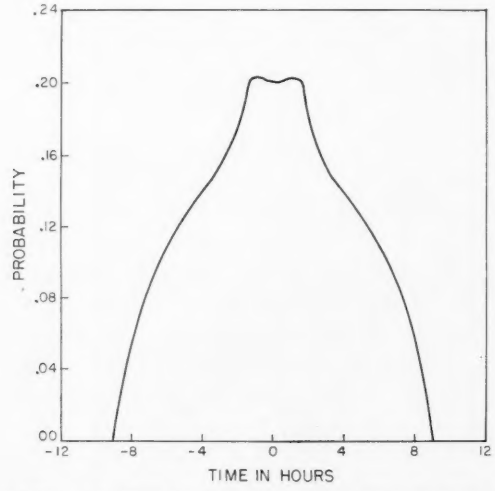

Fig. 4. The probability of finding the satellite over the target area as a function of time. At time $T = 0$ the most northerly part of the orbit is north of Ottawa, at 65°N, 75°W.

VOL. 22 1961

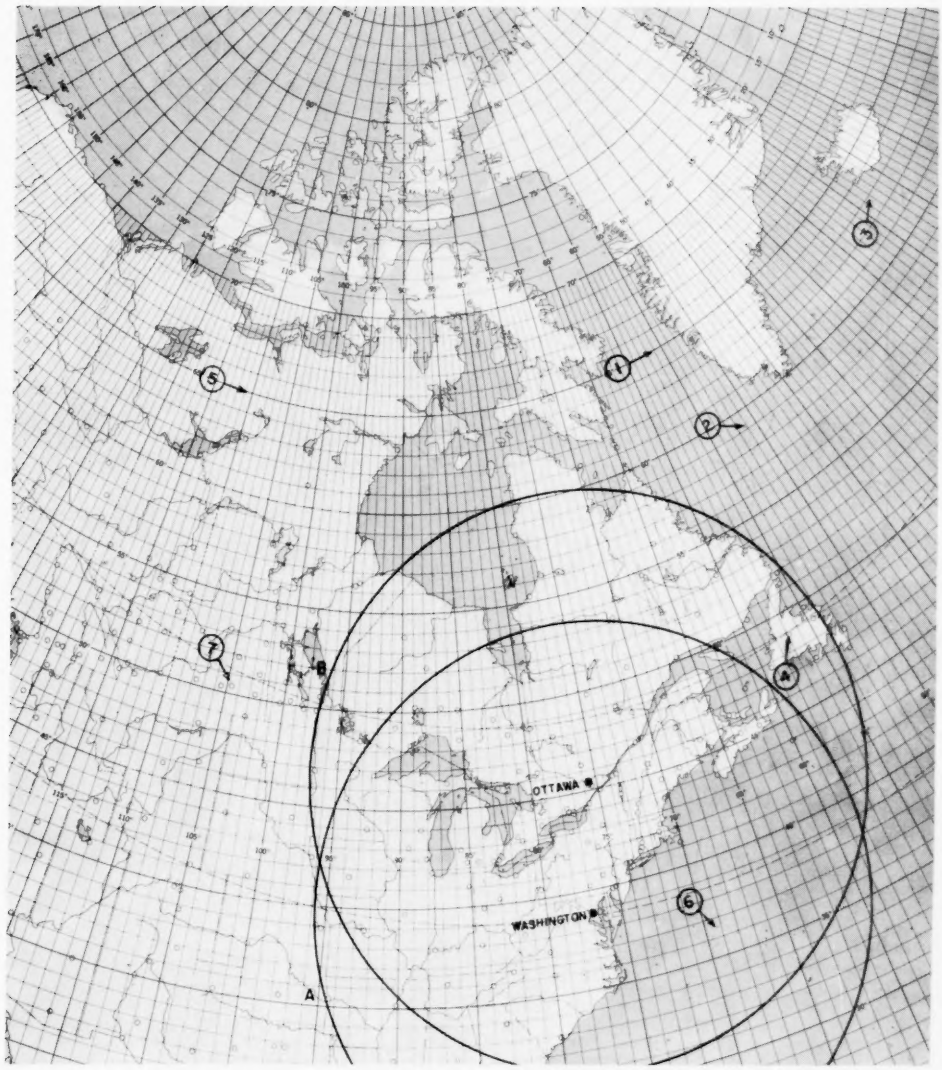

Fig. 5. The positions and headings of Sputnik III when the seven "hits" were recorded. The circles enclose the line-of-sight regions from Ottawa and Washington.

VOL.
22
1961

hits given in Table 1 showing the large bursts to be Numbers 3, 6 and 7. If satellite-reflected signals similar to those previously reported were recorded, these three bursts would be the most likely suspects.

The positions and directions of travel of Sputnik III when the seven hits were recorded are shown in Fig. 5. The encircled numbers on the map correspond to the numbers of the hits listed in Table 1. The range and direction of the satellite with respect to the transmitter and receiver is considerably different for each of the three large bursts.

Circle A in Fig. 5 is centred at Washington and encloses the region in which

Table 1

No.	Date	Time (E.S.T.)	Area	M.u.f. (Mc/s)
1	30 March	0510	2	16
2	30 March	0664	10	19
3	31 March	0038	84	13
4	1 April	0008	4	—
5	2 April	0736	8	14
6	4 April	0828	60	—
7	4 April	0968	48	20

the satellite was directly illuminated by the w.w.v. transmitter. The size of this circle was calculated for a satellite height of 100 miles using 4/3 of the Earth's radius. Circle B is the same as A but is centred at Ottawa. At a height of 100 miles over the common area of the two circles (A and B) a satellite could receive a signal directly from w.w.v. It would also be able to reflect this signal directly to Ottawa. Such is the case for the sixth and possibly the fourth hit. For any other position on the map one or more reflections from the ionosphere would be required to receive the satellite-reflected signal at Ottawa. The possibility of sending or receiving 20 Mc/s signals via one-hop *F*-reflections was examined for each hit (Radio Physics Laboratory, 1954). The maximum usable frequency for each hit is given in Table 1. These values of the m.u.f. are only predictions but they do indicate that 20 Mc/s signals are not likely to be propagated to or from the positions 1, 3 and 5.

Transmission over longer paths, however is possible at 20 Mc/s. Recent letters by Kraus (1960b,c) describe the reception of w.w.v. bursts when Sputnik III was near the auroral zones and the horns of the outer Van Allen belt. In order to test for this phenomenon the fifty-six positions of the satellite in Fig. 1 were separated according to latitude. The histogram of the latitude distribution using class intervals of 10° is shown in Fig. 6. The theoretical distribution in the same figure was calculated on the basis of fifty-six randomly-occurring w.w.v. bursts. The two curves match fairly well considering the number of samples in each class interval. The goodness of fit between these histograms can be demonstrated by the χ^2 test. This test, using Yates' correction and grouping the data into five sections (Fig. 6) indicates a probability of finding a worse fit by random samplings to be 60 per cent. Between the north latitudes of 55° and 65° however, twelve "hits" were observed while eight were expected. Again applying the test for a real change in frequency

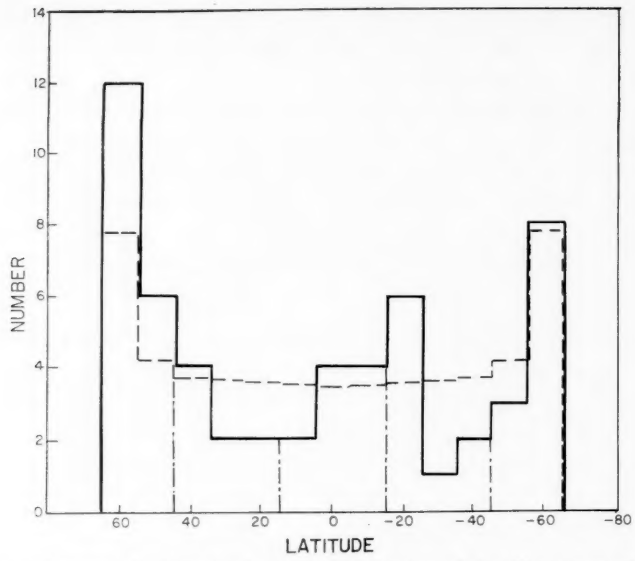

Fig. 6. A histogram showing the latitude distribution of the fifty-six satellite positions in Fig. 1. The dotted histogram is the theoretical distribution for fifty-six randomly-occurring w.w.v. bursts.

VOL. 22 1961

(BEER, 1956) shows that there is a 5 per cent probability of obtaining fourteen hits in this region due to random sampling.

A further check on the latitude distribution of Sputnik III was made after the weak w.w.v. bursts were excluded. If satellite-produced bursts of w.w.v. were large but infrequent, the smaller bursts due to scatter and meteor reflections would mask the effect of the wanted signals. A total of twenty-six bursts with an area of 10 units or more was recorded. Of these, eleven bursts had an area greater than 30 units. The positions of the satellite during the twenty-six larger bursts are plotted in Fig. 7. The corresponding histogram of the latitude distribution is

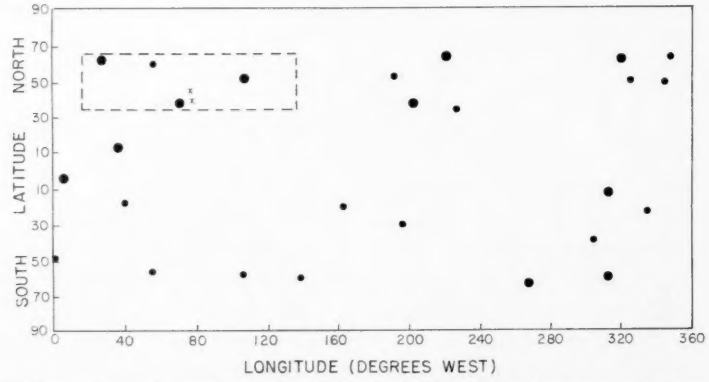

Fig. 7. The twenty-six positions of Sputnik III during the larger w.w.v. bursts. The eleven positions of the satellite when the area of the burst was greater than 30 units are positioned with larger dots.

shown in Fig. 8. This histogram also shows fairly good agreement with the theoretical values for randomly-occurring bursts. The goodness of fit was not tested in this case since there were only twenty-six samples. The increase over the expected values at the northern auroral latitudes, and also the slight increase at 60° do not appear to be significant.

The longitudinal distribution of the fifty-six burst positions in Fig. 1 was also tested for randomness. The Earth's surface was divided into six vertical sections of equal longitude (60°). The actual population of each sector was compared with the expected value (9·33 for random distribution), again using the χ^2 test. Then

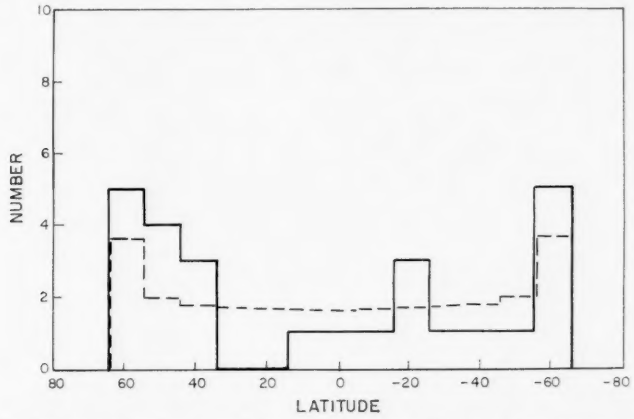

Fig. 8. The latitude distribution of the twenty-six satellite positions corresponding to the larger w.w.v. bursts. The dotted histogram was calculated for twenty-six randomly occurring bursts.

each sector was phase shifted 20° in the same direction and the test performed again. After two shifts the probabilities of obtaining distributions with larger discrepancies from the theoretical rectangular distribution were 25, 70 and 45 per cent. It is, therefore quite possible that the fifty-six bursts were taken from a population distributed randomly in longitude.

On two occasions high burst rates were recorded. An example of the frequent but short bursts is shown in Fig. 9. A total of 29 hr of this type of recording was obtained from 0100 to 0600 hours E.S.T. on 6 April and from 0800 E.S.T. on 3 April to 0800 E.S.T. on 4 April. An effort to correlate enhancements of this fine structure with the position of the satellite was made for two reasons. Firstly, 29 hr of recording represents a considerable amount of data. Secondly, this type of record was produced during the last few revolutions of Sputnik III. The satellite is believed to have fallen during the 5 hr period of rapid bursts on 6 April, shown in Fig. 9. The solid lines beneath the time scale indicate the times during which the satellite was expected north of the 45°N parallel. These times were predicted from the period of the satellite measured on previous days.

Fig. 9 shows several large bursts at 0415 E.S.T. Sputnik III at this time was expected to be over the southern tip of Greenland and heading S.E. However, the last official detection of the satellite was reported by the Millstone radar at

Prince Albert (Saskatchewan) at 0230 E.S.T. or one revolution earlier (CAMERON, 1960). From Fig. 9 it can be seen that no large bursts were recorded during this pass.

An attempt to correlate the short signals with the position of the satellite was carried out in the following manner. The numbers of bursts above two amplitude levels on the paper record were counted. The percentage of these bursts occurring while Sputnik III was north of 45°N was calculated for each amplitude level. The results are given in Table 2.

A satellite with an orbital inclination of 65° spends 21 per cent of its time north

Table 2

Date	Amplitude level	No. of bursts	Hits (%)
3–4 April	3	106	24
3–4 April	5	49	18
6 April	3	34	26
6 April	5	10	30

of 45°N. This is the average percentage of hits recorded on 3 and 4 April. On 6 April thé increase to an average of 28 per cent is the result of the few strong bursts at 0415 hours.

CONCLUSIONS

The results of this study indicate that detectable satellite induced enhancements of w.w.v. during a near pass of the satellite do not occur regularly, if at all. There are, of course, several w.w.v. bursts which, when examined singularly appear to and may be the result of a satellite crossing. The exact nature of the transmission of each of these bursts cannot be resolved with the data recorded by this experiment. It is possible, however, to show that collectively the w.w.v. burst rate does not increase when the satellite is near.

Examination of the positions of the satellite during w.w.v. bursts reveals latitude and longitude distributions similar to those produced by randomly-occurring bursts. When small bursts are included in this analysis more bursts than predicted occur when the satellite is in the northern auroral zone. Since the significance of this increase is doubtful, one of the following conclusions concerning the reception of 20 Mc/s bursts reflected by the distant satellite must be reached.

(a) If Sputnik III produced regular reflections that were detected above the background level its ability to do so was nearly, if not completely, independent of the satellite's position.

(b) If Sputnik III produced a few sporadic reflections that were detected, these signals probably occurred when the satellite was in the northern auroral zone. These signal bursts are so rare (compared with w.w.v. bursts propagated by "natural "modes) that considerably more than 100 hr of data are required to detect this effect by numbers alone.

(c) Sputnik III produced very weak reflections, none of which rose above the noise level and could be detected.

VOL. 22 1961

Acknowledgement—The author wishes to express his thanks to C. W. McLeish and K. Steele for their valuable assistance.

References

Beer S.	1956	*Engineer* **202,** 798.
Cameron E. A.	1960	Defence Research Telecommunications Establishment (Can.) Technical Memorandum No. 317.
Hendricks C. D.	1958	*Proc. I.R.E.* **46,** 1763.
Kraus J. D.	1958a	*Proc. I.R.E.* **46,** 611.
Kraus J. D.	1958b	*Proc. I.R.E.* **46,** 612.
Kraus J. D.	1958c	*Proc. I.R.E.* **46,** 1580.
Kraus J. D.	1958d	*Proc. I.R.E.* **46,** 1534.
Kraus J. D.	1960a	*Proc. I.R.E.* **48,** 672.
Kraus J. D.	1960b	*Proc. I.R.E.* **48,** 1913.
Kraus J. D.	1960c	*Proc. I.R.E.* **48,** 2027.
McLeish C. W.	1958	*Electron. Radio Engng* **35,** 386.
Radio Physics Laboratory	1954	Radio Physics Lab. (Can.) Report No. 1-1-3
Roberts C.	1959	*Q.S.T.* **43** (8), 34.
Wolfe J. L.	1958	*J. Atmosph. Terr. Phys.* **13,** 155.

Journal of Atmospheric and Terrestrial Physics, 1961, Vol. 22, pp. 186 to 191. Pergamon Press Ltd. Printed in Northern Ireland

The interpretation of *F2* critical frequency measurements

L. H. Heisler and J. D. Whitehead
Radio Research Board Laboratory, Electrical Engineering School,
University of Sydney, Australia

(*Received* 29 *June* 1961)

Abstract—During winter daylight hours changes in f_0F2 are almost continuous due to the presence of travelling ionospheric disturbances. It is suggested that variation in hourly values of f_0F2 from day to day on magnetically quiet days is due mainly to this cause and it is shown that these values are only reliable to $\pm$ 0·5 Mc/s. The resultant error in estimated maximum usable frequencies has been determined. Critical frequencies as read from ionogram records are not true vertical incidence values but are reflected at an angle θ from the vertical because of sloping isoionic contours. This angle has been estimated as well as the amount by which average measured values of f_0F2 must be decreased to give real vertical incidence values of f_0F2.

1. Introduction

The study of travelling ionospheric disturbances has shown that the ionosphere is a dynamic medium in which almost continuous changes in ion density are occurring. This is particularly so during winter daylight hours when ion density changes of the order of 30 per cent are not uncommon, disturbances occur approximately at the rate of one each hour, and duration of disturbances may be as long as 30 min (Heisler, 1958). It is felt that the observed variability in *F2* critical frequencies is not fully appreciated by many workers due to the practice of using 10 min ionosonde records or resorting to tabulated hourly values of f_0F2 for research purposes.

This paper shows that the variation of f_0F2 during winter daylight hours is considerable and that failure to take account of these large deviations in median values of f_0F2 gives rise to systematic errors in maximum usable frequency estimations. Furthermore resultant distortion in isoionic contours lead to off vertical reflections so that measured values of f_0F2 are seldom representative of the ionosphere immediately overhead, but at some angle θ to the vertical, the average value of which can be calculated.

2. Observational Data

Values of *F2* critical frequency have been scaled from ionograms recorded on a panoramic type ionosonde previously described (Heisler, 1955). This recorder provides a 15 sec scan every minute and each ionogram has been scaled to the nearest 0·1 Mc/s between the hours 0600–1800 for five magnetically quiet days during June 1955. Most changes in f_0F2 are due to cusp-type travelling ionospheric disturbances and the highest penetration frequency on the ionogram has therefore been read as the correct value of f_0F2 (Munro and Heisler, 1956). Fig. 1 shows the variation of f_0F2 on 11 June 1955 at Camden (150°40′E, 34°03′S). The values have been plotted every 3 min to conserve space, and considerable variation is evident. For the five days considered the frequent changes observed correspond to an average electron density change of $\pm$ 1·2 $\times$ 10^4 electrons/cm^3/min or 2 per

VOL.
22
1961

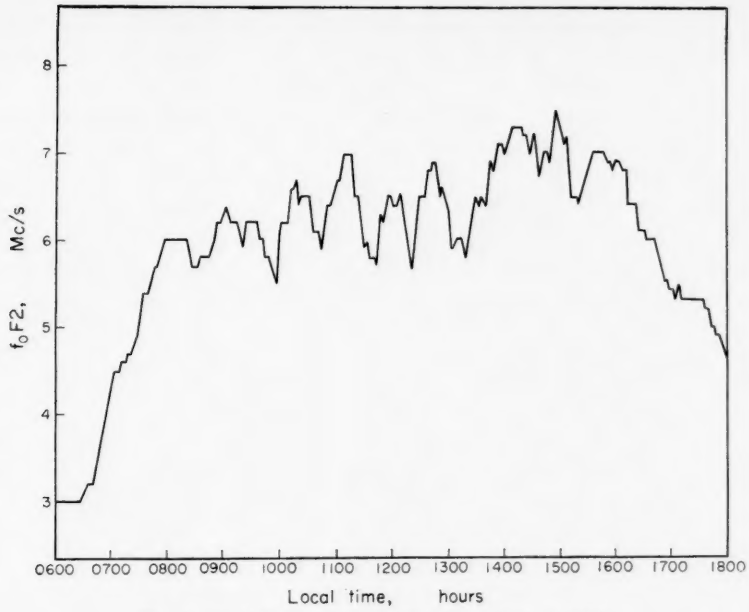

Fig. 1. Variation of f_0F2 at Camden, 11 June 1955.

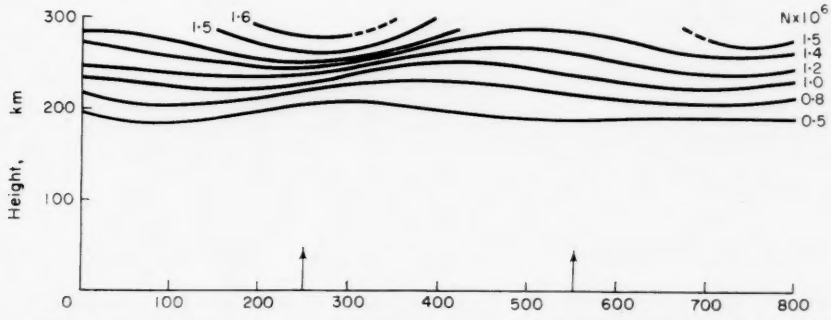

Fig. 2. Cross section of a travelling disturbance in the *F*-region of the ionosphere. (Lines represent isoionic surfaces or surfaces of equal ionization).

cent of the total electron density per minute. The main cycle change in f_0F2 has an average amplitude of 0·5 Mc/s and an average period of 61·5 min.

3. Average off Vertical Deviation during f_0F2 Measurement

A cross section of travelling disturbance in the *F*-region of the ionosphere is shown in Fig. 2, where the lines represent isoionic surfaces or surfaces of equal ionization. Between 250 and 450 km from the origin reflections will be possible from the 1·6 contour whereas actually the true vertical maximum ion density at 450 km is represented by the 1·4 contour. Over this distance the measured maximum ion density should fall steadily but because of curvature in isoionic contours off vertical reflections occur and measured values tend to remain constant. This is

evident in Fig. 1, where it can be seen that peak values of f_0F2 tend to remain constant giving the crests of the f_0F2 variation a flat-topped appearance. In practice the main cycle variation possesses a small superimposed random fluctuation. In Fig. 3 the dotted curve represents diagrammatically the observed variation in which this fluctuation is only shown near the maxima and minima. It is assumed that the fluctuation is of the order of 0·2 Mc/s and the intervals occupied by the maxima and minima have been defined as the time in which f_0F2 departs from the extreme peak values by less than this amount. Over the period considered the average duration of f_0F2 maxima is 20·2 min while the average period occupied by

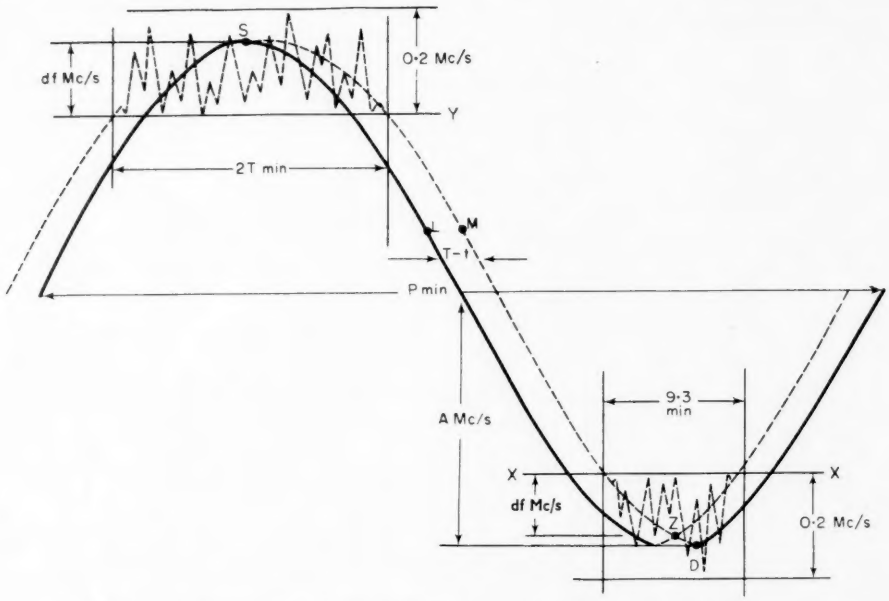

Fig. 3. A diagrammatic representation of average cyclic variation of f_0F2.

a minima is 9·3 min. From these values it is possible to estimate approximately the average angular deviation θ of measured values of f_0F2 from the vertical.

If we assume that the true variation of f_0F2 is sinusoidal in form, then this is represented by the full line in Fig. 3. (If the electron density rather than f_0F2 is assumed to have a sinusoidal variation, the off vertical angle and the corrections given are reduced to about 90 per cent of their values). At Y the observed f_0F2 has fallen to a certain magnitude in a time T minutes, where T is half the average duration of f_0F2 maxima. If we assume that the smoothed value of f_0F2 has fallen df Mc/s to the same magnitude in a time t minutes then

$$t = \frac{P}{2\pi}\left(\cos^{-1}\frac{A - df}{A}\right)$$

where A is the amplitude and P the period of the sine curve variation. The displacement in time therefore of observed variation from actual variation is $T - t$ minutes.

VOL. 22 1961

At point Z if we neglect superimposed fluctuations the observed f_0F2 reaches a minimum at a point of phase difference ϕ degrees from the sine wave minimum at D. However, due to presence of fluctuations the average duration of f_0F2 minima is measured along the line XX, corresponding to a magnitude df Mc/s greater than at Z. The angle ϕ is given by

$$\phi = \frac{2\pi(T - t)}{P}$$

and therefore the magnitude of the sine wave at Z is $-A \cos \phi$. The amplitude corresponding to the line XX is $-A \cos \phi + df$ corresponding to a phase angle β where

$$\cos \beta = \frac{-A \cos \phi + df}{A}.$$

The difference in phase angles $\beta - \phi$ is a measure of half the average duration time r of f_0F2 minima where

$$r = \frac{2P(\beta - \phi)}{\pi} \text{ minutes.}$$

r has been computed for various assumed values of df. Displacement $T - t$ giving the observed value of 4·67 min for r can then be determined by plotting corresponding values of $T - t$ against r. This displacement is 3·05 min and if we assume a disturbance velocity of 10 km/min (HEISLER, 1958) this represents a spatial distance of 30·5 km. If the virtual height of *F2* maxima is 250 km, the average angular deviation θ of f_0F2 measurements is 7°. Refraction which is probably considerable has been neglected and the above value of θ therefore is a minimum figure, and deviation is probably greater.

Presence of non-vertical reflections from the *F2*-region of the ionosphere has already been confirmed by BRAMLEY and ROSS (1951) who show that the *F*-layer at any point is usually tilted in a random direction, the r.m.s. magnitude of the varying tilt being of the order 1·5–2·0°. However these measurements were made on frequencies well below critical where slope of iosionic contours would be expected to be appreciably less than that at maximum ion density. Moreover the particular experimental method used, would be expected to fail when double reflections at a given frequency occurred, a usual phenomenon in the presence of large tilts.

4. MAXIMUM USABLE FREQUENCY ESTIMATIONS

These are usually estimated for a great circle path of 3000 km, and reflection from the ionosphere is considered to take place at the mid-point D between the two stations B and E in Fig. 4. However, due to the presence of travelling disturbances reflection may take place at some point A. If C is the centre of the earth then the largest permissible value of γ is determined by the position of AC such that angle AEC is a right angle, when

$$t^2 = (R + h)^2 - R^2$$

and $\sin(\alpha + \gamma) = t/(R + h)$. R, the radius of the earth, is 6370 km/sec and if h the height of ionospheric maximum is 250 km/sec then $\alpha + \gamma$ is 15·8°.

Also $$2\alpha = \frac{3000}{R} = 26{\cdot}98^\circ$$

therefore $\alpha = 13{\cdot}49^\circ$ and the maximum value of γ is $2{\cdot}31^\circ$. Ionospheric reflection can therefore be received over an arc of the ionosphere corresponding to angular measure $4{\cdot}62^\circ$ or 533 km.

Since the average disturbance periodicity is 61·5 min and the assumed velocity is 10 km/min, there would be on the average one maxima of ionization every 615 km

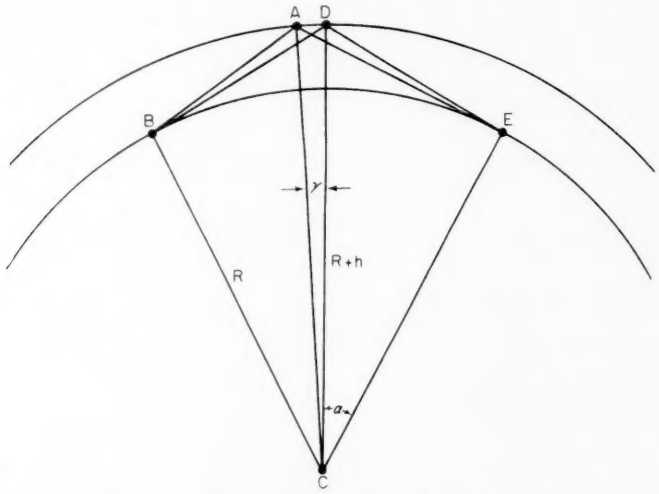

Fig. 4. Diagram showing possible mode of transmission between two stations when a travelling disturbance is present in the ionosphere.

therefore making it almost certain that one such maximum lies within the arc defined above. Therefore the maximum usable frequency should be estimated from the peak value of f_0F2 rather than the median. The mean critical frequency over the five days considered is 6·6 Mc/s and since the amplitude of the variation of f_0F2 is 0·5 Mc/s, the m.u.f. should be increased approximately 7 per cent above the value estimated from the median f_0F2. Since the angle of incidence on the ionosphere is greater at A than at D it would be expected that for the same electron density a slightly lower frequency would be reflected at A. However, there is negligible effect on the calculation of m.u.f. for the distances considered.

5. Mean Value of *F2* Critical

The measured value of *F2* critical differs from the true overhead value of f_0F2 because probing ionosonde rays tend to "cling" to high value off angle isoionic contours. This is obvious in the example of the flat topped nature of f_0F2 plots as shown in Fig. 3 when f_0F2 does not commence to fall until $t - T$ minutes after the maximum value is reached. Over the half cycle S to Q the measured value of f_0F2 is always greater than the vertical value by an amount δF the approximate average value of which is given by the amplitude multiplied by the area $SLDM$. The time

VOL. 22 1961

displacement $t - T$ is 3 min corresponding to a phase angle of 17·9°. The area $SLDM$ is therefore 17·9/180 and over a whole cycle δF is 0·09 Mc/s. Thus the true vertical critical frequency is 0·09 Mc/s less than the observed mean value, a drop of nearly 2 per cent.

6. Conclusions

During the daylight hours in winter months there is considerable variability in measured values of f_0F2. This is due to large travelling disturbances which introduce a cyclic change in f_0F2. For the five days considered this had an amplitude of 0·5 Mc/s and period 61·5 min.

Resultant distortion of isoionic contours causes non-vertical deflection of ionosonde transmissions such that on the average f_0F2 measurements are seldom vertical values but correspond to regions of the ionosphere 7° or more from the zenith. The true vertical critical frequency is approximately 2 per cent less than the observed mean value. Both of these corrections are likely to have time and spatial variations which add to their importance.

Use of hourly values of f_0F2 to determine maximum usable frequencies will result in estimates which are at least 7 per cent too low.

Acknowledgements—This work has been carried out in the Electrical Engineering School of the University of Sydney as part of the research program sponsored by the Radio Research Board of the Commonwealth Scientific and Industrial Research Organization.

We wish to express our appreciation to the University of Sydney and in particular to Professor W. N. Christiansen for provision of facilities in the Electrical Engineering School.

References

Bramley E. N. and Ross W. 1951 *Proc. Roy. Soc.* A **207,** 251.
Heisler L. H. 1955 *Aust. J. Appl. Sci.* **6,** 1.
Heisler L. H. 1958 *Aust. J. Phys.* **11,** 79.
Munro G. H. and Heisler L. H. 1956 *Aust. J Phys.* **9,** 343.

Journal of Atmospheric and Terrestrial Physics, 1961, Vol. 22, pp. 192 to 199. Pergamon Press Ltd. Printed in Northern Ireland

The geographical distribution of the harmonics of the annual variation in the critical frequency of the *F2*-layer at noon

G. H. Bazzard and C. M. Minnis
D.S.I.R. Radio Research Station, Ditton Park, Slough, Bucks.*

(*Received* 1 *July* 1961)

Abstract—At any location, the monthly median critical frequency of the *F2*-layer at noon can be represented by $f_{F2} = p(\theta) + q(\theta)\, I_{F2}$, in which $p(\theta)$ and $q(\theta)$ are oscillating functions which have a fundamental period of 1 year, and I_{F2} is an index of solar activity. The amplitudes of the first and second harmonics of $p(\theta)$ and $q(\theta)$ have been evaluated at sixty-one locations and contour maps of these and of the constant term have been drawn. The phase of the first harmonic does not reverse at the equator as might be expected on simple theory. The phase of the second harmonic is the same over the whole world except for a narrow range of latitudes. This is in accordance with simple theory, but the amplitude of the second harmonic is greater than expected. The contours of the constant term follow those of constant dip angle more closely than do those of f_{F2}.

1. Introduction

It is well known that the variations in the critical frequency (f_{F2}) of the *F2*-layer contain a cyclic component which has a period of 1 year. The amplitude of this component varies with geographical location and with solar activity, and at many stations it is evident that there is also a strong second harmonic. These cyclic variations are often inaccurately called seasonal components, but in this paper they are referred to, more correctly, as annual and semi-annual components. The further distinction between the seasonal and non-seasonal components of each harmonic will not be discussed.

Yonezawa (1959) has examined the amplitudes of the annual and semi-annual components in both the Northern and Southern Hemispheres. His results were obtained by grouping the data from small numbers of stations having roughly equal latitudes but widely different longitudes. Some information on the annual component alone has also been obtained by Mariani (1959), but his results and those of Yonezawa give only a very limited amount of information on the geographical distribution of the amplitudes of the different components.

Minnis and Bazzard (1960) have described the geographical distribution of f_{F2} at noon throught the year by using statistical relations of the form

$$f_{F2} = p(\theta) + q(\theta)\, I_{F2} \qquad (1)$$

in which $p(\theta)$, $q(\theta)$ are oscillating functions with a fundamental period of 1 year. The values of these functions at noon have been determined for each month of the year for sixty-one ionospheric observatories and the purpose of this paper is to show how the amplitudes of the harmonic components of $p(\theta)$ and $q(\theta)$, and hence of f_{F2}, vary with the location of the observatory. The results which have been obtained make it possible to present a more detailed picture of the annual and solar cycle variations in f_{F2} in all parts of the world than has hitherto been possible.

* Official communication.

VOL. 22 1961

2. Method of Analysis

A visual inspection of the experimentally determined values of $p(\theta)$ and $q(\theta)$ showed that both the first and second harmonic components could be expressed, with a sufficient degree of accuracy, by using cosine terms alone if it was assumed that $\theta = 0$ in mid-January. With this proviso, the two functions can be represented by

$$p(\theta) = \alpha_1 \cos\theta + \beta_1 \cos 2\theta + \gamma_1 \tag{2}$$

$$q(\theta) = \alpha_2 \cos\theta + \beta_2 \cos 2\theta + \gamma_2 \tag{3}$$

where α, β, γ are constants for a given location.

The minimum and maximum epochs of a typical solar cycle correspond

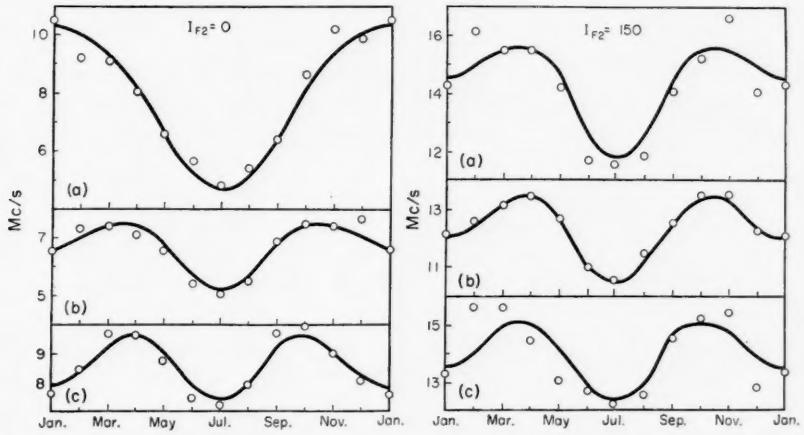

Fig. 1. The annual variation of f_{F2} at noon at (a) Rarotonga, (b) Johannesburg and (c) Panama C.Z. (○) Experimental values; (————) Fitted curves.

approximately to $I_{F2} = 0$ and 150 respectively in equation (1), and a combination of equations (1), (2) and (3) then gives:

$$f_{F2}\,(\min) = \alpha_1 \cos\theta + \beta_1 \cos 2\theta + \gamma_1 \tag{4}$$

$$f_{F2}\,(\max) = (\alpha_1 + 150\alpha_2)\cos\theta + (\beta_1 + 150\beta_2)\cos 2\theta + (\gamma_1 + 150\gamma_2) \tag{5}$$

$$= \alpha_3 \cos\theta + \beta_3 \cos 2\theta + \gamma_3 \tag{6}$$

The coefficients α, β, γ in equations (2) and (3) were derived for sixty-one observatories and are tabulated in Appendix 1. From these values, the coefficients in equation (6) were computed.

Fig. 1 shows the observed values of f_{F2} (min) and f_{F2} (max) for three typical observatories, together with the fitted curves represented by equations (4) and (6). Near the minimum epoch at Rarotonga and Panama, the first and second harmonics respectively are predominant; at Johannesburg, the two harmonics are approximately equal in amplitude.

Figs. 2 and 3 were constructed by plotting the coefficients in equations (4) and (6) for the sixty-one stations and interpolating smooth contours which are intended to

represent the way in which the amplitudes of the different coefficients vary over the world. These two figures illustrate conditions near the minimum and maximum of the solar circle respectively. The contours in Fig. 4 represent the coefficients in equation (3) and allow the amplitude of the components to be interpolated for any intermediate level of solar activity. In Figs. 2, 3 and 4, changes in the signs of α and β are denoted by thicker contour lines.

A peculiar anomaly was noticed in the results for Singapore where the coefficient for the annual component is negative, indicating a peak in July. All other stations, except those in high latitudes, have positive coefficients. It is worth noting, however, that the corresponding coefficients at Guam, Madras, Delhi, Puerto Rico and Panama are all small but positive. It seems probable that there is a narrow belt, to the north of the geographic equator, where the amplitude of the first harmonic is very much smaller than it is at locations on either side of this belt.

A second peculiarity in the Singapore data is that the phase of the annual component differs by about 45° from that of other stations. This can be represented by the introduction of both cosine and sine terms in equations (4) and (6). At Singapore the amplitude of the sine term is approximately equal to that of the cosine term.

3. Results

The phase of the first harmonic has been chosen so that a positive value of α indicates a maximum in f_{F2} in January and a minimum in July. Similarly, a negative value of β indicates maxima in April and October, and minima in January and July. Given the information contained in Figs. 2 and 3, it is possible to draw several conclusions concerning the observed annual and semi-annual variations of noon f_{F2} throughout the world at different epochs of solar activity.

VOL. 22 1961

3.1. At the minimum of the solar cycle, there is no reversal in the phase of the annual component at the equator. Such a reversal would be expected to occur if this component were caused by seasonal changes, that is by annual changes which are opposite in phase in the Northern and Southern Hemispheres. The phase in the observed annual component is such that, except for a small area near the northern polar cap, f_{F2} tends to be least in July in both the Northern and Southern Hemispheres as was first pointed out by Berkner *et al.* (1936).

The annual change in the distance between the sun and the earth is such that it might produce an annual change in f_{F2} with the same phase as that observed; the expected amplitude of this change is, however, only about one sixth of the mean observed amplitude for the stations included in this analysis.

3.2. At the maximum of the solar cycle, the first harmonic again has a minimum in July which occurs over most of the world except for an area in the Southern Hemisphere. The reversal in phase occurs much farther south than would be expected for a purely seasonal variation. This result explains an observation made by Rastogi (1960) who pointed out that the annual variations of f_{F2} at pairs of stations at similar locations north and south of the equator have the same phase near the minimum of the solar cycle, but are opposite in phase near the maximum. The Southern Hemisphere stations chosen by Rastogi for his analysis happen to be situated in the area which shows negative values of α_3 in Fig. 3.

A comparison of Figs. 2 and 3 shows that, over part of the Southern Hemisphere,

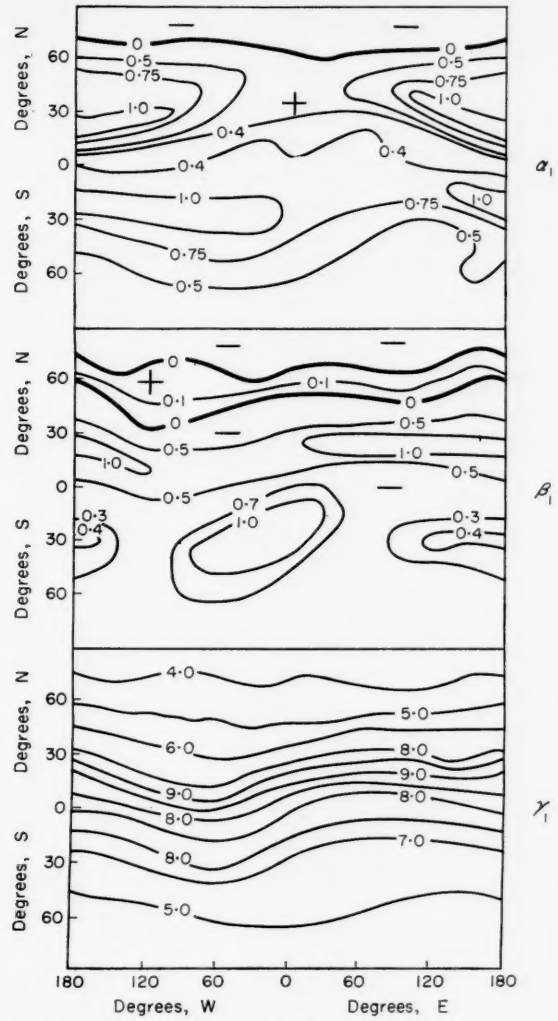

Fig. 2. Contour maps of the coefficients α_1, β_1, γ_1, defined in equation (2).

there is a reversal in the phase of the annual component somewhere between the minimum and the maximum of the solar cycle. It is clear from Fig. 4 that this is due to the reversal, which occurs near the equator, in the phase of the annual component (α_2) of the rate of change of f_{F2} with solar activity, $q(\theta)$.

3.3. Except in a small range of high northern latitudes, the phase of the semi-annual component is the same over the whole world throughout the solar cycle. It follows that f_{F2} tends everywhere to pass through secondary maxima in April and October, and minima in January and July.

If the rate of production of electrons in the *F2*-layer is proportional to cos χ, the phase of the second harmonic in cos χ would be such as to lead to peaks near the

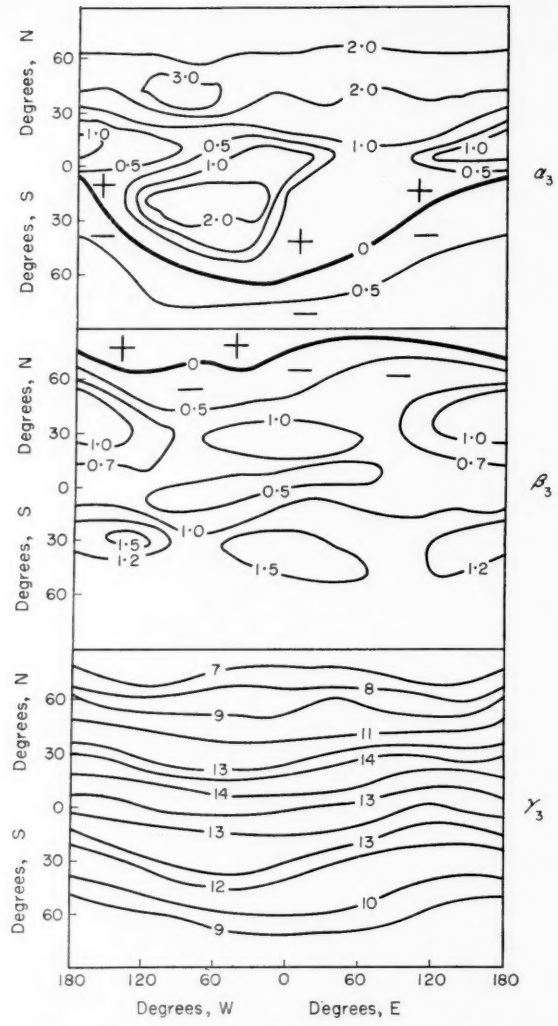

Fig. 3. Contour maps of the coefficients α_3, β_3, γ_3, defined in equation (6).

equinoxes. In this respect the observed characteristics of the second harmonic agree with expectations, but on the other hand the amplitude, relative to that of the first harmonic, is much greater than would be expected on this simple assumption. Figs. 2 and 3 show that there is a tendency, which has also been noted by Yonezawa (1959), for the amplitude of the semi-annual component to be somewhat larger in the Southern than in the Northern Hemisphere throughout the solar cycle.

3.4. In all cases, the contours of the constant term, γ, show a much closer similarity to the lines of constant magnetic dip angle than do the contours of f_{F2}. This observation suggests that the geographical distribution of f_{F2} may be thought

VOL. 22 1961

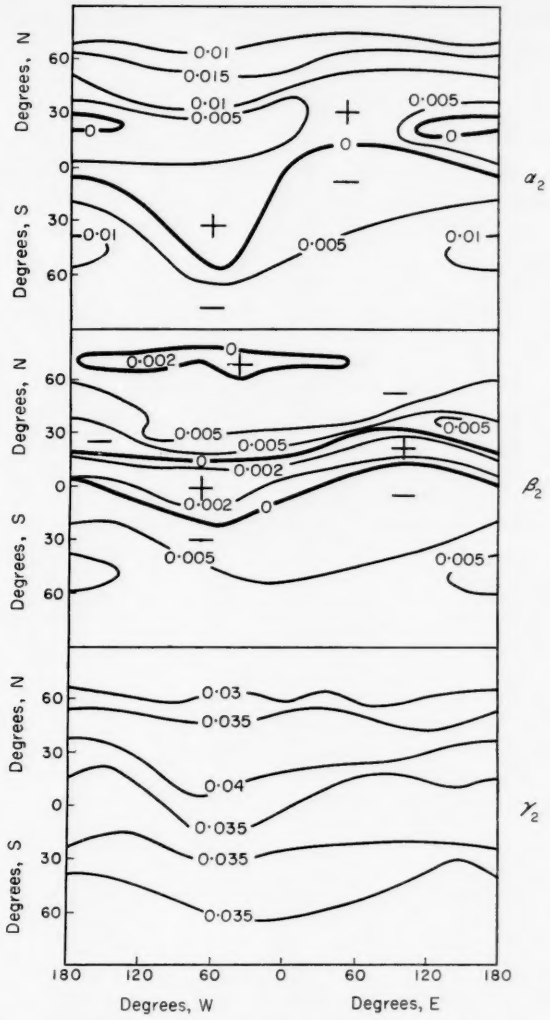

Fig. 4. Contour maps of the coefficients α_2, β_2, γ_2, defined in equation (3).

of as a constant background, which is represented by γ_1 or γ_3 and is closely controlled by dip-angle, upon which are superimposed annual and semi-annual variations the amplitudes of which are not so closely controlled by geomagnetic influences.

4. Conclusions

The first and second harmonics of the annual variation of f_{F2} at noon have been calculated at sixty-one locations and contour maps of their amplitudes have been drawn. Contrary to simple theoretical expectations, the first harmonic has the same phase in both the Northern and Southern Hemispheres except near the poles.

The phase of the second harmonic is as expected but the amplitude, relative to that of the first harmonic, is much greater.

Acknowledgments—The authors acknowledge the assistance of Mrs. M. D. Vickers who made many of the calculations.

The work described was carried out as part of the programme of the Radio Research Board. The paper is published by permission of the Director of Radio Research of the Department of Scientific and Industrial Research.

References

Berkner L. V., Wells H. W. and Seaton S. L. 1936 *Terr. Magn. Atmos. Elect.* **41,** 173.
Mariani F. 1959 *Nuovo Cim.* **12,** 218.
Minnis C. M. and Bazzard G. H. 1960 *J. Atmosph. Terr. Phys.* **18,** 181.
Rastogi R. G. 1960 *J. Geophys. Res.* **65,** 857.
Yonezewa T. 1959 *J. Radio Res. Lab., Tokyo* **6,** 651.

Appendix 1

Coefficients in Equations (2) and (3)

Station	α_1	β_1	γ_1	$\alpha_2 \times 100$	$\beta_2 \times 100$	$\gamma_2 \times 100$
Adak	0·75	−0·10	5·20	1·2	−0·7	3·6
Akita	0·60	−0·75	6·20	0·6	−0·2	3·6
Anchorage	0·40	0·08	4·40	1·5	0·2	3·0
Baguio	0·40	−0·85	8·65	0·8	0·4	3·2
Baker Lake	0·20	0·05	4·35	0·8	−0·2	2·7
Bombay	0·75	−1·28	10·00	0·7	0·9	3·0
Brisbane	0·75	−0·40	6·35	−0·1	−0·4	3·7
Buenos Aires	1·30	−1·33	8·05	0·6	0·1	3·3
Campbell Is.	0·50	−0·05	4·90	−1·1	−0·4	3·1
Canberra	0·55	−0·35	5·70	−0·6	−0·7	3·4
Capetown	0·75	−1·00	6·50	−0·3	−0·2	3·7
Casablanca	0·45	−0·35	6·00	0·2	−0·5	3·9
Churchill	0·30	0·05	4·65	1·6	0·1	3·2
Dakar	0·50	−0·95	10·05	0·4	0	4·2
De Bilt	0·30	−0·25	5·10	1·2	−0·5	3·7
Delhi	0·20	−1·08	8·05	0·6	0·2	3·9
Fairbanks	0·20	−0·03	4·23	1·4	0·3	2·8
Freiburg	0·50	−0·15	5·40	1·0	−0·5	3·6
Godley Head	0·60	−0·35	5·50	−0·8	−0·3	3·3
Graz	0·30	−0·23	5·50	0·7	−0·1	3·4
Guam	0·30	−0·96	8·75	0·5	0·2	3·5
Hobart	0·45	−0·30	5·45	−0·9	−0·4	2·6
Huancayo	0·55	−0·65	7·00	0·9	0·2	3·5
Ibadan	0·40	−0·68	7·20	0	0·2	3·7
Inverness	0·45	0	4·85	1·0	0·1	3·1
Johannesburg	0·80	−0·70	6·75	−0·1	−0·2	3·6
Leopoldville	0·70	−1·00	9·05	−0·1	0·1	3·4
Lindau	0·55	0	5·10	1·0	−0·4	4·0
Lulea	−0·05	0·13	4·60	1·2	−0·5	2·6
Madras	0·35	−0·45	7·70	0·7	−0·3	3·4

VOL. 22 1961

Appendix (*continued*)

Station	α_1	β_1	γ_1	$\alpha_2 \times 100$	$\beta_2 \times 100$	$\gamma_2 \times 100$
Macquarie Is.	0·70	−0·13	4·75	−1·5	−0·2	2·7
Maui	1·80	−1·08	9·30	−0·2	−0·2	3·3
Narsarssuak	0·30	−0·05	4·40	1·7	0·2	3·3
Okinawa	1·85	−1·38	8·15	−0·9	−0·6	4·2
Oslo	0·35	0·13	4·75	1·4	−0·1	3·0
Ottawa	0·55	0·05	5·15	1·9	−0·4	3·5
Panama C.Z.	0·15	−0·98	8·60	0·3	−0·2	3·5
Point Barrow	−0·30	−0·08	3·80	0·8	0	2·2
Poitiers	0·40	−0·10	5·35	0·8	−0·5	3·6
Port Lockroy	0·55	−0·70	4·90	−0·6	−0·9	2·8
Port Stanley	0·75	−0·98	5·95	0·2	−0·5	3·8
Puerto Rico	0·05	−0·85	7·25	0·1	−0·1	3·7
Rarotonga	2·80	−0·30	7·80	−1·0	−0·6	4·2
Resolute Bay	−0·35	−0·03	3·80	0·6	0·1	2·0
Reykjavik	0·40	+0·15	4·15	1·0	−0·3	3·0
San Francisco	0·70	0·05	5·90	1·3	−0·7	3·8
Schwarzenburg	0·60	−0·13	5·25	1·0	−0·3	3·8
Singapore	−0·40*	−0·60	8·60	0·1	0·2	2·5
Slough	0·45	0	5·00	1·3	−0·4	3·8
Taipei	2·10	−1·40	9·10	−0·9	0·5	4·2
Tiruchirapalli	0·50	−0·53	7·20	−0·3	0	3·4
Tokyo	0·65	−0·70	6·50	0·5	−0·7	4·0
Townsville	1·35	−0·25	7·15	−0·5	−0·4	3·4
Tromsø	−0·20	−0·13	4·30	1·2	−0·4	2·8
Uppsala	0·35	0·05	4·80	1·5	−0·3	3·5
Wakkanai	0·85	−0·23	5·60	0·9	−0·8	3·5
Washington	0·70	−0·15	5·55	1·8	−0·4	3·5
Watheroo	0·45	−0·45	5·95	−0·4	−0·5	3·7
White Sands	1·15	−0·23	6·15	0·4	−0·3	3·8
Winnipeg	0·55	0·18	4·90	1·7	−0·3	3·2
Yamagawa	1·15	−0·95	6·85	0·8	−0·1	4·1

* $+0{\cdot}35 \sin \theta$.

Journal of Atmospheric and Terrestrial Physics, 1961, Vol. 22, pp. 200 to 217. Pergamon Press Ltd. Printed in Northern Ireland

The effect of collisions on the propagation of radio waves in the ionosphere

J. E. TITHERIDGE*
Cavendish Laboratory, Cambridge

(*Received* 15 *July* 1961)

Abstract—Curves are given showing the effect of the electron collision frequency ν on the group refractive index, for both the ordinary and extraordinary rays, under a wide variety of conditions. It is shown that collisions do not significantly affect the virtual height of radio waves reflected in the E- and F-layers of the ionosphere. It is also shown that the absorption of a radio wave reflected in the ionosphere can be obtained by integrating an absorption coefficient k_0, equal to ν times the value of k/ν at $\nu = 0$, up to the classical height of reflection. This simple procedure yields the same result as a full-wave calculation of the absorption.

1. INTRODUCTION

MOST of the methods which have been proposed for determining the electron density as a function of height in the ionosphere assume that the effect of the collisions made by the electrons can be ignored. This assumption is made primarily because of the difficulty of including the effect of collisions in the calculations. The purpose of the present paper is to investigate this assumption, and to present some graphs showing the effect of collisions on the group refractive index and on the absorption of a radio wave.

The effect of collisions on the phase refractive index μ has been considered by TAYLOR (1933). Calculations showed that electron collisions increase the value of μ, but that this increase is very small except near reflection. Largely on the basis of these results, it is usually assumed (e.g. SCHMERLING, 1957) that the effect of collisions is negligible in the F-region, where the collision frequency is much less than the wave frequency, but may be important in the E-region.

Curves showing how the group refractive index μ' varies with the electron density, the wave frequency and the strength and direction of the magnetic field, for the particular case of no collisions, have been given by SHINN and WHALE (1952) and BECKER (1957).

Some calculations of the group refractive index μ' at a frequency of 6 Mc/s, including the effect of collisions, were made by DE VOOGT (1948). The values of $1/\mu'$ were found to fluctuate wildly, through positive and negative values, near the reflection point. The curves given by DE VOOGT were, however, drawn on the assumption that $1/\mu'$ is a finite, continuous function of the electron density N. In fact, when the collision frequency ν is not zero, μ' can become zero but is never infinite for real values of N.

GIBBONS and RAO (1957) used approximate methods to calculate μ' at frequencies of 75, 150 and 500 kc/s. The results showed that the effect of collisions is greatest at large values of N; when ν and N are both large the value of μ' actually decreases as N increases.

* Now at the Seagrove Radio Research Station, University of Auckland, New Zealand.

VOL. 22 1961

While the above calculations indicate the effect of collisions under some particular conditions, they do not show whether this effect must be allowed for in the analysis of ionospheric records. The electronic computer EDSAC 2 was therefore used to carry out some accurate calculations of the effect of collisions on the group refractive index. μ' was calculated as a function of X (where $X = Ne^2/\pi mf^2$) for values of X up to $1 + Y$ for both the ordinary and extraordinary rays. These calculations were carried out for at least six different values of the collision frequency, and six different values of the wave frequency, at dip angles of 0°, 49°, 67°, 79° and 89°. This produced a total of about 400 curves showing the variation of μ' with X under different conditions. Only a few of these curves can be shown in the present paper; the general conclusions given in this paper are however based on an examination of all the curves. Tables giving the calculated values of μ' under different conditions can be obtained from the author.

2. The Relations Used

For a vertically propagated wave the Appleton–Hartree relation for the phase refractive index μ can be written

$$M = \mu - j\frac{ck}{2\pi f} = \left(1 - \frac{X}{A - jB}\right)^{\frac{1}{2}} \tag{1}$$

where M is the complex refractive index, k is the absorption coefficient,

$$X = Ne^2/\pi mf^2, \quad Y = f_H/f, \quad Z = \nu/2\pi f, \quad A - jB = 1 - jZ - (a + jb)$$
$$\pm [(a + jb)^2 + Y^2 \sin^2 I]^{\frac{1}{2}} \text{ and } a + jb = \tfrac{1}{2} Y^2 \cos^2 I/(1 - X - jZ).$$

ν is the electron collision frequency, f_H is the electron gyrofrequency and I is the magnetic dip angle. For $X < 1$ the upper and lower alternative signs refer to the ordinary and extraordinary waves respectively.

The calculation of μ from this relation was divided into the following steps:

$$u + jv = (a + jb)^2 + Y^2 \sin^2 I \qquad 2w^2 = u + (u^2 + v^2)^{\frac{1}{2}}$$
$$A = 1 - a \pm w \qquad E = \tfrac{1}{2} - AX/2(A^2 + B^2)$$
$$B = Z + b \mp v/2w \qquad F = BX/2(A^2 + B^2)$$

and $$\mu^2 = (E^2 + F^2)^{\frac{1}{2}} + E$$

Writing D for the operator $\frac{1}{2}f\partial/\partial f$ we have

$$\mu\mu' = \mu^2 + D(\mu^2)$$
$$= (E^2 + F^2)^{\frac{1}{2}} + E + D(E) + [ED(E) + FD(F)]\,(E^2 + F^2)^{-\frac{1}{2}} \tag{2}$$

where $D(u) = (4a/Y^2 \cos^2 I)\,[3b^2X - a^2 - b^2Z^2/(1 - X)] + 3b^2 - Y \sin^2 I$

$$D(v) = (4b/Y^2 \cos^2 I)\,[b^2X - 2a^2X - a^2 + a^2 Z^2/(1 - X)] - 3ab$$
$$D(A) = (u^2 + v^2)^{-\frac{1}{2}}[w^2 D(u) + ab\,D(v)]/2w$$
$$D(B) = (u^2 + v^2)^{-\frac{1}{2}}[ab\,D(u) - w^2 D(v)]/2w$$
$$- \tfrac{1}{2}Z - \tfrac{3}{2}b + 2ab[Z^2/(1 - X) - 2X]/Y^2 \cos^2 I$$
$$D(E) = (\tfrac{1}{2} - E)\{1 - D(A)/A + 2[A\,D(A) + B\,D(B)]/(A^2 + B^2)\}$$

and $$D(F) = -F\{1 - D(B)/B + 2[A\,D(A) + B\,D(B)]/(A^2 + B^2)\}$$

To avoid small difference errors, w should be calculated from $v^2/2w^2 = (u^2 + v^2)^{\frac{1}{2}} - u$ when u is negative. Calculations with ten significant figures then give errors in μ' of less than 0·004 per cent for X less than 0·999. When ν is not small the error is everywhere much less than this.

The ordinary ray is normally defined as that for which the value of μ decreases to zero as X increases to unity at $\nu = 0$. At larger values of X the nomenclature can be confusing. In the present work a value of μ' will be labelled ordinary or extraordinary according as it tends continuously to the normal ordinary or extraordinary value as X decreases, the collision frequency remaining constant. For an

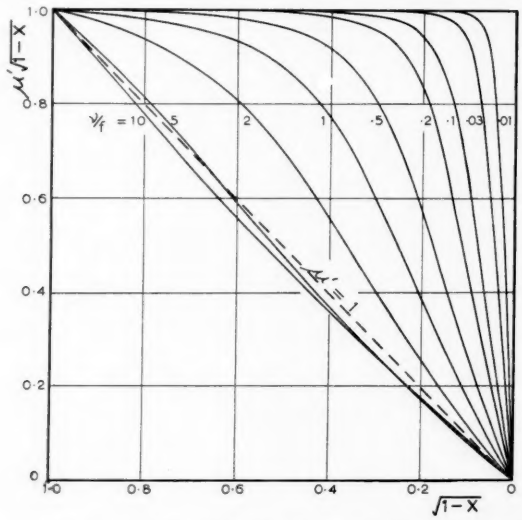

Fig. 1. The group refractive index for the ordinary ray at $I = 0°$.

ionosphere with a constant collision frequency, a given ray then has the same name throughout its path. For the ordinary ray at $X < 1$, this requires that the real and imaginary parts of the square root in the expression for $A - jB$ be given positive and negative signs respectively. For the ordinary ray at $X > 1$, the real and imaginary parts must be both negative or both positive according as ν is less than or greater than the critical value $\nu_c = \frac{1}{2} f_H \cos I \cot I$. The signs for the extraordinary ray are, in all cases, the opposite of those for the ordinary ray with the same values of X and ν.

3. The Group Refractive Index for the Ordinary Ray

Fig. 1 shows the effect of collisions on the group refractive index for vertical propagation at the magnetic equator. $\mu'\sqrt{(1 - X)}$ is plotted against $\sqrt{(1 - X)}$ so that the plotted function is always finite, and the important region near $X = 1$ is shown on an expanded scale. When collisions are neglected $\mu'\sqrt{(1 - X)} = 1$. When the collision frequency ν is small it affects the value of μ' only near reflection, where μ' is prevented from becoming infinite.

For values of ν greater than about $4f$, μ' becomes less than 1. This does not

VOL. 22 1961

require that a pulse travels faster than the free space velocity, since in such a highly absorbing region the group velocity defined by c/μ' is no longer the same as the signal velocity (BRILLOUIN, 1932). The values of μ' may also be unreliable at large collision frequencies because of errors in the Appleton–Hartree relation (HUXLEY, 1937; JANCEL and KAHAN, 1954; SEN and WYLLER, 1960).

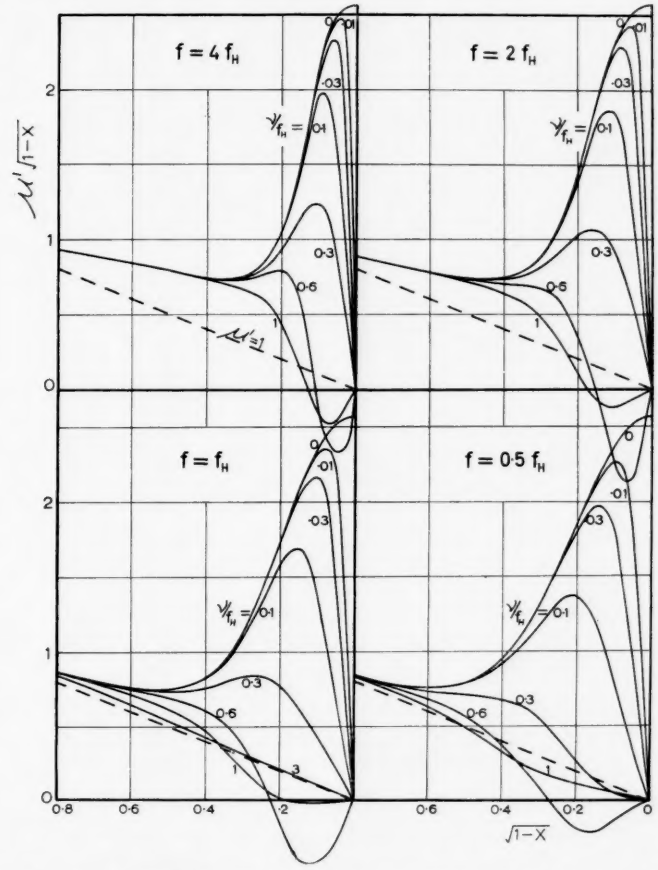

Fig. 2. The group refractive index for the ordinary ray at $I = 67°$ ($\nu_e = 0{\cdot}52\, f_H$).

Figs. 2 and 3 give the values of $\mu'\sqrt{(1-X)}$ for dip angles of 67° and 89° respectively. For a given value of ν/f the collisions have the same general effect as at $I = 0°$. The reduction in the value of $\int_0^1 \mu' dX = 2\int_0^1 \mu'\sqrt{(1-X)}\, d\sqrt{(1-X)}$ is however slightly greater due to the greater relative importance of that part of the curves near $X = 1$, where the effect of collisions is largest.

The effect of the collisions is mainly to counteract the increase in $\mu'\sqrt{(1-X)}$ which occurs near $X = 1$. At large dip angles this increase is confined to values of X very near 1. Consequently at $I = 89°$ (Fig. 3) the effect of collisions, even for

collision frequencies as large as 10^6, is quite unimportant for values of X less than about 0·98 ($\sqrt{(1-X)} > 0{\cdot}15$). By contrast, at $I = 49°$ a collision frequency of 10^6 considerably reduces the value of μ' when $X = 0{\cdot}7$.

Some of the curves in Figs. 2 and 3 show a sudden drop near $X = 1$, with μ' becoming small or negative. This occurs whenever ν is near the critical value given

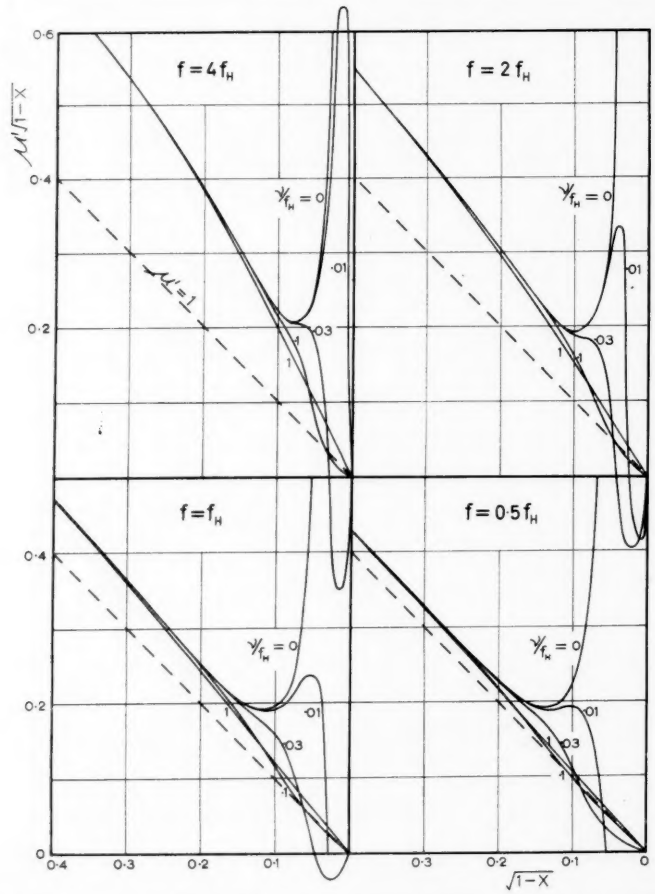

Fig. 3. The group refractive index for the ordinary ray at $I = 89°$ ($\nu_c = 0{\cdot}001\, f_H$).

by $\nu_c = \frac{1}{2} f_H \cos I \cot I$. On ray theory, coupling between the ordinary and extraordinary waves occurs only at $\nu = \nu_c$ and $X = 1$, but wave theory calculations show that it is important over an appreciable range (DAVIDS and PARKINSON, 1955). The Appleton–Hartree relation is incorrect whenever there is appreciable coupling. The present calculations show anomalous values of μ' whenever, approximately, $\frac{1}{2}\nu_c < \nu < 2\nu_c$ and $0{\cdot}9 < X < 1{\cdot}0$. This may indicate the range of conditions under which coupling is important. Under the same conditions the values of μ' for the extraordinary wave increase by an amount approximately equal to the decrease in the ordinary ray values (Figs. 7 and 8).

VOL. 22 1961

The values of μ' for $f = 2f_H$ at $I = 67°$ are shown in Fig. 4 for values of X up to $1 + Y$. When ν is less than the critical value of $0{\cdot}52f_H$, μ' becomes very large at $X = 1$ and the ray is reflected there. For larger values of ν the wave is reflected at $X = 1 + Y = 1{\cdot}5$, and μ' has a second maximum just below this value. The irregular variations near $X = 1$ for $\nu/f_H = 0{\cdot}5$ and $0{\cdot}6$ are due to the coupling effects when $\nu \doteqdot \nu_c$.

The broken lines in Fig. 4 show the values of μ' obtained if ν decreases and becomes less than ν_c once the level at which $X = 1$ has been passed. These broken

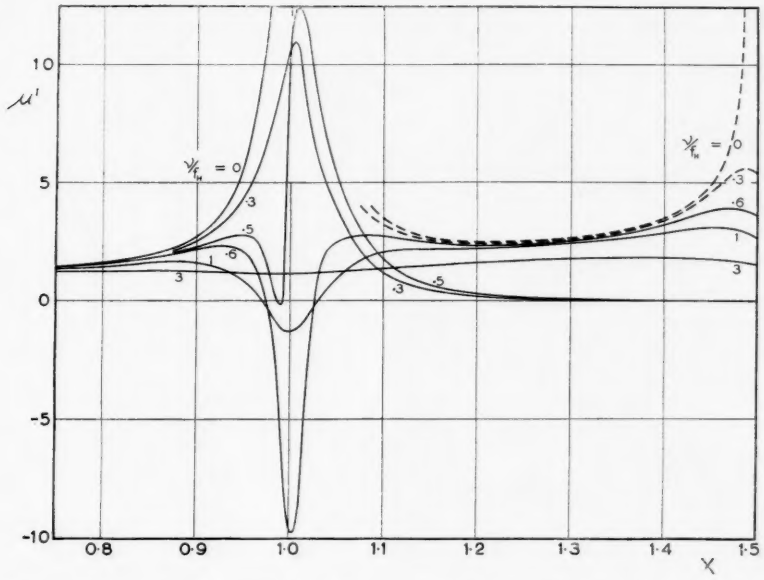

Fig. 4. The group refractive index for the ordinary ray at $f = 2\ f_H$ and $I = 67°$ ($\nu_c = 0{\cdot}52\ f_H$).

curves are continuous with the extraordinary wave curves, with the same value of ν, for $X < 1 - Y$. So when the value of ν falls below ν_c (at $X > 1$) the name of the wave must be changed from ordinary to extraordinary. There are, however, no sudden changes in the value of μ' or in the absorption coefficient (Fig. 11), so the wave will not be reflected at this point.

The values of μ' at $f = \frac{1}{2}f_H$ are shown in Fig. 5. The curves have the same general shape as at $f = 2f_H$ (Fig. 4) except that the values of μ' for $\nu < \nu_c$ decrease more rapidly at $X > 1$, and become large and negative. For $\nu > \nu_c$ the curves are much smoother than at $f = 2f_H$; the vertical scale in Fig. 5 is four times as large as in Fig. 4.

4. The Group Refractive Index for the Extraordinary Ray

For small collision frequencies, the extraordinary ray is reflected at $X = 1 - Y$ or $X = 1 + Y$ according as Y is less than or greater than one. If we define a function X' such that $X' = X/(1 - Y)$ when $Y < 1$, and $X' = X/(1 + Y)$ when

$Y > 1$, the extraordinary ray is always reflected at $X' = 1$. Graphs of $\mu'\sqrt{(1 - X')}$ for four different frequencies at the magnetic equator are shown in Fig. 6. The effect of collisions is of about the same order as for the ordinary wave, and (for $f > f_H$) μ' again becomes less than 1 when ν is greater than about $4f$.

Fig. 7 shows the corresponding curves at $I = 67°$. For $f > f_H$ the curves at given values of f and of ν are almost independent of the magnetic dip angle, at medium and high latitudes. Thus at $I = 89°$ the curves for $f > f_H$ are almost exactly the same as in Fig. 7. for all values of ν, except that the values of μ' near $X' = 1$ are about 4 per cent smaller than at $I = 67°$.

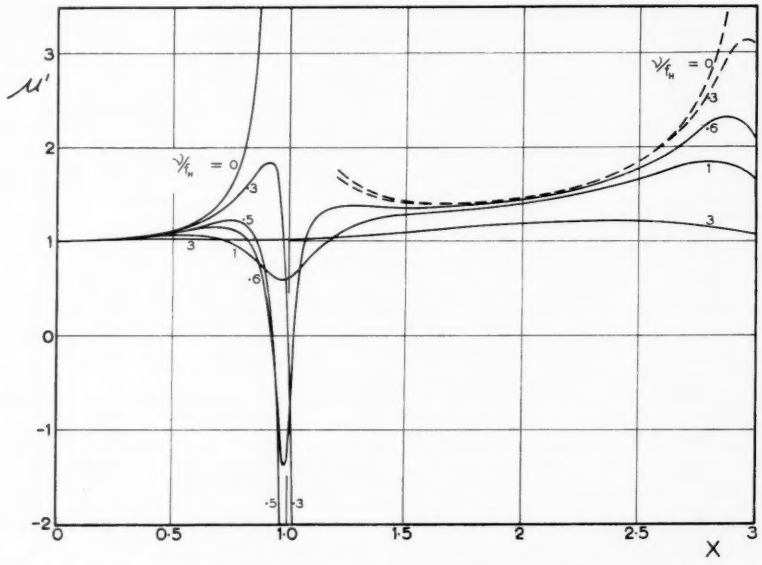

Fig. 5. The group refractive index for the ordinary ray at $f = \frac{1}{2}f_H$ and $I = 67°$ ($\nu_c = 0{\cdot}52\,f_H$).

For $f < f_H$ the value of μ' varies considerably with the dip angle. At medium latitudes μ' has a maximum near $X = 1$, corresponding to $\sqrt{(1 - X')} = 0{\cdot}82$ at $f = \frac{1}{2}f_H$ (Fig. 7). For collision frequencies greater than the critical value the extraordinary wave is reflected at $X = 1$, and the value of μ' drops rapidly at this point. At $I = 89°$ the critical collision frequency is only $0{\cdot}0001f_H$, so the extraordinary wave is normally reflected at $X = 1$. The curve for $\nu = 0$ (at $I = 89°$) has an extremely large peak at $X = 1$, but for collision frequencies greater than the critical value μ' is small or negative near this point.

The behaviour of the extraordinary wave at medium latitudes for $f < f_H$, is shown in Fig. 8, where μ' is plotted against $X' = X/(1 + Y)$. Collision frequencies less than ν_c cause the value of μ' near $X = 1$ to be greater than at $\nu = 0$. When f is small this increase almost balances the decrease in μ' near reflection, so that the value of $\int_0^1 \mu'\,dX'$ is not greatly affected by collisions. When $f > 0{\cdot}8\,f_H$, however, μ' becomes very large near $X = 0$ and these large values are considerably reduced by collisions.

VOL. 22 1961

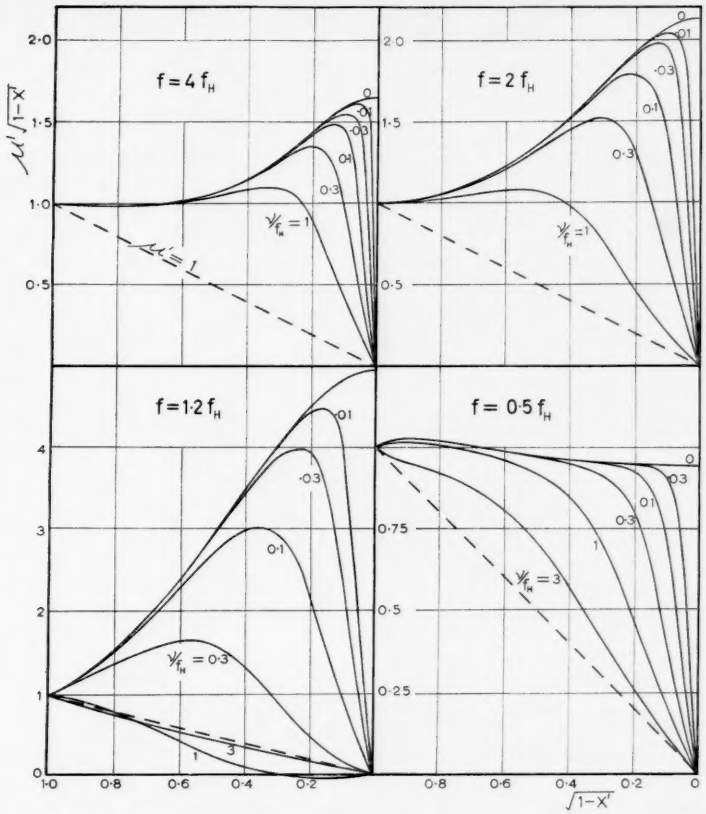

Fig. 6. The group refractive index for the extraordinary ray at $I = 0°$

5. The Virtual Height of Reflection of the Ordinary Ray

On simple ray theory the virtual height of a wave reflected in the ionosphere is obtained by integrating μ' up to the height at which the phase refractive index μ becomes zero. In the presence of collision, however, μ never becomes zero and some other method must be used to calculate the retardation of a reflected wave.

Gibbons and Rao (1957) used some fairly exact wave solutions by Davids and Schragg (1951) to calculate the virtual heights at 150 kc/s, and compared these with the height calculated by integrating μ' up to various levels. They found that good agreement could be obtained by integrating μ' up to the classical reflection level, at which μ becomes zero in the absence of collisions. They also found that μ' drops sharply above this level, so that any uncertainty in the limit of integration produces a negligible effect.

On the basis of these results the virtual heights for the ordinary wave at $\nu < \nu_c$ were calculated by integrating μ' up to the height at which $X = 1$. The effect of collisions was found to be quite large in the E-region of the ionosphere, altering the calculated size of the E-layer by about 20 per cent. For the F-region the errors were about 5 per cent.

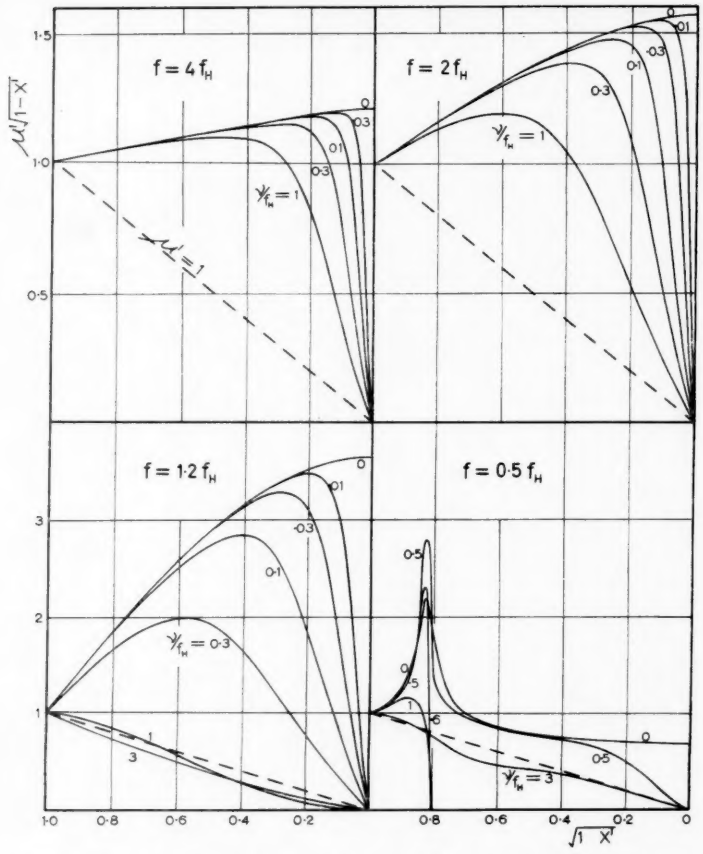

Fig. 7. The group refractive index for the extraordinary ray at $I = 67°$ ($\nu_c = 0{\cdot}52 f_H$).

However it has been shown by BUDDEN (1961) that the phase path P in the presence of collisions is equal to the real part of the contour integral of the complex refractive index M from $X = 0$ to the point in the complex plane at which M becomes zero. This is at $X = 1 - jZ$, where $Z = \nu/2\pi f$. Since the virtual height h' is equal to $P + f\,\partial P/\partial f$, h' can be found by integrating $M' = M + f\,\partial M/\partial f$ up to $X = 1 - jZ$. We therefore have:

$$h' = \mathscr{R}\int_0^{1-jZ} M' \frac{dh}{dX}\,dX = \int_0^1 \mu' \frac{dh}{dX}\,dX + \mathscr{R}\int_1^{1-jZ} M' \frac{dh}{dX}\,dX \qquad (3)$$

where $\mathscr{R}$ denotes the real part of the following function, and $\mu' = \mathscr{R}M'$. The virtual heights obtained by integrating μ' up to $X = 1$ are, therefore, only correct if the last integral in equation (3) is small.

For the simple case of propagation at the magnetic equator it can be shown that this integral is in fact quite large and, for a linear layer, is just equal to the amount by which the integral from $X = 0$ to $X = 1$ is reduced by the collisions. At $I = 0°$

VOL. 22 1961

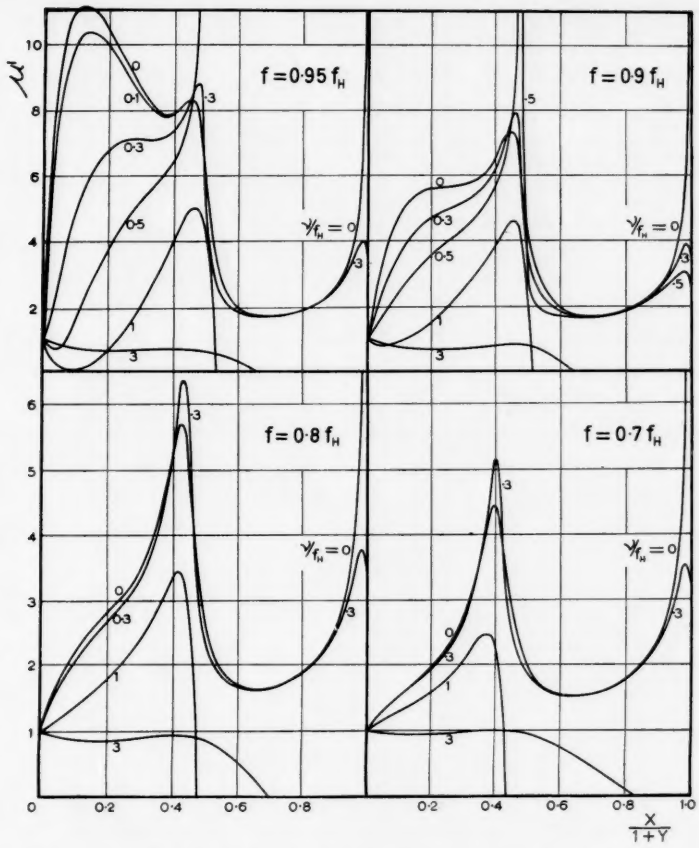

Fig. 8. The group refractive index for the extraordinary ray at $I = 67°$ ($\nu_e = 0{\cdot}52\, f_H$).

we have $M^2 = 1 - X/(1 - jZ)$. The phase path for the linear layer $h = X$ is then

$$P = \mathscr{R}\int_0^{1-jZ} M\, dX = \mathscr{R}\int_0^1 \sqrt{(1-s)}\,.\,(1-jZ)\, ds = \int_0^1 \sqrt{(1-s)}\,.\,ds$$

where $s = X/(1 - jZ)$. P is therefore the same at all frequencies as the value $P_0 = \int_0^1 \sqrt{(1-X)}\, dX$ in the absence of collisions. So the virtual height $h' = P + f\,\partial P/\partial f$ must also be the same as in the absence of collisions.

For a layer in which dh/dX increases with height a similar calculation shows that the virtual height is slightly reduced by collisions, and the reduction is approximately proportional to $(\nu/f)^2$. This reduction will only be important near the peak of a layer, where dh/dX is changing rapidly with height. Otherwise that part of the layer near reflection, where the effect of collisions is important, can be approximated to by a linear increase for which the virtual height is unaffected by collisions. This conclusion agrees with the results given by RYDBECK (1944) who

used wave theory calculations to determine the virtual heights for a parabolic layer in the absence of a magnetic field.

In the general case, including the effect of the magnetic field, the virtual height for the linear layer $h = X$ is given by

$$h' = \mathscr{R}\int_0^{1-jZ} M'\,dX = \int_0^1 \mu'\,dX + \mathscr{R}\int_1^{1-jZ} M'\,dX.$$

Writing $X = 1 - jpZ$ the second integral becomes

$$\mathscr{R}\left[-jZ\int_0^1 M'\,dp\right] = Z\int_0^1 \mathscr{I}(M')\,.\,dp$$

where $\mathscr{I}(M')$ is the imaginary part of the complex group refractive index M'. This integral must be added to the normal integral of μ' from $X = 0$ to $X = 1$ to give the correct virtual height.

The values of M' for $X = 1 - jpZ$, for values of p from 0 to 1, were calculated from the relations

$$M^2 = \tfrac{1}{2}(R - pZ)[\sqrt{(1 + R^2)} \pm R]/(1 + R^2)$$

and

$$\frac{M'}{M} = 1 \pm \frac{T}{\sqrt{(1 + R^2)}} + \frac{T - R}{R - pZ} + \frac{p(RS - pSZ - Y^2\sin^2 I)}{SZ(1 - p)(R - pZ)} + 2\,\frac{RS - SZ - Y^2\sin^2 I + RSTpZ - RSTZ}{SZ(1 - p)(1 + R^2)} \qquad (4)$$

where $R = Z + Y^2\cos^2 I/2Z(1 - p) - S$

$$S = [Y^4\cos^4 I/4Z^2(1 - p)^2 - Y^2\sin^2 I]^{\frac{1}{2}}$$

$$T = [p(Y^2\sin^2 I + SZ) - RS]/2(1 - p)$$

The plus and minus signs, in the expressions for M and M', give the real and imaginary parts respectively.

The imaginary part of M' at $f = f_H$ and $I = 67°$ is given as a function of p in Fig. 9(a). M' is quite large and tends to infinity at the "reflection point" $p = 1$. M' varies approximately as $(1 - p^2)^{-\frac{1}{2}}$ near this point, so that graphs of $M'\sqrt{(1 - p^2)}$ against $\sqrt{(1 - p^2)}$ remain finite (Fig. 9b). The broken lines show the corresponding curves at the equator, where the real and imaginary parts of M' near $X = 1$ are only about one third as large as at $I = 67°$.

The integral of M' from $X = 1$ to $X = 1 - jZ$ was evaluated numerically from the curves of Fig. 9(a) for values of p less than 0·6. For larger values the curves of Fig.9(b) were used to obtain

$$\int_{0\cdot6}^{1\cdot0} M'\,dp = \int_0^{0\cdot8} M'\,\frac{\sqrt{(1 - p^2)}}{p}\,d\sqrt{(1 - p^2)}.$$

The results for $f = f_H$ and $f = 2f_H$ are given in Table 1. The values in this table are accurate to one or two units of the last decimal place.

It is seen that the virtual heights calculated simply by integrating μ' up to $X = 1$ vary considerably with the collision frequency. When, however, these heights are corrected by adding the integral from $X = 1$ to $X = 1 - jZ$, the result is almost independent of the collision frequency. The conclusions obtained at

VOL. 22 1961

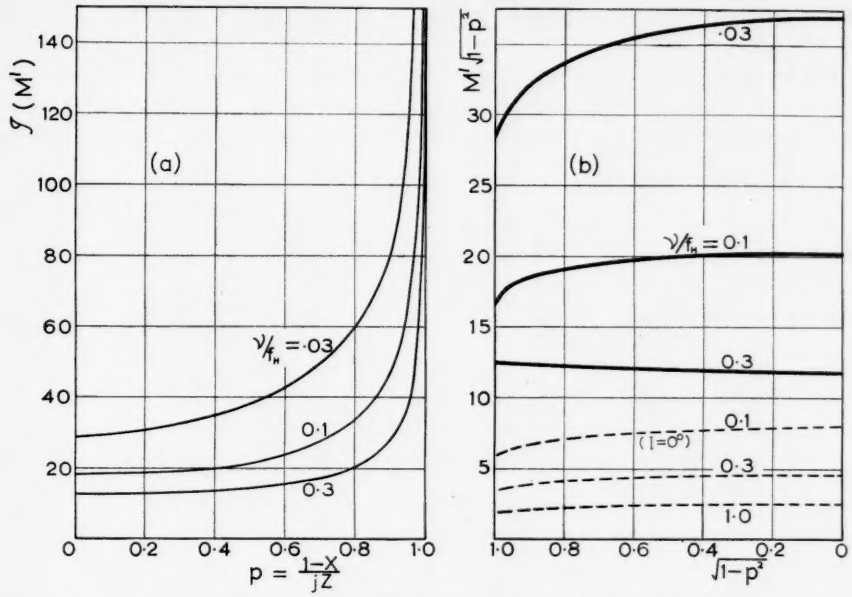

Fig. 9. The imaginary part of the complex group refractive index M', for the ordinary ray, from $X = 1$ to $X = 1 - jZ$. $f = f_H$, $I = 67°$.

Table 1. Virtual heights for the linear layer $h = X$ at $I = 67°$

	$f = f_H$				$f = 2f_H$			
ν/f_H	0	0·03	0·1	0·3	0	0·03	0·1	0·3
$\int_0^1 \mu' \, dX$	2·3908	2·1370	1·9121	1·4834	2·2852	2·1056	1·9524	1·6631
$\mathscr{R}\int_r^{1-jZ} M' \, dX$	0	0·2541	0·480	0·911	0	0·1790	0·333	0·622
$h' = \mathscr{R}\int_0^{1-jZ} M' \, dX$	2·3908	2·3911	2·392	2·394	2·2852	2·285	2·285	2·285

$I = 0°$ are therefore true quite generally, and the effect of collisions on the virtual heights will be appreciable only very near the peak of a layer.

6. The Absorption of the Reflected Wave

The absorption of a radio wave reflected from the ionosphere is usually calculated by using various approximate expressions for the absorption coefficient k. With the aid of an electronic computer, however, the exact values of k can be calculated from equation (1).

The values of kt/ν for the ordinary wave at $f = f_H$, $I = 0°$ and $I = 67°$ are given in Fig. 10 as a function of $t = \sqrt{(1 - X)}$. It is seen that as ν increases the value of kt/ν is reduced near $X = 1$ ($t = 0$) while as I increases the value of kt/ν near $X = 1$ is considerably increased. These changes are very similar to the corresponding

changes in the group refractive index μ', and at $X = 1$ and $\nu = 0$ it can be shown that $3kt/\nu = 5\mu' t = 5 \sec I$.

Fig. 11 shows the value of k up to $X = 1 + Y$ at $f = f_H$ and $I = 67°$. For ν less than the critical value of $0{\cdot}52 f_H$, k increases to a large maximum value near $X = 1$, where the wave is reflected. As ν increases above this value the size of the maximum

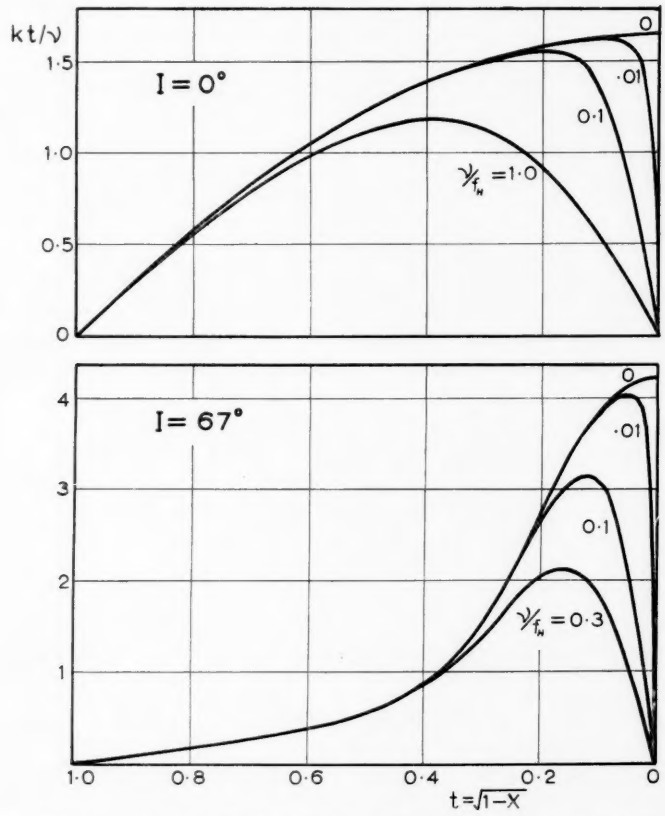

Fig. 10. The absorption coefficient k for the ordinary ray at $f = f_H$. k is in nepers/km and ν in 10^6 sec^{-1}.

near $X = 1$ decreases, until at large values of ν the value of k increases smoothly to the reflection point at $X = 1 + Y$. The broken lines in Fig. 11 strictly belong to the extraordinary wave. They show the values obtained when an ordinary wave penetrates the level $X = 1$ and the collision frequency then decreases to less than the critical value.

For exact calculations of the total absorption of a reflected wave the complex refractive index M must be integrated up to the complex height at which $X = 1 - jZ$. The total absorption is then proportional to minus the imaginary part of this integral (Budden, 1961). At $I = 0°$ the total absorption A for a linear layer is proportional to $-\mathscr{I}\int_0^{1-jZ} M\, dX = Z\int_0^1 \sqrt{(1-s)}\, ds$, where $s = X/(1 - jZ)$ as

before. The integral is independent of the value of Z, so that A/ν is independent of ν. The decrease in $\int_0^1 (k/\nu)\, dX$ when ν is large is thus exactly balanced by the increase in $\mathscr{I}\int_1^{1-jZ} (M/\nu)\, dX$.

At $I = 67°$, the value of k/ν for $X = 1$ to $X = 1 - jZ$ at $f = f_H$ is shown in

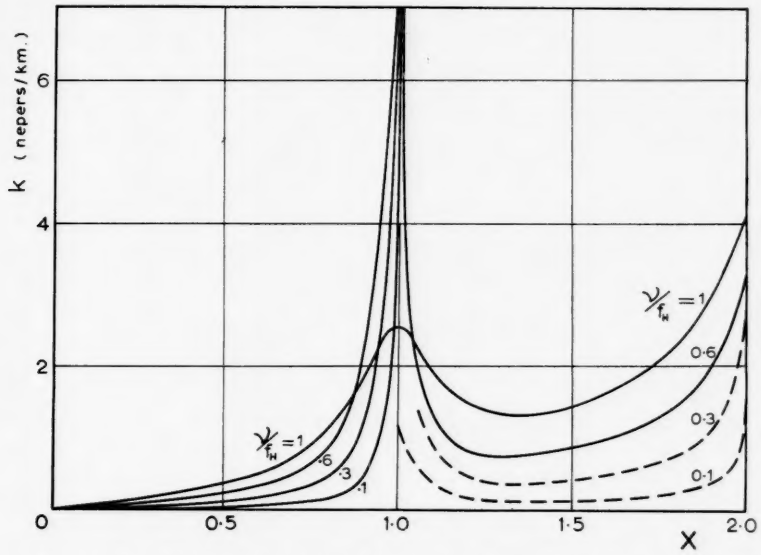

Fig. 11. The absorption coefficient k for the ordinary ray at $f = f_H$ and $I = 67°$.

Fig. 12. These curves were calculated from the real part of M, since the absorption is given by the imaginary part of $\int M\, dX = -jZ\int M\, dp$. Fig. 12 differs radically from the corresponding curves for M' (Fig. 9) since both the real and imaginary parts of M tend to zero at $X = 1 - jZ$. The integral of k/ν from $X = 1$ to $X = 1 - jZ$ is however still sufficient to balance the reductions in k/ν near $X = 1$ (Fig. 10). This is shown in Table 2. For $\nu > 0$ the numerical integrals used were accurate to about 1 per cent and it is seen that, to this accuracy, the value of A/ν is independent of ν.

We are thus led to the conclusion that, except for waves reflected very near the peak of a layer, the total absorption is given by ν times the integral, up to the height at which $X = 1$, of the value of k/ν at $\nu = 0$.

The absorption can therefore be accurately calculated from curves of the type shown in Fig. 13. This figure gives the value of $k_0 t/\nu$, where k_0 is ν times the value of k/ν at $\nu = 0$, for a number of different frequencies at $I = 67°$. The total absorption of a reflected wave is then

$$2\int_0^1 k_0(dh/dX)\, dX = 4\nu\int_0^1 (k_0 t/\nu)(dh/dX)\, dt.$$

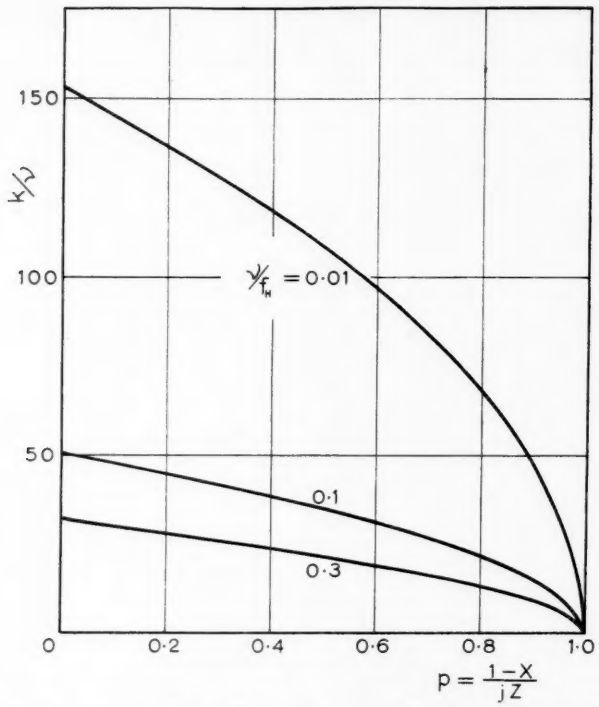

Fig. 12. The absorption coefficient k from $X = 1$ to $X = 1 - jZ$, at $f = f_H$ and $I = 67°$.

Table 2. The total absorption A of a wave reflected from the linear layer $h = X$ at $I = 67°$. f_H and f are in Mc/s and A is in nepers

	$f = f_H$			$f = 2f_H$		
ν/f_H	0	0·1	0·3	0	0·1	0·3
$\frac{2}{\nu}\int_0^1 k\,dX$	5·100	4·068	3·120	4·830	4·194	3·566
$\frac{2}{\nu}\int_1^{1-jZ} k\,dX$	0	1·05	1·95	0	0·67	1·27
$\frac{A}{\nu} = \frac{2}{\nu}\int_0^{1-jZ} k\,dX$	5·100	5·12	5·07	4·83	4·86	4·84

The curves of Fig. 13 show that the total absorption for a linear layer (with a fixed value of dh/dX) is not greatly affected by the wave frequency, although the ratio of the deviative to the non-deviative absorption varies considerably. The broken line in Fig. 13, giving the value of $k_0 t/\nu$ for $f \gg f_H$, also applies to all frequencies at $I = 0°$ and is given by $k_0 t/\nu = 5X/3$. For other values of I the value of k_0 is obtained from

$$k_0 = \frac{X\nu}{2cA^2}\left[1 + \frac{a(A-1)}{(A+a-1)(1-X)}\right]\left(1 - \frac{X}{A}\right)^{-\frac{1}{2}} \qquad (5)$$

where $a = \frac{1}{2}Y^2\cos^2 I/(1-X)$ and $A = 1 - a + (a^2 + Y^2\sin^2 I)^{\frac{1}{2}}$

VOL. 22 1961

A procedure for accurately determining the total absorption of a wave reflected from the ionosphere has also been given by FEJER and VICE (1959). By considering full wave theory they obtained a second order differential equation giving the correction to the total absorption calculated by integrating k up to $X = 1$. This differential equation was solved numerically for the particular case of $dh/dX = 5{\cdot}2$, $I = 62{\cdot}7°$, $f = 2{\cdot}13f_H$ and $\nu = 0{\cdot}335f_H = 0{\cdot}287$ Mc/s, and gave a correction of 15 dB.

In the present work this correction was calculated by integrating the complex refractive index M from $X = 1$ to $X = 1 - jZ$. At $I = 67°$, $f = 2{\cdot}13f_H$ and

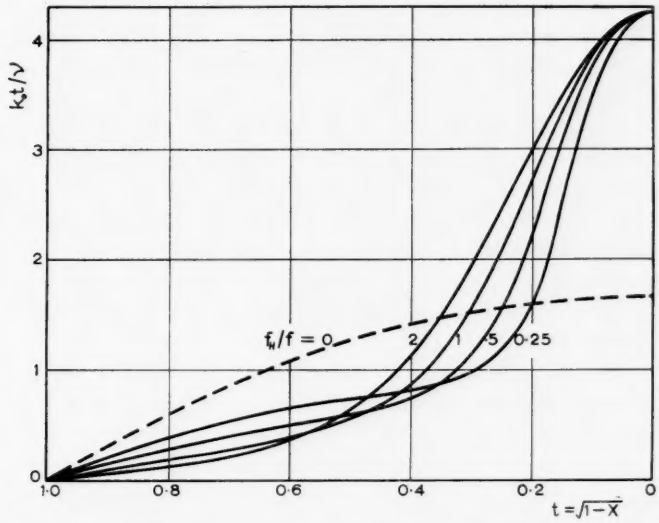

Fig. 13. The absorption coefficient k_0, equal to ν times the value of k/ν at $\nu = 0$, at $I = 67°$. The broken line also gives the value of k_0 for all frequencies at $I = 0°$. k_0 is in nepers/km and ν in 10^6 sec^{-1}.

$\nu = 0{\cdot}335f_H$, Table 2 indicates a correction of about $1{\cdot}29\nu = 0{\cdot}37$ nepers for $dh/dX = 1$. This is equivalent to 16·7 dB at $dh/dX = 5{\cdot}2$. Since the values of k near $X = 1$ vary approximately as sec I, the correction at $I = 62{\cdot}7°$ will be nearer 16·7 sec 62·7°/sec 67° = 14·2 decibels, agreeing well with the correction obtained by FEJER and VICE. A full wave calculation of the total absorption therefore gives the same result as the integral, up to the height at which $X = 1$, of the comparatively simple value of k_0 given by equation (5).

7. CONCLUSIONS

Curves are given showing the effect of the collision frequency ν on the group refractive index μ', for different values of the wave frequency f and magnetic dip angle I.

For the ordinary ray, the general effect of collisions is to prevent μ' from becoming infinite at $X = 1$. The reduction in the value of μ' depends mainly on the

value of ν/f. At large dip angles this reduction occurs only when X is very near 1, while at $I = 0°$ the reduction is important at all values of X.

For the extraordinary ray, at frequencies less than the gyrofrequency f_H, the values of μ' near $X = 1$ are increased in the presence of collisions. This increase is of the same order as the decrease in the values of μ' near reflection. When $f > 0{\cdot}8 f_H$ the values of μ' at $\nu = 0$ become very large near $X = 0$, but these large values are considerably reduced by collisions.

For the extraordinary ray at $f > f_H$ the effect of collisions is to reduce the value of μ' near reflection, as for the ordinary ray. At given values of f and of ν the values of μ' for the extraordinary ray are almost independent of the magnetic dip angle at medium and high latitudes.

The values of μ' for both the ordinary and extraordinary rays become less than 1 when the collision frequency is greater than about four times the wave frequency. Anomalous values of μ' also occur whenever X is between about 0·9 and 1·0 and ν is between half and twice the critical value ν_c; this suggests that coupling between the ordinary and extraordinary rays is important under these conditions.

For the usual case of the ordinary ray reflected at $\nu < \nu_c$ it was found that the virtual height of reflection from a linear layer with a constant collision frequency ν is independent of the value of ν. This result holds exactly at the magnetic equator ($I = 0°$) and was shown by numerical calculations to hold to within 0·1 per cent at $I = 67°$. It can therefore be assumed, in the analysis of virtual height records, that the collision frequency is zero.

A similar result was obtained by considering the absorption coefficient for the ordinary ray. It was found that, for a wave reflected from a linear layer with a constant collision frequency ν, the total absorption of the reflected wave is proportional to ν. Again this result holds exactly at $I = 0°$ and was shown numerically to hold within 1 per cent at $I = 67°$. This means that the total absorption can be calculated by integrating an absorption coefficient k_0, equal to ν times the value of k/ν at $\nu = 0$, up to the height at which $X = 1$. This greatly simplifies the accurate calculation of the absorption of a reflected wave since (1) the calculation of the value of k/ν at $\nu = 0$ is much simpler than the calculation of k when $\nu \neq 0$, and (2) it is not necessary to apply a full-wave correction to the absorption obtained by integrating k_0 to $X = 1$.

These results were obtained by considering the particular case of a linear layer with a constant collision frequency. Since, however, departures from simple ray theory are important only near reflection, the results will hold whenever the electron density can be assumed to increase approximately linearly with height near the point of reflection. This assumption will be seriously in error only for waves reflected very near the peak of a layer, where dh/dN is large and changes rapidly with height. Under these conditions, however, the virtual height and the absorption are large and variable, so that they cannot be measured accurately. Departures from the results given above should therefore not be important in practice.

Acknowledgements—This work was carried out during the tenure of an Overseas Scholarship awarded by the Commissioners for the Exhibition of 1851. Thanks are due to the Director of the Cambridge Mathematical Laboratory for permission to use the electronic computer EDSAC 2 in these calculations.

VOL. 22 1961

References

Becker W.	1957	*Arch. Elektr. Übertr.* **11,** 166.
Brillouin L.	1932	*Rep. Congr. Int. Elect. Paris,* Vol. 2.
Budden K. G.	1961	*Radio Waves in the Ionosphere,* Chap. 16. Cambridge University Press.
Davids N. and Parkinson R. W.	1955	*J. Atmosph. Terr. Phys.* **7,** 173.
Davids N. and Schragg R. L.	1951	*J. Atmosph. Terr. Phys.* **2,** 355.
Fejer J. A. and Vice R. W.	1959	*J. Atmosph. Terr. Phys.* **16,** 307.
Gibbons J. J. and Rao B. R.	1957	*J. Atmosph. Terr. Phys.* **11,** 151.
Huxley L. G.	1937	*Phil. Mag.* **23,** 210, 442.
Jancel R. and Kahan J.	1954	*J. Phys. Radium* **15,** 26.
Rydbeck O. E. H.	1944	*Trans. Chalmers. Univ. Tech.* No. 34, p. 139.
Schmerling E. R.	1957	*Sci. Rep.* No. 94. Pennsylvania State University.
Sen H. K. and Wyller A. A.	1960	*J. Geophys. Res.* **65,** 3931.
Shinn D. H. and Whale H. A.	1952	*J. Atmosph. Terr. Phys.* **2,** 85.
Taylor M.	1933	*Proc. Phys. Soc. Lond.* **45,** 245.
De Voogt A. H.	1948	*Tijdschr. Ned. Radiogenoot.* **13,** 183.

Journal of Atmospheric and Terrestrial Physics, 1961, Vol. 22, pp. 218 to 220. Pergamon Press Ltd. Printed in Northern Ireland

RESEARCH NOTES

A new versatile ionospheric recorder

(*Received* 8 *July* 1961)

THE ionospheric recorder or ionosonde is readily accepted as an extremely valuable ground-based instrument for upper atmosphere research. However its widespread use in many countries has been restricted by the high cost of commercial equipment available. Moreover such equipment often lacks facilities for specific research purposes, and bulk and consequent difficulty of transportation are prohibitive when observations are required at a number of localities. The purpose of this note is to describe briefly a new ionosonde developed at this laboratory which overcomes many of these limitations. This recorder is the culmination of a continuous development of recorders over a period of 10 years to provide more detailed information for use in the ionospheric research program. It is a far more versatile piece of equipment than those at present in service but retains features necessary to produce good clear records of the reflection characteristics of the ionosphere.

The ionosonde is panoramic in form and similar in principle to existing American type C4 recorders (BROWN, 1959). A description of the design techniques involved in panoramic recorders in general is given by HEISLER and WILSON (1961). This particular recorder is unique in that it features electronic scan of the observed frequency range. No cams are used, and an electronically generated linear or logarithmic frequency scan law may be selected at will by a switch. Frequency scan may be set by two controls to cover any range within the maximum range of 0·5–20 Mc/s. This useful facility enables the trace to be set so as to cover most of the ionogram using the normal f_0F2 predictions, thus increasing the accuracy of reductions, or to cover a limited frequency range as for instance may be required in sporadic-E studies (BRIGGS, 1958). The recorder may also be set to operate at any particular fixed frequency by a manual control, or a series of discrete fixed frequencies by application of an external "stepped" waveform. Normal scan period is 15 sec repeated at a scan rate of one per minute. However scan period and scan rate are both variable using panel controls and scan period can be made as short as 2 sec and this can be repeated almost continuously. This feature is particularly valuable for studying rapid changes and movements in the ionosphere, such as are often apparent in the F-region, particularly in winter daytime records (HEISLER 1958). Ionograms on 16 mm film may be projected to study the nature of such changes.

Weight and size of the equipment have been reduced to a minimum through the use of wide band ferrite cored transformers in the driver and output stages of the transmitter which is capable of delivering 5·5 kW pulse peak power input to a 600 Ω balanced antenna over the frequency range. Most of the power supplies are electronically voltage regulated. Total power consumption of the equipment is 675 W.

The complete recorder weighs approximately 150 lb and is contained in 22 in. square cubicle which stands 34 in. high (without camera or camera box). It is quite transportable and can readily be handled by one man. Particular attention has been paid to service accessibility and chassis are arranged to hinge forward from the housing to expose all working components. The use of standard television type valves throughout has led to a

VOL.
22
1961

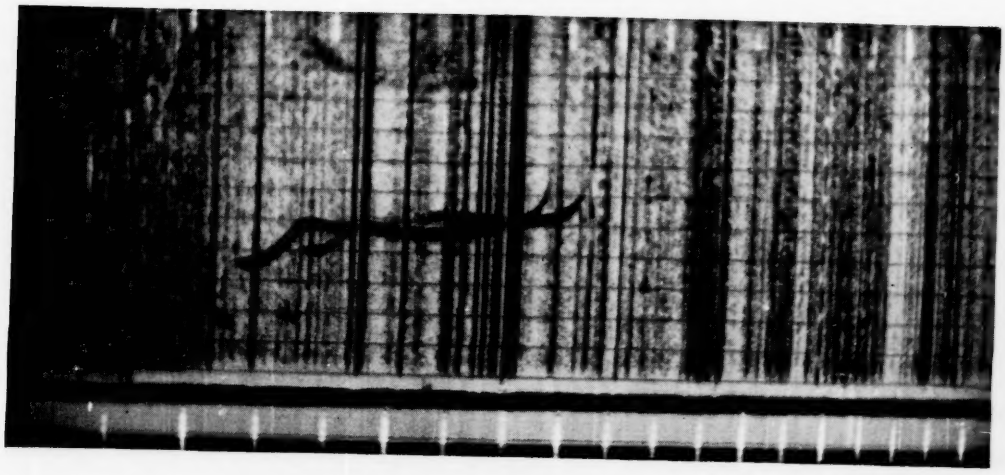

Fig. 1. A 15 sec logarithmic scan covering the range 1–20 Mc/s. Camden (150° 40′E, 34° 03′S) 1208 hours, 16 June 1961.

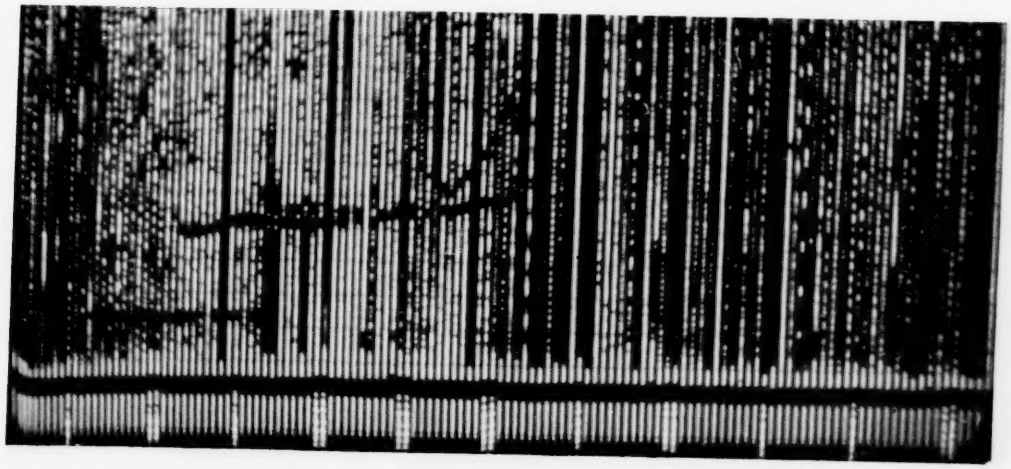

Fig. 2. A 2 sec linear scan covering the range 2–12 Mc/s. Camden (150° 40′E, 34° 03′S) 1448 hours, 14 June 1961.

VOL.
22
1961

very economical design and it is estimated that not considering cost of aerial systems or camera it could be produced for less than £800 (Australian).

Positive prints of typical records are shown in Figs. 1 and 2. Fig. 1 is a 15 sec logarithmic scan* covering the range 1–20 Mc/s, while Fig. 2 shows a 2 sec linear scan covering the range 2–12 Mc/s. DIEMINGER (1959) discusses loss of detail in rapid scan records due to deterioration in integrated signal noise ratio. In Fig. 2 it will be noticed that although the scan period is fast enough to show individual time base sweeps, considerable detail is still present in the ionogram, sufficient to warrant use of the technique in studying rapid ionospheric changes. A complete technical description of the equipment will be published at a later date.

L. H. HEISLER
L. D. WILSON

Radio Research Board Laboratories
School of Electrical Engineering
University of Sydney, Australia

REFERENCES

BRIGGS B. H.	1958	Agardograph 34, p. 151. (N.A.T.O. Advisory groups for aeronautical research and development.)
BROWN J. N.	1959	*Proc. I.R.E.* **47**, 296.
DIEMINGER W.	1959	*J. Atmosph. Terr. Phys.* **16**, 179.
HEISLER L. H.	1958	*Aust. J. Phys.* **1**, 79.
HEISLER L. H. and WILSON L. D.	1961	*J. Res. Nat. Bur. Stand.* D. In press.

* The logarithmic scan law in Fig. 1 is only approximate. The equipment has recently been modified to provide an exact scan law.

On the apparent long term negative correlation between scintillations and spread-*F*

(*Received* 1 *August* 1961)

IN a recent paper CHIVERS (1960) pointed out that whereas DAGG'S (1957) earlier observations on Cassiopeia from Jodrell Bank indicated that scintillation and spread-*F* (as observed at Inverness) have similar monthly mean diurnal distributions of percentage occurrence, the correlation between the monthly mean scintillation index and percentage occurrence of spread-*F* appears to be negative when carried out over half a sunspot cycle. CHIVERS tacitly assumes that the spread-*F* information from Inverness is characteristic of the irregularity configuration over the whole range of latitudes involved in the scintillation observations. It is the purpose of this note to question the validity of this assumption.

In the course of a day the line of sight from Jodrell Bank to the radio source cuts the *F2*-region of the ionosphere at points which range from 58° to 65° geomagnetic latitude. Consequently the monthly average scintillation index is an integrated measure of *F2*-region irregularity activity over this field of view. SINGLETON (1960) has shown that the percentage occurrence of spread-*F* increases rapidly from less than 20 per cent at 60° geom. to over 80 per cent at 70° geom. Thus the irregularity configuration in the northern part of the field of view will be predominant in determining the mean scintillation index integrated over the whole field of view. Further, while the percentage occurrence of spread-*F* correlates

negatively with sunspot number at Inverness, this situation changes as the pole is approached (SINGLETON, 1957); the correlation becoming positive for higher latitudes. The locus of points at which the sunspot number correlation changes from negative to positive, the spread-*F* invariant (REBER, 1956), certainly passes to the north of Scotland and most likely between Scotland and Greenland. Consequently, the northern part of CHIVERS' field of view will be situated in a region for which the spread-*F* versus sunspot number correlation is less negative than at Inverness. Indeed it may be that the most northern part of the field of view is associated with an *F*-region for which the spread-*F* versus sunspot number correlation is positive. Hence CHIVERS' mean scintillation index would be expected to correlate with sunspot number less negatively than does the percentage occurrence of spread-*F* at Inverness.

BRIGGS (1958) and KOSTER and WRIGHT (1960), by assuming that the same system of irregularities in the *F2*-region gives rise to both spread-*F* and scintillations, have shown that the percentage occurrence of spread-*F*, ϕ, and the scintillation index, S, are related by

$$S \propto z \sec^{\frac{1}{2}} i \, f_0 \, \phi$$

where z is the distance from the irregularities to the radio telescope and i is the angle of incidence of the extraterrestrial radiation on an *F2*-region of critical frequency f_0. At any particular point in the field of view $z \sec^{\frac{1}{2}} i$ will be roughly constant throughout the sunspot cycle and hence the scintillation index appropriate to this point will be proportional to $f_0 \, \phi$ at the point. The critical frequency varies with sunspot number, R, in the following way (RATCLIFFE, 1960):

$$f_0^2 \propto (1 + 0{\cdot}02 \, R).$$

During the period of interest (1955–1957) R increases from 20 to 200 which implies a twofold increase in both f_0 and the scintillation index associated with a given percentage occurrence of spread-*F*. Consequently, the change from negative to positive scintillation versus sunspot number correlation occurs at latitudes for which the spread-*F* versus sunspot number correlation is negative to the extent that the percentage occurrence at sunspot minimum is twice that at sunspot maximum. Thus even if the northern part of the field of view considered above does not extend beyond the region associated with the spread-*F* invariant, where the spread-*F* versus sunspot number correlation is small, the scintillation sunspot number correlation may still be substantially positive and cause the index, integrated over the whole field of view, to be positively correlated also.

It appears therefore that a positive monthly average scintillation index versus sunspot number correlation is not unexpected for the case of Cassiopeia viewed from Jodrell Bank even though the occurrence of spread-*F* as observed at Inverness shows a negative correlation with sunspot number.

D. G. SINGLETON

Department of Physics
University of Queensland
Australia

REFERENCES

BRIGGS B. H.	1958	*J. Atmosph. Terr. Phys.* **12,** 89.
CHIVERS H. J. A.	1960	*J. Atmosph. Terr. Phys.* **19,** 54.
DAGG M.	1957	*J. Atmosph. Terr. Phys.* **10,** 204.
KOSTER J. R. and WRIGHT R. W.	1960	*J. Geophys. Res.* **65,** 2303.
RATCLIFFE J. A.	1960	*Physics of the Upper Atmosphere*, p. 433. Academic Press, London.
REBER G.	1956	*J. Geophys. Res.* **61,** 157.
SINGLETON D. G.	1957	*Aust. J. Phys.* **10,** 60.
SINGLETON D. G.	1960	*J. Geophys. Res.* **65,** 3615.

VOL. 22 1961

Journal of Atmospheric and Terrestrial Physics, 1961, Vol. 22, pp. 221 to 227. Pergamon Press Ltd. Printed in Northern Ireland

BOOK REVIEWS

Science in Space: Edited by L. V. BERKNER and H. ODISHAW. McGraw-Hill, New York, 1961. 458 pp., $7.

THIS authoritative volume appears under the distinguished sponsorship of the Space Science Board of the American National Academy of Sciences. Its various chapters have been already circulated, in separate off-print form, to interested scientists throughout the world; and the reviewer, as one of the fortunate recipients, wishes warmly to acknowledge here his appreciation of this generous pre-publication gesture on the part of the Space Science Board. Nevertheless it is most convenient to have these memoirs assembled now in volume form, and, of course, available to scientists everywhere.

The Space Science Board has naturally been fortunate in its ability to invite twenty outstanding authorities, all intimately associated with American space research, to write the seven sections of the book which are entitled, respectively, (1) A General Review; (2) Gravity; (3) The Earth; (4) The Moon and the Planets; (5) Fields and Particles in Space; (6) The Stars; and (7) The Life Sciences. These sections serve to remind us of the very notable discoveries in the field of pure science which have attended American efforts in this field, even if Russia has to its credit the more spectacular technological achievements. Quite rightly the American discovery of the two Van Allen radiation belts, in the course of which both satellites and deep space probes were employed, is counted the outstanding disclosure of space research so far.

A reviewer could not possibly omit to commend specially the first section of the book, the authors of which are the editors, L. V. BERKNER and HUGH ODISHAW, Chairman and Executive Director, respectively, of the Space Science Board. This is a brilliant and thoughtful essay on the whole philosophy of space research, and on the experimental possibilities of an age when man's instruments, and even man himself, are no longer earthbound.

E. V. APPLETON

Antarctic Meteorology: Proceedings of the Melbourne Symposium, February 1959. Pergamon Press, Oxford, 1960. xviii + 483 pp., 105s.

THIS splendidly-produced book reflects great credit on the editors, printers and publishers who have collaborated in this assemblage of forty papers, contributed by scientists representative of ten nations at the Symposium on Antarctic Meteorology held in Melbourne in February 1959. These provide us with some of the first results, in the minds of a number of meteorologists, of the extensive Antarctic observational programme undertaken during the International Geophysical Year. Ten of the twelve participating nations were represented at this meeting.

It was fitting that the Australian Bureau of Meteorology should sponsor such a meeting at the first opportunity. For a hundred years or so the great grasslands of the Southern Hemisphere have produced food and raw materials subject to the hazards of drought. In spite of the apparent monotony of the endless eastward flow of frontal systems over the two thousand miles of ocean north of Antarctica, it is increasingly evident that decided irregularities occur in the vigour and persistence with which they affect the continents to the northward. The causes of such irregularities may be many, but the Antarctic continent as a cooling agent of variable potency is a primary object of study.

Beyond the meteorological problems of the Antarctic itself, including that of the nourishment of the ice cap, the question arises, how far can the lessons learnt in the Northern Hemisphere be applied to southern temperate latitudes? These papers make it clear how much attention is now focussed on the constraints applicable to a belt of two thousand miles of turbulent surface flow; how often, when, and why do anticyclones develop in latitudes around 50–60°S? Are such blocking systems related to the upper-air circulation over Antarctica itself; are variations in the surface outflow from that continent a significant element in the genesis of depressions, or, for example, in the onset of "cold outbreaks" in southern Australia?

The sessions were framed around seven topics: (1) local effects in the Antarctic, (2) synoptic analyses and forecasting, (3) synoptic influences in lower latitudes, (4) circulation studies, (5) snow and ice characteristics, (6) heat and mass exchanges, (7) climatological studies. To each sessional group of papers a brief and excellently-edited summary of the subsequent discussion is appended. This is of great value to the reader who wants to acquaint himself with the flux of ideas at such a meeting.

Many meteorological readers will turn with interest to the synoptic studies affecting the general circulation, e.g. papers by LANGFORD, KERR and VAN LOON. That the sudden warming of the polar stratosphere appears to take place in early October in the Antarctic, but late January in the Arctic, is very provocative. As few can read Russian, ASTAPENKO's summary of Russian ideas of the Antarctic circulation is welcome. Many details provoke thought, e.g. the very considerable backing with height of the surface wind at Halley Bay and the extent of katabatic effects at the South Pole. Physicists will be glad to have an opportunity to study MELLOR's work on drifting snow. LOEWE draws the interesting conclusion that the present budget for Antarctica seems to show a gain of substance.

If a criticism can be offered it is that more reference to already established ideas might have been forthcoming. After all Antarctic meteorology did not begin with the I.G.Y. For example in more than one paper on the Southern Hemispheric circulation no reference is made to LAMB's work ten years earlier. In general the earlier work of MEINARDUS and the extensive contributions of the Falkland Islands Meteorological Service received little attention, except in a paper by BERSON and RADOK who make reference not only to LAMB but also to the work of MANSFIELD and GLASSEY; among other things we are reminded that Sir GEORGE SIMPSON's pressure waves are still to be discussed. What is very clear is that more data from the sub-Antarctic islands are needed with regard to the variability that the Southern Hemispheric circulation shows; and many geophysicists will ask for more study of the part played by oceanographical factors.

There are commendably few slips: a misprint of "Arctic air" (p. 420) and the use of "phenomena" and "data" as singular nouns might have been taken care of editorially. The lack of an index is rather inconvenient, but in such a collection of papers supported by references the contents-list goes far to assist the informed reader.

In sum, this book makes a stimulating and a quite indispensable adjunct for all those who are interested in Antarctic meteorology. The subject is so vast that an assemblage of papers of this kind is very necessary; it is too much to expect such a collection to appear in the journals. Our knowledge has grown so rapidly that it might well be a decade before a comprehensive study can be expected; hence this book is to be thoroughly commended.

G. MANLEY

Some Ionospheric Results obtained during the International Geophysical Year: Scientific Editor: W. J. G. BEYNON. Elsevier Publishing Company, Amsterdam, 1960. 400 pp., 72s.

THE International Geophysical Year (IGY) was the title assigned to the period 1 July 1957 to 31 December 1958, during which the scientists of some sixty-six nations worked at over 4000 observatories throughout the world on co-operative programme concerned with the physical properties of the earth and its atmosphere, and with the related solar and terrestrial phenomena. In the past few years the results of the great international scientific effort expended during the

VOL. 22 1961

IGY have tended to be overshadowed by the more limited but much more spectacular development of space research with artificial earth satellites. It is therefore all the more important that the results of the vast quantity of observations made during the IGY should be carefully studied and analysed and made generally available in the form of permanent scientific publication.

From this standpoint, the volume under review is very welcome, and is a credit to the International Scientific Radio Union (URSI) which played the major part in planning and coordinating the programme of the IGY. The magnitude of the task of interpreting the results is appropriately indicated in the preface to the present volume in the following form. "The fruits of the operational phase of the IGY radio programme amount to many millions of radio observations, now stored in the four World Data Centres, at Washington, Moscow, Slough and Tokyo, where these are available to bona fide scientific workers. Further scientific progress in the way of insight and understanding will be the reward of those investigators who are able to formulate the right questions, to be answered by way of accumulated data."

With this understanding of the nature and magnitude of the task, it is of interest to note that the URSI committee which, with Sir EDWARD APPLETON as Chairman and Dr. (now Professor) W. J. G. BEYNON as Secretary, had planned the observational programme, also took the initiative in holding a Symposium in Brussels in September 1959. It is the Proceedings of this Symposium that comprise the present volume, which is divided into eight sections corresponding to the subject grouping adopted for the successive sessions of the meeting.

Each section of the volume contains a number of prepared scientific contributions from authors in widely scattered observatories throughout the world, and is followed by a brief summary (one or two pages) of the salient points brought out in the discussion at the Brussels meeting. The titles of the sections with the number of papers in each are as follows:—I: *F2*-Layer Phenomena (9); II: High Latitude Studies (6); III: Disturbance Phenomena (10); IV: Ionospheric Irregularities (7); V: $N(h)$ Profiles (6); VI: Absorption (7); VII: Drifts (8); VII: Noise, Whistlers, Rockets, Satellites (7). The texts of the papers are in English while in some, but not all, cases a "Résumé" is given in the French language. The production of this work is eminently satisfactory and reflects great credit on the committee, the editor and publishers alike.

R. L. SMITH-ROSE

W. SULLIVAN: **Assault on the Unknown.** McGraw-Hill, New York, 1961. 460 pp., $7.95.

THIS is the second book published providing a comprehensive assessment of the scientific harvest of the International Geophysical Year 1957–8. The first one was written, appropriately enough, by Professor SYDNEY CHAPMAN, the principal planner of the year's concerted geophysical experiments and observations. This was published last year under the title *I.G.Y: Year of Discovery* and provides the reader with a succinct yet readable account of I.G.Y. discoveries.

The volume under present review, by a distinguished American journalist, WALTER SULLIVAN, Chief Science Writer of the New York Times, has been written with a different objective from that of Professor CHAPMAN's. Mr. SULLIVAN tells us a story—the story of "the single most significant peace-time activity of mankind since the Renaissance and the Copernican Revolution." In telling that story he deals almost as much with people as with things, almost as much with human, as with scientific, situations. To do this the author naturally has to rely on his own personal contact with American I.G.Y. projects. As he says in his own words: "To season the scientific accounts with personal experience, the author has included a number of events that he witnessed and, because of this and the broad scope of the American programme, more space has been devoted to the United States effort than to that of any other nation." Nevertheless the international pooling of resources and techniques, which was such a striking feature of the I.G.Y., receives adequate attention and emphasis.

Readable and reliable, Mr. SULLIVAN's book is an outstanding success. It will both entertain and inform the scientist who himself took part in the I.G.Y., while it cannot fail to fire the scientific schoolboy with a desire to participate in the next I.G.Y.

E. V. APPLETON

Handbook of Aviation Meteorology: Air Ministry, Meteorological Office. H.M. Stationery Office, London, 1960. 404 pp., 25s.

This book has been prepared to replace Dr. Sutcliffe's *Meteorology for Aviators* which for more than 20 years has been widely used not only by the airmen to whom it was addressed but also by students generally, for, when it was first published, it provided the best short introduction to the subject available in English. This is an entirely new book, about twice the length of its predecessor but the main aim remains the same, namely "to provide a work suitable for the use of pilots and navigators undergoing intermediate and advanced courses of instruction at flying training schools".

The first and longest of the five parts into which the book is divided gives the basic physical theory, developed in much the same sequence as was first used by Sutcliffe. The remaining parts deal with meteorological observations, synoptic meteorology, meteorological organization and climatology and there is an appendix giving the derivation of some of the formulae used in the text.

Applications of meteorological principles in air navigation that are described include pressure pattern flying, flight through thunderstorms, flight procedure in airframe icing conditions and flying conditions in the stratosphere, but the use of this book is not likely to be limited to the airman. It is a useful elementary text book in general meteorology.

J. Paton

I. S. Shklovsky: **Cosmic Radio Waves.** Harvard University Press; Oxford University Press, 1961. xvi + 444 pp., 65s.

VOL. 22 1961

The barrier of language is often supposed to be of little consequence for scientists. However when Soviet astrophysicists, Shklovsky amongst them, solved the problem of the origin of radio emission from the Galaxy and most of the discrete radio sources at one stroke, the importance of their work was not realized for some 2 years after publication. Even with the full recognition now accorded to the astrophysical theorists in U.S.S.R. it is only too easy for Western radio astronomers to skim through abstracts, or merely to read the titles of papers and books in Russian. The publication in 1956 of the only up-to-date survey of radio astronomy, as seen by a theorist, was scarcely noticed in the West: it was written in Russian. The present publication, a translation made in U.S.A. in 1958, will be widely welcomed and may still come as a surprise to those who do not know much of the first-rate Russian theoretical work.

But what a pity it was not published in English earlier. In 1956 it was all new and exciting; radio astronomy changes fast. There are indeed revisions and additions, but they are a sad patching up for the most part. Thus on page 178: "One may assert with considerable confidence that Hydra A is actually variable" is a direct translation from the original text. But on page 179 comes an added paragraph with "the highly important question as to the true variability of Hydra A remains open". (The modern evidence is that it does not vary at all.) Even this patching up has not been applied consistently, for example the 1956 result about the "radio red-shift" of Cygnus A, since disproved, stands uncorrected as a glaring anachronism in the text.

There is also some occasional unkindness: page 308 "In September 1955, the proprietors of the greatest telescope in the world finally expressed active interest in the problems of the polarisation of the Crab". But we are after all being treated in this book to an exposition by the leading theoretical radio-astronomer, who is almost bound to find himself in conflict with others, particularly the leading observers.

Accepting these two limitations, the one of date and the other of a necessarily personal viewpoint, we have here a very valuable book. It is the only one of its kind, and it is a fine text-book. We can only hope that we shall be treated to an up-to-date version one day.

F. G. Smith

Satellite Environment Handbook: Edited by F. S. JOHNSON. Stanford University Press, 1961. 155 pp., $5.50.

THE available data relating to the geophysical environment encountered by earth satellites are assembled in this volume. Such data are presented in a series of eight essays, each of which is lucid, brief and comprehensive. The editor himself sets his colleagues an admirable example with an opening chapter on the structure of the Upper Atmosphere. This is followed by seven further chapters, each by a different author, on the structure of the Ionosphere, Penetrating Radiation, Solar Radiation, Micrometeorites, Radio Noise, Thermal Radiation from the Earth and Geomagnetism.

Although most of the data relating to upper-atmospheric conditions has been compiled from the scientific literature, and many references are cited, some of the information included here is available for the first time.

The volume can be recommended with confidence as an up-to-date guide for workers in the fields of space-systems development, geophysics, meteorology and communications.

E. V. APPLETON

G. R. MICZAIKA and W. M. SINTON: **Tools of the Astronomer.** Harvard University Press; Oxford University Press, 1961. 294 pp., 62s.

THE present volume, the most recent addition to the well-known series of Harvard Books on Astronomy, attempts to provide on just under 300 pages and with the help of some 190 photographs and diagrams a comprehensive review of the various types of instrumentation which are in common use in present-day astronomy. Like the other books of the same series, it is addressed primarily to non-specialists; it is descriptive throughout, and in this way cannot give more than the general principles of instruments which in many cases involve highly complicated techniques.

There are eight chapters. The first is devoted to an introduction into the fundamentals of optics. A discussion of the properties of the photographic plate as a receiver of radiation forms the subject of the second chapter. In the following chapters the authors discuss telescopes, the optics of refractors, mirrors and Schmidt cameras, their mountings, drives and housing. The fifth and sixth chapters deal with stellar photometry and spectroscopy, that is with fields in which post-war developments in optics and electronics have brought about great advances in accuracy and sensitivity. Instruments for solar research are given a chapter of their own which includes a discussion of high-resolution vacuum spectrographs, the magnetograph and polarizing filters. The last chapter attempts to give on some thirty pages a brief survey of radio telescopes.

The authors have purposely refrained from dealing with instruments for observations from balloons, rockets or satellites. Restricting themselves to what is well established, they have also had to omit any discussion of such fundamental present developments as image tubes or new techniques for data processing. The chapter on radio astronomy contains no reference to recent improvements in interferometry. All in all, however, the book gives a very readable, through purely descriptive account of observational methods and their development up to about three or four years ago.

H. A. BRÜCK

M. NEIBURGER, D. S. JOHNSON and CHEN-WU-CHIEN: **Studies of the Structure of the Atmosphere over the Eastern North Pacific in Summer—I. The Inversion over the Eastern North Pacific Ocean.** (University of California Publications in Meteorology, Vol. 1, No. 1). University of California Press, 1961. 94 pp., $2.50.

THIS is the first of a new series of publications in meteorology, and describes a phenomenon, the temperature inversion, which is closely associated with many aspects of the weather in California

from its famous sunshine to the smog which has earned a certain notoriety in recent years for San Francisco.

The temperature inversion, in which the usual decrease of temperature with height above the earth's surface is replaced by an increase, occurs on many days of summer (70 per cent or more) over a wide area of the North East Pacific including the Western seaboard of the United States. All available information on this temperature inversion has been assembled in this booklet, including the results obtained from special cruises by craft operated by the University of California Scripps Institution of Oceanography. A digest of the data is also given and the average characteristics of the structure of the atmosphere in the first few thousand metres over the Eastern Pacific are demonstrated in many charts and diagrams with a discussion of the vertical motions, turbulent diffusion, surface heating and radiation exchanges leading to the observed distributions. Some of the general results have been known for many years, for example that the height of the inversion, usually a few hundred metres over the coast, rises to seawards. As in many meteorological investigations the data are comparatively few and have had to be combined to give a general picture of a phenomenon which is changing from day to day; many of the interesting features therefore appear somewhat blurred. Nevertheless this monograph seems likely to be the standard descriptive reference on the subject for many years.

J. K. Bannon

Space Astrophysics: Edited by W. Liller. McGraw-Hill, New York, 1961. 272 pp., $10.

In this volume there is assembled a series of articles dealing with astronomical and astrophysical problems investigated from *above* the atmosphere. In the first half of the book the experimental methods, involving the aid of rockets and satellites, are described in detail; while the second half is devoted to theoretical discussions of such topics as the solar corona, interplanetary gas, solar winds and lunar conditions.

Most of the contributions were presented at a symposium on space astrophysics, organized in 1959–60 by the Department of Astronomy of the University of Michigan. They have been written by experts for experts, and the claim made on the book cover that "many can be understood by the intelligent layman" can scarcely be admitted. Nevertheless the volume is the first planned collection of articles on a very young subject, the study of space with instruments that are situated there.

E. V. Appleton

Dissertations in Physics: An indexed bibliography of all doctoral theses accepted by American universities, 1861–1959. Compiled by M. L. Marckworth. Stanford University Press, 1961. xii + 803 pp., $17.50.

According to the Introduction to this imposing volume, 8418 doctorates in physics have been awarded by American universities since Yale conferred the degree of Ph.D. on Arthur Williams Wright in 1861 for a thesis entitled "Having given the velocity and direction of motion of a meteor on entering the atmosphere of the earth, to determine its orbit about the sun, taking into account the attractions of both these bodies". Ninety-seven institutions have been involved in this degree-giving, from the University of California with 535 doctors, to Colorado State, Smith College, Wayne State and Western Reserve with one each. More than 5000 of these higher degrees have been awarded in the decade 1950–1959.

This up-to-date bibliography of a century's theses was compiled, as it would appear from the Foreword, partly from the conviction that it was a timely contribution to the tools of research, partly—even primarily—as an experiment in information processing by machine. Part I is an

VOL. 22 1961

alphabetical list by authors' names; Part II (pp. 397–791) a "permutation subject index" produced on the 704 computer of the International Business Machines Corporation of San Jose, California, who hold the copyright of the work as a whole. The code designation of this type of indexing is KWIK (key word in context). The promoters say of it "It provides an index that is both consistent and exhaustive for the material on which it is based: the words in the titles themselves. The program cannot index a document beyond the depth of the words supplied . . ." Out of the machine, in this particular case, have come more than 40,000 index entries, some 600, for example, with "electron" or "electronic" as key-word—together with an unavoidable residue of grotesques such as "DRIVEN—A study of the time-dependent wind-driven ocean circulation. 7500". The number, of course, provides the reference to the alphabetical list by authors' names.

Without the impersonal machine, indexing of these theses would have been a truly formidable task. Its use has undoubtedly diminished the incidence of human error in the undertaking, but the sly jest is absent—as by definition: only the occasional grotesque remains. That is not to deny the value of the final product to the researcher. He will find it all here—except what is "beyond the depth of the words supplied". For that he must rely on his own nose.

N. Feather

Journal of Atmospheric and Terrestrial Physics, 1961, Vol. 22, p. 228. Pergamon Press Ltd. Printed in Northern Ireland

NOTICE

Carnegie Institution of Washington
1530 P Street, Northwest, Washington 5, D.C., U.S.A.

Publication No. 620, "Equatorial Electrojet in Peru," by SCOTT E. FORBUSH and MATEO CASAVERDE. 1961. Quarto, v + 135 pp., 98 tables.

MAGNETOGRAMS with H, D, and Z traces were obtained on the west coast of South America between the geographic equator and latitude 22°S at fifteen temporary survey stations, at four IGY observatories, and at Huancayo. Analysis of these and other data shows that the primary S_q electrojet near midday is a band, about 660 km wide, of eastward current at about 100 km height centred over the dip equator, near which it accounts for about half the total range of S_q in H.

The induced field of the S_q jet is compatible with that of its negative image at 600 km depth and consistent with results from an analysis of a bay disturbance in the auroral zone. No jet effects are found at night, and there is no evidence for seasonal changes in the location of the jet.

The centre of the jet follows the secular change in the geographic latitude of the dip equator. There is no evidence for jet effects in D_{ST}. Jet effects are found near midday for sudden commencements, for solar-flare effects (crochets), and for sudden changes, probably associated with S_D disturbances. For the average of solar-flare effects near midday the ratio of the jet effect near the dip equator to the "normal" for the jet effect is about twice the corresponding ratio for the average S_q jet. For sudden commencements at night the vertical field changes sign at geographic latitude 8°S, which corresponds to the location of Simpson's cosmic-ray equator at the same longitude; the change in sign of ΔZ for these sudden commencements occurs within a narrow range of latitude, indicating that the current system responsible for sudden commencements probably flows in the upper atmosphere.

VOL. 22 1961

Publication No. 175, Volume XXI: "Cosmic-Ray Results." Huancayo, Peru, January 1956–December 1959; Cheltenham, Maryland, January 1956–4 October 1956; Fredericksburg, Virginia, 5 October 1956–December 1959; Christchurch, New Zealand, January 1956–June 1959; Godhavn, Greenland, January 1954–July 1959; Universidad Nacional de Mexico, July 1957–December 1958. By LISELOTTE BEACH and S. E. FORBUSH. 1961. Quarto, v + 226 pp., 221 tables.

THIS is a third volume of cosmic-ray publications which includes data obtained through 1959 from Huancayo and Cheltenham-Fredericksburg. Bi-hourly means and summaries for Huancayo and Cheltenham-Fredericksburg are included. Summaries for Christchurch are for the period January 1956 to June 1959. Bi-hourly means and summaries for Godhavn are for the period January 1954 to July 1959. Also included are bi-hourly means and summaries from Universidad Nacional de Mexico, Instituto de Geofisica, for the IGY period July 1957 to December 1958.

Note: Carnegie Institution of Washington will be happy to supply the above volumes without charge to research organizations and research workers in the field.

Journal of Atmospheric and Terrestrial Physics, 1961, Vol. 22, pp. 229 to 231. Pergamon Press Ltd. Printed in Northern Ireland

Indices of geomagnetic activity

of the Observatories HARTLAND (*Ha*), ESKDALEMUIR (*Es*) and LERWICK (*Le*) May–July 1961

The figures given on pages 229 to 231 represent the K-indices for three-hour intervals, beginning with 00–03 hrs for the first and ending with 21–24 hrs for the eighth figure.

May 1961

Day	*Ha* *Range for* $K = 9{:}500\gamma$			*Es* *Range for* $K = 9{:}750\gamma$			*Le* *Range for* $K = 9{:}1000\gamma$			*Day*
	K-Indices		*Sum*	*K-Indices*		*Sum*	*K-Indices*		*Sum*	
1	2313	3403	19	2313	3413	20	3312	3313	19	1
2	5322	1211	17	5423	2211	20	5522	1211	19	2
3	1200	1100	5	0111	1121	8	0110	1110	5	3
4	0001	0234	10	1121	2333	16	0121	1235	15	4
5	2332	2543	24	2232	3543	24	2222	2534	22	5
6	3544	4244	30	2444	3234	26	2443	4344	28	6
7	3243	3433	25	3343	3433	26	3233	3323	22	7
8	2222	2333	19	2222	2343	20	3221	2333	19	8
9	1234	3322	20	0224	3322	18	1223	2312	16	9
10	2111	2123	13	2112	2222	14	2212	2224	17	10
11	4332	3342	24	3332	4442	25	4322	3332	22	11
12	3322	2333	21	3323	2333	22	3332	2324	22	12
13	5422	3322	23	4433	4332	26	5422	3222	22	13
14	3423	2211	18	3323	2221	18	3422	2211	17	14
15	0011	1222	9	0002	2321	10	0101	1223	10	15
16	4443	4432	28	4442	4432	27	4442	4432	27	16
17	3112	3311	15	3123	3311	17	3112	3211	14	17
18	1010	1110	5	1111	1221	10	1011	1211	8	18
19	2122	2334	19	2122	3324	19	2212	2214	16	19
20	3432	3331	22	3432	3331	22	4432	2231	21	20
21	2211	1232	14	1121	2232	14	1111	1222	11	21
22	2222	2332	18	2222	2342	19	2222	1331	16	22
23	2323	4431	22	3323	4432	24	1322	3321	17	23
24	3210	2313	15	3212	2322	17	3311	1313	16	24
25	3552	3441	27	3553	4342	29	4553	4342	30	25
26	3211	3212	15	3022	3212	15	3221	2212	15	26
27	3222	1101	12	3222	2212	16	3221	2211	14	27
28	1112	3333	17	1112	3433	18	1012	3333	16	28
29	1221	1121	11	1311	1221	12	1321	1121	12	29
30	2113	3323	18	2122	3323	18	1122	3312	15	30
31	3333	4433	26	3333	4433	26	3333	4333	25	31

June 1961

Day	*Ha* Range for $K = 9$: 500γ			*Es* Range for $K = 9$: 750γ			*Le* Range for $K = 9$: 1000γ			*Day*
	K-Indices		*Sum*	*K-Indices*		*Sum*	*K-Indices*		*Sum*	
1	3324	5532	27	3334	5532	28	3323	5533	27	1
2	3233	4441	24	3234	4441	25	4233	4441	25	2
3	2322	2112	15	2333	2212	18	2432	2111	16	3
4	1222	3201	13	1222	3211	14	1222	3201	13	4
5	1311	1222	13	1322	3322	18	1322	2322	17	5
6	1221	2543	20	2222	3543	23	1122	2532	18	6
7	2234	5433	26	2234	5433	26	1233	4433	23	7
8	3232	3332	21	3233	4322	22	4323	3332	23	8
9	1112	1232	13	0122	2322	14	1111	2222	12	9
10	2111	2000	7	1221	2200	10	1111	2101	8	10
11	0101	2110	6	0101	1220	7	0101	1110	5	11
12	1322	2210	13	1322	3321	17	1331	2210	13	12
13	0111	2111	8	0102	2222	11	0112	2111	9	13
14	2000	0013	6	2012	1113	11	1011	1012	7	14
15	2223	3321	18	2223	4332	21	2213	3331	18	15
16	4213	2332	20	3213	3332	20	4213	3332	21	16
17	1101	3212	11	1212	3212	14	1102	3112	11	17
18	1112	2435	19	1123	3434	21	1112	3334	18	18
19	2311	1232	15	2322	2232	18	2331	1232	17	19
20	1322	0333	17	1322	1333	18	1221	1334	17	20
21	4444	4445	33	4434	5455	34	6534	4557	39	21
22	5433	3554	32	6534	3554	35	7744	3454	38	22
23	3110	2322	14	3222	2322	18	4311	2323	19	23
24	2211	2121	12	2212	2222	15	2211	2221	13	24
25	1213	2223	16	1213	3333	19	1222	2333	18	25
26	1100	3330	11	1111	4331	15	1101	3221	11	26
27	0132	3200	11	1232	3211	15	0123	3201	12	27
28	0111	1111	7	1112	2211	11	1112	2211	11	28
29	3533	3321	23	2533	3321	22	3652	3222	25	29
30	2000	1111	6	2111	1121	10	2111	1011	8	30

VOL. 22 1961

July 1961

Day	*Ha* *Range for* $K = 9{:}500\gamma$		*Sum*	*Es* *Range for* $K = 9{:}750\gamma$		*Sum*	*Le* *Range for* $K = 9{:}1000\gamma$		*Sum*	*Day*
	K-Indices			*K-Indices*			*K-Indices*			
1	2122	2311	14	2223	3312	18	3222	2311	16	1
2	1222	2443	20	1223	2443	21	1112	2333	16	2
3	3234	4431	24	2233	4432	23	2132	4421	19	3
4	2222	3335	22	2122	3335	21	2122	3236	21	4
5	5533	4433	30	4533	4433	29	7743	3423	33	5
6	2322	2432	20	2323	3521	21	3322	2532	22	6
7	3233	3321	20	3133	4321	20	4433	3321	23	7
8	2122	3312	16	2223	3322	19	2222	2223	17	8
9	2232	1310	14	2232	2311	16	3232	2221	17	9
10	3432	2322	21	3332	2422	21	3332	2322	20	10
11	3212	2232	17	3221	2332	18	3311	1432	18	11
12	1124	1120	12	2123	1120	12	2123	2121	14	12
13	0116	7765	33	0126	7765	34	1115	6777	35	13
14	4367	5553	38	4367	6653	40	6357	7764	45	14
15	2322	4343	23	3433	4344	28	3433	5335	29	15
16	5322	3442	25	5422	4442	27	6522	3333	27	16
17	2223	3356	26	2223	4356	27	4323	4355	29	17
18	4554	6645	39	4554	7655	41	6663	7657	46	18
19	5410	2220	16	5410	2221	17	7631	2121	23	19
20	1332	1344	21	1232	2344	21	1333	2335	23	20
21	4542	2332	25	4542	3333	27	5553	4442	32	21
22	2232	3311	17	2233	3311	18	2233	2311	17	22
23	1123	3543	22	1113	4543	22	1122	4443	21	23
24	2332	3222	19	2233	3322	20	2333	3322	21	24
25	4233	3322	22	4322	3322	21	5432	2222	22	25
26	4421	2254	24	4422	3253	25	4321	1146	22	26
27	3478	5446	41	3478	5547	43	5367	4567	43	27
28	4233	3443	26	4333	3442	26	4333	2442	25	28
29	1321	2222	15	2321	3222	17	2321	3122	16	29
30	3221	1232	16	2232	2232	18	2121	2132	14	30
31	1111	3221	12	1012	3322	14	1012	3222	13	31

Journal of Atmospheric and Terrestrial Physics, 1961, Vol. 22, p. 232. Pergamon Press Ltd. Printed in Northern Ireland

Papers to be published in future issues

T. ONDOH: Variations of the earth's exosphere and geomagnetic disturbances during the geomagnetic storm of 4 September 1958

G. S. KENT: High frequency fading of the 108 Mc/s wave radiated from an artificial earth satellite as observed at an equatorial station

R. NAISMITH and P. A. SMITH: Further evidence of a long term variation in the relationship of solar activity to the ionosphere

W. BECKER: The varying electron density profile of the F-region during magnetically quiet nights

R. K. SURYANARAYANA: Effect of radio fade-out on the $F2$-layer

R. G. RASTOGI: The morphology of lunar semi-diurnal variation of f_0F2 near solar noon

R. G. FLAVELL and J. A. LANE: The application of potential refractive index in tropospheric wave propagation

M. A. UMAN: Bead lightning and the pinch effect

R. E. BARRINGTON and E. THRANE: The determination of D-region electron densities from observations of cross modulation

B. HULTQVIST: On the orientation of auroral arcs

J. K. HARGREAVES: The behaviour of the lower ionosphere near sunrise

M. W. CHIPLONKAR, R. N. KAREKAR and P. R. MARWADI: Midnight fall in atmospherics activity of 27 kc/s band at Poona

VOL.
22
1961

Journal of Atmospheric and Terrestrial Physics. 1961, Vol. 22, pp. 233 to 254. Pergamon Press Ltd. Printed in Northern Ireland

Variations of the earth's exosphere and geomagnetic disturbances during the geomagnetic storm of 4 September 1958

T. ONDOH
Geophysical Institute, Kyoto University, Kyoto, Japan

(*Received* 5 *July* 1961)

Abstract—The time variations of D_S and D_{st} for the geomagnetic storm of 4 September 1958 have been calculated using hourly values of the horizontal component of the geomagnetic field over the world. These D_{st} and D_S have been compared with the observation of the earth's exosphere by Explorer IV and that of auroral radio echoes during the same period. During this geomagnetic storm marked decrease in the intensity of trapped radiations was observed in the outer zone and brilliant auroral displays were observed at latitudes well below the auroral zone. The time variations of D_S at geomagnetic latitudes of 57–58° have indicated the largest deviation of all ones at other latitudes. All peaks of D_S at high latitudes and auroral radio echoes at Jodrell Bank occurred for the main phase of this geomagnetic storm. The time variations of D_S at low latitudes have shown only a little deviation and have been almost relatively unvariable compared with ones at high latitudes during the geomagnetic storm. From the analyses of D_S at high latitudes it is deduced that the exospheric region within the inner boundary of the outer zone, where is is located along the geomagnetic lines of force intersecting the earth's surface at geomagnetic latitudes of about 50°, was not so much disturbed by the invasion of solar plasma cloud. It is considered that the dumping of part of the contents of the outer earth's exosphere, which interprets well the reduction in the intensity of trapped radiations in the outer exosphere, produces regions of comparatively high ionization which are detectable as auroral radio echoes and D_S of geomagnetic disturbances. It has been shown that the time variations of D_S at the auroral and the sub-auroral zones represent reasonably well the extent of disturbance of trapped radiations in the outer exosphere during the geomagnetic storm. The equatorward shifting of latitude of the maximum strength of chorus and hiss during the geomagnetic storm may be due to the inaction of generation mechanism of v.l.f. emissions in the exospheric region where the geomagnetic lines of force intersecting the auroral zone pass through during the geomagnetic quiet period, in addition to the equatorward shifting of precipitation of auroral particles during the geomagnetic storm. Statistical results of v.l.f. emission suggest that the electron density distribution given by the gyrofrequency model may not exist along the geomagnetic lines of force intersecting the earth's surface at the auroral zone during the geomagnetic storm. D_{st} at the auroral zone has shown larger deviation from the prestorm level for the main phase, sharper recovery after the main phase, and earlier recovery for the recovery phase than ones at the middle and the equatorial zones. This slow and late recovery of equatorial D_{st} and small variation of equatorial D_S may support the existence of the equatorial ring current around the earth. A simple model of the state of earth's exosphere during the main phase of the storm has been proposed.

1. INTRODUCTION

THE relation of polar ionospheric phenomena to the decrease in the intensity of trapped radiations in the outer zone and the invasion of auroral particles during geomagnetic storms has become an important geophysical problem in recent years. ANDERSON (1958) observed a close correlation between the occurrence of X-rays at high altitude and a geomagnetic storm. WINCKLER *et al.* (1959) found that strong X-ray bursts recorded at balloon altitude appeared coincident with large magnetic bays, strong cosmic absorption, and passage across the zenith of a very large amount of auroral luminosity. ROTHWELL and MCILWAIN (1960) have suggested that the intensity decreases in the outer radiation zone are due largely to increased scattering and absorption of trapped charged particles produced by atmospheric heating and expansion at fairly high latitudes during geomagnetic storms. ARNOLDY *et al.* (1960) have shown that the radiation dumped from the outer zone during the geomagnetic storm coincides very well with the intensity and latitude distribution

required to account for balloon observation of auroral X-rays. It is well known that the auroral display and the geomagnetic bay have a close correlation at high latitudes and that the polar geomagnetic storm is composed of some polar elementary storms which are almost the same as the geomagnetic bay and are well represented by an overhead current system composed of an intense westward current with narrow longitudinal width along the auroral zone (NAGATA and FUKUSHIMA, 1952; FUKUSHIMA, 1959). BULLOUGH *et al.* (1957) and WATKINS (1961) have confirmed that the geomagnetic disturbances are associated with comparatively high ionization regions which move in an east–west direction and which are detectable as auroral radio echoes. It is considered that these polar elementary storms are almost composed of D_S component. The purpose of this paper is to study the relation of D_S at high latitudes to the intensity decrease of the trapped radiations in the outer zone, auroral phenomena and v.l.f. emissions and that of D_{st} to the existence of a ring current around the earth during the geomagnetic storm.

CROUCHLEY and BRICE (1960), YOSHIDA (1960) and ONDOH *et al.* (1961) have found that the region of maximum average chorus strength and occurrence moves towards lower latitudes during the geomagnetic storm. ALLCOCK (1957), POPE (1960) and ONDOH (1961) have suggested that the origin of dawn chorus lies on the Störmer's orbit of protons in the earth's exosphere. The presence of such protons is confirmed by the auroral displays and auroral zone blackouts (HAKURA *et al.*, 1958; OBAYASHI and HAKURA, 1960). As for the ring current around the earth, its presence has been discovered using the deviation of observed geomagnetic field from the geomagnetic dipole field with Explorer VI and Pioneer V (SMITH *et al.*, 1960).

VOL. 22 1961

2. METHOD OF ANALYSIS AND THE DATA USED

The total geomagnetic disturbance D during the geomagnetic storm is represented as follows:

$$D = D_{st} + D_S + S_q$$

where D_{st} is the storm time variation, D_S the disturbance longitudinal inequality and S_q the quiet daily variation. When D_S is averaged over a whole day, these variations are called disturbance daily variations S_D. The solar daily variation of the geomagnetic field at geomagnetic latitudes above the auroral zone is in general very small except for the mid-summer, but there is some deviation from the base value of each observatory on the geomagnetic quiet day even at high latitudes. Therefore to take up quantitatively the pure geomagnetic storm effect on D_{st} and D_S, we must take into consideration S_q as the quiet daily deviation from the base value even at high latitudes. The geomagnetic data used in this study are the hourly values of the horizontal component of the geomagnetic field over the world and K-indices for some parts of the polar region. The observatories of above mentioned geomagnetic data are given in Table 1.

The data of auroral radio echoes used in this study were obtained by WATKINS (1961) at Jodrell Bank which was approximately geomagnetically south of the geomagnetic observatories Eskdalemuir and Lovö on 4–5 September 1958. These auroral radio echoes are compared with D_{st} and D_S in Fig. 17 and Fig. 1. Analyses

Table 1. The list of geomagnetic observatories

Observatory	Abbrev.	Geomag. lat.	Geomag. long.	Observatory	Geomag. lat.	Geomag. long.
Tikhaya Bay		71° 31′	153° 15′	Odessa	43° 42′	111° 00′
College	Co	64° 42′	256° 30′	Memambetsu	34° 06′	208° 18′
Murmansk	Mu	64° 06′	126° 30′	Tashkent	32° 30′	143° 48′
Dixon Is.		63° 00′	161° 24′	Vladivostock	32° 18′	197° 54′
Lerwick		62° 30′	88° 36′	San Juan	29° 54′	3° 18′
Tixie Bay	Ti	60° 36′	191° 18′	Honolulu	21° 00′	266° 24′
Sitka	Si	60° 00′	275° 24′	Guam	3° 54′	212° 48′
Lovö	Lo	58° 12′	105° 48′	Addis Ababa	4° 46′	109° 44′
Leningrad	Le	56° 12′	117° 18′	Luanda	−7° 06′	80° 36′
Yakutsk	Ya	51° 00′	198° 48′	Trivandrum	−18° 36′	145° 33′
Fredericksburg	Fr	49° 36′	349° 54′	Amberley	−47° 36′	252° 36′
Kazan	Ka	49° 18′	130° 30′	Macquarie Is.	−61° 06′	243° 06′
Lvov	Lv	48° 06′	105° 54′	Scott Base	−78° 50′	245° 32′
Tihany		46° 24′	99° 06′			

of observations from Explorer IV given by ROTHWELL and MCILWAIN (1960) are used as the data of the outer radiation zone during the same period. It is well known that about two-thirds of the geomagnetic variation is of external origin, but we shall not pay attention to this factor in this paper hereafter.

3. Variations of the Outer Radiation Zone and D_{st} at High Geomagnetic Latitudes

The satellite and balloon observations during the I.G.Y. have shown that the bursts of auroral X-rays which are associated with the passage of large auroral luminosity across the zenith, correspond closely to the intensity decrease of trapped radiations in the outer zone, where the geomagnetic lines of force intersecting the auroral zone and below pass through, during the geomagnetic storm (WINKLER, 1960). Such observations are briefly reviewed and then the relation between latitude distribution of D_{st} over the world and the aboved-mentioned phenomena is indicated in this Section.

On the night of 16/17 August 1959 a typical strong storm aurora, which has always been correlated with the occurrence of an auroral X-ray burst, was observed visibly from geomagnetic latitudes of 58–54°. After *sc* on 16 August a large loss of radiation from the outer zone that corresponded to about two-thirds of the detectable radiation existing in the outer zone before *sc*, was observed during the first 24 hr of this storm. On the assumption that it is discharged down along the corresponding geomagnetic lines of force, the location on the earth's surface where this radiation must be precipitated has been computed. Its result has indicated that the radiation lost from the outer zone (electrons of approximately 50 keV energy) is dumped between geomagnetic latitudes of 52° and 62° with a peak intensity around ~57–58° and that enough radiation is lost from the outer zone to account completely for balloon observations of auroral X-rays (ARNOLDY *et al.*, 1960).

The probability of detecting auroral radio echoes has been dependent on the degree of geomagnetic disturbances. Moderate and severe geomagnetic disturbances are associated with regions of comparatively high ionization which move in an east–west direction and which are detectable as the large majority of auroral radio echoes (BULLOUGH *et al.*, 1957; WATKINS, 1960). It is well known that the auroral

display means the invasion of auroral protons which ionize particles in the polar ionosphere.

The auroral zone black-out during the geomagnetic storm is regarded as the invasion of low energy solar protons due to reduced geomagnetic cut-off energies by the geomagnetic perturbations (HAKURA *et al.*, 1958; OBAYASHI and HAKURA, 1960). HAKURA *et al.* (1961) have suggested the presence of an auroral zone current at the level of 100 km where both the auroral zone blackout and E_s appear. Low energy solar cosmic rays were also detected when the auroral display and the auroral X-rays occurred at the sub-auroral zone (WINCKLER and BHAVSAR, 1960). Thus we can certainly consider the invasion of protons during the geomagnetic storm as the cause of geomagnetic disturbances. But as FERMI (1950) has indicated

$$\left(\frac{dE}{dx}\right)_{\text{ion.}} \Big/ \left(\frac{dE}{dx}\right)_{\text{rad.}} = \frac{800}{ZE}$$

where Z is the atomic number of stopping matter and E is the electron energy in MeV, the ionization loss for the electrons producing auroral X-rays ($E = 50 \sim 100$

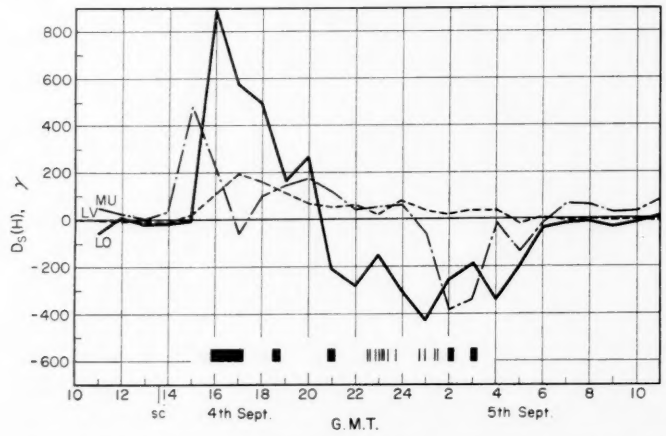

Fig. 1. Time variations of D_S at Murmansk (64° 06′, 126° 30′), Lovö (58° 12′, 105° 48′) and Lvov (48° 06′, 105° 54′) on 4 and 5 September 1958. *sc*: 1339 GMT, 4 September 1958.

keV) is greater than the radiation loss in the ionosphere. Therefore we can consider that geomagnetic disturbances are caused by the invasion of electrons which raises the conductivity of the ionosphere E-layer and produces auroral X-rays, as well as by that of auroral protons into the polar ionosphere.

A "double" geomagnetic storm occurred at 0848 U.T. on 3 September and 1339 U.T. on 4 September 1958. The former was weak and the latter was great. The time variations of D_S of the horizontal geomagnetic field during this geomagnetic storm at high geomagnetic latitudes are shown from Figs. 1–4. Intermittent bands of the lower part in Fig. 1 show the durations of the auroral radio echoes observed at Jodrell Bank which is approximately geomagnetically south of

VOL. 22 1961

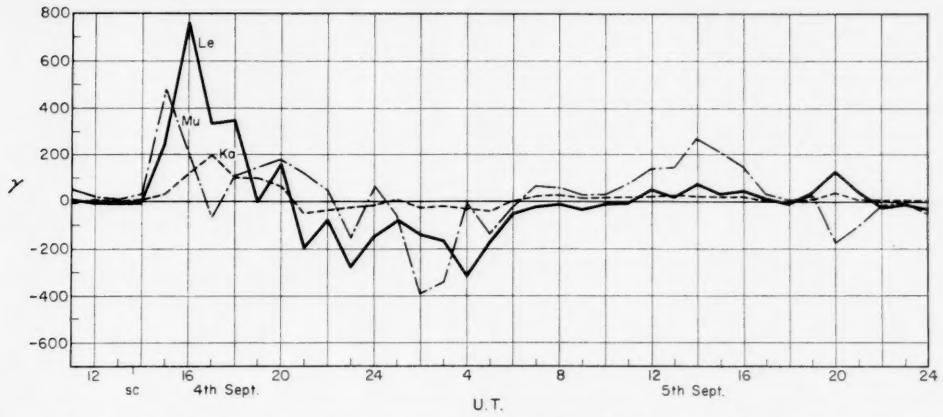

Fig. 2. Time variations of D_S at Murmansk, Leningrad and Kazan on 4 and 5 September 1958.

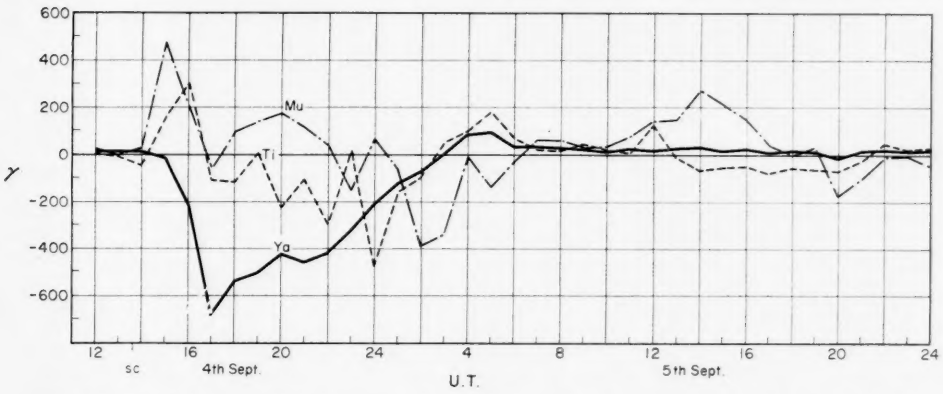

Fig. 3. Time variations of D_S at Murmansk, Tixie Bay and Yakutsk on 4 and 5 September 1958.

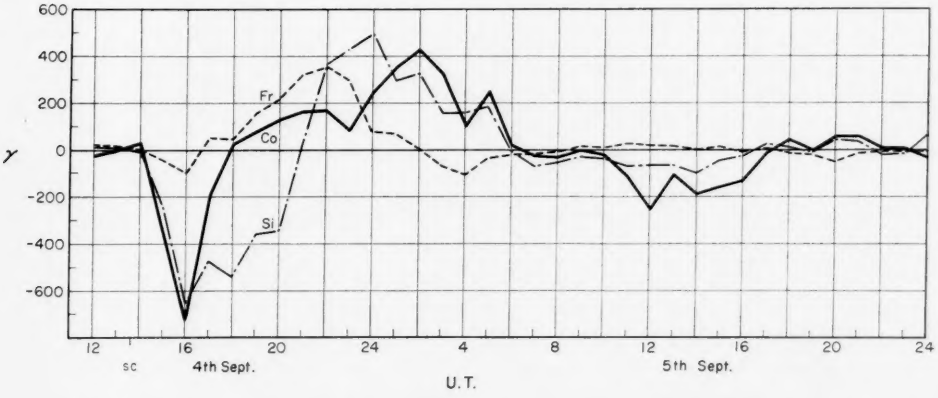

Fig. 4. Time variations of D_S at College, Sitka and Fredericksburg on 4 and 5 September 1958.

Lovö. The durations of auroral radio echoes correspond well to positive and negative peaks of D_S at Lovö (geomag. lat. 58°12′) which is well below the auroral zone during the geomagnetic storm of 4 September. In fact brilliant auroral displays were observed at latitudes well below the auroral zone in many parts of the world on the night of 4/5 September 1958. Before this "double" storm there was a broader maximum in counting rate of the unshielded counter carried in Explorer IV at about 50° latitude in the outer zone. But from 4 to 5 September after the second *sc* there was a large decrease in the intensity of trapped particles in the outer zone and in the Argus shell: over North America the outer zone peak practically disappeared, and over Australia its intensity diminished by about an order of magnitude. The drag data on Explorer IV (SCHILLING and WHITNEY, 1959) have shown that there is a general dependence of satellite drag on magnetic activity that is greater at higher than at lower latitudes. The orbital acceleration of satellite is usually assumed to be approximately proportional to the air density at perigee. The strong decrease in the intensity of the outer zone during the same period occurred soon after the sharp increase in orbital acceleration at high latitudes (JACCHIA, 1959).

The increased atmospheric density at relatively low altitudes causes increase of scattering and absorption of trapped particles with low mirror points. Therefore the intensity decreases are observed at the lower tips of the trapped radiation belt and intensity increase may be found beneath the outer zone (ROTHWELL and MCILWAIN, 1960).

In Figs. 1–3 the time variations of D_S at geomagnetic latitudes of about 58–54°, such as Lovö, Leningrad and Yakutsk, represent larger excursions than ones at the auroral zone and at the geomagnetic latitude of about 48° for the main phase of the geomagnetic storm on 4 September. In Fig. 4 D_S at Sitka (60°00′) is not considerably different from one at College (64°42′) but is much different from one at Fredericksburg (49°36′).

The above facts suggest the conclusion obtained by WATKINS (1961) that the north–south extent of comparatively high ionization is less than about 3° of latitude. It is likely that the increased particles (electrons of 50 $\sim$ 100 keV energy) observed beneath the outer zone invade the polar ionosphere and produce the regions of comparatively high ionization of which movement is detected as D_S at high latitudes (around 57° in our case).

In Figs. 1–4 it is shown that the first positive or negative peak of D_S at all high latitudes occurred from about 1·5 to 2·5 hr after *sc* on 4 September and its maximum excursion occurred at the sub-auroral zone. This result means that the radiation (electrons) dumped from the outer zone or the invasion of auroral protons occurred along the geomagnetic latitude around 57° during this period. Such an explanation of D_S at high latitudes may account for the conclusion reached by ANDERSON (1959) that, although strong X-ray bursts are observed under visible auroras in latitudes below the auroral zone, balloon observations of auroras in the auroral zone show only weak X-rays.

The time variations at Fredericksburg (geomag. lat. 49°36′), Kazan (49°18′) and Lvov (48°06′) have shown small variations compared with ones at geomagnetic latitudes above 51° during this geomagnetic storm. This fact suggests that the

exospheric region within the inner boundary of the outer zone, which is approximately located along the geomagnetic lines of force intersecting the earth's surface at geomagnetic latitude of about 50°, was not so much disturbed by the invasion of solar corpuscular stream and did not lose much trapped radiation existing there during the geomagnetic storm.

Comparing the time variations of D_S at high latitudes with those of D_{st} at three zones in Fig. 17, we can find that variations of D_S at latitudes below about 60° recovered soon after the end of the main phase but those at latitudes above 60° still showed disturbances for the recovery phase and that the time variations at latitudes below about 50° recovered earlier than those at latitudes from 60° to 50°. These results indicate that the geomagnetic disturbed state in the earth's exosphere recovers gradually from the inside of it. The counting rates of the unshielded counter in the outer zone returned nearly to prestorm level after the geomagnetic storm. The shielded counter showed considerably higher counting rates over both North America and Australia after the storm. The increase in the counting rates of the shielded counter which suggests the increase of the average energy of particles in the outer zone, began late on 5 September (ROTHWELL and MCILWAIN, 1960). The time variations of D_S at geomagnetic latitudes above 60° showed again relatively small variations late on 5 September as shown in Figs. 1–4. These variations of D_S at latitudes above 60° for the recovery phase may be caused by the direct invasion of very low energy solar protons or the invasion of charged particles having the increased energy from the external side of the outer radiation zone. The average energy of trapped particles in the outer zone may increase as a result of perturbation of the magnetic field due to the arrival of solar plasma cloud. The sharp-crested hydromagnetic waves have been observed at geocentric distances of 12·3–14·6 earth radii by Pioneer I. The observations of the diminution in the amplitudes of these waves in the earth's exosphere have indicated that they are dissipative and lose a large fraction of their energy in the region of 7–13 earth radii (COLEMAN *et al.*, 1960; SONETT *et al.*, 1960). Therefore we can expect the presence of such as Fermi acceleration for the charged particles due to these waves in the exosphere.

Observations by Explorer VI and VII have shown that later in the storm the outer zone increased to much in excess of its prestorm level and such a situation developed over 2 days. This fact provides strong evidence for the local acceleration of trapped electrons within the geomagnetic field with a characteristic time of the order of 1 day (ARNOLDY *et al.*, 1960; VAN ALLEN and LIN, 1960). Pioneer III and Pioneer IV also observed the intensity increase of the outer radiation zone at large distances from the earth after the geomagnetic storm (VAN ALLEN and FRANK, 1959). The sign of D_S variations in Fig. 4 are opposite to that in Figs. 1–3. In other words this represents the phase difference with respect to the time among different points in the longitude and corresponds to S_D current system in the ionosphere at high latitudes.

Next we analyse D_S at high latitudes during the small geomagnetic storm of 3 September 1958 which preceded the geomagnetic storm of 4 September 1958. As shown in Figs. 5–8 and in Fig. 18, the geomagnetic storm of 3 September recovered approximately to its prestorm level about 20 hr after *sc* and this storm possibly did

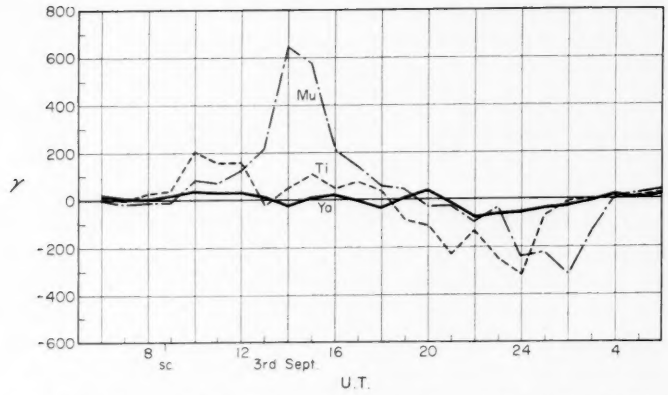

Fig.5. Time variations of D_S at Murmansk, Tixie Bay and Yakutsk on 3 September 1958.

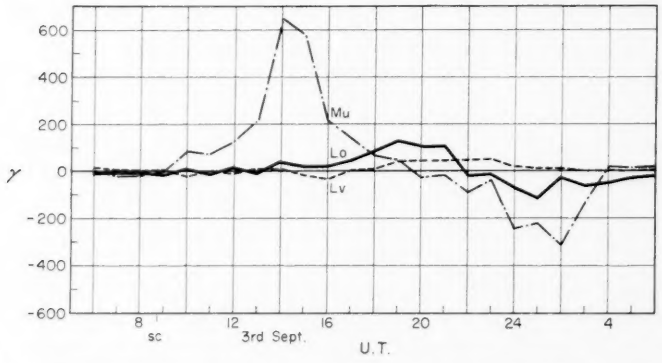

Fig. 6. Time variations of D_S at Murmansk, Lovö and Lvov on 3 September 1958.

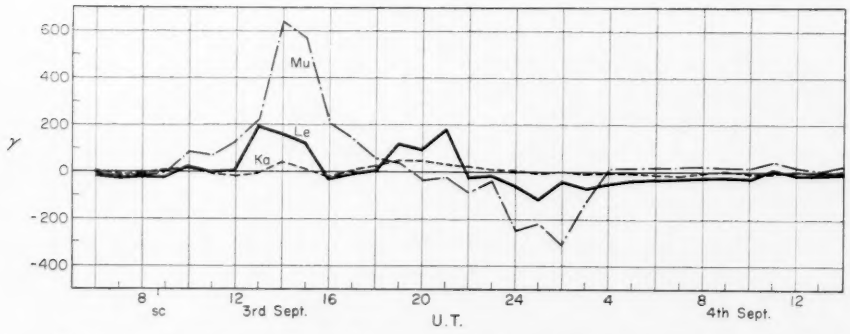

Fig. 7. Time variations of D_S at Murmansk, Leningrad and Kazan on 3 September 1958.

VOL.
22
1961

not have so much after-effect on the geomagnetic storm of 4 September. In other words it is deduced that the geomagnetic state of the outer zone was relatively calm from about 0500 to 1200 U.T. on 4 September.

It is shown in Figs. 5–8 that variations of D_S at the auroral zone were markedly larger than those at latitudes below the auroral zone during the course of this storm. After *sc* of the geomagnetic storm of 3 September 1958 some decreases in the outer zone and in two Argus electron shells were observed and the high latitude increase in the shielded counter rate disappeared (ROTHWELL and MCILWAIN, 1960). The smaller decrease of trapped radiation in the outer zone compared with the case of

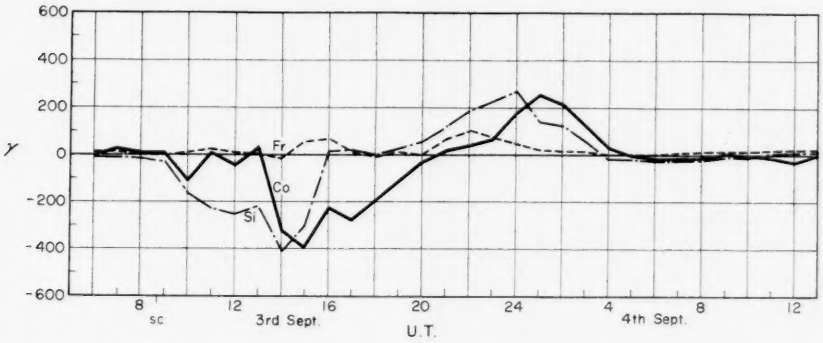

Fig. 8. Time variations of D_S at College, Sitka and Fredericksburg on 3 September 1958.

4 September may explain small variations of D_S at latitudes below the auroral zone. The radiation dumped from the external part of the outer zone or the direct invasion of solar protons which was not observed with the satellite, may be able to explain the time variations of D_S at the auroral zone during the geomagnetic storm of 3 September. From the above results we can deduce that the exospheric region within the boundary which is located along the geomagnetic lines of force intersecting the earth's surface at geomagnetic latitudes of ~53–51°, was not considerably disturbed by the solar corpuscular stream and did not lose a large amount of the trapped radiation during this storm. A small increase in counting rate in the shielded counter was seen at high latitudes along the satellite orbit in both northern and southern hemispheres on 1–3 September. But we can not detect this effect on D_S and D_{st} on 3 September. Positive or negative peaks of D_S at high latitudes occurred first 4–5 hr after *sc* which started at 0843 U.T. on 3 September. On the one hand positive or negative peaks of D_S at high latitudes occurred first 1·5–2·5 hr after *sc* which started at 1339 U.T. on 4 September. This earlier occurrence of the first positive or negative peak of D_S after *sc* on 4 September was due to the after-effect of the geomagnetic storm of 3 September or the earlier arrival of large amount of solar plasma cloud on 4 September. It is likely that the external part of the outer zone had become sensitive to the geomagnetic excitation by the impact of solar plasma cloud on the geomagnetic field, in addition to the invasion of a large amount of the solar plasma due to the decrease of the strength of geomagnetic field that was caused by the decayed equatorial ring current of the preceded storm

around the earth. In order to know the situation in the polar cap region during these storms, we show graphs of the time variation of the K-index in Figs. 9 and 10. It is shown that K-indices, i.e. the geomagnetic activities in the polar cap region, were small compared with those at latitudes of the auroral zone and below during this double storm. The geomagnetic activity in the polar cap region is always smaller than that at the auroral zone during the geomagnetic storm (ONDOH and MAEDA, 1961).

WATKINS (1961) has found that the occurrence of auroral radio echoes, which

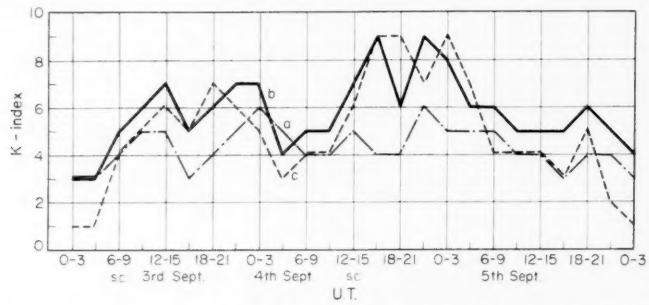

Fig. 9. Time variations of K-index at (a) Tikhaya, (b) Dixon Is. and (c) Leningrad on 3–5 September 1958.

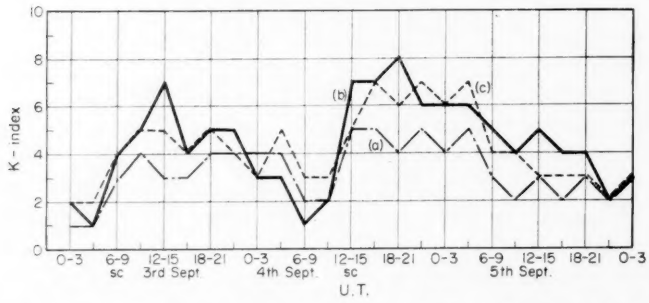

Fig. 10. Time variations of K-index at (a) Scott Base, (b) Macquarie Is. and (c) Amberley on 3–5 September 1958.

is a parameter of the invasion of charged particles into the ionosphere, is closely related to the local geomagnetic activity, i.e. K-index. Therefore it is deduced that the amount of charged particles invading into the polar cap region was small during the geomagnetic storms of 3 and 4 September. The variations of D_S during the geomagnetic storms of 3 and 4 September recovered completely about 24 hr after *sc*. Thus the elapsed time of D_S variation agrees well to one from the beginning to the maximum of the intensity decrease of trapped radiation in the outer zone. From the above analyses we have found that D_S observed at high geomagnetic latitudes from about 60–51° corresponds well with the radiation dumped from the outer zone.

Next we try to explain the density variation of charged particles trapped by the geomagnetic field in the earth's exosphere during the geomagnetic storm. The

VOL. 22 1961

plasma particles spiralling around the geomagnetic lines of force have magnetic moments which tend to reduce the magnetic field in the interiors of their orbits. Such diamagnetic effects of trapped particles (protons or electrons) in the earth's exosphere were first pointed out by KELLOG (1959). Inside the earth's exosphere, next expression will hold good as

$$B = H - 4\pi N \frac{\frac{1}{2}.mV_{\perp}^2}{B} \tag{1}$$

when

$$\frac{1}{B}|(r.\mathrm{grad})B| < 1 \text{ and } \frac{T}{B}\left|\frac{dB}{dt}\right| < 1$$

where B is the flux density of the geomagnetic field, H the applied magnetic field strength (the geomagnetic field in the vacuum), N the number density of particles, m the mass of a particle, $V_{\perp}$ the velocity component of particles perpendicular to the direction of B, $r = mV_{\perp}c/eB$ the radius of gyration, $T = 2\pi mc/eB$ the period of gyration, e the electric charge of a particle and c the velocity of light. We neglect the effect near the edges of the plasma. We solve the equation (1) with respect to B. Then we obtain solutions of B as

$$B = \frac{H \pm \sqrt{(H^2 - 8\pi N m V_{\perp}^2)}}{2}. \tag{2}$$

A solution of $B = [H - \sqrt{(H^2 - 8\pi N m V_{\perp}^2)}]/2$ becomes $B = 0$ when $N = 0$. Such a situation is physically unreasonable and so we neglect this solution having a negative sign at the plus or minus sign of solution (2). Particle density N is expressed as

$$N = \frac{1}{2\pi m V_{\perp}^2} B(H - B).$$

When H and $V_{\perp}$ are constant, N becomes the maximum of $H^2/8\pi m V_{\perp}^2$ and the minimum of zero at $B = H/2$ and $B = H$ respectively. In other words the magnetic flux B reaches the minimum of $H/2$ when the energy density of the plasma is equal to one-half of the energy density of the applied magnetic field. The above results are shown as

$$0 \leqq N \leqq \frac{H^2}{8\pi m V_{\perp}^2} \text{ for } H \geqq B \geqq \frac{H}{2}. \tag{3}$$

The applied magnetic field (the geomagnetic field in the vacuum) is decreased by the ring current around the earth mainly for the main phase and the recovery phase of the storm. Considering always only particles which have constant value of $V_{\perp}$ at a given point in space, from expression (3) we can expect that the allowable maximum density of particles which have constant value of $V_{\perp}$ at a given point in space and trapped by the geomagnetic field there, decreases with decreasing the strength of geomagnetic field for the main and the recovery phases of the storm. Especially the effect of the ring current around the earth on the magnetic field may be most effective in the outer radiation zone.

Therefore a part of particles which have a given energy and are trapped at a

given point in the outer radiation zone for the geomagnetically quiet period, may become unable to be confined by the geomagnetic field at that point in space for the main phase of the storm. Such particles being unable to be trapped by the geomagnetic field at a given point will move down along the geomagnetic lines of force passing through there because charged particles can move most easily in the direction of the geomagnetic line of force. When the geomagnetic field B is decreased by the ring current and the kinetic energy of particles is constant, the angle between the velocity vector of trapped particles and the geomagnetic field θ becomes small following the expression of $\sin^2 \theta/B = \text{const}$. Therefore we can expect the penetration of trapped particles into the polar ionosphere during the geomagnetic storm without the variation of their magnetic moments. But such effects can become effective only after the formation of the ring current. And so the first peaks of D_S which occurred uniformly along the auroral and the sub-auroral zones 1·5–2·5 hr after *sc* on 4 September may be due to the direct invasion of so-called auroral particles.

4. Variations in the Inner Radiation Zone and D_S at Low Geomagnetic Latitudes

The flight of Pioneer IV was preceded by five consecutive nights of strong auroral activity, whereas the periods preceding the flights of Pioneer III were especially quiet geophysical periods. On the occasions of the two flights the inner zone was not significantly different. From this fact Van Allen and Frank (1959) have concluded that the inner zone, lying as it does in the region of strong geomagnetic field, is relatively well isolated from direct solar influence. Explorer IV, orbiting rather close to the earth, cut through the inner zone at low latitudes during 3–5 September and observed that the inner zone intensity apparently remained unchanged (Rothwell and McIlwain, 1960). It is shown in Figs. 11–16 that

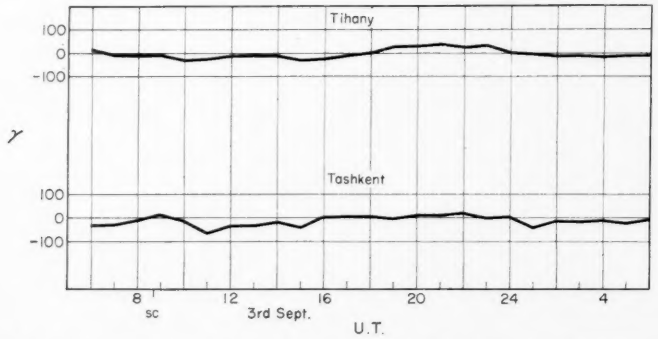

Fig. 11. Time variations of D_S at Tihany and Tashkent on 3 September 1958.

variations of D_S at low geomagnetic latitudes were within ± 100 gammas during the course of the geomagnetic storms on 3 and 4 September and that the time variations of D_S at low geomagnetic latitudes remained relatively unvariable as the geomagnetic storms developed. The satellite observations have shown that the outer boundary of the inner radiation zone is located along the geomagnetic lines

VOL. 22 1961

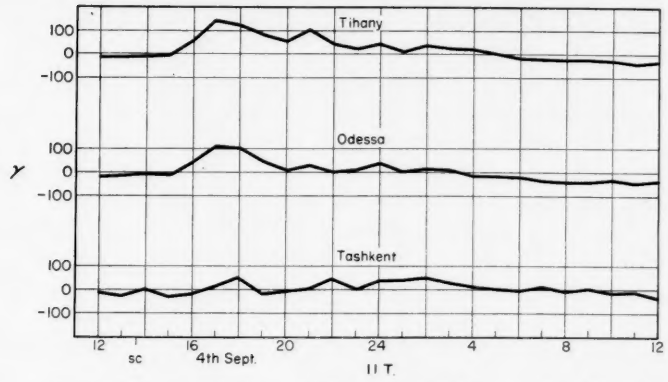

Fig. 12. Time variations of D_S at Tihany, Odessa and Tashkent on 4 September 1958.

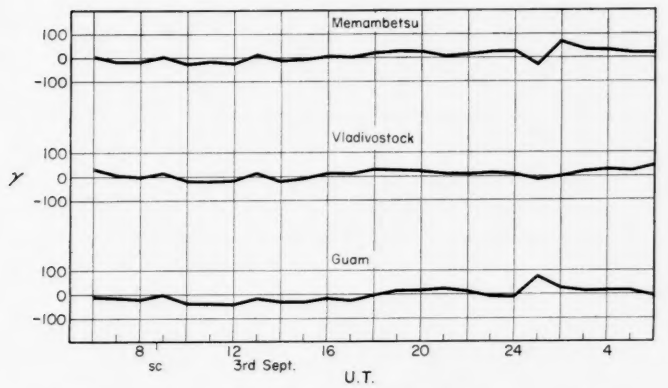

Fig. 13. Time variations of D_S at Memambetsu, Vladivostock and Guam on 3 September 1958.

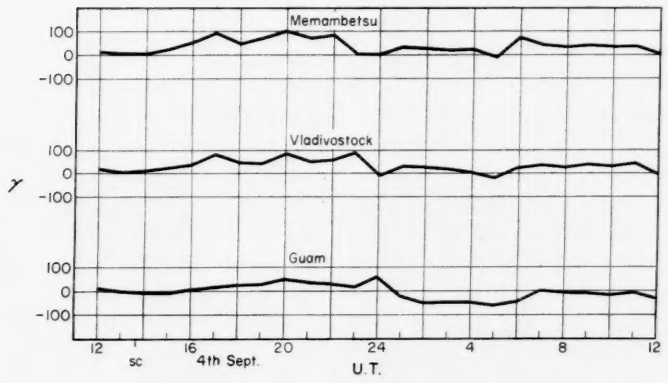

Fig. 14. Time variations of D_S at Memambetsu, Vladivostock and Guam on 4 September 1958.

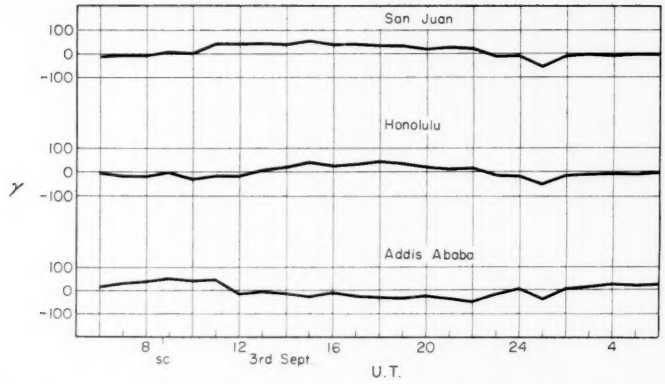

Fig. 15. Time variations of D_S at San Juan, Honolulu and Addis Ababa on 3 September 1958.

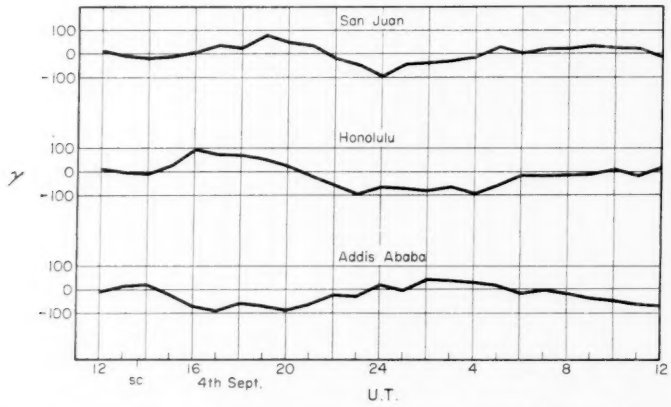

Fig. 16. Time variations of D_S at San Juan, Honolulu and Addis Ababa on 4 September 1958.

of force intersecting the earth's surface at geomagnetic latitude of about 45° (VAN ALLEN and FRANK, 1959; VERNOV and CHUDAKOV, 1959).

The above results of D_S at low latitudes are explained by consideration of the fact that the inner zone had suffered little influence of the solar corpuscular stream and that the radiations dumped from the inner zone were very small during the geomagnetic storm.

Figs. 12–14 show a tendency for variations of D_S at low latitudes to increase slightly with increasing geomagnetic latitude during the geomagnetic storm of 4 September. But Fig. 16 shows that there was little difference among the magnitude of variations of D_S at geomagnetic latitudes below 30° during this double storm. Comparing Figs. 11, 13 and 15 with Figs. 12, 14 and 16 respectively, we find that variations of D_S on 4 September were larger than those on 3 September even at low geomagnetic latitudes.

From the above analyses of D_S at low geomagnetic latitudes we can deduce that the cause of D_S at low latitudes during the geomagnetic storm may be mainly

VOL. 22 1961

the ionospheric current having leaked from the origin at high latitudes of the so-called S_D current system and that when the geomagnetic storm is great, this leakage current in the ionosphere may be also strengthened by the larger amount of ionization in high latitude ionosphere due to the invasion of charged particles from the outer radiation zone, in addition to the invasion of auroral particles.

5. V.L.F. Emissions and the Variation of the Earth's Exosphere During the Geomagnetic Storm

The geomagnetic latitude effect of time of maximum occurrence of chorus means that chorus is generated by the incoming protons from the sun (Allcock, 1957; Pope, 1956, 1960; Crouchley and Brice, 1960). Therefore the origin of chorus may lie on the Störmer's orbit of protons at distances less than about 4 earth radii from the centre of the earth where the condition of the generation of chorus holds good (Gallet, 1959; Ondoh, 1961).

The amplification of v.l.f. radio waves of whistler mode by the mechanism similar to the travelling wave tube can exist in the earth's exosphere (Bell and Helliwell, 1959; Barrington, 1959; Maeda and Kimura, 1961). Crouchley and Brice (1960) and Yoshida (1960) have found that the average strength or the occurrence probability of chorus increases with increasing value of K-index at lower latitude stations and shows a maximum at moderate value of K-index at geomagnetic latitudes of the auroral zone. The latter fact has been also found using the data at College, Alaska by Ondoh *et al.* (1961).

The variation of the electron density in the earth's exosphere, the equatorward shifting of the incidence of protons, the distortion of the geomagnetic field and the absorption of radio waves in the polar ionosphere are considered as the causes of the strength decrease of chorus received at the auroral zone during the geomagnetic storm. On the one hand the strength of chorus has a negative correlation to that of auroral radio echoes during the geomagnetic storm (Ondoh *et al.*, 1961).

The magnitudes of the horizontal component of geomagnetic disturbances between the northern and the southern geomagnetic conjugate points around the auroral zone have shown close correlations at all geomagnetic storm-time phases (Ondoh and Maeda, 1961). Assuming that the geomagnetic disturbances around the auroral zone are mainly caused by the incoming charged particles along the geomagnetic lines of force intersecting the earth's surface at the auroral zone during the geomagnetic storm, we can deduce that the geomagnetic lines of force are symmetrical around the geomagnetic equatorial plane. The geomagnetic data of Explorer VI have shown that the geomagnetic field retains its essentially dipolar character out to 8 earth radii during the geomagnetic storm (Smith *et al.*, 1960).

From the above facts we can expect that protons invade enough to cause chorus into the earth's exosphere and that the geomagnetic lines of force do not so much deviate from the state of the geomagnetically quiet period during the geomagnetic storm. The absorption of v.l.f. radio waves in the polar ionosphere is generally small. The condition for the coupling between the beam modes of charged particles and the radio waves of whistler mode to occur is expressed as

$$V = \frac{c}{n} \tag{4}$$

where V is the velocity of charged particles, n the local refractive index, and c the velocity of light (GALLET, 1959). The local refractive index for the radio waves of whistler mode is given by $n \simeq f_0/\sqrt{(ff_H)}$, where $f_0 = \sqrt{(Ne^2/\pi m)}$ is the plasma frequency, f the radio wave frequency, $f_H = eB/2\pi mc$ the electron gyrofrequency, N the electron density, B the flux density of the geomagnetic field, e the electronic charge and m the mass of an electron (STOREY, 1953).

The average geomagnetic storm is nearer to the geomagnetic storm of 3 September, 1958 than that of 4 September in scale and characteristics. As shown in Section 4, D_S at geomagnetic latitudes of 63–60° will show comparatively large variations during the average geomagnetic storm. The intensity of trapped radiation in the outer zone where the geomagnetic lines of force intersecting the earth's surface at latitudes of 63–60° pass through during the geomagnetically quiet period, will decrease considerably during the average geomagnetic storm. The decrease of electron density in the outer zone will result in the break-down of the condition (4), in other words the inaction of generation mechanism of v.l.f. emissions.

The data observed by Explorer VII during the geomagnetic storm of 1 April 1960 have shown a great depletion of the outer zone, its movement to much lower latitudes, the nearly complete absence of soft radiation at high geomagnetic latitudes, and the presence of an abnormal intensity of relatively penetrating radiation which is confined to geomagnetic latitudes exceeding 57° (VAN ALLEN and LIN, 1960).

YOSHIDA (1960) has found that the occurrence probability of hiss also shows a maximum at geomagnetic latitude 55° on storm days and a maximum at geomagnetic latitude around 60° on geomagnetically quiet days. At present the generation of hiss is explained by the same mechanism as chorus. In order to explain the steady tone of hiss of which the frequency characteristic is given by $f = f_0^2/f_H(V/c)^2$, the gyrofrequency model for the electron density distribution in the earth's exosphere has been postulated as $\dfrac{f_0^2}{f_H} \propto \dfrac{N}{B} = \text{const.}$ (GALLET, 1959; SMITH, 1960; DOWDEN, 1961). But YOSHIDA's result suggests that the electron density distribution postulated by the gyrofrequency model can not exist in the exospheric region along the geomagnetic lines of force intersecting the earth's surface at geomagnetic latitudes of 63–60° on the storm days. ELLIS (1960a) has proposed a possible explanation of v.l.f. emissions that Čerenkov radio emissions caused by the passage of high-speed charged particles through the earth's exosphere are superimposed on a steady background of radio noise due to the Van Allen particles in the v.l.f. range, and these superimposed radio waves are much more intense radio bursts than each one separately. As was pointed out by GALLET (1959) the frequency–time characteristic of hiss has no restriction such as the frequency bandwidth of chorus at any moment. This fact suggests that we may consider comparatively large-scale radio emissions as the origin of hiss. And so we consider Čerenkov radio emissions from an ionization column along the geomagnetic line of force, which consists of a number of high-speed electrons (10^2–10 per cm^3) dumped from the outer radiation zone and is several thousands kilometres in length, as the origin of hiss. In the earth's exosphere relatively near the earth,

VOL. 22 1961

i.e. less than about 4 earth's radii from the earth's centre, there is lateral stability of such high-speed electron beams (ONDOH, 1961).

Next supposing that the superimposed radio waves, which consist of the above-mentioned Čerenkov radio emissions and a background of radio noise due to Van Allen particles, are amplified by incoming auroral protons in a manner similar to the travelling wave tube at distances less than about 4 earth radii from the centre of the earth (ONDOH, 1961), we can obtain the incident power flux of hiss observed at the ground and the frequency characteristic of it under an assumption of a gain of amplification of several tens of decibels.

We now consider protons (1 MeV or less energy) which are related to auroral displays and the occurrence of the auroral zone blackouts. The auroral zone blackout which frequently occurs during the main phase of a geomagnetic storm and correlates with visible auroras and local geomagnetic disturbances, shows considerable equatorward shifting as the geomagnetic storm progresses (OBAYASHI and HAKURA, 1960). Such shifting of the auroral zone blackout may also correlate with that of hiss during the geomagnetic storm. The occurrence of the auroral zone blackouts do not always correspond to type IV outbursts of the solar radio waves. This fact also requires the hydromagnetic acceleration of charged particles in the earth's exosphere. ELLIS (1960b) has found that many *sc*'s were followed by bursts of v.l.f. noises or storms of them after an average delay of 8·5 hr, and many isolated noise bursts of less than 4 hr duration were associated with positive bays in the geomagnetic horizontal component at Camden, N.S.W. SUGIURA and CHAPMAN (1958) have obtained the results that the north component of D_S attains its maximum at about 9 hr of the storm time in all geomagnetic storms. These results suggest a close correlation between D_S and the occurrence of v.l.f. noise burst or storm at geomagnetic latitudes below the auroral zone during the geomagnetic storm. We cannot expect the invasion of auroral protons at low geomagnetic latitudes, therefore the v.l.f. emissions observed at low geomagnetic latitudes (OUTSU and IWAI, 1961) are explained only by the propagation of wave guide mode of v.l.f. radio waves penetrating the polar ionosphere between the ionosphere and the ground as tweek.

6. D_{st} of the Geomagnetic Storms on 3 and 4 September 1958

Graphs of the time variation of D_{st} during the geomagnetic storm of 3 and 4 September 1958 at the auroral, the middle, and the equatorial zones are given in Figs. 17 and 18. Common features of D_{st} on 3 and 4 September are that the recovery of D_{st} at the auroral zone was sharper than ones at the middle and the equatorial zones from the end of main phase to the initial part of recovery phase, and that D_{st} at the auroral zone recovered earlier than ones at other zones for the recovery phase. But recovery rate of D_{st} with respect to time was approximately constant for the recovery phase at each zone. Small differences of the magnitude of D_{st} variation among three zones except for differences between that at the auroral zone and ones at other zones for the main phase, and the same tendency of the time variation of D_{st} at three zones, suggest that D_{st} represents the effect of a large-scale geomagnetic phenomenon occurring distant from the earth such as

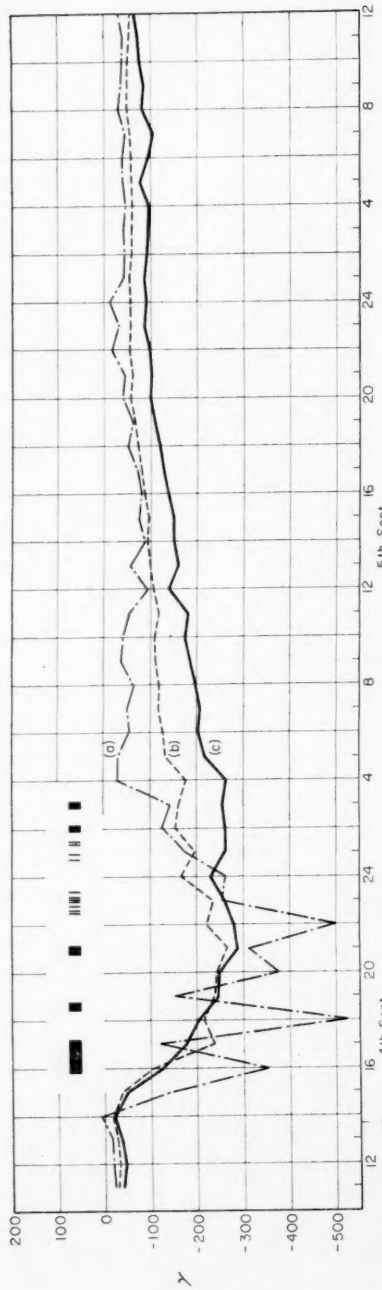

Fig. 17. Time variations of D_{st} at (a) the auroral, (b) the middle, and (c) the equatorial zones on 4 September 1958.

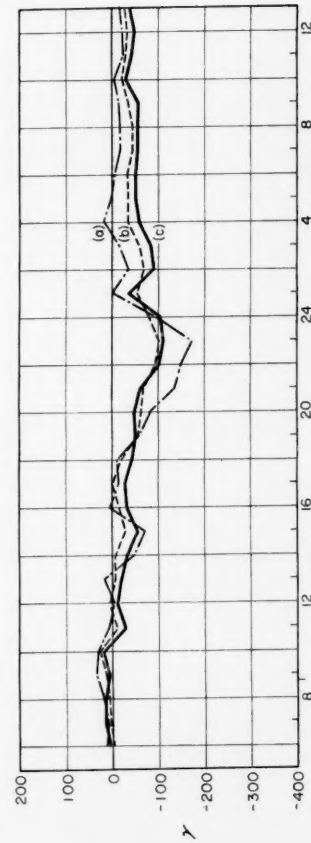

Fig. 18. Time variations of D_{st} at (a) the auroral, (b) the middle, and (c) the equatorial zones on 3 September 1958.

VOL.
22
1961

the ring current. From D_{st} on 3 and 4 September, the following deductions are derived:

(1) The main part of the origin of D_{st} for the main phase lies in the outer earth's exosphere and is unstable.
(2) The strength of the origin of D_{st} in the outer earth's exosphere is strong for the main phase but is very weak for the recovery phase.
(3) The life time of main origin of D_{st} for the main phase is short (about 12–20 hr).
(4) The main origin of D_{st} for the recovery phase lies distant from the earth and is stable for a long period.

VAN ALLEN and LIN (1960) have observed the rapid recovery of the outer zone, and the great enhancement of intensity of trapped radiation that followed the events of 31 March to 1 April 1959. This observation seems to support deductions (2) and (3) above. The intermittent bands at the upper part of Fig. 17 show the durations of auroral radio echoes observed at Jodrell Bank during the geomagnetic storm of 4 September 1958 (WATKINS, 1961). Comparing D_{st} at the auroral zone with the durations of auroral radio echoes, we can deduce that the invasion of charged particles from the sun or ones accelerated in the exosphere may have occurred along the auroral zone and below due to the decrease of the strength of geomagnetic field in the exosphere caused by the ring current around the earth for the main phase.

The elapsed time from *sc* to the maximum decrease of D_{st} on 4 September was shorter than that on 3 September. This fact may mean that the residual solar plasma particles of the geomagnetic storm on 3 September still remained on 4 September and the external part of the exosphere, or the boundary region between the earth's exosphere and the interplanetary space, had become sensitive to the geomagnetic excitation by the impact of solar plasma cloud on the geomagnetic field, in addition to the earlier arrival of a large amount of solar plasma particles on 4 September.

Charged particles which acquire large energy from the sharp-crested hydromagnetic waves in the boundary region (7–13 earth radii), invade deeply into the earth's exosphere and oscillate back and forth along the geomagnetic lines of force between the southern and the northern mirror points. Such motions of charged particles along the geomagnetic lines of force stress outwards the geomagnetic field (DESSLER and PARKER, 1959; AKASOFU, 1960). Such a situation may be observed as the decrease of the horizontal geomagnetic field at the earth's surface.

The observation of the geomagnetic field during the geomagnetic storm by Explorer VI has shown the following results (SMITH *et al.*, 1960):

(1) The geomagnetic field is strongly perturbed in the external part of the exosphere but retains an essentially dipolar character out to 8 earth radii.
(2) The distant field participates in the long period variations of D_{st}.
(3) The amplitude of the magnetic field decrease at 4 earth radii is several times larger than that at the earth's surface for the main phase.

From the above results SMITH *et al.* (1960) have concluded that a westward ring current (around 10 earth radii on the geomagnetic equatorial plane) gives

rise to a major large-scale perturbation of the distant geomagnetic field and has a radius about 3 earth radii.

Considering the above satellite observations and analysis of the geomagnetic data, we can deduce that the external part of the earth's exosphere acts as trigger mechanism against the solar corpuscular stream and as the acceleration one for the charged particles during the geomagnetic storm, and that the solar plasma cloud arriving in the neighbourhood of the earth during or after the main phase of the storm has a more magnetized character than one arriving before the main phase, and the deeper into the earth's exosphere the solar plasma particles invade, the earlier they become unstable and lose their energy.

7. Concluding Remarks

The time variations of D_S of the geomagnetic horizontal component observed at latitudes of 63–54° correspond well to the intensity decrease of trapped radiation in the outer exosphere during the geomagnetic storm. From the time variations of D_S, it is deduced that the exospheric region within the boundary which is located along the geomagnetic lines of force intersecting the earth's surface at a geomagnetic latitude of about 50° had not been much disturbed by the invasion of solar corpuscular stream during the geomagnetic storm of 4 September 1958. The fact that the average strength of the occurrence probability of chorus decreases with increasing geomagnetic activity at the auroral zone may be explained by the inaction of generation of the chorus mechanism in the exosphere where it is connected to the auroral zone by the geomagnetic lines of force. Therefore the electron density distribution given by the gyro-frequency model can not possibly exist in the exospheric region along the geomagnetic lines of force intersecting the earth's surface at the auroral zone during the geomagnetic storm. Solar plasma particles having large momentum invade deep into the exosphere and set up the broad westward ring current about which charged particles oscillate back and forth between lowered mirror points and stress the geomagnetic field outwards. Such a state of which hydromagnetic propagation may be observed as the decrease of D_{st} at the earth's surface during the main phase of geomagnetic storm, is possibly unstable and decay soon afterwards. The westward ring current relatively near the earth may begin to decay from the inside of the earth's exosphere. But the ring current may be stable for long periods in the boundary region between the earth's exosphere and the interplanetary space because of the lesser loss of charge and energy of charged particles.

Acknowledgements—The author wishes to express his sincere thanks to Professor Y. Tamura and Dr. H. Maeda for their kind direction and support of this work, to Professor K. Maeda and Dr. Y. Inoue for their valuable discussions and criticism, to Miss K. Tsuda and Miss T. Ozaki for their assistance, and also to the I.G.Y. World Data Centre C2 at Kyoto University for supply of geomagnetic data.

References

Akasofu S.	1960	*J. Geophys. Res.* **65,** 535.
Allcock G. M.	1957	*Aust. J. Phys.* **10,** 286.
Anderson K. A.	1958	*Phys. Rev.* **111,** 1397.
Anderson K. A.	1959	Preprint SUI-59-22, Dept. Phys. Astr. State Univ. Iowa.

VOL. 22 1961

Arnoldy R. L., Hoffman R. A. and Winckler J. R.	1960	*J. Geophys. Res.* **65,** 1361, 3004.
Barrington R. E.	1959	*Proceedings of the Symposium on Physical Processes in the Sun–Earth Environment,* p.223. Defence Research Board, Canada.
Bell T. F. and Helliwell R. A.	1959	*Proceedings of the Symposium on Physical Processes in the Sun–Earth Environment,* p.215. Defence Research Board, Canada.
Bullough K., Davidson T. W., Kaiser T. R. and Watkins C. D.	1957	*J. Atmosph. Terr. Phys.* **11,** 237.
Coleman P. J. Jr., Sonett C. P., Judge D. L. and Smith E. J.	1960	*J. Geophys. Res.* **65,** 1856.
Crouchley J. and Brice N. M.	1960	*Planet. Space Sci.* **2,** 238.
Dessler A. J. and Parker E. N.	1959	*J. Geophys. Res.* **64,** 2239.
Dowden R. L.	1961	*J. Atmosph. Terr. Phys.* **20,** 122.
Ellis G. R. A.	1960a	*J. Geophys. Res.* **65,** 1705.
Ellis G. R. A.	1960b	*Proc. IRE* **48,** 1650.
Fermi E.	1950	*Nuclear Physics,* p. 47. The University of Chicago Press.
Fukushima N.	1959	*J. Geomagn. Geoelect. Kyoto* **10,** 164.
Gallet R. M.	1959	*Proc. IRE* **47,** 211.
Hakura Y., Nagai M. and Sano K.	1961	*J. Radio Res. Lab. Japan* **8,** 81.
Hakura Y., Takenoshita Y. and Otsuki T.	1958	*Rep. Ionos. Res. Japan* **12,** 459.
Jacchia L.	1959	*Nature, Lond.* **183,** 1662.
Kellogg P. J.	1959	*Nouvo Cim.* **11,** 48.
Maeda K. and Kimura I.	1961	*Rep. Ionos. Space Res. Japan.* In press.
Nagata T. and Fukushima N.	1952	*Rep. Ionos. Res. Japan* **6,** 85.
Obayashi T. and Hakura Y.	1960	*J. Geophys. Res.* **65,** 3131.
Ondoh T.	1961	*J. Geomagn. Geoelect. Kyoto* **12,** 77.
Ondoh T., Kitamura T. and Maeda H.	1961	*J. Geomagn. Geoelect. Kyoto* **12,** 115.
Ondoh T. and Maeda H.	1961	Lecture at the 29th Annual Meeting of Society of Terrestrial Magnetism and Electricity of Japan.
Outsu J. and Iwai A.	1961	Lecture at the 29th Annual Meeting of Society of Terrestrial Magnetism and Electricity of Japan.
Pope J. H.	1957	*Nature, Lond.* **180,** 433.
Pope J. H.	1960	*Nature, Lond.* **185,** 87.
Rothwell P. and McIlwain C. E.	1960	*J. Geophys. Res.* **65,** 799.
Schilling G. F. and Whitney C. A.	1959	*Planet. Space Sci.* **1,** 136.
Smith E. J., Coleman P. J. Jr., Judge D. L. and Sonett C. P.	1960	*J. Geophys. Res.* **65,** 1858.
Smith R. L.	1960	Technical Report No. 6, p. 110. Stamford University.
Sonett C. P., Smith E. J. and Sims A. R.	1960	*Space Research,* p. 921 North-Holland Publishing Co., Amsterdam.
Storey L. R. O.	1953	*Phil. Trans.* A **246,** 113.
Sugiura M. and Chapman S.	1958	Geophys. Inst., Univ. Alaska Publ. AFCRC-TR-58-266.
Van Allen J. A. and Frank L. A.	1959	*Nature, Lond.* **184,** 219.
Van Allen J. A. and Lin W. C.	1960	*J. Geophys. Res.* **65,** 2998.

VAN ALLEN J. A., MCILWAIN C. E. and LUDWIG G. H.	1959	*J. Geophys. Res.* **64,** 271.
VERNOV S. N. and CHUDAKOV A. E.	1959	*Dokl. Akad. Nauk SSSR* **125,** 304.
WATKINS C. D.	1961	*J. Atmosph. Terr. Phys.* **20,** 131.
WINCKLER J. R.	1960	*J. Geophys. Res.* **65,** 1331.
WINCKLER J. R. and BHAVSAR P. D.	1960	*J. Geophys. Res.* **65,** 2637.
WINCKLER J. R., PETERSON L., HOFFMAN R. A. and ARNOLDY R. L.	1959	*J. Geophys. Res.* **64,** 597.
YOSHIDA S.	1960	*Uchusen-Kenkyu* **5,** 397, 483.

VOL.
22
1961

Journal of Atmospheric and Terrestrial Physics, 1961, Vol. 22, pp. 255 to 269. Pergamon Press Ltd. Printed in Northern Ireland

High frequency fading of the 108 Mc/s wave radiated from an artificial earth satellite as observed at an equatorial station

G. S. KENT
University College, Ibadan, Nigeria

(*Received* 14 *July* 1961)

Abstract—A study has been made of the high frequency fading observed on the 108 Mc/s wave radiated from satellite 1959η. This fading had a frequency of a few cycles per second and is believed to be caused by the passage of the waves through irregularities in the F-region of the ionosphere. These irregularities are found to occur only at night and to have a dependence upon magnetic activity and latitude similar to that found for spread-F irregularities. In addition they are found to have a tendency to be concentrated into regions with dimensions of the order of 100 km. The size and shape of the irregularities have been deduced from observations on the fading and from spaced aerial measurements. They are elongated along the magnetic lines of force with axial ratios of not less than 5:1 and have dimensions perpendicular to the lines of force of about half a kilometre.

1. INTRODUCTION

SEVERAL workers have observed fading on the signals received from artifical earth satellites. This fading has been divided into three classes. In two of these the fading is periodic, being caused by rotation of the satellite and by Faraday rotation of the plane of polarization of the wave as it passes through the anisotropic ionosphere. In addition there is an irregular fading caused by the presence in the ionosphere of irregularities the same as, or similar to, those responsible for spread-F and radio star scintillation (SLEE, 1958; KENT, 1959; YEH and SWENSON, 1959; SINGLETON *et al.*, 1961).

This paper contains an account of observations made at an equatorial station on the 108 Mc/s wave radiated from satellite 1959η. The received signal was found to exhibit the three types of fading referred to above and an analysis has been made of the characteristics of the irregular component.

2. THE EXPERIMENTAL CONDITIONS

2.1. *The observations*

Observations were made on nearly all of the transits within range of Ibadan (Geographic Latitude 7° 26′ N, Longitude 3° 54′ E.) between 21 September and 24 November 1959. On the average about six useful transits a day were observed, the times of observation varying over all hours of the day and night during the 2 month period of observation.

Most of the observations were made using a Microlock receiver, of the type developed by the Jet Propulsion Laboratory, California, in conjunction with a d.c. amplifier and a pen-recorder capable of responding to frequencies of up to 2 c/s. The noise bandwidth of the receiver was 3 kc/s and an automatic frequency control circuit with a bandwidth of about 7 c/s enabled the receiver to follow the signal accurately as the frequency varied due to Doppler shift. The aerial was at ground level and of helical design, giving an approximately isotropic pattern in a horizontal plane. Recordings were also made using a low noise 108 Mc/s pre-amplifier and

converter followed by an Eddystone Model 750 receiver with a bandwidth of about 5 kc/s. In addition to the pen recordings, records were taken on film of the signal displayed on an oscilloscope in order to study the fading in detail.

The satellite possessed an elliptical orbit with a perigee of about 500 km and an apogee of about 4000 km, it thus at nearly all times lay above the maximum of the *F*-layer. The irregular high frequency fading was almost entirely observed only at night. On one or two occasions such fading was present during the day but on these occasions the satellite was at a great distance and it is not possible to state positively that the fading was not due to noise. Fig. 1 shows a typical chart record.

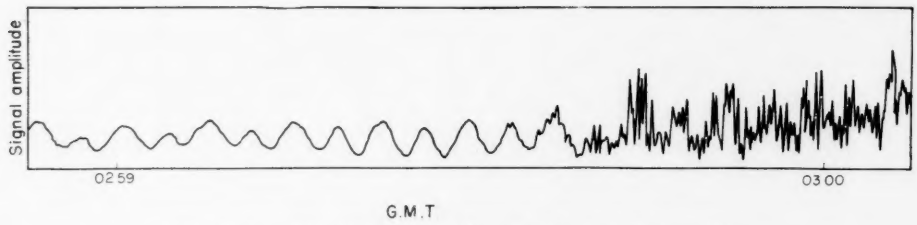

Fig. 1. Example of the fading of the signal showing the transition from slow to high frequency fading.

In the figure the rapid high frequency fluctuations occurring after about 0259·6 GMT show the high frequency fading under discussion. Photographic records showed that under these conditions the fading rate was about 5 c/s; the slower fading with a period of about $3\frac{1}{2}$ sec is attributed to the rotation of the satellite.

To describe the high frequency fading a fluctuation index S has been defined. This has a value of 0 if there is no fading, a value of 1 if the signal as shown on the chart record is less than 100 per cent modulated, and a value of 2 if the signal is 100 per cent modulated. Normally the index was either 0 or 2 as the transition occurred extremely rapidly.

VOL. 22 1961

2.2. *Scattering by ionospheric irregularities*

When a wave passes through a region in which there are irregularities of refractive index these produce irregular fluctuations in phase across the wavefront. The magnitude of the fluctuations produced depends upon the number of irregularities traversed and their refractive index (RATCLIFFE, 1956). As the wave travels downwards from the ionosphere the phase fluctuations develop into amplitude fluctuations whose depth depends upon the distance travelled. These amplitude fluctuations constitute a diffraction pattern which may be observed on the ground.

If the source is a radio star, movements of the irregularities will cause the diffraction pattern to move over the ground and fading of the signal will be observed. If the source is a satellite, its motion will also cause the diffraction pattern to move and since the velocity of a satellite is much greater than the velocity of ionospheric irregularities this is the more important factor. The theory of the production of the diffraction pattern will be discussed in detail in Section 4.2 where it will be used in a study of the fading.

3. The Occurrence of the Irregularities

3.1. *Introduction*

Fig. 2 shows the observed transits of the satellite between 1200 GMT on 9 October and 10 October 1959. The dotted lines are the projection of the orbit onto the surface of the earth, the full parts of the lines showing those parts of the orbit from which signals were received. To show the position of the satellite when the high frequency fading was observed these lines have been marked with crosses.

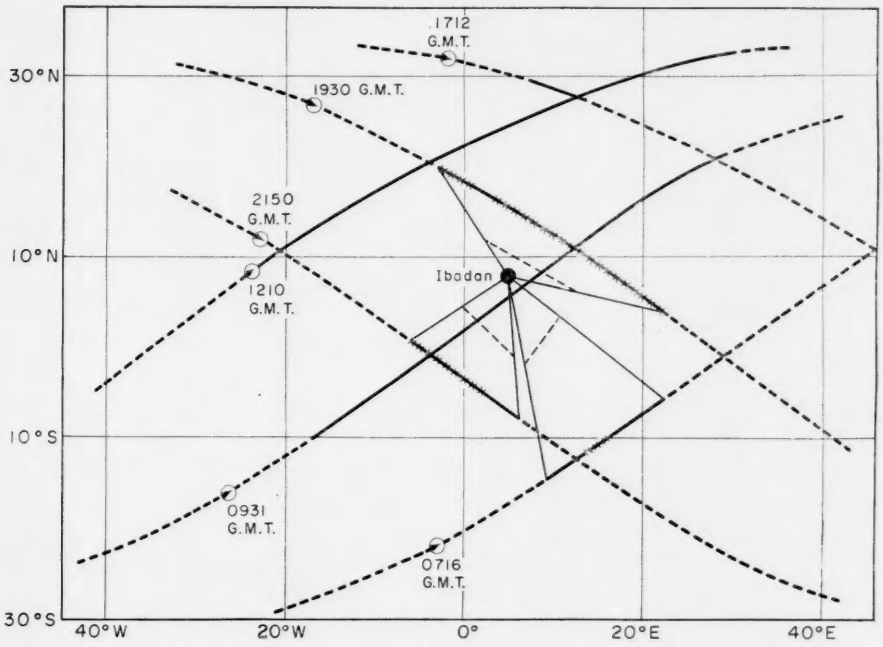

Fig. 2. Map showing the satellite tracks on 9–10 November. The parts of the orbit from which signals were received are shown by solid lines, the remainder by dotted lines. The crosses show the position of the satellite when the high frequency fading was observed. The dashed lines are the loci of the points of intersection with the ionosphere of lines joining the receiver to the satellite tracks.

The satellite was generally well above the *F*-region and in order to obtain an estimate of the geographical position in the ionosphere of the irregularities it was assumed that they occurred at a height of 400 km. In Fig. 2 the dashed lines are the points of intersection with the ionosphere, at a height of 400 km, of lines joining the satellite to the receiver. These are only shown for transits on which the high frequency fading was observed.

The range of latitudes observed was from about 20° N, geographic, to about 5° S and the main facts which emerged from a study of the occurrence of the irregularities are as follows:

(a) The irregularities only occurred between 1800 and 0600 hours local time.
(b) There was a slight dependence upon latitude.
(c) The occurrence of the irregularities was inversely correlated with magnetic activity.

(d) The occurrence of the irregularities is correlated with the occurrence of spread-F at Ibadan.
(e) The irregularities are grouped into regions of the order of 100 km in size.

3.2. *Dependence of the irregularities on local time, latitude and magnetic activity*

In order to study the way in which the occurrence of the irregularities depends upon local time, latitude and magnetic activity it has been supposed that they have always occurred at a height of 400 km. Over the 2 months of observation there are insufficient results to be able to analyse them for dependence upon each of the above characteristics separately. It has therefore been supposed that to a first order of approximation the fluctuation index on any occasion is proportional to the product $S(T)\,.\,G(C_p)\,.\,H(\theta)$ where $S(T)$, $G(C_p)$ and $H(\theta)$ are functions of local time T, C_p the magnetic character figure for the previous 24 hr, and θ the magnetic latitude, the first and last of these functions being taken at the point in the ionosphere under examination. The results have then been analysed by an iterative method to find the functions $F(T)$, $G(C_p)$ and $H(\theta)$ which form the best fit. For this purpose $G(C_p)$ and $H(\theta)$ have been normalized so that their mean values are unity. The resultant values obtained are shown in Fig. 3(a) and the following characteristics emerge:
(1) That the irregularities only occur at night.
(2) That the occurrence of the irregularities is inhibited by strong magnetic activity.
(3) That there is a slight but definite decrease with increasing magnetic latitude.

In Fig. 3(b) is shown the behaviour of spread-F as observed at Ibadan over the same period of time. Fig. 3(b)(i) shows the mean value of the spread-F index, defined on a scale of 0–3, averaged for constant local mean time over the period of observation. Fig. 3(b)(ii) shows the mean value of the sum of the spread-F indices for the same nights plotted as a function of C_p. The variation with latitude shown in Fig. 3(b)(iii) is an estimate obtained from the paper of LYON *et al.* (1960) on the morphology of equatorial spread-F.

It can be seen that there is a close correspondence between Figs. 3(a) and 3(b) showing that the irregularities responsible for the fluctuations on the signals received from the satellite must be related to, if not the same as, those responsible for spread-F.

3.3. *The concentration of the irregularities into limited regions*

In many transits it was found that the fluctuation index would alternate between the values of 0 and 2 indicating that the satellite was passing over successive clouds of irregularities. In order to obtain an estimate of the size of these clouds two methods of analysis have been adopted. In the first the auto-correlation coefficient of the fluctuation index has been calculated as a function of the distance along each single satellite track (when projected onto the 400 km level) and the results averaged over all the observed tracks. In the second the cross-correlation coefficient between the spread-F index at Ibadan at the time of observation and the fluctuation index has been calculated for different distances of the irregularities from Ibadan.

The results from these two methods of analysis are shown in Fig. 4. The dots

VOL. 22 1961

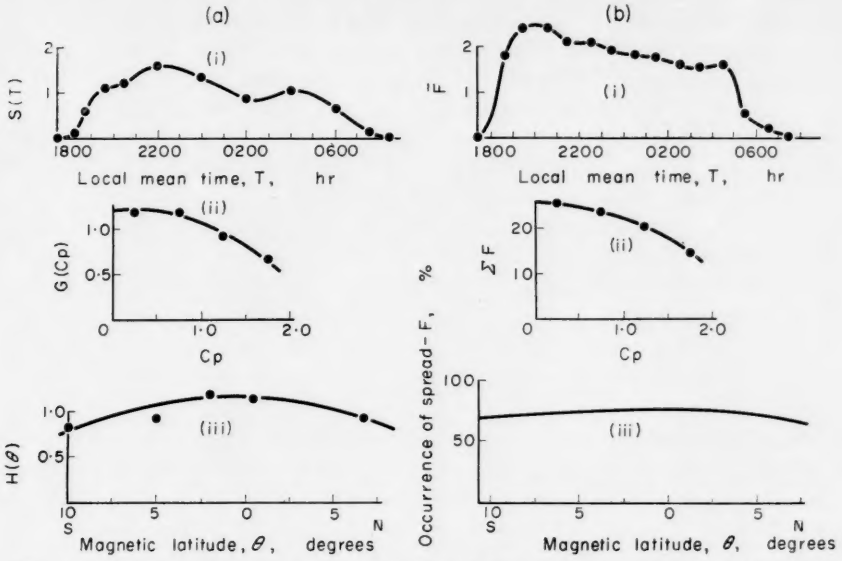

Fig. 3. (a) Characteristics of the high frequency fading observed on the signals from the satellite. (b) Corresponding characteristics of spread-F during the same period of time.

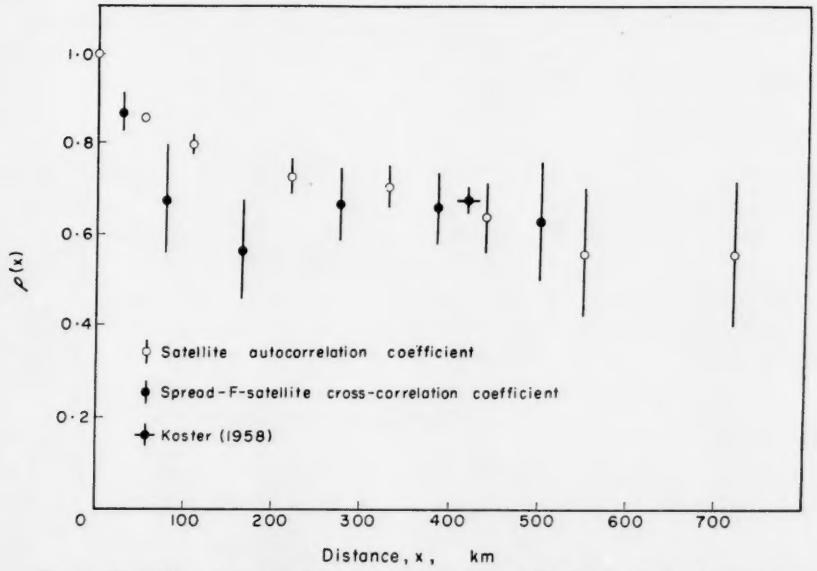

Fig. 4. Variation of the correlation of the intensity of the fading along the satellite tracks and the cross-correlation of the fading and spread-F index with distance.

represent the values of the correlation obtained and the lines their estimated standard deviation. Two significant facts emerge. The first is that the values obtained by the two methods agree well, giving support to the hypothesis that the irregularities responsible for the fluctuations and those responsible for spread-F

are probably the same. On the same graph there is a star representing the value obtained by KOSTER (1958) for the correlation coefficient between radio star scintillation at Accra and spread-F at Ibadan, a separation of 420 km. This value agrees extremely well with the other values plotted. The second point is that there is a sharp fall in correlation near the origin followed by a very slow decrease. This fall near the origin indicates that often the irregularities must be grouped into regions of the order of only 100 km in size. The very gradual decrease which follows would be expected as it is known (WRIGHT and SKINNER, 1959) that even between stations separated by several thousand kilometres along the equator there is still a high degree of correlation in the occurrence of spread-F, due mainly to the high inverse correlation of spread-F at each station with magnetic activity.

4. THE FADING OF THE RECEIVED SIGNAL

4.1. *Introduction*

In order to examine the fading in detail the signal was taken from the intermediate frequency stage of the receiver and applied to the Y-plates of a cathode ray oscilloscope. A photographic record was then taken by moving a film in a camera past the face of the oscilloscope in the X-direction. An example of a record obtained in this way is shown in Fig. 5 which shows the fading observed as the satellite passes across one of the clouds of irregularities discussed in Section 3.3. The slow fading with a period of about 7 sec is attributed, as explained in Section 2.1 to the rotation of the satellite. The fast fading, due to the irregularities, can be seen to have a fading rate varying from less than 1 c/s up to about 6 c/s; fading rates up to about double this have been observed. Interpreted in terms of a diffraction pattern moving over the ground this means a pattern size from peak to peak varying between about 0·5 and 5 km.

Five occasions were recorded in which the satellite passed behind or emerged from behind a cloud of irregularities. On each of these occasions, as would be expected, a gradual change in modulation depth occurred: the transition from 0 to 100 per cent modulation taking place in a few seconds. In addition, on each occasion a change in fading rate was also observed, the slower fading occurring with the shallow modulation and the faster fading only occurring when the modulation was 100 per cent. This can be seen in Fig. 5 and will be discussed in detail in Section 4.3.

4.2. *Production of the diffraction pattern*

The problem of the production of the diffraction pattern and its relation to the fading depth is of some complexity. It may be divided into the following series of steps:

(1) The wave on passing through the ionosphere suffers an irregular change of phase across the wavefront. The spatial auto-correlation function of the complex amplitude and the root mean square value of the phase fluctuations can be related to the characteristics of the medium. This is discussed in Section 4.2.1.

(2) As the wave travels from the ionosphere the phase fluctuations develop into amplitude fluctuations, the degree of development depending upon the distance travelled. The spatial auto-correlation of the complex amplitude at the ground

VOL. 22 1961

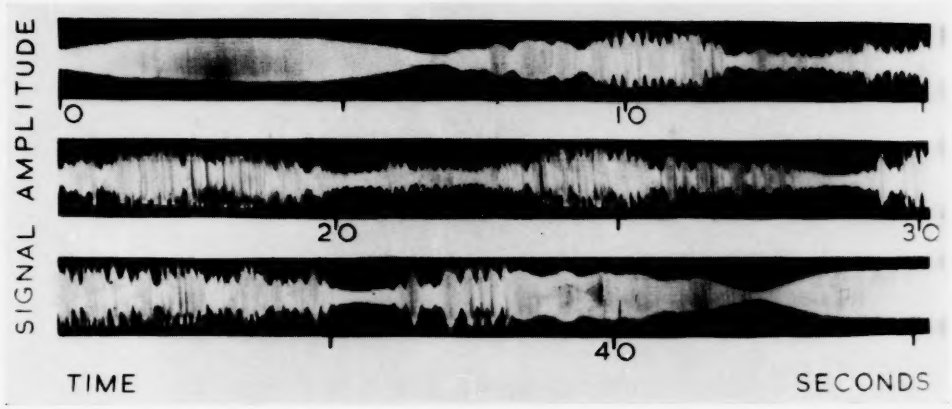

Fig. 5. Photographic record of the signal amplitude showing the passage of the satellite behind a cloud of irregularities.

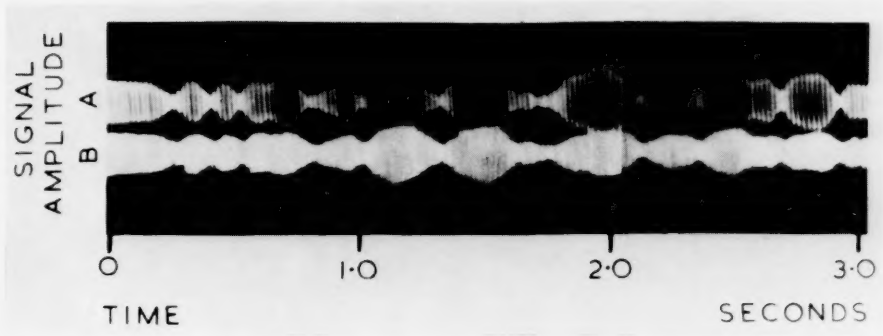

Fig. 11. Example of a record showing the fading on two spaced aerials.

VOL.
22
1961

may be related to the corresponding function at the ionosphere and the signal to noise ratio may be related to the amplitude of the phase fluctuations at the ionosphere. This is discussed in Section 4.2.2.

(3) The actual measured functions which are the time auto-correlation function and the fading depth of the amplitude of the signal may be found in terms of the functions obtained in (2). This is discussed in Section 4.2.3.

4.2.1. *The effect of the ionosphere.* Consider an ionosphere in which the electron density varies in a random manner in a vertical and in one horizontal direction (x-direction) and is constant in the other direction. Let the variation in the x-direction $\Delta N(x)$ be a function with a normal distribution of standard deviation N_m and spatial auto-correlation function

$$\rho_{\Delta N}(\xi) = \exp(-\xi^2/\xi_0^2). \tag{4.1}$$

A wave passing through this medium will emerge with the phase across a wavefront randomly distributed so that the root mean square value of its departure from its mean is equal to ϕ_m

where
$$\phi_m \propto (z_0 l)^{1/2} N_m \tag{4.2}$$

and z_0 = distance travelled by the wave inside the layer
l = average size of an irregularity along the path of the wave

(Ratcliffe, 1956; Bramley, 1954).

Let the complex amplitude across the emergent wavefront be $f(x)$ then the auto-correlation $\rho_f(\xi)$ of $f(x)$ is given by

$$\left.\begin{aligned} \rho_f(\xi) &= (b+1) r_f(\xi) - b \\ \text{where} \quad r_f(\xi) &= \exp[-\phi_m^2\{1 - \exp(-\xi^2/\xi_0^2)\}] \\ \text{and} \quad b &= 1/[\exp(\phi_m^2) - 1] \end{aligned}\right\} \tag{4.3}$$

b may be shown to be the signal to noise ratio in the wave (Ratcliffe, 1956).

The value of ξ for which $\rho_f(\xi)$ falls to $\exp(-1)$ may be taken as the scale of the fluctuation in the emergent diffraction pattern and will be denoted by ξ_0'. The ratio (ξ_0'/ξ_0) is obviously a function of ϕ_m and Fig. 6(a) shows the way in which it varies. Fig. 6(b) shows the variation of b with ϕ_m. Points to note in these figures are firstly that for low values of ϕ_m the ratio (ξ_0'/ξ_0) is approximately unity whereas for high values it tends towards $1/\phi_m$ and secondly that b varies extremely rapidly for small changes in ϕ_m.

4.2.2. *The development of the amplitude fluctuations.* As the wave travels from the ionosphere the fluctuations in phase develop into amplitude fluctuations (Hewish, 1952). It can be shown that the distance z taken for this development is of the order of $8\xi_0^2/\lambda$ where λ is the wavelength used. If we denote the value of $\rho_f(\xi)$ at a distance z from the ionosphere by $\rho_{fz}(\xi)$ then it can also be shown that for an infinitely distant source $\rho_{fz}(\xi)$ is independant of z, regardless of this development of the phase fluctuations into amplitude fluctuations. The signal to noise ratio is also a constant independant of z, the distribution of power between the phase and amplitude components will however vary. Beyond the critical distance

an equilibrium will be reached and the amplitude probability distribution takes the form of a Rice distribution (RICE, 1945). The probability $P(A)\,dA$ of the amplitude lying between A and $A + dA$ is given by

$$P(A) = 2Ab \,.\, \exp\left[-b(A^2 + 1)\right] \,.\, I_0(2Ab) \tag{4.4}$$

where I_0 is a Bessel of zero order and imaginary argument. The form of the distribution here has been normalized so that the amplitude of the constant component is unity.

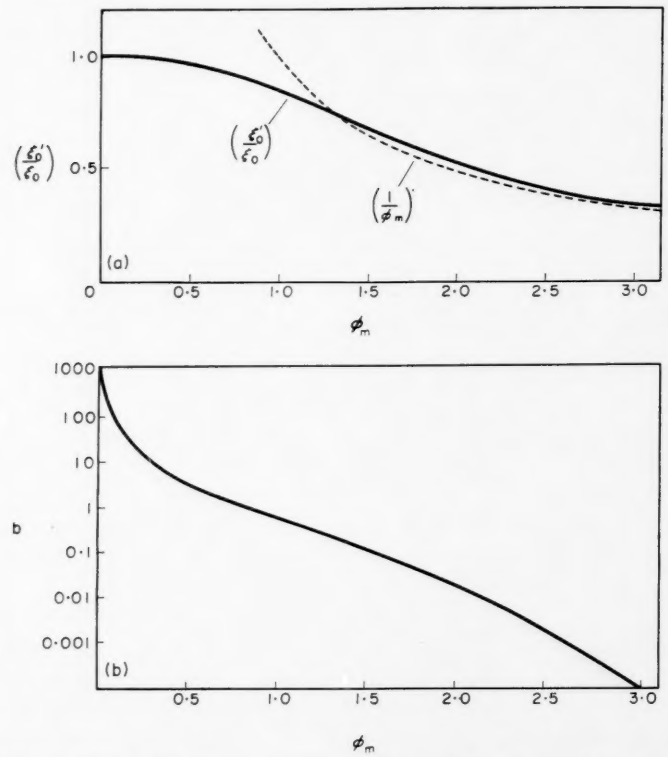

Fig. 6. (a) Ratio of the diffraction pattern size immediately beneath the ionosphere to the irregularity size within it as a function of the depth of phase modulation. (b) The signal to noise ratio of the wave leaving the ionosphere as a function of the depth of phase modulation.

In the case of a satellite a modification is necessary to the theory developed by HEWISH and also to the statement made about the constancy of $\rho_{fz}(\xi)$ with distance from the ionosphere. It can be shown (RATCLIFFE, 1956) that if the source and receiver are at finite distances z_1 and z_2 from the ionosphere, as shown in Fig. 7, then the factor z must be replaced by $z_1z_2/(z_1 + z_2)$ and the scale of the diffraction pattern is increased by the factor $(z_1 + z_2)/z_1$.

4.2.3. *The observations made at the ground.* The fading observed at an aerial on the ground is produced by the movement of the diffraction pattern across it. If, as in Fig. 7, the satellite is moving horizontally with velocity v the diffraction

VOL. 22 1961

pattern on the ground will move in the opposite direction with velocity $v(z_2/z_1)$. If therefore $\rho_f(\tau)$ is the time auto-correlation function of the complex amplitude then

$$\rho_{fz_2}(\tau) = \rho_{fz_2}(\xi)$$

if

$$\xi = \left(\frac{z_2}{z_1}\right) v\tau$$

hence

$$\rho_{fz_2}(\tau) = \rho_{f,0}(\xi)$$

if

$$\xi = \left(\frac{z_2}{z_1 + z_2}\right)\tau. \tag{4.5}$$

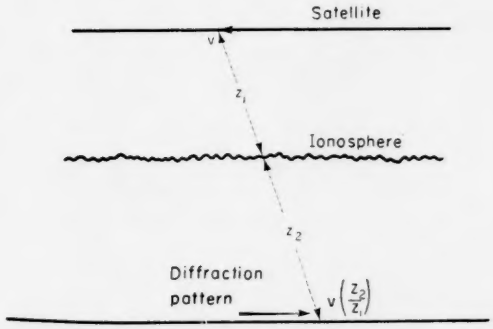

Fig. 7. Figure illustrating the geometry of the formation of the diffraction pattern.

The function of the signal which is actually recorded is the amplitude, and the auto-correlation functions of the amplitude $\rho_A(\xi)$ may be related to $\rho_f(\xi)$ (BRAMLEY, 1951).

If b is large then $\rho_{Az_2}(\xi)$ is approximately equal to $\rho_{fz_2}(\xi)$.

If b is small then $\rho_{Az_2}(\xi)$ is approximately equal to $[\rho_{fz_2}(\xi)]^2$.

Making the approximation $\rho_{Az_2}(\xi) = \rho_{fz_2}(\xi)$ would in the second case result in an estimate of the pattern size too small by a factor of about 1·5. Since in the comparison with experiment made in the next Section we shall be dealing with pattern sizes which vary over a range of 5 to 1 this factor will not be of very great importance. Approximate corrections will however be applied to obtain a rather truer value of $\rho_{fz_2}(\xi)$ from $\rho_{Az_2}(\xi)$ than would be obtained by merely equating the two.

Since the amplitude of the signal alone is measured we shall also be unable to obtain directly a value for the signal to noise ratio b. Instead the ratio

$$b_A = \bar{A}^2/\overline{(A - \bar{A})^2} \tag{4.6}$$

where the bars denote mean values, has been evaluated. Using equation (4.4) this may be related to b and the result is shown in Fig. 8(a). It may be noted that for large b, b_A is approximately equal to $2b$ and for small b, b_A tends to the constant value of 3·66 for a Rayleigh distribution.

4.2.4. *Summary.* We have obtained graphs showing how both the ratio of the diffraction pattern size just underneath the ionosphere to the irregularity size inside it (ξ_0'/ξ_0) and the signal to noise ratio b vary with the depth of phase modulation ϕ_m. We have also seen that the width of the time auto-correlation function at a point on the ground is simply related to ξ_0' by a scaling factor. A final graph has been obtained showing how the value of the function b_A varies with the signal to noise ratio provided the wave travels sufficiently far for the

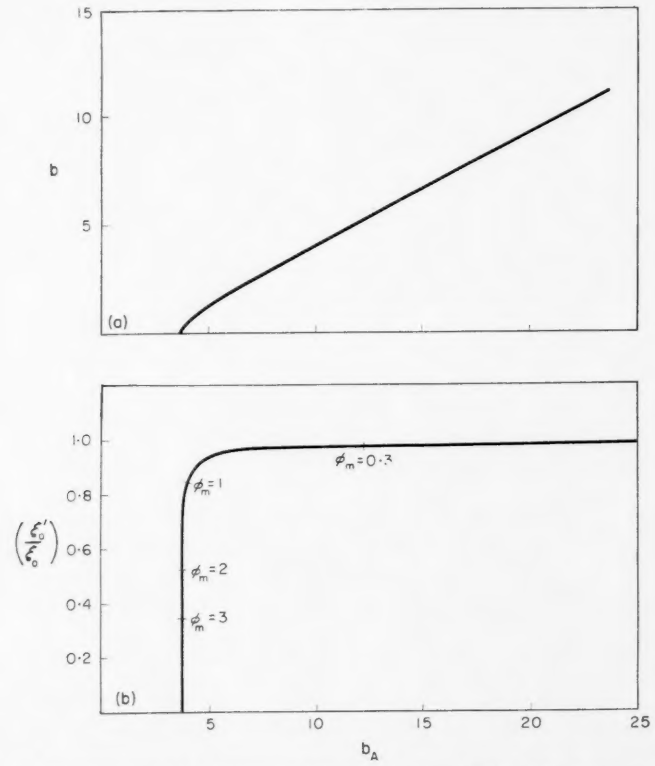

Fig. 8. (a) Graph of the relation of the measured variable b_A to the true signal to noise ratio b. (b) Graph showing the relation between b_A and the diffraction pattern size.

modulation to develop fully. A further graph can thus be drawn relating b_A and (ξ'_0/ξ_0) and this is shown in Fig. 8(b). It can be seen to form a curve with a very sharp bend in it where ϕ_m is about unity. Comparison of this curve with the experimental results will be made in the next Section.

4.3. *Comparison of theory and experiment*

In Section 4.1 it was stated that on occasions on which the satellite passed behind or emerged from behind a cloud of irregularities a simultaneous change of fading depth and fading rate occurred as shown in Fig. 5. On one transit, at 2320 GMT on the 16 November, the transition was rather slower than usual and this has been analysed in detail.

VOL. 22 1961

The record was divided into lengths of about 7 sec each and the auto-correlation function of the fading $\rho_A(\tau)$ and the parameter b_A, defined in the previous Section, calculated for each length. The auto-correlation function $\rho_A(\tau)$ was used, in the way explained in the previous Section, to provide an estimate of $\rho_f(\tau)$ the auto-correlation function of the complex amplitude and hence of τ_0 the value of τ for which $\rho_f(\tau)$ has fallen to $1/e$. τ_0 is related to the diffraction size immediately under the ionosphere $\xi_0{}^1$ by the equation

$$\xi_0{}' = v\tau_0 \left(\frac{z_2}{z_1 + z_2}\right).$$

On this occasion

$$\text{mean value of} \quad z_1 = 1000 \text{ km}$$
$$z_2 = 1000 \text{ km}$$
$$v = 6{\cdot}0 \text{ km/sec}$$

therefore
$$\frac{vz_2}{z_1 + z_2} = 3{\cdot}0 \text{ km/sec}.$$

Twelve values for τ_0 and b_A were obtained covering the transition period and in Fig. 9(a) and (b) these are plotted against time, measured here from an arbitrary zero.

It can be seen that the values for τ_0 fall into two groups, the first with a mean value of about 0·12 sec and the second with a mean value of about 0·05 sec; the transition between the two groups occurs at a time of about 40 sec when, in the second graph, b_A has just fallen to the limiting value of about four. Fig. 9(c) shows a graph of τ_0 plotted against b_A.

τ_0 is proportional to $\xi_0{}'$ and if we assume for the moment that ξ_0, the irregularity size in the ionosphere, is constant then the experimental points in Fig. 9(c) should be expected to fit the theoretical curve in Fig. 8(b). The dotted line shows this curve fitted to the experimental points and it can be seen that the agreement is extremely good.

The assumption just made that ξ_0 is constant has really no more justification than that there is no reason to expect it to vary. In the absence of a theoretical model to explain the existence of the irregularities there is no way of predicting the way in which their size will behave. The change in fading depth can obviously be explained in terms of an increase either in the number of irregularities or in the magnitude of the variations in electron density. We have just seen that the change in diffraction pattern size can be explained in the same way, so while it is possible that the irregularity size does vary with distance from the edge of a cloud there is no need to postulate this in order to explain the experimental results.

Assuming that ξ_0 is a constant it is possible to calculate its value from Fig. 9(c). The maximum value of τ_0 will correspond to the maximum value of $\xi_0{}'$ which will then be equal to ξ_0. Taking $\tau_{0\,\max} = 0{\cdot}13$ sec and the conversion factor of 3·0 km/sec obtained earlier in this Section this gives a value for ξ_0 of 0·4 km. This is of course the dimension of the irregularities along the direction of motion of the satellite, no information has been obtained about the size perpendicular to this.

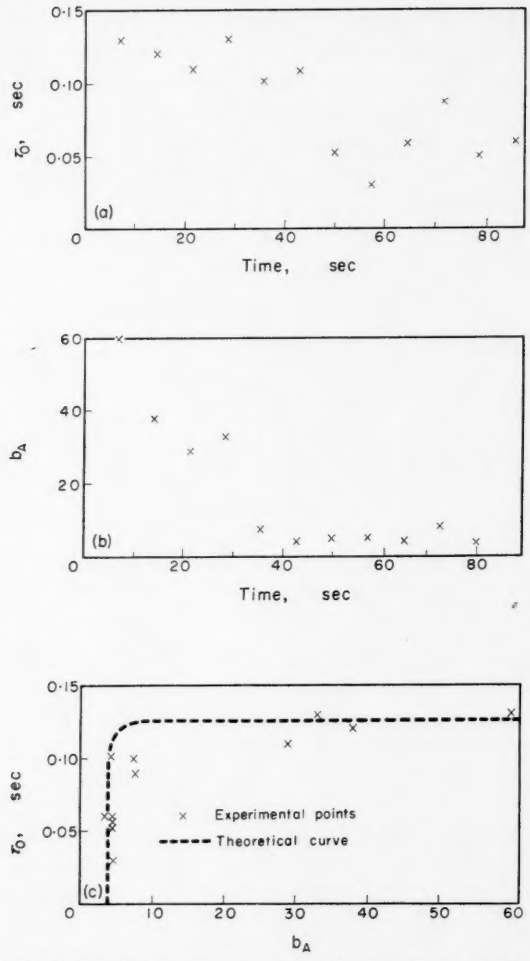

Fig. 9. (a) Half-width τ_0 of the time auto-correlation function of the fading of the complex amplitude during a transit on 16 November. (b) Values of b_A for the same transit as in (a). (c) τ_0 plotted against b_A together with the theoretical curve relating them.

We are now in a position to test the assumption that has been made that the receiver was sufficiently far from the ionosphere for the phase fluctuations to develop into amplitude fluctuations. The condition for this was that

$$\frac{z_1 z_2}{z_1 + z_2} > \frac{8\xi_0^2}{\lambda}.$$

The left hand side of this equation is equal to 500 km while the right hand side is about 400 km, the assumption is therefore probably justified.

One other constant may be obtained from Fig. 9(c). This is ϕ_m the depth of phase modulation of the wave as it leaves the ionosphere. Comparison of this figure with Fig. 8(b) shows that values of ϕ_m exceeding 3 rad occurred.

VOL. 22 1961

4.4. *Measurement of the diffraction pattern size*

Towards the end of the period of recording an additional aerial was erected about 0·5 km north of the original aerial; the plan of the arrangement is shown in Fig. 10. Using the two receivers described earlier, the signals were displayed simultaneously on the face of a double beam oscilloscope and photographed in the same way as for a single trace. An example of a record taken on 16 November is shown in Fig. 11. It is immediately clear that the cross-correlation was very high; in practice, since there was rather a lot of noise on the second aerial, it was impossible to distinguish its value from unity even when very high fading speeds were observed.

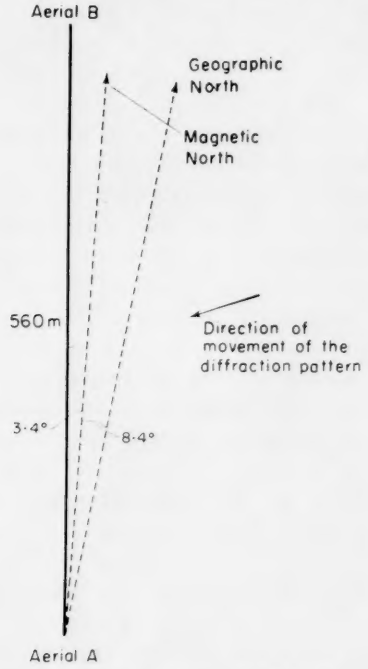

Fig. 10. Plan of the aerial arrangement used in the spaced aerial experiment.

In the example shown the value of the cross-correlation for zero time displacement was 0·93. The width of the time auto-correlation function was 0·105 sec to the point where the correlation had fallen to $1/e$. The velocity of the pattern across the ground was about 6 km/sec giving a pattern size of 0·7 km. Comparing this to the value found for the cross-correlation between the two aerials it is evident that the pattern was very elongated in a north–south direction. Assuming that the shape of the space auto-correlation function was the same north–south and east–west these figures give a minimum elongation of four to one.

It is also possible to use the records to determine whether the irregularities are elongated along the magnetic or the geographic north–south axis. The directions of these axes together with the direction of movement of the pattern are shown in Fig. 10. Because of their different orientations with respect to the line joining the

two aerials small but different time shifts would be expected in the fading of the signals arriving at the two aerials for irregularities aligned along these two directions. These time shifts are:

For geographic alignment—the delay of the signal at aerial B with respect to aerial A will be 22 msec.
For magnetic alignment—the corresponding delay is 6 msec.

These values are calculated on the assumption that the irregularities are horizontal; if the irregularities are not horizontal then the orientation of the pattern on the ground will vary depending upon the position of the satellite. In order to eliminate this effect a transit has been chosen in which the satellite passed almost overhead and an equal number of points taken for analysis in which the satellite was east and west of this position.

The display on the oscilloscope was intensity modulated at a frequency of 50 c/s enabling measurement of the amplitude to be made accurately at intervals of 20 msec. The cross-correlation function between the signals received on the two aerials was calculated for six sections of record taken from the chosen transit, one of them being that shown in Fig. 11. The time delays taken from the cross-correlation functions were averaged and gave a mean value of 2 ± 3 msec for the time delay of the signal at aerial B behind that at aerial A. This value is consistent with the theory of magnetic alignment but not with that of geographic alignment.

Values of the maximum cross-correlation were obtained from the same analysis and used in conjunction with observations on the fading rate to provide an estimate of the elongation of the irregularities. The values, which can only be regarded as minimum estimates, varied between ratios of 2:1 and 10:1 with a mean value of 6:1. Using the value for ξ_0 obtained in the previous Section this gives an irregularity size in the ionosphere of about 0·4 km in the east–west direction and at least 2·0 km along the magnetic north–south axis.

There are unfortunately no results available on the sizes of the irregularities causing equatorial spread-*F* or radio-star scintillation with which the values just obtained may be compared. It is known however, that the ordinary irregularities in the *F*-region at Ibadan are considerably elongated along the magnetic axis with axial ratios of the order of 10:1 (SKINNER *et al.*, 1958). Information is also available on the irregularities responsible for spread-*F* and radio star scintillation in temperate latitudes (HEWISH, 1952; LITTLE and MAXWELL, 1951; SPENCER, 1955; KENT, 1959) and the values are similar to those obtained above.

5. CONCLUSION

In this paper results have been presented which were obtained on the fading of the signals received from an artificial earth satellite. These have been analysed on the assumption that the fading was produced by the passage of the waves through irregularities in the ionosphere similar or the same as those responsible for spread-*F* and radio star scintillation. Those irregularities have been found to occur only at night and to be inhibited by high magnetic activity, there also appears to be a slight variation with latitude. In these characteristics their behaviour is very similar to that of the irregularities causing spread-*F*. The irregularities have also

VOL. 22 1961

been found to exist often in the form of clouds with dimensions of the order of 100 km.

A detailed analysis of the fading has been made and the fading rate and the fading depth have been found to behave in the manner predicted by diffraction theory. A deduction of the irregularity size and shape from this and from spaced aerial observations shows the irregularities to be elongated along the magnetic lines of force with dimensions of about 0·5 km perpendicular to them and not less than 2 km along them.

References

Bramley E. N.	1951	*Proc. Inst. Elect. Engrs* **1,** 98, 19.
Bramley E. N.	1954	*Proc. Roy. Soc.* A **225,** 515.
Hewish A.	1952	*Proc. Roy. Soc.* A **214,** 494.
Kent G. S.	1959	*J. Atmosph. Terr. Phys.* **16,** 10.
Koster J. R.	1958	*J. Atmosph. Terr. Phys.* **12,** 100.
Little C. G. and Maxwell A.	1951	*Phil. Mag.* **42,** 267.
Lyon A. J., Skinner N. J. and Wright R. W. H.	1960	*J. Atmosph. Terr. Phys.* **19,** 145.
Ratcliffe J. A.	1956	*Rep. Progr. Phys.* **19,** 188.
Rice S. O.	1945	*Bell Syst. Tech. J.* **24,** 46.
Singleton D. G., Lynch G. J. and Thomas J. A.	1961	*Nature, Lond.* **189,** 30.
Skinner N. J., Hope J. and Wright, R. W.	1958	*Nature, Lond.* **182,** 1363.
Slee O. B.	1958	*Nature, Lond.* **181,** 1610.
Spencer M.	1955	*Proc. Phys. Soc. Lond.* B **68,** 493.
Wright R. W. and Skinner N. J.	1959	*J. Atmosph. Terr. Phys.* **15,** 121.
Yeh K. C. and Swenson G. W.	1959	*J. Geophys. Res.* **64,** 2281.

Journal of Atmospheric and Terrestrial Physics, 1961, Vol. 22, pp. 270 to 274. Pergamon Press Ltd. Printed in Northern Ireland

Further evidence of a long term variation in the relationship of solar activity to the ionosphere

R. NAISMITH and P. A. SMITH
D.S.I.R. Radio Research Station,
Slough, Bucks.*

(*Received* 24 *July* 1961)

Abstract—Ionospheric measurements indicate that during the last 20 years there has been a progressive decrease in F-region ionization corresponding to a given sunspot number. In a previous paper it was shown that there was a corresponding decrease in the E-region. It is pointed out that this represents a progressive change in the nature of solar radiation or in the atmosphere.

INTRODUCTION

EVIDENCE of a progressive decrease in E-region ionization corresponding to a given sunspot number over two and a half sunspot cycles has already been described (NAISMITH *et al.*, 1961). We now consider a similar decrease in the F-region ionization corresponding to a given sunspot number (R) or solar noise flux measured

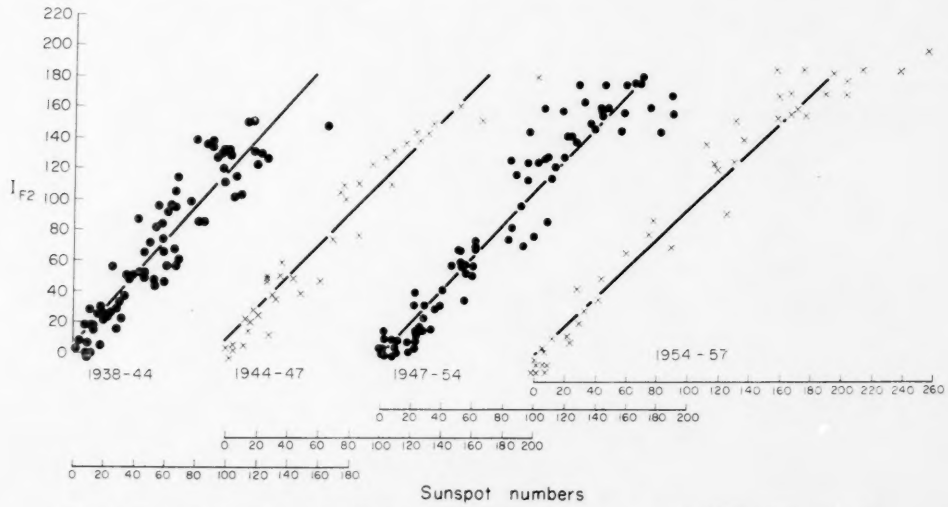

Fig. 1. The relationship of I_{F2}/R for each half cycle in the period 1938–1957 and the calculated regression lines.

on 10 cm wavelength (Φ). The use of the more quantitative measurement Φ supports the reality of the observation and by using two solar indices based on observations on such very different wavelengths the identification of the effect as primarily solar or primarily ionospheric could be assisted.

There is, unfortunately, no F-region index corresponding to the E-region character figure (Ch_E) used in the former discussion, which effectively removes the

* Official communication.

VOL. 22 1961

marked seasonal variation in the F-region measurements. It is therefore necessary to make some more empirical approach to the problem and MINNIS and BAZZARD (1960) have described an $F2$-region index, (I_{F2}), based on ionospheric measurements, which is free from seasonal variations and is therefore suitable for our present purpose. Values of this latter index are, however, only available for the period 1938–1959 but this is long enough to enable us to decide if the long term variation referred to above has also occurred in the F-region.

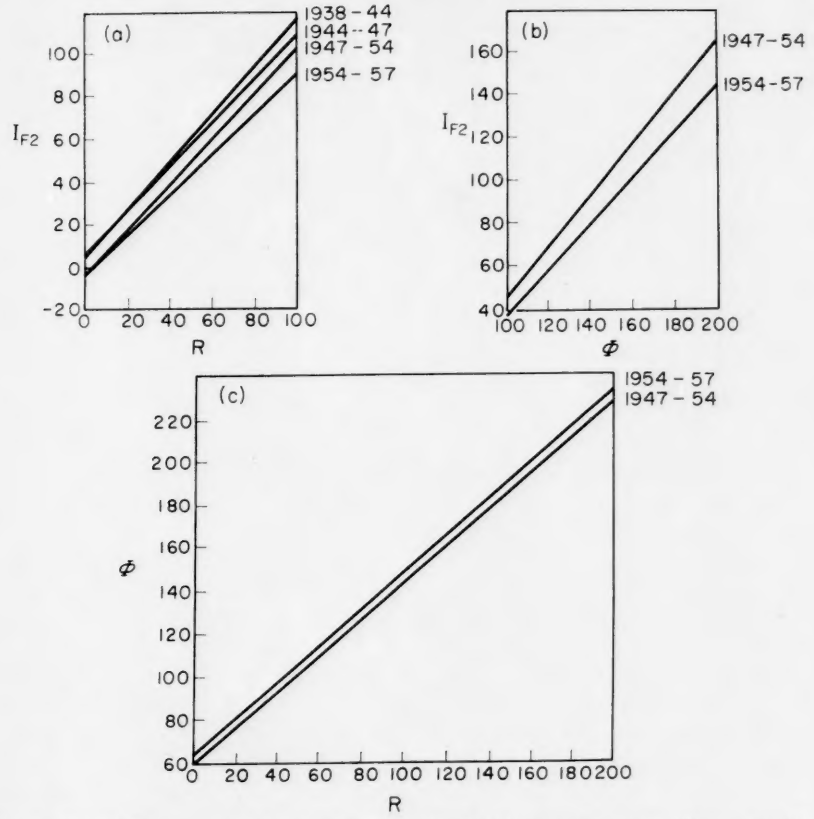

Fig. 2. Calculated regression lines for the relationships (a) I_{F2}/R, (b) I_{F2}/Φ and (c) Φ/R.

An important difference between the index Ch_E and the index I_{F2} is that the former is derived from measurements made at one station while the latter is derived from measurements made at ten different stations and is regarded as a world index.

TREATMENT OF THE DATA

The data have been divided as before into half sunspot cycles. A plot of the relationship of I_{F2} to R for each of the four available half cycles is given in Fig. 1 and the calculated regression line has been drawn on each. The slope and intercept of these regression lines are the quantities considered in the discussion below. The index I_{F2} is similarly compared with the solar Noise Flux measured on 10 cm

wavelength. The latter measurements are only available since 1947 and the comparison is correspondingly limited. The zero on the I_{F2} scale is not defined, but the range of values extends from -15 to 195 as shown in Fig. 1. The index has an annual variation, but this does not affect its use in the present context. The values of Ch_E extend from 106 to 355 and one unit on this scale is therefore approximately equal to a unit on the I_{F2} scale.

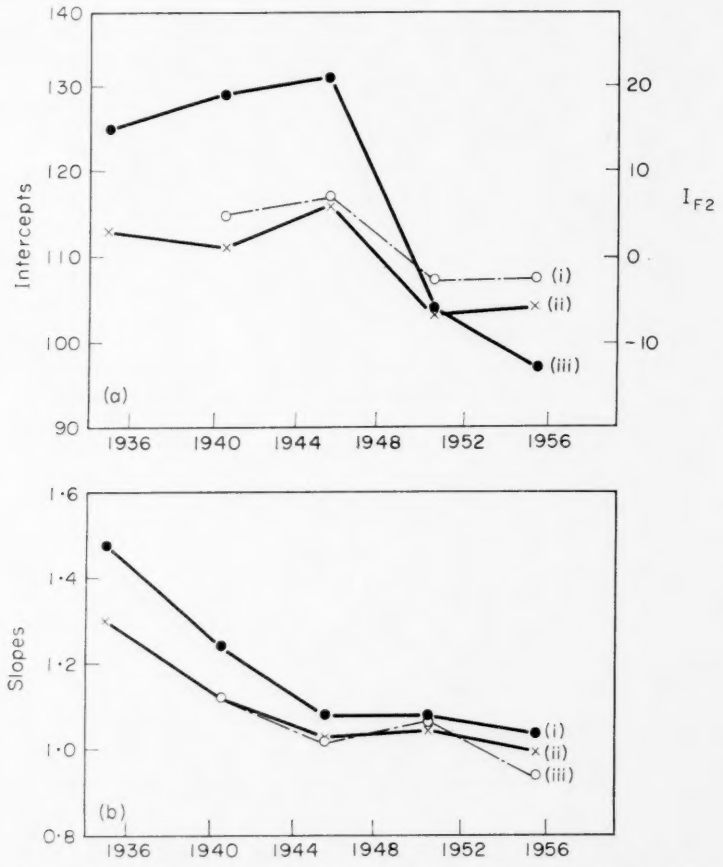

Fig. 3. The variation of slopes and the intercepts of regression lines for $R = 0$. (a)(i) I_{F2}/R World, (ii) Ch_E/R Slough, (iii) Ch_E/R Washington. (b) (i) Ch_E/R Washington, (ii) Ch_E/R Slough, (iii) I_{F2}/R World.

DISCUSSION

The calculated regression lines of I_{F2} on R taken from Fig. 1 are re-plotted in Fig. 2(a). For a fixed value of R there is a progressive decrease in the value of I_{F2} in each succeeding half cycle. In Fig. 2(b) the calculated regression lines of I_{F2} on Φ are plotted for the only two half cycles available and these also show that for a constant value of Φ the value of I_{F2} was less in the latter half cycle than in the earlier.

VOL. 22 1961

Since the effect is observed to occur with both solar indices (R and Φ) it is included in observations of the visible and the 10 cm wavelength parts of the spectrum. It is relevant to consider the relation between these two solar indices. For this purpose the regression lines of Φ on R have been calculated and plotted in Fig. 2(c). In this case the lines are parallel indicating that for any fixed value of Φ the corresponding value of R was slightly less in the latter period. Although this effect is too small to allow definite conclusions to be deduced by extrapolating towards the ionizing wavelengths, the possibility remains that the secular effect disclosed could be due to a change in the relative emission on different parts of the

Table 1. Noon median critical frequencies in Mc/s corresponding to the same sunspot number (0·5)

Observatory	February f_0E			February f_0F2		
	1944	1954	Difference	1944	1954	Difference
Burghead	—	—	—	5·1	4·7	−0·4
Canberra	3·3	3·2	−0·1	5·6	5·5	−0·1
Christchurch	3·3	3·1	−0·2	5·7	5·4	−0·3
Churchill	2·8	2·5	−0·3	4·7	4·6	−0·1
Delhi	—	—	—	8·2	6·4	−1·8
Fairbanks	2·3	2·0	−0·3	4·3	4·3	0
Ottawa	2·9	2·8	−0·1	5·7	5·0	−0·7
Huancayo	3·6	3·4	−0·2	8·0	8·0	0
Slough	2·7	2·6	−0·1	5·5	5·3	−0·2
Tromso*	—	—	—	4·9	4·25	−0·65
Washington	3·1	2·9	−0·2	6·0	5·7	−0·3
Watheroo	3·1	3·1	0	6·8	5·9	−0·9

* These are mean values.

spectrum. A second possibility is that a secular change in the conditions between the earth and the sun has occurred and a third possibility is that the change occurs in the ionosphere itself. These explanations are still under consideration but it is noted that the secular changes occur both at sunspot maximum and at sunspot minimum and in both the E-region and the F-region.

The computed values of the intercepts on the axis for $R = 0$ are plotted in Fig. 3(a) for the relationship I_{F2}/R and on the same diagram the corresponding values in the relationship Ch_E/R are plotted for Slough and Washington to illustrate the general similarity in the trends of both quantities.

The computed values of the slopes for the same relationships as for the intercepts are plotted in Fig. 3(b) and these indicate a long period downward trend in the I_{F2}/R relationship and its similarity to the corresponding Ch_E/R relationships in the data for Slough and Washington.

At a high level of sunspot activity ($R = 100$) the changes in Ch_E and in I_{F2} with time are shown in Fig. 4 to illustrate the steady decrease which has taken place in the measured values of the critical frequencies for both regions over the years.

A decrease with time in the measured values near sunspot minimum ($R = 0{\cdot}5$) is shown in Table 1. All stations at which measurements were made in both 1944

and 1954 are included in the table. The seasonal variation has been eliminated by considering only the same month in the two epochs. The table shows that there was an average reduction of about 7 per cent in the measured value.

CONCLUSIONS

A study of the relationship of sunspot numbers to F-region measurements as denoted by the world ionospheric index I_{F2} reveals a long-term variation corresponding to that described for the E-region. The secular variation thus disclosed

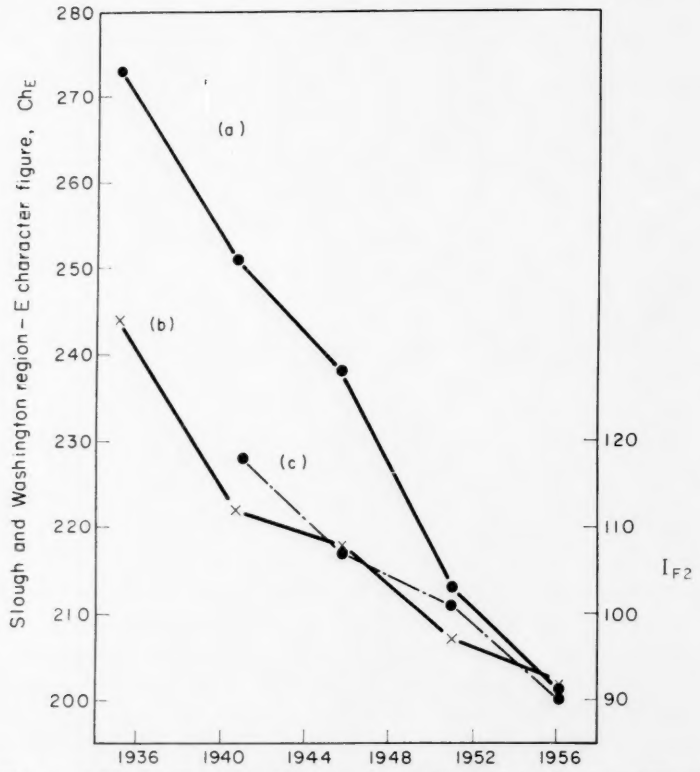

Fig. 4. Values of Ch$_E$ for Slough and Washington and World I_{F2} for $R = 100$. (a) Ch$_E$ Washington, (b) Ch$_E$ Slough, (c) I_{F2}.

requires that consideration be given to the dates on which ionospheric measurements have been made.

Acknowledgements—The work described was carried out as part of the programme of the Radio Research Board. The paper is published by permission of the Director of Radio Research of the Department of Scientific and Industrial Research.

REFERENCES

MINNIS C. M. and BAZZARD G. H. 1960 *J. Atmosph. Terr. Phys.* **18**, 297.
NAISMITH R., BEVAN H. C. and SMITH P. A. 1961 *J. Atmosph. Terr. Phys.* **21**, 167.

VOL. 22 1961

Journal of Atmospheric and Terrestrial Physics, 1961, Vol. 22, pp. 275 to 289. Pergamon Press Ltd. Printed in Northern Ireland

The varying electron density profile of the F-region during magnetically quiet nights

W. Becker
Max-Planck-Institut für Aeronomie, Institut für Ionosphären-Physik,
(20b) Lindau/Harz über Northeim/Hann., Germany

(*Received* 4 *August* 1961)

Abstract—Ionogrammes taken at Lindau and at two field stations (average distance from Lindau 125 km) on magnetically quiet nights were reduced to $N(h)$-profiles of the F-layer. The normalized profiles showed maximum height changes of about 60 km lasting for about 2 hr; they also showed layer height differences on comparable nights of more than 100 km. No seasonal influence on the rise and descent of these profiles in the late evening and early morning hours respectively could be found. The ionogrammes of the field stations did not show any local difference or temporal displacement. Generally, the electron loss rate at the F-layer peak is closely related with the height of the peak and therefore dependent on season. Spread-F echoes of high intensity are occasionally observed at Lindau even on magnetically quiet nights; they are not necessarily associated with vertical movements of the F-layer. No spread-F echoes were observed during vertical movements of the F-layer induced by positive magnetic bay disturbances. Both observations do not allow to decide whether vertical movements cause instability-conditions within the F-layer or not.

1. Introduction

A study of the behaviour of the night-time ionosphere is important because the electron density profile of the ionosphere is monotonic at night so that accurate real height calculations can be made. A second important point suggesting such a study is the fact that after sunset there is no prominent ionizing agent present leading to a reformation of an otherwise disturbed F-region.

The reason for studying the behaviour of the F-region on a magnetically quiet night was an electron density profile of the F-region which varied during a positive magnetic bay disturbance as shown in Fig. 1.

Fig. 1 shows the real height* variation of constant ionization ratios f_0/f_{c0}. f_0 is the plasma frequency of each level and f_{c0} the ordinary critical frequency of the F-region. The intensity variation of the earth's magnetic field and the observed spread-F intensities (given in an arbitrary scale 0, 1, 2, 3), are shown in the lower part of Fig. 1. The striking feature of Fig. 1 is the delay of $\frac{3}{4}$ hr between the end of the bay disturbance and the maximum heights of the ionization levels. Theory (Martyn, 1953; Kohl, 1960) and other observations allow for a delay of no more than a few minutes but not for $\frac{3}{4}$ hr. The suggestion is made that a mechanical disturbance initially compensated the induced rise. So investigations were started on the varying electron density profile of the F-region during magnetically quiet nights.

In the second part of this paper real height variations lasting only for a few hours are reported. The third part of the paper demonstrates striking height differences which occur from night to night and from season to season. Spread-F observations and the stability of the F-region are discussed in Section 4 of this paper.

* As to the procedure used for calculating the $N(h)$ profile see Becker (1959).

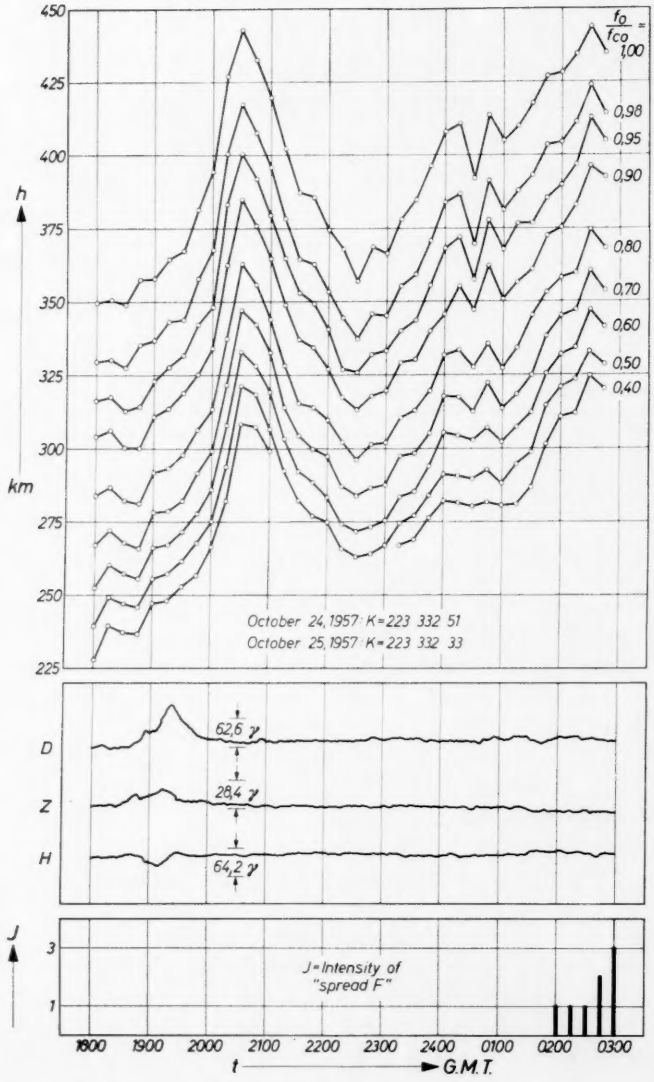

Fig. 1. Real heights, h, deduced from quarter-hourly ionogrammes taken at Lindau/Harz. f_0 measures the plasma frequency, and $f_{c0} = f_{c0}F2 = f_0F2$ the ordinary critical frequency of the F-layer. The D(East–West)-, H(North–South)-, Z(vertical)-components of the earth's magnetic field were observed at Göttingen (30 km from Lindau). The Bartels' K-figures were supplied by the Geomagnetic Observatory at Wingst (250 km to the north of Lindau).

VOL. 22 1961

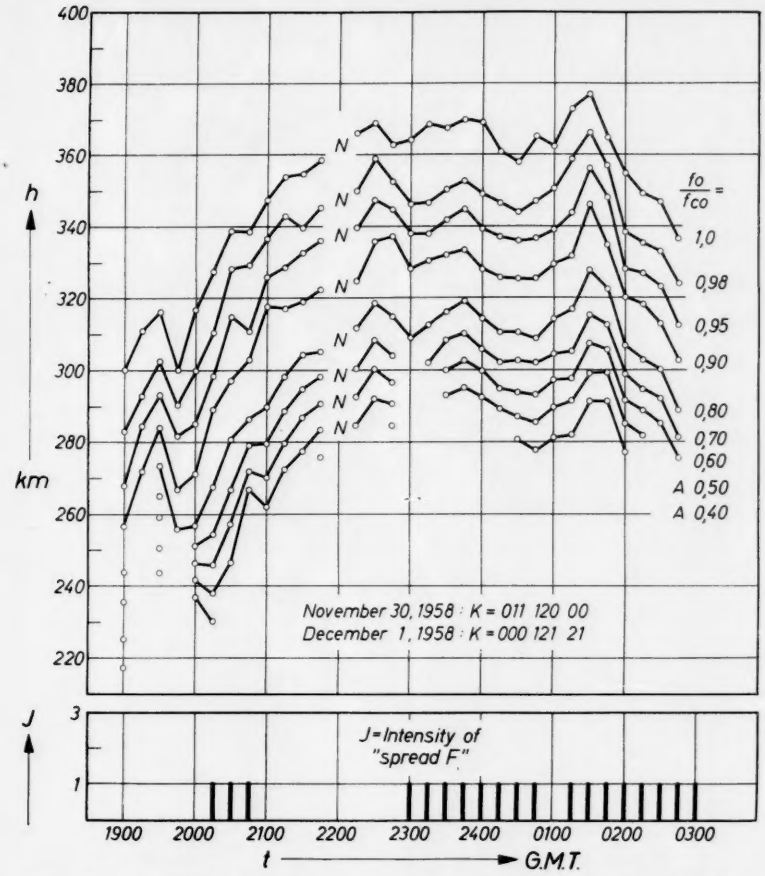

Fig. 2. Real heights, h, deduced from quarter-hourly ionogrammes taken at Lindau/Harz. f_0 measures the plasma frequency, and $f_{c0} = f_{c0}F2 = f_0F2$ the ordinary critical frequency of the F-layer. The D(East–West)-, H(North–South)-, Z(vertical)-components of the earths' magnetic field were observed at Göttingen (30 km from Lindau). The Bartels' K-figures were supplied by the Geomagnetic Observatory at Wingst (250 km to the north of Lindau).

2. Short-term Height Variations

During the night of 30 November to 1 December the earth's magnetic field was extremely quiet. The Wingst K-figures for these days were:

30 November 1958, K = 011 120 00;
1 December 1958, K = 000 121 21.

Fig. 2 shows the varying ionospheric electron density for quarter-hourly intervals on that night. The curve with $f_0/f_{c0} = 1$ refers to the F-layer peak. The time variation of the real heights shows no striking features; on the contrary, it is very smooth and seems to be typical of an undisturbed ionosphere. The same is true for

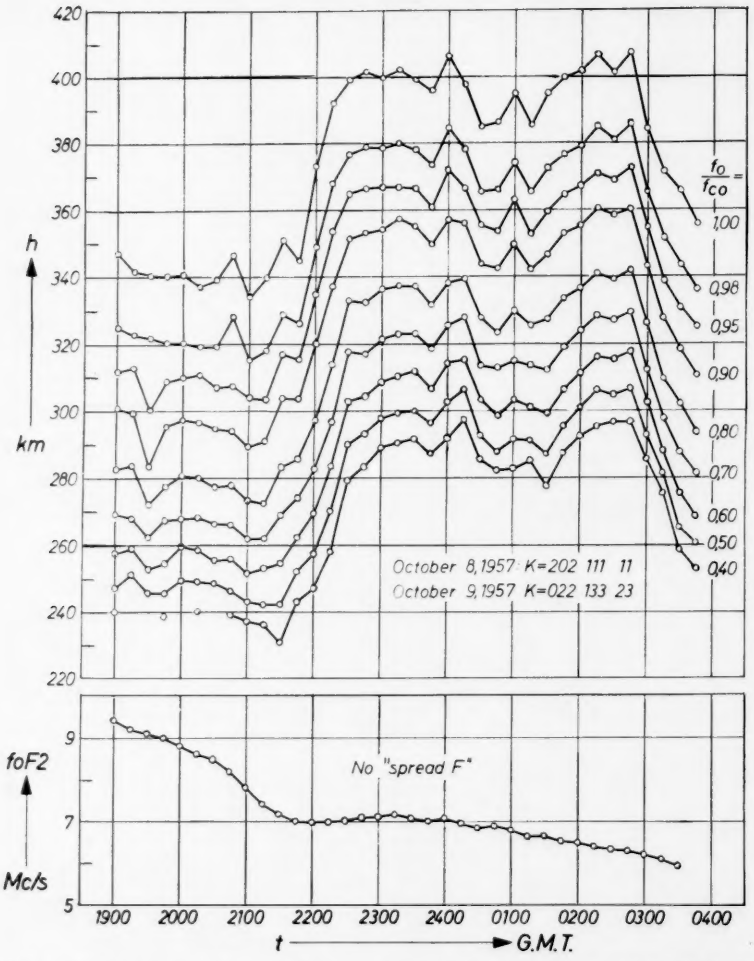

Fig. 3. Real heights, h, deduced from quarter-hourly ionogrammes taken at Lindau/Harz. f_0 measures the plasma frequency, and $f_{c0} = f_{c0}F2 = f_0F2$ the ordinary critical frequency of the F-layer. The D(East–West)-, H(North–South)-, Z(vertical)-components of the earth's magnetic field were observed at Göttingen (30 km from Lindau). The Bartels' K-figures were supplied by the Geomagnetic Observatory at Wingst (250 km to the north of Lindau).

the heights themselves. Their maximum value at about midnight is no greater than 375 km. The presence of spread-F echoes of low intensity was noted, as shown in Fig. 2. It should be stressed that this example of ionospheric behaviour during a magnetically quiet night is rather an exception. This is demonstrated in the figures of this Section.

Fig. 3 is such an example. The K-figures for the days concerned were also very low:

8 October 1957, K = 202 111 11;

9 October 1957, K = 022 133 23.

VOL. 22 1961

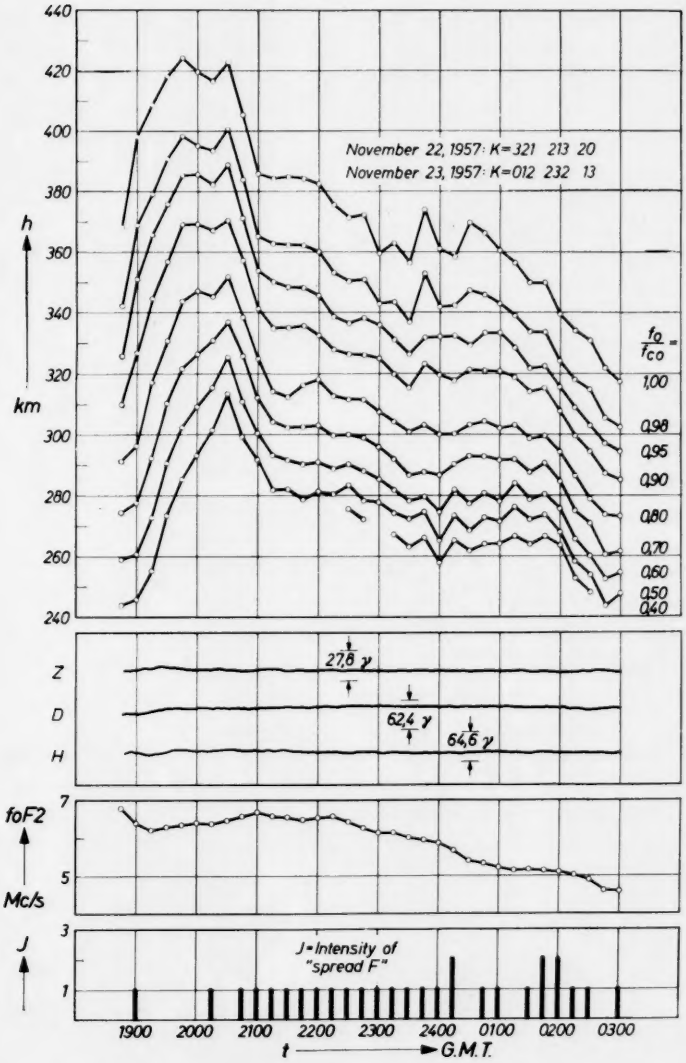

Fig. 4. Real heights, h, deduced from quarter-hourly ionogrammes taken at Lindau/Harz. f_0 measures the plasma frequency, and $f_{c0} = f_{c0}F2 = f_0F2$ the ordinary critical frequency of the F-layer. D(East–West)-, H(North–South)-, Z(vertical)-components of the earth's magnetic field were observed at Göttingen (30 km from Lindau). The Bartels' K-figures were supplied by the Geomagnetic Observatory at Wingst (250 km to the north of Lindau).

They characterize the night 8/9 October as a quiet night. Fig. 3 shows, however, that even at 1900 hours the ionization levels were higher by about 40 km than at the same time on 30 November/1 December. These heights remain constant for about $2\frac{1}{2}$ hr and then increase very fast by about 50 km within $\frac{1}{2}$ hr. About 3 hr after midnight the ionization levels drop, but much faster than after midnight on 1 December (Fig. 2). It is interesting to see this fast height change being reflected in the time variation of the critical frequency of the F-layer. No spread-F echoes (even during the sudden height change) were observed throughout this night.

Another sudden change in ionization level heights was observed in the early evening hours on 22/23 November (Fig. 4). No reason for this phenomenon can be found in the D-, H-, Z-intensities of the earth's magnetic field for the same interval. After midnight there is a good correspondence in layer heights with those of Fig. 2, i.e. those of 1 December 1957. Spread-F echoes were observed on 22/23 November 1957. Again we can see this fast height variation being reflected in the time variation of the critical frequency of the F-layer.

K-figures for the above days:

22 November 1957, K = 321 213 20;
23 November 1957, K = 012 232 13.

A similar picture was obtained for the night 22/23 December as is shown in Fig. 5.

According to the intensity of the earth's magnetic field or the K-figures:

22 December 1957, K = 221 111 10;
23 December 1957, K = 121 221 11.

The night was undisturbed so that the reason for this rise must be looked for elsewhere. Spread-F echoes of low, mean and high intensities were observed.

The earth's magnetic field was extremely quiet during the night 1/2 January as the K-figures show:

1 January 1959, K = 000 110 00;
2 January 1959, K = 000 221 21.

What was observed is shown in Fig. 6.

The presence of intense spread-F echoes did not allow accurate critical frequency measurements. For this season, the ionization parameters in Fig. 6 refer to particular values of plasma frequencies f_0 rather than f_0/f_{c0}. Contrary to Fig. 4 and Fig. 5 the level heights remain constant till midnight and then increase very abruptly.

These height variations are also being studied by a three sounding station network. Our two field stations, Ostenland (westwards of Lindau) and Gedern (in the South of Lindau) are 100 and 150 km from Lindau respectively.

Fig. 7 shows the data for the $f_0/f_{c0}F2 = 0{\cdot}95$ ionization level, the critical frequencies and the optical sunrise (S.R.) and sunset (S.S.) data versus height for the stations Lindau and Ostenland.

VOL. 22 1961

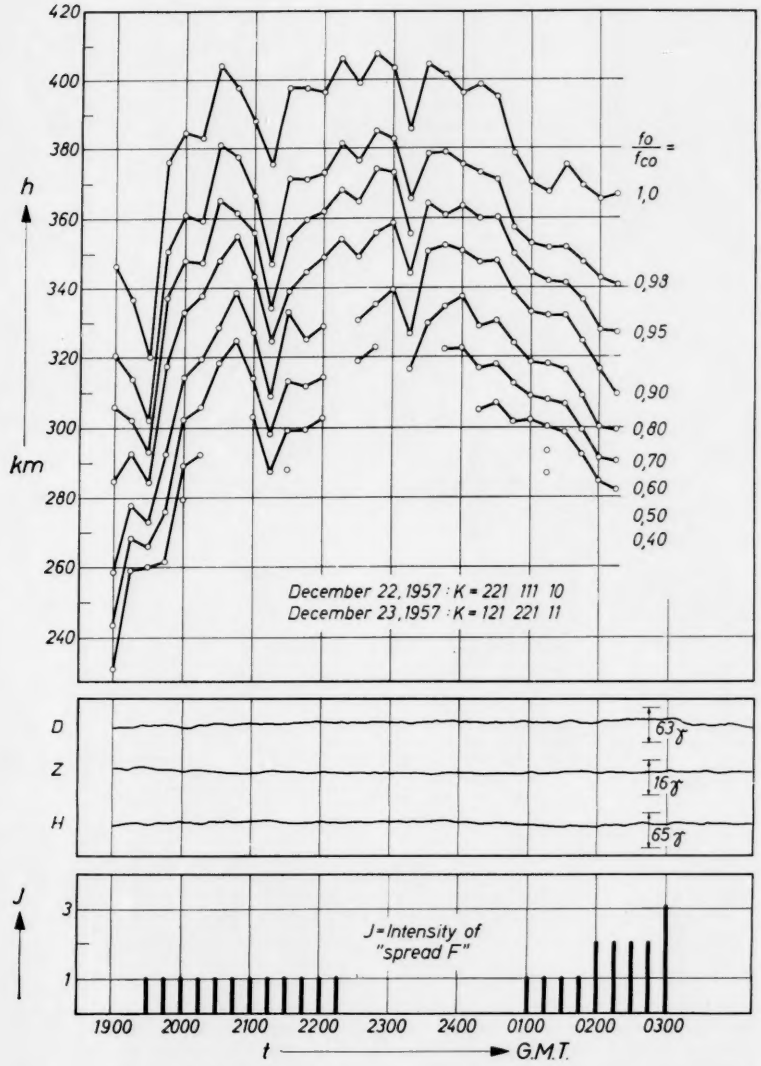

Fig. 5. Real heights, h, deduced from quarter-hourly ionogrammes taken at Lindau/Harz. f_0 measures the plasma frequency, and $f_{c0} = f_{c0}F2 = f_0F2$ the ordinary critical frequency of the F-layer. The D(East–West)-, H(North–South)-, Z(vertical)-components of the earth's magnetic field were observed at Göttingen (30 km from Lindau). The Bartels' K-figures were supplied by the Geomagnetic Observatory at Wingst (250 km to the north of Lindau).

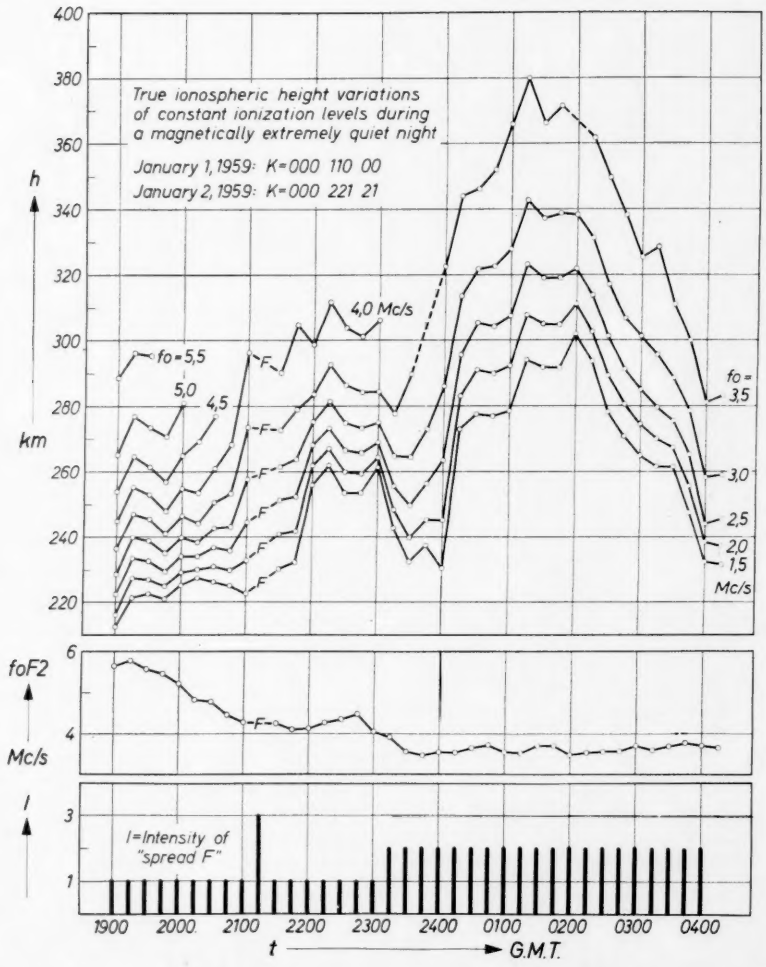

Fig. 6. Real heights, h, deduced from quarter-hourly ionogrammes taken at Lindau/Harz. f_0 measures the plasma frequency, and $f_{c0} = f_{c0}F2 = f_0F2$ the ordinary critical frequency of the F-layer. The D(East–West)-, H(North–South)-, Z(vertical)-components of the earth's magnetic field were observed at Göttingen (30 km from Lindau). The Bartels' K-figures were supplied by the Geomagnetic Observatory at Wingst (250 km to the north of Lindau).

VOL. 22 1961

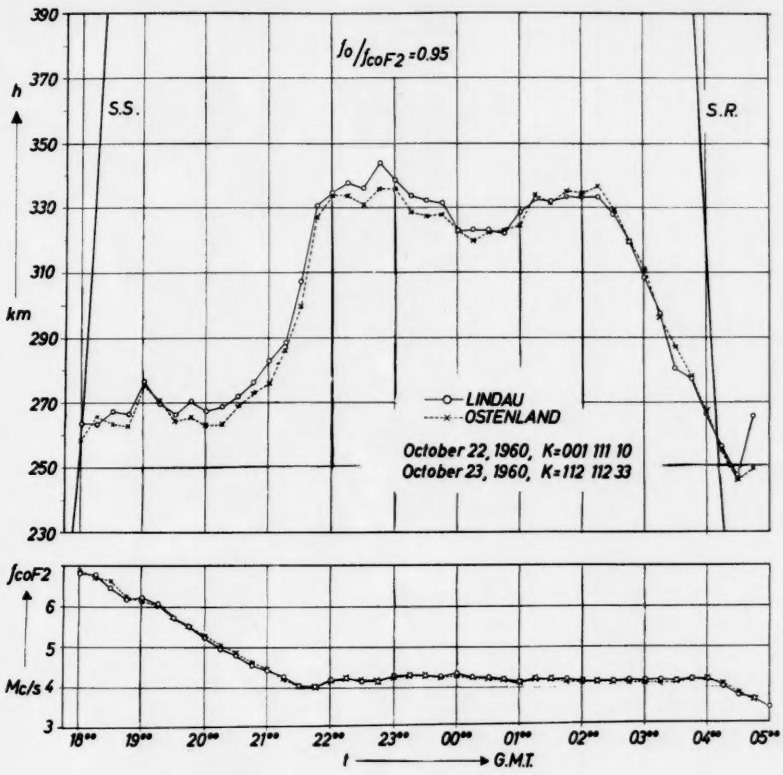

Fig. 7. Real heights, h, deduced from quarter-hourly ionogrammes taken at Lindau/Harz and Ostenland (100 km westward of Lindau/Harz). Optical sunrise- (S.R.) and sunset-data (S.S.) versus height. f_0 = plasma frequency, $f_{c0}F2$ = critical frequency of the F-layer.

Gedern was not in operation during that night, 22/23 October 1960. During this night the earth's magnetic field was very quiet as the K-figures show:

22 October 1960, K = 001 111 10;

23 October 1960, K = 112 112 23.

As expected, the correspondence between the data of both stations is extremely good. Also a fast height change at about 2130 GMT was observed as on 8/9 October 1957. This too is reflected in the time variation of the critical frequency of the F-layer. Here again there is no obvious correlation between the times of rise and descent of the layer and the times of optical sunrise and sunset respectively. This phenomenon is not a local one at least not for an area defined by our three stations. A full description is being given elsewhere.

3. Day-to-day and Season-to-season Real Height Variations

It was mentioned in Section 2 of this report that there may be considerable height differences between equal ionization levels for different days in the same

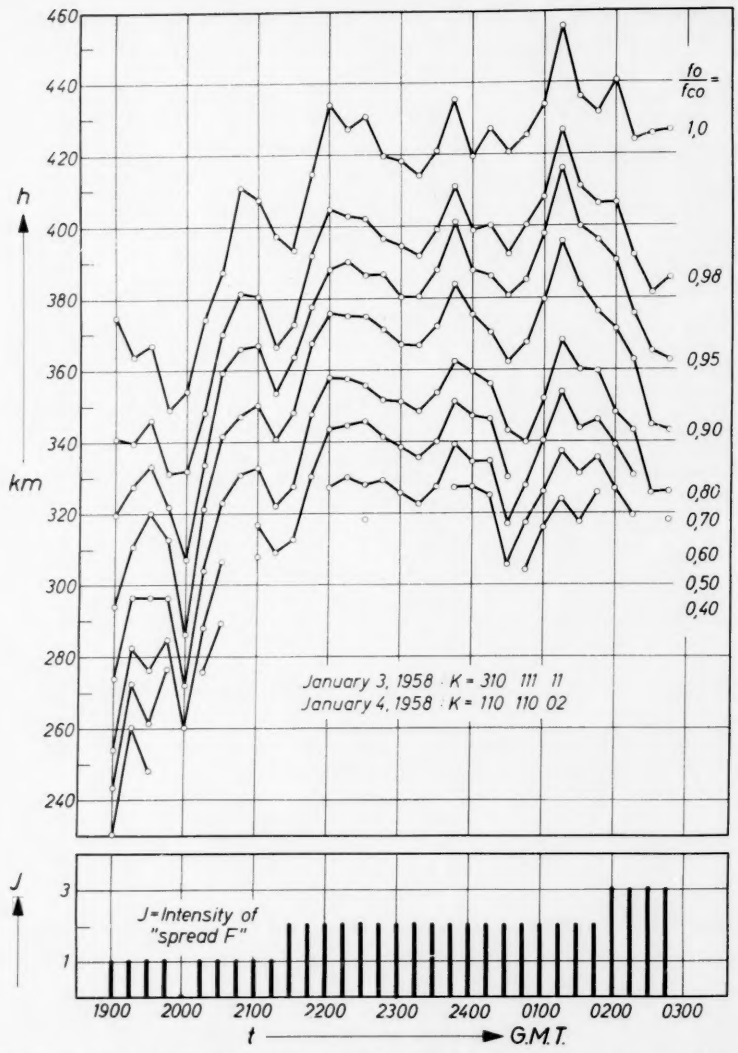

Fig. 8. Real heights, h, deduced from quarter-hourly ionogrammes taken at Lindau/Harz. f_0 measures the plasma frequency, and $f_{c0} = f_{c0}F2 = f_0F2$ the ordinary critical frequency of the F-layer. The D(East–West)-, H(North–South)-, Z(vertical)-components of the earth's magnetic field were observed at Göttingen (30 km from Lindau). The Bartels' K-figures were supplied by the Geomagnetic Observatory at Wingst (250 km to the north of Lindau).

season. Fig. 8 shows the real height data for another quiet winter night, 3/4 January 1958. The K-figures for both days were:

3 January 1958, K = 310 111 11;

4 January 1958, K = 110 110 02.

Comparing Fig. 8 with Fig. 7 one finds a maximum height difference for the F-layer peaks of 90 km. This difference gets even greater by 60 km, if Fig. 8 and

VOL. 22 1961

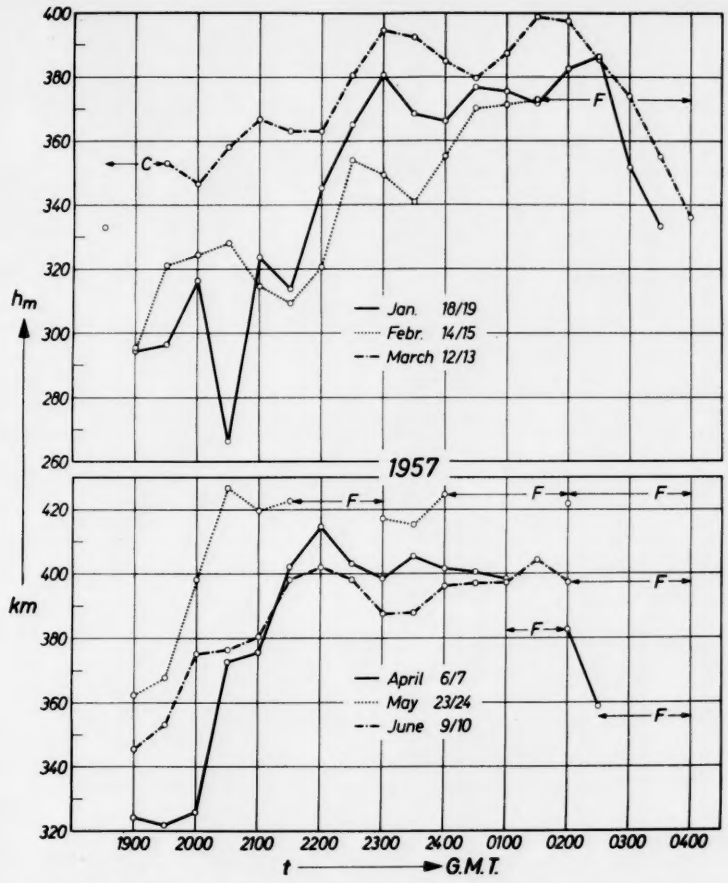

Fig. 9. Real height variation of the F-layer peak (h_m) deduced from ionogrammes taken at Lindau/Harz. The letter "F" means, that h_m-values could not be deduced because of intense spread-F.

Fig. 6 are compared with each other. We have not yet any explanation for these height variations on magnetically quiet nights.

Figs. 9 and 10 may demonstrate the seasonal phenomenon. They show the real height variation of the F-layer peak during one night per month of the year 1957. The magnetically quietest night of each month was selected. The other ionization levels are not reproduced in these figures, because their additional information would concern only fine-structure differences which are not of interest here.

Fig. 9 and Fig. 10 show that the curves for the summer months differ only slightly from each other. This is quite reasonable, because during these months the F-region is constantly reformed by incident radiation. On 15 June 1957 for example, optical sunrise and sunset coincided at a height of 173 km above Lindau. The nights of the winter months and the equinoctial months may differ enormously.

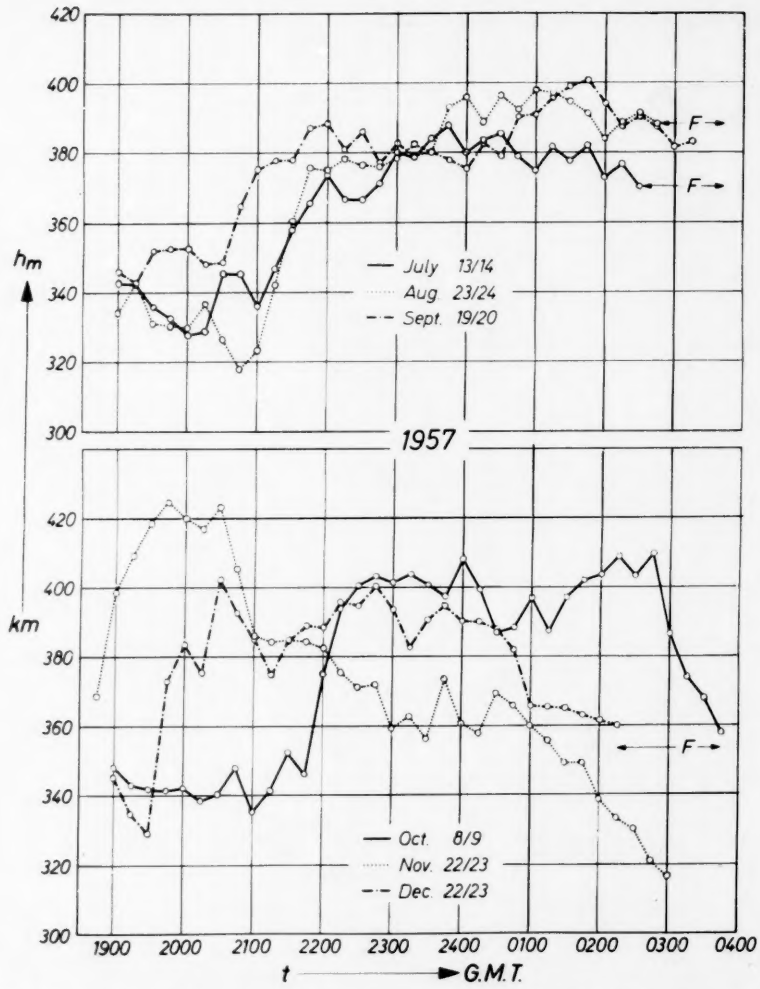

Fig. 10. Real height variation of the F-layer peak (h_m) deduced from ionogrammes taken at Lindau/Harz. The letter "F" means that h_m-values could not be deduced because of intense spread-F.

Height differences of about 100 km may be observed even on magnetically extremely quiet nights. Both Figs. 9 and 10 underline our above statement that there is a general rise of the F electron density profile between 2000 and 2100 hours and that this rise is independent on any seasonal influence. The same is approximately true for the descent of the profile.

4. Vertical Movements of the F-region and the Occurrence of Spread-F

Vertical movements of the F-region due to positive magnetic bay disturbances, that is to say due to a horizontal electric field do not induce turbulence in the F-region giving rise to spread-F echoes.

VOL. 22 1961

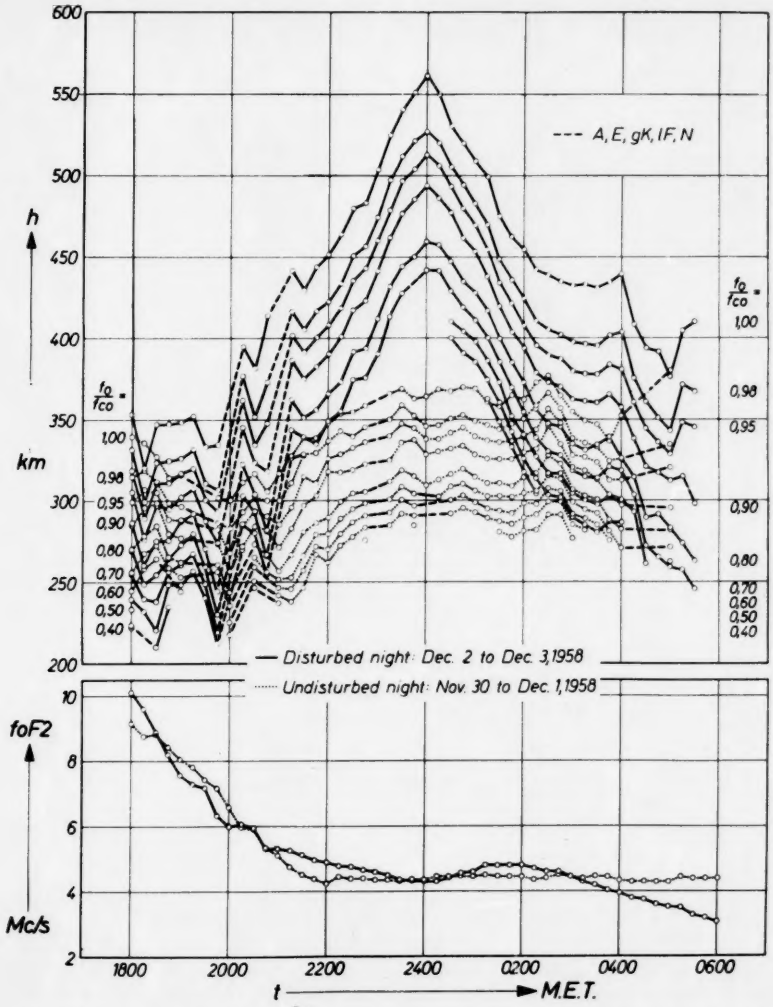

Fig. 11(a). Real heights, h, deduced from quarter-hourly ionogrammes taken at Lindau/Harz for a magnetically quiet (30 November/1 December 1958) and a disturbed night (2/3 December 1958). f_0 = plasma frequency; $f_{c0} = f_0F2$ = ordinary critical frequency. Dashed lines mean that accurate real heights could not be deduced as a consequence of either blanketing by sporadic-E, high absorption, spread-F or experimental failures.

Figs. 11(a) and (b) show a total rise of the F-layer peak during a severe magnetic bay disturbance on 2/3 December 1958 of about 200 km if the magnetically quiet night 30 November/1 December may be taken as a reference night (see Fig. 2). Fig. 12(a) shows the ionogram taken at Lindau on 2 December 1958, 2300 hours, during the main phase of the vertical layer rise. This record is representative of all the other records. The corresponding ionogram for the magnetically extremely quiet night 30 November/ 1 December is shown in Fig. 12(b). Only the latter

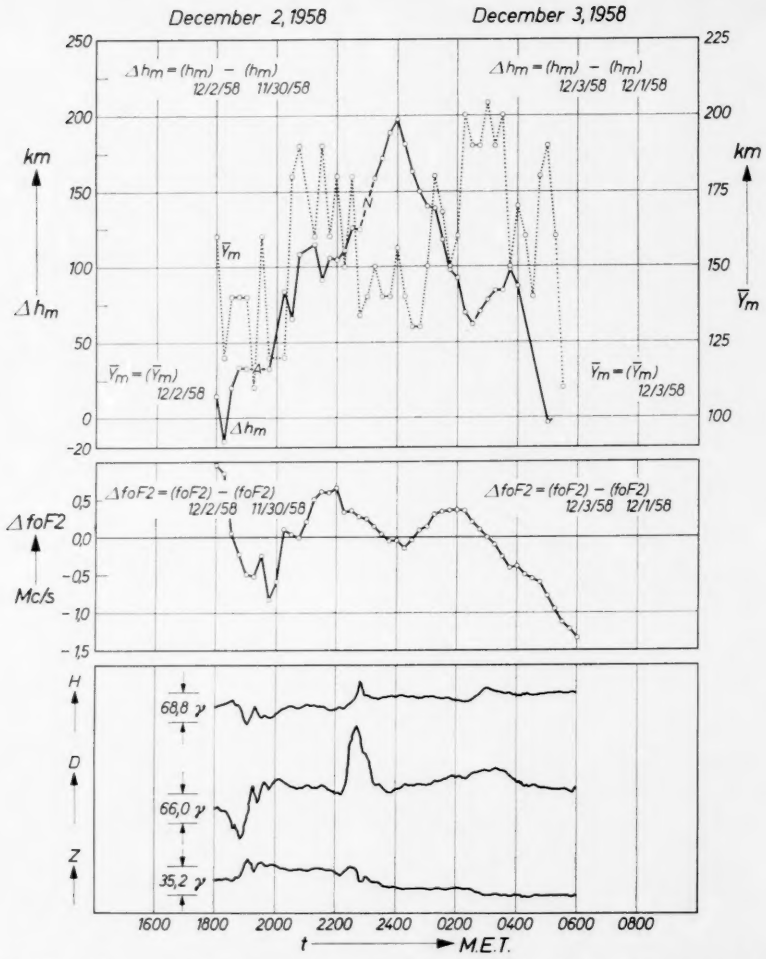

Fig. 11(b). Δh_m means the difference between the real heights of the F-layer peaks of the magnetically disturbed and undisturbed nights (Fig. 11a). Y_m measures the half-layer thickness of a parabolic fit to the maximum of the F-layer electron density profile as deduced from quarter-hourly ionogrammes taken at Lindau/Harz during the magnetically disturbed night. D, H, and Z measure the intensities of the components of the earth's magnetic field and refer to the disturbed night.

shows spread-F echoes. These observations do not seem to settle the question, whether vertical movements of the F-region prevent any formation of inhomogeneities within the F-layer or not (MARTYN, 1959; DOUGHERTY, 1959). If the latter is true, the electrical fields inducing the above mentioned vertical movements (KOHL, 1960) must be responsible for the failure of spread-F echoes.

It is well known (WRIGHT, 1959) that there is no correlation between magnetic activity and the occurrence of spread-F echoes at equatorial regions but an excellent correlation at polar stations. The preceding figures show that we seem to participate in both phenomena at our latitude. This again is in agreement with the results

VOL. 22 1961

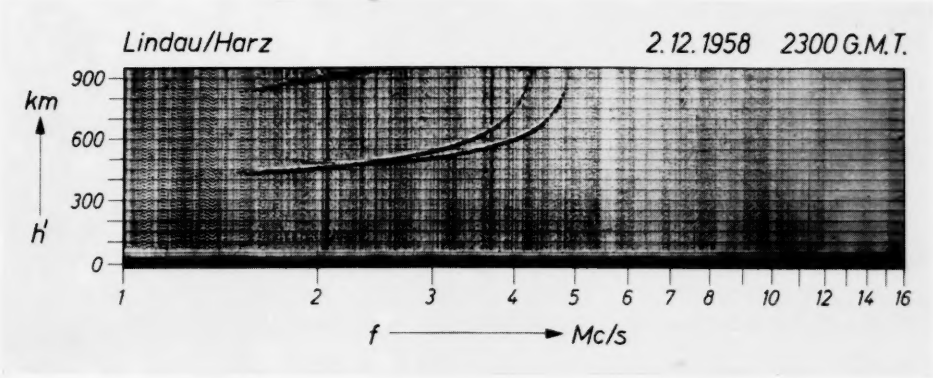

Fig. 12(a). Ionogram taken at Lindau/Harz on 2 December 1958, 2300 hours GMT.

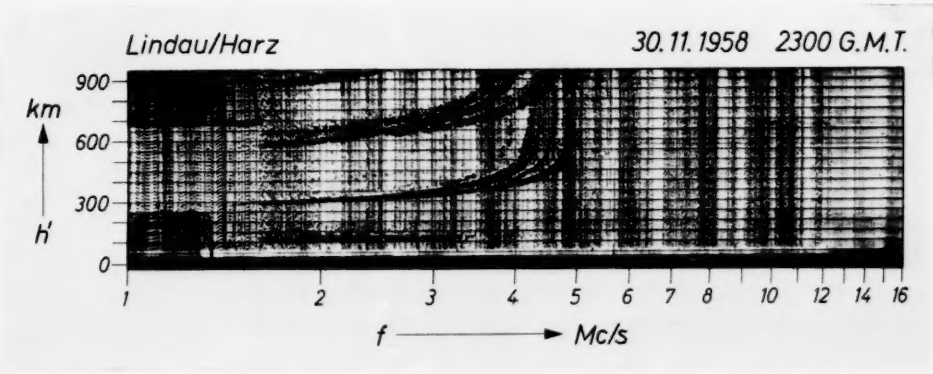

Fig. 12(b). Ionogram taken at Lindau/Harz on 30 November 1958, 2300 hours GMT.

VOL.
22
1961

of SINGLETON (1960) who reported a geographical dependence of the occurrence of spread-F. BOWMAN (1960) reported a correlation between spread-F intensity and the height of the F-layer above Brisbane. There is no evidence from the real height data which have been presented in this paper that such a correlation exists for magnetically quiet nights.

5. CONCLUSION

F-layer real height data of magnetically quiet nights revealed maximum changes of about 60 km lasting for about 2 hr and differences between comparable nights of more than 100 km. No seasonal influence on the rise and descent of the F-electron density profile at night could be found. These phenomena are not of a local nature at least not for an area of 150×100 km^2.

Acknowledgements—The work described in the paper was carried out with special financial assistance of the Max-Planck-Gesellschaft zur Förderung der Wissenschaften e.V., Gottingen, which is gratefully acknowledged. The author is indebted both to his colleagues K. H. GEISWEID and W. BARKE for maintaining the sounding stations and to Miss U. GOLLMER and to Miss R. TETZLAFF for the reduction work.

REFERENCES

BECKER W.	1959	*J. Atmosph. Terr. Phys.* **16,** 67.
BOWMAN G. G.	1960	*Aust. J. Phys.* **13,** 69.
DOUGHERTY J. P.	1959	*J. Geophys. Res.* **64,** 2215
KOHL H.	1960	*Mitt. aus dem Max-Planck-Inst. f. Aeronomie* Nr. 3. Springer, Berlin.
MARTYN D. F.	1953	*Proc. Roy. Soc.* A **218,** 1.
MARTYN D. F.	1959	*J. Geophys. Res.* **64,** 2178.
SINGELTON D. G.	1960	*J. Geophys. Res.* **65,** 3615
WRIGHT R. W. H.	1959	*J. Geophys. Res.* **64,** 2203.

Journal of Atmospheric and Terrestrial Physics, 1961, Vol. 22, pp. 290 to 297. Pergamon Press Ltd. Printed in Northern Ireland

The morphology of lunar semi-diurnal variation in f_0F2 near solar noon

R. G. RASTOGI
High Altitude Observatory, Boulder, Colorado

(*Received* 14 *August* 1961)

Abstract—The variations of the midday critical frequency of the *F2*-layer, f_0F2, with the phase of the moon are computed for eighteen stations within about $\pm 40°$ latitude during a period of low sunspot activity. The results show that the phase of the lunar variation of f_0F2 is determined by the magnetic and not by the geomagnetic or the geographic latitude. The reversal from the equatorial type of variation with a maximum near 04 lunar hour to the higher latitude type with a maximum near 10 lunar hour occurs at about $\pm 11°$ magnetic latitude. The variation of amplitude with latitude shows a sharp maximum on the magnetic equator, associated with the equatorial electro-jet, and two broad maxima at about $\pm 20°$ magnetic latitude. The latter are closely associated with the well-known maxima in the variation of noon f_0F2 with latitude.

INTRODUCTION

THE first direct evidence of lunar tidal phenomena in the *F2*-layer was given by MARTYN (1947) who found tidal changes in both the height of maximum, h_mF2, minimum virtual height, $h'F2$, and the critical frequency, f_0F2, at Huancayo. The maximum deviation of noon f_0F2 was 4 per cent at about 03 lunar hour after transit. However, later studies of f_0F2 at other stations showed that there were large changes in both the phase and the amplitude with position (APPLETON and BEYNON, 1948; MARTYN, 1948; MCNISH and GAUTIER, 1949). Detailed studies at particular stations show that the lunar perturbations also varies with solar time (MARTYN, 1947; BURKARD, 1951; BROWN, 1956). In this report, the analysis is restricted to data obtained near midday.

The published values of the amplitude and phase of the lunar semi-diurnal variations of f_0F2 as measured near noon are summarized in Table 1. This has been divided into two parts; stations with phases near 3·8 lunar hours are collected together as are those with phases near 9·8 lunar hours. The systematic grouping with approximately 180° phase difference (6 lunar hours) is very obvious.

MCNISH and GAUTIER (1949) have suggested that the phase might depend on geomagnetic latitude but RASTOGI (1961) has shown that the agreement is much better when magnetic latitude is used. This is confirmed by the present analysis. The main objective of the present analysis is to delineate the variations of lunar perturbations of f_0F2 near noon with magnetic latitude for a period of relatively low solar activity, 1952–1955.

METHOD OF ANALYSIS

From the published hourly values of f_0F2, daily averages of the three values at 1100, 1200 and 1300 L.S.T. are computed. These give our individual midday values. The average monthly means are subtracted from the individual day values to obtain the deviations for the particular days. The phases of the moon "μ" for each day are derived from the tables given by BARTELS and FANSELAU (1937). For our purposes, the phases are expressed in units of the nearest integral lunar hour, 00 to 23 and the data are grouped accordingly. The data for days having A_p

VOL. 22 1961

Table 1. Amplitude and phase of lunar semi-diurnal variation in midday value of f_0F2 at different stations available in literature

Station	Latitude			P_2		t_2 (lunar hour)	Period studied	Reference
	Geog. (degr.)	Geom. (degr.)	Magn. (degr.)	(Mc/s)	(%)			
Huancayo	−12·1	−0·6	+1	—	4·2	3·3	1942–1944	Martyn (1947)
Leyte	+11·0	−0·2	+4	0·53	—	4·2	—	McNish and Gautier (1949)
Huancayo	−12·1	−0·6	+1	0·45	—	4·0	—	McNish and Gautier (1949)
Tiruchy	+10·2	+1·0	+2·4	0·13	1·8	2·2	Jan. 1954–Dec. 1954	Kotadia and Ramanathan (1956)
Christmas Is.	+1·9	+2·1	+3	0·33	—	4·7	—	McNish and Gautier (1949)
Madras	+13·1	+3·1	+6·3	0·14	1·8	3·8	Jan. 1954–Dec. 1954	Kotadia and Ramanathan (1956)
Singapore	+1·3	−10·0	−9	0·30*	—	4·0*	Nov. 1948–June 1951	Osborne (1952)
Ibadan	+7·4	+10·4	−2·5	0·33*	4·2*	3·3	Dec. 1951–Apr. 1954	Brown (1956)
Leopoldville	−4·4	−3·1	+18	0·33	3·2	10·5	Nov. 1953–Oct. 1956	Rastogi (1961)
Bombay	+19·0	+9·8	+13	0·24	2·6	10·0	Jan. 1954–Dec. 1954	Kotadia and Ramanathan (1956)
Ahmedabad	+23·0	+13·6	+18·6	0·35	3·9	10·2	Jan. 1954–Dec. 1954	Kotadia and Ramanathan (1956)
Maui	+20·8	+20·8	+23	0·36	—	9·1	—	McNish and Gautier (1949)
Trinidad	+9·7	+22·0	+24	0·31	—	9·2	—	McNish and Gautier (1949)

* These values are derived from the curves given in the original report.

values greater than 50 are rejected so as to avoid the large perturbations associated with the magnetic disturbances. The average deviations are then found for each lunar hour. The first two Fourier components of the resultant variation are computed giving the phases and amplitudes of the lunar diurnal and semi-diurnal variations of f_0F2. The resultant phases are corrected for the errors due to the movement of the moon between Greenwich and local noon. The amplitude of the first harmonic is usually small compared with the second harmonic as expected on

Table 2. Amplitude and phase of Lunar semi-diurnal variation in midday value of f_0F2 at different stations analysed by the author

Station	Latitude			P_2		t_2 (lunar hour)	Period studied
	Geog. (degr.)	Geom. (degr.)	Magn. (degr.)	(Mc/s)	(%)		
Ibadan	+7·4	+10·6	−2·5	0·22	3·0	3·2	Jan. 1952–Dec. 1954
Nha Trang	+12·2	+0·7	+3	0·36	4·95	3·1	Jul. 1952–Oct. 1954
Djibouti	+11·6	+7·0	+3	0·21	2·4	2·5	Jan. 1952–Dec. 1953
Khartoum	+15·6	+12·9	+7	0·22	2·3	2·1	Mar. 1952–Feb. 1954
Guam Is.	+13·5	+3·9	+7	0·13	1·6	2·9	Jan. 1952–Dec. 1954
Singapore	+1·3	−10·0	−9	0·21	2·3	3·5	Jan. 1952–Dec. 1954
Baguio	+16·4	+5·1	+10	0·22	2·5	3·4	May 1952–Apr. 1955
Dakar	+14·7	+21·2	+11	0·12	1·01	10·8	Jan. 1952–Dec. 1953
Sao Paulo	−23·6	−12·9	−12	0·22	2·2	12·4	May 1953–Dec. 1956
Nairobi	−1·3	−4·4	−14	0·22	2·9	10·6	Mar. 1952–Dec. 1954
Lwiro	−2·3	−4·0	−16	0·22	2·4	9·4	May 1952–Dec. 1954
Buenos Aires	−34·6	−23·3	−17	0·21	2·5	10·8	Jan. 1952–Dec. 1954
Leopoldville	− 4·4	−3·1	−18	0·36	3·8	11·0	Feb. 1952–Dec. 1954
Panama	+9·4	+20·6	+20	0·33	3·7	11·6	Jan. 1952–Dec. 1955
Okinawa	+26·3	+15·5	+21	0·37	4·1	10·1	Jan. 1952–Dec. 1955
Yamagawa	+31·2	+20·3	+25	0·17	2·3	10·0	Jan. 1952–Dec. 1954
Tokyo	+35·7	+25·4	+30	0·05	1·5	9·7	Jan. 1952–Dec. 1954
Tananarive	−18·9	−23·7	−36	0·15	2·0	9·2	Apr. 1952–Nov. 1954

theoretical grounds. The amplitudes of the semi-diurnal lunar variation, P_2, of f_0F2 for all the stations studied by the author are given in Table 2 both as deviations in Mc/s and as a percentage of the mean value of f_0F2 for the period studied. The phases t_2 show the times of maximum positive deviation of f_0F2 in lunar hours after transit. The stations are arranged in order of increasing magnetic latitude. The table also shows geographic and geomagnetic latitude and the period analysed.

The Phase of the Semi-Diurnal Variation

The mean lunar semi-diurnal variation can be best shown by combining the data for lunar hour n and lunar hour $n + 12$. Some of the resultant distributions of the f_0F2 deviations with lunar time are shown in Figs. 1 and 2 together with the semi-diurnal component given by the harmonic analysis. The agreement between the curves and the points is remarkably good.

In Fig. 1 are presented the variations for four stations at low magnetic latitude and four stations at relatively high magnetic latitudes, all of which are in Africa,

VOL. 22 1961

where the differences between geographic, geomagnetic and magnetic latitudes are great.

Comparing the latitudes, Table 2, it is clear that the curves are consistent in magnetic coordinates but not consistent in geomagnetic or geographic coordinates. It is noted, in particular, that Nairobi, Lwiro, and Leopoldville behave as high latitude stations despite their low geographic and geomagnetic latitudes.

In Fig. 3 are plotted the phase of the P_2 oscillation for all the stations given in Tables 1 and 2, as functions of geographic, geomagnetic and magnetic latitude.

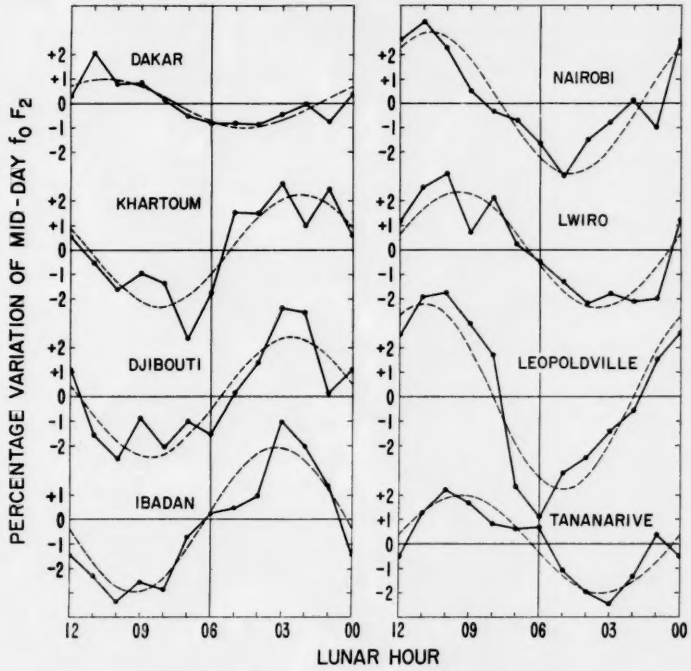

Fig. 1. Lunar semi-diurnal variations in midday values of f_0F2 at stations in Central Africa

Both the geographic and geomagnetic distributions show two distinct and incompatible groups at latitudes below about 10°. The anomaly disappears in the plot against magnetic latitude which shows a rapid decrease in phase between 10° and 11° followed by a more gradual decrease at higher latitudes. It may be noted that the distribution of points in the change-over region strongly supports our curve and makes it unlikely that the phase really increased through 06–07 hours to the higher latitude value. Thus, in Fig. 2, the three stations in the transition zone, Panama, Buenos Aires and Sao Paulo, show maxima near 12 hours and not near 06 hours. No station near the transition zone has a phase angle between 04 and 10 hours.

It is concluded that the phase of lunar semi-diurnal perturbation for midday values of f_0F2 is controlled by magnetic latitude and that the phase decreases from 04 to 09 hours through 12 hours and not through 06 hours lunar time.

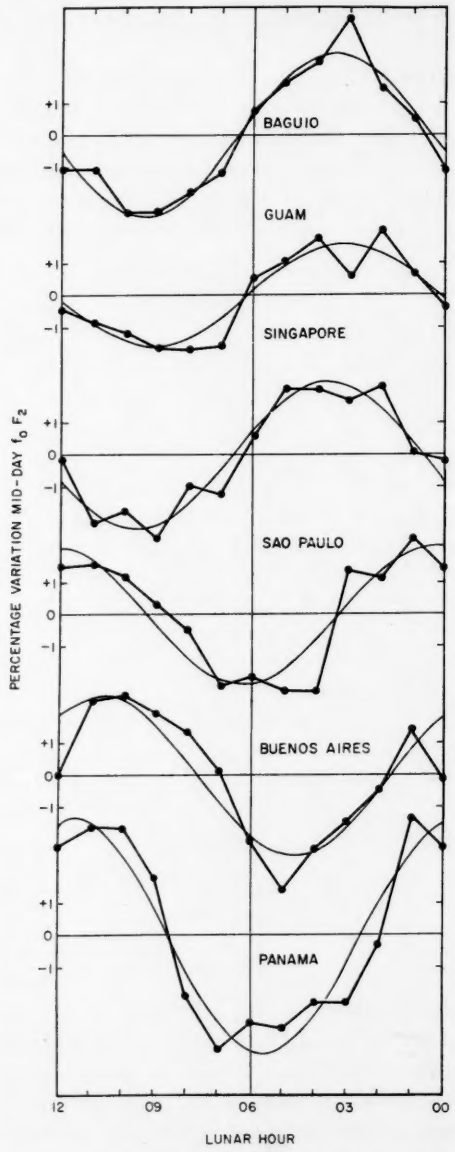

Fig. 2. Lunar semi-diurnal variations in midday values of f_0F2 at some low latitude stations.

THE AMPLITUDE OF THE SEMI-DIURNAL VARIATION

The very large amplitude of the lunar variation in f_0F2 found at Huancayo, Christmas Island and Leyte, Table 1, has led to the idea that the amplitude increases at the lower latitudes. BOSSOLASCO and ELENA (1960) suggested that the amplitude P_2, deduced from all solar hours, varies roughly as a cosine function of

VOL. 22 1961

magnetic dip up to about 75° dip. They have, however, only two stations below 18° magnetic latitude. The present detailed studies at low latitudes, Fig. 4, show that the variation is considerably more complicated at latitudes below about 20°. Owing to the effect of luni-solar terms, our noon values near the magnetic equator are approximately three times greater than means for all hours quoted by above authors. There is thus a large drop in amplitude between 4° and 17° magnetic latitude relative to the values suggested by the cosine rule.

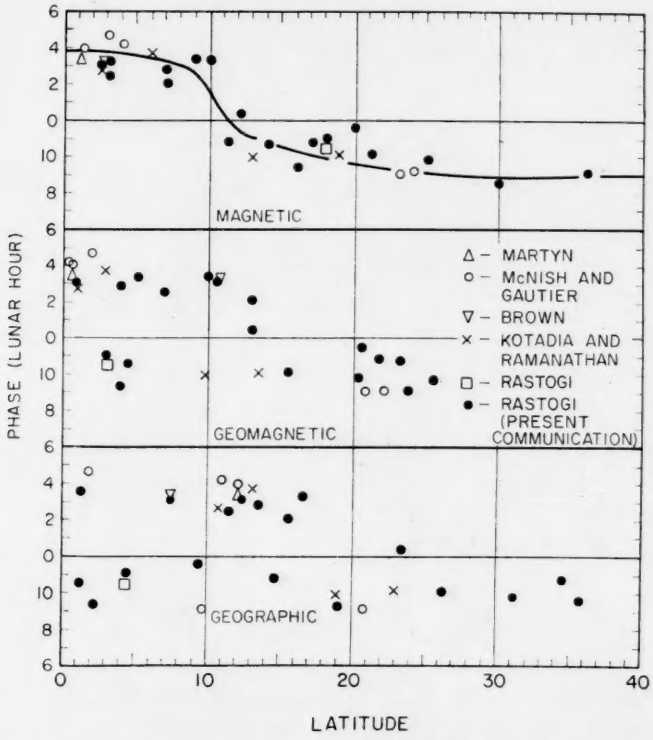

Fig. 3. The phase of lunar semi-diurnal variation of midday values of f_0F2 as functions of geographic, geomagnetic and magnetic latitudes.

Both the absolute deviation and the percentage change of f_0F2, Fig. 4, show the presence of a narrow belt within $\pm 3°$ latitude of the magnetic equator in which the amplitude is abnormally great. Somewhat wider maxima are found centred near magnetic latitudes $\pm 20°$. The three maxima are separated by zones in which the amplitude is almost constant.

It may be noted that the belt of intense equatorial sporadic-E (MATSUSHITA, 1951) is also restricted to $\pm 3°$ in magnetic latitude (KNECHT, personal communication) and is associated with the equatorial electro-jet (SKINNER and WRIGHT, 1957).

BARTELS and JOHNSTON (1940) showed the lunar variations in the horizontal component of the quiet day magnetic field at Huancayo is abnormally large during

the daytime but very small at night. This result is also found at Ibadan, which is near the magnetic equator (ONWUMECHILLI and ALEXANDER, 1959). This is best regarded as a large lunar perturbation of the well-known equatorial electro-jet.

Taking the data as a whole, it appears probable that the abnormally large amplitudes of the lunar perturbations of f_0F2 near the magnetic equator are closely connected with the electro-jet.

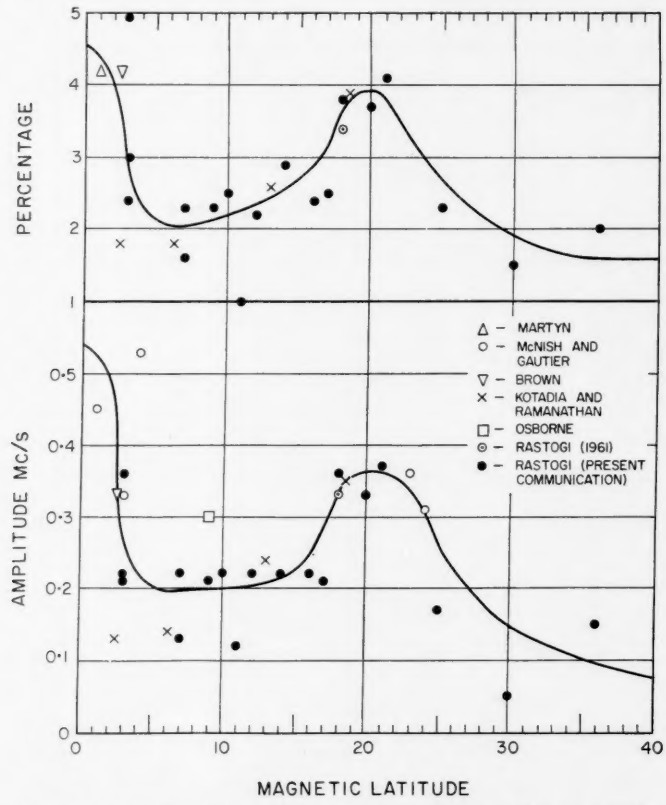

Fig. 4. The amplitude of lunar semi-diurnal variation of midday value of f_0F2 as a function of magnetic latitude.

The stations near 20° magnetic latitude with abnormally high lunar amplitudes, Okinawa, Ahmedabad, Leopoldville and Panama have been shown by RASTOGI (1959a, b) to have the highest noon values of f_0F2 in their respective longitude zones. Since the lunar anomaly shows in the percentage deviation of f_0F2, it is not due only to the local increase in f_0F2. We may conclude that the lunar perturbation is abnormally large in tropical latitudes where f_0F2 at noon itself is abnormally large.

The diurnal variation of f_0F2 at low latitudes and the very high values of f_0F2 near the tropics have been explained (RASTOGI, 1959c) in terms of combined vertical and horizontal transport of electrons. These ideas have been used to

explain other features of the *F2*-layer (RASTOGI, 1959d; DUNCAN, 1960; APPLETON, 1960). Our phenomena suggest that there is a lunar controlled movement of ionization between low and high latitudes of the same general type.

Acknowledgements—The author is indebted to Mr. A. H. SHAPLEY and Dr. W. O. ROBERTS for arranging his visit to Boulder; to the High Altitude Observatory, for awarding him a Post-Doctorate Fellowship; and to the Central Radio Propagation Laboratory of the U.S. National Bureau of Standards for giving him the facilities in the World Data Center A. Part of the work was done during the author's stay at the National Research Council of Canada as a Post-Doctorate Fellow. Thanks are due to Mr. W. R. PIGGOTT for very stimulating discussions and for valuable help in the preparation of this paper. The author is further pleased to acknowledge the valuable discussions and suggestions from Dr. S. MATSUSHITA, Mr. J. W. WRIGHT and Mr. R. A. DUNCAN.

REFERENCES

APPLETON E. V.	1948	*Some Ionospheric Results Obtained during IGY* (Ed. W. J. G. BEYNON), p. 3. Elsevier, Amsterdam.
APPLETON E. V. and BEYNON W. J. G.	1948	*Nature, Lond.* **162,** 486.
BARTELS J. and FANSELAU G.	1937	*Z. Geophys.* **13,** 311.
BARTELS J. and JOHNSTON H. F.	1940	*Trans. Amer. Geophys. Un.* (1940), 273.
BOSSOLOSCO M. and ELENA A.	1960	*Geofis. Pur. Appl.* **46,** 167.
BROWN R. A.	1956	*J. Atmosph. Terr. Phys.* **9,** 144.
BURKARD O.	1951	*J. Atmosph. Terr. Phys.* **1,** 349.
DUNCAN R. A.	1960	*J. Atmosph. Terr. Phys.* **18,** 89.
KOTADIA K. M. and RAMANATHAN K. R.	1956	*Proc. Ind. Acad. Sci.* **43,** 394.
MARTYN D. F.	1947	*Proc. Roy. Soc.* A **190,** 273.
MARTYN D. F.	1948	*Proc. Roy. Soc.* A **194,** 429.
MATSUSHITA S.	1951	*J. Geomagn. Geoelect.* **3,** 44.
MCNISH A. G. and GAUTIER T. N.	1949	*J. Geophys. Res.* **162,** 486.
ONWUMECHILLI C. A. and ALEXANDER N. S.	1959	*J. Atmosph. Terr. Phys.* **16,** 115.
OSBORNE B. W.	1952	*Nature, Lond.* **169,** 661.
RASTOGI R. G.	1959a	*J. Atmosph. Terr. Phys.* **14,** 31.
RASTOGI R. G.	1959b	*Canad. J. Phys.* **37,** 874.
RASTOGI R. G.	1959c	*J. Geophys. Res.* **64,** 727.
RASTOGI R. G.	1959d	Proc. Symp. on *Physical Processes in Sun-Earth Environment,* Ottawa, July, 1959. D.R.T.E. Publication No 1025.
RASTOGI R. G.	1961	*Nature, Lond.* **189,** 214.
SKINNER N. J. and WRIGHT R. W.	1957	*Proc. Phys. Soc. Lond.* B **70,** 833.

Journal of Atmospheric and Terrestrial Physics, 1961, Vol. 22, pp. 298 to 302. Pergamon Press Ltd. Printed in Northern Ireland

RESEARCH NOTE

The heat balance of the *F*-region and the saturation effect

(*Received* 22 *August* 1961)

FROM the work of various authors, based on the original work of BATES and MASSEY (1947) and RATCLIFFE (1956), it appears possible to develop a consistent theory of the ionospheric *F*-region if this region is due primarily to monochromatic radiation acting on an atmosphere in diffusive equilibrium. The *F*-region bifurcates as a result of a transition in loss mechanism from predominantly a recombination type lower in the atmosphere to an attachment-like type higher up, while the heat balance of this region is governed by the input from the ionizing source and conduction downwards.

In this note it is proposed to give a qualitative picture of the variations of atmospheric scale height and electron production rates over the course of a sunspot cycle and show that the "saturation" effect in the maximum electron density of the *F*-region, as reported by CHUN-MING HUANG (1960), is a natural consequence of these postulates. It will also be shown that the simple postulate of heat loss by conduction only, is inadequate for the lower *F*-region and that BATES's (1951) suggestion of radiative cooling by infra-red emission from atomic oxygen will have to be included in any complete analysis of the problem.

VOL. 22 1961

Let us assume that equilibrium conditions have been established and that only one atmospheric constituent is ionized. Let us fix our coordinate system within this ionizable constituent. Then following CUMMACK (1961) the equation of heat flow under equilibrium conditions may be written in the form

$$K\left(\frac{mg}{k}\right)^{\frac{3}{2}} H^{\frac{1}{2}} \frac{\partial H}{\partial h} = \gamma I_\infty \{1 - \exp[-(P\sigma \operatorname{Ch}\chi)]\} \tag{1}$$

where $K\left(\frac{mgH}{k}\right)^{\frac{1}{2}}$ is the thermal conductivity and K is a function of atmospheric composition

H is the scale height of the ionizable constituent
γ the thermal equivalent of each photon
I_∞ the photon flux
P the partial pressure of the ionizable constituent
σ is proportional to the mass absorption coefficient
$\operatorname{Ch}\chi$ the "Chapman" function.

It has also been shown that if this equation is put in terms of the "reduced height" z, it becomes directly integrable.

Thus putting $P\sigma \operatorname{Ch}\chi = e^{-z}$

where $$z = \int \frac{dh}{H} \quad \text{and} \quad z = 0 \quad \text{at} \quad P\sigma \operatorname{Ch}\chi = 1$$

also putting $$A = \frac{\gamma}{K_{z=0}} \left(\frac{k}{mg}\right)^{\frac{3}{2}} (e - 1) \tag{2}$$

then equation (1) may be integrated to give

$$H^{\frac{1}{2}} - H_0^{\frac{1}{2}} = A\phi(z)\frac{1}{e}I_\infty \tag{3}$$

where

$$\phi(z) = \tfrac{1}{2}\int_0^z \frac{K_{z=0}}{K}\frac{\{1-\exp[-(\exp -z)]\}}{1-\exp(-1)}\,dz. \tag{4}$$

Further, from the general Chapman theory it is easily shown that

$$I_\infty = eq_0H_0 \tag{5}$$

where q_0 and H_0 are the values of the electron production rate and scale height at $P\sigma\,\mathrm{Ch}\chi = 1$. The product q_0H_0 will be taken as a measure of the incident ionizing flux throughout the rest of the paper.

Equation (3) thus takes the form

$$H^{\frac{1}{2}} - H_0^{\frac{1}{2}} = A\phi(z)q_0H_0. \tag{6}$$

If a suitable lower boundary can now be chosen it is possible to find the form of the variation of both q_0 and H_0 over the course of a sunspot cycle when the incident flux, denoted by q_0H_0, varies. As an initial working hypothesis, let us assume that there is a virtual heat sink situated at a constant partial pressure of the ionizable constituent and that the temperature variation at this sink over the course of a sunspot cycle is negligible. Let us denote the temperature and position of this sink by H_s and z_s. Further assume that $H_s < H_0$. Consequently z_s and $\phi(z_s)$ are negative.

Equation (6) thus becomes

$$H_s^{\frac{1}{2}} - H_0^{\frac{1}{2}} = A\phi(z_s)q_0H_0. \tag{7}$$

From equation (7)

$$\frac{\partial H_0^{\frac{1}{2}}}{\partial(q_0H_0)} = -A\phi(z_s). \tag{8}$$

By further manipulation of equation (7)

$$\frac{\partial q_0}{\partial(q_0H_0)} = \frac{1}{H_0}\left[2\left(\frac{H_s}{H_0}\right)^{\frac{1}{2}} - 1\right]. \tag{9}$$

Thus q_0 increases to a maximum, at a time when $H_0 = 4H_s$ and then declines.

When $H_0 = 4H_s$ we may derive the condition

$$H_0^{\frac{1}{2}} = -2A\phi(z_s)q_0H_0. \tag{10}$$

A further relation of interest which may be derived is

$$\Gamma_0\phi(z_s) = -\tfrac{1}{2}. \tag{11}$$

Here Γ_0 denotes the value of $\partial H/\partial h$ at $z = 0$.

It is now required to see if the previous theoretical model is applicable to the ionosphere.

The constant A may be computed on the assumption that the ionospheric F-region is formed from the absorption of He II photons at 304 Å and that the thermal energy given to the atmosphere is 40·6 eV per electron formed. The thermal conductivity constant K is taken as that corresponding to an atmosphere predominantly in atomic form. Both these estimates are probably too high. It is further assumed that the ionizable constituent is atomic oxygen. Under these conditions we can compute $A \simeq 1{\cdot}1 \times 10^{-7}$ cm$^{5/2}$ per electron.

Table 1

	Sunspot number	
	130	20
q_0 (electrons/cm^3)	1400	350
H_0 (km)	70	35
q_0H_0 (electrons/cm^2)	$9{\cdot}8 \times 10^9$	$1{\cdot}2 \times 10^9$

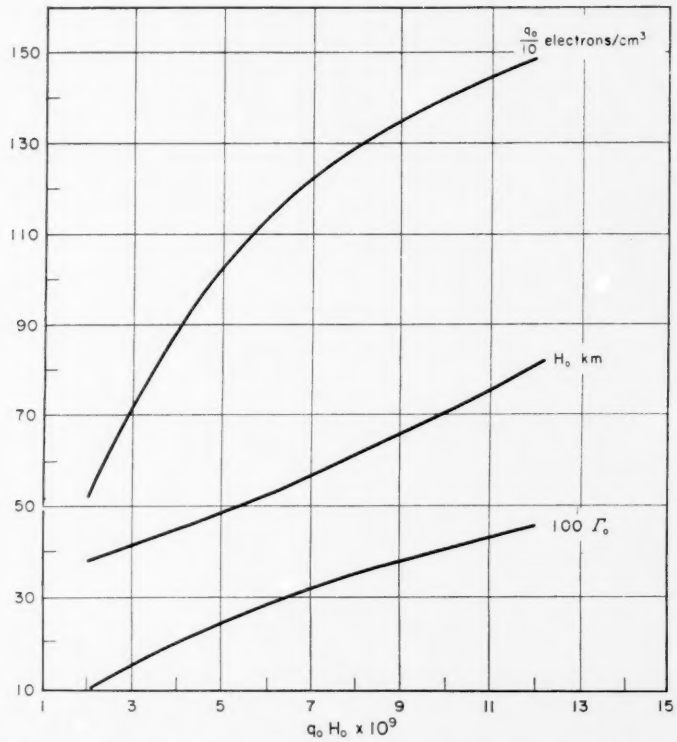

Fig. 1. The variation of q_0, H_0 and Γ_0 plotted against the incident ionizing flux, as measured by the product q_0H_0.

The estimates of q_0 and H_0 will be taken as those given by KING (1961) which were derived from transition theory. These are given in Table 1.

Now substituting these values in equation (7) we obtain $H_s = 30$ km and $\phi(z_s) = -0{\cdot}83$. From this value of $\phi(z_s)$ and equation (4) it is possible to show that $z_s \simeq -1{\cdot}2$ and that this value is not particularly sensitive to composition variations.

Using these values of H_s and $\phi(z_s)$ it is now possible to compute the variation of q_0, H_0 and Γ_0 with q_0H_0. This is shown in Fig. 1.

Further we are able to predict that the critical conditions which occur when $H_0 = 4H_s$ correspond to a value of $q_0H_0 \simeq 2 \times 10^{10}$ electrons/cm^2.

The curve of H_0 in Fig. 1 shows that H_0 is less than the critical value of $4H_s$ over the

VOL. 22 1961

plotted portion of the curve. q_0 is thus increasing with q_0H_0 though it is showing a marked flattening at higher values of q_0H_0. It is now suggested that this flattening effect is also observable in a plot of the maximum electron density of the *F2*-layer, N_m, against sunspot number and that the "saturation" effect observed at high sun-spot number may be explained in terms of the model here presented.

Since no data are available on the variation of the ionizing flux with sunspot number and N_m is related in some way to q_0 then Fig. 1 may be taken as a plot of N_m against sunspot number in unspecified units.

The previous analysis has been performed in coordinates fixed in atomic oxygen with $z = 0$ defined as the level where $P\sigma\ \mathrm{Ch}\chi = 1$, but if we wish to examine variations under different solar zenith angles, then equation (7) must be transformed. Now, if the virtual sink remains at a fixed partial pressure of atomic oxygen then the reduced height difference between the level $P\sigma\ \mathrm{Ch}\chi = 1$ and the sink becomes $z_s - \log \mathrm{Ch}\chi$. Also values of q_0H_0 must be normalized by $\mathrm{Ch}\chi$. Equation (7) thus becomes

$$H_s^{\frac{1}{2}} - H_0^{\frac{1}{2}} = A\phi(z_s - \log \mathrm{Ch}\chi)\,\frac{q_0H_0}{\mathrm{Ch}\chi}\,. \tag{12}$$

The saturation effect then occurs where

$$q_0H_0 = \frac{H_s^{\frac{1}{2}}\,\mathrm{Ch}\chi}{A\ \phi(z_s - \log \mathrm{Ch}\chi)} \tag{13}$$

and for constant values of H_s and z_s this occurs at higher values of q_0H_0 in temperate latitudes than those near the equator. There is evidence for this in CHUN-MING HUANG's description of the saturation effect.

BULLEN (1961) has shown that the height of maximum electron density of the *F2*-layer continues to climb with increasing sunspot number, even though the maximum electron density is flattening off. The height of maximum electron density is a crude index of atmospheric scale height since the whole atmosphere expands on heating. This result is thus in agreement with the postulated model.

This theory is open to criticism. Many factors which may affect the results have been overlooked purely for the sake of simplicity. BATES (1951) has shown that for the upper *F*-region at least the cooling by infra-red emission from atomic oxygen is probably next to conduction in importance. Also, since the values of H_s and z_s computed above put the effective sink at about one scale height below the maximum of electron production, it is not rigorously permissible to replace a distributed sink by one at fixed z although it is probably a reasonable approximation. From this, however, it is inferred that the thermal loss from the *F*-region is roughly that of thermal conduction downwards to a height of perhaps 140 km where radiative cooling becomes important.

The assumption of a fixed temperature at the sink may not be justified but this may be tested by considering a larger body of data.

Should the assumption of monochromatic radiation acting on an atmosphere composed predominantly of atomic oxygen be inadequate, then provided the atmospheric composition at *F*-region heights remains unchanged over the course of a sunspot cycle, equation (7) remains unchanged, save for a constant factor in the coefficient A and a modification in the integral $\phi(z_s)$. The conclusion that a "saturation" effect exists at some value of incident flux, however remains unchanged.

This description of the variations of the ionospheric parameters q_0 and H_0 with varying ionizing flux, though only qualitative, is able to give a reasonable form to these variations as well as predict the existence of a saturation effect and to some extent its variation with

latitude. The theory also shows the necessity for a mechanism of heat loss other than conduction which could be satisfied by BATES's suggestion of radiation from atomic oxygen.

Acknowledgements—This work is part of the research programme of the Christchurch Geophysical Observatory of the New Zealand Department of Scientific and Industrial Research, Superintendent, Mr. J. W. BEAGLEY. Thanks are due to Mr. G. A. M. KING and Miss J. M. BULLEN for many helpful discussions.

C. H. CUMMACK

Geophysical Observatory
Christchurch, New Zealand

REFERENCES

BATES D. R. and MASSEY H. W. S.	1947	*Proc. Roy. Soc.* A **192,** 1.
BATES D. R.	1951	*Proc. Phys. Soc. Lond.* B **64,** 805.
BULLEN J. M.	1961	*N.Z. J. Geol. Geophys.* In press.
CHUN-MING HUANG	1960	*J. Geophys. Res.* **65,** 897.
CUMMACK C. H.	1961	*J. Geophys. Res.* In press.
KING G. A. M.	1961	*J. Geophys. Res.* In press.
RATCLIFFE J. A.	1956	*J. Atmosph. Terr. Phys.* **8,** 260.

VOL.
22
1961

Journal of Atmospheric and Terrestrial Physics, 1961, Vol. 22, p. 303. Pergamon Press Ltd. Printed in Northern Ireland

Indices of geomagnetic activity

of the Observatories HARTLAND (*Ha*), ESKDALEMUIR (*Es*) and LERWICK (*Le*)

August 1961

The figures given on this page represent the K-indices for three-hour intervals, beginning with 00–03 hrs for the first and ending with 21–24 hrs for the eighth figure.

August 1961

Day	*Ha* *Range for* $K = 9{:}500\gamma$			*Es* *Range for* $K = 9{:}750\gamma$			*Le* *Range for* $K = 9{:}1000\gamma$			*Day*
	K-Indices		*Sum*	*K-Indices*		*Sum*	*K-Indices*		*Sum*	
1	3310	1122	13	3221	1223	16	3311	1122	14	1
2	5534	3432	29	5544	4432	31	6543	3334	31	2
3	2333	3333	23	2223	3333	21	3332	3334	24	3
4	5323	3322	23	4333	3332	24	5433	3332	26	4
5	2223	3223	19	1123	3223	17	1122	3222	15	5
6	3212	3222	17	3112	3323	18	2112	2222	14	6
7	0010	1122	7	0011	3223	12	1111	2122	11	7
8	1233	2341	19	1232	3341	19	1233	3341	20	8
9	1210	1110	7	1211	1110	8	1211	1110	8	9
10	3221	3221	16	3321	3222	18	3312	4322	20	10
11	3423	3334	25	3323	4334	25	4423	4344	28	11
12	1211	1233	14	1210	2233	14	3201	1223	14	12
13	2110	0010	5	2111	0111	8	2211	1110	9	13
14	0011	3430	12	0021	3431	14	0012	3431	14	14
15	1132	2322	16	1122	3323	17	1122	2222	14	15
16	2210	0111	8	2221	1211	12	2211	1211	11	16
17	0002	2222	10	1112	2231	13	1111	1121	9	17
18	1001	2311	9	1111	3312	13	1011	2211	9	18
19	2332	2101	14	2333	2312	19	2332	2201	15	19
20	1002	1431	12	1003	2422	14	0002	2331	11	20
21	2101	1210	8	2212	2221	14	1111	1211	9	21
22	1010	0001	3	1110	2111	8	0011	0011	4	22
23	0010	1112	6	1011	1211	8	0011	0112	6	23
24	0010	2332	11	0001	2332	11	0001	1222	8	24
25	2222	3223	18	2122	3213	16	2122	3212	15	25
26	2213	3234	20	2213	3334	21	1213	2234	18	26
27	3131	1221	14	3231	2312	17	4231	1211	15	27
28	2211	1021	10	2212	2222	15	2111	1211	10	28
29	2001	2444	17	2102	2454	20	2101	2345	18	29
30	5323	5444	30	4323	5445	30	4323	4645	31	30
31	4433	3434	28	4432	3434	27	5541	3434	29	31

Journal of Atmospheric and Terrestrial Physics, 1961, Vol. 22, p. 304. Pergamon Press Ltd. Printed in Northern Ireland

Papers to be published in future issues

R. K. Suryanarayana: Effect of radio fade-out on the *F2*-layer

R. G. Flavell and J. A. Lane: The application of potential refractive index in tropospheric wave propagation

M. A. Uman: Bead lightning and the pinch effect

R. E. Barrington and E. Thrane: The determination of *D*-region electron densities from observations of cross modulation

B. Hultqvist: On the orientation of auroral arcs

J. K. Hargreaves: The behaviour of the lower ionosphere near sunrise

M. W. Chiplonkar, R. N. Karekar and P. R. Marwadi: Midnight fall in atmospherics activity of 27 kc/s band at Poona

R. W. Ditchburn and P. A. Young: The absorption of molecular oxygen between 1850 and 2500 Å

T. Watanabe: Law of electric conduction for waves in the ionosphere

K. M. Kotadia: The equatorial sporadic-*E* layer and the electrojet

J. W. King and C. Graham: The relationship between f_0F2 and magnetic phenomena

T. Rikitake and T. Yukutake: A theory of s.f.e. current systems

A. Omholt, W. Stoffregen and H. Derblom: Hydrogen lines in auroral glow

J. E. Titheridge: The stratification of the lower ionosphere

J. E. Titheridge: The electron density in the lower ionosphere

J. Taubenheim: Information on the ionizing radiation of solar flares from the ionospheric absorption effect

M. V. Wilkes: The solar and luni-solar harmonic components of geomagnetic variation at San Fernando

A. Onwumechilli and P. O. Ogbuehi: Fluctuations in the geomagnetic horizontal field

O. Burkard: Recombination in the upper ionosphere

B. P. Sandford: Polar-glow aurora in polar cap absorption events

R. J. Hynds: Time variations of the electronic component of the cosmic radiation

M. K. Rao, S. C. Mazumdar and S. N. Mitra: Investigation of ionospheric absorption at Delhi

VOL.
22
1961

OL.
22
961

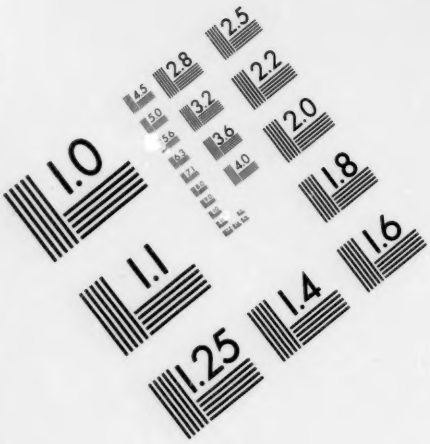

NATIONAL MICROGRAPHICS ASSOCIATION

MS303-1980

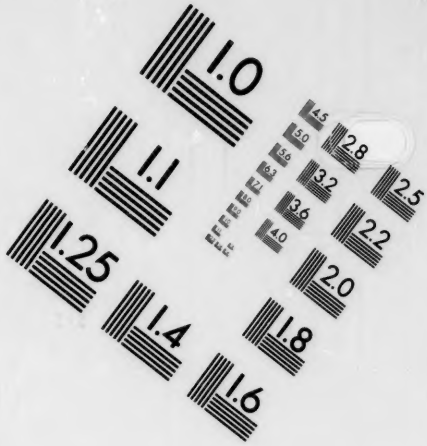

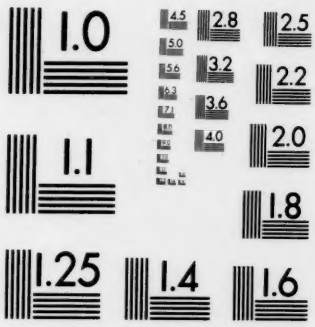

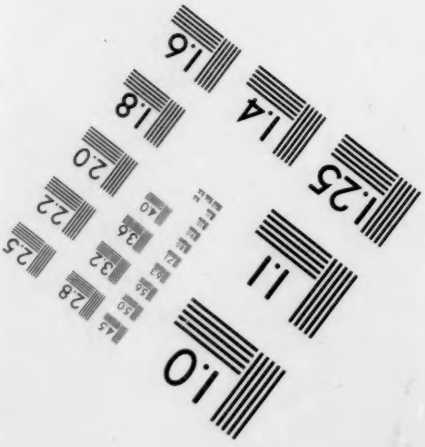

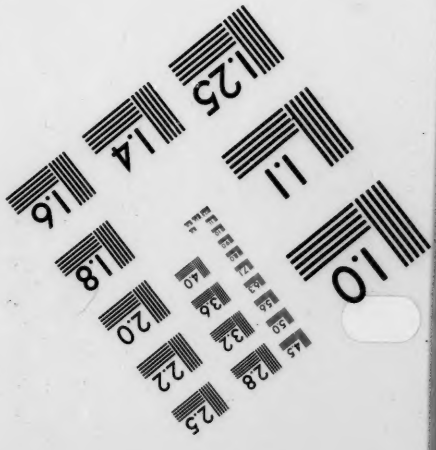

PERGAMON PRESS INC.

MICROFORMS INTERNATIONAL
MARKETING CORPORATION
FAIRVIEW PARK, ELMSFORD, NEW YORK 10523

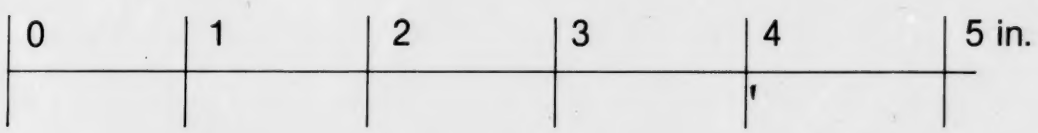

PRODUCED AT

MIMC MICROFORMS LABORATORY
ELMSFORD, NEW YORK